Stony Brook University

OFFICIAL COPY

The official electronic file of this thesis or dissertation is maintained by the University Libraries on behalf of The Graduate School at Stony Brook University.

© All Rights Reserved by Author.

Design, Synthesis and Biological Evaluation of Novel Tumor-targeting Taxane-based Drug Delivery Systems

A Dissertation Presented

by

Manisha Das

to

The Graduate School

in Partial Fulfillment of the

Requirements

for the Degree of

Doctor of Philosophy

in

Chemistry

Stony Brook University

August 2010

Copyright by
Manisha Das
2010

STONY BROOK UNIVERSITY

THE GRADUATE SCHOOL

Manisha Das

We, the dissertation committee for the above candidate for the

Doctor of Philosophy degree, hereby recommend

acceptance of this dissertation.

Iwao Ojima – Dissertation Advisor
Distinguished Professor, Department of Chemistry

Kathlyn A. Parker – Chairperson of Defense
Professor, Department of Chemistry

Peter J. Tonge – Third Member
Professor, Department of Chemistry

Howard Crawford – Outside Member
Associate Professor, Department of Pharmacological Sciences
Stony Brook University, Stony Brook, New York

This dissertation is accepted by the Graduate School

Lawrence Martin
Dean of the Graduate School

Abstract of the Dissertation

Design, Synthesis and Biological Evaluation of Novel Tumor-targeting Taxane-based Drug Delivery Systems

by

Manisha Das

Doctor of Philosophy

in

Chemistry

Stony Brook University

2010

Cancer continues to be a leading cause of death in the U.S. after heart disease and has become the leading cause of death for people younger than 85. Cancer chemotherapy relies on the hypothesis that rapidly proliferating cancer cells will be the more likely target of cytotoxic agents. However, cytotoxic agents have very little or no specificity towards cancer cells leading to systemic toxicity causing severe undesirable side effects. A tumor-targeting drug delivery system (DDS) that can distinguish between normal and cancer cells by utilizing their physiological and/or morphological differences is amongst the most promising protocols. Tumor cells overexpress many receptors and biomarkers which can be targeted to deliver chemotherapeutic agents specifically inside the cancer cells. Generally, a tumor-targeting DDS consists of a tumor-targeting moiety (TTM) connected to a cytotoxic agent directly or through a suitable linker.

A novel tumor-targeting DDS using folic acid as the TTM conjugated to a potent novel second-generation taxoid via a novel mechanism-based self-immolative linker has been successfully developed. In vitro internalization studies using confocal fluorescence microscopy (CFM) and flow cytometry as well as cytotoxicity assays against several folate receptor positive and negative cancer cell lines exhibited excellent specificity. Immunofluorescent assays demonstrated the release of the potent taxane and its binding to microtubules.

Another DDS using functionalized single-walled carbon-nanotubes (f-SWNT) as the drug delivery vehicle and biotin as the TTM was successfully developed to study dual therapy effects of thermal ablation and cytotoxicity. The intrinsic property of SWNT to absorb light at near-IR range and thermally ablate cells was successfully utilized in these studies. CFM studies demonstrated specific internalization and thermal ablation of biotin-receptor positive cancer cells.

The stability of disulfide linkers while in circulation and the effective disulfide bond cleavage to liberate the potent drug after the prodrug reaches the targeted tumor site is crucial in the design of successful linkers. A novel series of disulfide linkers have been designed and synthesized to study substituent effects and other key factors in their stability. The blood plasma stability of several DDS with biotin as TTM has also been determined.

Table of Contents

Chapter 1

Anticancer Drug Paclitaxel and Semi-synthesis of Taxoid using the *β*-Lactam Synthon Method

Chapter 2

Synthesis of C-3'-Difluorovinyl Taxoid SB-T-12851

Chapter 3

Synthesis and Stability Studies of Novel Disulfide Linkers

Chapter 4

Tumor-targeted Drug Delivery using Folate as the Tumor-targeting Moiety

Chapter 5

Functionalized SWNT (*f*-SWNT) as a Versatile Platform for Tumor-targeted Drug Delivery and Dual Therapy

Chapter 6

Synthesis of Novel Taxoid for PET Studies

List of Figures

Chapter 1

Chapter 2

Chapter 3

Chapter 4

Chapter 5

Chapter 6

List of Schemes

Chapter 1

Chapter 2

Chapter 3

Chapter 4

Chapter 5

Chapter 6

List of Tables

Chapter 2

Chapter 3

Chapter 4

Chapter 5

Chapter 6

List of Abbreviations

5-FU	5-fluorouracil
10-DAB III	10-deacetylbaccatin III
10-HCPT	10-hydroxycamptothecin
Å	angstrom
Ac	acetyl
AcOH	acetic acid
AGM	aminoglutethimide
AML	acute myelogenous leukemia
Anal	analysis
atm	atmosphere
ATP	adenosine triphosphate
AuNPs	gold nanoparticles
bd	broad doublet
Bn	benzyl
b.p.	boiling point
br	broad
bs	broad singlet
Boc	*tert*-butoxycarbonyl
t-Bu	tert-butyl
n-BuLi	n-butyllithium
Bz	benzoyl
Calcd	calculated
CAN	cerium(IV) ammonium nitrate
CDR	complementarity determining region
CFM	confocal fluorescence microscopy
CNT	carbon nanotube
CPT	camptothecin
CVD	chemical vapor deposition
CW	continuous wave
d	doublet
DCC	*N*,*N*'-dicyclohexylcarbodiimide
DCM	dichloromethane
dd	doublet of doublet
DDS	drug delivery system
de	diastereomeric excess
DHA	docosahexaenoic acid
DIC	*N*,*N*-diisopropylcarbodiimide
DIPEA	*N*,*N*-diisopropylethylamine
DM1	methyldithio-maytansinoid
DMAP	4-*N*,*N*'-dimethylaminopyridine
DMF	*N*,*N*'-dimethylformamide
DMS	dimethyl sulfide
DMSO	dimethyl sulfoxide
DNA	deoxyribonucleic acid

DOS	density of states
DOX	doxorubicin
DTPA	diethylentriaminepentaacetic acid
DTT	dithiothreitol
EC_{50}	concentration of drug that produces 50 % effect
EDC.HCl	1-ethyl-3-(3-dimethylaminopropyl)carbodiimide hydrochloride
ee	enantiomeric excess
EE	ethoxyethyl
e.g.	for example
EGFR	epidermal growth factor receptor
EPR	enhanced permeability and retention
eq	equivalent
ESI	electrospray ionization
Et	ethyl
et al.	and others
EtOAc	ethyl acetate
EtOH	ethanol
EVE	ethyl vinyl ether
FA	folic acid
FDA	Food and Drug Administration
FITC	fluorescein isothiocyanate
FR	folate receptor
fs	femto second
F-SWNT	fluorinated single-walled carbon nanotube
f-SWNT	functionalized single-walled carbon nanotube
FTIR	fourier tranform infrared spectroscopy
g	gram
GC	gas chromatography
GDP	guanosine 5'-diphosphate
GI	gastrointestinal
GlcNAc	*N*-acetyl-D-glucosamine
GlcUA	D-glucuronic acid
GSH	glutathione
GSH-OEt	glutathione mono ethyl ester
GTP	guanosine 5'-triphosphate
h	hour
HA	hyaluronic acid
HATU	2-(1H-7-azabenzotriazol-1-yl)-1,1,3,3-tetramethyl uronium
HEX	hexanes
HiPCO	high pressure carbon monoxide
HMPA	hexamethylphosphoramide
HOBT	1-hydrobenzotriazole hydrate
HOSu	*N*-hydroxysuccinimide
HPLC	high performance liquid chromatography
HPMA	*N*-(2-hydroxypropyl)methacrylamide copolymer
HRMS	high resolution mass spectrometry

HAS	human serum albumin
Hz	hertz
IC_{50}	concentration for 50 % inhibition
i.e.	that is
iPr	isopropyl
IR	infrared spectroscopy
J	coupling constant
Kd	dissociation constant
kDa	kilodalton
kg	kilogram
KHMDS	potassium 1,1,1,3,3,3-hexamethyldisilazide
L	liter
LC	liquid chromatography
LDA	lithium diisopropylamide
LiHMDS	lithium 1,1,1,3,3,3-hexamethyldisilazide
m	multiplet
M	molar or molarity
mAb	monoclonal antibody
MALDI–TOF	matrix-assisted laser desorption ionization time-of-flight
MAPs	microtubule associated proteins
MDR	multi-drug resistance
MDS	methyldisulfanyl
Me	methyl
MeOH	methanol
mg	milligram
MHz	megahertz
min	minute
mL	milliliter
MMAE	monomethyl auristatin E
mM	millimolar
mmol	millimole
MMPNs	multifunctional magneto-polymeric nanohybrids
MNP	magnetic nanoparticles
mol	mole
m.p.	melting point
MPA	methylpyridinium acetate
MRI	magnetic resonance imaging
MS	mass spectrometry
MTD	maximum tolerated dose
MTX	methotrexate
MWNT	multi-walled carbon nanotube
NCI	National Cancer Institute
ND	no data
NaHMDS	sodium 1,1,1,3,3,3-hexamethyldisilazide
NIR	near infra-red
nJ	nano joule

NLS	nuclear localization sequence
nM	nanomolar
NMO	*N*-methylmorpholine-*N*-oxide
NMR	nuclear magnetic resonance
OEG	oligoethylene glycol
PABC	*p*-aminobenzyloxycarbonyl
PAMAM	polyamidoamine
PBS	phosphate buffered saline
PDT	pyridyldithio
PEG	poly(ethylene glycol)
Pgp	P-glycoprotein
Ph	phenyl
PLAP	pig liver acetone powder
pM	picomolar
PMA	phosphomolybdic acid
PMP	*p*-methoxyphenyl
ppm	parts per million
PSMA	prostate-specific membrane antigen
p-TSA	*p*-toluenesulfonic acid
Py	pyridine
q	quartet
QD	quantum dot
RF	radiofrequency
RNA	ribonucleic acid
r.t.	room temperature
s	singlet
SA	streptavidin
SAR	structure-activity relationship
SCID	severe combined immunodeficiency
SPION	superparamagnetic iron oxide nanoparticle
SPP	*N*-succinimidyl-4-(2-pyridyldithio)pentanoate
SPR	surface plasmon resonance
SST	somatostatin
SWNT	single-walled carbon nanotube
t	triplet
t1/2	half time
TAP	tumor activated prodrug
TBDMS	*tert*-butyldimethylsilyl
TEA	triethylamine
TEM	transmission electron microscopy
tert	tertiary
TES	triethylsilyl
Tf	triflouromethanesulfonate
TFA	trifluoroacetic acid
THF	tetrahydrofuran
TIPS	triisopropylsilyl

TLC	thin layer chromatography
TMS	trimethylsilyl
TOPO	trioctylphosphine oxide
TTM	tumor-targeting molecule
U.S.	United States
USDA	U.S. Department of Agriculture
U-tube	ultra short carbon nanotube
UV	ultraviolet-visible
W/cm^2	$Watt/cm^2$
wt	weight
[α]	specific optical rotation
β-LSM	*β*-Lactam Synthon Method
δ	chemical shift
µg	microgram
µL	microliter
µM	micromolar
µm	micrometer
µmol	micromole
USPION	ultrasmall superparamagnetic iron oxide nanoparticle

Acknowledgments

This dissertation would not have been complete without the support and cooperation from various individuals at various stages and I owe them all everlasting gratitude. First and foremost, I would like to express my deepest and most sincere gratitude to my dissertation advisor Distinguished Professor Iwao Ojima for his invaluable guidance and continuous support throughout my graduate study. He has been most instrumental in ensuring my academic and professional well being and none of this work would have been possible without him. Professor Ojima set the perfect example of a dedicated scientist with his relentless commitment to excellence in research and his extremely valuable contributions to chemistry. His creative ideas, remarkable perseverance and steadfast meticulousness have truly inspired me. I would like to thank Professor Ojima for giving me the opportunity to be a part of his group and making my graduate days at Stony Brook the most academically enriching and memorable years of my life.

I would like to extend my heartfelt thanks to the chair of my committee, Professor Kathlyn Parker for her help and insightful comments throughout my graduate study. I would like to express my deepest thanks to the third member of my committee, Professor Peter Tonge for all his help and I greatly appreciate his invaluable suggestions. I would also like to thank Professor Howard Crawford of the Department of Pharmacological Sciences for taking the time out of his busy schedule to be the fourth member of my committee.

I would like to thank all the professors of the Chemistry department for providing me insights into various aspects of Chemistry. I would like to thank all the past and current ICB&DD members for their help especially Dr. Bela Ruzsicska for all the analytical support and help. I would like to thank Ms. Rebecca Rowehl and Dr. Anne Savitt, Cell Culture and Hybridoma Facility for all their help and valuable comments. I would like to thank our collaborator, Professor Jon Longtin from the Department of Mechanical Engineering for sharing his expertise in his discipline with me.

A special thanks to our NMR specialist, Dr. James Marecek, for his kind assistance in NMR spectroscopy and many insightful discussions on my research. I thank Mrs. Katherine Hughes, Student Affairs Coordinator, for her timely assistance and help during my stay at Stony Brook.

I want to express my true appreciation to all of the past and present members of the Ojima group for their support throughout my graduate study at Stony Brook. I thank them for their valuable discussions as well as warm relationships.

I would like to express my thanks to Mrs. Yoko Ojima for her gracious hospitality and kindness. She has made every Ojima group traditional event memorable with her generosity, attention to detail and aesthetic sensibilities. I would like to thank Mrs. Patricia Marinaccio, our Project Staff Assistant for her kindness, support and words of advice throughout my stay; she is truly the “Mom” of the Ojima Group.

I am most grateful to my parents, grandparents and uncle for their unconditional love and support over all the years. I would like to specially acknowledge my parents for all the sacrifices they have made for me. A very special thanks goes to my husband for his undying encouragement, love and support throughout my graduate studies and always.

I thank you very much for believing in me and encouraging me to pursue my childhood dream. I admire your endurance and commitment and the extreme sacrifice you made for me; I feel truly blessed.

I would like to thank my friends, Krithika, Neelam, Rupa and Mike for always being there for me and for making this difficult and challenging journey enjoyable for me. Krithika, I thank you for all the patience, support and kindness that you have extended towards me over the years. Neelam, I thank you for your constant encouragement, support and for being there for me. Rupa, I thank you for all your help. Mike you have been there whenever I needed a friend and I thank you for that.

Finally, I would like to acknowledge the financial support from the National Institutes of Health, National Cancer Institute, and the Department of Chemistry at Stony Brook.

Chapter 1
Anticancer Drug Paclitaxel and Semi-synthesis of Taxoid using the *β*-Lactam Synthon Method

1.1 Introduction: Cancer and its Treatment

Cancer is the second leading cause of death in the United States after heart disease and affects millions of people worldwide. According to the statistics released by the American Cancer Society in 2010 it is estimated that more than 1.4 million new cases of cancer will be diagnosed and more than half a million people will die from it in the United States alone i.e. more than 1500 people per day are going to die from cancer.[1] There is an estimated more than 12 million new cases of cancer and more than 7 million deaths worldwide. It is projected that more than 21 million new cases will be diagnosed globally by 2030 (up 69 % compared to 2008) and more than 13 million deaths will occur globally by 2030 (up 72 % compared to 2008).[2] In fact cancer has surpassed heart disease as the leading cause of death for people younger than 85 years of age. Though there has been a decline in the incidence of cancer by 1.8 % per year from 2001-2005 in men and a decline of 0.6 % per year from 1998-2005 in women in the United States[1] much remains to be done to combat this deadly disease.

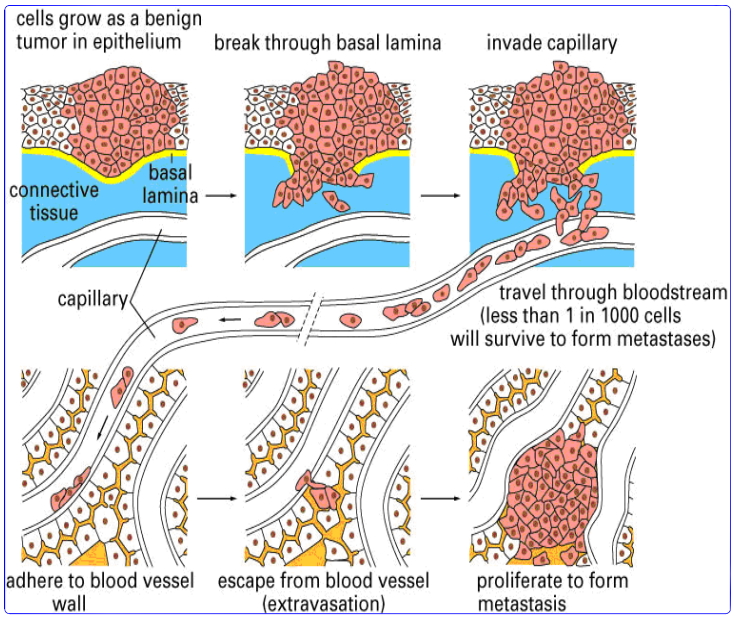

Figure 1-1. Schematic illustration of cancer formation and metastasis[3] (Adapted from http://64.202.120.86/upload/image/articles/2008/smart-bombing-cancer/cell-grow.jpg)

The Greek physician Hippocrates (460-370 B.C.) used the word *carcinos* and *carcinoma* to describe tumors and is credited for the origin of the word *cancer*. In Greek these words mean a *crab* probably because of the spreading projections associated with cancer. Celsus, the Roman physician later translated the word to *cancer* which is the Latin word for *crab*. Cancer is the collective term for a group of diseases which are characterized by an unrestrained division of cells and the ability of these cells to proliferate and invade other tissues either by direct invasion into the neighboring tissues or by metastasizing to distant sites.

Cancer can be caused by various external (chemicals, radiation, viruses, etc) and internal (mutation, immune conditions, hormones, etc) factors which cause mutations to genes that encode for the proteins controlling the cell division. This mutation results in accelerated and uncontrolled growth of cells which causes the formation of tumor mass or neoplasm i.e. a discrete population of cells which grow independently. Tumors can be benign or malignant whereas cancer is by definition malignant. A benign tumor is usually composed of cells that bear a strong resemblance to the normal cells of the organs from where it originates and if required can be easily removed by surgery in most cases. A benign tumor is usually harmless and grows slowly whereas a malignant tumor grows much faster and invades neighboring tissues and can metastasize i.e. break away or dislodge from the parent tumor and spread to other organs or distant parts of the body through the bloodstream or lymph system. A malignant tumor or cancer is made up of cells that are different from the normal cells around them and grows much faster than the normal cells.

Physicians use different names to identify cancers and naming conventions are not standardized. Cancers are usually named based on one of the following:

a) Site of the body where it originated (breast, lung, liver, etc)
b) Type of tissue involved (carcinoma, adenocarcinoma, etc)
c) Type of cancer cell (basal cell, squamous cell, etc)
d) Stage of cancer

Cancer can be treated by surgery, radiation therapy, chemotherapy and other methods as well as combination therapy like surgery and chemotherapy. The choice of therapy usually depends on various factors like the stage of the cancer, location and type of cancer as well as the medical history of the patient.

a) Surgery

   Surgery is used to remove the malignant tumor or the organ where the tumor is located. However often cases the tumor cannot be entirely excised and it can grow back. Complete surgical removal of tumor is usually impossible when the tumor metastasizes prior to surgery.

b) Radiation therapy

   Radiation therapy uses ionizing radiation to kill the malignant cells and shrink the tumor and can be used to treat solid tumors. However it is not effective against other types of tumor like leukemia and radiation can also damage neighboring tissue causing undesirable side effects.

c) Chemotherapy

Chemotherapy is the treatment of disease with drugs; cancer chemotherapeutic drugs or cytotoxic drugs impair mitosis or cell division and effectively target the fast dividing cells causing apoptosis or other forms of cell death. These cytotoxic chemotherapeutic drugs however make little or no distinction between normal and cancer cells and thus systemic non-cancerous fast-dividing cells like those for hair growth, bone marrow, intestinal lining, etc are often affected. This often results in severe undesirable side effects which is a major drawback of chemotherapy. Some of the common side effects are depressed immune system, hair loss, nausea, vomiting, anemia, diarrhea or constipation, cardiotoxicity, hemorrhage, etc. Since chemotherapy affects cell division malignant tumors like aggressive lymphomas, acute myelogenous leukemia, etc which have higher growth rate are more sensitive to chemotherapy while malignant tumors with slower growth rate respond much slowly to chemotherapy. Tumors that are more differentiated or younger tumors are affected more by chemotherapy than older tumors where differentiation is typically lost and the growth is not as regulated. Chemotherapy can be used to prolong life by ameliorating symptoms and decreasing tumor load or to cure the condition. There are different strategies for administering chemotherapeutic drugs. In neoadjuvant or preoperative chemotherapy the tumor is usually shrunk by administering drugs and then surgery or radio therapy is used which is more effective. Adjuvant or postoperative chemotherapy is used when there is a risk of cancer recurrence to destroy any remaining cancerous cells. Combination chemotherapy involves using different drugs which can differ in mechanism. Combined modality chemotherapy involves using drugs with other forms of treatment like surgery or radiation therapy. Chemotherapy is the most prevalent form of treatment and the drugs can be divided into different categories like plant alkaloids (e.g. taxanes, vinca alkaloids), anthracycline antibiotic (e.g. doxorubicin, daunorubicin), DNA targeting agents (e.g. cisplatin, carboplatin), topoisomerase inhibitors (e.g. topotecan, irinotecan), antimetabolites (e.g. methotrexate), antitumor antibiotics (e.g. dactinomycin). Some of the chemotherapy drugs are shown in Figure 1-2.

d) Immunotherapy

Immunotherapy uses the body's own system to reject the cancer like using therapeutic antibodies to modulate the body's natural defense mechanism.

e) Hormonal therapy

Hormonal therapy is a form of systemic therapy which can be used to help reduce the risk of cancer recurrence after treatment or after the cancer has spread. It is used for treating cancers of the breast, prostate, etc by lowering hormone levels or sometimes by supplying certain hormones.

f) Cancer vaccines

Cancer vaccines can be prophylactic/preventive or therapeutic. The prophylactic vaccines are intended to prevent cancer from developing in healthy people and therapeutic vaccines are intended to treat existing cancers by fortifying the body's natural defenses against cancer.

g) Bone marrow transplant

In bone marrow transplant the diseased bone marrow of the patient is destroyed and replaced with healthy bone marrow from the donor. In a successful transplant the bone marrow then migrates to the cavities of the bones and starts producing healthy normal cells.

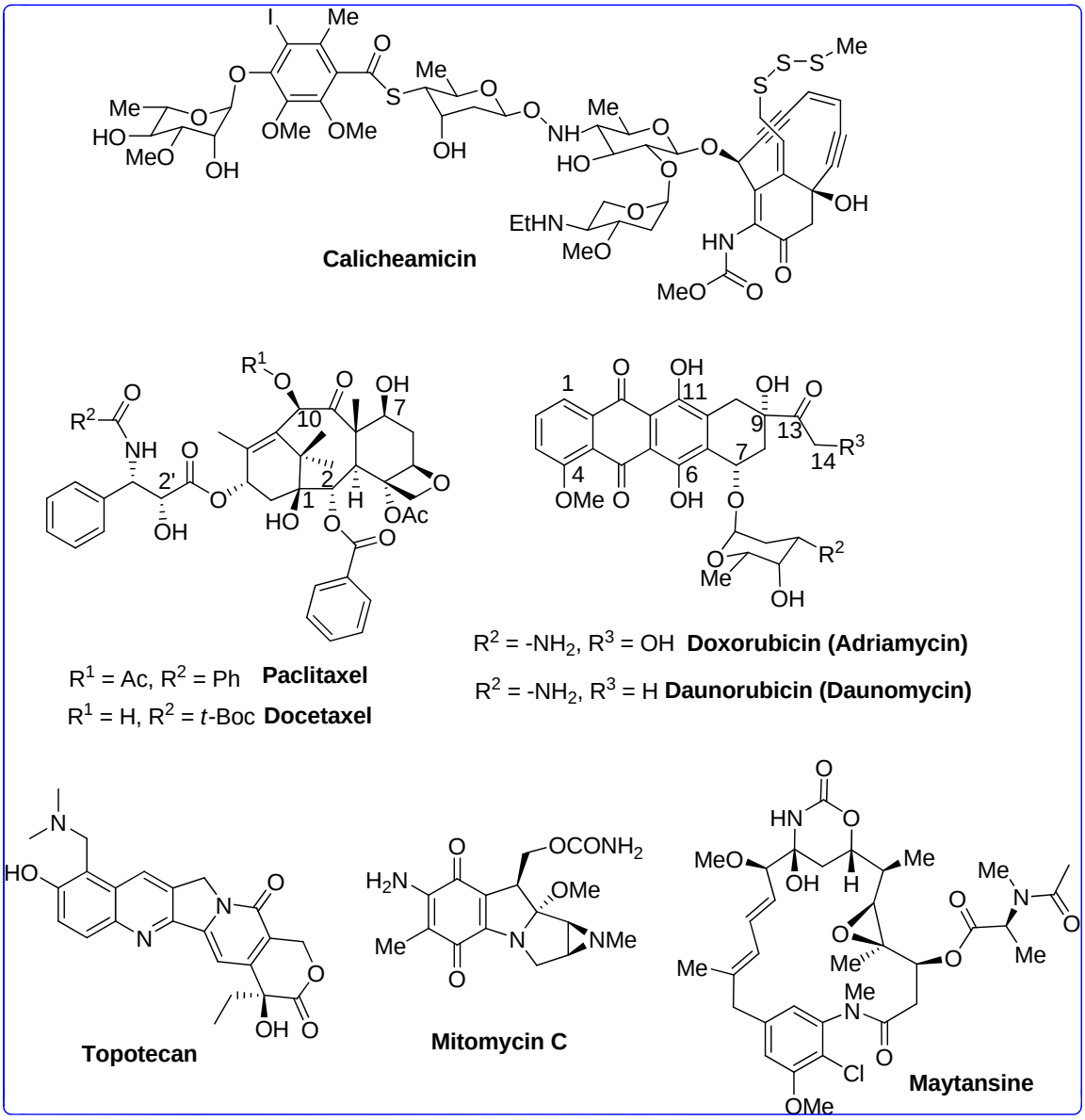

Figure 1-2. Examples of some chemotherapeutic drugs

1.2 Anticancer Drug Paclitaxel

1.2.1 Discovery and Development

Paclitaxel is a mitotic inhibitor and is used in cancer treatment. In the 1950s the National Cancer Institute (NCI) started an exploratory plant screening program. The objective was to identify and evaluate potential anticancer drug sources in nature. In 1960 NCI commissioned the United States Department of Agriculture (USDA) to collect plant species for screening.[4] More than 35000 plant species were screened for anticancer activity.[5] One sample was collected from the Pacific Yew tree - *Taxus brevifolia* Nutt. growing in the Gifford Pinchot National forest in the state of Washington. The extract from the bark of this tree was found to have tumor inhibitory properties and potent cytotoxicity against mouse leukemia. The extract was sent to the laboratory of Wall and Wani in Research Triangle Park, North Carolina for identification and characterization and it was not until 1971 that Wall, Wani and their coworkers succeeded in the identification of the active component of this natural extract.[6] Taxol® (paclitaxel) is a complex diterpene and has a tetracyclic framework including an oxetane D-ring with an *N*-benzoylphenylisoserine side chain attached to the C-13 hydroxy group. There are 11 chiral centers and 14 oxygen atoms present in the molecule. Paclitaxel has a molecular weight of 853.90 and a molecular formula $C_{47}H_{51}NO_{14}$. Paclitaxel is one of the best selling anticancer drugs with annual sales of $ 1.6 billion in 2000.

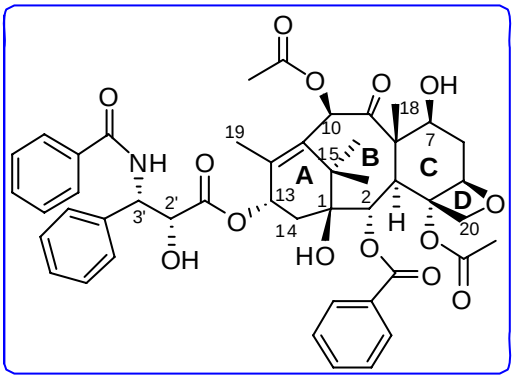

Figure 1-3. Structure of paclitaxel

1.2.2 Mechanism of Action of Paclitaxel

Paclitaxel was believed to be a typical spindle poison with a mechanism similar to other known vinca alkaloids.[7] However, in 1979 Susan Horwitz and her coworkers[8-10] discovered that paclitaxel possesses a unique mechanism of action unlike the other naturally occurring microtubule poisons like vinca alkaloids, colchicine, etc.[11] Microtubule is an important structural component of cells and plays a critical role in cytoskeletal formation and cell division. The biological role of microtubules is regulated

mainly by the polymerization dynamics.[12] Paclitaxel disrupts the tubulin-microtubule equilibrium by actually promoting polymerization unlike the vinca alkaloids which inhibit polymerization of tubulins to form microtubules thereby disrupting cell division cycle and causing apoptosis and cell death. Paclitaxel promotes polymerization, stabilizes the resulting microtubules and prevents depolymerization thereby inhibiting the normal dynamic reorganization of microtubular network required for mitosis, which eventually induces apoptosis and cell death.[8] The cell cycle and role of microtubule-targeting anticancer agent is shown in Figure 1-4.[5]

Cells have a characteristic life cycle that can be divided into two major phases based on cellular activity – *interphase* and *mitosis* and microtubules play a very important role in cell division governing the location of membrane-bound organelles and other cell components[13] which makes it one of the best known targets in cancer chemotherapy. *Interphase* is the first phase and is the period of time between successive cell divisions. During *interphase*, the size of the cell increases as new proteins are synthesized and the genetic material is duplicated. *Interphase* is characterized by three subphases G1-S-G2. The G1 (GAP 1) is the first growth phase and lasts for 8-10 hours. During this phase the cell increases organelle numbers and cytoplasm grows in volume. S-phase is the synthesis of new proteins and duplication of the genetic material under slow microtubule dynamics. This stage is completed in 6-8 hours. The G2 - "GAP 2" is the second growth phase before mitosis stage. The G2 is generally shorter than G1, it lasts for 4-6 hours, and it is more uniform in duration among the different cell types. This is illustrated in the cell cycle diagram in Figure 1-5. The cell then enters the *mitosis* phase where the actual division occurs.

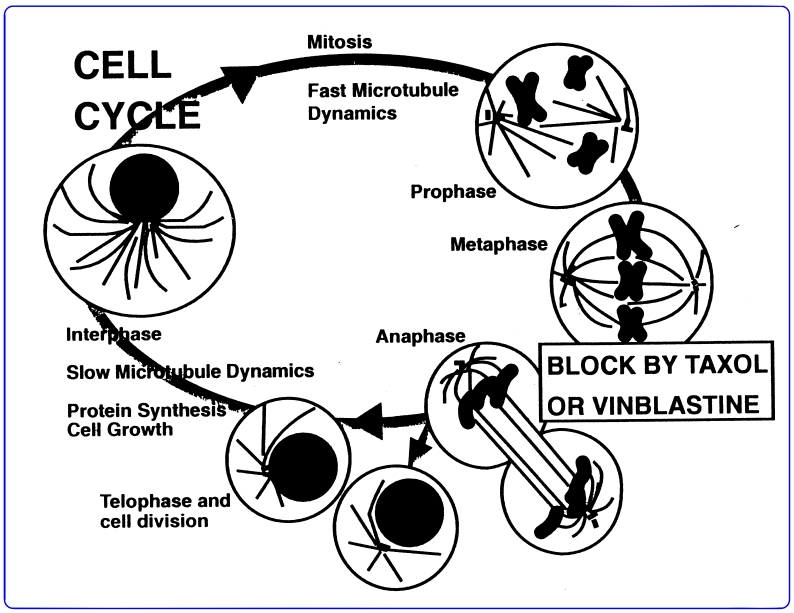

Figure 1-4. Cell cycle and microtubule targeting anticancer agent[5] (Adapted from Ref. 5)

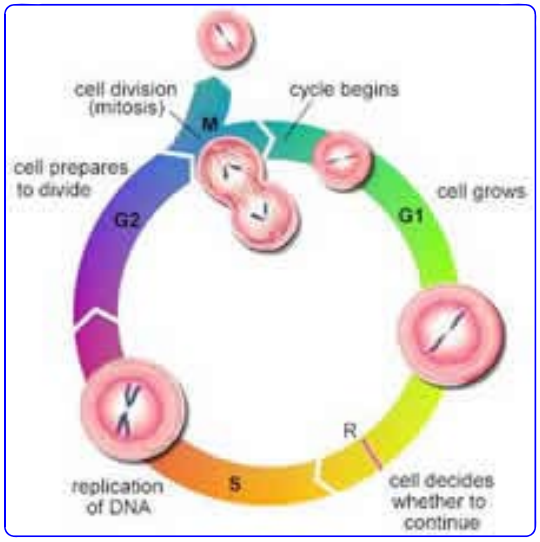

Figure 1-5. Cell cycle diagram[14] (Adapted from Ref. 14)

Mitosis can be further divided into several small phases lasting an hour or less. During the first stage of mitosis or *prophase*, the duplicated chromatin condenses into discrete chromosomes, each composed of two identical sister chromatids. The centrosome splits into two daughter centrosomes which serve as the spindle poles of the dividing cell later. Then in a "sun-burst" arrangement, spindles, composed of microtubules, start to radiate out from each centrosome to reach into the nucleus as the nuclear membrane breaks down. The process of mitosis is shown in Figure 1-6 where a cultured epithelial cell line stained with immunofluorescent antibodies for actin and microtubules and a DNA-specific dye for chromosomes.[15]

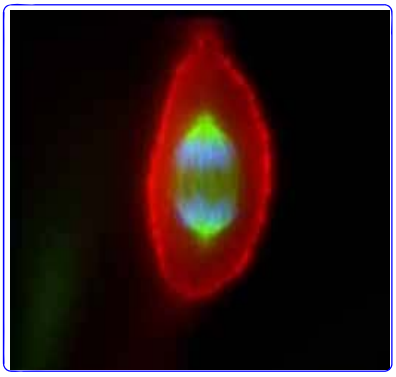

Figure 1-6. Process of mitosis visualized (Adapted from http://www.itg.uiuc.edu/technology/atlas/structures/actin/images/actin_microtubules.jpg&imgrefurl)

The cell reaches the *metaphase* stage once the spindles attach onto the sets of chromosomes and help align them along the "equator" of the cell. During *anaphase* the sister chromatids of each chromosome split apart and begin their poleward movement. The migration of each chromosome toward a pole is facilitated by the shortening of the microtubules to which they are attached. It is between *metaphase* and *anaphase* that microtubule-targeting agents such as paclitaxel or vinblastine disrupt the regular dynamics required for *mitosis*. As a result of this mitotic block, apoptosis or programmed cell death is eventually induced.[16]

When the chromosomes nearly reach their respective poles on each side of the mother cell, the cell enters *telophase*. At this phase the nuclear envelope reforms around each set of chromosomes and the cell membrane pinches off to form two daughter cells. After *mitosis* phase, cell can either enter the dormant G_0 phase or re-enter the cell cycle. G_0 phase is a stage outside the normal cell division cycle where cells can remain dormant for a long time before they suddenly become active and start rapid proliferation when necessary.

Horwitz and her co-workers[8, 9] further investigated the mechanism of action of paclitaxel at the molecular level and found that paclitaxel enhances the rate, extent, and nucleation phase of tubulin polymerization and stabilizes the microtubules arresting cell division at the G2/M phase. The process of microtubule formation and the mechanism of action of paclitaxel are illustrated in Figure 1-7. Microtubules are linear polymers of the globular protein tubulin and consist of two polypeptide subunits – α- and β-tubulin. α, β-tubulin heterodimer is the basic structural unit of microtubule. α- and β-tubulin are homologous but not identical with a molecular weight of 50 kDa each. α-tubulin has a bound molecule of GTP which is not hydrolyzed and β-tubulin may have bound GTP or GDP which can hydrolyze under certain conditions.[17] In the presence of magnesium ions, guanosine 5'-triphosphate (GTP), and microtubule-associated proteins (MAPs), the α- and β-tubulin form dumb-bell shaped heterodimers that could grow both along and perpendicular to the axis until the two edges join to form a microtubule. This microtubule is composed of 13 protofilaments with an average diameter of about 24 nm. This tubulin heterodimer is the binding target of a number of drugs such as colchicine, podophyllotoxin, *Vinca* alkaloids, vinblastine and vincristine that inhibit tubulin polymerization. However, paclitaxel binds to the tubulin heterodimer aggregate in a 1:1 ratio[18] and promotes polymerization thereby stabilizing the microtubules, either in the presence or in the absence of GTP, MAPs and magnesium ion. The microtubule thus formed differs from the one produced by MAP induction in that only 12 protofilaments are present with a mean diameter of about 22 nm, and is irreversibly stabilized to regular microtubule depolymerization conditions (calcium ions or cooling to 0-4 ^{o}C).[5]

The mechanism of action of paclitaxel is very complex and paclitaxel kills cancer cells by morphologically altering the microtubules thereby inducing apoptosis or cell death. However, the biochemical events that take place downstream of paclitaxel binding to microtubules that lead to apoptosis are not well understood. Apoptosis induced by paclitaxel can occur either directly after a mitotic arrest or after an aberrant mitotic exit into a G1-like multinucleated state.[19-22] When cells are treated with high concentration of paclitaxel then paclitaxel-induced abnormal centrosome function interferes with bipolar

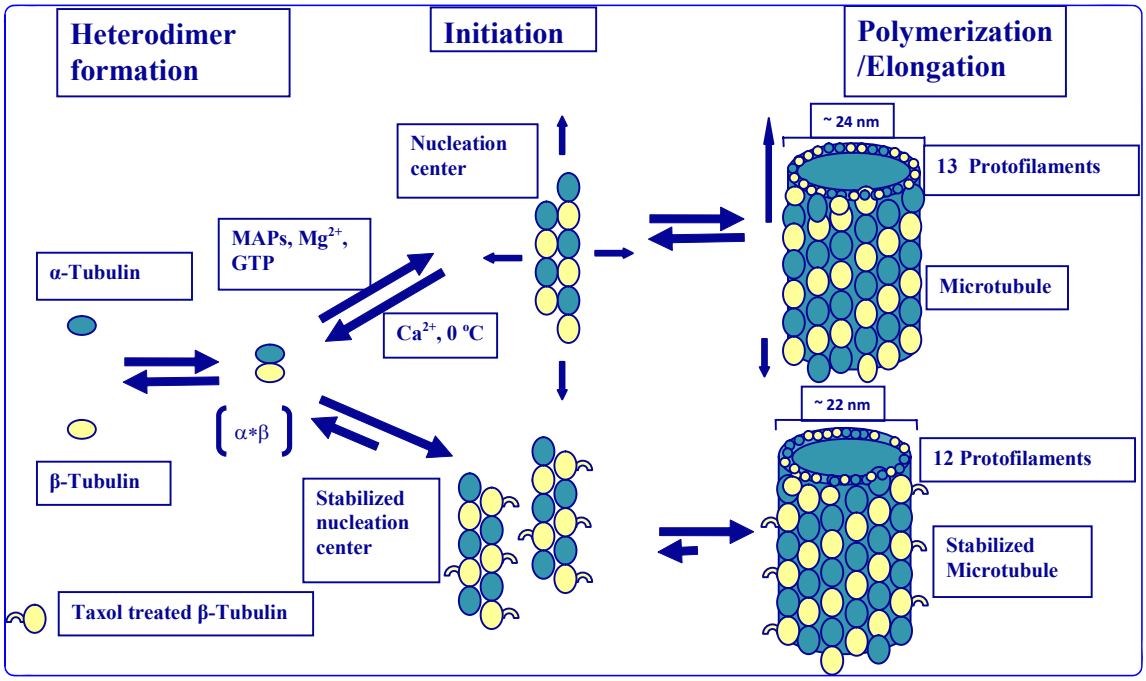

Figure 1-7. Microtubule formation and mechanism of action of paclitaxel[8] (Adapted from Ref. 8 with modification)

spindle formation and monopolar and multipolar spindles are formed. When cells are treated with low concentration of paclitaxel the normal centrosome functions remain unperturbed and bipolar spindle formation takes place but microtubule dynamics and accurate chromosome segregation are impaired. Sustained mitotic block may lead to apoptosis, whereas mitotic slippage may lead to multinucleated G1-like state and the activation of apoptosis as illustrated in Figure 1-8.[11] G2/M arrest is characterized by $p34^{cdc2}$ activation[23-26] and Bcl-2 phosphorylation[27-30], both contributing to apoptosis. Also there is accumulating evidence that suggests that the arrest of cell cycle at the G2/M phase is not the only mechanism for paclitaxel induced apoptosis.[31, 32] There is enough evidence to suggest that the microtubule network integrates both apoptosis and cell cycle[33-35] and therefore paclitaxel has multiple effects on the modulation of apoptosis and cell cycle.[36]

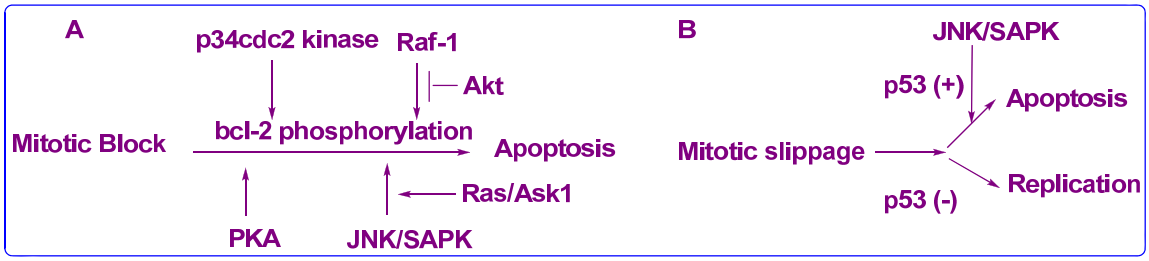

Figure 1-8. Possible molecular mechanism in paclitaxel-induced apoptosis[11]

1.2.3 Synthesis of Paclitaxel

The unique mechanism of action and novel structure of paclitaxel have attracted extensive research over the past few decades. Paclitaxel is used to treat various cancers when other existing treatments have failed. It has been approved by the US Food and Drug Administration (FDA) for the treatment of refractory ovarian cancer (December 1992, approved for first line treatment in April 1998), breast cancer (April 1994), AIDS related Kaposi's sarcoma (1997), and non-small cell lung cancer (1998). Phase II and Phase III clinical trials for the treatment of other cancers such as prostate, colon, head and neck cancers as well as combination therapy with other chemotherapeutic drugs are currently in progress. Paclitaxel (Taxol®) and docetaxel (Taxotere®) are among the most successful anticancer drugs currently in the market. Despite its overwhelming promise, large scale clinical trials of paclitaxel were hampered because of the limited supply of the drug from natural resources. Paclitaxel was originally isolated from the extracts of the bark of the pacific yew tree (*Taxus brevifolia*) which is a slow-growing coniferous tree populating the old growth forest of the American Pacific Northwest[37] and this was the major source of the drug. However harvesting the bark of the tree is fatal to the tree and poses a major ecological and environmental hazard especially because the trees are slow growing making this a limited and nonrenewable natural source. Moreover the extraction process is slow and difficult as well as low yielding which makes this process very expensive. Approximately 3,000 yew trees have to be sacrificed to obtain 10,000 kg of bark which can yield 1 kg of paclitaxel[38] (0.01 % yield) – a supply sufficient to treat approximately 500 patients. Accordingly, alternate methods of producing paclitaxel were explored to secure a sustainable supply of this novel anticancer drug.

Total synthesis of paclitaxel has been successfully attempted by Danishefsky, Nicolaou,[39-43] Holton,[44, 45] Wender,[46, 47] Kuwajima,[48] Mukaiyama[49-51] research groups. While these syntheses were remarkable academic achievements they are not economically viable and thus not suitable for large scale production of paclitaxel. Cell culture fermentation[52, 53] is one promising alternative to producing paclitaxel. Since the first report of producing paclitaxel from *Taxus* cell cultures[54] there has been some progress in increasing the yield of paclitaxel *in vitro*. Cell suspension cultures,[55-57] plant tissue culture,[58] hairy root cultures,[59] recombinant microorganisms[60] and the induction of

paclitaxel biosynthesis in cell culture systems[61] have been reported. A paclitaxel producing endophytic fungus, *Taxomyces andreanae*, isolated from yew trees[62-64] has also been reported though the yield of paclitaxel is low.

Fortunately in 1980 a natural product 10-deacetyl baccatin III (10-DAB III) was isolated from the leaves of the ubiquitous European yew (*Taxus baccata*), a renewable natural source, in a relatively good yield (1 g/ 1 Kg of fresh leaves).[65, 66] The 10-DAB III is the most difficult to synthesize tetracyclic core of paclitaxel and thus it was identified as a suitable starting material for the semisynthesis of paclitaxel and its congeners. The discovery of 10-DAB III, ensured a long term supply of paclitaxel which could be semi-synthesized by attaching the chiral C-13 side chain to the appropriately modified baccatin core (10-DAB III). The semi synthetic approach opened the doors for readily producing paclitaxel and its analogs with superior potency and better pharmacological properties.

In 1988 Potier and Greene[65] reported the first semisynthesis of paclitaxel. The four hydroxyl groups on the 10-DAB III exhibited different reactivities which allowed for the modification of the C-7 and C-10 positions sequentially. The C-13 hydroxyl group was then esterified with (2*R*,3*S*)-*N*-benzoyl-phenylisoserine as shown in Scheme 1-1. The isoserine acid precursor was synthesized in 8 steps from *trans*-cinnamyl alcohol with a modest 76-80% ee and later improved to 98%.[67, 68] However, partial epimerization occurred at the C-2' position of the side chain under harsh reaction conditions (73 ^{o}C, 100 h) which was necessary because of the steric hindrance at the C-13 position and the esterification of the C-13 hydroxyl group with the protected chiral side chain precursor gave modest yields of the protected paclitaxel.

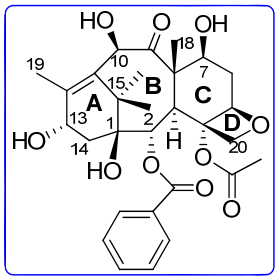

Figure 1-9. Structure of 10-DAB III

Numerous reports have since been made on various methodologies for the asymmetric synthesis of (2'*R*,3'*S*)-*N*-benzoyl-3-phenylisoserine and its analogs such as Sharpless'[69] and Jacobsen's asymmetric epoxidation,[70] Sharpless' dihydroxylation,[71] Sharpless' asymmetric aminohydroxylation,[72] aldol reaction,[73] Chen's chemoenzymatic synthesis *via* lipase-mediated trans-esterification,[74] Kobayashi's chiral Lewis acid catalyzed Mannich-type reaction.[75]

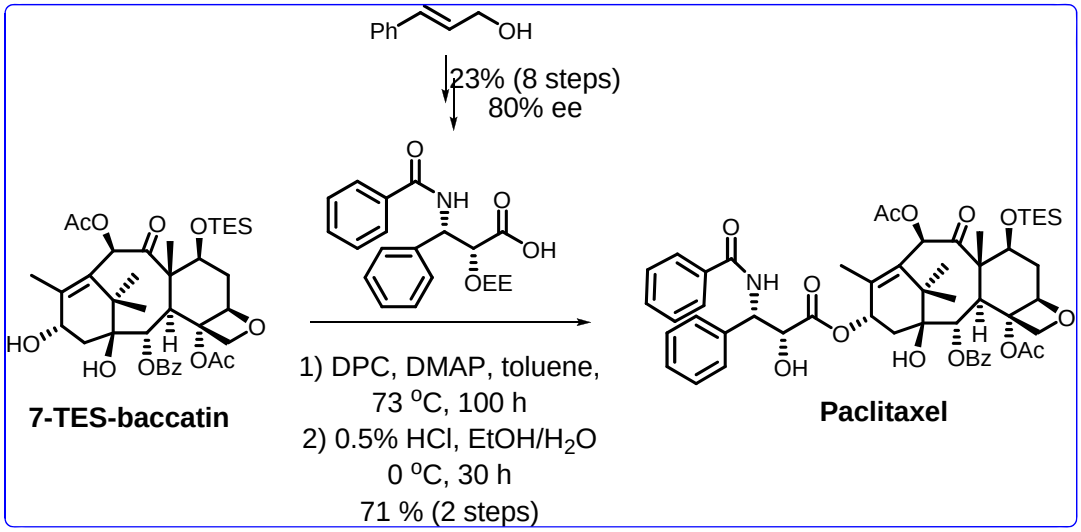

Scheme 1-1. First semi-synthesis of paclitaxel by Potier and Greene[65]

Several new methods for the coupling of modified baccatin and phenylisoserine moiety have been reported such as Commerçon oxazolidinecarboxylic acid coupling (Scheme 1-2),[76] Ojima-Holton *β*-lactam coupling,[77-79] Green-Potier esterification,[65] Holton oxazinone coupling[79, 80] and Kingston oxazolinecarboxylic acid coupling.[81] The Ojima-Holton *β*-lactam coupling has been the most efficient amongst all the coupling methods and is frequently used for the semi-syntheses of paclitaxel as well as other taxoids for SAR studies.

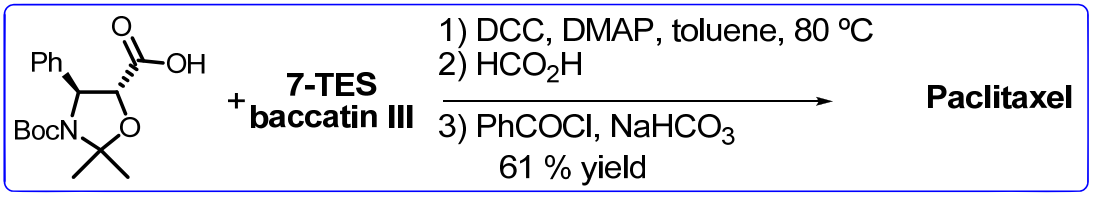

Scheme 1-2. Semi-synthesis of paclitaxel by Commerçon

Holton proposed direct coupling of (3*R*,4*S*)-*N*-benzoyl-3-*O*-EE-4-phenylazetidin-2-one (5 eq; EE = 1-ethoxyethoxyl) with 7-TES-baccatin III in the presence of 4-dimethylaminopyridine (DMAP) and pyridine to generate the 7-TES-2'-*O*-EE-paclitaxel in 92% yield. The (3*R*,4*S*)-*N*-benzoyl-3-*O*-EE-4-phenylazetidin-2-one was obtained through classical optical resolution of racemic *cis*-3-hydroxy-4-phenylazetidin-2-one. Paclitaxel was obtained in 90% yield by subsequent deprotection as shown in Scheme 1-2. There were limitations in Holton's protocol like the necessity of using a large excess of

β-lactam, slow reaction, and being limited *N*-benzoyl group protected β-lactam although no epimerization was observed and the overall yield was high.

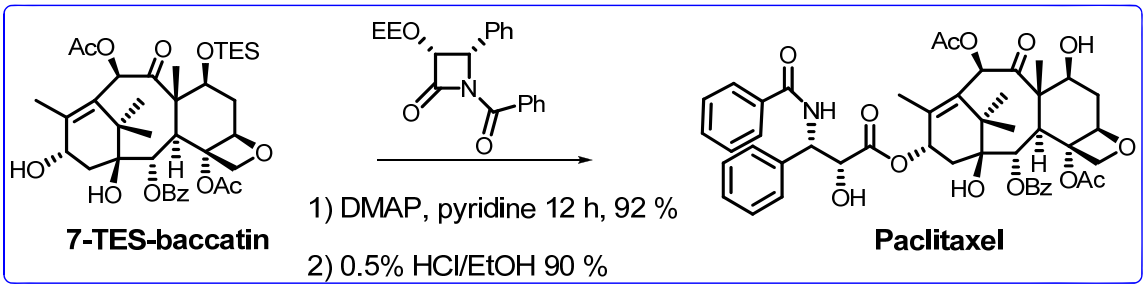

Scheme 1-3. Semi-synthesis of paclitaxel by Holton

Ojima *et. al.* introduced a very practical and efficient way to semi-synthesize paclitaxel by using the "β-Lactam Synthon Method"[82, 83] which was developed in our laboratories (Scheme 1-4). The optically pure β-lactam (3*R*,4*S*)-4-phenylazetidin-2-one was prepared *via* a highly efficient lithium chiral ester enolate-imine cyclocondensation in high yield and with high enantioselectivity (> 96% ee).[78, 84, 85] A ring-opening coupling of *N*-acyl-β-lactams with 13-*O*-metalated derivatives of 7-TES-baccatin III was achieved in the presence of strong bases. Amongst the numerous bases examined such as NaH in THF and DME, *n*-BuLi, LDA, LiHMDS, NaHMDS, and KHMDS in THF, NaHMDS proved to be the best base for these ring-opening couplings which proceeded smoothly at -30 ~ 0 ^{o}C with only a slight excess of *N*-acyl-β-lactam to give the desired coupled product within 30 min in excellent yield which was followed by deprotection to afford paclitaxel in high overall yield.

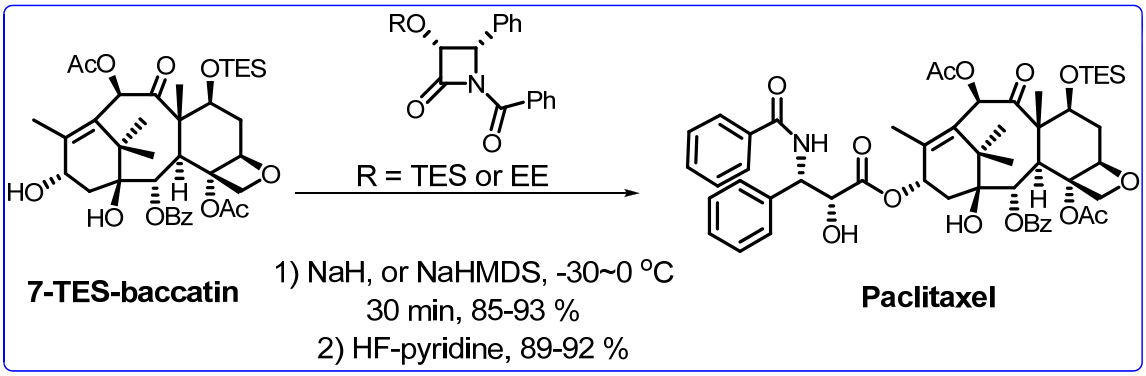

Scheme 1-4. Ojima coupling protocol

1.2.4 Structure-Activity Relationship (SAR) Studies

The efficient semi-synthetic route not only ensured a steady supply of the drug but also allowed for a practical synthetic route for generating paclitaxel analogs for structure-activity relationship (SAR) studies. In 1984 docetaxel (Taxotère®) was discovered by Potier *et. al.* and developed by a French pharmaceutical company, Rhone-Poulenc Rorer.[86-88] This paclitaxel analog has a C3'-*N*-*tert*-butoxycarbonyl moiety in place of the benzoyl group and a free C-10 hydroxyl group in place of the acetoxyl group of paclitaxel.

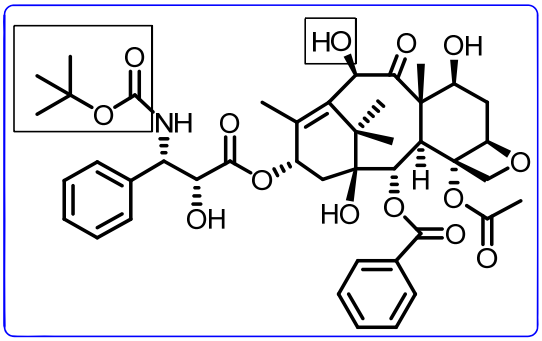

Figure 1-10. Docetaxel

Docetaxel has the same mechanism of action as paclitaxel and is twice as potent as paclitaxel. It was approved by the FDA for the treatment of breast cancer in 1996 and is currently undergoing clinical trials for breast and lung cancers.[5] Despite their enormous success and extensive use in cancer chemotherapy they cause numerous undesirable side effects like infections due to low white blood cell count, hair loss, joint and muscle pain, upset stomach and diarrhea, neuropathy and allergic reactions. Often multi-drug resistance (MDR)[89] renders these drugs ineffective and thus it is imperative to develop new analogs (taxoids) with superior pharmacological profiles which can bypass MDR. Accordingly, SAR studies have been performed by the Ojima group as well as others[79, 86, 90-93] and Figure 1-11 summarizes the results performed on paclitaxel. SAR studies of the C-13 side chain and the baccatin core of paclitaxel are discussed below.

(i) C-13 side chain

SAR studies have revealed that the C-13 side chain (2*R*,3*S*)-*N*-acyl-3-phenylisoserine moieties of paclitaxel and docetaxel are crucial for retaining their cytotoxicity and antitumor activity. The loss of this isoserine moiety results in >1,000-fold reduction in their potency and the deletion of any substituent or introduction of any other stereochemistry also substantially lowers their potency by >500 times in some cases.[94, 95]

Studies have indicated that a free hydroxyl group at the C-2' position of the isoserine moiety is required for the biological activity of the compounds. Recent studies

indicate hydrogen bonding between the free C-2' hydroxyl group and either Arg 369 or Gly 370 of the *β*-tubulin backbone.[96] Thus any protection, deletion or acylation at this position caused significant decreases in *in vitro* activity.[97] However, groups which can undergo hydrolysis in the presence of esterases in the cells can be used at this position as the *in vivo* activity is comparable to the parent compound which led to the development of a "prodrug".[37, 91, 98-100]

C-3'-*N* position is more tolerable to structural changes and can lead to more potent compounds as is evidenced by docetaxel which has *tert*-butoxycarbonyl group in place of the C-3'-*N*-benzoyl group.[91, 101-103] C-3'-*N* acyl analogs have significantly increased activity compared to the free amine group or replacement with *n*-alkanoyl groups at this position.[90, 101, 104] However, analogs with lipophilic and hydrophilic acyl groups both exhibit activity similar to paclitaxel.[104] Some analogs bearing *N*-cycloalkenoyl substituents also possess improved biological activity.[105]

C-3' phenyl group has been extensively studied[90-92] and has been replaced with a range of heteroaromatic groups which led to numerous analogs that exhibit activity comparable to or better than paclitaxel.[104] Second-generation taxoids bearing C-3' alkyl, alkenyl, fluorinated alkyl, and epoxy groups have been extensively studied and developed in our laboratory and were found to be extremely potent, especially against multidrug resistant cancer cell lines.[91, 92, 101-103, 106, 107]

The effect of stereochemistry at the C-2' and C-3' positions of the side chain on the potency of paclitaxel has also been investigated. Studies have shown that a departure from the natural configuration of 2'*R*, 3'*S* have resulted in significant loss of activity. However, epimerization at one of the two stereocenters resulted in analogs with activity comparable to that of the parent compound.

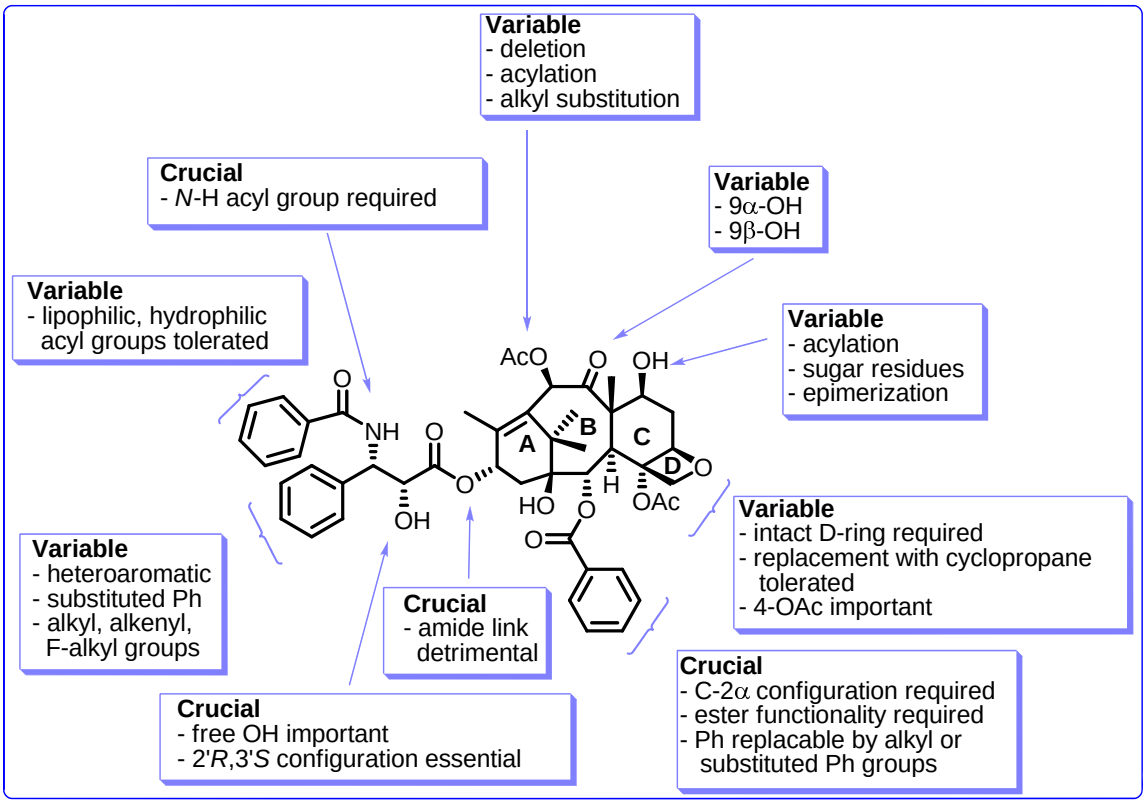

Figure 1-11. SAR summary for paclitaxel

(ii) Baccatin core

Studies on the modification of the baccatin skeleton such as altering ring sizes and structural integrity as well as deletion and/or modification of various oxygen functionalities have been extensively reported (Figure 1-11).[108-110] Modifications to the A ring such as contraction[111, 112] or cleavage[113, 114] significantly decreases activity compared to the intact structure. The contraction of B-ring, however, maintains a certain level of cytotoxicity[115] but contracted C-ring analogs exhibit considerably decreased activity. C-seco taxoids obtained through an oxidation-reduction protocol have been reported and one of the analogs, IDN5390 (Figure 1-12) exhibited a slightly diminished cytotoxicity compared to paclitaxel but possess potent antiangiogenic and antimetastatic activity.[116, 117]

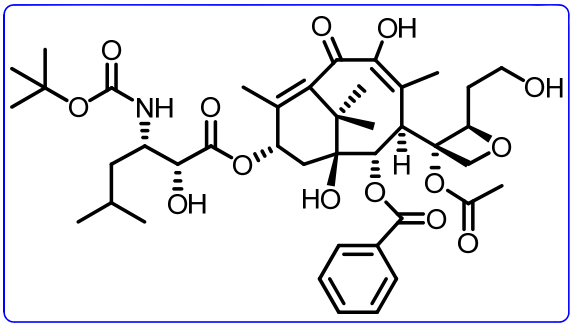

Figure 1-12. Structure of C-seco taxoid IDN5390

Extensive SAR studies of this novel semi-synthetic analog are ongoing in our laboratory. An intact D-ring is crucial in maintaining the high level of activity; modifications such as ring-opening,[115-117] formation of azetidine ring,[118, 119] replacement of oxygen with sulfur,[120] results in loss of activity. The activity of the analog, in which the oxetane ring is replaced with a cyclopropane ring, remains similar to that of paclitaxel.[121]

Several SAR studies have found that the C-2 position is essential for cytotoxicity. There is a drastic decrease in activity when there is epimerization at C-2 as well as hydrolysis of the ester functionality at C-2.[122] Substitution at the *meta* position ($F>Cl>OMe>N_3>Me>CH=CH_2$) of the C-2 benzoyl group results in analogs with greater cytotoxicity than that of paclitaxel while substitution at the *para* position of the C-2 benzoyl group is detrimental to activity. It has been found that *meta* position of C-2 benzoyl group is involved in the metabolism of paclitaxel,[123, 124] therefore, a slower metabolic rate of *meta* substituted derivatives may be responsible for the higher activity. It is believed that substitution at the *para* position of the C-2 benzoyl group disrupts the hydrophobic interactions between the C-2 benzoate residue and the phenyl group at C-3' which is necessary for the conformation of the active compounds, while substitution at the *meta* position enhances them.[125] Studies in our laboratory have shown that the incorporation of an alkyl or alkenyl group in place of the phenyl group may lead to improved activity. However, a majority of these analogs exhibited muted activity.[126]

The C-4 functionality is also important to maintain the activity. The loss of acetoxy group and hydrolyzation of C-4 ester functionalities resulted in significant decrease in cytotoxicity.[127-129] Analogs bearing a cyclopropanoyl group in place of acetyl group exhibited slightly increased activity, whereas analogs bearing a benzoyloxy group at C-4 showed greatly reduced activity.[130] Unlike the southern part of the taxane skeleton, the northern part, particularly C-7, C-9 and C-10, are more tolerable to modifications and most of the resulting analogs possess similar or even better biological activity.

Extensive SAR studies have been performed on the C-7 hydroxyl group.[130-132] Acylation, epimerization as well as deoxygenation at the C-7 position do not significantly alter the *in vitro* activities though there have been reports that *in vitro* data do not necessarily correlate with *in vivo* activity of such analogs.[130]

Reduction of the C-9 ketone of paclitaxel analogs to either an α- or β-hydroxyl group has little effect on the cytotoxicity,[133, 134] while a C-9, C-10 diol results in decreased activity.[135-137]

Studies have shown that modification of C-10 position has little effect on the *in vitro* cytotoxicity.[138, 139] However, the SAR studies in our group on the second-generation taxoids revealed that the exceptional activity of these analogs against the drug resistant cell lines is clearly ascribed to the modification at C-10 position.[101, 102] Besides, studies of the advanced second-generation taxoids indicated that the combination of C-10 and C-2 modifications virtually overcame the P-glycoprotein based MDR in several cancer cell lines.[140]

SAR studies performed on paclitaxel indicate that the upper part of the taxane skeleton appears to be much more flexible and tolerable to various modifications compared to the lower part of the molecule (Figure 1-11). The exact roles of each part of the molecule towards the anticancer activity of paclitaxel are not completely clear. Thus further studies are required to study the roles of each part in order to develop new generation anticancer agents with fewer side effects, superior pharmacological properties, and improved activity against various classes of tumors, especially against drug-resistant human cancers.

1.3 β-Lactam Synthon Method

1.3.1 Introduction

The β-lactam skeleton is the core structure of natural and synthetic β-lactam antibiotics and hence has attracted significant interest among synthetic and medicinal chemists over the years.[141] These antibiotics include various structural classes such as carbapenems, cephems, monobactams, penams, penems, trinems, etc[142, 143] as shown in Figure 1-13.

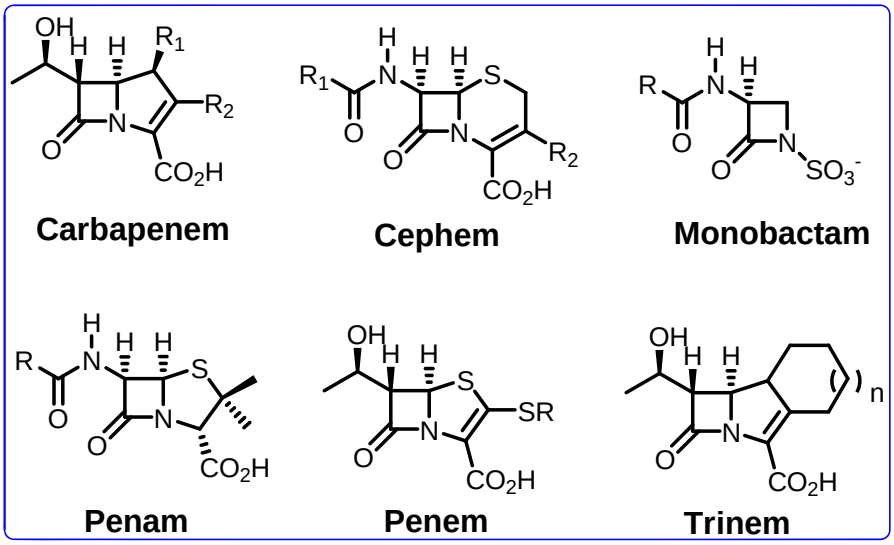

Figure 1-13. Structures of *β*-lactams

However, the ability of *β*-lactams to serve as synthetic intermediates was not fully realized until the early 1980s, when the Ojima group started to develop the "*β*-lactam Synthon Method (*β*-LSM)". Through 1980s and 1990s, Ojima and others have successfully demonstrated that enantiopure *β*-lactam serve as versatile intermediates for the asymmetric synthesis of various natural and unnatural amino acids, peptides, peptide mimetics and taxoid anticancer agents.[83, 144, 145]

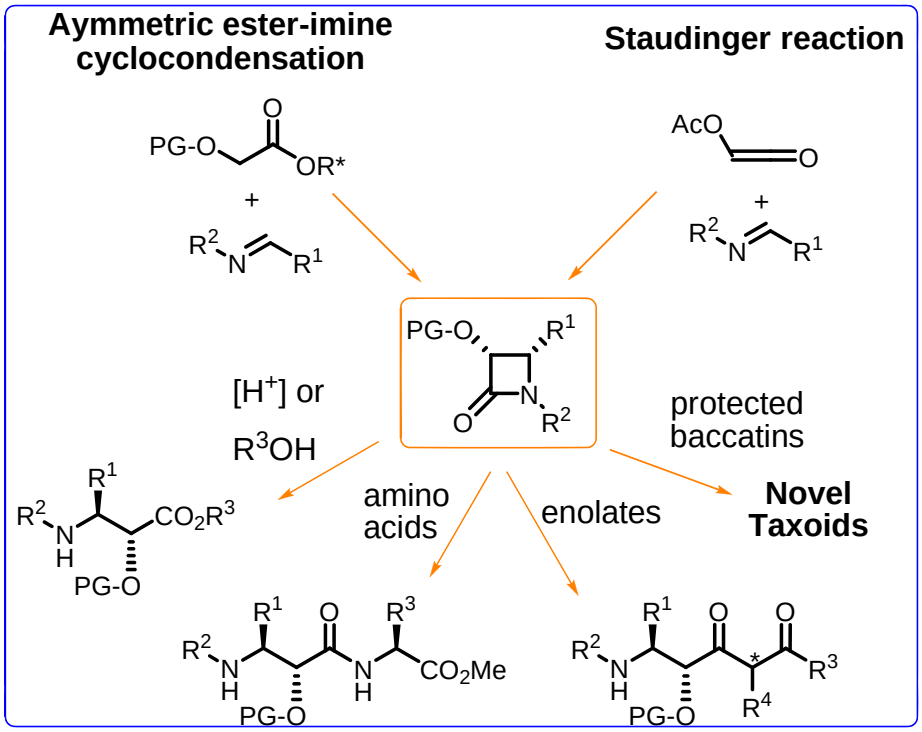

Scheme 1-5. *β*-Lactam Synthon Method

Several research groups have extensively studied the semisynthesis of paclitaxel, docetaxel and their analogs *via* the coupling of a phenylisoserine moiety with DAB.[91, 92, 94, 146-148] Among the various coupling protocols, the Ojima-Holton *β*-lactam coupling protocol is the most efficient and versatile method.[39, 45, 47, 149, 150] Our strategy has been to apply the *β*-lactam synthon method[82, 83, 145] for the asymmetric synthesis of a (2'*R*,3'*S*)-*N*-benzoyl-3-phenylisoserine moiety in high yield and excellent enantiopurity followed by ring-opening coupling of (3*R*,4*S*)-*N*-benzoyl-*β*-lactam with an appropriately modified DAB (Scheme 1-6).

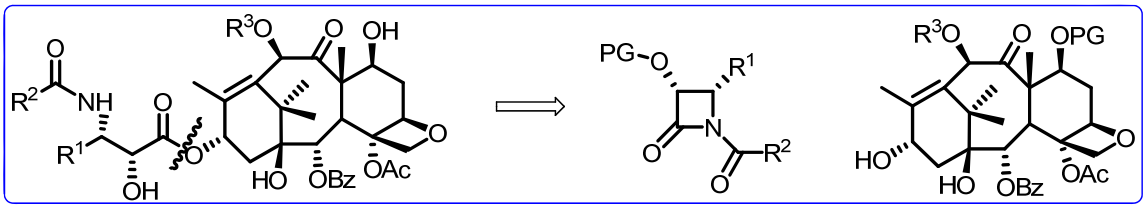

Scheme 1-6. Retro-synthesis of taxane-based anticancer agents

Our efforts on the development and applications of the *β*-LSM have been well reviewed.[82, 83, 91, 92, 144, 145, 151] In addition to its industrial application for the synthesis of paclitaxel, the Ojima-Holton protocol has opened an extremely efficient and practical route for the synthesis of a diverse array of new taxoids which paved the way for extensive structure-activity relationship (SAR) studies of taxoid anticancer agents. The most important issue for the *β*-LSM to be successfully applied to taxoid syntheses is to secure the supply of enantiopure *β*-lactams with the appropriate substituents and correct absolute configuration. Various synthetic methods have been explored to synthesize *β*-lactams[152-154] such as metalloester enolate-imine condensation,[155-159] hydroxamate cyclization,[160] isocyanate-alkene cycloaddition,[161] chromium carbene-imine reaction,[162] ketene-imine cycloaddition, also known as the Staudinger reaction.[163] We employed two methods for the synthesis of *β*-lactams –

(a) asymmetric ester–imine cyclocondensation

(b) Staudinger reaction followed by enzymatic optical resolution.

1.3.2 Synthesis of enantiomerically pure *β*-lactam *via* asymmetric ester–imine cyclocondensation

1.3.2.1. Introduction

The *β*-Lactam Synthon Method has been successfully utilized for the preparation of C-13 side chain precursors in the semi-synthesis of paclitaxel,[77] docetaxel[85] and a great number of taxoids possessing extremely high antitumor activity.[91, 92] Investigations in our laboratory showed that the desired *β*-lactams can be synthesized in good yields and high enantiomeric purity through an efficient chiral TIPS-ester enolate-imine cyclocondensation reaction.[84, 150] The chiral auxiliaries that have been successfully employed in the *β*-LSM for the synthesis of highly optically pure *β*-lactams include (-)-trans-2-phenylcyclohexanol (Whitesell's chiral auxiliary) (Figure 1-14 a),[164, 165] or (-)-10-dicyclohexylsulfamoyl-D-isoborneol (Oppolzer's chiral auxiliary) (Figure 1-14 b).[166, 167]

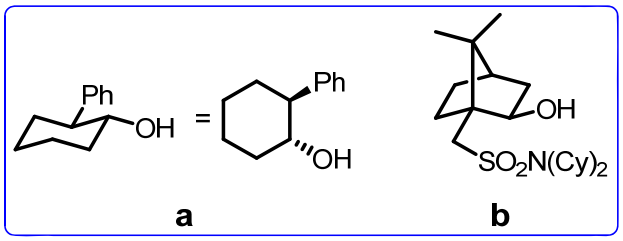

Figure 1-14. Structure of chiral auxiliaries

Numerous novel taxoids have been synthesized using the efficient coupling of *β*-lactams following the Ojima coupling protocol with appropriately protected and functionalized baccatins followed by deprotection[101-103, 106, 107, 168, 169] (Scheme 1-7).

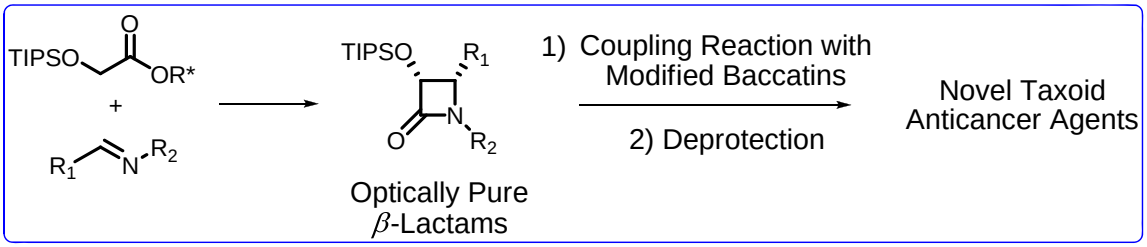

Scheme 1-7. Synthesis of novel taxoids using *β*-lactam

1.3.2.2. Results and discussion

Chiral TIPS ester (**1-7**) was synthesized as the first step towards the synthesis of *β*-lactam. (-)-*trans*-2-Phenylcyclohexanol (Whitesell's chiral auxiliary) (**1-2**) was synthesized according to Whitesell's methods[164, 170] and used as the source of chirality. CuI-catalyzed ring opening of cyclohexene oxide (**1-1**) with phenylmagnesium bromide afforded racemic *trans*-2-phenylcyclohexanol (**1-2**). Acetylation of this alcohol followed by enzymatic kinetic resolution of the resultant racemic acetate (**1-3**) using pig liver acetone powder (PLAP) afforded (-)-(**1-2**) (Scheme 1-8).

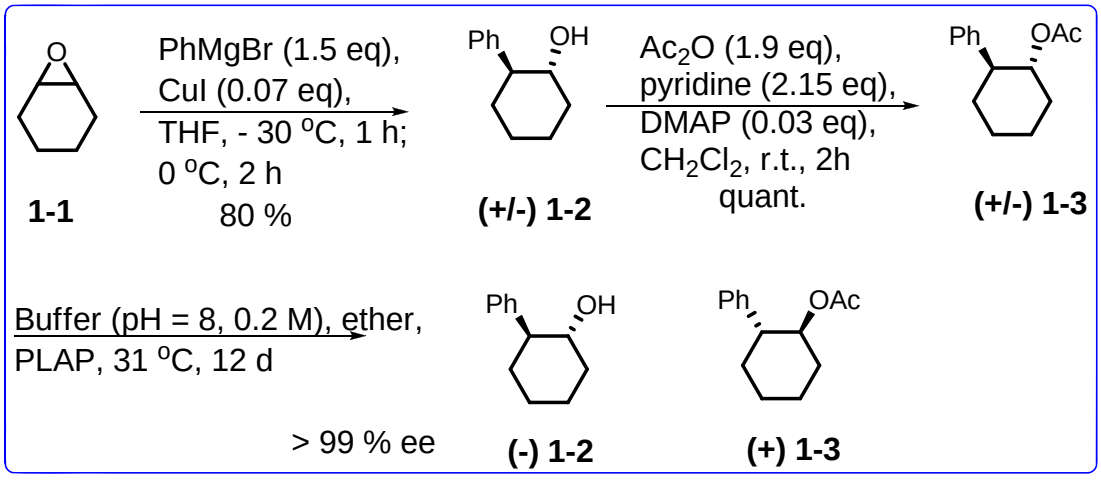

Scheme 1-8. Synthesis of Whitesell's chiral auxiliary

Benzyloxyacetic acid (**1-4**) was obtained by reacting bromoacetic acid with the sodium benzyl alkoxide. Chiral alcohol (-)-(**1-2**) was then reacted with benzyloxyacetic acid (**1-4**) in the presence of *p*-toluenesulfonic acid (*p*-TSA), yielding the esterified

product (**1-5**). Subsequent hydrogenolysis of the benzyloxyacetic ester with palladium on carbon at 45 ^{o}C in methanol gave hydroxyacetate (**1-6**) as a white solid (Scheme 1-9). Protection of the free hydroxyl group of (**1-6**) with chlorotriisopropylsilane (TIPSCl) yielded the chiral (-)-ester (**1-7**) bearing Whitesell's chiral auxiliary in good overall yield after vacuum distillation as a colorless, viscous liquid.

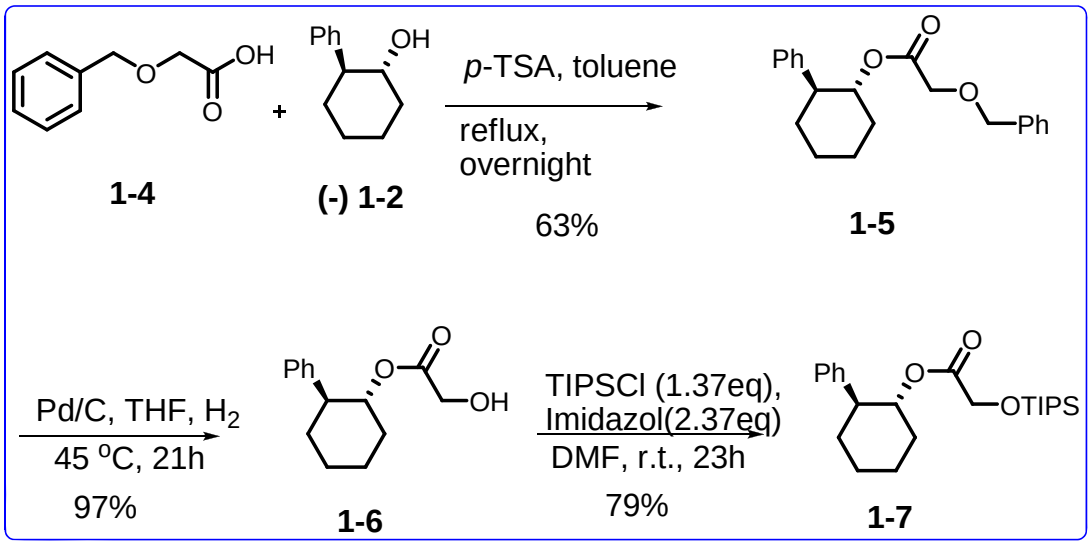

Scheme 1-9. Synthesis of TIPS ester

One of the advantages of the *β*-LSM is that it can be applied to the syntheses of a variety of *β*-lactams bearing different substituent groups at the C-4 position. *β*-lactams with phenyl group,[78, 85] substituted phenyl groups,[171] isobutenyl group,[101, 169, 171] and even long-chain alkenyl moieties at C-4 positions[171] have been synthesized in high yields and enantiopurities.

p-Methoxyphenyl (PMP) *β*-lactam (**1-9**) was synthesized as shown in Scheme 1-10. 3-Methyl-2-butenal was reacted with *p*-anisidine in methylene chloride to generate *N*-*p*-methoxyphenyl-iso-butenylaldimine (**1-8**). TIPS ester **1-7** in THF was slowly added to LDA and the resulting enolate was then reacted with the **1-8** to yield *β*-lactam (**1-9**). The *p*-methoxy phenyl group was removed by a ceric ammonium nitrate (CAN) oxidation in aqueous acetonitrile. Subsequent standard acylation with di-*tert*-butyldicarbonate anhydride yield the desired *β*-lactam, 4-isobutenyl-1-(*tert*-butoxycarbonyl)-3-(triisopropylsilyl)oxyazetidin-2-one(**1-11**) (Scheme 1-10).[82]

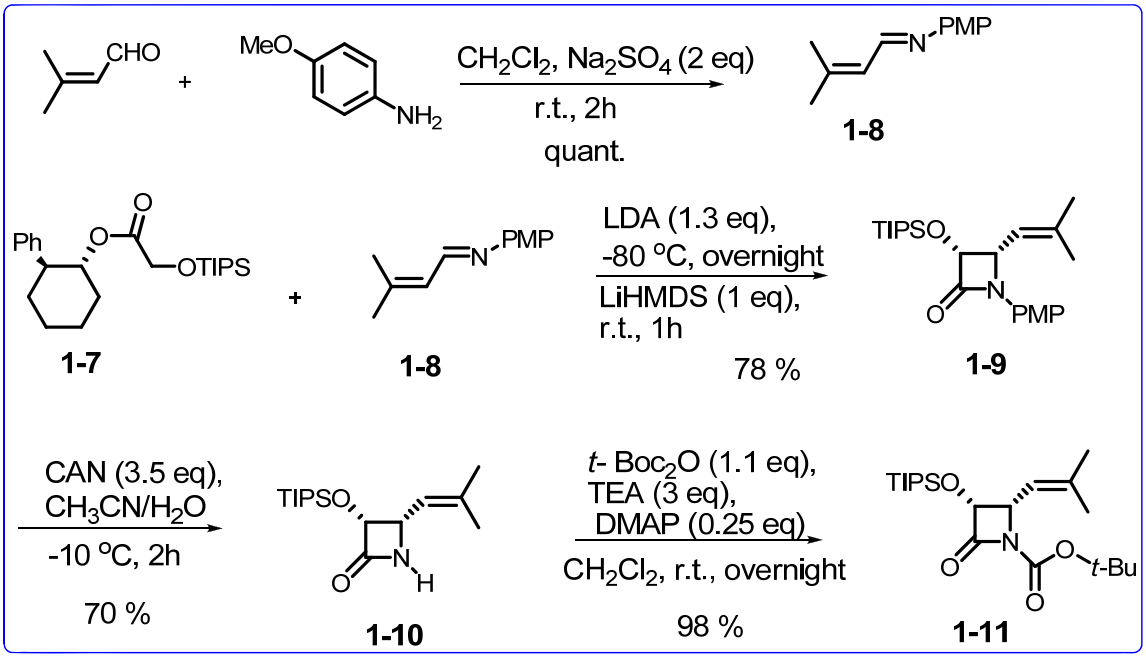

Scheme 1-10. Synthesis of C-4-isobutenyl *β*-lactam

The selective formation of cis-*β*-lactam with high enatiomeric purity could be explained by the 6-member-ring transition state proposed in Scheme 1-11.[150] At low temperature, (*E*)-enolate is predominantly formed and the initial enolate addition to imine would occur from the least hindered face, thus forming the *β*-amino ester intermediate which could be isolated upon quenching the reaction at low temperature. When warmed up to room temperature, this intermediate cyclizes to give the chiral *β*-lactam and release the chiral auxiliary.

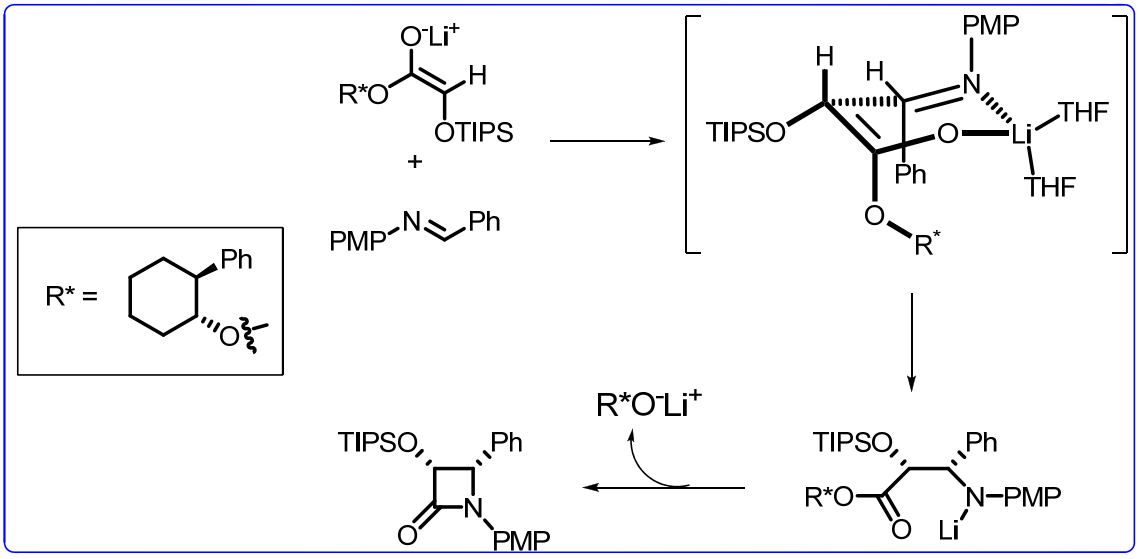

Scheme 1-11. Proposed mechanism of chiral TIPS-ester enolate-imine condensation

1.3.3 Synthesis of enantiomerically pure *β*-lactam *via* Staudinger cycloaddition reaction followed by enzymatic kinetic resolution

1.3.3.1. Introduction

Although our laboratory already developed optically pure *β*-lactams in high yield with high enantioselectivity (> 96% ee) *via* a highly efficient lithium chiral ester enolate-imine cyclocondensation,[78, 84, 85] asymmetric Staudinger reaction provides an alternative way to generate optically active *β*-lactams, due to the ready availability of both Schiff bases and ketenes.[172, 173]

Staudinger reaction or ketene-imine cycloaddition, is one of the most versatile approaches for the formation of diversely functionalized *β*-lactams. The reaction between acyl chlorides and imines is assumed to proceed *via in situ* formation of a ketene, followed by reaction with the imine to form a zwitterionic intermediate, which undergoes an electrocyclic conrotatory ring closure to give the *β*-lactam ring (Figure 1-15).[174] In general, (*E*)-imines preferentially lead to the more hindered cis-*β*-lactams, while (*Z*) imines give predominantly the corresponding trans isomers (Figure 1-15).[175-177] The theoretical studies undertaken to establish the origin of the cis/trans stereoselection reveal that the relative energies of the rate-determining transition states, led from the zwitterions to *β*-lactams, are dictated not necessarily by steric effects, but by electronic torquoselectivity.[178-180] For instance, it has been calculated[179] at the RHF/6-31G* level that the zwitterionic intermediate having an electron-donating group in the ketene fragment (R1 = OH, CH_3) has a barrier for conrotatory closure to the *β*-lactam that is 8-12 kcal/mol lower when it adopts an "outward" rotation. This situation translates as a

preference for the imine attack opposite (exo) to the R1 group and, therefore, the formation of cis-β-lactams from (*E*) imines. The origin of the chiral control of the Staudinger reaction, arising from the presence of chiral substituents (R1, R2 and/or R3), has also been investigated at a semiempirical level (AM1) for chiral amino ketenes and chiral α-hydroxy- and α-amino-imines.[180]

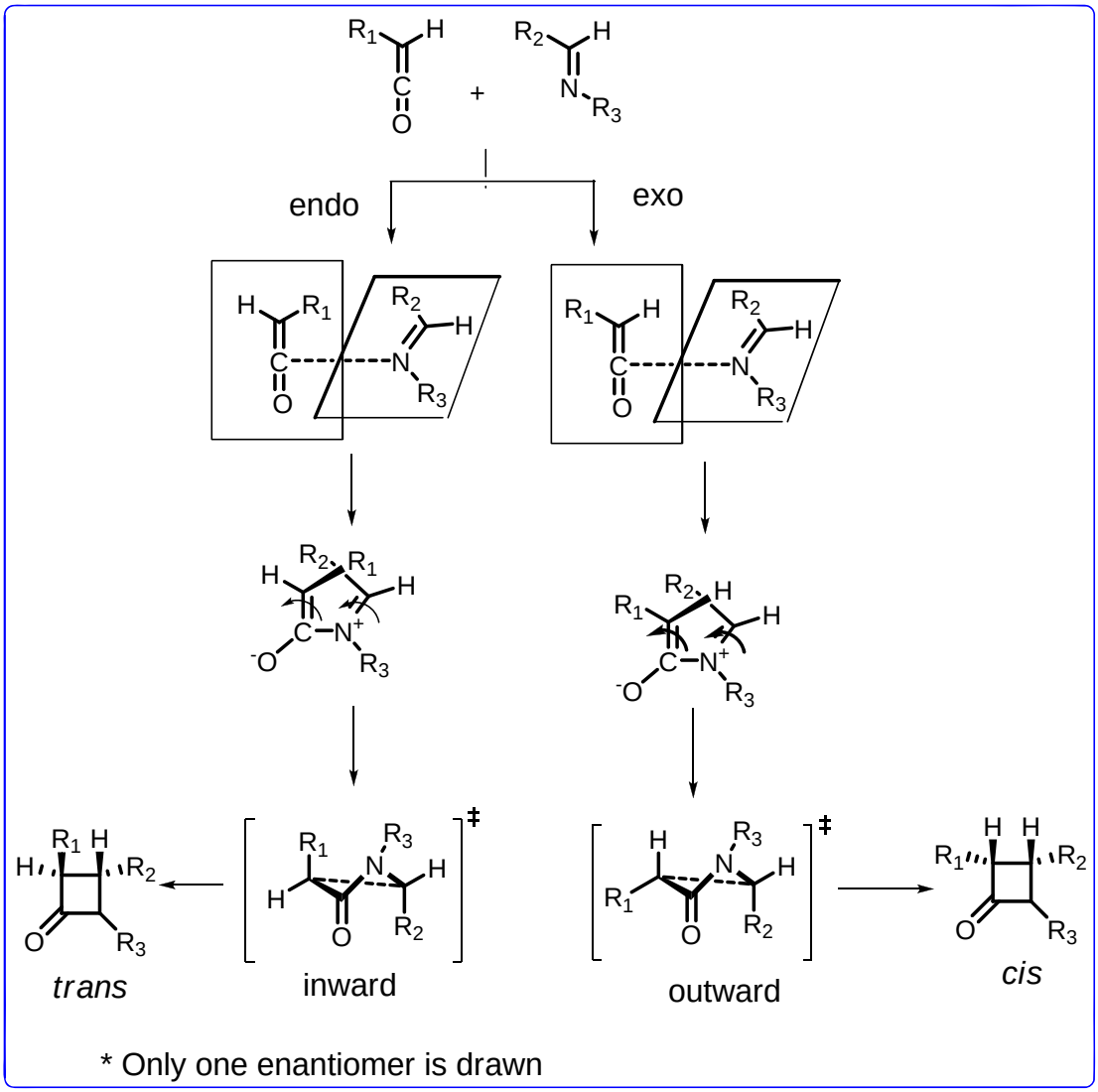

Figure 1-15. Synthesis of β-lactams by Staudinger reaction

Optically pure α-hydroxy β-lactams can be obtained by chemical[181] or enzymatic[38] resolution of the corresponding racemic derivatives. It was reported that racemic phenyl β-lactams underwent selective kinetic hydrolysis with several

Pseudomonas lipases and two penicillinases and the enantiomeric excess was determined by NMR with chiral shift reagents.

1.3.3.2. Results and discussion

Hydrolytic enzymes are being increasingly used to produce optically active compounds, particularly lipases which are being used for the kinetic resolution of racemic alcohols and carboxylic esters. These lipases also catalyze the cleavage of the *β*-lactam ring to produce (2*R*,3*S*)-phenylisoserine derivatives in high enantiomeric excess which are important intermediates in the C-13 paclitaxel side chain synthesis. The lipases are an attractive class of catalysts for industrial-scale kinetic resolution process because of their commercial availability and relative stability. The following are application of lipases in the synthesis of optically active 3-hydroxy-4-aryl-*β*-lactam derivatives. In both cases [2+2] ketene-imine cycloaddition is followed by enzymatic resolution to produce *β*-lactams with different substituents.

p-Methoxyphenyl (PMP) *β*-lactam (**1-13**) was synthesized using Staudinger reaction as shown in Scheme 1-12. Acetoxyacetylchloride was cyclocondensed with *N*-(4-methoxyphenyl)benzaldimine (**1-12**) in presence of tertiary amine to give the racemic (**1-13**). PS-Amano preferentially hydrolyzed the C-3 acetate moiety of the (3*S*, 4*R*) enantiomer of (**1-13**). A common approach for improving the biocatalytic reaction rates of water-insoluble substrates is the use of cosolvents. Acetonitrile (10%) was used as the cosolvent to enhance the rate and enantioselectivity of the reaction. The *p*-methoxyphenyl group was eventually removed by oxidation with ceric ammonium nitrate followed by hydrolysis of the acetoxy group to give (**1-16**) and subsequent protection of the hydroxyl group by ethoxyethyl (EE). The smaller EE group facilitates the coupling of *β*-lactam to baccatin.

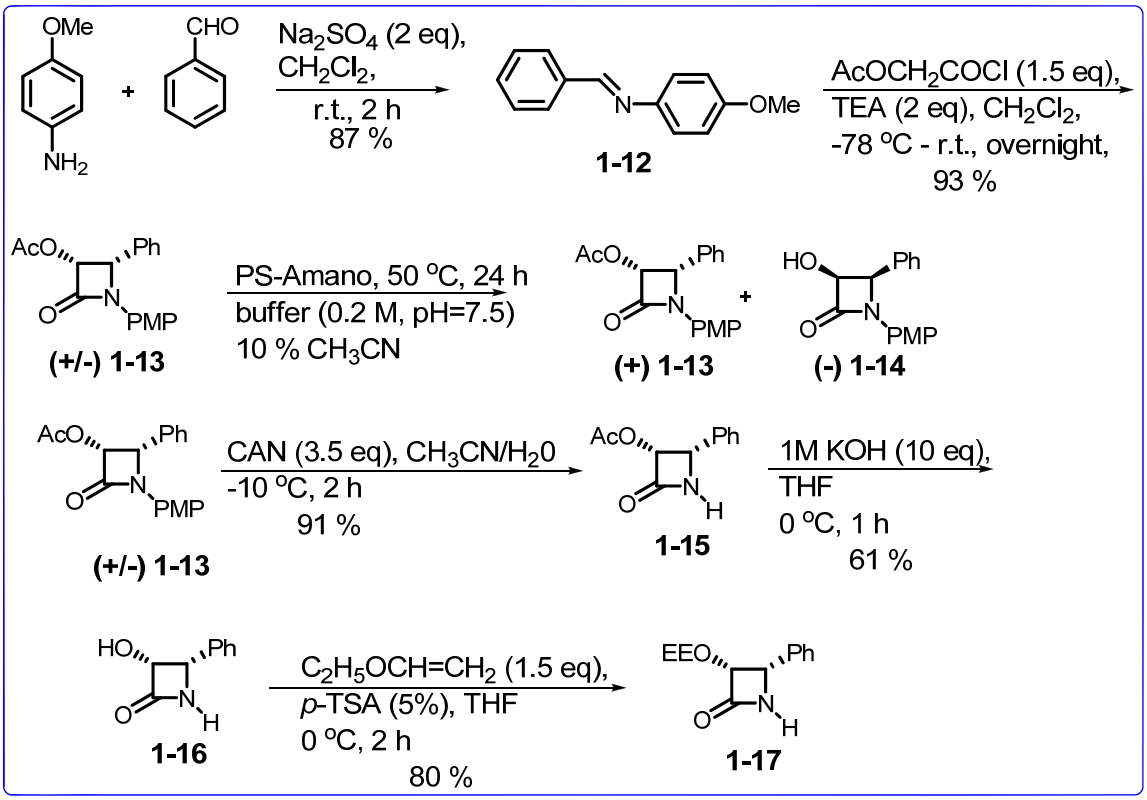

Scheme 1-12. Synthesis of *Z*-3(*R*)-Ethoxyethoxy–4(*S*)-phenylazetidin-2-one (**1-17**)

The isobutenyl *β*-lactam (**1-11**) was also synthesized in a similar way as shown in Scheme 1-13. Acetoxyacetylchloride was cyclocondensed with imine (**1-8**) in the presence of tertiary amine to obtain the racemic (**1-18**). PS-Amano preferentially hydrolyzed the C-3 acetate moiety of the (3*S*, 4*R*) enantiomer of (**1-18**). Acetonitrile (10%) was used as the cosolvent to enhance the rate and the enantioselectivity of the reaction. The racemic acetate (**1-18**) was hydrolyzed followed by protection with TIPSCl. *p*-Methoxyphenyl group is then removed by oxidation with ceric ammonium nitrate followed by protection of the amine with di-tert-butyl dicarbonate yielding (**1-11**). The optical purity of 3-acetoxy-*β*-lactam (+)-**1-18** was determined by chiral HPLC and by comparison to the reported specific rotation.[38]

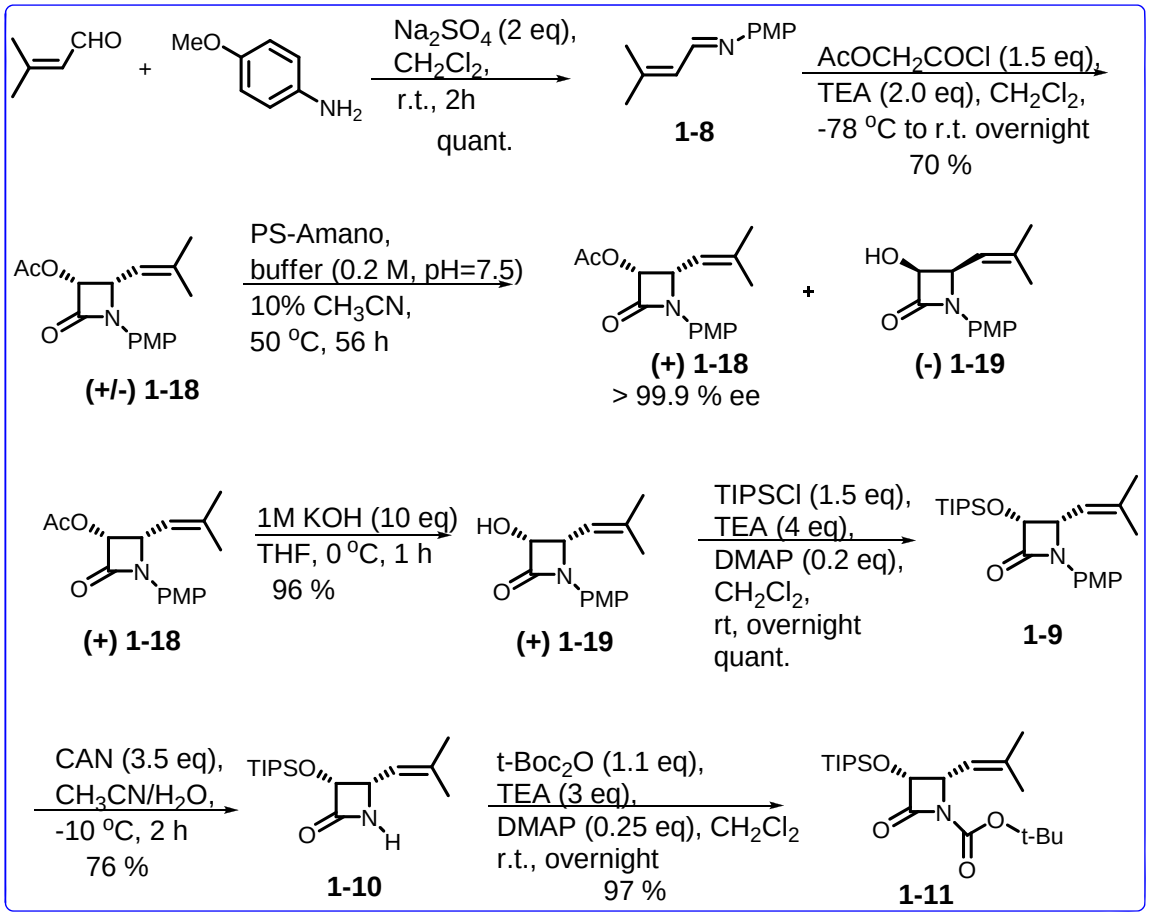

Scheme 1-13. Synthesis of 4-isobutenyl-1-(*t*-butoxycarbonyl)-3-[(triisopropylsilyl)oxy] azetidin-2-one (**1-11**)

1.3.4 Synthesis of second generation taxoid SB-T-1214 by *β*-LSM

1.3.4.1. Introduction

Paclitaxel (Taxol®) and its semisynthetic analog docetaxel (Taxotére®) are two of the most important drugs used in cancer chemotherapy.[91] Both these drugs exhibit excellent anti-tumor activity against various cancer cell lines due to their unique antimitotic mechanism of action and are approved by the FDA for treatment of several different types of cancers. However, treatment with these drugs often result in various undesired side effects and multi-drug resistance (MDR).[182] Therefore, it is essential to develop novel taxoids with superior pharmacological properties, greatly reduced and fewer side effects and greatly improved activity against various classes of tumors,

especially against drug-resistant human cancers. Extensive structure-activity relationship (SAR) studies on paclitaxel, docetaxel as well as on a series of highly active second-generation taxoids were explored by Ojima and coworkers through collaboration with world-leading experts in oncology, pharmacology, cell biology, hematology, and toxicology. The structures of some of the novel taxoids are summarized in Figure 1-16.[107, 113, 126, 183-189]

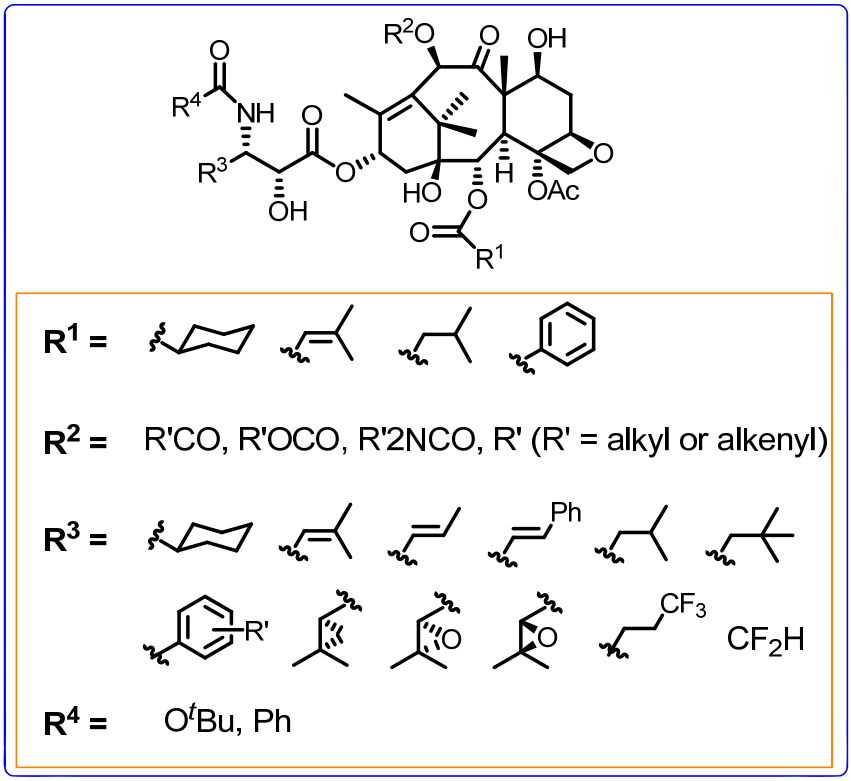

Figure 1-16. Structure of some novel second-generation taxoids

SAR studies in our group led to the discovery of novel second-generation taxoids most of which possess one order of magnitude higher potency than paclitaxel and docetaxel against drug-sensitive cancer cell lines and 2-3 orders of magnitude higher potency than their parent compounds against drug-resistant cell lines expressing MDR phenotypes. These SAR studies indicate that there are three key factors responsible for the enhanced anticancer activity of these novel taxoids:[102, 126]

(1) presence of a *t*-butoxycarbonyl group at C-3'-N in place of a benzoyl group;
(2) replacement of C-3' phenyl with an alkenyl or alkyl group;
(3) proper modification at C-10 position.

Another novel taxane diterpenoid, 14*β*-hydroxy-10-deacetylbaccatin III (14*β*-OH-10-DAB-III, Figure 1-17) was isolated from the needles and other parts of the plant *Taxus wallichiana Zucc*.[190]

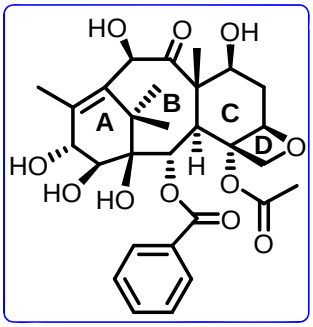

Figure 1-17. Structure of 14*β*-OH-10-DAB-III

This baccatin possessed an extra hydroxyl group at the C-14 position, allowing another modification site for the SAR studies as well as rendering it more water soluble than the 10-DAB-III. Thus new taxoids developed from modifications of 14*β*-OH-10-DAB-III could be expected to have improved water solubility, bioavailability, and less hydrophobicity-related drug resistance.[191]

A new series of second-generation taxoids has also been designed and synthesized based on this novel taxane. These taxoids have a 1,14-carbonate moiety and various substituents at the C-10, C-3' and C-3'-*N* positions and exhibit potent anticancer activities.[101] One of these compounds, SB-T-110131 (IDN5109; BAY59-8862; Ortataxel) (Figure 1-19) has a promising pharmacological profile and has been the focus of extensive biological studies. It is orally active, showed excellent pharmacological profile in preclinical studies and is in human clinical trials sponsored by Bayer Corporation and Spectrum Pharmaceuticals.[192-194]

Studies showed that modification to the *meta*-position of C-2 benzoyl group showed significantly improved activities against the P-388 cell line.[195] A new series of second-generation taxoids bearing a substituent on the C-2-benzoyl group and modifications at C-3'/C-10 positions has been synthesized and their cytotoxicity evaluated based on this result and our study. It is noteworthy that a couple of taxoids shows virtually no difference in activity against drug-resistant and drug-sensitive cell lines, which are categorized as “advanced second generation taxoids” (Figure 1-18). The synthesis of a novel taxoid with substitution at the *meta*-position SB-T-121402 (Figure 1-19) is discussed in Chapter 6.

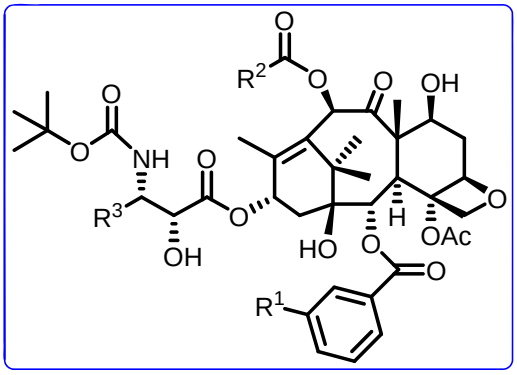

Figure 1-18. Structure of advanced second generation taxoids

During the development of the "second generation taxoids", our group members realized that these taxoids might have MDR reversal activity and they can modulate Pgp efflux, which might also be responsible for the modulation of Pgp in the intestine of animals that would enhance the uptake of the drug from intestine to blood stream. This hypothesis was then proven by investigating a possible Pgp modulation by IDN-5109, SB-T-1213, SB-T-1250, and SB-T-101187 using the rhodamin 123 fluorescent probe. Thus these taxoids have dual functions in one molecule, i.e., cytotoxicity and MDR reversal activity. This exciting discovery identified a new class of anticancer agents. SB-T-1214, SB-T-1103, SB-T-1104 and SB-T-1216 were chosen for further development. Structures of some novel taxoids are shown in Figure 1-19. This chapter describes the synthesis of SB-T-1214.

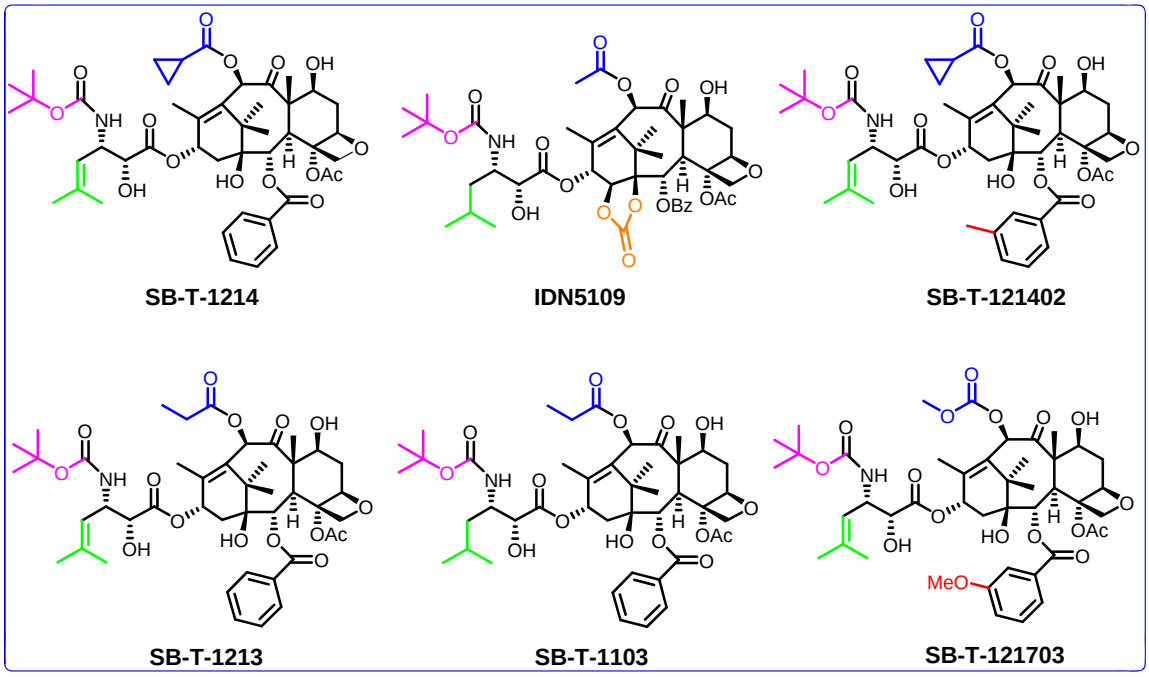

Figure 1-19. Structure of some novel taxoids

1.3.4.2. Results and discussion

The synthesis of second-generation taxoid SB-T-1214 was carried out using the *β*-LSM *via* *β*-lactam ring-opening coupling with modified baccatin. The 10-DAB III was selectively protected at the C-7 OH with triethylsilyl choride (TESCl) in presence of imidazol in DMF to yield 7-TES-DAB III (**1-12**) in excellent yield.[102] This was then modified at C-7 position by treating with cyclopropanoyl chloride to yield **1-13** followed by ring opening coupling of *β*-lactam (**1-11**) with lithium bis(trimethylsilyl)amide (LiHMDS) to afford the protected taxoid **1-14** which was then subjected to a global silyl deprotection with HF/pyridine to yield **SB-T-1214** as shown in Scheme 1-14 .

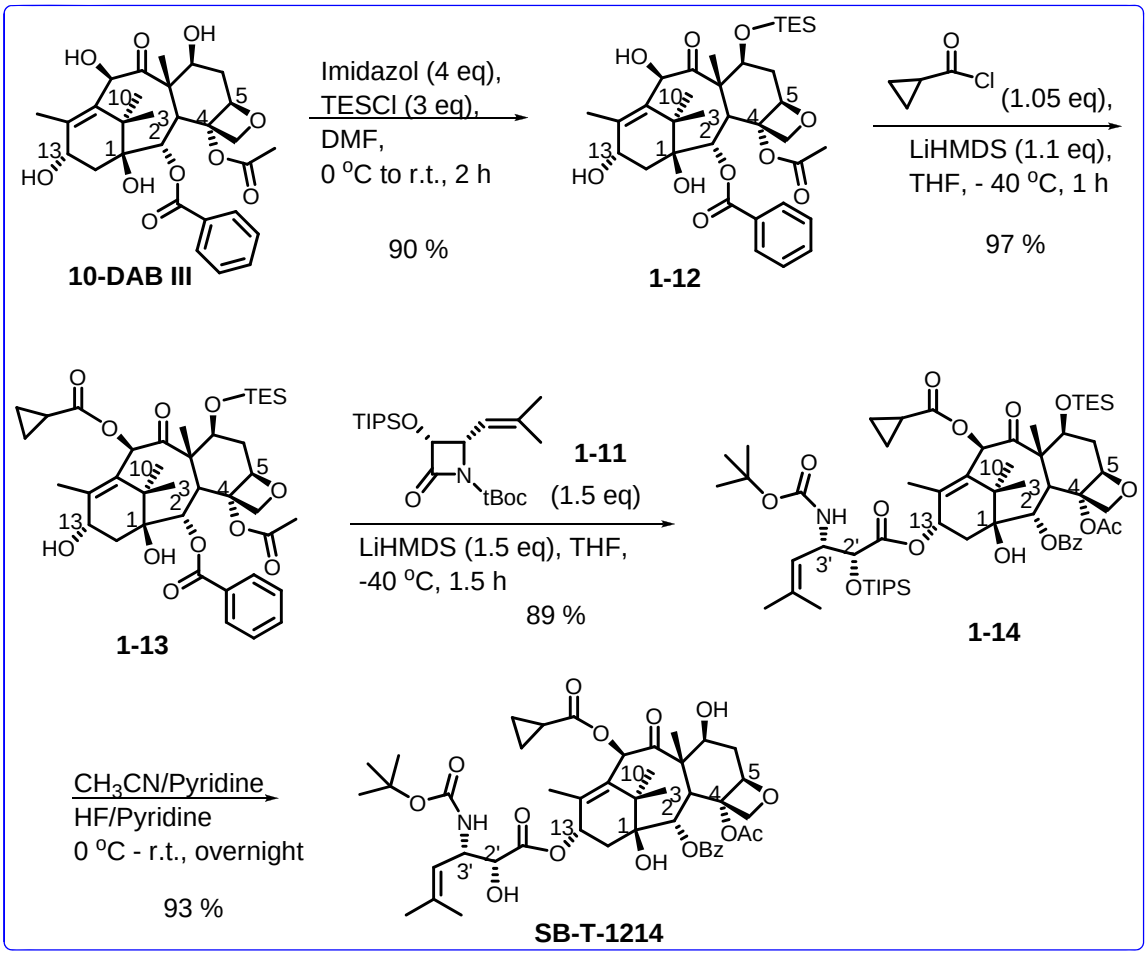

Scheme 1-14. Synthesis of SB-T-1214

1.4 Experimental section

General Methods: ^{1}H, ^{13}C and ^{19}F NMR spectra were measured on a Bruker AC-250 NMR spectrometer or a Varian 300, 400, 500, or 600 MHz NMR spectrometer. The melting points were measured on a "Uni-melt" capillary melting point apparatus from Arthur H. Thomas Company, Inc. Optical rotations were measured on a Perkin-Elmer Model 241 polarimeter. High-resolution mass spectrametric analyses were conducted at the Mass Spectrometry Laboratory, University of Illinois at Urbana-Champaign, Urbana, IL. GC-MS analyses were performed on an Agilent 6890 Series GC system equipped with the HP-5HS capillary column, (50 m X 0.25 mm, 0.25 μm) and with the Agilent 5973 network mass selective detector. LC-MS analyses were carried out on an Agilent 1100 Series Liquid Chromatograph Mass Spectrometer. IR spectra were measured on a

Shimadzu FTIR-8400s spectrophotometer. TLC analyses were performed on Merck DC-alufolien with Kieselgel 60F-254 and were visualized with UV light, iodine chamber, 10 % sulfuric acid and 10% PMA solution. Column chromatography was carried out on silica gel 60 (Merck; 230-400 mesh ASTM). Chemical purity was determined with a Waters HPLC assembly consisting of dual Waters 515 HPLC pumps, a PC workstation running Millennium 32, and a Waters 996 PDA detector, using a Phenomenex Curosil-B column, employing CH_3CN/water as the solvent system with a flow rate of 1 mL/min, or Shimadzu HPLC. Chiral HPLC analysis for the determination of enantiomeric excess was carried out with a Waters HPLC assembly, comprising Waters M45 solvent delivery system, Waters Model 680 gradient controller, Water M440 detector (at 254 nm) equipped with a Spectra Physics Model SP4270 integrator. The system uses a DAICEL-CHIRACEL OD chiral column (25 x 0.46 cm i.d.), employing hexan/2-propanol as the solvent system with a flow rate of 1.0 mL/min.

Materials: The chemicals were purchased from Sigma Aldrich Company or Acros Organic Fischer Company. 10-Deacetyl baccatin III (DAB) was donated by Indena, SpA, Italy. Dichloromethane and methanol were dried before use by distillation over calcium hydride under nitrogen or argon. Ether and THF were dried before use by distillation over sodium-benzophenone ketyl under nitrogen or argon. Toluene and benzene were dried by distillation over sodium metal under nitrogen or argon before use. Dry DMF was purchased from EMD chemical company, and used without further purification. PURE SOLV^{TM}, Innovative technology Inc, provided an alternative source of dry toluene, THF, ether, and dichloromethane. The glasses were dried in a 110 ^{o}C oven and allowed to cool to room temperature in a desiccator over "*Drierite*" (calcium sulfate) and assembled under inert gas nitrogen or argon atmosphere.

1.4.1 Synthesis of *β*-lactam (1-11) by chiral TIPS-ester enolate-imine cyclocondensation method

Racemic trans-2-phenylcyclohexanol [(±)-1-2]:[164]

A solution of phenylmagnesium bromide in 150 mL of THF was prepared from 7.07 g (0.29 mol) of magnesium and bromobenzene (31 mL, 0.294 mol) using standard conditions. After cooling the Grignard solution to -30 ^{o}C, CuI (2.52 g, 13.2 mmol) was added. The resulting solution was stirred for approximately 10 min, and a solution of cyclohexene oxide (20 mL, 0.2 mol) **1-1** in 200 mL of THF was added dropwise over a period of 1 h. The reaction mixture was then allowed to warm to 0 ºC and was stirred for an additional 2 h. The reaction was quenched at 0 ºC with a saturated aqueous NH_4Cl solution and extracted with ethyl acetate. The organic layer was washed with a saturated aqueous NH_4Cl solution until there was no longer any color change in the aqueous layer. The combined aqueous layers were extracted with ether and the combined organic layers dried over anhydrous $MgSO_4$, filtered and concentrated *in vacuo*. Recrystallization from hexane gave 28.35 g (80 % yield) of **1-2** as a white solid. M.p. 55-56 °C. ^{1}H NMR (300

MHz, $CDCl_3$) 1.25-1.53 (m, 4 H)(H on C2,C4,OH), 1.62 (s, 1 H)(H on C6), 1.76 (m, 1 H)(H on C3), 1.84 (m, 2 H)(H on C3), 2.11 (m, 1 H)(H of C6), 2.42 (ddd, J = 16.6 Hz, 10.8 Hz, 5.4 Hz, 1 H)(H on C2), 3.64 (ddd, J = 16.6 Hz, 10.8 Hz, 5.4 Hz, 1 H)(H on C1), 7.17-7.35 (m, 5 H)(H on benzene ring). All data are in agreement with literature values.[164]

Racemic trans-2-phenylcyclohexyl acetate [(±)-(1-3)]:[164]

Racemic alcohol **1-2** in (27.85 g, 157 mmol), 4-dimethylaminopyridine (DMAP) (0.419 g, 4.71 mmol), pyridine (17 mL) was dissolved in CH_2Cl_2 (23 mL) in a flask and a solution of acetic anhydride (17 mL) in 28 mL of CH_2Cl_2 was added dropwise over a period of 2 h. The reaction was then poured into a mixture of 49 mL 6 N HCl, 73 mL of ice and 150 mL of ether. The organic layer was washed with 2 N HCl aqueous solution and the combined aqueous layers were extracted with ether. The combined organic layers were washed with a saturated aqueous $NaHCO_3$ solution and dried over anhydrous $MgSO_4$, filtered and concentrated *in vacuo* to afford 39.02 g (quantitative yield) of **1-3** as pale yellow oil. ^{1}H NMR (300 MHz, $CDCl_3$) 1.35 (m, 1 H)(H on C4), 1.41 (m, 1 H) (H on C4), 1.46 (m, 1 H)(H on C2), 1.56 (m, 1 H) (H on C6), 1.74 (s, 3 H) (H on CH3), 1.78 (m, 1 H) (H on C3), 1.84 (m, 1 H) (H on C3), 1.93 (m, 1 H) (H of C6), 2.65 (ddd, J = 16.6 Hz, 11.0Hz, 5.4 Hz, 1 H)(H on C2), 4.98 (ddd, 1 H)(H on C1), 7.17-7.35 (m, 5 H)(H on benzene ring). All data are in agreement with literature values.[164]

(+)-*trans*-2-Phenylcyclohexyl acetate [(+)-1-3] and (-)-*trans*-2-phenylcyclohexanol [(-)-1-2]:[164]

The racemic acetate **1-3** (39 g, 0.178 mol) in 161 mL of ether was added to 1.21 L of 0.5 M aqueous buffer with pH = 8 (KH_2PO_4/K_2HPO_4) at 31 ºC. After stirring for 30 min, 9.2 g of pig liver acetone powder (PLAP) was added. The mixture was stirred for 7 days at 31 ºC, until ^{1}H NMR of the crude organic layer showed <50/50 ratio of alcohol (-)-**1-2** and acetate (+)-**1-3**. The reaction mixture was quenched by acidifying to pH = 4 with 2 N HCl solution. To the resulting mixture was added 200 mL of ether with stirring for 1 h. After the PLAP was allowed to settle, the supernatant organic layer was removed (addition of ether and removal of the organic layer was repeated 3 times). The organic and aqueous layers were filtered and the aqueous layer was extracted with ether. The combined organic layers were dried over anhydrous $MgSO_4$, filtered and concentrated *in vacuo*. Some (-)-alcohol was crystallized out from the resulting brown solution. The remainder of the crude product was purified *via* column chromatography on silica gel using hexane/ethyl acetate (15/1) as the eluant to afford acetate (+)-**1-3** as a slightly yellow oil (15.2 g, 39 %) and 7.23 g (23 %) of pure (-)-**1-2** as a white solid. M.p.: 63-65 ºC.

Benzyloxyacetic acid (1-4):[196]

Sodium metal (5.4 g, 0.236 mol) was added gradually to benzyl alcohol (88 mL, 0.848 mol) at room temperature with stirring. After most of the sodium had reacted, the reaction mixture was heated to 150 ºC till complete reaction of the sodium was observed. Bromoacetic acid (14.20 g, 0.103 mol) in 20 mL of THF was added dropwise to the reaction mixture. The reaction mixture was stirred at 150 ºC for 3 h and then cooled to

room temperature. Cold water was added and the two layers separated. The aqueous layer was carefully extracted with dichloromethane to remove any remaining benzyl alcohol. The water layer was acidified with 10 % HCl until a pH of 2-3 and extracted with ether. The organic layer was then dried over magnesium sulfate, filtered and concentrated *in vacuo*. The oil residue was distilled under reduced pressure to afford 5.4 g (32 %) of **1-4** as a colorless oil: B.p. 138-140 ºC (0.3 mm Hg); ^{1}H NMR (300 MHz, $CDCl_3$,) δ 4.17 (s, 2 H)(H on benzyl group), 4.67 (s, 2 H)(H on C1), 7.38 (m, 5 H)(H on benzene ring). All data are in agreement with literature values.[196]

(1*R*,2*S*)-(-)-2-Phenylcyclohexyl benzyloxyacetate (1-5):[196]

(-)-trans-2-Phenylcyclohexanol (**1-2**) (5.50 g) and a catalytic amount of (p-TSA) p-toluenesulfonic acid was taken in a flask which was then inerted (vacuum/nitrogen). Distilled toluene (75 mL) was then syringed into the flask to dissolve the solids. Benzyloxyacetic acid (**1-4**, 5.20 g) was dissolved in distilled toluene and added to the reaction flask. The reaction mixture was refluxed (130 ^{o}C) overnight. The water produced in the reaction along with some toluene was condensed and collected in a Dean-Stark apparatus. The toluene was evaporated off *in vacuo* and the reaction mixture was diluted with ether and washed with saturated sodium bicarbonate solution. The organic and aqueous layers were separated and the organic layer was washed with saturated sodium chloride solution and dried over anhydrous magnesium sulfate solution, filtered and concentrated *in vacuo*. The crude product was purified *via* flash chromatography (50:1 pentane/ ethylacetate) to yield 6.3 g (63 %) of **1-5** as a white solid. ^{1}H NMR (400 MHz, $CDCl_3$) δ 1.26-1.63 (m, 4 H)(H on C2,C4,C6), 1.76-1.99 (m, 3 H)(H on C3,C5,C6), 2.10-2.20 (m, 2 H)(H on C6), 2.70 (dt, J = 11.0, 4.1 Hz, 1 H)(H on C2), 3.73 (d, J = 16.5 Hz, 1 H)(H on acetic acid), 3.84 (d, J = 16.5 Hz, 1 H) (H on acetic acid), 4.25 (s, 2 H) (H on benzyl group), 5.13 (td, J = 11.0Hz, 4.1 Hz, 1 H) (H on C1), 7.17-7.36 (m, 10 H) (H on benzene ring). All data are in agreement with literature values.[196]

(1*R*,2*S*)-(-)-2-Phenylcyclohexyl hydroxyacetate (1-6):[141]

(-)-Benzyloxyacetate (**1-5**) (3.5 g) and 0.807 g of 10% palladium on carbon (Pd-C) was added in a flask which was inerted (vacuum/nitrogen) and then filled with hydrogen gas. 50 mL of distilled THF and 3 mL of methanol was added to the reaction flask. The reaction mixture was stirred for 40 h at 45 ºC under hydrogen. When TLC monitor (2:1 hexane/ethylacetate) indicated no starting material the reaction mixture was filtered through celite and concentrated *in vacuo*. The crude product was purified *via* flash chromatography (20:1 pentane/ethylacetate) to afford 2.49 g (97 % yield) of **1-6** as a white solid. ^{1}H NMR (300 MHz, $CDCl_3$) δ 1.30-1.66 (m, 4 H) (H on C2,C4,C6), 1.78-2.00 (m, 3 H) (H on C3,C5,C6), 2.14-2.20 (m, 2 H) (H on C6), 2.67 (dt, J = 11.0, 4.2 Hz, 1 H) (H on C2), 3.72 (d, J = 17.0 Hz, 1 H)(H on acetic acid), 3.92 (d, J = 17.0 Hz, 1 H) (H on acetic acid), 5.07 (td, J = 11.0 Hz, 4.2 Hz, 1 H)(H on C1), 7.15-7.32 (m, 5 H) (H on benzene ring). All data are in agreement with literature values.[141]

(1*R*,2*S*)-(-)-2-Phenylcyclohexyl triisopropylsilyloxyacetate (1-7):[141]

Hydroxy-acetate (**1-6**) (2.48 g), 1.7 g of imidazole was taken in a flask which was inerted (vacuum/nitrogen) and 5.4 mL of DMF was added to dissolve the solids. 3 mL of chlorotriisopropylsilane (TIPSCl) was then syringed into the flask. The reaction was stirred under nitrogen overnight at room temperature. TLC monitor (6:1 hexane/ ethylacetate) was performed and the reaction quenched with saturated ammonium chloride solution. The aqueous layer was extracted with dichloromethane (3 x 20 mL). The collective organic layers was washed with saturated sodium chloride solution, dried over anhydrous magnesium sulfate, filtered and concentrated *in vacuo*. The oil residue was distilled under reduced pressure to afford 3.1 g (79 % yield) of **1-7** as a colorless oil: B.p.: 155-160 ºC (0.1 mm Hg). ^{1}H NMR (300 MHz, $CDCl_3$) δ 0.94-1.25 (m, 21 H)(H on TIPS group), 1.35-1.70 (m, 4 H)(H on C2,C4,C6), 1.80-2.04 (m, 3 H)(H on C3,C5,C6), 2.10-2.20 (m, 1 H)(H on C6), 2.70 (dt, J = 11.0 Hz, 4.2 Hz, 1 H)(H on C2), 3.91 (d, J = 16.5 Hz, 1 H)(H on acetic acid), 4.08 (d, J = 16.5 Hz, 1 H)(H on acetic acid), 5.07 (td, J = 11.0 Hz, 4.2 Hz, 1 H)(H on C1), 7.16-7.30 (m, 5 H)(H on benzene ring). All data are in agreement with literature values.[141]

_N_-(4-Methoxyphenyl)-3-methyl-2-butenaldimine (1-8):[101]

p-Anisidine (0.44 g) and anhydrous Na_2SO_4 (2 eq) was added in a flask which was inerted (vacuum/nitrogen). 20 mL of distilled dichloromethane was syringed in the flask to dissolve the *p*-anisidine. 0.41 mL of 3-Methylbut-2-eneal was added dropwise, and then the reaction mixture was stirred at room temperature for 2 h. When TLC monitor (1:1 hexane/ethylacetate) indicated no starting material the reaction mixture was filtered and the solvent was evaporated, then put under vacuum to yield imine **1-8** as yellow, viscous oil, which was immediately used for the synthesis of *β*-lactam without further purification. ^{1}H NMR (300MHz, $CDCl_3$) δ 1.95 (s, 3 H)(H on CH_3), 2.01 (s, 3 H)(H on CH_3), 3.81 (s, 3 H)(H on CH_3O group), 6.20 (d, J = 9.5 Hz, 1 H)(H on C2), 6.89 (d, J = 7.0 Hz, 2 H)(H on benzene ring), 7.11 (d, J = 7.0 Hz, 2 H)(H on benzene ring), 8.38 (d, J = 9.5 Hz, 1 H)(H on C1). All data are in agreement with literature values.[101]

1-*p*-Methoxyphenyl-3-triisopropylsilyloxy-4-(2-methylpropen-2-yl)azetidin-2-one (1-9): [101]

Distilled diisopropylamine (0.44 mL) in 10 mL of distilled THF was added in an inerted flask which was cooled to –15 ^{o}C. 1.26 mL (2.5 M in hexanes) of *n*-butyllithium was then added to the flask and the mixture was stirred for 1 h at – 15 ^{o}C. The reaction mixture was then cooled to -80 ^{o}C. A solution of the TIPS-Ester **1-7** (0.93 g) in 10 mL distilled THF was slowly added *via* cannula over a period of 1 h. After stirring for an additional hour, a solution of the imine (**1-8**) (in 10 mL distilled THF) was carefully added *via* a cannula over a period of 2 h. The reaction was stirred overnight at -80 ^{o}C. LiHMDS (1 eq) was added the next day and the reaction was allowed to stir at -80 ^{o}C for 1 h. TLC monitor (10:1 hexane/ethyl acetate) was performed and the reaction was then quenched with a saturated ammonium chloride solution. The aqueous layer was extracted with dichloromethane and the combined organic layers were washed with saturated sodium chloride solution and dried over magnesium sulfate and concentrated *in vacuo*. The crude product was then purified by column chromatography on silica gel (40:1 hexane/ethyl

acetate) to yield 0.75 g 1-*p*-methoxy-phenyl-3-triisopropylsiloxy-4-(2-methylpropen-2-yl)azetidin-2-one (**1-9**) in 78 % yield. ^{1}H NMR (300 MHz,$CDCl_3$): δ 0.97-1.24 (m, 21 H)(H on TIPS group), 1.84 (d, J = 2.3 Hz, 3 H)(H on CH3), 1.88 (d, J = 2.3 Hz, 3 H)(H on CH_3), 3.77 (s, 3 H)(H on CH_3O group), 4.82 (dd, J = 9.9, 5.1 Hz, 1 H)(H on C1'), 5.04 (d, J = 5.1 Hz, 1 H)(H on C4), 5.33 (d, J = 9.9 Hz, 1 H)(H on C3), 6.84 (d, J = 8.7 Hz, 2 H)(H on benzene ring), 7.32 (d, J = 8.7 Hz, 2 H)(H on benzene ring). All data are in agreement with literature values.[101]

3-Triisopropylsilyloxy-4-(2-methylpropen-2-yl)azetidin-2-one (1-10):[102]

The compound **1-9** (0.97 g) was dissolved in 94 mL of acetonitrile and 19 mL of water and cooled to - 10 ^oC. Ammonium cerium nitrate (CAN) (4.6 g) in 75 mL water was added dropwise over a 30 min period using a dropping funnel. The reaction mixture was then stirred for 2 h and quenched with 140 mL of saturated sodium sulfite solution when TLC monitor indicated no starting material. The reaction mixture was filtered using a buchner funnel and the aqueous layer was extracted with dichloromethane (3 x 100 mL). The combined organic layers was washed with saturated sodium chloride solution, dried over anhydrous magnesium sulfate, filtered and concentrated *in vacuo*. The crude was purified using flash chromatography on silica gel (7:1 pentane/ethyl acetate). 0.5 g of the pure **1-10** was obtained in 70 % yield. ^{1}H NMR (400 MHz,$CDCl_3$) δ 0.97-1.18 (m, 21 H)(H on TIPS group), 1.19 (d, J = 2.3 Hz, 3 H)(H on CH_3), 1.68 (d, J = 2.3 Hz, 3 H)(H on CH_3), 4.45 (dd, J = 9.5, 4.7 Hz, 1 H) (H on C1'), 4.98 (dd, J = 4.7, 2.3 Hz, 1 H) (H on C4), 5.31 (d, J = 9.5 Hz, 1 H) (H on C3). All data are in agreement with literature values.[102]

1-(*t*-Butoxycarbonyl)-3-triisopropylsiloxy-4-(2-methylpropen-2-yl)azetidin-2-one (1-11):[102]

The compound **1-10** (0.406 g) and a catalytic amount of DMAP (0.25 eq) was added in a flask and inerted (vacuum/nitrogen). 8 mL of distilled dichloromethane was then syringed into the flask to dissolve the solids. Triethylamine (0.6 mL, 3 eq) was then syringed in dropwise followed by 0.324 g of di-*t*-butyl-dicarbonate (1.1 eq) in 5 mL dichloromethane. The reaction was allowed to stir overnight at room temperature and quenched with 10 mL saturated ammonium chloride solution. The organic and aqueous layer was separated and the aqueous layer was extracted with dichloromethane (3 x 30 mL). The combined organic layers was washed with saturated sodium chloride solution, dried over anhydrous magnesium sulfate, filtered and concentrated *in vacuo*. The crude was purified using flash chromatography (40:1 pentane/ethyl acetate) to give 0.459 g of **1-11** as a clear oil in 98 % conversion yield. ^{1}H NMR (300 MHz, $CDCl_3$) δ 1.02-1.2 (m, 21 H)(H on TIPS group), 1.48 (s, 9 H)(H on Boc group), 1.77 (d, J = 1.0 Hz, 3 H)(H on CH3), 1.79 (d, J = 1.0 Hz, 3 H)(H on CH3), 4.75 (dd, J = 9.8, 5.6, 1 H) (H on C'), 4.97 (d, J = 5.6 Hz, 1 H) (H on C4), 5.28 (dd, J = 9.8, 1.0 Hz, 1 H)(H on C3). All data are in agreement with literature values.[102]

1.4.2 Synthesis of *Z*-3(R)-Ethoxyethoxy-4(S)-phenylazetidin-2-one (1-17) *via* [2+2] ketene-imine cycloaddition

_N_-(4-Methoxyphenyl)benzaldimine (1-12):
Benzaldehyde (2.95 mL, 29 mmol) was added dropwise to a solution of *p*-anisidine (3.180 g, 26 mmol; recrystalized once from methanol) and anhydrous Na_2SO_4 in 60 mL CH_2Cl_2 and then the reaction mixture was stirred at room temperature for 2 h. The solution was filtered and evaporated to remove the solvent. After recrystallzation, 4.49 g *N*-(4-methoxyphenyl)benzaldimine **1-12** was obtained as a white solid (87 % yield).

cis-1-*p*-Methoxyphenyl-3-acetoxy-4-phenylazetidin-2-one (1-13):
A solution α-acetoxyacetyl chloride (3.134 g, 23 mmol) in 30 mL CH_2Cl_2 was added dropwise to a solution of *N*-(4-methoxyphenyl)benzaldimine **1-12** (4.430 g, 20 mmol) and triethylamine (4.46 mL, 15.4 mmol) in 90 mL of CH_2Cl_2 at –78 ^oC. The reaction mixture was allowed to warm to 25 ^oC over 18 h, then diluted with 50 mL of CH_2Cl_2, and organic layer was washed with 30 mL of water and 30 mL of saturated aqueous sodium bicarbonate, dried over magnesium sulfate, and concentrated to provide a solid product. The product **1-13** was then purified by column chromatography on silica gel (hexane:ethyl acetate = 3/1) to give a white crystal (5.53 g, 93 % yield). ^1H NMR (300 MHz, $CDCl_3$) δ 7.35-7,26 (m, 7 H)(H on benzene group), 6.81 (d, J = 9.0 Hz, 2 H)(H on PMP group), 5.81(d, 1 H)(H on C3), 5.34 (d, J = 4.9 Hz, 1 H)(H on C4), 3.75 (s, 3 H)(H on CH*3*O group), 1.68 (s, 3 H)(H on acetate group).

Enantioselective hydrolysis of *β*-lactam (1-13):[38]
The racemic **1-13** (5.5 g) was suspended in 480 mL of potassium phosphate buffer (pH = 7.5) and 48 mL of acetonitrile. PS-Amano lipase (1.5 g) was added to it and the mixture was stirred at 50 ^oC for 25 h. The reaction was terminated when NMR monitor indicated 50:50 ratio of the acetate and the alcohol. Extraction was performed with ethyl acetate (4 x 50 mL). The organic layers was washed with saturated sodium chloride solution, dried over magnesium sulfate, and concentrated to provide solid product mixture which was then separated using column chromatography on silica gel (dichloromethane and dichloromethane/0.1% methanol) to yield (+)-cis-l-(*p*-methoxyhenyl)-3-acetoxy-4-phenylazetidin-2- one **1-13** 2.2 g with the yield of 40 % and (-)-cis-l-(*p*-methoxyhenyl)-3-hydroxy-4- phenylazetidin-2-one **1-14** 0.9 g with 23 % yield.

Z–3(*R*)-Acetoxy-4(*S*)-phenylazetidin-2-one (1-15):[38]
The compound **1-13** (1.004 g) was dissolved in 96 mL of acetonitrile and 16 mL of water and cooled to -10 ^oC. Ammonium cerium nitrate (CAN) (6.189 g) in 96 mL water was added dropwise over a 30 min period using a dropping funnel. The reaction mixture was then stirred for 2 h afterwards and quenched with 143 mL of saturated sodium sulfite solution when TLC monitor (2:1 hexane/ethylacetate) indicated no starting material. The reaction mixture was filtered using a buchner funnel and the aqueous layer was extracted with dichloromethane (3 x 100 mL). The combined organic layers was washed with

saturated sodium chloride solution, dried over anhydrous magnesium sulfate, filtered and concentrated *in vacuo*. The product **1-15** (0.6 g) was obtained as a white solid in 91 % yield. ^{1}H NMR (300 MHz, $CDCl_3$): δ 1.68 (s, 3 H)(H on acetate group), 5.05(d, 1 H)(H on C4), 5.87 (dd, J = 2.7Hz, 4.7Hz, 1 H)(H on C3), 6.21 (s, exchangeable, 1 H)(H on NH), 7.30-7.38 (m, 5 H)(H on benzene ring). All data are consistent with literature data.[38]

Z-3(*R*)-Hydroxy–4(*S*)-phenylazetidin-2-one (1-16):
The compound **1-15** (0.48 g) was dissolved in 30 mL THF and cooled to 0 ^{o}C. A solution of 24 mL of 1 M KOH in 20 mL of THF was added dropwise to the reaction flask *via* a dropping funnel. The mixture was kept stirring at 0 ^{o}C for 1 h. TLC monitor was performed with (1:1 hexane/ethylacetate) and the reaction was quenched when no starting material was indicated with saturated ammonium chloride solution (pH ~ 7). The organic and aqueous layers were separated and the aqueous layer was extracted with dichloromethane (4 x 50 mL). The collective organic layers was washed with saturated sodium chloride solution, dried with anhydrous magnesium sulfate, filtered and concentrated *in vacuo* to yield 0.23 g of pure **1-16** in 61 % yield. ^{1}H NMR (300 MHz, $CDCl_3$) δ 2.10 (d, 1 H)(H on OH), 4.94 (d, J = 4.7 Hz, 1 H)(H on C4), 5.04 (d, J = 4.7 Hz, 1H)(H on C3), 6.20 (s exchangeable, 1 H)(H on NH) 7.25-7.35 (m, 5 H)(H on benzene ring); All data are consistent with literature data.

Z-3(*R*)-Ethoxyethoxy-4(*S*)-phenylazetidin-2-one (1-17):
The flask containing **1-16** (0.21 g) and a catalytic amount of *p*-TSA (5 %) was inerted (vacuum/nitrogen). Distilled THF (5 mL) was used to dissolve the solids in the flask and 0.18 mL of ethoxy vinyl ether was added dropwise *via* syringe. The reaction was monitored by TLC (1:1 hexane/ethylacetate). The reaction was stirred at room temperature for 2 h and quenched with saturated sodium bicarbonate solution when no starting material was observed in TLC. The aqueous layer was extracted with dichloromethane (4 x 30 mL). The collective organic layers was washed with saturated sodium chloride solution, dried with anhydrous magnesium sulfate, filtered and concentrated *in vacuo*. The pure product **1-17** was obtained using flash chromatography (1:1 hexane/ethyl acetate) on silica gel as a white solid in 80 % yield (0.244 g). ^{1}H NMR (300MHz, $CDCl_3$) δ 0.98 (d, J = 5.4 Hz), 1.05 (d, J = 5.4 Hz), 3H (H on CH_3 of ethyl group), 1.11 (t, J = 7.1 Hz), 1.12 (t, J = 7.1 Hz), 3H (H on CH_3 of OCO), 3.16-3.26 (m), 3.31-3.42 (m), 3.59-3.69 (m), 2H (H on CH_2 of ethyl group), 4.47 (q, J = 5.4 Hz), 4.68 (q, J = 5.4 Hz), 1H (H on OCO), 4.82 (d, J = 4.7 Hz), 4.85 (dd, J = 4.7 Hz), 1H (H on C3), 5.17-5.21 (m, 1 H)(H on C4), 6.42 (s, 1 H)(H on NH), 7.35 (m, 5 H)(H on benzene ring). All data are consistent with literature data.

1.4.3 Synthesis of 1-(*t*-Butoxycarbonyl)-3-triisopropylsiloxy-4-(2-methyl propen-2-yl)azetidin-2-one (1-11) *via* [2+2] ketene-imine cycloaddition

(+)-1-(4-Methoxyphenyl)-3-acetoxyl-4-(2-methylprop-1-enyl)azetidin-2-one (1-18):

p-Anisidine (6 g, 48.72 mmol) and anhydrous sodium sulfate (27.68 g, 4 eq) were added in a flask which was inerted (vacuum/nitrogen). The flask was covered by aluminum foil. 194 mL of distilled dichloromethane was then added while stirring to dissolve the solid reactant. 3-methyl-2-butenal (5.5 mL, 56.7 mmol) was added dropwise into the flask and the reaction mixture was kept stirring at room temperature for 3 h. The reaction was monitored by TLC every half hour using 2:1 hexane/ethyl acetate. When the TLC indicated no starting material the reaction was stopped. The inorganic solid was filtered off using sintered glass funnel. The precipitate was washed with dichloromethane. The filtrate was concentrated *in vacuo* and the unreacted 3-methyl-2-butenal was pumped out using a vacuum pump to obtain **1-8**.

The flask containing **1-8** was inerted (vacuum/nitrogen) and 270 mL of distilled dichloromethane was added to dissolve **1-8**. The solution was cooled to -78 ^{o}C. Triethylamine (13.8 mL, 97.9 mmol, 2 eq) was added using syringe followed by acetoxyacetyl chloride (6 mL, 55.9 mmol, 1.14 eq). The reaction mixture was allowed to warm up to room temperature overnight. The reaction was quenched after TLC monitor (1:1 hexane/ethyl acetate) with 120 mL saturated ammonium chloride solution and extracted with dichloromethane (3 x 170 mL). The organic and aqueous layers were separated using a separating funnel. The combined organic layers were washed with distilled water, saturated sodium chloride solution, dried over anhydrous magnesium sulfate and concentrated *in vacuo*. Flash column chromatography of the crude compound was performed on silica gel (5:1 hexane/ethyl acetate) to give 11.86 g of pure **1-18** as a pale yellow solid in 84 % yield. ^{1}H NMR (300 MHz, $CDCl_3$) 1.70 (s, 3 H)(H on CH_3), 1.72 (s, 3 H)(H on CH_3), 2.01 (s, 3 H)(H on CH_3 of acetate), 3.67 (s, 3 H)(H on CH_3 of PMP), 4.83 (dd, J = 9.9Hz, 4.8 Hz, 1 H)(H on CH of isobutenyl), 5.02 (d, J = 9.3 Hz, 1 H)(H on C4), 5.67 (d, J = 4.8 Hz, 1 H)(H on C3), 6.74 (d, J = 8.9 Hz, 2 H)(H on benzene ring), 7.20 (d, J = 8.9 Hz, 2 H) (H on benzene ring).

Enzymatic kinetic resolution of 1-18:[38]

Racemic **1-18 (**2.03 g) was suspended in 238.5 mL of 0.2 M potassium phosphate buffer (pH = 7.5) and 25 mL acetonitrile. PS-Amano lipase (1.07 g) was added to it and the mixture was vigorously stirred using a mechanical stirrer at 50 ^{o}C (using oil bath). The reaction was monitored by NMR and stopped after 56 h when 50% of the acetate had converted to the alcohol. The reaction mixture was filtered using a sintered glass funnel to remove the enzyme. The enzyme was washed with dichloromethane and the organic and aqueous layers were separated using separating funnel. The aqueous layer was washed with dichloromethane (4 x 100 mL) and the organic layer collected with the previous organic layers. The collective organic layers was washed with saturated sodium chloride solution, dried with anhydrous magnesium sulfate, filtered and concentrated *in vacuo*. The pure compounds were obtained by performing flash chromatography on silica gel (5:1 and 2:1 hexane/ethyl acetate). 0.849 g of the (+)-cis-1-(4-methoxyphenyl)-3-acetoxyl-4-(2-methylprop-1-enyl)azetidin-2-one (**1-18**) was obtained as colorless solid in 41 % yield (> 99.99 % ee) and (-)-cis-1-(4-methoxyphenyl)-3-hydroxy-4-(2-methylprop-1-enyl)azetidin-2-one (-)-(**1-19**) was obtained in 55 % yield (0.950 g) as a reddish colored solid.

(3*R*,4*S*)-1-(4-Methoxyphenyl)-3-hydroxy-4-(2-methylprop-1-enyl)azetidin-2-one (1-19):[197]

The pure (+)-**1-18** (4.24 g) was dissolved in 255 mL THF and cooled to 0 ^{o}C. A solution of 156.4 mL of 1 M KOH (10 eq) and 174 mL of THF was added dropwise using a dropping funnel over 30 min period at 0 ^{o}C. The mixture was then stirred for 2.5 h at 0 ^{o}C and monitored by TLC (1:1 hexane/ethyl acetate). The reaction was quenched with saturated ammonium chloride solution (pH ~ 7) when TLC monitor showed no starting material. The organic and aqueous layers were separated and the aqueous layer was washed with dichloromethane (4 x 250 mL). The organic layers were collected with the previous organic layers. The combined organic layers was washed with saturated sodium chloride solution, dried with anhydrous magnesium sulfate, filtered and concentrated *in vacuo* to give 3.6 g of (+) **1-19** as colorless solid in quantitative yield and > 99.9% ee. (Daicel-Chiracel ODH, hexane/2-propanol (85:15 v/v) as solvent system, 0.9 mL/min flow rate). ^{1}H NMR (300 MHz, $CDCl_3$) δ 1.86 (s, 6H on isobutenyl CH_3), 3.78 (s, 3H on OCH_3), 4.84 (d, J = 4.7 Hz, 1 H)(H on C4), 5.04 (d, J = 4.7 Hz, 1 H)(H on C3), 7.25-7.35 (m, 5 H)(H on benzene ring). All data are consistent with literature data.[197]

1-*p*-Methoxyphenyl-3-triisopropylsilyloxy-4-(2-methylpropen-2-yl)azetidin-2-one (1-9):[101]

To 0.498 g of **1-19** was added 0.0492 g of DMAP (0.2 eq) and the flask was inerted (vacuum/nitrogen). Distilled dichloromethane (7 mL) was added to dissolve the solids in the flask and 1.12 mL of triethylamine (4 eq) was added using syringe. TIPSCl (0.65 mL, 1.5 eq) was then added dropwise and the mixture was stirred at room temperature overnight. TLC monitor was performed using 2:1 hexane/ethyl acetate and the reaction quenched with saturated ammonium chloride solution (pH ~ 7) when TLC monitor showed no starting material. The organic and aqueous layers were separated and the aqueous layer was washed with dichloromethane (3 x 30 mL) and the organic layer collected with the previous organic layers. The collective organic layers was washed with saturated sodium chloride solution, dried with anhydrous magnesium sulfate, filtered and concentrated *in vacuo*. The pure product was obtained using flash chromatography (15:1 pentane/ethyl acetate) on silica gel as a colorless crystal in quantitative yield (0.869 g). ^{1}H NMR (300 MHz, $CDCl_3$) δ 0.97-1.24 (m, 21 H)(H on TIPS group), 1.84 (d, J = 2.3 Hz, 3 H)(H on CH_3), 1.88 (d, J = 2.3 Hz, 3 H)(H on CH3), 3.77 (s, 3 H)(H on CH_3O group), 4.82 (dd, J = 9.9, 5.1 Hz, 1 H)(H on C1'), 5.04 (d, J = 5.1 Hz, 1 H)(H on C4), 5.33 (d, J = 9.9 Hz, 1 H)(H on C3), 6.84 (d, J = 8.7 Hz, 2 H)(H on benzene ring), 7.32 (d, J = 8.7 Hz, 2 H)(H on benzene ring). All data are in agreement with literature values.[101]

3-Triisopropylsilyloxy-4-(2-methylpropen-2-yl)azetidin-2-one (1-10):[102]

The compound **1-9** (0.812 g) was dissolved in 80 mL of acetonitrile and 16 mL of water and cooled to -10 ^{o}C. Ammonium cerium nitrate (CAN) (3.86 g) in 63 mL water was added dropwise over a 30 min period using a dropping funnel. The reaction mixture was then stirred for 2 h and quenched with 120 mL of saturated sodium sulfite solution when TLC monitor indicated no starting material. The reaction mixture was filtered using a

buchner funnel and the aqueous layer was extracted with dichloromethane (3 x 100 mL). The combined organic layers was washed with saturated sodium chloride solution, dried over anhydrous magnesium sulfate, filtered and concentrated *in vacuo*. The crude was purified using flash chromatography on silica gel (7:1 pentane/ethyl acetate) and 0.456 g of the pure **1-10** was obtained in 76 % yield. ^{1}H NMR (400 MHz, $CDCl_3$) δ 0.97-1.18 (m, 21 H)(H on TIPS group), 1.19 (d, J = 2.3 Hz, 3 H)(H on CH_3), 1.68 (d, J = 2.3 Hz, 3 H)(H on CH_3), 4.45 (dd, J = 9.5, 4.7 Hz, 1 H) (H on C1'), 4.98 (dd, J = 4.7, 2.3 Hz, 1 H) (H on C4), 5.31 (d, J = 9.5 Hz, 1 H) (H on C3). All data are in agreement with literature values.[102]

1-(*tert*-Butoxycarbonyl)-3-triisopropylsiloxy-4-(2-methylpropen-2-yl)azetidin-2-one (1-11):[102]

The pure compound **1-10** (0.424 g, 1.42 mmol) and a catalytic amount of DMAP (0.25 eq) was added in a flask and inerted (vacuum/nitrogen). Distilled dichloromethane (8 mL) was then syringed into the flask to dissolve the solids. Triethylamine (0.6 mL, 3 eq) was then syringed in dropwise followed by di-tert-butyl-dicarbonate (0.3469 g, 1.1 eq) in 5 mL dichloromethane. The reaction was stirred overnight at room temperature and quenched with 10 mL saturated ammonium chloride solution. The organic and aqueous layer was separated and the aqueous layer was extracted with dichloromethane (3 x 30 mL). The combined organic layers was washed with saturated sodium chloride solution, dried over anhydrous magnesium sulfate, filtered and concentrated *in vacuo*. The crude was purified using flash chromatography (40:1 pentane/ethyl acetate) to give 0.550 g of **1-11** as clear oil in 97 % yield. ^{1}H NMR (300 MHz,$CDCl_3$) δ 1.02-1.2 (m, 21 H)(H on TIPS group), 1.48 (s, 9 H)(H on Boc group), 1.77 (d, J = 1.0 Hz, 3 H)(H on CH_3), 1.79 (d, J = 1.0 Hz, 3 H)(H on CH_3), 4.75 (dd, J = 9.8, 5.6, 1 H) (H on C'), 4.97 (d, J = 5.6 Hz, 1 H) (H on C4), 5.28 (dd, J = 9.8, 1.0 Hz, 1 H)(H on C3). All data are in agreement with literature values.[102]

1.4.4 Synthesis of novel second-generation taxoid, SB-T-1214

7-Triethylsilyl-10-deacetylbaccatin III (1-12):[102]

A flask containing 10-deacetyl baccatin III (380 mg, 0.71 mmol) and imidazol (194 mg, 2.8 mmol) was inerted. Anhydrous DMF (18 mL, c 0.04 M) was added *via* syringe to dissolve the solids in the flask. The temperature of the flask was maintained at 0 ˚C. Triethylsilylchloride (0.36 mL, 3 eq) was then added dropwise *via* syringe in the flask. The reaction was monitored by TLC (1:1 hexane:ethyl acetate) and quenched with saturated ammonium chloride solution after 2 h. The reaction mixture was diluted with ethyl actetate and the organic and aqueous layer was separated. The organic layer was washed with brine, dried over anhydrous magnesium sulphate and concentrated *in vacuo*. The pure product **1-12** was obtained by performing flash chromatography (4:1, 1:1 hexane:ethyl acetate) as a white solid in 90 % (420 mg) yield. ^{1}H NMR (300 MHz, $CDC1_3$) δ 0.56 (m, 6 H), 0.94 (m, 9 H), 1.08 (s, 6 H), 1.59 (d, J = 2.5 Hz, 1H), 1.73 (s, 3H), 1.90 (dt, 1 H) (H6a), 2.05 (d, J = 4.8 Hz, 1H), 2.08 (s, 3 H), 2.24 (s, 1 H), 2.28 (s, 3

H) (OAc), 2.48 (ddd, 1 H) (H6b), 3.95 (d, J = 7.1 Hz, 1 H) (H3), 4.16 (d, J = 8.3 Hz, 1 H) (H20a), 4.25 (s, 1 H), 4.31 (d, J = 8.3 Hz, 1 H) (H20b), 4.40 (dd, J = 6.4, 10.5 Hz, 1 H) (H7), 4.85 (t, 1 H) (H13), 4.95 (d, J = 8.0 Hz, 1 H) (H5), 5.17 (s, 1 H) (H10), 5.60 (d, J = 7.0 Hz, 1 H) (H2), 7.47 (t, J = 7.5 Hz, 2 H), 7.60 (t, J = 7.5 Hz, 1 H), 8.10 (d, J = 7.3 Hz, 2 H); ^{13}C NMR (400 MHz, $CDCl_3$) δ 5.1, 6.7, 9.9, 15.1, 19.5, 22.6, 26.8, 37.2, 38.6, 42.7, 47.0, 57.9, 67.9, 72.9, 74.6, 74.8, 76.5, 78.8, 80.7, 84.2, 87.6, 128.6, 129.4, 130.0, 133.6, 135.1, 141.8, 167.0, 170.7, 210.3. All data are in agreement with literature values.[102]

7-Triethylsilyl-10-cyclopropanecarbonyl-10-deacetylbaccatin III (1-13):[102]

A flask containing 7-TES-10-DAB III **1-12** (303 mg, 0.46 mmol) was inerted and dry THF (c 0.06 M) was added to dissolve it. The flask was cooled to -40 ^{o}C. LiHMDS 1.0 M in THF (0.51 mL, 1.1 eq) was added dropwise *via* syringe. The mixture was stirred at -40 ^{o}C for 5 min, and then cyclopropanoyl chloride (44.2 μL, 1.05 eq) was added dropwise. After 50 min, the reaction was quenched with aqueous saturated NH_4Cl (10 mL), extracted with CH2Cl2 (20 mL x 3), and the combined organic layers were dried over anhydrous $MgSO_4$ and concentrated *in vacuo*. The crude product was purified on a silica gel column (hexane : ethylacetate = 4 : 1 followed by 2 : 1 and then 1 : 1) to afford **1-13** as a white solid in 97 % yield (332 mg). ^{1}H NMR (300 MHz, $CDC1_3$) δ 0.55 (m, 6 H), 0.90 (m, 9 H), 1.00 (s, 3 H), 1.16 (s, 3 H), 1.64 (s, 3 H), 1.73 (m. 1 H), 1.82 (m, 1 H) (H6a), 2.14 (s, 3 H), 2.23 (m, 2 H), 2.24 (s, 3 H) (OAc), 2.49 (m, 1 H) (H6b), 3.84 (d, J = 6.9 Hz, 1 H) (H3), 4.11 (d, J = 8.0 Hz, 1 H) (H20a), 4.26 (d, J = 8.2 Hz, 1 H) (H20b), 4.45 (dd, J = 6.7, 10.3 Hz, 1 H) (H5), 4.77 (t, J = 7.8 Hz, 1 H) (H13), 4.92 (d, J = 8.6 Hz, 1 H) (H5), 5.59 (d, J = 7.0 Hz, 1 H) (H2), 6.43 (s, 1H) (H10), 7.43 (t, J = 7.4 Hz, 2 H), 7.56 (t, J = 7.6 Hz, 1 H), 8.05 (d, J = 7.3 Hz, 2 H). All data are consistent with the reported values.[102]

3'-Dephenyl-3'-(2-methyl-1-propenyl)-10-cyclopropanecarbonyl-10-deacetyl-2'-TIPS-7-TES docetaxel (1-14):

A flask containing **1-13** (511 mg, 0.703 mmol) was inerted and dry THF (55 mL) was added to dissolve it. *β*-lactam **1-11** (419.3 mg, 1.5 eq) was dissolved in 15 mL of dry THF and added to the reaction flask. The flask was cooled to -40 ^{o}C and LiHMDS (1 M in THF solution, 1.5 eq) was added dropwise *via* syringe and the reaction was monitored by TLC (2:1 hexane:ethyl acetate). The reaction was quenched after 1.5 h with saturated ammonium chloride solution and extracted with dichloromethane three times. The combined organic layers was dried with brine and anhydrous magnesium sulphate and concentrated *in vacuo*. The pure product **1-14** was obtained by performing flash chromatography (20:1, 4:1 hexane:ethyl acetate) as a white solid in 89 % (717 mg) yield. ^{1}H NMR (300 MHz, $CDC1_3$) δ 0.55 (m, 9H), 1.11-1.39 (m, 47 H), 1.69 (s, 3 H), 1.69-1.93(m, 6 H), 2.02 (s, 3 H), 2.04 (s, 3 H), 2.36 (m, 5 H), 2.51 (m, 1 H), 3.84 (d, J = 6.9 Hz, 1 H), 4.20 (d, J = 8.4 Hz, 1 H), 4.30 (d, J = 8.4 Hz, 1 H), 4.47 (m, 2 H), 4.77-4.87 (m, 2 H), 4.93 (d, J = 8.4 Hz, 1 H), 5.69 (d, J = 7.2 Hz, 1 H), 6.09 (t, J=9, 1H), 6.49 (s, 1H), 7.46 (t, J = 7.5 Hz, 2 H), 7.60 (t, J=7.2, 1 H), 8.10 (d, J = 6.9 Hz, 2 H).

3'-Dephenyl-3'-(2-methyl-1-propenyl)-10-cyclopropanecarbonyl-10-deacetyldocetaxel, SB-T-1214:

A flask containing **1-14** (717 mg, 0.628 mmol) was inerted and 30 mL of dry pyridine/acetonitrile (1:1) was added to dissolve it. The flask was cooled to 0 ^{o}C and HF/pyridine (70:30, 7.5 mL) was added dropwise at 0 ^{o}C. The mixture was stirred at room temperature for 15 h. The reaction was quenched with aqueous saturated sodium carbonate solution (30 mL) and diluted with ethyl acetate (100 mL), washed with aqueous saturated copper sulfate solution (50 mL x 3) and water (50 mL), dried over anhydrous magnesium sulfate and concentrated *in vacuo* to afford **SB-T-1214** as a white solid in 93 % yield (500 mg, > 98 % purity). ^{1}H NMR (300 MHz, $CDC1_3$) δ 0.98-1.05 (m, 2 H), 1.13-1.21 (m, 2 H), 1.27 (m, 2 H), 1.37 (s, 9 H), 1.42 (m, 1 H), 1.69 (s, 3 H), 1.69-1.1.93(m, 4 H), 1.91 (s, 3 H), 2.06 (s, 1 H), 2.37 (s, 3 H), 2.55 (m, 1 H), 2.63 (d, J = 3.9 Hz, 1 H), 3.82 (d, J = 7.2 Hz, 1 H), 4.21 (m, 2H), 4.33 (d, J = 8.1 Hz, 1 H), 4.43 (m, 1 H), 4.76 (t, J = 6, 1 H), 4.85 (d, J = 8.4 Hz, 1 H), 4.97 (d, J = 9.3 Hz, 1 H), 5.33 (d, J = 8.4 Hz, 1 H), 5.68 (d, J = 7.2 Hz, 1 H), 6.19 (t, J=7.6, 1H), 6.32(s, 1H), 7.49 (t, J = 8.1 Hz, 2 H), 7.61 (t, J=7.2, 1 H), 8.11 (d, J = 8.4 Hz, 2 H). All data are consistent with the reported values. [102]

Chapter 2
Synthesis of C-3'-Difluorovinyl Taxoid SB-T-12851

2.1 Introduction

2.1.1 The Relevance of Fluorine in Medicinal Chemistry

Fluorine is an important heteroatom used in drug design and its importance in bioorganic and medicinal chemistry has been demonstrated by the numerous fluorinated compounds approved by the FDA for medical use for both human and veterinarian use.[1, 2] There are only a few organic compounds found in nature that contain fluorine (Figure 2-1).[3] There are, however, more than a hundred FDA approved fluorine-containing drugs for human diseases (Figure 2-2) and 33 are currently approved for veterinary use.[4] The two most notable examples, 5-flurouracil (anticancer drug) and 9α-fluorohydrocortisone, were discovered and developed in the 1950s and the introduction of one fluorine atom resulted in remarkable pharmacological properties. In 2006, Lipitor®/atorvastatin calcium, an anticholesteremic agent was the best selling drug in the world. Risperidone used for schizophrenia and lansoprazole which is a proton pump inhibitor are also very successful drugs currently available in the market.

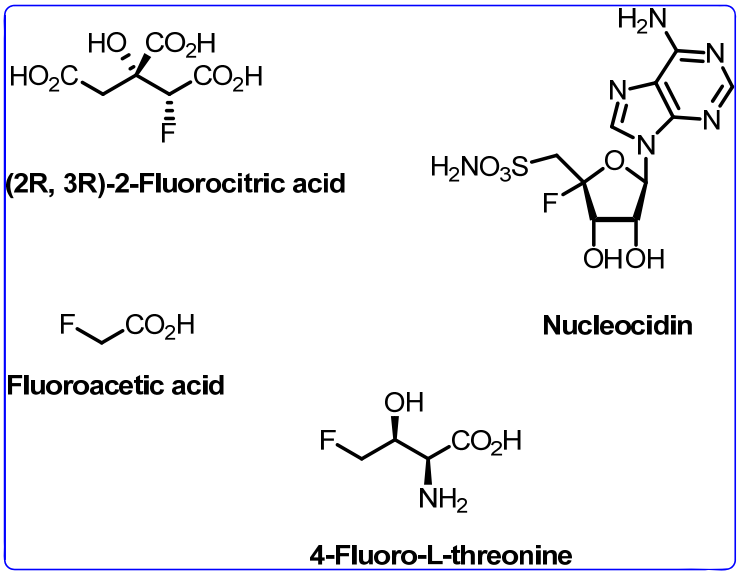

Figure 2-1. Structures of naturally occurring fluoro-compounds

Fluorine is considered to be the second favorite heteroatom in drug design after nitrogen because of its favorable properties.[5] Fluorine is a unique atom with attractive properties that has potential beneficial application to medicinal chemistry. Fluorine has very small size with very high electronegativity and its van der Waals radius is 1.47 Å[6]

which is larger than hydrogen atom but smaller than a lot of functional groups such as methyl, hydroxyl and amino group. Its nuclear spin of ½ and low polarizability of the C–F bond are also among the special properties that render fluorine so attractive. The replacement of a C–H or C–O bond with a C–F bond in fluoroorganic compounds often leads to increased binding to target molecules, higher metabolic stability, increased lipophilicity and membrane permeability all of which translate to appealing attributes of biologically active compounds.[7, 8, 9] The recognized value of fluorine has contributed to the study of fluoro-analogs of lead compounds under development in drug discovery.[10]

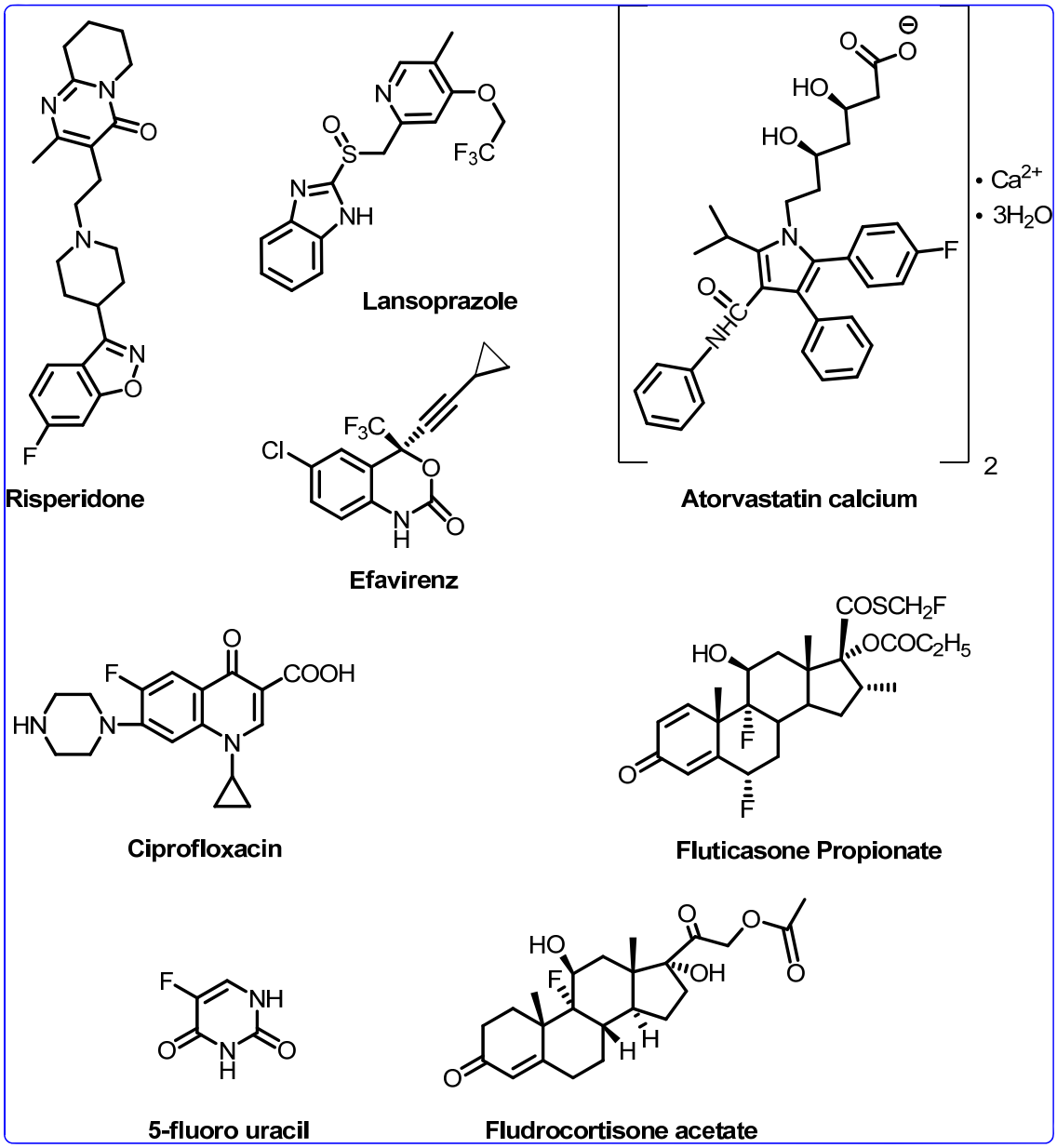

Figure 2-2. Structure of some FDA approved fluorine containing drugs

Medicinal chemists have long introduced fluorine into bioactive molecules on the basis of experience and intuition, however, it is recent experimental and computational studies that have given a better understanding as to how the introduction of fluorine into small drug molecules results in higher binding affinities and selectivity.[11] It is essential to have an understanding of how the replacement of H with F affects the electronic nature and conformation of small molecules to be able to predict the interaction of the fluorine-containing molecules with proteins and enzymes. Since the size of F atom is only slightly more than H atom replacing H with F will introduce minimal steric alterations. The C-F bond is at least 14 Kcal/mole stronger than C-H bond making it much less susceptible to metabolic oxidation compared to the C-H bond. Oxidative metabolism by the liver enzymes, especially the cytochrome P450, often leads to undesirable pharmacological profile. The carbon-fluorine bond length is 1.39 Å while carbon-oxygen bond is 1.43 Å. The fluorine can be a hydrogen bond acceptor and as the most electronegative element, fluorine can significantly affect the basicity and acidity of neighboring groups altering the physicochemical properties of the molecule.[7] Fluorine atom can significantly change the hydrophobicity of groups such as the trifluoromethyl and difluoromethyl making them highly lipophilic and modulate the properties of bioactive molecules for a substantially improved pharmacological profile.[9] Thus, a fluorine atom can be introduced at the active site to block the enzymatic cleavage and enhance the lipophilicity of the molecule, increase hydrophobic binding and membrane permeability. Moreover, the introduction of fluorine(s) into the bioactive molecules as marker(s) provides a unique and valuable tool for *in vitro* and *in vivo* ^{19}F NMR studies of protein structures and drug-protein interactions which has found numerous applications to molecular imaging and promoted the development of molecular probes for imaging. The sensitivity of ^{19}F NMR spectroscopy, the large $^{19}F–^{1}H$ coupling constants and the virtual absence of ^{19}F in living tissues,[12] makes incorporation of fluorine into bioactive compounds a particularly powerful tool for the investigation of biological processes.[13, 14] Thus, the rational design of fluoro-compounds will lead to the generation of new and effective biochemical tools.

2.1.2 The Applications of Fluorine in Novel 2nd-generation Taxoids

The *β*-lactam skeleton is found in numerous pharmacologically active molecules possessing antifungal,[15] antibacterial,[16] antitumor[17] and plasma cholesterol lowering activities.[18, 19] Thus fluorine-containing *β*-lactams have inherent importance as a pharmacophore of various therapeutic agents and have attracted considerable attention in the past few decades. The fluoro-*β*-lactams could be utilized as versatile synthetic intermediates and the development and applications of the *β*-Lactam Synthon Method (*β*-LSM) carried out in our group have been well reviewed.[20-25] The Ojima-Holton coupling protocol is an extremely efficient and practical route to synthesize a diverse array of new taxoids which has paved the way for extensive structure-activity relationship (SAR) studies of taxoids besides its industrial application. As part of our continuing efforts, the *β*-LSM has been applied for the syntheses of fluorinated α-hydroxy-*β*-amino acids, dipeptides, and fluoro-taxoids. Figure 2-3 illustrates representative transformations of *N*-*t*-Boc-3-PO-4-R_f-*β*-lactams (P = hydroxyl protecting group).

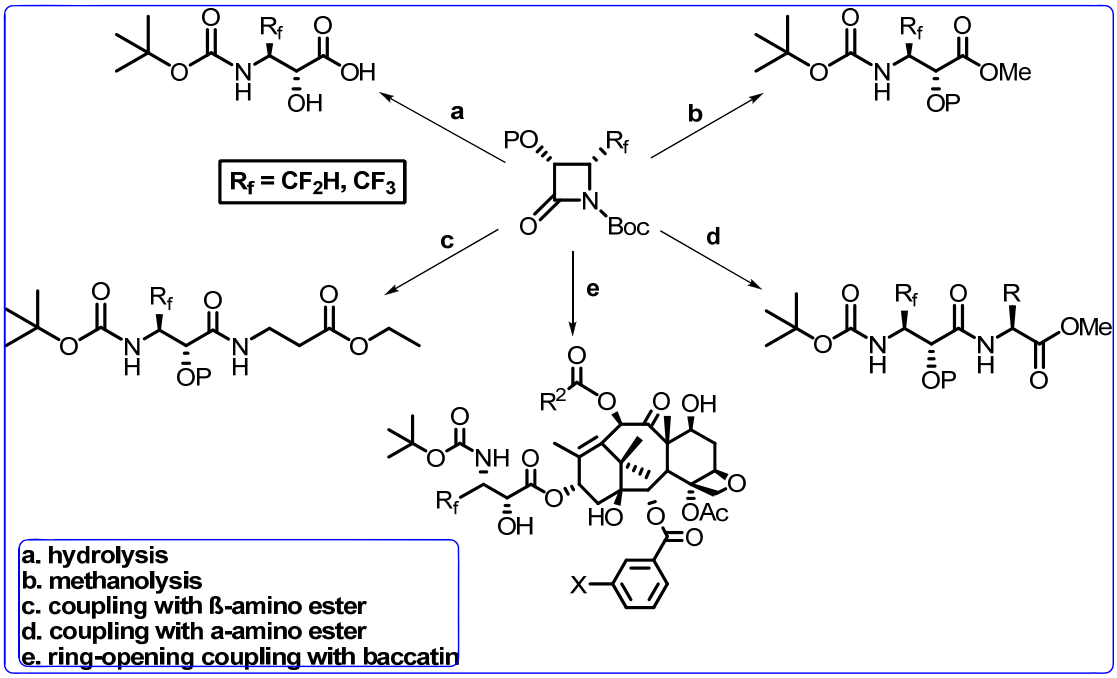

Figure 2-3. Representative transformations of *N*-*t*-Boc-3-PO-4-R_f-*β*-lactams

Several fluorine-containing second-generation taxoids have been prepared in our laboratory. The new fluoro-taxoids, **SB-T-12842-4** and **SB-T-128221-3**, were found to possess more than two orders of magnitude higher cytotoxicity than paclitaxel against the drug-resistant cell lines, MCF7-R and LCC6-MDR,and several times higher potency than paclitaxel against the drug-sensitive cell lines, MCF7-S and LCC6-WT (Figure 2-4, Table 2-1).

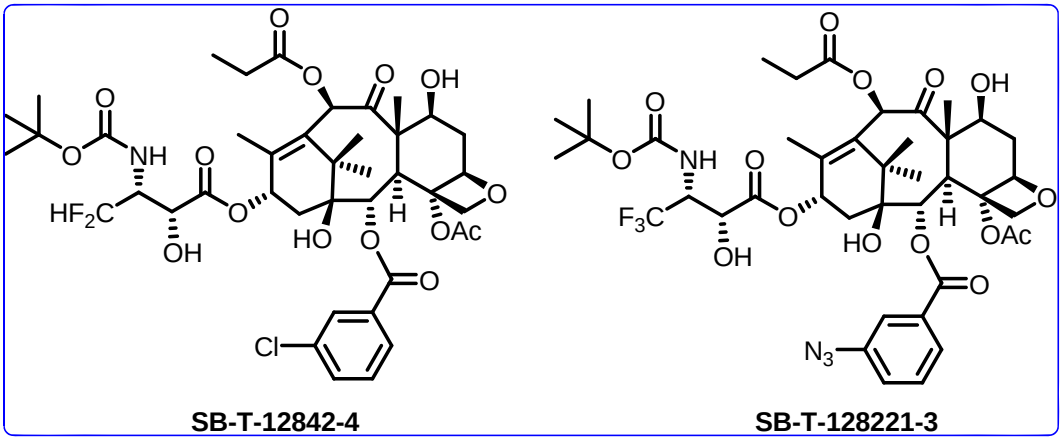

Figure 2-4. Structure of SB-T-12842-4 and SB-T-128221-3

Taxoid	MCF7-S (breast)	MCF7-R (breast)	R/S[b]	LCC6-WT (breast)	LCC6-MDR (breast)	R/S[b]	H460 (ovarian)	HT-29 (colon)
Paclitaxel	1.8	484	269	3.4	216	64	5.5	3.6
SB-T-12842-4	0.6	6.4	11	0.6	3.1	5.2	0.3	0.5
SB-T-128221-3	0.4	2.6	6.5	1.2	1.6	1.3	0.2	0.4

Table 2-1. *In vitro* cytotoxicity (IC_{50} nM)[a] of fluoro-taxoids[26]

[a] The concentration of compound which inhibits 50% (IC_{50}) of the growth of the human tumor cell line after 72 h drug exposure.
[b] R/S = drug-resistant factor = IC_{50} (drug-resistant cell line)/IC_{50} (drug-sensitive cell line).

Metabolism studies on paclitaxel have shown that the *para* position of the C-3' phenyl, *meta* position of the C-2 benzoate, C-6 methylene, and C-19 methyl groups are the primary sites of hydroxylation by the cytochrome P450 family of enzymes. Among them, the predominant site is the hydroxylation of the C-3' phenyl at *para* position by cytochrome 3A family.[27] The metabolism studies on the second generation taxoids containing C3'-N t-Boc, and C3'-isobutyl groups which were developed in our group showed that cytochrome P450 does not attack t-Boc, which is most likely the only oxidation observed for docetaxel in the first place.[27] Instead, CYP 3A4 of the cytochrome P450 primarily attacks the two allylic methyl groups of the C-3′-isobutenyl (SB-T-1214, SB-T-1216) and the methine moiety of the 3′-isobutyl (SB-T-1103) group as shown in Figure 2-5.[28, 29] Accordingly, C3′-difluorovinyl-taxoids to replace C3'-isobutenyl group were synthesized to block the allylic oxidation by CYP 3A4 which should enhance the metabolic stability and activity *in vivo*.

This chapter describes the large scale preparation of enantiopure 4-difluorovinyl *β*-lactam and the corresponding fluorine-containing second-generation taxoid **SB-T-12851** (Figure 2-6). Three other fluorine-containing taxoids **SB-T-12852**, **SB-T-12853**, and **SB-T-12854** (Figure 2-6) were synthesized by Dr. Jin Chen, Dr. Xianrui Zhao, Dr. Liang Sun and Dr. Shuyi Chen. The fluorine-containing *β*-lactam and second-generation taxoid were synthesized in multi-gram scale for the first time in our group for preclinical animal studies.

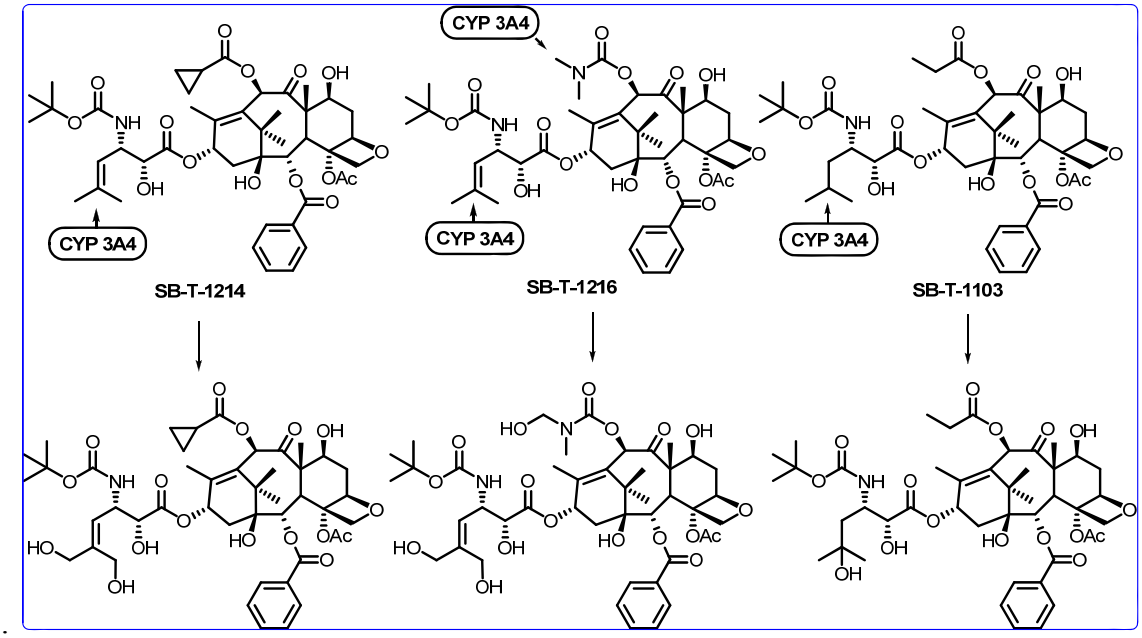

Figure 2-5. Primary sites of hydroxylation on the second-generation taxoids by the P450 family of enzymes

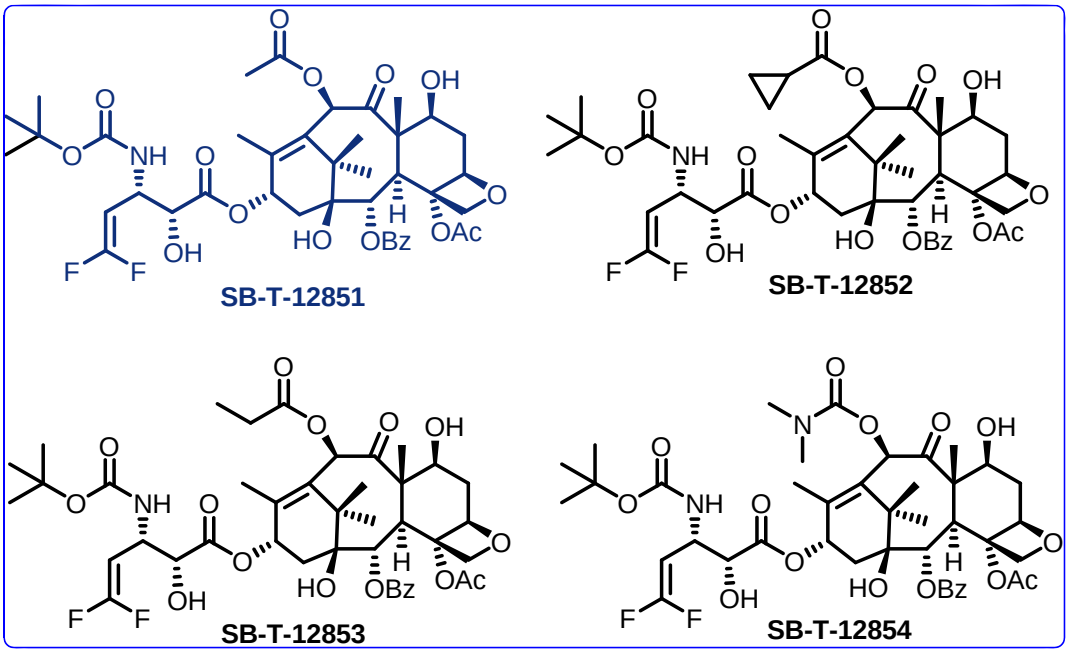

Figure 2-6. Structures of some 2nd-generation fluoro-taxoids

2.2 Results and Discussion

2.2.1 Synthesis of 4-Difluorovinyl *β*-lactam

The enantiopure (3*R*,4*S*)-*N*-Boc-3-TIPSO-4-difluorovinylazetidin-2-one was prepared *via* [2+2] ketene-imine cycloaddition followed by kinetic enzymatic resolution (please refer to Chapter 1 for more details). The TIPS protected *β*-lactam, (+)-(3*R*,4*S*)-1-PMP-3-TIPSO-4-(2-methyl-1-propenyl)-azetidin-2-one (**A**) (Scheme 2-1, please refer to Chapter 1 for synthesis) was first subjected to ozonolysis to give (3*R*,4*S*)-1-PMP-3-TIPSO-4-formylazetidin-2-one. The resulting aldehyde was then converted to fluorinated *β*-lactam, (3*R*,4*S*)-1-PMP-3-TIPSO-4-difluorovinylazetidin-2-one by Wittig reaction using CBr_2F_2, hexamethylphosphoroustriamide (HMPA) and Zn in THF solution.[30, 31] The PMP group was then removed with cerium ammonium nitrate (CAN) to obtain enantiopure (3*R*,4*S*)-3-TIPSO-4-difluorovinylazetidin-2-one which was subjected to acylation with Boc_2O to yield desired *β*-lactam (3*R*,4*S*)-*N*-Boc-3-TIPSO-4-difluorovinylazetidin-2-one in excellent overall yield (Scheme 2-2).

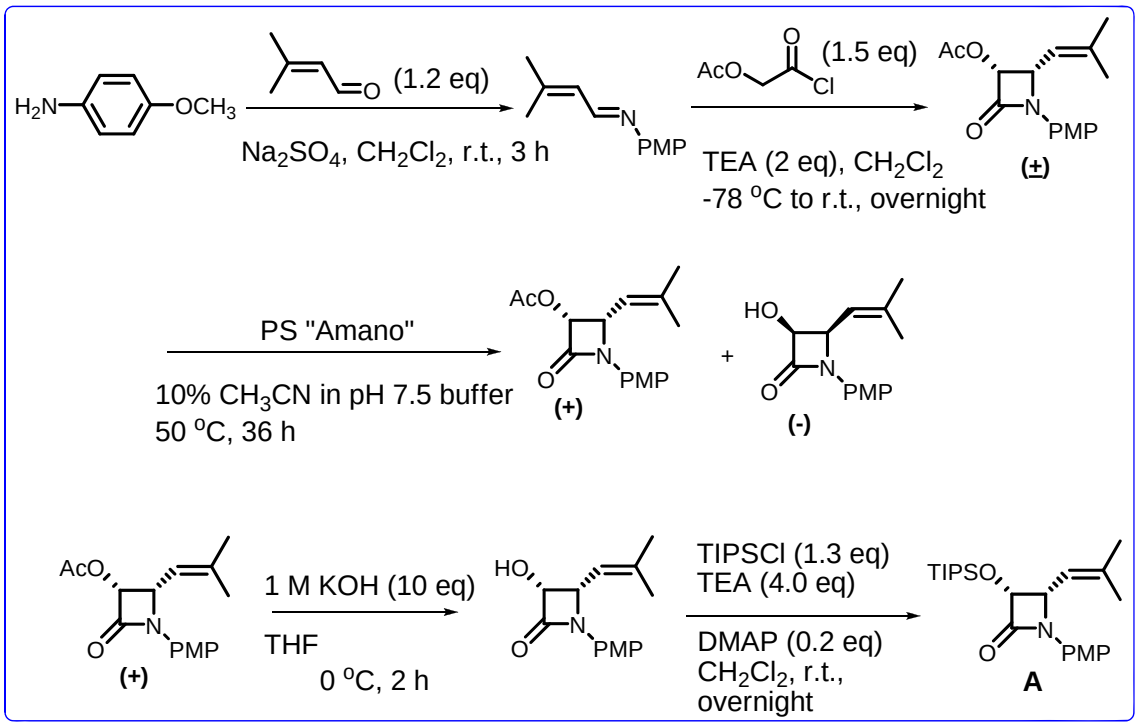

Scheme 2-1. Synthesis of TIPS protected *β*-lactam

The difluorination reaction is the key step of this synthesis. The synthesis of difluorovinyl compounds proceeds through the formation of $[Ph_3P^+\text{-}CF_2Br]Br^-$ **(B)** generated in situ by the reaction of Ph_3P and CBr_2F_2 in THF. A highly exothermic reaction occurs immediately due to the formation of the quasicomplex with zinc **(C)** and then ylide system **(D)**. The ylide conversion is fast and yields the desired fluorocarbon within a short period of time (Scheme 2-3).[32]

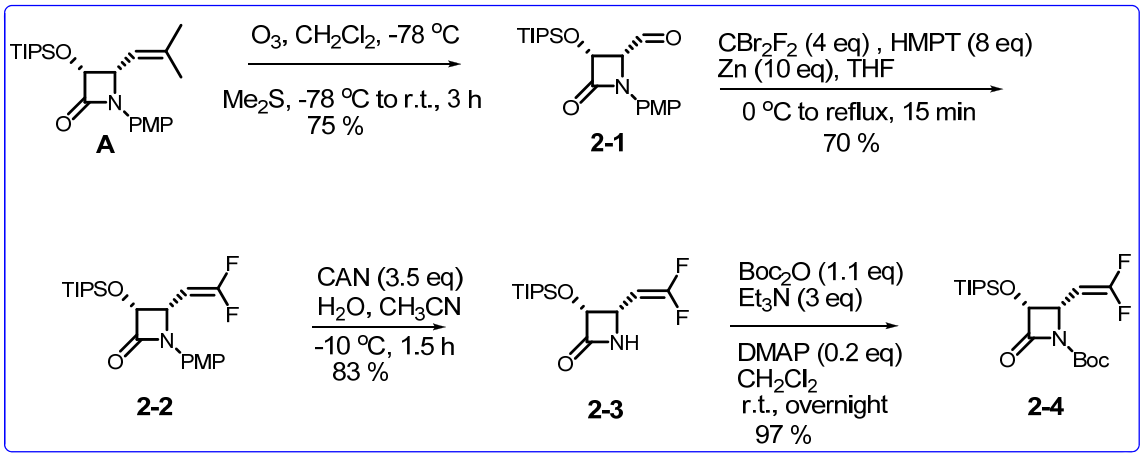

Scheme 2-2. **Synthesis of difluorovinyl *β*-lactam**

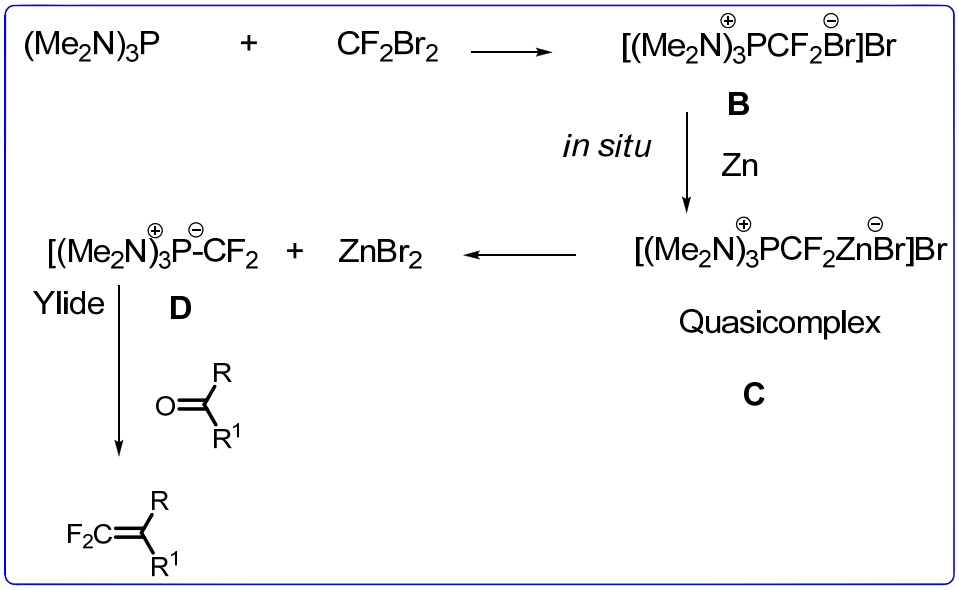

Scheme 2-3. Mechanism of difluoroolefin formation

2.2.2 Synthesis of SB-T-12851

The synthesis of baccatin core started from **10-DAB-III** with acetylation of the C-10 position followed by TES protection of C-7 position **2-6** (Scheme 2-4).

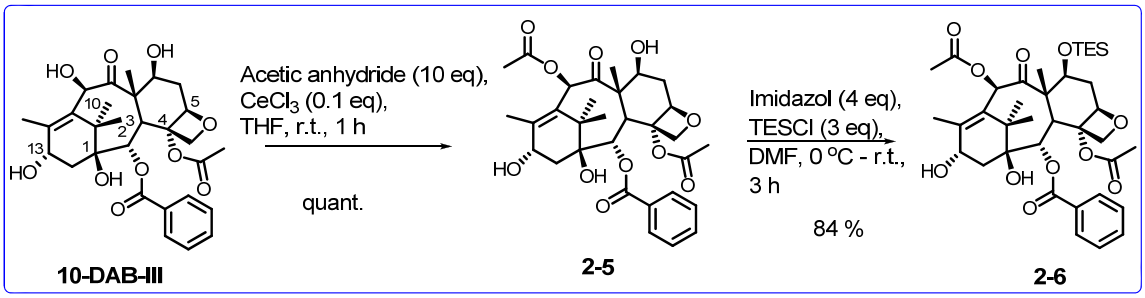

Scheme 2-4. Modification of baccatin core

The ring-opening coupling of *β*-lactams with modified baccatin **2-6** was carried out at -40 °C in THF using LiHMDS.[33, 34] The subsequent removal of the silyl protecting groups with HF/pyridine gave the corresponding new difluorovinyl-taxoid **SB-T-12851** in good overall yields (Scheme 2-5).

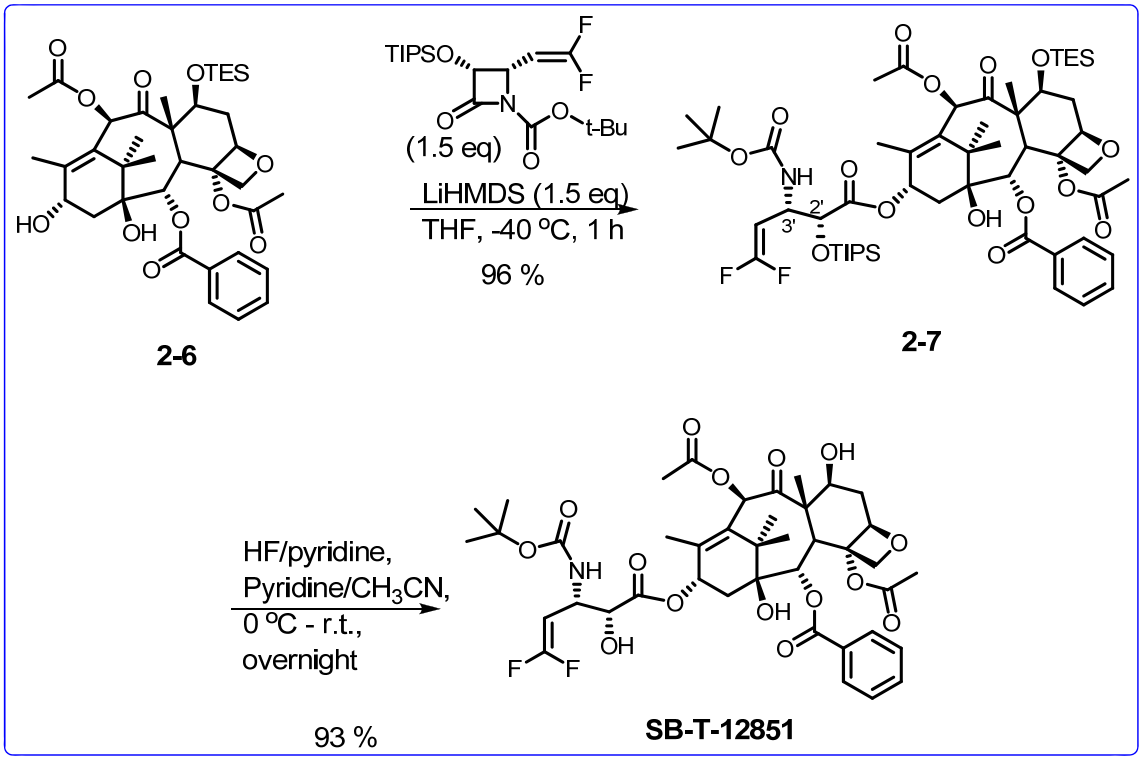

Scheme 2-5. Synthesis of SB-T-12851

2.2.3 Biological Evaluation of SB-T-12851

The novel fluoro-taxoids **SB-T-12851**, **SB-T-12852**, **SB-T-12853**, and **SB-T-12854** were previously synthesized by Dr. Larisa Kuznetsova and sent to the Department of Pharmacology and Therapeutics in Roswell Park Center Institute for biological

evaluations. Cytotoxicity of the difluorovinyl second-generation taxoids was evaluated *in vitro* against both types of human breast cancer cell lines, drug sensitive and drug resistant, MCF7-S and MCF7-R respectively. The IC_{50} values were determined through 72 h exposure of the fluoro-taxoids to the cancer cells according to protocol developed by Skehan et al.[35] The data is summarized in Table 2-2.

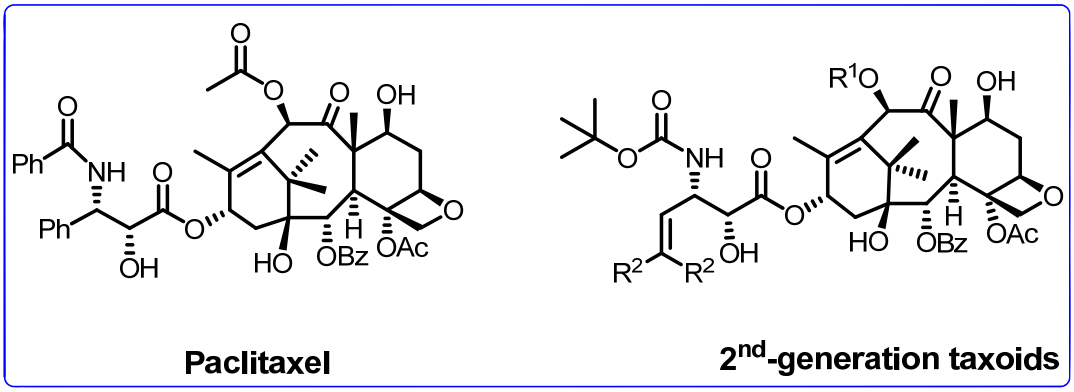

Taxoid	R^1	R^2	MCF7-S (breast)	MCF7-R (breast)	R/S
Paclitaxel			1.7	300	176
SB-T-1213	Et	CH_3	0.18	2.2	12
SB-T-12851	Ac	F	0.14	0.95	6.7
SB-T-12852	*c*-Pr-CO	F	0.17	6.03	35.5
SB-T-12853	Et-CO	F	0.17	1.2	7.06
SB-T-12854	Me_2N-CO	F	0.19	4.27	22.5

Table 2-2. *In vitro* cytotoxicity (IC_{50} nM) of C-3'-difluorovinyl-taxoids

According to Table 2-2, C-3' difluorovinyl taxoids possess one order of magnitude higher potency than paclitaxel, and comparable cytotoxicity with second-generation taxoid **SB-T-1213,** against the drug-sensitive cell line MCF7-S. The biological activity against drug-resistant cell line MCF7-R was two to three orders of magnitude better compared with paclitaxel and several times higher activity than non-fluorinated second-generation taxoid **SB-T-1213** (except **SB-T-12852, SB-T-12854**).

Newly synthesized difluorovinyl taxoids **SB-T-12851** and **SB-T-12854** were tested against two drug-resistant pancreatic cancer cell lines, CFPac and Panc1, with the help of Jennifer Curato in Professor Weixing Zong's research group in the department of molecular genetics and microbiology at Stony Brook University. The preliminary results are summarized in Table 2-3.

Taxoids	CFPac	Panc1
Paclitaxel	15.8	4.7
SB-T-12851	0.0056	1.3
SB-T-12854	2.2	0.83

Table 2-3. *In vitro* cytotoxicity (IC_{50} nM) of C-3'-difluorovinyl-taxoids against pancreatic cancer cell lines

The two taxoids were tested and shown to have IC_{50} values that ranged between 0.0056-2.2 nM, from several times to 4 times more potent than paclitaxel against CFPac and Panc1 cell lines. The efficacy of the compounds did not appear to be affected by the expression of multidrug resistance proteins.

2.3 Conclusion

C-3'-difluorovinyl second-generation taxoids were successfully synthesized in large scale. These taxoids were previously evaluated for their antitumor activity against the drug-sensitive human breast tumor cell line MCF7-S and the drug-resistant human breast tumor cell line MCF7-R. It was found that C-3'-difluorovinyl taxoids have one order of magnitude better antitumor activity against drug sensitive MCF7-S cell line and more than two orders of magnitude better activity against drug-resistant MCF7-R cell line. Also these analogs were tested against drug-resistant pancreatic cancer cell lines, CFPac and Panc1. **SB-T-12851** and **SB-T-12854** exhibited much higher cytotoxicity than paclitaxel. These results showed that C-3'-difluorovinyl taxoids are very promising candidates for preclinical studies and further development.

2.4 Experimental Section

General Methods: ^{1}H, ^{13}C and ^{19}F NMR spectra were measured on a Bruker AC-250 NMR spectrometer or a Varian 300, 400, 500, or 600 MHz NMR spectrometer. The melting points were measured on a "Uni-melt" capillary melting point apparatus from Arthur H. Thomas Company, Inc. Optical rotations were measured on a Perkin-Elmer Model 241 polarimeter. High-resolution mass spectrometric analyses were conducted at the Mass Spectrometry Laboratory, University of Illinois at Urbana-Champaign, Urbana, IL. GC-MS analyses were performed on an Agilent 6890 Series GC system equipped with the HP-5HS capillary column, (50 m X 0.25 mm, 0.25 um) and with the Agilent 5973 network mass selective detector. LC-MS analyses were carried out on an Agilent 1100 Series Liquid Chromatograph Mass Spectrometer. IR spectra were measured on a Shimadzu FTIR-8400s spectrophotometer. TLC analyses were performed on Merck DC-alufolien with Kieselgel 60F-254 and were visualized with UV light, iodine chamber, 10 % sulfuric acid and 10% PMA solution. Column chromatography was carried out on

silica gel 60 (Merck; 230-400 mesh ASTM). Chemical purity was determined with a Waters HPLC assembly consisting of dual Waters 515 HPLC pumps, a PC workstation running Millennium 32, and a Waters 996 PDA detector, using a Phenomenex Curosil-B column, employing CH_3CN/water as the solvent system with a flow rate of 1 mL/min, or shimazu HPLC.

Materials: The chemicals were purchased from Sigma Aldrich Company or Acros Organic Fischer Company. 10-Deacetyl baccatin III (DAB) was donated by Indena, SpA, Italy. Dichloromethane and methanol were dried before use by distillation over calcium hydride under nitrogen or argon. Ether and THF were dried before use by distillation over sodium-benzophenone and kept under nitrogen or argon. Toluene and benzene were dried by distillation over sodium metal under nitrogen or argon before use. Dry DMF was purchased from EMD chemical company, and used without further purification. PURE SOLV™, Innovative Technology Inc, provided an alternative source of dry toluene, THF, ether, and dichloromethane. The glasses were dried in a 110 ^oC oven and allowed to cool to room temperature in a desiccator over "*Drierite*" (calcium sulfate) and assembled under inert gas nitrogen or argon atmosphere.

2.4.1 Synthesis of Difluorovinyl *β*-lactam

(3*R*,4*S*)-1-*p*-Methoxyphenyl-3-triisopropylsilyloxy-4-formylazetidin-2-one (2-1):
Compound **A** (598 mg, 1.48 mmol) was dissolved in distilled dichloromethane (c 0.02 M) in a two-necked flask. Nitrogen was bubbled through the solution for 5 min. The temperature of the flask was brought down to – 78 °C using acetone and dry ice. Ozone was then passed through the mixture till a faint blue color was observed. Nitrogen was then bubbled through the mixture to make it colorless. Dimethyl sulfide (5 eq, 0.24 mL) was then added and the acetone bath removed after 5 min. The reaction was allowed to stir (~ 3 h) and monitored by TLC (2:1 hexane:ethyl acetate). The organic layer was washed with distilled water several times and then washed with brine and dried over anhydrous magnesium sulphate. The organic layer was then concentrated *in vacuo* and the pure product was obtained by performing flash chromatography (20:1, 10:1 hexanes:ethyl acetate) in 75 % yield (420 mg) as a white solid. ^1H NMR (300 MHz, $CDCl_3$): δ 1.11-1.27 (21 H, m) (H on TIPS group), 3.84 (3 H, s) (H on CH_3O group), 4.53 (dd, J = 9.6, 4.2 Hz, 1 H)(H on C4), 5.36 (d, J = 5.4 Hz, 1 H)(H on C3), 6.93 (d, J = 9.3 Hz, 2 H)(H on benzene ring), 7.32 (d, J = 9.3 Hz, 2 H)(H on benzene ring), 9.83 (d, J = 4.8 Hz, 1 H)(H on aldehyde).

1-(4-Methoxyphenyl)-3-triisopropylsiloxy-4-(2,2-difluorovinyl)azetidin-2-one (2-2):[31]
The compound **2-1** (300 mg, 0.79 mmol) was taken in a flask and inerted. An empty two necked round bottom flask fitted with a condenser was inerted, THF (5 mL) was added to it and cooled to 0 °C. CF_2Br_2 (2 eq, 0.15 mL) was added using a syringe cooled to – 78 °C followed by HMPT (hexamethyl phosphorus triamide) (4 eq, 0.58 mL) and the flask shaken to break up the clumps of ylid formed. The starting material **2-1** was dissolved in the remaining THF (c 0.05M) and introduced in the flask containing the ylid. Zinc powder (6 eq, 314 mg) was then added to it and the flask was refluxed in an oil bath at 80 °C. The reaction mixture turned reddish brown and the reaction was monitored by TLC

(5:1 hexane:ethyl acetate). The reaction was stirred till TLC indicated no starting material (~ 30 min). The reaction mixture was then cooled to room temperature and the Zn filtered out using celite lined frit funnel. The THF was removed using a rotary evaporator and the mixture diluted with dichloromethane. The organic layer was washed several times with distilled water to remove the salt, dried over anhydrous magnesium sulphate and concentrated *in vacuo*. The pure product was then obtained by performing flash chromatography (30:1, 25:1 hexanes:ethyl acetate) in 70 % yield (231 mg) as a transparent oil/white solid. ^{1}H NMR (300 MHz, $CDCl_3$): δ1.08-1.15 (21 H, m), 3.79 (3 H, s), 4.54 (1 H, ddd, J = 1.5, 6.3, 16.5 Hz), 4.83 (1 H, m), 5.14 (1 H, d, J = 5.1 Hz), 6.87 (2H, d, J = 9.0 Hz), 7.32 (2H, d, J = 9.0 Hz); ^{13}C NMR (400 MHz, $CDCl_3$): 12.1, 17.9, 54.1 (d, J = 8.5 Hz), 55.8, 75.8 (dd, J = 5.0, 22.1 Hz), 76.9, 77.4, 114.8, 118.6, 130.9, 156.7, 164.9; ^{19}F NMR (300 MHz, $CDCl_3$): δ-80.80 (d, 1F, J = 32.7 Hz), -86.34 (dd, 1F, J = 2.8 Hz, J = 28.2); HRMS (FAB^+, m/z): Calcd. for $C_{21}H_{31}F_2NO_3Si{\cdot}H^+$, 412.2114; Found, 412.2127.

3-Triisopropylsiloxy-4-(2,2-difluorovinyl)azetidin-2-one (2-3):[36]

The compound **2-2** (216 mg, 0.52 mmol) was taken in a flask and dissolved in acetonitrile (18 mL) and water (3 mL). The flask was then cooled to – 10 °C. A solution of cerium ammonium nitrate (CAN, 3.5 eq, 1 g) in distilled water (16 mL) was then added dropwise *via* a dropping funnel over a 30 min period. The reaction mixture was then stirred for 2 h and periodically monitored by TLC (2:1 hexane:ethyl acetate). When no starting material was observed the reaction was quenched with saturated solution of sodium sulfite resulting in an orange precipitate. This was filtered using a Buchner funnel and the precipitate washed well with ethyl acetate. The organic and aqueous layers were then separated and the organic layer was washed with brine, dried over anhydrous magnesium sulphate and concentrated *in vacuo*. The crude was then purified by performing flash chromatography (15:1, 10:1 hexanes:ethyl acetate) to yield a transparent oil in 83 % yield (132 mg). ^{1}H NMR ($CDCl_3$, 400 MHz): δ1.03-1.18 (21 H, m), 4.44-4.54 (2 H, m), 5.04 (1 H, dd, J = 1.6, 2.4 Hz), 6.59 (1 H, bs); ^{13}C NMR ($CDCl_3$, 100 MHz): 12.1, 17.8 (d, J = 4.6 Hz), 50.4 (d, J = 7.6 Hz), 77.1 (dd, J = 15.9, 23.5 Hz), 79.3, 157.6 (t, J = 289.9 Hz), 169.4; ^{19}F NMR (282 MHz, $CDCl_3$): δ -82.33 (d, 1F, J = 34.7 Hz), -87.50 (dd, 1F, J = 9.3 Hz, J = 25.7).

(3*R*,4*S*)-1-(*tert*-Butoxycarbonyl)-3-triisopropylsilyloxy-4-difluorovinylazetidin-2-one (2-4):[36]

The compound **2-3** (266 mg, 0.87 mmol) and a catalytic amount of DMAP (0.25 eq, 26.59 mg) were added in a flask and inerted (vacuum/nitrogen). 5 mL of distilled dichloromethane was then added into the flask to dissolve the solids. Triethylamine (3 eq, 0.36 mL) was then added dropwise followed by di-*tert*-butyldicarbonate (1.1 eq, 209 mg) in 2 mL dichloromethane. The reaction was allowed to stir overnight at room temperature and quenched with 10 mL saturated ammonium chloride solution. The organic and aqueous layer was separated and the aqueous layer was extracted with dichloromethane (3 x 30 mL). The combined organic layers was washed with saturated sodium chloride solution, dried over anhydrous magnesium sulfate, filtered and concentrated *in vacuo*. The crude was purified using flash chromatography (50:1 hexane:ethyl acetate) to give 344 mg of the pure product as a clear oil in 97 % yield. ^{1}H NMR (300 MHz, $CDCl_3$): δ

1.04-1.17 (21 H, m), 1.50 (9 H, s), 4.49 (1 H, ddd, J = 1.6, 13.8, 23.7 Hz), 4.75 (1 H, dddd, J = 0.9, 2.4, 5.1, 9.0 Hz), 5.04 (1 H, d, J = 5.7 Hz), 6.59 (1 H, bs); ^{13}C NMR (400 MHz, $CDCl_3$): δ 12.0, 17.8 (d, J = 5.3 Hz), 28.2, 53.6 (d, J = 8.4 Hz), 74.5 (dd, J = 10.6, 26.5 Hz), 77.2, 83.9, 147.9, 158.5 (t, J = 292.2 Hz), 165.3; ^{19}F NMR (300 MHz, $CDCl_3$): δ -81.20 (d, 1F, J = 31.0 Hz), -85.83 (dd, 1F, J = 5.6 Hz, J = 29.3). HRMS (FAB^+, m/z): Calcd. for $C_{19}H_{33}F_2NO_4SiNa^+$, 428.2039; Found, 428.2050.

2.4.2 Synthesis of SB-T-12851

10-Acetylbaccatin III (2-5):
A flask containing 10-DAB-III (10-deacetylbaccatin III, 860 mg, 1.57 mmol), cerium trichloride heptahydrate (0.1 eq, 60 mg) was inerted. Distilled THF (c 0.03 M) was added to dissolve the solids. Acetic anhydride (10 eq, 1.48 mL) was then added dropwise at room temperature and the reaction was monitored by TLC (1:4 hexane:ethyl acetate). The reaction was stopped after 3 h when no starting material was observed. The THF was evaporated off and distilled water was added to dissolve the inorganic solids. Dichloromethane was used for extraction and the organic layer was washed with brine, dried over anhydrous magnesium sulfate and concentrated *in vacuo*. The white crude product **2-5** thus obtained in quantitative yield was then subjected to 7-TES protection. ^{1}H NMR (300 MHz, $CDCl_3$): δ 1.1 (3H, s, C-16), 1.25 (3H, m, C-17), 1.67 (3H, s, H-19), 1.75 (bs, 1 H, OH), 1.88 (4H, m, H-6b, H-18), 2.24 (3H, s, 10-OAc), 2.33 (2H, m, H-14), 2.39 (3H, s, 4-OAc), 2.49 (1H, d, *J*= 3.6 Hz, OH), 2.55 (1H, ddd, *J*= 6.4, 9.6, 14.8 Hz, H-6a), 3.72 (1H, OH), 3.81 (1H, d, *J*= 7.2 Hz, H-3), 4.17 (1H, d, *J*= 8.4 Hz, H-20b), 4.31 (1H, d, *J*= 8.4 Hz, H-20a), 4.44 (1H, m, H-7), 5.66 (1H, d, *J*= 7.2 Hz, H-2), 6.24 (1 H, t, *J*= 8.8 Hz, H-13), 6.30 (1H, s, H-10), 7.49 (2H, t, *J*= 7.6 Hz), 7.61 (1H, t, *J*= 7.2 Hz), 8.11 (2H, d, *J*= 7.6 Hz).

7-TES-10-acetylbaccatin III (2-6):
A flask containing modified baccatin **2-5** (921 mg, 1.57 mmol) and imidazol (4 eq, 430 mg) was inerted. DMF (c 0.04 M) was added *via* syringe to dissolve the solids in the flask. The temperature of the flask was maintained at 0 °C. Triethylsilylchloride (3 eq, 0.8 mL) was then added dropwise *via* syringe in the flask. The ice bath was removed after 5 min. The reaction was monitored by TLC (1:1 hexane:ethyl acetate) and quenched with saturated ammonium chloride solution after 2.5 h. The reaction mixture was diluted with ethyl acetate and the organic and aqueous layer was separated. The organic layer was washed with brine, dried over anhydrous magnesium sulphate and concentrated *in vacuo*. The pure product **2-6** was obtained by performing flash chromatography (4:1, 1:1 hexane:ethyl acetate) as a white solid in 84 % (920 mg) yield. ^{1}H NMR (300 MHz, $CDCl_3$): δ 0.52- 0.93 (m, H on TES), 1.15 (3H, s, C-16), 1.25 (3H, m, C-17), 1.67 (3H, s, H-19), 1.75 (bs, 1 H, OH), 1.88 (4H, m, H-6b, H-18), 2.24 (3H, s, 10-OAc), 2.33 (2H, m, H-14), 2.39 (3H, s, 4-OAc), 2.49 (1H, d, *J*= 3.6 Hz, OH), 2.55 (1H, ddd, *J*= 6.4, 9.6, 14.8 Hz, H-6a), 3.81 (1H, d, *J*= 7.2 Hz, H-3), 4.17 (1H, d, *J*= 8.4 Hz, H-20b), 4.31 (1H, d, *J*= 8.4 Hz, H-20a), 4.44 (1H, m, H-7), 5.66 (1H, d, *J*= 7.2 Hz, H-2), 6.24 (1 H, t, *J*= 8.8 Hz, H-13), 6.30 (1H, s, H-10), 7.49 (2H, t, *J*= 7.6 Hz), 7.61 (1H, t, *J*= 7.2 Hz), 8.11 (2H, d, *J*= 7.6 Hz)

10-Acetyl-3'-dephenyl-3'-(2,2-difluorovinyl)-2'-TIPS-7-TES docetaxel (2-7):
10-Acetyl-7-TES baccatin III (**2-6**) (722 mg, 1.03 mmol) was taken in a flask which was inerted and dry THF (c 0.01 M) 50 mL was added to dissolve it. *β*-Lactam **2-4** (1.5 eq, 630 mg) was inerted in a separate flask and dissolved in the remaining dry THF and syringed into the reaction flask containing the modified baccatin. The flask was cooled to - 40 °C using dry ice and acetone. Then LiHMDS (1 M in THF solution, 1.5-2 eq, 2 mL) was added dropwise *via* syringe and the reaction monitored by TLC (2:1 hexane:ethyl acetate). The reaction was quenched after 2 hr with saturated ammonium chloride solution and extracted with dichloromethane three times. The combined organic layers was dried with brine and anhydrous magnesium sulphate and concentrated *in vacuo*. The pure product **2-7** was obtained by performing flash chromatography (13:1, 5:1 hexane:ethyl acetate) as a white solid in 96 % (1.1 g) yield. ^{1}H NMR (300 MHz, $CDCl_3$): δ 0.52- 0.93 (m, H on TES), 1.08 – 1.3 (m, H on TIPS), 1.15 (3H, s, C-16), 1.25 (3H, m, C-17), 1.30 (9H, s, Boc), 1.68 (3H, s, H-19), 1.88 (4H, m, H-6b, H-18), 2.24 (3H, s, 10-OAc), 2.33 (2H, m, H-14), 2.39 (3H, s, 4-OAc), 2.49 (1H, d, *J*= 3.6 Hz, OH), 2.55 (1H, ddd, *J*= 6.4, 9.6, 14.8 Hz, H-6a), 3.81 (1H, d, *J*= 7.2 Hz, H-3), 4.17 (1H, d, *J*= 8.4 Hz, H-20b), 4.28 (1 H, s, *J*= 2.8 Hz, H-2'), 4.31 (1H, d, *J*= 8.4 Hz, H-20a), 4.44 (1H, m, H-7), 4.58 (1H, ddd, *J*= 1.2, 9.6, 24.8 Hz, H-3'-vinyl), 4.87 (1H, t, *J*= 8.8 Hz, H-3'), 4.96 (2 H, d, *J*= 9.6, H-5, NH-3'), 5.66 (1H, d, *J*= 7.2 Hz, H-2), 6.24 (1 H, t, *J*= 8.8 Hz, H-13), 6.30 (1H, s, H-10), 7.49 (2H, t, *J*= 7.6 Hz), 7.61 (1H, t, *J*= 7.2 Hz), 8.11 (2H, d, *J*= 7.6 Hz)

10-Acetyl-3'-dephenyl-3'-(2,2-difluorovinyl)docetaxel (SB-T-12851):
The compound **2-7** (1.1 g, 0.99 mmol) was taken in a flask which was inerted and cooled to 0 °C. Acetonitrile and dry pyridine (22 mL each, 1:1) was added to dissolve the solid compound. Then HF/Pyridine was added (11 mL) dropwise, the reaction was allowed to warm to room temperature and stirred overnight. TLC (1:1 hexane:ethyl acetate) indicated complete conversion and the reaction was quenched with saturated $NaHCO_3$ slowly and stirred. The reaction mixture was diluted with ethyl acetate and the organic layer was washed with saturated $NaHCO_3$ several times to remove unreacted HF. The combined organic layers were then washed with copper sulphate solution to remove pyridine till no color change was observed. The organic layer was then washed with distilled water to remove copper sulphate, dried over brine and anhydrous magnesium sulphate and concentrated *in vacuo*. The pure product was obtained by performing flash chromatography (5:1, 2:1 pure hexane:ethyl acetate) as a white solid in 93 % (770 mg) yield. (HPLC purity > 97 %, mp 155-160 °C) ^{1}H NMR (CDCl3, 300 MHz): δ 1.15 (3H, s, C-16), 1.25 (3H, m, C-17), 1.30 (9H, s, Boc), 1.68 (3H, s, H-19), 1.75 (bs, 1 H, OH), 1.88 (4H, m, H-6b, H-18), 2.24 (3H, s, 10-OAc), 2.33 (2H, m, H-14), 2.39 (3H, s, 4-OAc), 2.49 (1H, d, *J*= 3.6 Hz, OH), 2.55 (1H, ddd, *J*= 6.4, 9.6, 14.8 Hz, H-6a), 3.52 (1H, d, *J*= 5.6 Hz, OH), 3.81 (1H, d, *J*= 7.2 Hz, H-3), 4.17 (1H, d, *J*= 8.4 Hz, H-20b), 4.28 (1 H, s, *J*= 2.8 Hz, H-2'), 4.31 (1H, d, *J*= 8.4 Hz, H-20a), 4.44 (1H, m, H-7), 4.58 (1H, ddd, *J*= 1.2, 9.6, 24.8 Hz, H-3'-vinyl), 4.87 (1H, t, *J*= 8.8 Hz, H-3'), 4.96 (2 H, d, *J*= 9.6, H-5, NH-3'), 5.66 (1H, d, *J*= 7.2 Hz, H-2), 6.24 (1 H, t, *J*= 8.8 Hz, H-13), 6.30 (1H, s, H-10), 7.49 (2H, t, *J*= 7.6 Hz), 7.61 (1H, t, *J*= 7.2 Hz), 8.11 (2H, d, *J*= 7.6 Hz); ^{13}C NMR ($CDCl_3$, 400 MHz) δ 9.8, 14.4, 15.1, 21.1, 22.1, 22.5, 26.9, 28.3, 35.7 (d, *J*= 13.7 Hz), 43.5, 45.7, 48.2, 58.8, 72.4, 72.9, 75.8, 76.7, 79.3, 80.7, 81.3, 84.6, 128.9,

129.3, 130.4, 133.4, 133.9, 142.4, 155.1, 156.7, 158.0, 167.3, 170.5, 171.5, 172.7, 203.9; ^{19}F NMR, ($CDCl_3$, 282 MHz) δ –84.29 (1 F, dd, *J*= 25.7, 36.4 Hz), –86.22 (1 F, dd, *J*= 34.7 Hz); HRMS (FAB^+, *m/z*): Calcd. for $C_{41}H_{51}F_2NO_{15}\cdot H^+$, 836.3300; Found, 836.3278.

Chapter 3
Synthesis and stability studies of novel disulfide linkers

3.1 Introduction

The therapeutic activity of most anticancer drugs used in chemotherapy is restricted because of the nonspecific toxicity they generate by killing rapidly proliferating cells including normal cells. This results in a low therapeutic index and a narrow therapeutic window. Most chemotherapeutic drugs have to be used near their maximum tolerated dose (MTD) to achieve desired therapeutic effect and using multidrug therapy has become a standard practice.[1] Thus the intensive chemotherapy required because of the lack of selectivity and specificity for tumors results in systemic toxicity and effective therapeutic results are achieved only in a small number of cancers. Besides the lack of tumor selectivity drug development is also hampered because of multi-drug resistance (MDR). Thus it is critical to develop target-specific agents which can utilize the physiological and morphological differences between normal and tumor cells and potent cytotoxic drugs which would be able to bypass or overcome MDR.

Small molecules that can specifically inhibit enzymes which play a key role in the development of tumors have received clinical success. Imatinib or Gleevec® was approved by the Food and Drug Administration (FDA) in 2001 and is the first small molecule tyrosine kinase inhibitor used in treating chronic myeloid leukemia (CML).[2, 3] Imatinib competitively inhibits ATP binding to the kinase domain of target proteins[4] and gave encouraging and impressive results in late stage clinical trial for blast crisis CML. However, these positive results were annulled by the emergence of drug resistance[5, 6] which arose mainly due to the mutations in BCR-ABL kinase domain which alter binding.[7, 8] Thus promising opportunities are met by challenges as was evidenced by the failure of other such kinase inhibitors. Another tumor-specific approach is to develop drugs or prodrugs that can specifically recognize and target receptors or other biomarkers that are overexpressed on the surface of tumor cells. Thus a tumor-targeted drug delivery system (DDS) (please refer to chapter 4 for details) which consists of a tumor-targeting moiety (TTM) conjugated to a potent, cytotoxic drug through an appropriate linker is a promising way to overcome the challenges faced by conventional chemotherapy. Mylotarg® (gemtuzumab-ozogamicin) which has an anti-CD33 antibody (hP67.6) conjugated to calicheamicin was the first mAb-drug immunoconjugate approved by the FDA in 2000 for the treatment of acute myelogenous leukemia (AML).[9]

3.2 Linker

The first generation tumor-targeted DDS were designed by conjugating clinically used anticancer drugs such as methotrexate, doxorubicin, vinca alkaloids, etc with TTM like monoclonal antibodies (mAb) to enhance tumor specificity.[10] In general, after the conjugate internalizes into the target cell the drug has to be released efficiently from the TTM. This efficient cleavage of the drug from the TTM requires a linker with certain desirable features. A summary of some of the desired features of the key parts of a tumor-targeting moiety are show in Figure 3-1.

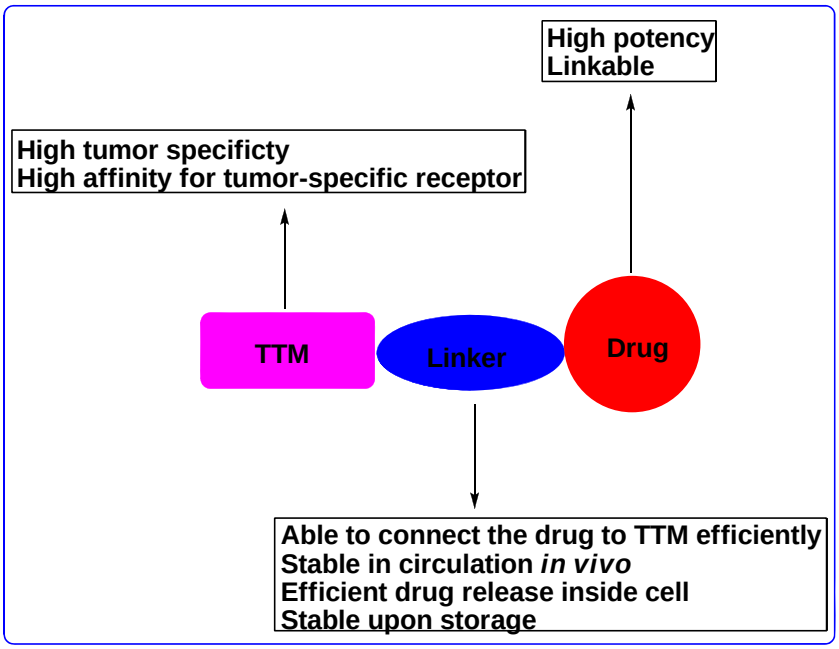

Figure 3-1. Key features of a tumor-targeting DDS

The linker has a critical significance in the design of a successful DDS and must meet some stringent criteria. Firstly, the linker should be designed such that it can connect the drug to the TTM effectively and under mild chemistry conditions. Secondly, the linker must be stable in circulation *in vivo* but get efficiently cleaved inside cancer cells once the DDS has internalized. The desired stability of the linker also depends on the type of tumors the DDS is targeting. If a linker is too labile then it will release the drug before the prodrug conjugate reaches the target site causing high systemic toxicity and if it is too stable it will prevent the drug from being released which will cause substantially decreased or insufficient potency. The whole conjugate must remain intact during storage in aqueous solution to allow formulations for administration. Early work on immunoconjugate involved direct connection of a drug and a monoclonal antibody (mAb) through an amide bond, which suffered from the insufficient release of the active drug. Thirdly, the linkers should be exposed in a way such that they can be readily cleaved inside cancer cells. The selection of an appropriate linker depends on the type of tumor and the required cytotoxic agent. There is no universal linker and each of them has its advantages and disadvantages. The most frequently used linkers can be categorized into four classes in accordance with their modes of cleavage, *i.e.* (i) acid labile, (ii) proteolytic, (iii) disulfide exchange, and (iv) hydrolytic. Several types of cleavable linkers have been evaluated and some examples of the commonly used linkers are shown on Figure 3-2.

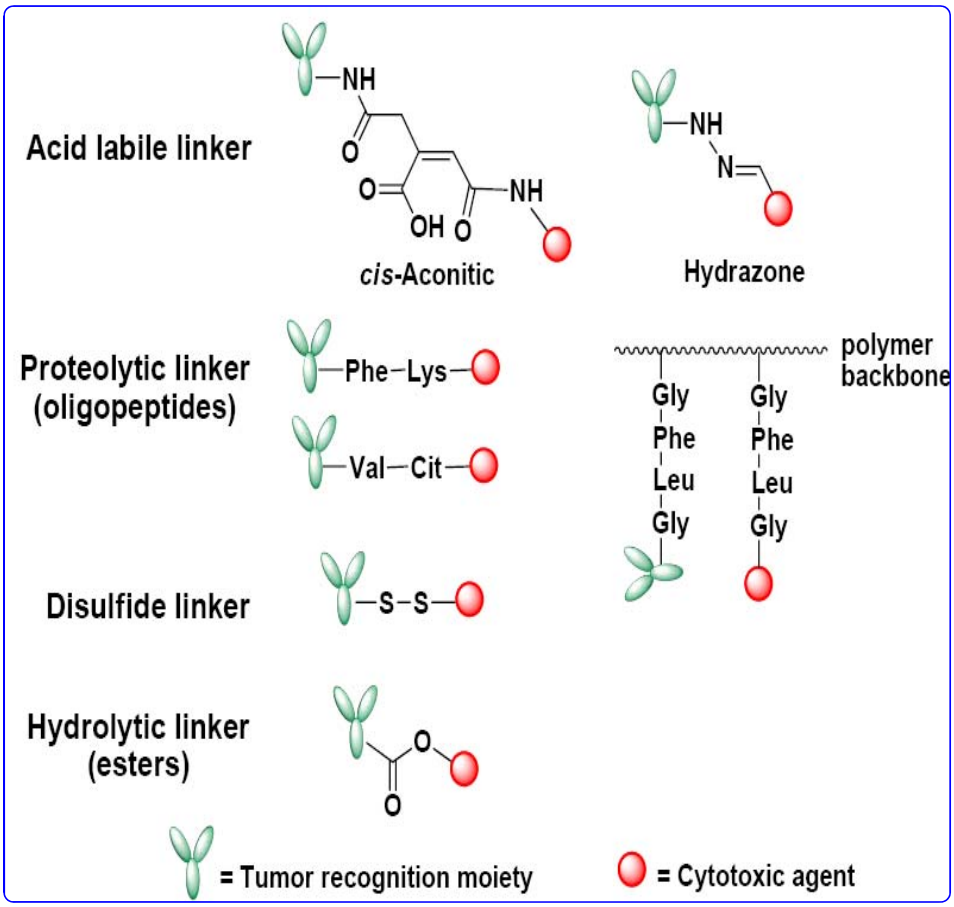

Figure 3-2. Examples of some commonly used linkers[11]

3.2.1 Acid Labile Linker

The acid labile linker takes advantage of the low pH (~ 5) or acidic conditions in the endosomes and lysosomes which can release the potent drug from the prodrug conjugate via non-enzymatic hydrolysis. The most extensively studied linkers are *cis*-aconitic acid and hydrazone linkers. *cis*-Aconitic acid linker was used to attach daunorubicin to poly(D-lysine)[12] and also to attach daunorubicin to anti T-cell mAb.[13, 14] It is one of the first acid labile linkers used in immunoconjugates.

Hydrazone linkers are also widely used acid labile linkers. The cytotoxic drug or the TTM should have an appropriate carbonyl group such as ketone or aldehyde moiety to form the hydrazone. Several cytotoxic agents such as doxorubicin,[15, 16] daunorubicin,[17] calicheamicin,[18] vinblastine[19] and chlorambucil[17] have been used in tumor-targeting conjugates containing a hydrazone linker. Doxorubicin (Dox) attached to a mAb via a hydrazone linker was used for the first time in 1990.[20] A hydrazone linker was also used to attach Dox to a chimeric mAb BR96 that recognizes Lewis Y antigens that are overexpressed on lung, colon, breast and various other human carcinomas. This BR96-Dox conjugate had 8 molecules of Dox and was rapidly internalized into the target cell upon binding to the antigen.[10] Phase II clinical trials showed that single-agent treatment

did not bring about complete responses for patients with large solid tumors though complete regressions was observed in animal models with human lung, colon and breast tumor xenografts.[15, 21] Follow-up studies with the xenograft models in animals showed significant synergistic antitumor effect with combination therapy using BR96-Dox and paclitaxel or docetaxel.[22] Conjugates with hydrazone linker exhibited higher release rate under slightly acidic conditions as compared to neutral conditions. However, premature cleavage of the hydrazone linker at physiological pH was also observed[16] which indicates instability of the linker during circulation.

Nevertheless, hydrazone linker has proven to be successful in Mylotarg® which is used for the treatment of AML. In this immunoconjugate the TTM is CDR-grafted humanized mAb hP67.6 targeting CD33 in leukemia cells and the cytotoxic agent is calicheamicin. This immunoconjugate contains 2 or 3 molecules of the cytotoxic agent and has a sophisticated linker system with both a hydrazone linker and a disulfide moiety. The lysine residue in mAb was coupled to a 4-(4-acetyl-phenoxy) butanoic acid via a stable amide bond and the carbonyl group of the acetophenone moiety was then linked to the cytotoxic agent via an alkanoylhydrazone linker serially connected to a disulfide moiety. Studies showed that cleavage by disulfide exchange is not sufficient and hydrazone linker is the actual cleavage site.[23] Studies showed that this conjugate was 2000-fold more potent than the parent cytotoxic agent and its remarkable activity was also confirmed *in vivo*. It became the first anticancer immunoconjugate in the market.[9] Unfortunately, in June 2010 the FDA withdrew Mylotarg® from the market because a recent clinical trial designed to determine whether adding Mylotarg® to standard chemotherapy demonstrated an improvement in clinical benefit (survival time) to AML patients showed no improvement in clinical benefit. Also, a greater number of deaths occurred in the group of patients who received Mylotarg® compared with those receiving chemotherapy alone.[24]

An acid labile thiocarbamoyl linker for conjugating daunorubicin to a polymeric carrier has also been reported. Structures of some representative examples of acid labile linkers are shown in Figure 3-3.

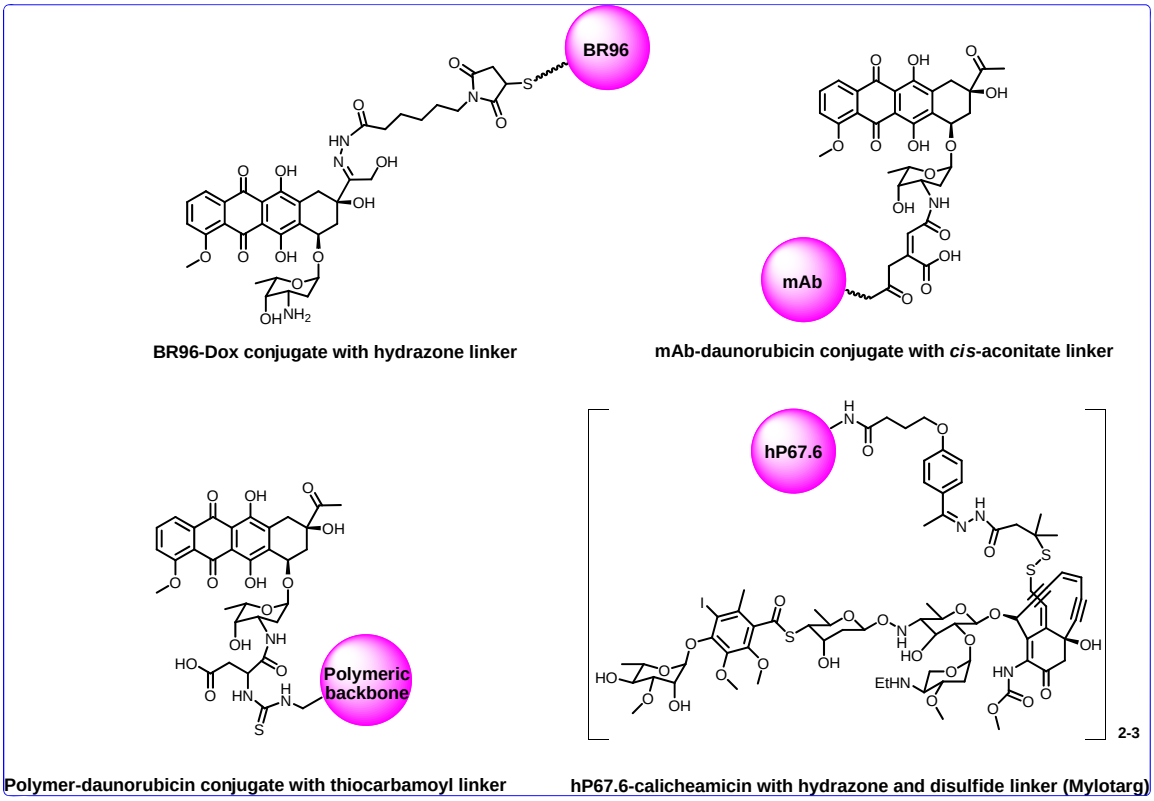

Figure 3-3. Structures of representative acid labile linkers

3.2.2 Proteolytic Linker

The proteolytic or peptide linkers are designed to have high serum stability and undergo rapid lysosomal hydrolysis. When a DDS is delivered to the lysosomes in cancer cells *via* internalization they are exposed to many proteases, mostly belonging to the cathepsin family and a number of exopeptidases. Therefore, numerous short peptide sequences were explored for their suitability as cleavable linkers. These peptide linkers should contain 2 to 5 amino acid residues with at least two hydrophobic, preferably aromatic residues.[25] There are several examples of peptide linkers such as dipeptides Phe-Lys and Val-Cit (Cit = citrulline)[26] and tetrapeptide Gly-Phe-Leu-Gly.[27] The dipeptide linkers Phe-Lys and Val-Cit were employed for BR96-Dox immunoconjugate with a self-immolative spacer (*p*-aminobenzyloxycarbonyl, PABC) inserted between the dipeptide and the drug. The self-immolation of the spacer is triggered by a proteolytic cleavage of the linker by cathepsin B, which is present in lysosomes of cancer cells.[28] These conjugates did not cleave when incubated in fresh human plasma for over 7 h and the half-lives of Phe-Lys-PABC and Val-Cit-PABC linkers were 8 and 240 min, respectively. The *in vitro* assay showed potent antigen-specific cytotoxicity of both immunoconjugates with IC_{50} values of 0.15 μM and 0.4 μM respectively. Dipeptide linker-PABC constructs have also been used for BR96-Dox[28] and cAC10-monomethylauristatin E (MMAE)[29] and the peptide linkers seemed to be more stable compared to the hydrazone linker containing conjugates prepared earlier. The *in vitro*

cytotoxicity assay of mAb-MMAE conjugate against Karpas 299 cell line gave an IC_{50} value of 4.5 ng/mL and a specificity ratio (*i.e.* the IC_{50} ratio of nonbinding conjugates to the binding control) of more than 500. The *in vivo* antitumor activity assay against Karpas 299 lymphoma in severe combined immune deficiency (SCID) mice showed that effective dose was 60-times lower than the maximum tolerated dose (MTD). Thus, 35 µg of MMAE component/kg/injection achieved 100 % tumor cure in human Karpas 299 anaplastic large cell lymphoma. Figure 3-4 shows the structure BR96-MMAE conjugate with Val-Cit linker and PABC spacer.

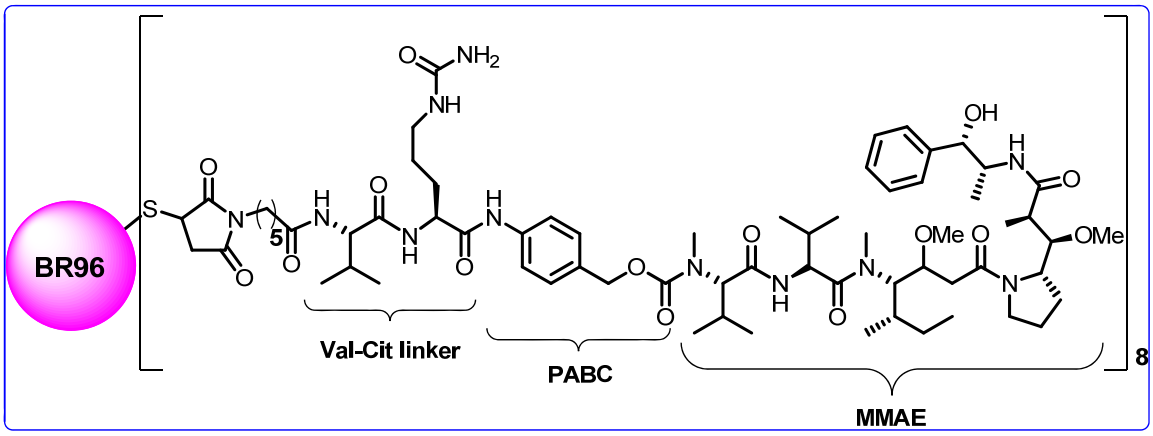

Figure 3-4. Structure of BR96-MMAE conjugate with Val-Cit linker and PABC spacer

3.2.3 Hydrolytic Linker

Hydrolytic linker such as ester linker is cleaved due to pH sensitivity or by lipase-catalyzed hydrolysis *in vivo*. The ester linkers are highly labile and have limited use in prodrug design without appropriate modifications. Sterically hindered secondary alcohols are used to circumvent this problem. A mAb C225 which specifically recognizes EGFR was conjugated to paclitaxel for tumor-targeting therapy.[30, 31] This conjugate was synthesized by conjugating the mAb to the C2'-hydroxyl group of paclitaxel through an ester bond using succinic acid as a spacer Figure 3-5.

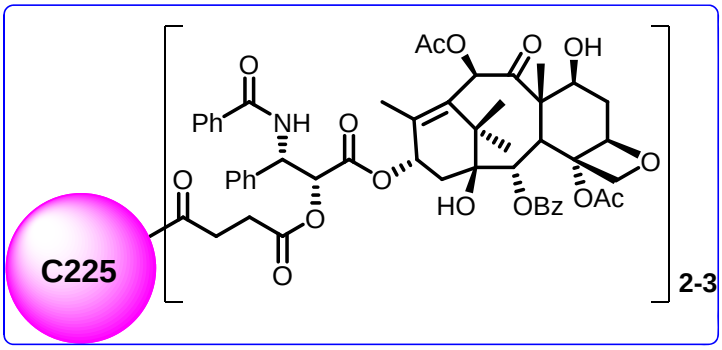

Figure 3-5. Structure of C225-paclitaxel

This conjugate induced more apoptosis than free drug alone in *in vitro* studies, however, *in vivo* studies showed no difference in tumor growth inhibition effects between the conjugate and C225. This phenomenon was likely caused due to the instability of the ester linker. Biodistribution and *in vitro* kinetic study using a ^{125}I-labeled C3'-OH-paclitaxel-C225 conjugate showed that the conjugate is not stable under physiological conditions with a half-life of about 2 h. The succinic acid moiety in the conjugate was replaced by glutaric acid to improve the systemic stability and the new prodrug showed better stability and indicated better antitumor activity than the original conjugate in *in vivo* studies.[31]

3.2.4 Disulfide Linker

Disulfide linkers are designed to cleave inside tumor cells through a disulfide exchange with an intracellular thiol such as glutathione which is an intracellular tripeptide with a thiol group. They are stable at physiological pH and take advantage of the high levels of reduced glutathione inside cancer cells that can cause scission of the disulfide bond and release the drug inside the cell. The concentration of reduced glutathione in circulation in blood is very low (typically in the micromolar range) while that in cancer cells is very high (typically in the millimolar range).[32] Sterically hindered disulfides are commonly used in the design of prodrugs to prevent premature cleavage of the disulfide bond and release of the drug while in circulation. There are several examples of disulfide linker containing conjugates which have superior efficacy compare to other linkers against numerous tumor xenografts such as colorectal cancer, pancreatic cancer, gastric cancer, small-cell lung cancer, non-small-cell lung cancer, prostate cancer and breast cancer in preclinical models.[33, 34]

A tumor-targeting drug conjugate with a humanized mAb huC242 which has high binding affinity to CanAg antigen expressed on most pancreatic, biliary and colorectal cancer cell membranes conjugated to a specially designed maytansine derivative DM1 bearing a methyldisulfanyl (MDS) group (Figure 3-6) showed remarkable potency and selectivity *in vitro* and *in vivo*. This mAb-DMI conjugate cured all mice bearing COLO 205 human colon tumor xenografts at much lower dose than the parent drug and also caused complete regressions of tumors of large size (260-500 mm^3).[33] A Phase I clinical trial on patients with CanAg-expressing solid malignancies showed some responses with

a terminal half-life of 41 (+/- 16) hours. Less than 1% of prematurely cleaved maytansoid DM1 was also detected in blood.[35]

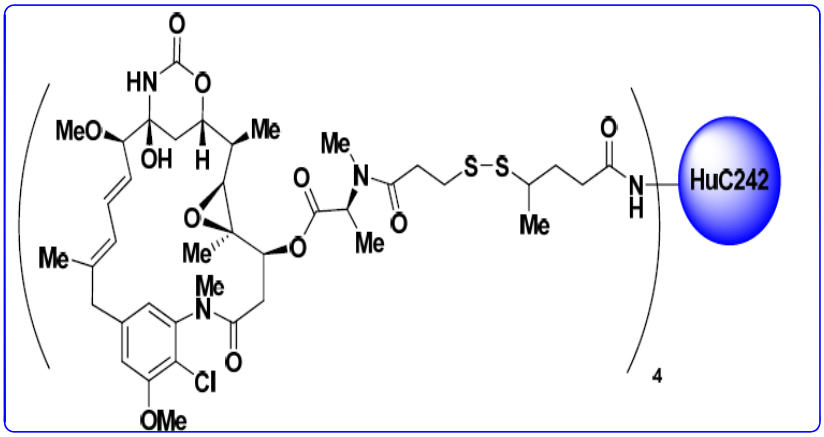

Figure 3-6. Structure of HuC242-DM1 conjugate

Disulfide-containing CC-1065 analog conjugated to anti-B4 targeting CD19 showed >700-fold potency against targeted cells. The disulfide linkage was stable and did not show any cytotoxicity to antigen-negative cells.[10] The disulfide bond linking the drug to the antibody can be manipulated to obtain maximum stability of the linker during blood circulation while cleaving efficiently inside the target cells. Varying degrees of steric hindrance could be obtained by introducing methyl substituents on the carbon atom geminal to the disulfide link.[36] Some structures of mAb-maytansinoid are shown in Figure 3-7.[37] Our group has developed mAb-taxoid conjugates containing disulfide linkers which showed remarkable antitumor activity[38] (discussed in chapter 4).

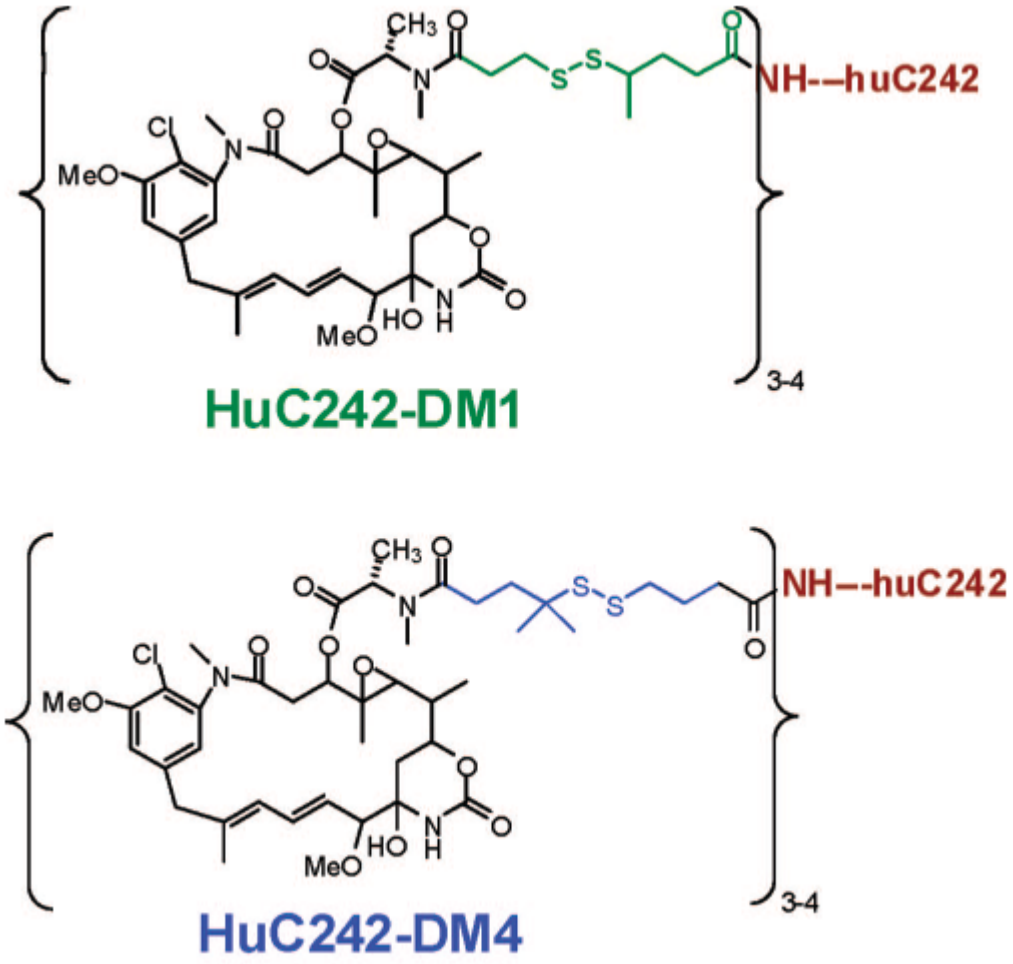

Figure 3-7. Structure of some mAb-maytansinoid conjugates[37]

3.3 Previous Achievements on Novel Disulfide Linkers

Despite the success of our first-generation mAb-taxoid immunoconjugates, the cytotoxicity of the active drug in cancer cell was 8 times weaker than the parent taxoid (SB-T-1213) and would not be potent enough for clinical use in humans. This was because the active drug, SB-T-12136-SH, was a derivative of the original taxoid molecule, SB-T-1213, with modification at C-10 position to attach the disulfide linker.[38, 39] Accordingly, novel second-generation mechanism-based disulfide linkers were developed which would release the potent drug in its original form efficiently and restore its extremely high cytotoxicity upon internalization to cancer cells. Several novel disulfide linkers were proposed as shown in Figure 3-8.

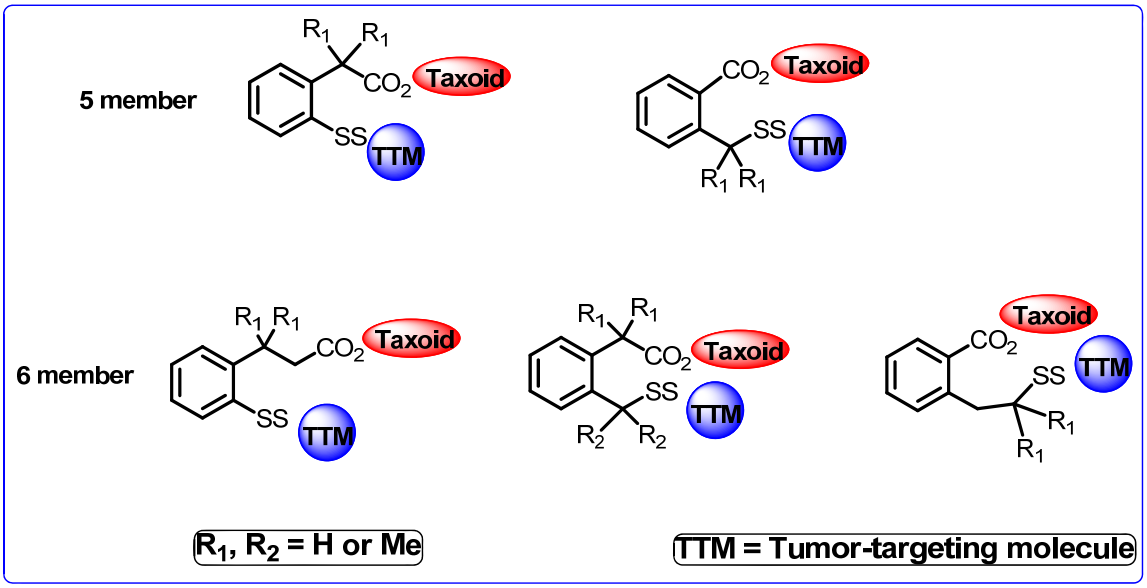

Figure 3-8. Structure of novel disulfide linkers

These novel mechanism-based self-immolative disulfide linkers are bifunctional and can be connected to various tumor-targeting moieties and various potent drugs. Upon target-specific internalization inside the cancer cells the glutathione triggered cascade releases the potent anticancer drug. The concentration of glutathione (GSH) in blood plasma is very low (~ 2 μM), while that in tumor tissues is 1,000 times higher (2-8 mM). Also, the concentration of GSH in tumor tissues is 2-10 fold higher than in normal tissues (10 fold higher in drug-resistant tumors).[32, 40-43] The disulfide bond is cleaved by glutathione or other thiols to generate a free sulfhydryl group on the linker moiety which can then undergo an intramolecular nucleophilic acyl substitution on the ester moiety to form a 5- or 6-membered ring thiolactone and release the taxoid molecule in its original active form. Like other linkers these disulfide linkers should be stable in blood circulation but readily cleave inside the tumor tissues and cells.

Model reactions were carried out to prove the mechanism-based release process and study the relative reactivity of the disulfide linkers towards a thiol-initiated fragmentation, the substitution effect on the aromatic ring and the release profile under different pH conditions. A commonly used protocol to perform dynamic studies of complex reaction systems is ^{19}F NMR because the fluorine tagged compounds and their behavior can be easily detected by ^{19}F NMR technique *in vivo*. Accordingly, model compounds were synthesized with *p*-fluorophenol as an alternative to the drug and a fluorine tag was also introduced into the aromatic ring to monitor the reaction progress with ^{19}F NMR.[44] The model reaction was carried out at 37 ^{o}C with acetonitrile as co-solvent in pH 7.4 buffer solution using cysteine to mimic glutathione present in cancer cells. The progress of the reaction was monitored by time-dependent ^{19}F NMR and the expected intramolecular thiolactonization went as expected and completed in about 90 min (Figure 3-9).[44, 45]

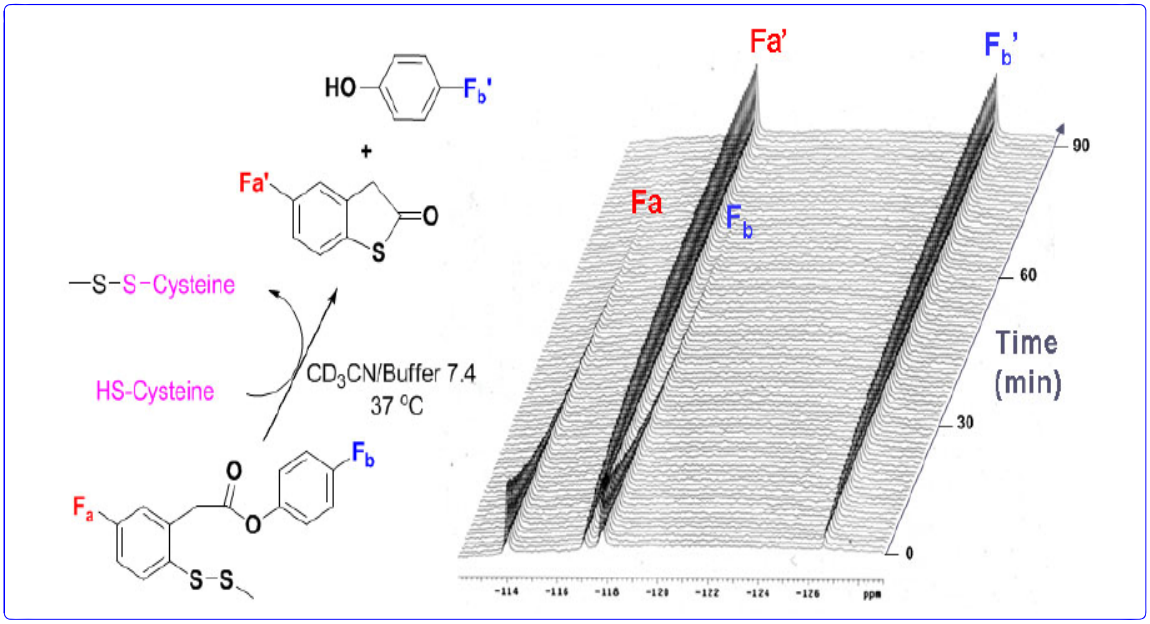

Figure 3-9. Mechanism-based release profile of model system[45]

The strategic design of placing the phenyl group attached to the disulfide bond directs the cleavage of the disulfide bond by a thiol to generate a desirable thiophenolate or sulfhydryl phenyl moiety for intramolecular thiolactonization. The mechanism of cleavage of disulfide bond is shown in Figure 3-10.

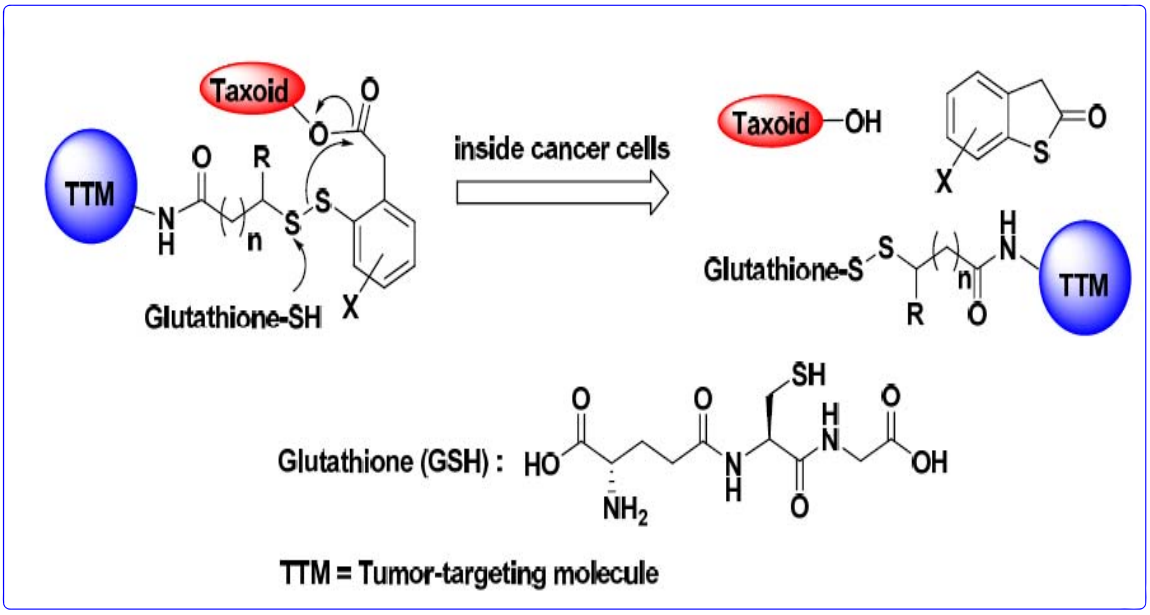

Figure 3-10. Mechanism of disulfide bond cleavage

This type of mechanism-based self-immolative disulfide linker is readily applicable to a wide range of tumor-targeting DDS as shown in Figure 3-11.

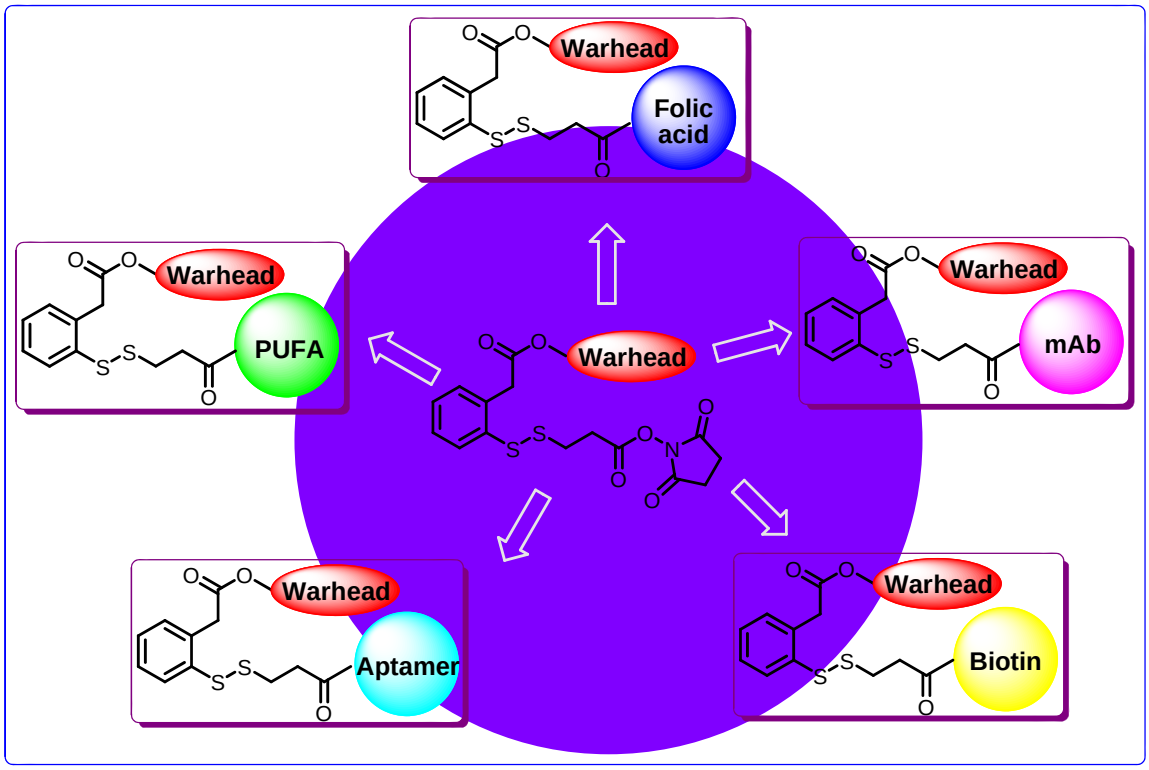

Figure 3-11. Applications of disulfide linker to various tumor-targeting conjugates

The promising preliminary results prompted the application of the original cytotoxic taxoid for the drug release study as shown in Figure 3-12. The reaction was performed in a similar manner to the model system and monitored by TLC, HPLC and NMR. The time-dependent ^{19}F NMR spectrum clearly indicated the disappearance of the starting material and formation of thiolactone and free taxoid.

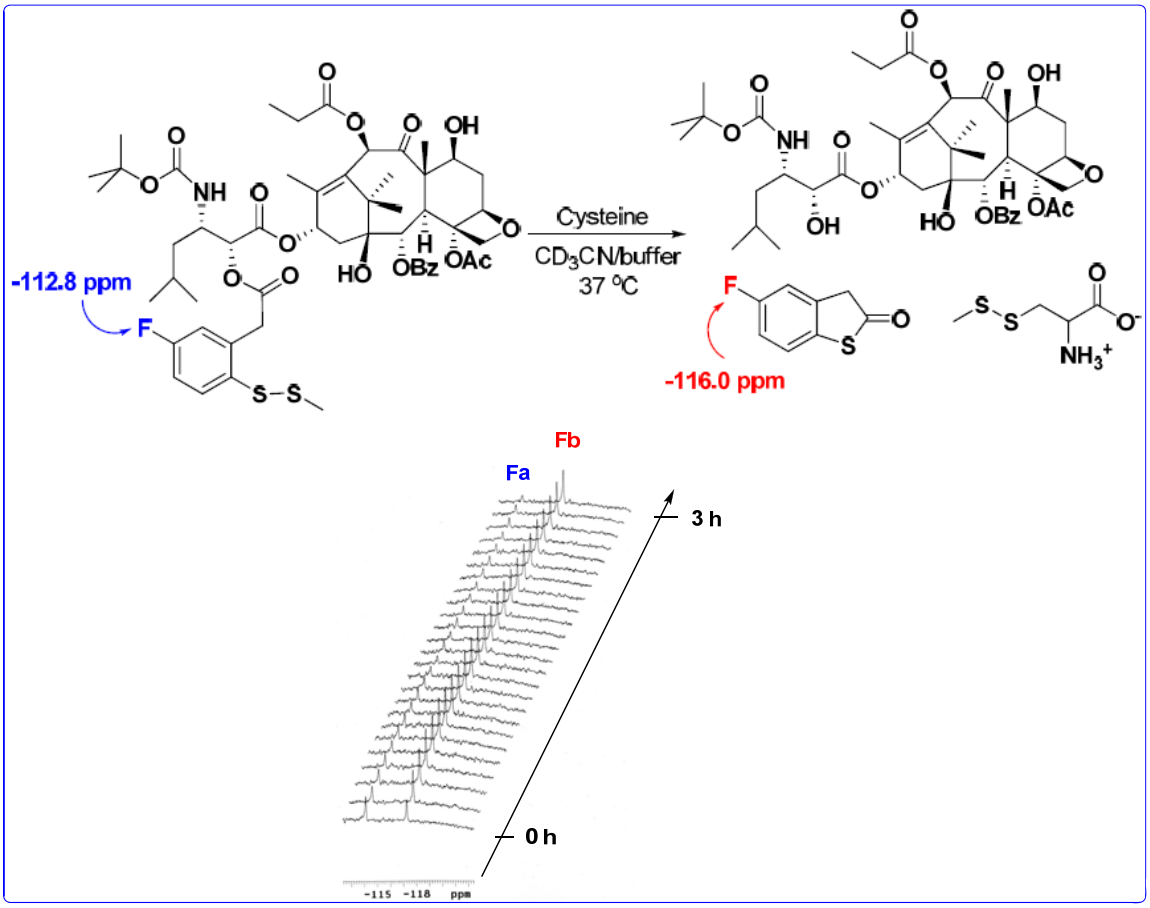

Figure 3-12. ^{19}F NMR profile of mechanism-based taxoid release[44]

Various buffer solutions (pH = 6.0, 7.0, 8.0) were used to investigate the pH dependent release profile and it was found that the reaction completed in 2 h at pH 7, within 1.5 h at pH 8 but the reaction went much slower at pH 6. At pH 6, only 84 % of conjugate was converted to thiolactone and taxoid even after 5 h (Table 3-1).

pH	Reaction time
6.0	> 5 h, at 5 h 84 % conversion
7.0	2.0 h
8.0	1.5 h

Table 3-1. Profile of pH dependent release

3.4 Results and Discussion

The mechanism of thiol-disulfide exchange reaction has been under investigation for a long time because of its great significance in biochemistry. Thiol-disulfide exchange reaction plays an important role in the folding of proteins, maintaining the redox state of cells, protecting organism from oxidative stress and in many other fundamental processes.[46-49] Thiol-disulfide exchange reaction can be schematically considered as shown in Scheme 3-1.

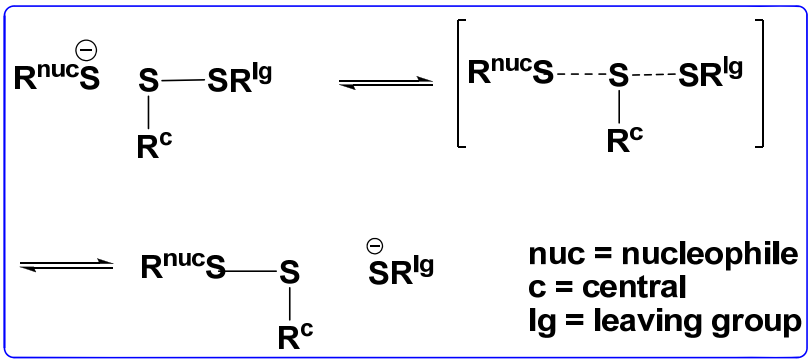

Scheme 3-1. Mechanism of thiol-disulfide exchange reaction

The thiol-disulfide exchange reaction is an S_N2 reaction in which the thiolate anion is the reactive species. The thiolate anion attacks the disulfide bond along the S–S axis.[46, 49] Consequently, introduction of bulky functional groups can affect the speed of the reaction. For example, introduction of methyl group at β position to the C–S bond of thiolate anion slightly slows down the reaction.[46] The reaction proceeds through the S_N2 transition state. The charge in the transition state is delocalized on the peripheral sulfur atoms with zero or small negative charge on central sulfur atom. It has been concluded that the charge is transferred directly from S_{nuc} to S_{lg} without significant accumulation on S_c. The concentration of the charge on S_{nuc} or S_{lg} (or reactants) will lead to better stabilization of reactant in polar solvents compared with the transition state where the charge is more evenly distributed. Thus, polar environment will increase the activation energy and slow down the thiol-disulfide exchange reaction.[49]

A systematic kinetic study, wherein a *p*-fluorophenol was used as an alternative to a real drug for simplicity, was performed towards the understanding of the drug release processes. Glutathione was utilized to mimic the *in vitro* reducing conditions in biological environment. All the model reactions were carried out at 37 ^{o}C and pH 7.4 conditions. The kinetic studies and the synthesis of model linkers were carried out in collaboration with Dr. Jin Chen, Dr. Stanislav Jaracz, Dr. Shuyi Chen and Dr. Xianrui Zhao.

3.4.1 Synthesis of Disulfide Linkers

Initially, the relative activity of disulfide linkers with variable lengths was investigated, as shown in Figure 3-13.

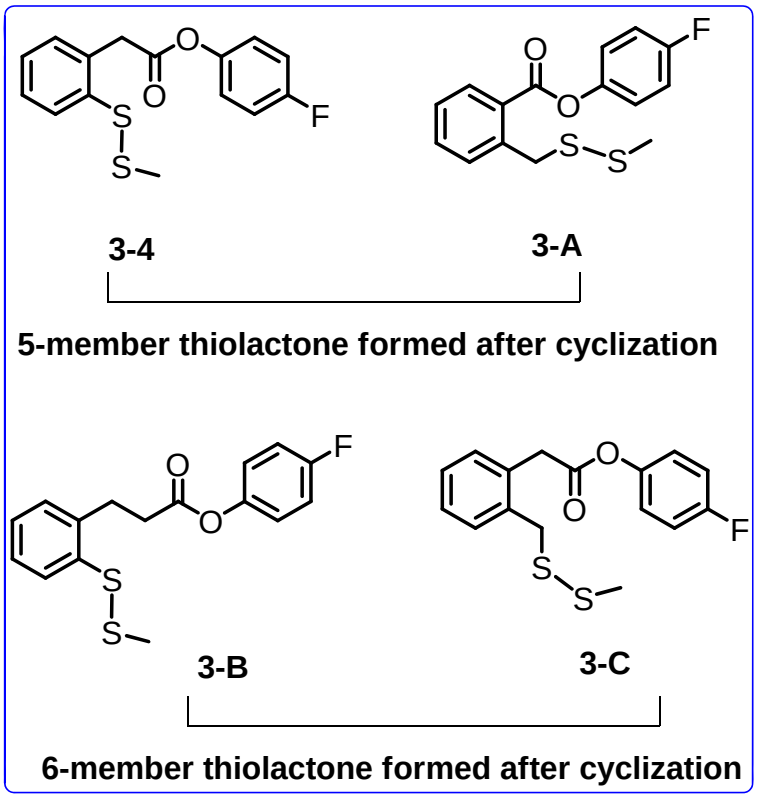

Figure 3-13. Structure of disulfide linkers with variable lengths

The disulfide linker **3-4** has been proven to be the most successful substrate in our model system. Its synthetic route is illustrated in Scheme 3-2. First, oxidation of benzo[b]thiophen-2-ylboronic acid with H_2O_2 in ethanol gave the 5-member ring thiolactone **3-1**, which was then hydrolyzed to yield the corresponding product 2-mercaptophenyl acetic acid **3-2** bearing a free sulfhydryl group. Methyl methanethiosulfonate was used in thiol-disulfide exchange reaction to afford methyl disulfide **3-3**, followed by esterification with *p*-fluorophenol in DIC/DMAP to give the desired final product **3-4** in good overall yield.

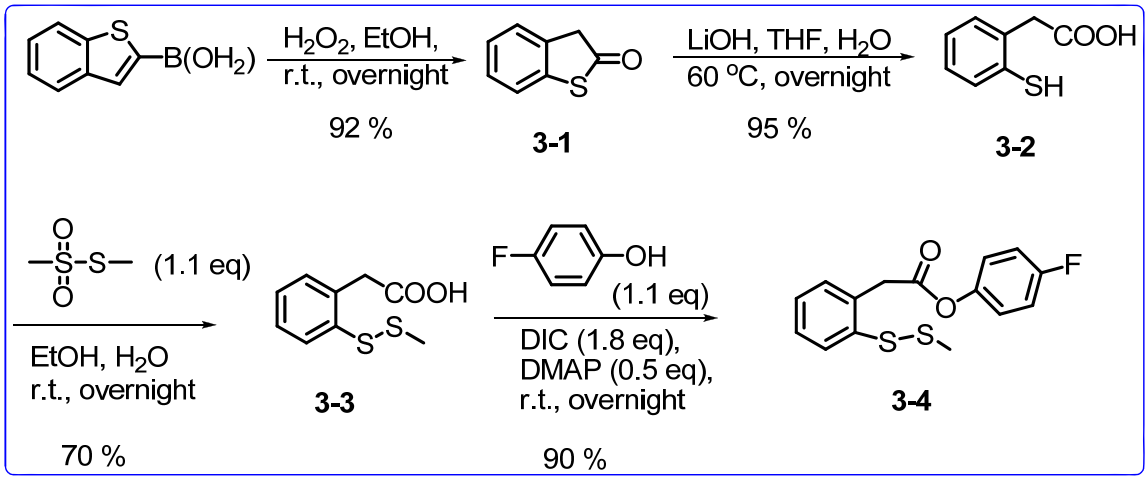

Scheme 3-2. Synthesis of 4-fluorophenyl 2-(2-methyldisulfanylphenyl)acetate (**3-4**)

The *gem*-dimethyl effect, also termed as Thorpe-Ingold effect was first reported in the early 1900s to accelerate cyclization rate by a *gem*-dialkyl moiety located on the framework of the acyclic carbon backbone.[50-53] A common application of this effect is the presence of a quaternary carbon, e.g. a *gem*-dimethyl group, in an alkyl chain, to increase the reaction rate of cyclization. In our attempts to elucidate the mechanism-based release process, we believed that the incorporation of *gem*-dimethyl effect may facilitate the intramolecular cyclization and thereby accelerate the drug release. Accordingly, a set of disulfide linkers bearing a *gem*-dimethyl group on the benzylic position was proposed, as illustrated in Figure 3-14.

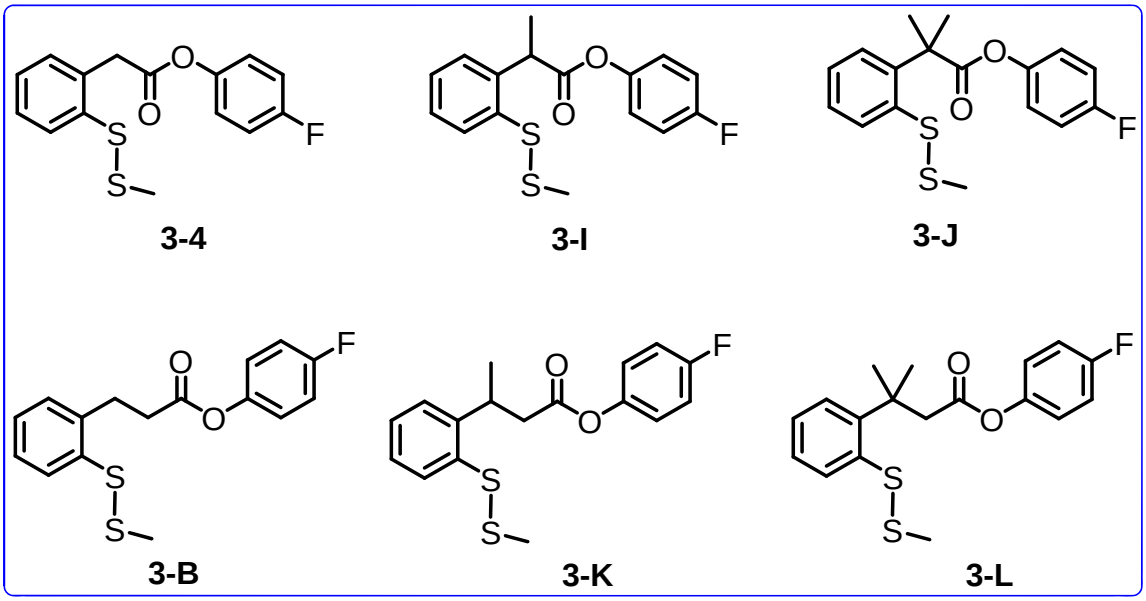

Figure 3-14. Structure of disulfide linkers with *gem*-mono/dimethyl groups

The afore-mentioned rate acceleration of cyclization reactions was attributed to the decrease in angle between the two reacting termini when the *gem*-dimethyl groups were located on the framework of the acyclic carbon backbone (Figure 3-15). This compression would subsequently result in bringing the two reacting termini closer to each other and thereby, increase the cyclization rate.

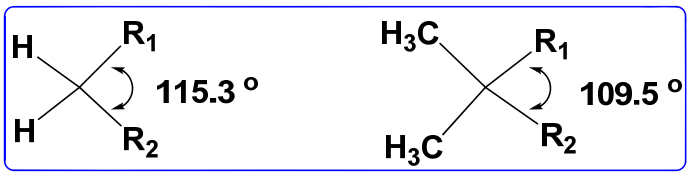

Figure 3-15. Decrease in angle between the two reacting termini upon introduction of *gem*-dimethyl groups

Several disulfide linkers were designed with various substituents on the aromatic ring as shown in Figure 3-16 to study the effect of substitution on the aromatic ring on the kinetics of the mechanism-based drug release.

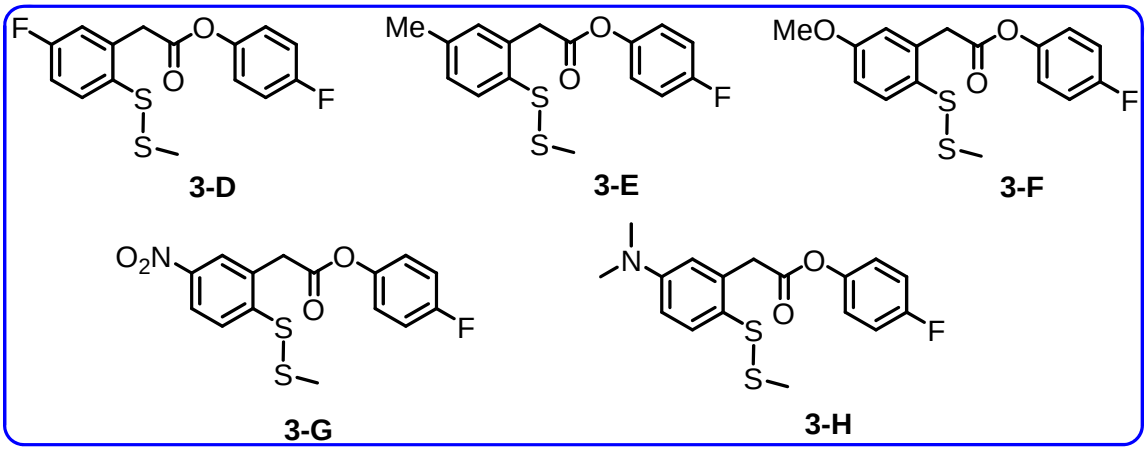

Figure 3-16. Structure of disulfide linkers with substituents on aromatic ring

Several disulfide linkers were designed and synthesized with different substituents on the S-S bond as shown in Figure 3-17 to compare the effect of the polarities of different disulfide bonds on the stability and mechanism-based release.

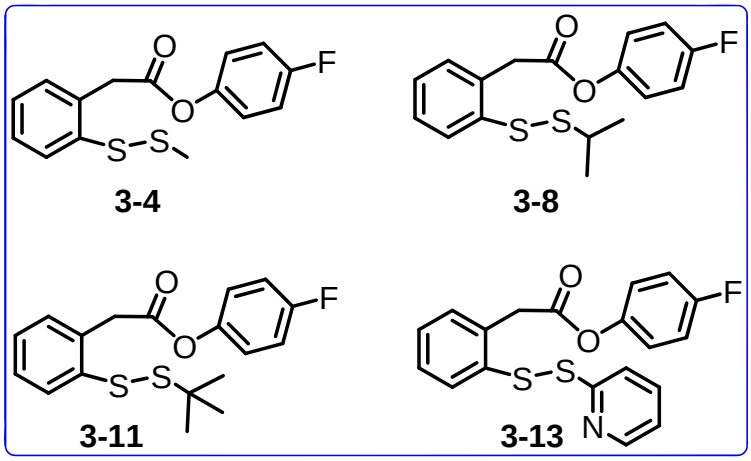

Figure 3-17. Structure of disulfide linkers with different substituents on the S-S bond

Scheme 3-3 shows the synthesis of 4-fluorophenyl 2-(2-isopropyldisulfanyl phenyl) acetate (**3-8**). *p*-Toluenesulfonhydrazide is reacted with bromine to yield tosyl bromide (**3-5**)[54] which was then reacted with propan-2-thiol[55] to yield **3-6**. This reaction did not proceed well with DCM as solvent. The compound **3-6** was then reacted with **3-2** to yield the acid **3-7**. The acid **3-7** was then reacted with 4-fluorophenol to form the desired compound **3-8** in excellent yields.

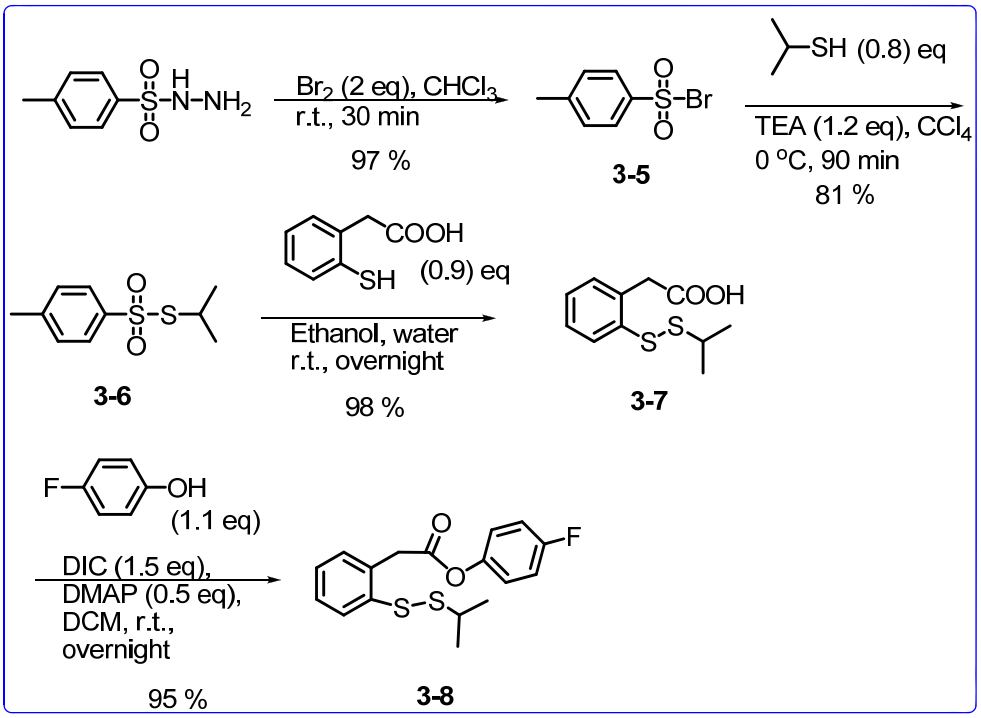

Scheme 3-3. Synthesis of 4-fluorophenyl 2-(2-isopropyldisulfanylphenyl)acetate (**3-8**)

Scheme 3-4 shows the synthesis of 4-fluorophenyl 2-(2-*tert*-butyldisulfanylphenyl) acetate (**3-11**). Tosyl bromide (**3-5**) was reacted with 2-methylpropan-2-thiol[55] to yield **3-9** which was then reacted with **3-2** to yield the acid **3-10**. The compound **3-10** was then reacted with 4-fluorophenol to form the desired compound **3-11** in excellent yields.

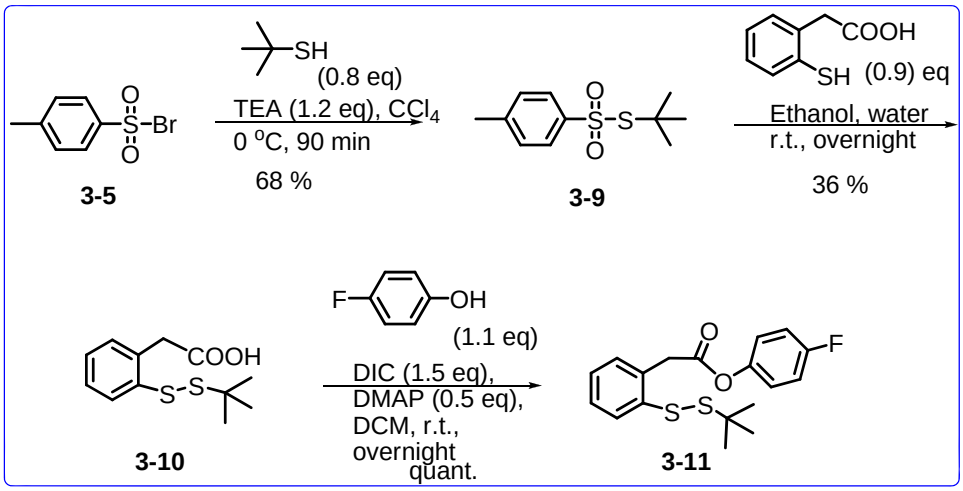

Scheme 3-4. Synthesis of 4-fluorophenyl 2-(2-*tert*-butyldisulfanylphenyl)acetate (**3-11**)

Scheme 3-5 shows the synthesis of 4-fluorophenyl 2-(2-pyridin-2-yldisulfanylphenyl)acetate (**3-13**). A disulfide exchange reaction was performed using the compound **3-2** and 2,2'-dithiodipyridine to form the acid **3-12** which was then reacted with 4-fluorophenol to form the desired compound **3-13**.

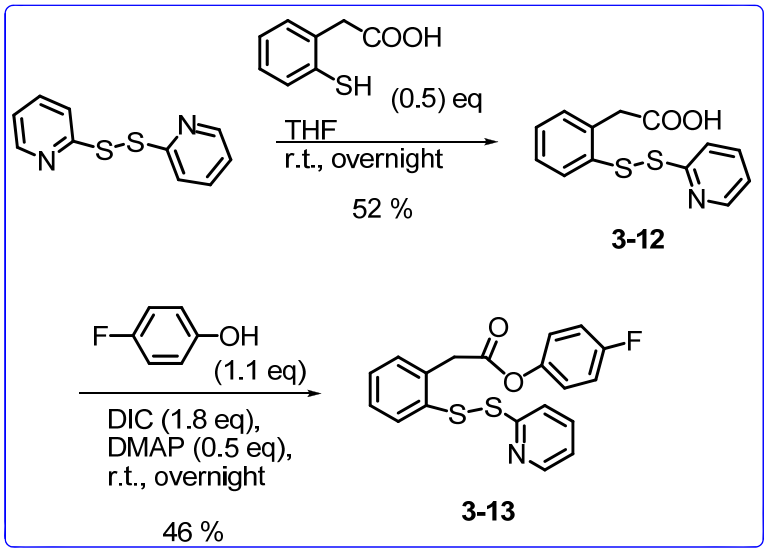

Scheme 3-5. Synthesis of 4-fluorophenyl 2-(2-pyridin-2-yldisulfanylphenyl)acetate (**3-13**)

3.4.2 Kinetic Study of Disulfide Linkers

A series of systematic kinetic studies to further elucidate the characteristics of this self-immolative disulfide linker including reaction rate constant determination and pH-dependent drug release profile were performed in our laboratory by previous group members. The reaction rate constant was determined based on HPLC assay as shown in Scheme 3-6. The reaction was carried out in the presence of excess glutathione, pH 7.4 buffer, at 37 ^{o}C to mimic biological conditions. Acetonitrile was used as the co-solvent to improve the poor solubility of the substrate in the buffer.

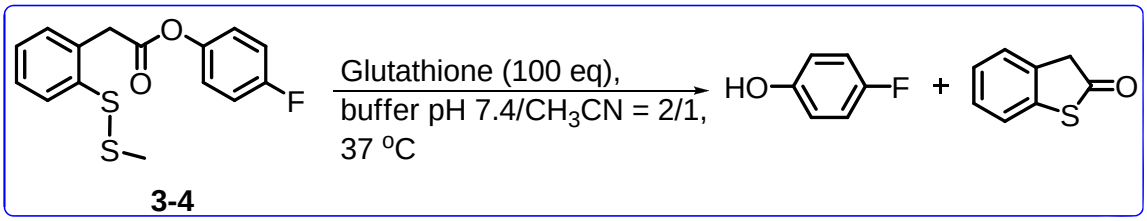

Scheme 3-6. Model reaction for determination of rate constant

The rate constant was calculated according to rate law, rate = -d[A]/dt = k[A][B]. When B is in large excess, rate = -d[A]/dt = q[A], wherein q = k[B]. As shown in Figure 3-18 (C), ln(A) exhibited a linear relationship with time, which indicated that this reaction can be considered as a pseudo-first order reaction. Consequently, $\ln(A_t) = \ln(A_0)^{-qt}$, q = 6.1×10^{-2} min^{-1}, half time $t_{1/2}$ = 11.4 min.

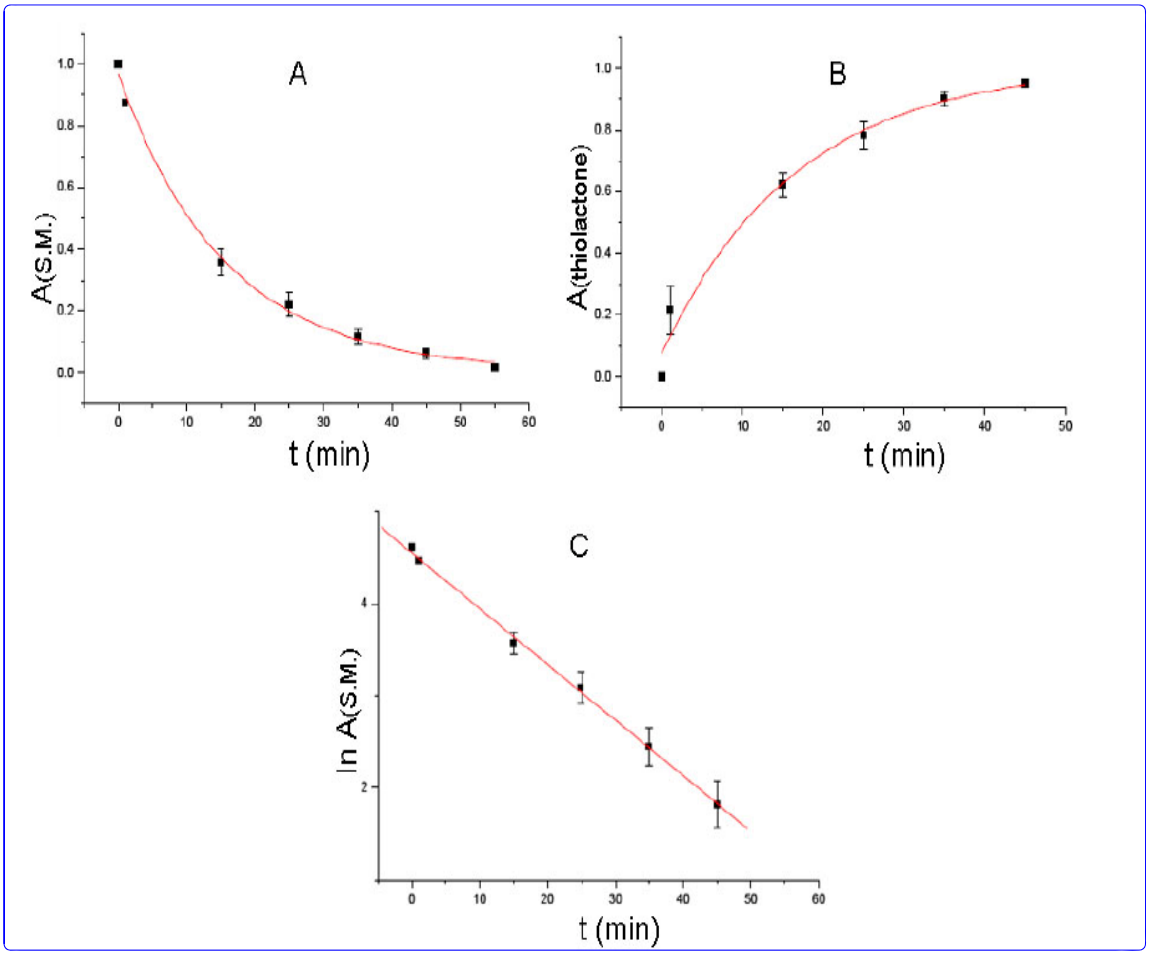

Figure 3-18. Measurement of model drug release rate constant for disulfide linker (**3-4**)

However, in the case of disulfide linkers (**3-A**) and (**3-C**) bearing S-S bond at the benzylic position, both reactions were extremely slow with incomplete conversion even after several days as shown in Scheme 3-7.

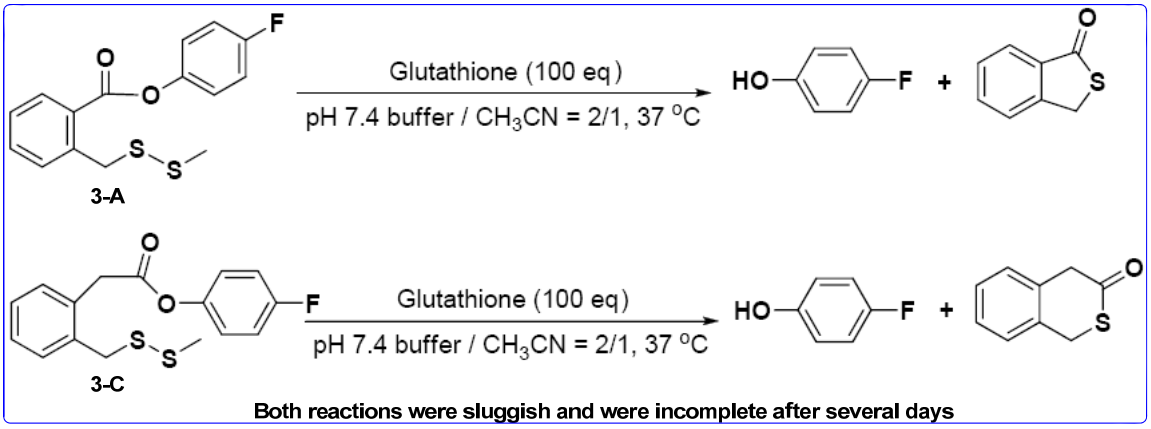

Scheme 3-7. Model reaction for drug release with different thiol-initiated fragmentation

The pH-dependence of drug release was also assayed by Dr. Jin Chen with disulfide linker (**3-4**) as shown in Figure 3-19. The pH in physiological environment is 7.4 while that in tumor tissues is usually lower than 7; therefore it is essential to explore this reaction under different pH conditions. As expected, the reaction was faster at pH 10.0 (green) than under physiological pH of 7.4 (red). The release rate is only slightly decreased at pH 5.0 (blue) than that at pH 7.4 (red).

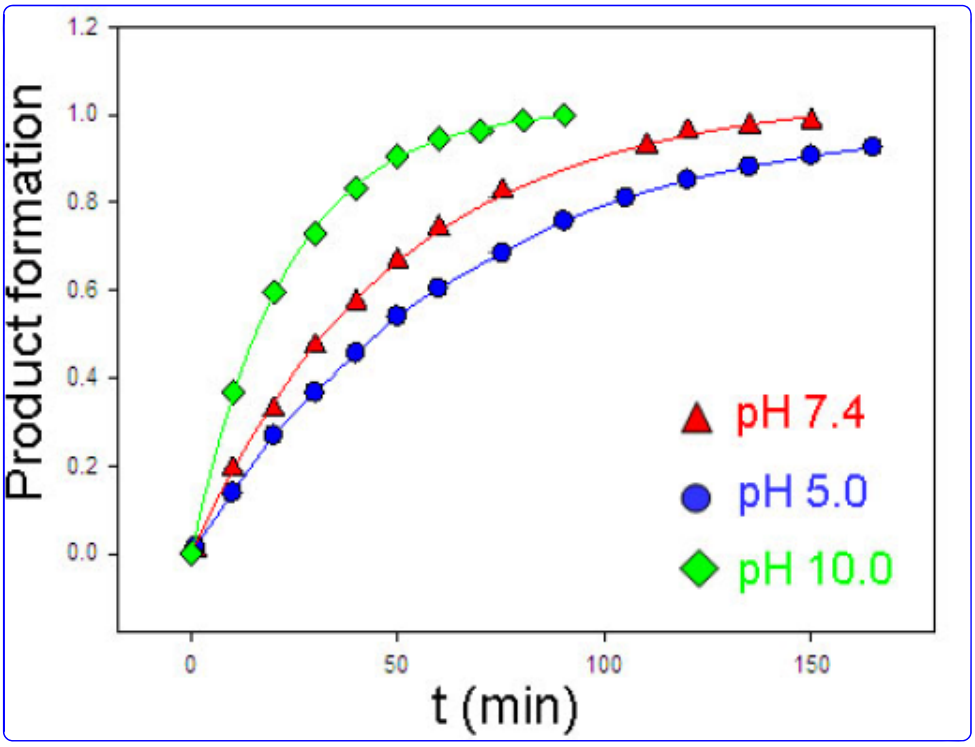

Figure 3-19. Profile of pH-dependent drug release for disulfide linker (**3-4**)

A preliminary evaluation of *gem*-dimethyl effect with disulfide linker (**3-28**) is illustrated in Scheme 3-8 and Figure 3-20. The rate constant (q) and release half time ($t_{1/2}$) were also calculated according to the rate law: $q = 9.6\times10^{-3}$ min^{-1} and $t_{1/2} = 72.1$ min, respectively.

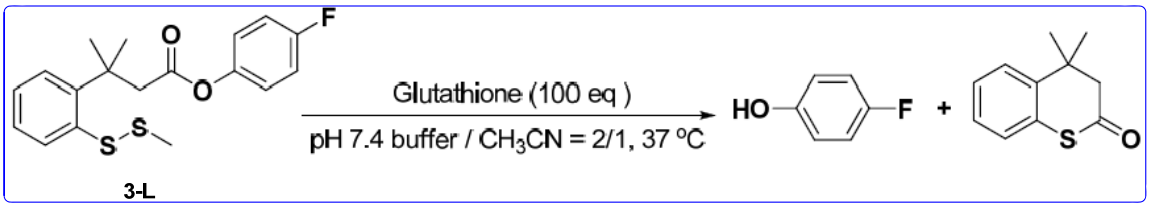

Scheme 3-8. Model reaction of **3-L**

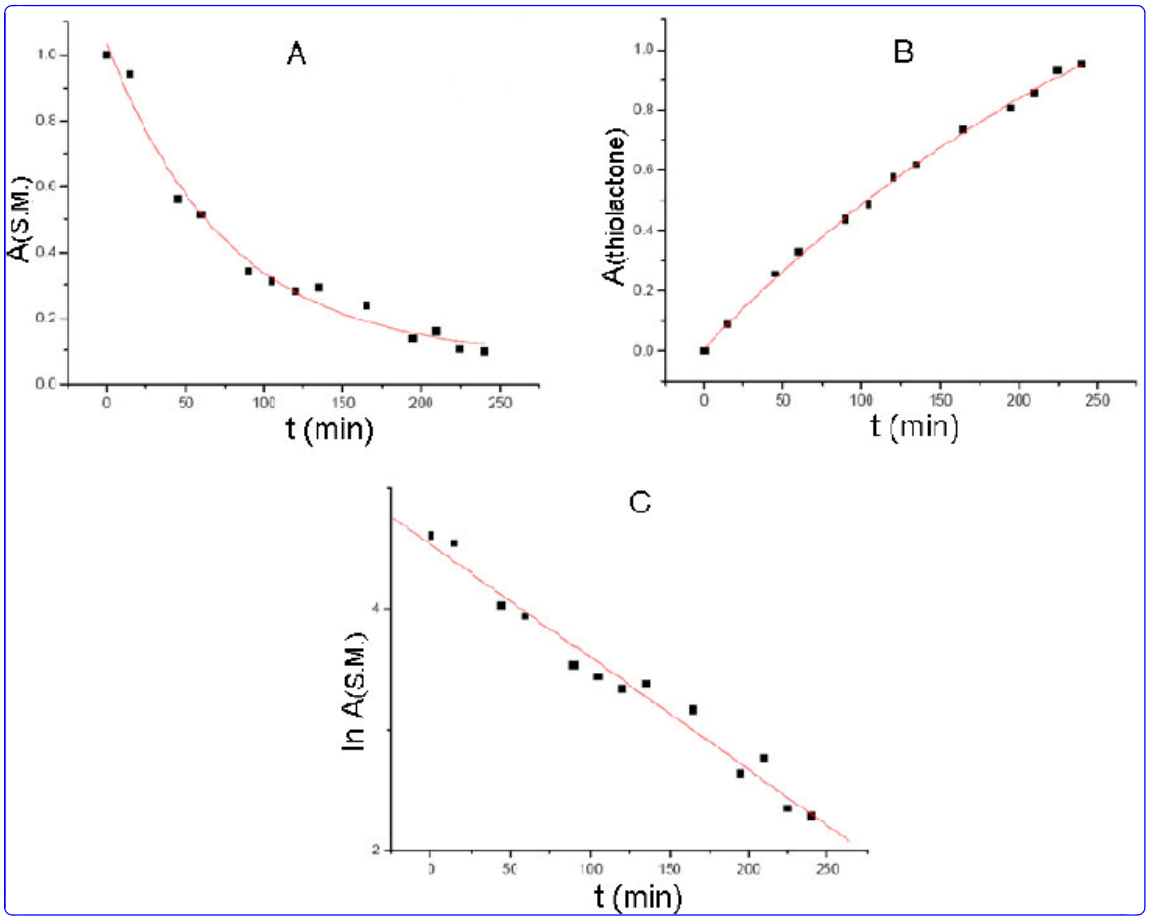

Figure 3-20. Measurement of *gem*-dimethyl effect on drug release for **3-L**

The substituent effects on the aromatic ring of the disulfide linker are described in Scheme 3-9. These substituents included H, F, Me, OMe, NO_2 and NMe_2. The reactions were carried out in the presence excess of glutathione, buffer pH 7.4, at 37 ^oC to mimic

physiological conditions. Acetonitrile was used as the co-solvent to improve the poor solubility of the substrates in the buffer. Preliminary results, wherein R = H, Me and OMe, are summarized in Table 3-2. The release rate decreased in the following order, R = H > R = OMe > R = Me.

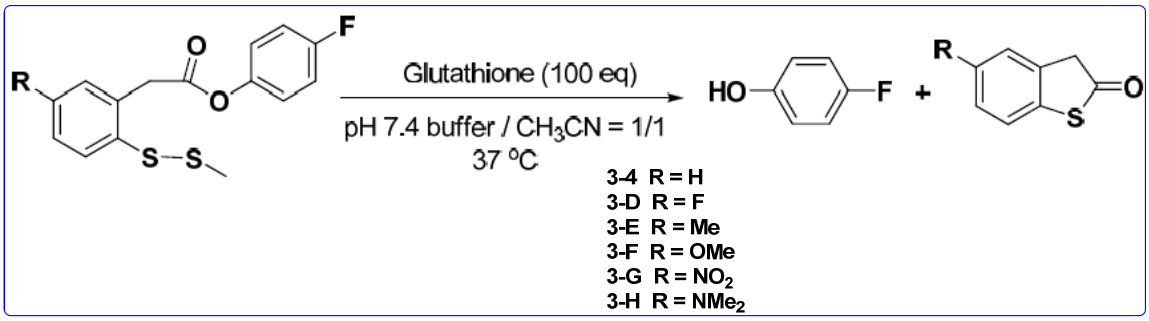

Scheme 3-9. Model reaction for comparison of substituent effect

R	Reaction Rate Constant (q, min^{-1})	Release Half Time ($t_{1/2}$, min)
H	6.1×10^{-2}	11.4
OMe	2.6×10^{-2}	22.6
Me	1.5×10^{-2}	46.2

Table 3-2. Aromatic ring substituent effect on drug release

Currently, it would be very difficult to make a convincing conclusion on the exact intrinsic characteristics of the mechanism-based drug release profile without extensive exploration of other substituents. Figure 3-21 describes the drug release profile only when R = OMe for simplicity.

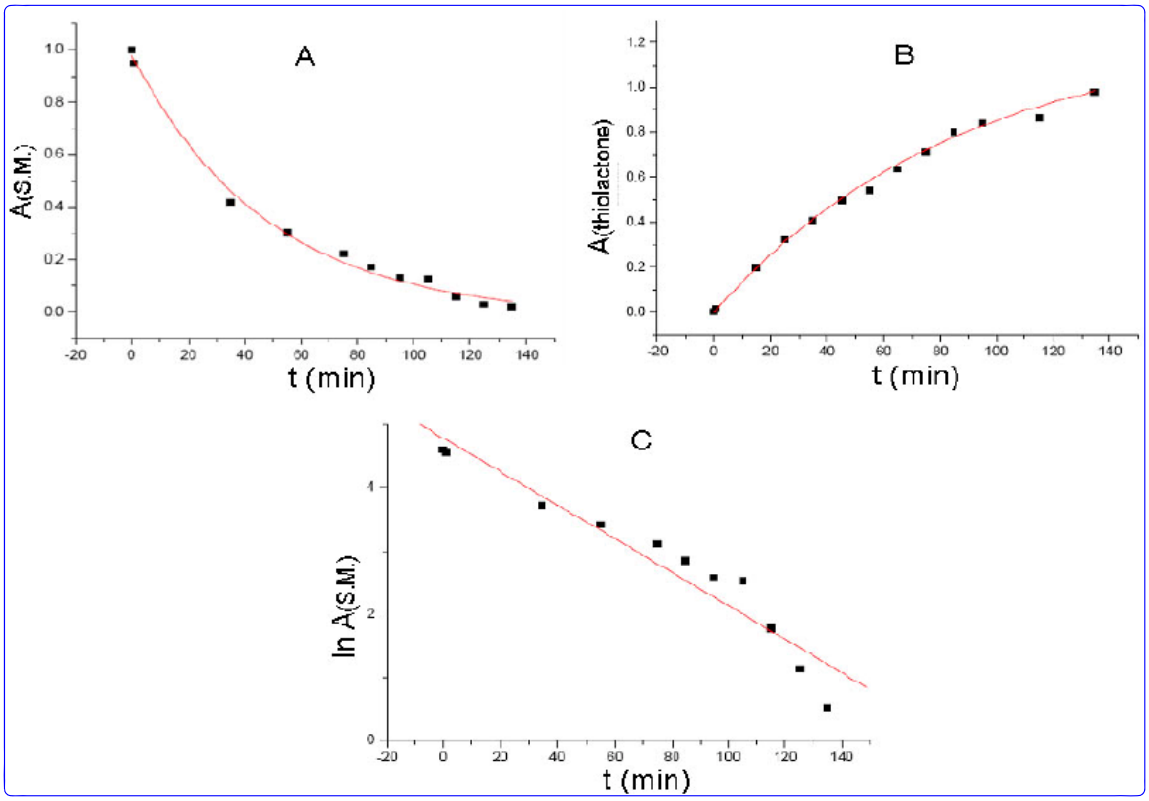

Figure 3-21. Measurement of substituent effect on drug release for **3-F**

Disulfide bonds with different polarities and steric hindrance environments may also significantly affect the thiol disulfide exchange reaction. Accordingly, an iso-propyl functionalized disulfide linker (**3-8**) was employed for comparison (Scheme 3-10). It was observed that this reaction was sluggish with only trace amounts of thiolactone formation even after 40 h. Another two disulfide linker substrates (**3-11**) and (**3-13**) with *tert*-butyl and pyridinyl substituents, respectively, are still under investigation.

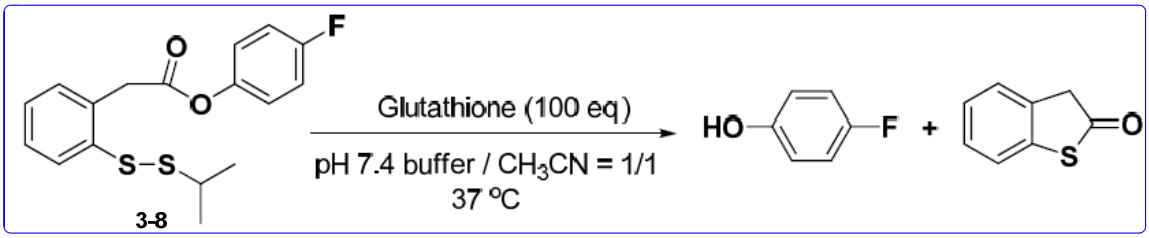

Scheme 3-10. Model reaction with **3-8**

3.4.3 Stability Studies

As mentioned before it is crucial that the linker remains stable in circulation and cleaves efficiently inside the target cells once the conjugate is internalized. Several stability studies were performed with model systems as well as with suitably tagged drug conjugate system. The stability studies were performed using the biotin-linker-taxoid conjugates in blood plasma. Prior to the blood plasma studies the stability of these conjugates were monitored in PBS (phosphate buffered saline) under physiological conditions (37 ^{o}C, pH ~7.4) using varying amounts of glutathione. This preliminary study allowed us to develop the LC-MS method as well as gave us some idea of the stability of these conjugates. The structures of the tumor-targeting conjugates are shown in Figure 3-22.

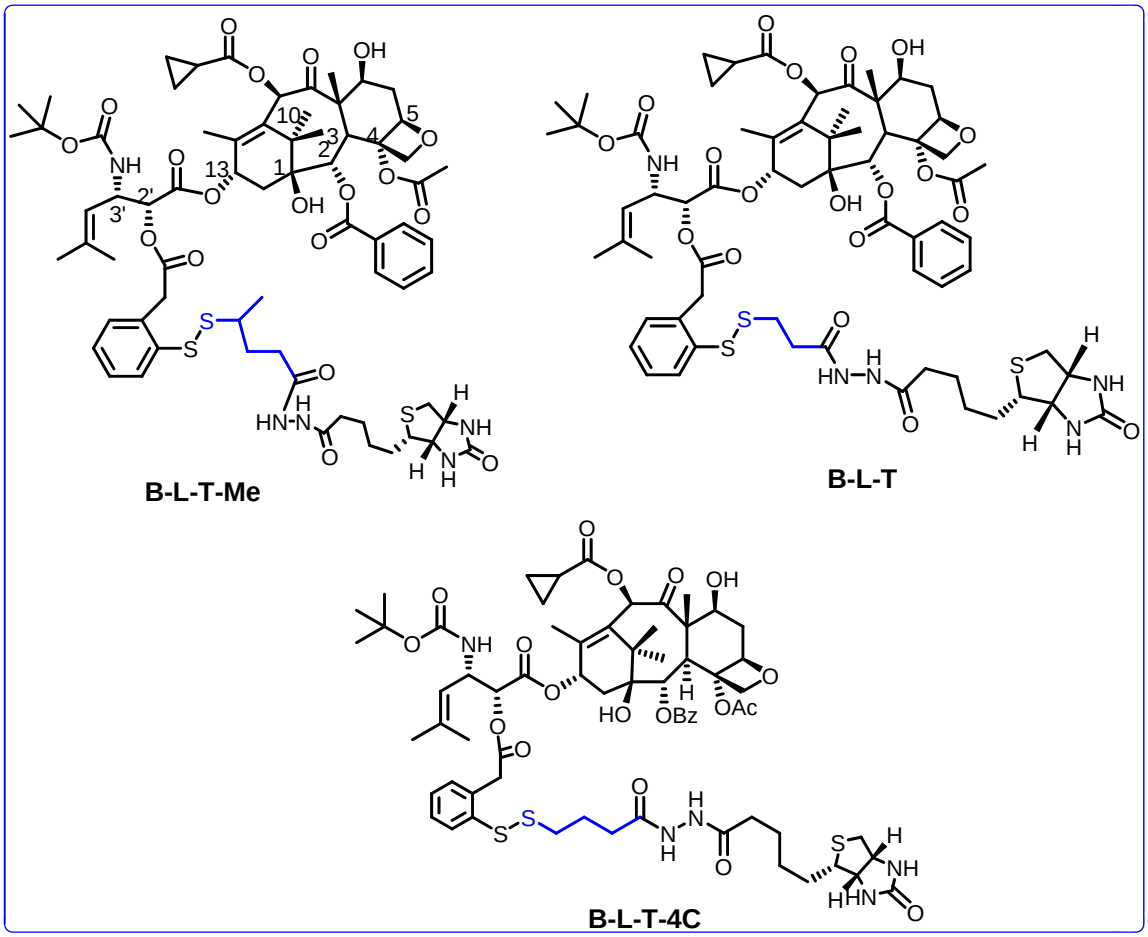

Figure 3-22. Structures of tumor-targeting conjugates for linker stability studies

The conjugates were incubated with PBS (pH ~ 7.4) or blood plasma at 37 ^{o}C and aliquots were taken at certain time intervals and monitored using HPLC. (Note: The human blood plasma used for the study was from the same lot.) The amount of taxoid released was compared to the decrease in the conjugate to determine the stability of the linkers. In the case of blood plasma the aliquots were treated with acetonitrile/0.1 % TFA

to precipitate out the plasma proteins which was then removed by centrifugation and the clear supernatant was used to monitor the stability. The linkers chosen for this study has different lengths and branching to study the effect on stability and drug release. Figure 3-23 shows the results of stability of two conjugates in presence of 10 eq of glutathione in PBS. Under these conditions the branched linker is more stable than the short chained unbranched linker.

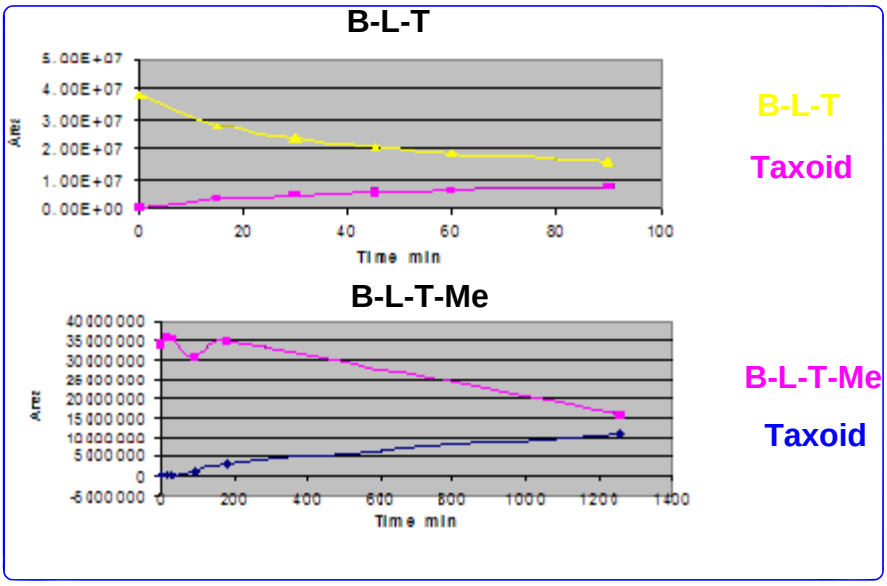

Figure 3-23. Preliminary study of conjugates using 10 eq glutathione in PBS

B-L-T was incubated with blood plasma and after 30 min there was some release of the drug from the conjugate. In 1 h 15 min there was an almost 1:1 ratio of conjugate to drug with the conjugate being in excess as shown in Figure 3-24, Figure 3-25. After 2 h 15 min the conjugate was consumed with the release of the taxoid.

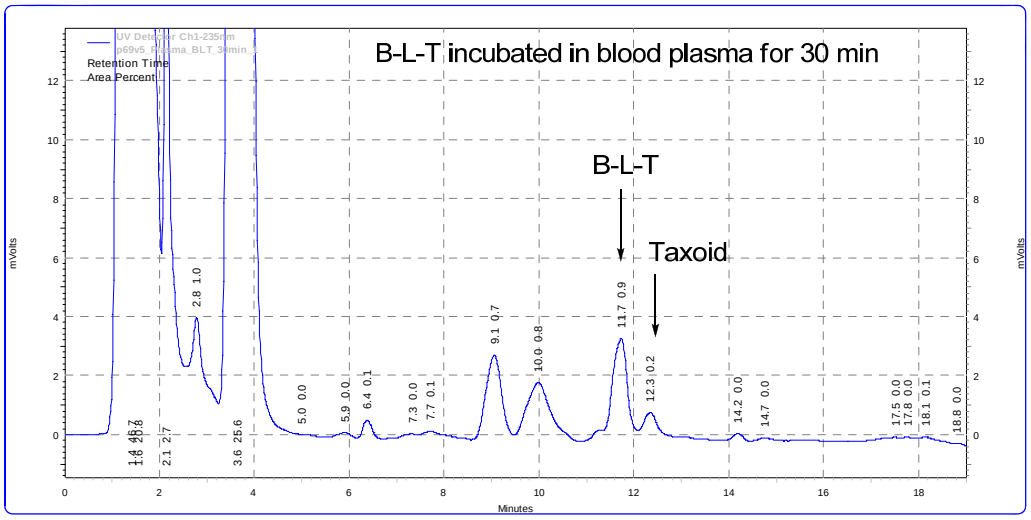

Figure 3-24. B-L-T after 30 min incubation in blood plasma

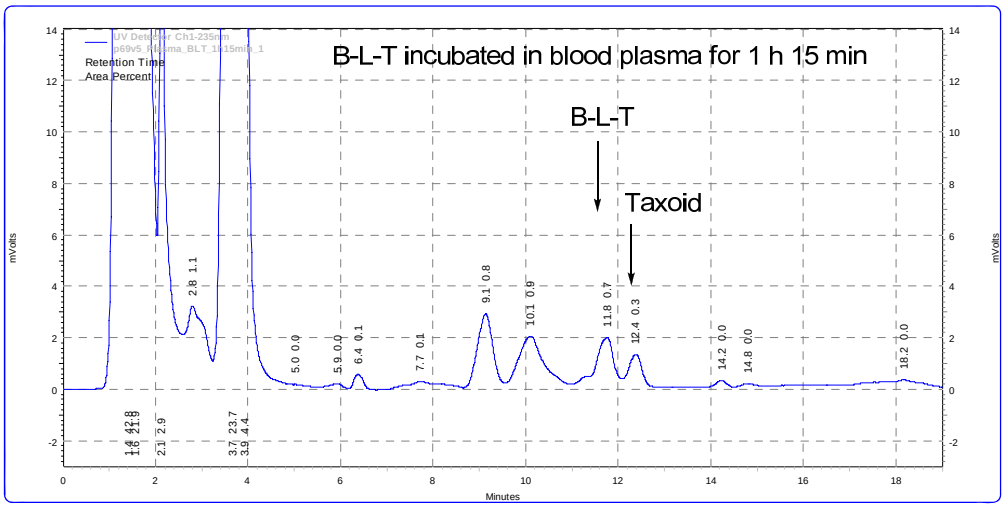

Figure 3-25. B-L-T after 1 h 15 min incubation in blood plasma

When B-L-T-4C was incubated in PBS (pH 7.4) with 1 eq of GSH it was stable and very little taxoid formed even after 24 h of incubation (Figure 3-26) while in 10 eq GSH there was almost 1:1 ratio of the conjugate and taxoid in 7 h and in 23 h there was a slight excess of taxoid as compared with the conjugate but still a 1:1 ratio of conjugate to taxoid was maintained (Figure 3-27). It seems that even after 23 h there was still no complete release of the taxoid under these conditions. While in blood plasma the conjugate was present in 1:1 ratio with the taxoid after 3 h 30 min incubation and was consumed after 5 h incubation as shown in Figure 3-28.

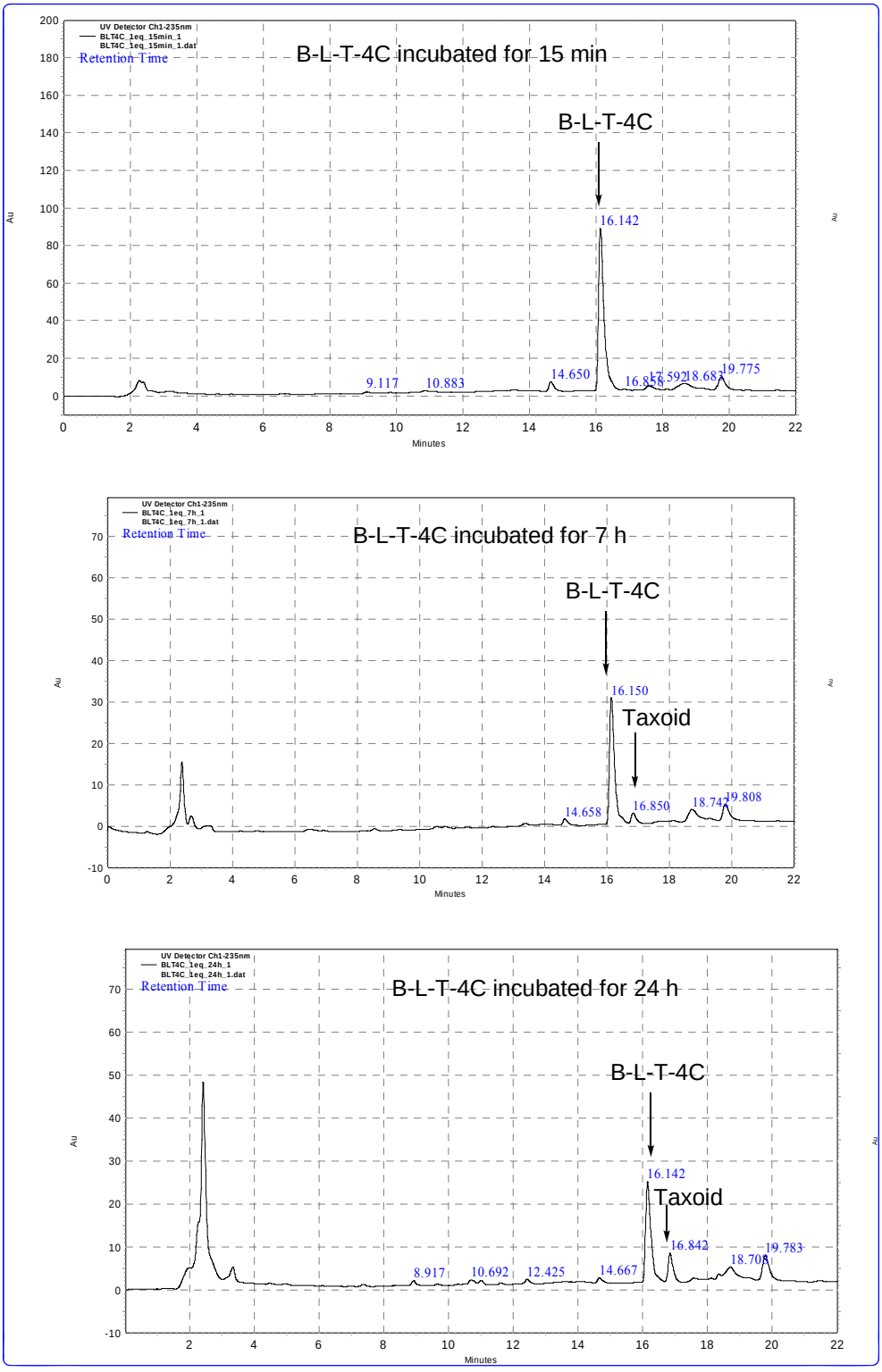

Figure 3-26. B-L-T-4C incubated in PBS with 1 eq GSH

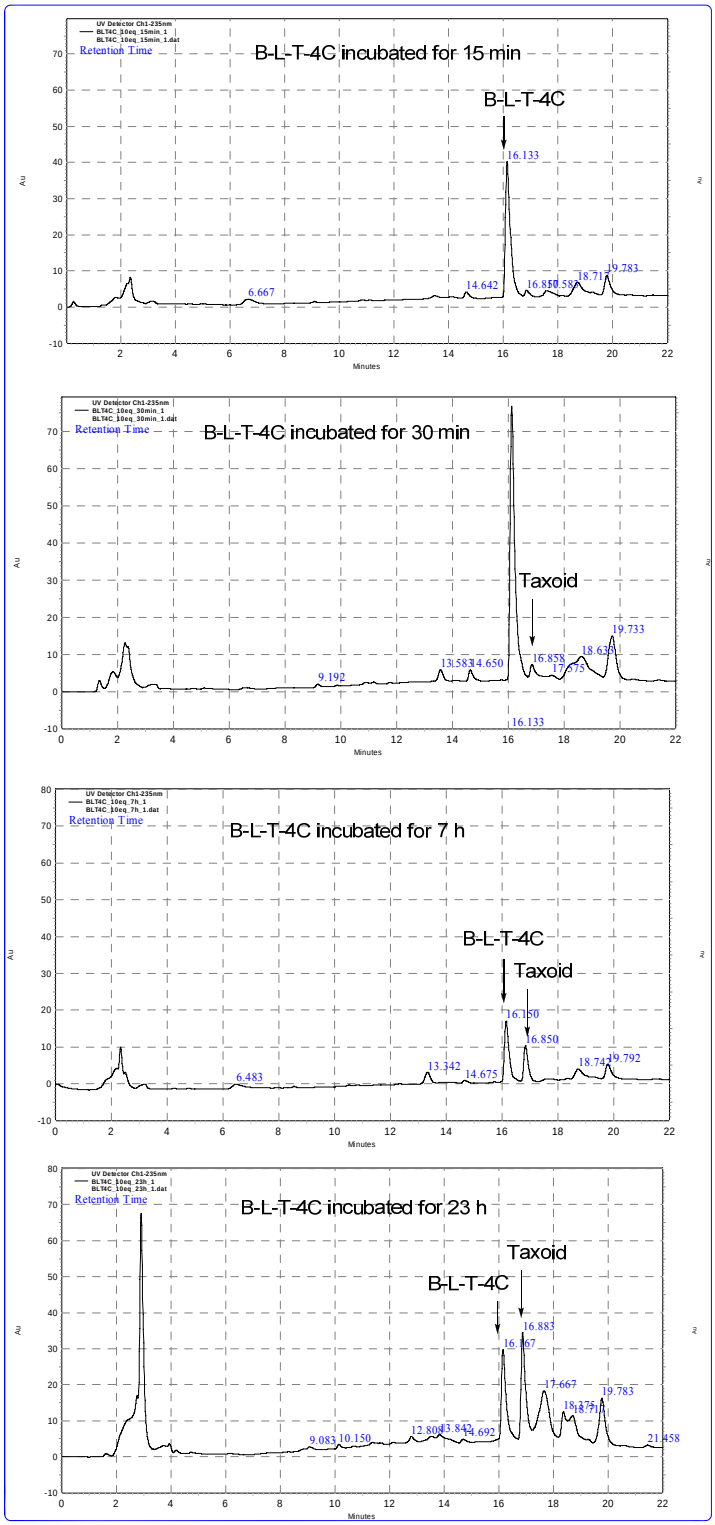

Figure 3-27. B-L-T-4C incubated in PBS with 10 eq GSH

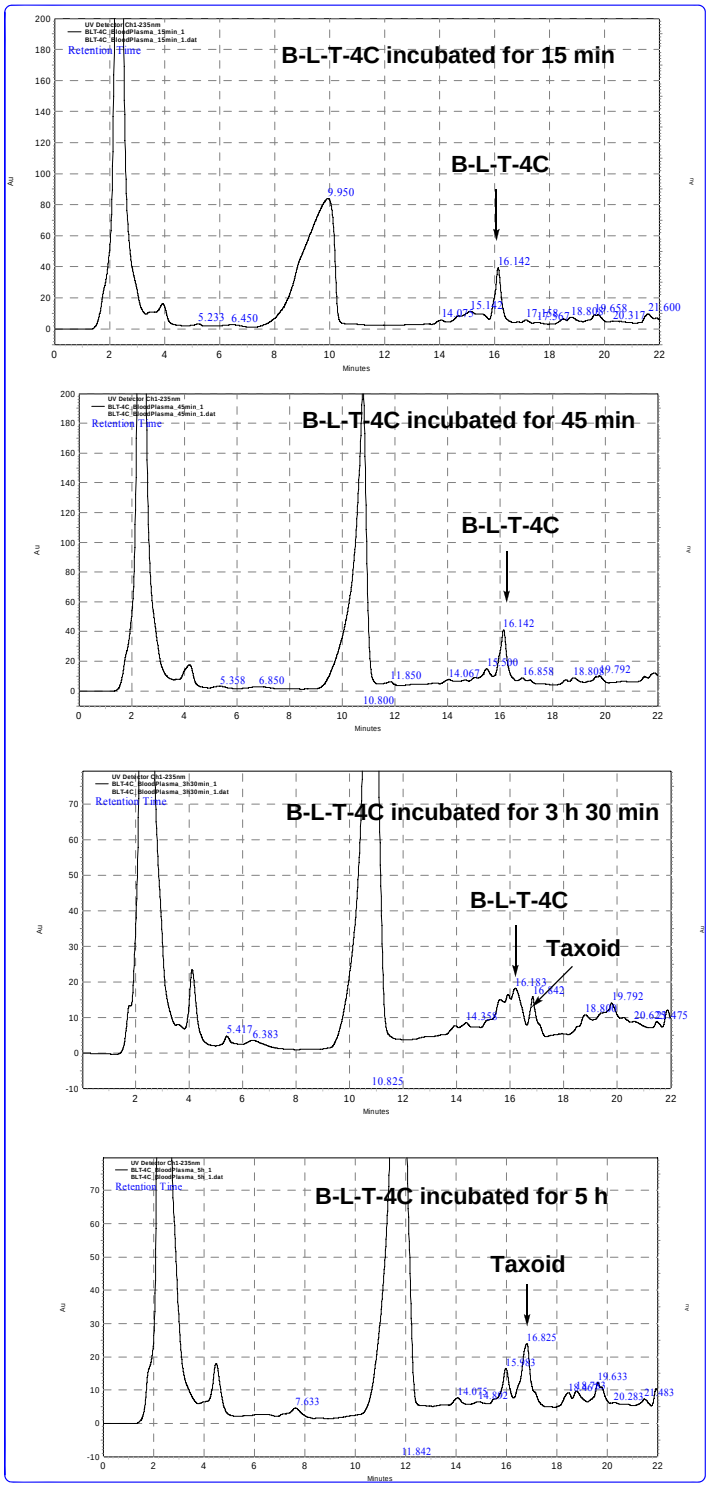

Figure 3-28. B-L-T-4C after incubation in blood plasma

When B-L-T-Me was incubated in PBS (pH 7.4) with 1 eq of GSH it was stable even after 6 h as shown in Figure 3-29.

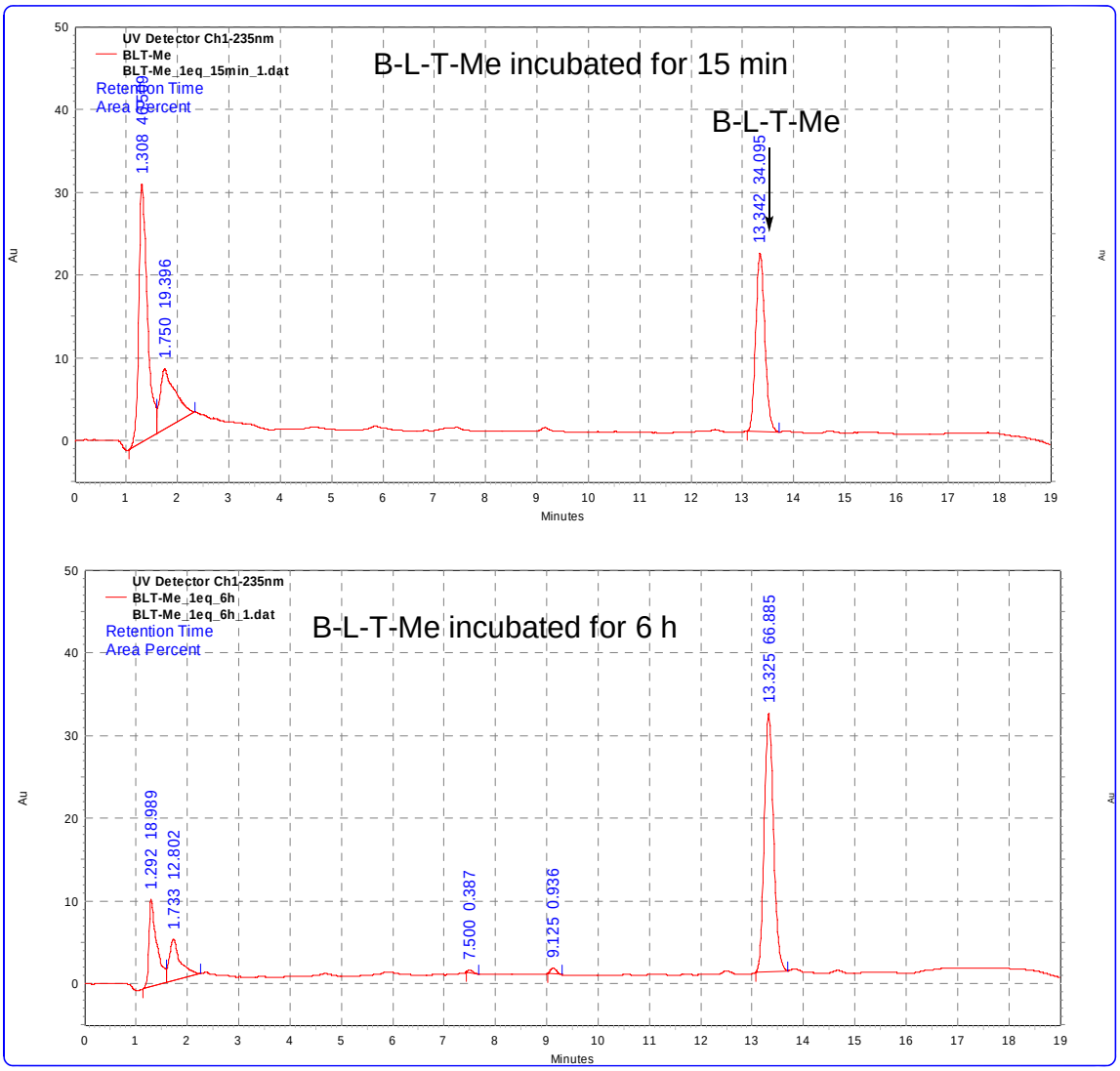

Figure 3-29. B-L-T-Me incubated in PBS with 1 eq GSH

When B-L-T-Me was incubated in PBS and 10 eq GSH there was a 2:1 ratio of conjugate to taxoid in 3 h and a 1:1 ratio in 6 h as shown in Figure 3-30. When this conjugate was incubated in blood plasma there was a 2:1 ratio of conjugate to drug in 4 h 20 min as shown in Figure 3-31.

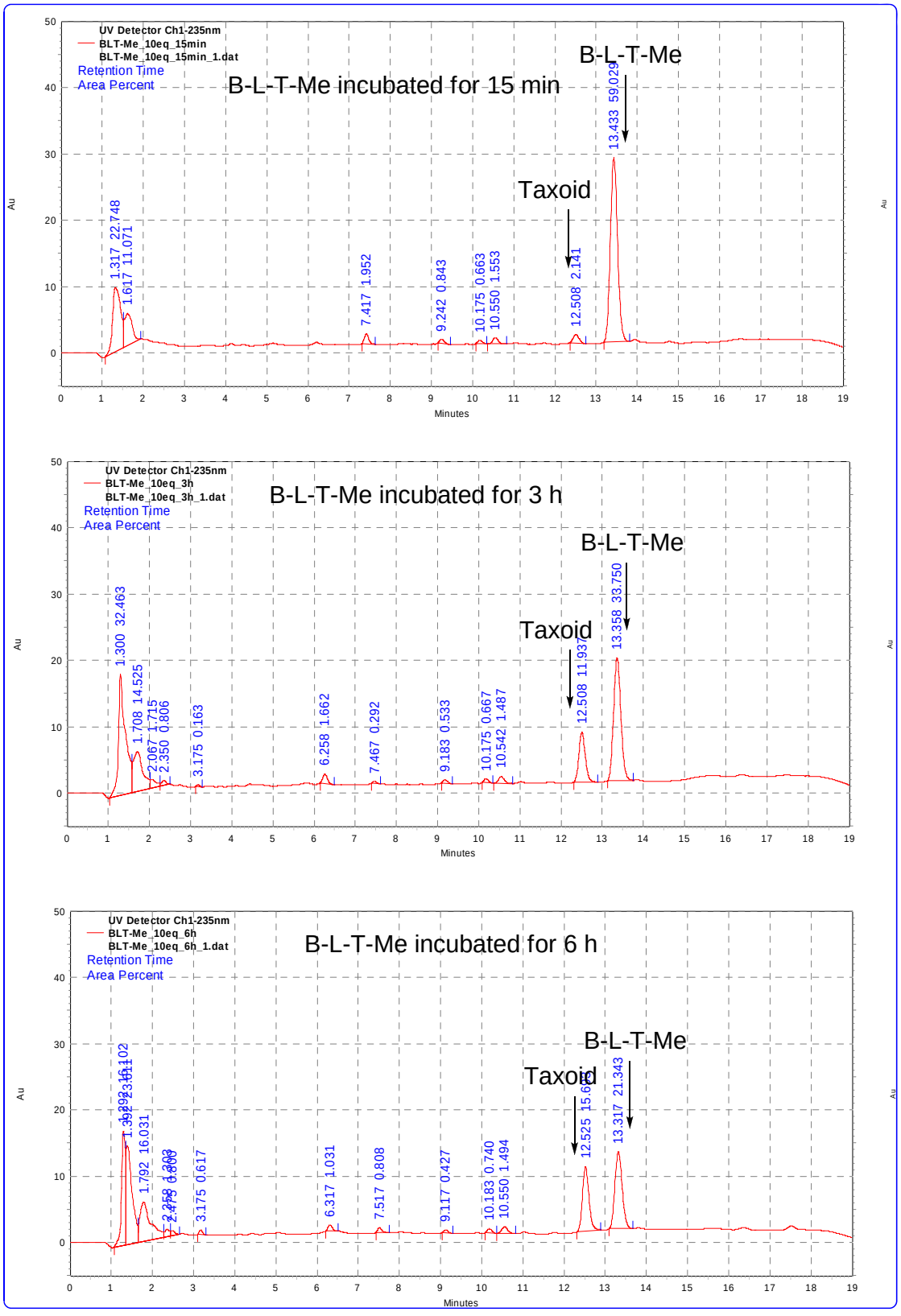

Figure 3-30. B-L-T-Me incubated in PBS with 10 eq GSH

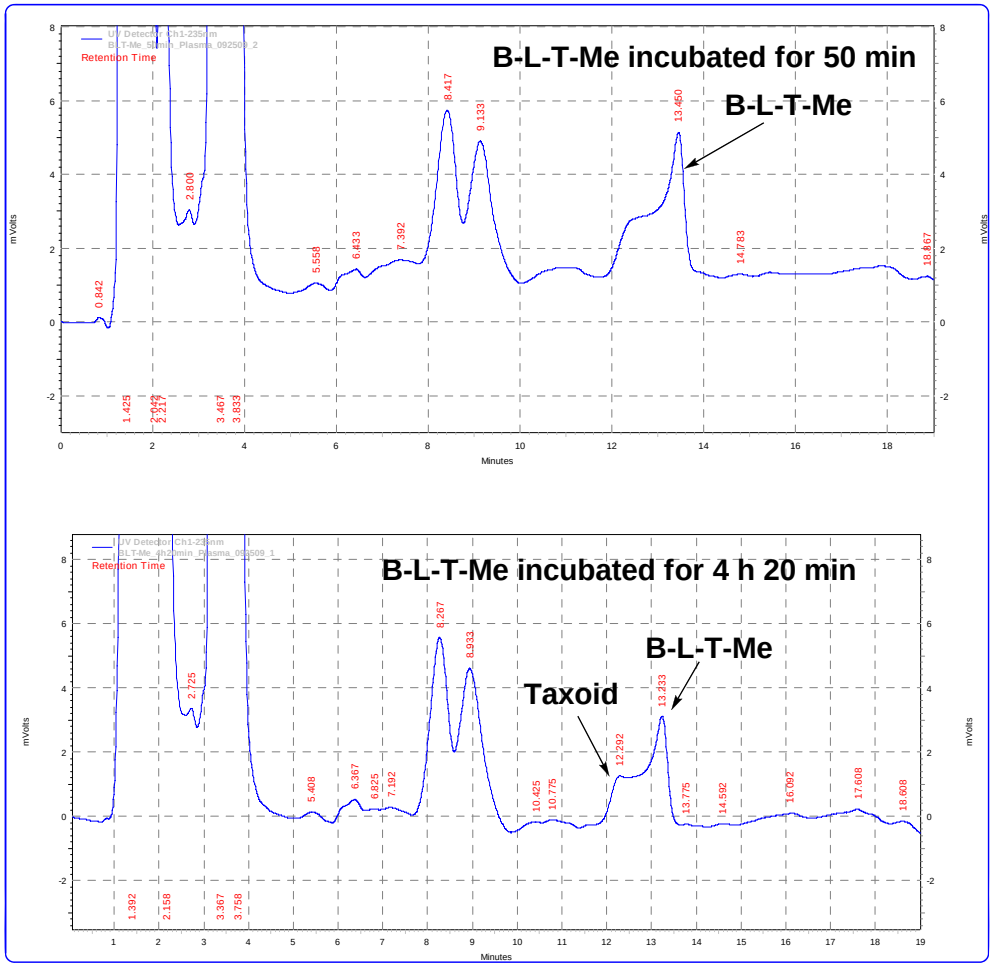

Figure 3-31. B-L-T-Me after incubation in blood plasma

3.5 Experimental Section

General Methods: ^{1}H, ^{13}C and ^{19}F NMR spectra were measured on a Bruker AC-250 NMR spectrometer or a Varian 300, 400, 500, or 600 MHz NMR spectrometer. The melting points were measured on a "Uni-melt" capillary melting point apparatus from Arthur H. Thomas Company, Inc. Optical rotations were measured on a Perkin-Elmer Model 241 polarimeter. High-resolution mass spectrometric analyses were conducted at the Mass Spectrometry Laboratory, University of Illinois at Urbana-Champaign, Urbana, IL. GC-MS analyses were performed on an Agilent 6890 Series GC system equipped with the HP-5HS capillary column, (50 m X 0.25 mm, 0.25 μm) and with the Agilent 5973 network mass selective detector. LC-MS analyses were carried out on an Agilent 1100 Series Liquid Chromatograph Mass Spectrometer. IR spectra were measured on a Shimadzu FTIR-8400s spectrophotometer. TLC analyses were performed on Merck DC-alufolien with Kieselgel 60F-254 and were visualized with UV light, iodine chamber, 10

% sulfuric acid and 10% PMA solution. Column chromatography was carried out on silica gel 60 (Merck; 230-400 mesh ASTM). Chemical purity was determined with a Waters HPLC assembly consisting of dual Waters 515 HPLC pumps, a PC workstation running Millennium 32, and a Waters 996 PDA detector, using a Phenomenex Curosil-B column, employing CH_3CN/water as the solvent system with a flow rate of 1 mL/min, or shimazu HPLC.

Materials: The chemicals were purchased from Sigma Aldrich Company or Acros Organic Fischer Company. 10-Deacetyl baccatin III (DAB) was donated by Indena, SpA, Italy. Dichloromethane and methanol were dried before use by distillation over calcium hydride under nitrogen or argon. Ether and THF were dried before use by distillation over sodium-benzophenone and kept under nitrogen or argon. Toluene and benzene were dried by distillation over sodium metal under nitrogen or argon before use. Dry DMF was purchased from EMD chemical company, and used without further purification. PURE SOLV™, Innovative Technology Inc, provided an alternative source of dry toluene, THF, ether, and dichloromethane. The glasses were dried in a 110 ^oC oven and allowed to cool to room temperature in a desiccator over "*Drierite*" (calcium sulfate) and assembled under inert gas nitrogen or argon atmosphere.

Benzo[b]thiophen-2(3H)-one (3-1):
Thianaphthene-2-boronic acid (1.81 g, 10 mmol) was dissolved in EtOH (17.5 mL) and hydrogen peroxide (30%, 3.3 mL) was added dropwise. The reaction mixture color changed from pink to reddish pink within 1 hr. The reaction mixture was stirred overnight at room temperature. TLC (eluant hexane/ethyl acetate 5:1) was performed. The reaction mixture was evaporated *in vacuo*. The reddish white crude residue was dissolved in saturated NaCl solution and extracted with chloroform (x3). The combined organic layer was dried over anhydrous $MgSO_4$ and concentrated *in vacuo*. The pure compound 4-8 was obtained as white solid by flash chromatography on silica gel (40:1 hexane/ethyl acetate) in 92 % yield (1.38 g). ^1H NMR (300 MHz, $CDCl_3$): δ 3.98 (s, 2 H), 7.2-7.4 (m, 4 H).

(2-Mercaptophenyl) acetic acid (3-2):
Benzo[b]thiophen-2(3H)-one (**3-1**) (953 mg, 6.35 mmol) was added in a flask which was inerted (vaccum/nitrogen) and dissolved with dry THF (c 0.2 M). Distilled water (6.3 mL) was added to the flask. (Both THF and water was degassed before addition). Lithium hydroxide monohydrate (6 eq) was dissolved in 25 mL distilled water and syringed into the flask. The reaction mixture was heated to 60 ^oC using an oil bath for 14 h (overnight). The reaction was checked by TLC (eluent hexane/ethyl acetate 2:1) the next day and stopped. The flask was cooled to room temperature and the reaction mixture was diluted with water (20 mL) and diethyl ether (45 mL). The organic and aqueous layer was separated and the yellow aqueous layer was acidified with 6N aqueous HCl to pH ~2. The aqueous layer became white on acidification and was extracted with diethyl ether (X 3). The combined organic layer was then washed with brine, dried over anhydrous $MgSO_4$ and concentrated *in vacuo*. The pure compound **3-2** was obtained by flash chromatography on silica gel (10:1 hexane/ethylacetate) in 95 % yield (1 g). ^1H NMR (300 MHz, $CDCl_3$): δ 3.49 (s, 1 H, S-H), 3.83 (s, 2 H on methylene carbon), 7.18-7.29

(m, 3 H), 7.41 (m, 1 H), 10.10 (b, 1 H), ^{13}C NMR (400 MHz, $CDCl_3$): δ 39.85, 126.94, 128.25, 130.74, 131.00, 132.41, 133.33, 176.16.

2-(2-Methyldisulfanylphenyl)acetic acid (3-3):
A flask containing **3-2** (93 mg, 0.55 mmol) was inerted. Degassed ethanol (3 mL) and water (0.78 mL) was added to dissolve the solid. Methyl methane thiosulfonate (MMTS) (1.1eq) was then added dropwise and the reaction was stirred overnight. The reaction was checked by TLC the next day (1:1 hexane/ethyl acetate). The reaction mixture was then diluted with ether and washed with 1N KOH solution (x 3). The combined yellow aqueous layers were then acidified with 5N HCl solution which becomes colorless on acidification. The aqueous layer was then extracted with DCM (x 3) and dried over anhydrous $MgSO_4$ and concentrated *in vacuo*. The pure compound **3-3** was obtained by flash chromatography on silica gel (10:1 hexane/ethylacetate) in 70 % yield (83 mg). ^{1}H NMR (400 MHz, $CDCl_3$): δ 2.41 (s, 3 H), 3.89 (s, 2 H), 7.2 (m, 1 H), 7.3 (m, 2 H), 7.76 (dd, 1 H).

4-Fluorophenyl 2-(2-methyldisulfanylphenyl)acetate (3-4):
A flask containing **3-3** (53 mg, 0.247 mmol), DMAP (0.5 eq) and *p*-fluorophenol (1.1 eq) was inerted. Anhydrous DCM (1 mL) was added to dissolve the solids and the flask was cooled to 0 0C using ice bath. DIC (1.5 – 2 eq) was added dropwise and the mixture was allowed to stir overnight and the flask was kept at room temperature. The reaction was checked by TLC the next day (5:1 hexane/ethyl acetate). The reaction mixture was filtered using Buchner funnel to remove the urea formed and concentrated *in vacuo*. The pure compound **3-4** was obtained by flash chromatography on silica gel (50:1 hexane/ethylacetate) in 90 % yield (69 mg, 97 % purity). ^{1}H NMR (300 MHz, $CDCl_3$): δ 2.43 (s, 3 H), 4.08 (s, 2 H), 7.05 (m, 4 H), 7.33 (m, 3 H), 7.79 (dd, 1 H).

Tosyl bromide (3-5):[54]
p-Methoxybenzenesulfonhydrazide (1.9 g, 0.01 mol) was taken in an Erhlenmeyer flask and dissolved in chloroform (20.5 mL). Few pieces of ice were added to the flask. Bromine (2 eq) was added in portions while vigorously stirring the reaction mixture. The orange color disappeared as the reaction proceeded and the temperature inside the flask was maintained at less than 10-15 ^{o}C. When the chloroform layer acquired a permanent orange color in ~ 30 min it was separated from the aqueous layer and washed with water. The chloroform was removed *in vacuo* and **3-5** was obtained as a white solid in 97 % yield (2.3 g, m.p. 93-96 ^{o}C). ^{1}H NMR (400 MHz, $CDCl_3$): δ 2.48 (s, 3H), 7.38 (d, 2H, J = 6.4 Hz), 7.87 (d, 2H, J = 6.3 Hz), ^{13}C NMR (400 MHz, $CDCl_3$): δ 21.81, 126.51, 130.08, 144.61, 146.72.

(*S*)-isopropyl 4-methylbenzenesulfonothioate (3-6):[55]
Tosyl bromide (1.2 eq, **3-5**) was taken in a flask which was inerted and 15 mL of carbontetrachloride was added to dissolve the solid. The reaction mixture was cooled to 0 ^{o}C and triethylamine (1.2 eq) was added to the flask. A solution of propan-2-thiol (0.18 mL, 2 mmol, 1 eq) was dissolved in 5 mL carbontetrachloride and added very slowly using addition funnel over a 30 min period. The mixture was stirred for 60 min and 50 mL of DCM was added to dissolve the yellowish white solid. This was then washed with

cold 5 % HCl (x 3), saturated $NaHCO_3$ (x 2), brine (x 1) and dried on anhydrous $MgSO_4$ and dried *in vacuo* to remove solvent and the thiol. The pure compound **3-6** was obtained by flash chromatography using silica gel (50:1 hexane/ethylacetate) as colorless liquid in 81 % yield (361 mg). ^{1}H NMR (400 MHz, $CDCl_3$): δ 1.28 (s, 3H), 1.30 (s, 3H), 2.43 (s, 3H), 3.46 (m, 1H), 7.32 (d, 2H, J = 8 Hz), 7.80 (d, 2H, J = 8 Hz), ^{13}C NMR (400 MHz, $CDCl_{3)}$: δ 21.55, 23.44, 42.48, 126.88, 129.72, 142.54, 144.50

2-(2-Isopropyldisulfanylphenyl)acetic acid (3-7):
A flask containing **3-2** (105 mg, 0.62 mmol) and **3-6** (1.1 eq) was inerted. Degassed ethanol (3.65 mL) and water (0.87 mL) was added to dissolve the solids. The reaction was stirred overnight at room temperature. The reaction was checked by TLC the next day (1:1 hexane/ethyl acetate). The reaction mixture was concentrated *in vacuo*. The pure compound **3-7** was obtained by flash chromatography on silica gel (10:1 hexane/ethylacetate) in 98 % yield (157 mg, 56-58 ^{o}C). ^{1}H NMR (400 MHz, $CDCl_3$): δ 1.27 (d, 6H, J = 6.8 Hz), 3.01 (m, 1H), 3.90 (s, 2H), 7.27 (m, 3H), 7.79 (d, 1H, J = 7.6 Hz), ^{13}C NMR (400 MHz, $CDCl_3$): δ 22.31, 38.86, 41.36, 127.24, 128.23, 129.64, 130.76, 132.66, 137.92, 177.38, HRMS: (EI+) *m/z* Calculated for $C_{11}H_{14}O_2S_2$: 242.0437 Found: 242.0435 (Δ = -0.2 ppm).

4-Fluorophenyl 2-(2-isopropyldisulfanylphenyl)acetate (3-8):
A flask containing **3-7** (75 mg, 0.31 mmol), DMAP (0.5 eq) and *p*-fluorophenol (1.1 eq) was inerted. Dry DCM (1.25 mL) was added to dissolve the solids and the flask was cooled to 0 ^{o}C using ice bath. DIC (1.5 – 2 eq) was added dropwise and the mixture was allowed to stir overnight and the flask was kept at room temperature. The reaction was checked by TLC the next day (5:1 hexane/ethyl acetate). The reaction mixture was filtered using frit funnel to remove the urea formed and concentrated *in vacuo*. The pure compound **3-8** was obtained as colorless oil by flash chromatography on silica gel (45:1 hexane/ethylacetate) in 95 % yield (98 mg, 97 % purity). ^{1}H NMR (400 MHz, $CDCl_3$): δ 1.30 (d, 6H, J = 6.8 Hz), 3.06 (m, 1H), 4.1 (s, 2H), 7.05 (m, 4H), 7.30 (m, 3H), 7.83 (d, 1H, J = 8 Hz), ^{13}C NMR (400 MHz, $CDCl_3$): δ 22.33, 39.23, 41.40, 115.81, 116.05, 122.79, 122.88, 127.41, 128.23, 129.77, 130.81, 132.95, 137.73, 146.55, 146.58, 158.95, 161.38, 169.42, ^{19}F NMR (400 MHz, $CDCl_3$): δ -67.23 (m, 1F), HRMS: (EI+) *m/z* Calculated for $C_{17}H_{17}O_2S_2F$: 336.0654 Found 336.0654: (Δ = 0.0 ppm).

(*S*)-*tert*-butyl 4-methylbenzenesulfonothioate (3-9):[55]
Tosyl bromide (1.2 eq, **3-5**) was taken in a flask which was inerted and 15 mL of carbontetrachloride was added to dissolve the solid. The reaction mixture was cooled to 0 ^{o}C and triethylamine (1.2 eq) was added to the flask. A solution of 2-methylpropan-2-thiol (0.22 mL, 2 mmol) was dissolved in 5 mL carbontetrachloride and added very slowly using addition funnel over a 30 min period. The mixture was stirred for 45 min and 50 mL of DCM was added to dissolve the yellowish white solid. This was then washed with cold 5 % HCl (x 3), saturated $NaHCO_3$ (x 2), brine (x 1) and dried on anhydrous $MgSO_4$ and dried *in vacuo* to remove solvent and the thiol. The pure compound 5-2 was obtained by flash chromatography using silica gel (50:1 hexane/ethylacetate) as white solid in 69 % yield (329 mg, m.p 67-68 ^{o}C). ^{1}H NMR (300

MHz, $CDCl_3$): δ 1.44 (s, 9H), 2.43 (s, 3H), 7.31 (d, 2H, J = 8.1 Hz), 7.83 (s, 2H, J = 8.7 Hz), ^{13}C NMR (400 MHz, $CDCl_3$): δ 21.60, 30.80, 55.12, 127.00, 129.62, 143.97, 144.28.

2-(2-*tert*-Butyldisulfanylphenyl)acetic acid (3-10):
A flask containing **3-2** (105 mg, 0.62 mmol) and **3-9** (1.1 eq) was inerted. Degassed ethanol (200 proof, 3.68 mL) and water (0.88 mL) was added to dissolve the solids. The reaction was stirred overnight at room temperature. The reaction was checked by TLC the next day (1:1 hexane/ethyl acetate). The reaction mixture was then diluted with ether and washed with 1N KOH solution (x 3). The combined yellow aqueous layers were then acidified with 5N HCl solution which becomes colorless on acidification. The aqueous layer was then extracted with DCM (x 3) and dried over anhydrous $MgSO_4$ and concentrated *in vacuo*. The pure compound **3-10** was obtained by flash chromatography on silica gel (10:1 hexane/ethylacetate) in 36 % yield (57 mg, m.p. 71-73 ^oC). ^1H NMR (300 MHz, $CDCl_3$): δ 1.26 (s, 9H), 3.91 (s, 2H), 7.18 (m, 2H), 7.29 (m, 1H), 7.84 (d, 1H, J = 9 Hz), ^{13}C NMR (400 MHz, $CDCl_3$): δ 29.75, 38.84, 49.35, 126.74, 128.10, 128.76, 130.65, 131.78, 138.42, 177.51, HRMS: (EI+) *m/z* Calculated for $C_{12}H_{16}O_2S_2$: 256.0592 Found: 256.0592 (Δ = 0.0 ppm)

4-Fluorophenyl 2-(2-*tert*-butyldisulfanylphenyl)acetate (3-11):
A flask containing **3-10** (40 mg, 0.15 mmol), DMAP (0.5 eq) and *p*-fluorophenol (1.1 eq) was inerted. Anhydrous DCM (0.64 mL) was added to dissolve the solids and the flask was cooled to 0 ^oC using ice bath. DIC (1.5 – 2 eq) was added dropwise and the mixture was allowed to stir overnight and the flask was kept at room temperature. The reaction was checked by TLC the next day (5:1 hexane/ethyl acetate). The reaction mixture was filtered using frit funnel to remove the urea formed and concentrated *in vacuo*. The pure compound **3-11** was obtained as a colorless oil by flash chromatography on silica gel (45:1 hexane/ethylacetate) in 95 % yield (98 mg, 98 % purity). ^1H NMR (400 MHz, $CDCl_3$): δ 1.29 (s, 9H), 4.11 (s, 2H), 7.05 (m, 4H), 7.263 (m, 3H), 7.87 (d, 1H, J = 8 Hz), ^{13}C NMR (400 MHz, $CDCl_3$): δ 24.57, 29.83, 39.19, 49.37, 115.82, 116.05, 122.81, 122.89, 126.95, 128.01, 129.00, 130.70, 132.17, 138.24, 146.57, 146.59, 158.96, 161.39, 169.39, ^{19}F NMR (300 MHz, $CDCl_3$): δ -67.24 (m, 1F), HRMS: (EI+) *m/z* Calculated for $C_{18}H_{19}O_2S_2F$: 350.0810 Found: 350.0811 (Δ = 0.1 ppm).

2-(2-Pyridin-2-yldisulfanylphenyl)acetic acid (3-12):
A flask containing **3-2** (46 mg, 0.27 mmol) was inerted and dry THF (c 0.1 M) was added to dissolve it. A solution of dithiodipyridine (2 eq, 0.54 mmol) in dry THF (c 0.1 M) was then added dropwise to the reaction flask and stirred overnight. The reaction mixture was concentrated *in vacuo* and the pure compound **3-12** was obtained by flash chromatography on neutral alumina (DCM/MeOH 5 % /Acetic acid 3 %) and then another silica gel column (2:1 hexane/ethylacetate) in 52 % yield (40 mg) m.p. 117-118 ^oC). ^1H NMR (300 MHz, $CDCl_3$): δ 4.01 (s, 2 H), 7.10 (m, 1 H), 7.26 (m, 3H), 7.64 (m, 3 H), 8.46 (dd, 1 H), ^{13}C NMR (400 MHz, $CDCl_3$): δ 39.05, 120.24, 121.11, 128.06, 128.64, 129.67, 130.93, 133.29, 136.10, 137.48, 149.39, 159.18, 176.10. HRMS: (EI+) *m/z* Calculated for $C_{13}H_{11}O_2NS_2$: 277.0231 Found: 277.0231 (Δ = 0.0 ppm).

4-Fluorophenyl 2-(2-pyridin-2-yldisulfanylphenyl)acetate (3-13):

A flask containing **3-12** (40 mg, 0.14 mmol), DMAP (0.5 eq) and p-fluorophenol (1.1 eq) was inerted. Anhydrous DCM (1 mL) was added to dissolve the solids and the flask was cooled to 0 ^{o}C. DIC (1.5 – 2 eq) was added dropwise and the mixture was allowed to stir overnight at room temperature. The reaction was monitored by TLC (5:1 hexane/ethyl acetate). The reaction mixture was filtered using Buchner funnel to remove the urea formed and concentrated *in vacuo*. The pure compound **3-13** was obtained by flash chromatography on silica gel (50:1 hexane/ethylacetate) in 46 % yield (24.6 mg). ^{1}H NMR (300 MHz, $CDCl_3$): δ 4.18 (s, 2 H), 7.08 (m, 5 H), 7.30 (m, 3H), 7.58 (m, 2 H), 7.70 (m, 1 H), 8.47 (dd, 1 H), ^{13}C NMR (300 MHz, $CDCl_3$): δ 39.36, 115.86, 116.17, 120.03, 121.05, 122.81, 122.92, 128.16, 128.51, 128.71, 129.85, 130.88, 131.01, 133.27, 136.19, 137.24, 149.61, 158.62, 159.18, 161.86, 169.38, ^{19}F NMR (300 MHz, $CDCl_3$): δ -67.05 (m, 1 F).

Chapter 4
Tumor-targeted Drug Delivery using Folate as the Tumor-targeting Moiety

4.1 Introduction

4.1.1 Tumor-targeted Drug Delivery

Despite the significant progress that has been made in the development of treatments and therapies for treating cancer, there is still no common cure for patients afflicted with this malignant disease. The most common forms of treatments used for treating patients suffer from many drawbacks. A long-standing problem associated with chemotherapy is the lack of specificity for tumors. Traditional chemotherapy relies on the premise that rapidly proliferating cancer cells will preferentially be killed over the normal cells by the cytotoxic agents used in chemotherapy. It has been reported that in cancer patients whose disease has spread there are about one trillion cells or 10^{12} cells. It is well established that it is necessary to kill at least 99% of these cells i.e. a two-log or greater reduction of these neoplastic cells is required to achieve complete remission. Thereafter, continued treatment during remission is required to completely eradicate the tumor.[1, 2] Unfortunately, clinically used chemotherapeutic agents have very little or no specificity for the tumor cells over other actively proliferating normal cells. Therefore the levels of drug required to destroy sufficient number of tumor cells to achieve the state of complete remission in cancer patients as well as maintain such a state leads to significant systemic toxicity towards rapidly proliferating non-malignant or normal cells. This results in severe undesirable side effects such as hair loss, damage to bone marrow, liver, kidney, gastrointestinal tract, etc. Also tumors which are young or more differentiated will be affected more by these cytotoxic chemotherapeutic agents than older tumors where the differentiation is typically lost. Experimental evidence also suggests that there are other factors such as drug-resistant cells, stem cells, pharmacological barriers, etc that have to be negotiated to overcome the final hurdle to achieve almost complete to complete eradication of the tumor. Thus it is required to develop new delivery methods for cytotoxic agents which will have better selectivity for tumor cells to avoid the collateral damage associated with their uptake by the healthy cells. Therefore, several drug delivery protocols and systems have been explored in the past few decades.

Cancer cells originate from the host unlike bacteria and viruses and thus do not contain molecular targets that are completely foreign to the host. However, it is important to recognize that there are inherent morphological and physiological differences between malignant and normal cells which can be potentially exploited to design an effective tumor-targeted drug delivery system which can be selective towards the cancer cells. The tumor-targeting approach can be broadly divided into two categories – a) passive tumor-targeting and b) active tumor-targeting. Passive tumor targeting relies on the accumulation of macromolecules in the tumor tissue by means of nonspecific trapping of such molecules in the tumor interstitium.[3] Active tumor targeting relies on the effective binding of ligands carrying cytotoxic drugs to the tumor-specific receptors overexpressed on the tumor cells.

The rapidly growing tumor cells have unique growth characteristics like rapid growth rate and ability to metastasize to distant sites in the body and hence require quick formation of new blood vessels to sustain such growth. The solid tumor has various vascular mediators which results in a defective tumor vasculature. The defective tumor vasculature allows macromolecules and lipids to easily enter the extravascular space in the tumors and the undeveloped and suppressed lymphatic drainage system in the tumors cannot release these macromolecules and lipids which are effectively retained inside the tumor tissues. It is reasonable to assume that the large interstitial space in tumors possibly serves as a reservoir for these macromolecules which can accumulate in this space and enhance vascular permeability and thus contribute to specific affinity for tumor cells.[4] The enhanced vascular permeability is considered to meet the enhanced nutritional demand as well as demand for oxygen by these actively growing cancer cells. This phenomenon was first described by Maeda *et. al.* in 1986 and is termed "*enhanced permeability and retention*" (EPR) effect.[5, 6] Almost all human cancers with the exception of hypovascular tumors such as prostate cancer or pancreatic cancer exhibit EPR effect.[7]

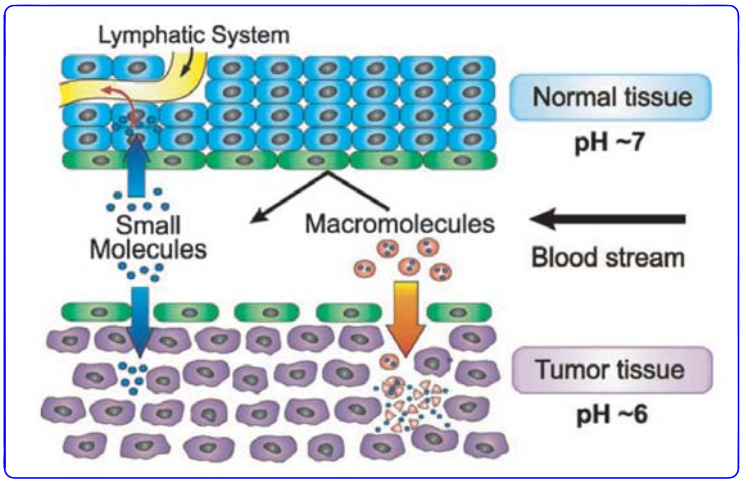

Figure 4-1. Schematic representation of EPR effect[8] (Adapted from Ref. 8)

The EPR effect is thus critical in the targeted delivery of macromolecular anticancer drugs to the tumor whose impaired lymphatic system can hamper the clearance of these drugs and retain them for a long time inside the tumor. The EPR effect is regarded as a "gold standard" in designing targeted anticancer drugs.[9-12] Extensive studies indicate that tumor blood flow appears to be an irregular event – blood flow in tumor can be seen only once in 15-20 min, then stops for a while or runs in the opposite direction which is in contrast to the normal organs or tissues.[13-15] Biocompatible macromolecules which have an average molecular size greater than 45 kDa accumulate at a much higher concentrations (> 6-fold) in tumor tissues than in normal tissues and in even much higher concentrations than in plasma.[9, 10, 16, 17] Thus while most conventional low molecular weight drugs have short plasma half-lives it takes about 6 h or longer for drugs in circulation to exert EPR effect. This requires drug candidates to have a large molecular weight which is above the renal clearance threshold so that it can circulate for a longer time.[5]

An actively developing tumor requires various vitamins and nutrients and therefore to meet the increased demand tumor cells overexpress many tumor-specific receptors. The lack of overexpressed tumor specific markers on the normal cells compared to the tumor cells forms the basis for active tumor targeting.[18] The logical outcome of this interesting difference between tumor cells and normal cells was to exploit the binding specificity of various ligands to these receptors or biomarkers. The basic approach to the design of a tumor-targeted drug delivery system is the conjugation of an anticancer drug to the tumor-specific molecule which renders the drug inactive till it reaches the tumor site. One of the important physiological characteristics of cancer cells is their enhanced metabolic rate which results in hypoxicity inducing anaerobic metabolism, resulting in lactate formation and thereby lowering the intracellular pH.[19, 20] Thus numerous conjugates can be designed which can release the cytotoxic agent upon acidification. These tumor-specific drug conjugates can be construed as molecular Trojan horse which can get internalized specifically inside the tumor cells. The basic principle of

these tumor-targeting drug delivery systems is that these tumor-targeting conjugates or prodrugs should be initially inactive. Once they reach the tumor site the tumor-targeting module then tightly bind to the specific receptor overexpressed on the surface of the tumor cells and get internalized via various mechanisms such as endocytosis and transcytosis. Thus these conjugates should have minimal systemic toxicity while in circulation. Once these prodrug conjugates are internalized the active drugs are liberated in their original potent form.

Conventionally, prodrugs have been designed to improve oral delivery by making the prodrug more water soluble or to overcome other physiological barriers such as rapid metabolism, etc with the expectation that improving the pharmacokinetic properties of the original drug will result in elevated levels of the drug in circulation and thus enhanced levels at the target site. Usually a tumor-targeted drug conjugate or "guided molecular missile"[21] (Figure 4-2) consists of a) tumor-targeting module b) missile or warhead (anticancer drug) and c) linker.

Figure 4-2. Tumor-targeting drug conjugate

Once the tumor-targeting conjugate is tightly bound to the receptor on the surface of the tumor cells it is then internalized via receptor mediated endocytosis. This process which involves several steps is illustrated in Figure 4-3. In the first step the drug conjugate binds to the tumor receptor and is internalized to form a vesicle coated by clathrin which is later removed by depolymerization. The uncoated vesicle thus formed fuses with an endosome in the cell to form an 'early endosome'. As the endosome matures the pH value gradually drops from 7 to ~5 in the late endosome stage. This drop in pH causes the receptor to change configuration and release the conjugate. Sometimes the receptor recycles back to the membrane to ferry in more of the conjugate. The fate of the rest of the conjugate is determined during a sorting process within the late endosome stage. The cytotoxic warhead is released from the conjugate by various mechanisms such as acid catalyzed hydrolysis, enzymatic hydrolysis, disulfide exchange, etc depending on the type of linker used.

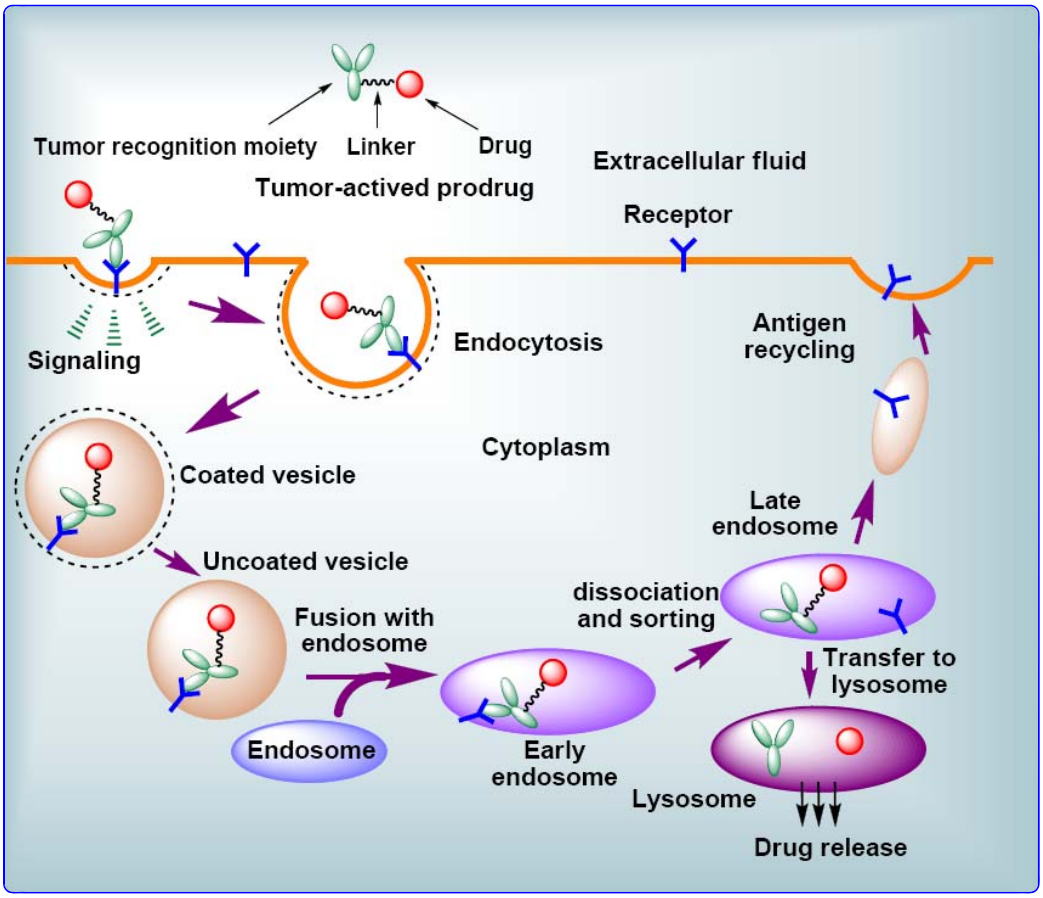

Figure 4-3. Schematic representation of receptor mediated endocytosis[22] (Adapted from Ref. 22)

The efficacy of such drug conjugates depend on several factors such as the efficiency of the targeting moiety, stability of the whole conjugate while in circulation, efficient release mechanism that regenerates the parent cytotoxic drug and potency of the drug. It is crucial for the tumor-targeting conjugate to possess a good pharmacokinetic profile, a broad therapeutic window and optimal biodistribution. Additionally, a key parameter to take into consideration is optimal drug loading per conjugate to maximize the number of drug molecules that can be safely internalized since there are only a limited number of receptors on the cancer cell surface.

4.1.2 Tumor-targeting Modules

Tumor-targeting drug delivery methods have received a lot of attention in the past few decades[23, 24] as it attempts to develop effective cures for cancer by trying to ameliorate the negative effects of chemotherapy. Several tumor-targeting and tumor specific moieties such as monoclonal antibodies,[22, 25-29] folic acid,[30-32] biotin,[33, 34] aptamers,[35, 36] oligopeptides,[37] hyaluronic acid,[38, 39] polyunsaturated fatty acids,[40, 41] etc (Figure 4-4) have been applied as tumor-targeting modules to construct "guided molecular missiles".

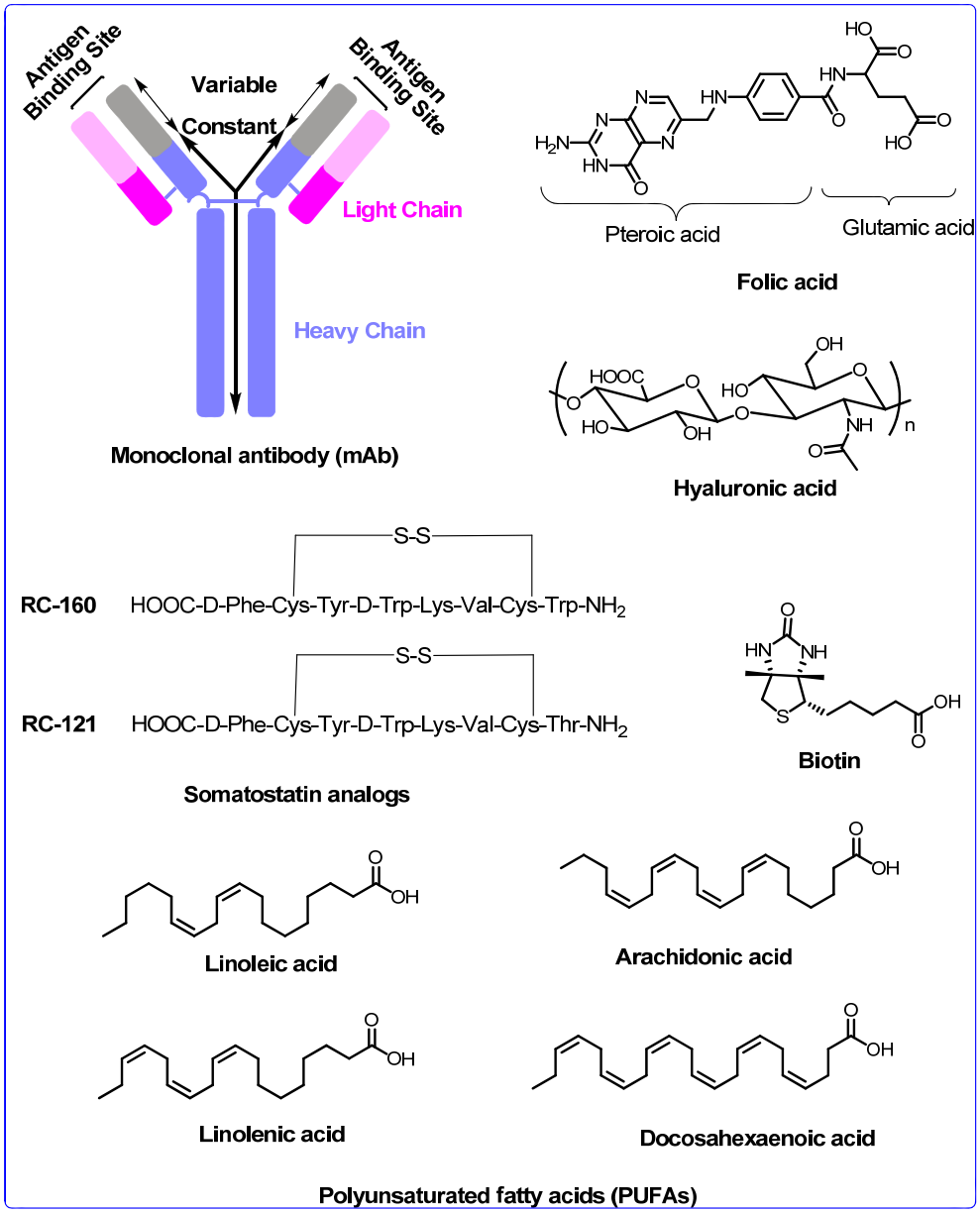

Figure 4-4. Tumor-targeting modules

Paul Ehrlich suggested the use of antibody conjugated to diphtheria toxins as far back as the early 1900s.[42] The discovery of antigens which are overexpressed on the surface of cancer cells opened up promising opportunities for tumor-targeted therapy. Early efforts towards this goal were hindered due to the technical difficulty in obtaining appropriate antibodies. However, pioneering work by Kohler and Milstein[43] on monoclonal antibodies (mAbs) using hybridoma technology significantly accelerated the progress in mAb-based cancer therapy. Monoclonal antibodies (mAbs) have a high binding specificity to tumor-specific antigens and thus can be used as a vehicle to deliver

cytotoxic drugs selectively inside the cancer cells. The high binding affinity of mAbs to their respective antigens makes them an attractive target because this would allow localization and retention of the drug in high concentrations at the tumor site. Eventually the mAb moiety carrying the drug payload binds to the tumor specific antigens on the cancer cells and gets internalized and subsequently the parent drug is released inside the cancer cells. Also, the long circulation time of the antibodies increases the probability of the drug to reach the tumor site. A mAb has a characteristic general structure consisting (Figure 4-4) of two light chains (25 kDa each) and two heavy chains connected by disulfide bonds (50 kDa each).

The therapeutic effects of the early mAb-drug conjugates were severely impaired because the murine antibody derived from the hybridoma technology caused human antimouse antibody (HAMA) response which resulted in the rapid clearance of these conjugates from the body. Accordingly, recombinant DNA protocol was developed to produce generations of chimeric and humanized mAbs which had decreased immunogenicity.[44] Also, large mAb conjugates impaired efficacy because of poor penetration in solid tumors which led to the development of truncated mAb which can penetrate into solid tumors much faster.[45-47] However, these truncated mAbs are cleared more rapidly in circulation but chA7Fab-neocarzinostatin bearing a truncated mAb fragment exhibited significantly better antitumor activity than A7-neocarzinostatin with whole mAb against human pancreatic carcinoma xenograft in nude mice.[48] Currently humanized antibodies which are generated by grafting the complementarity determining region (CDR) from a mouse mAb into a human IgG are most commonly used. The binding affinity of these humanized mAbs are also fully preserved as compared to the original murine mAb.[49]

The warhead or cytotoxic drug used in these immunoconjugates should be very potent (toxicity in the subnanomolar range) to be effective in humans[18, 50] because only a limited number of molecules can be loaded on the mAb without reducing its binding affinity. Another reason for using a highly potent cytotoxic drug is that there are only a limited number of antigens expressed on the surface of the tumor cells. During the early development stages of these mAb-drug conjugates several drugs such as vinca alkaloids,[51] vinblastine,[52] methotrexate,[28] mitomycin,[53] etc were linked to the mAbs but none of them showed any appreciable anticancer efficacy *in vivo*. This failure was attributed to the moderate cytotoxicity of the drugs used in these conjugates and consequently extremely cytotoxic agents such as calicheamicin,[54] second-generation taxoid,[27] monomethylauristatin E,[55] maytansine derivative DM1,[56] C-1065,[57] etc were used. Mylotarg® (gemtuzumab-ozogamicin) which has an anti-CD33 antibody (hP 67.6) conjugated to calicheamicin[54] (Figure 4-5) was the first mAb-drug immunoconjugate approved by the Food and Drug Administration (FDA) in 2000 for the treatment of acute myelogenous leukemia (AML). Several other mAbdrug conjugates, including maytansinoid-bearing huC242-DM1,[56] huN901-DM1,[58] MLN2704-DM1,[58] herceptin-DM1,[58] anti-CD44v6 antibody-DM1,[58] BR96–doxorubicin[59] and CTM01-calicheamicin,[60] are currently under human clinical trials.

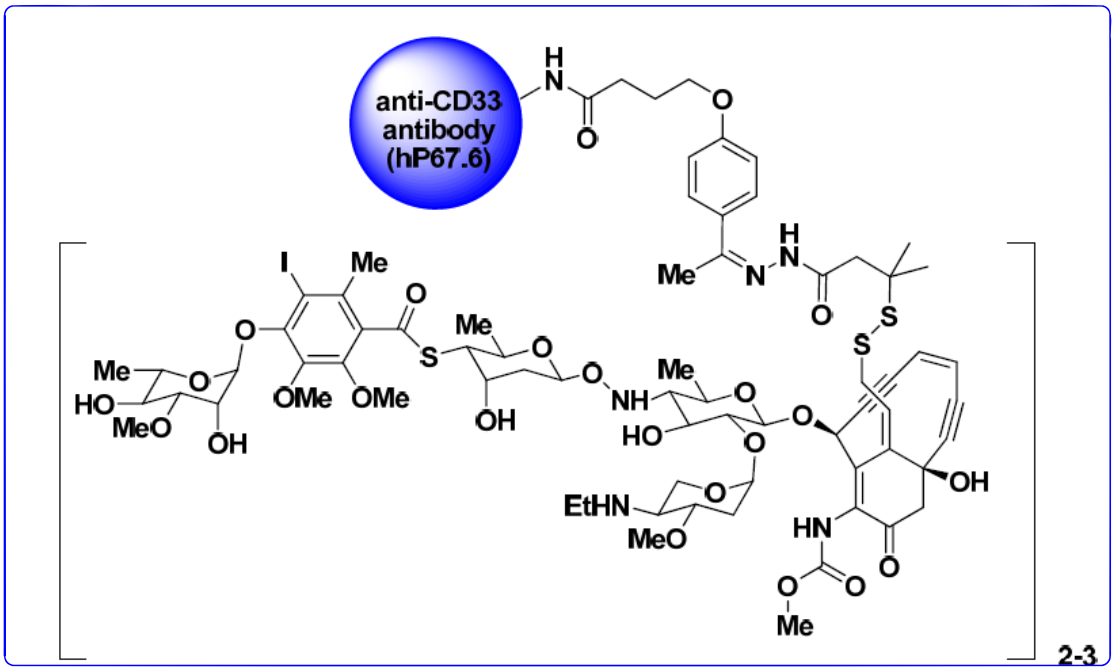

Figure 4-5. Mylotarg® (gemtuzumab-ozogamicin)

Hyaluronic acid or hyaluronan (HA) has a linear, negatively charged polysaccharide (Figure 4-4) with alternating units of D-glucuronic acid and *N*-acetyl-D-glucosamine. It is responsible for a wide range of physiologically important functions such as cell growth, cell differentiation, cell migration,[61] etc as is evidenced by the large number of HA-binding receptors such as cell surface glycoprotein CD44 (associated with lymphocyte activation), receptor for hyaluronic acid-mediated motility (RHAMM), hyaluronic acid receptor for endocytosis (HARE), lymphatic vessel endocytic receptor (LYVE-1), and also intracellular HA-binding proteins including CDC37, RHAMM/IHABP, P-32, and IHABP4.[62, 63] Various cancer cells have an elevated level of HA which is believed to be responsible for forming a less dense matrix enhancing the motility of the cell as well as its invasive ability into other tissues.[64, 65] Numerous tumors like ovarian, colon, epithelial, stomach, etc overexpress HA-binding receptors like CD44[66] and RHAMM[67] and consequently exhibit enhanced binding and internalization of HA.[68] While overexpression of hyaluronic acid synthases increases the HA level causing accelerated tumor growth and metastasis,[69, 70] exogenous oligomeric HA inhibits tumor progression most likely by competing with endogenous polymeric HA.[71] Although the mechanism of HA-CD44 is not fully understood studies show that larger oligomers (≥ HA_{20}) have higher binding affinity than smaller oligomers due to simultaneous multiple interactions with more than one CD44 receptor.[66, 71, 72]

Consequently, the high tumor specificity and exceptional biocompatibility of HA make it a desirable targeting module which can be coupled to potent anticancer drugs either directly or via a suitable polymer. HA has been directly conjugated to low molecular weight drug such as paclitaxel[39] and doxorubicin.[38] It has been shown that these conjugates are internalized into the cancer cells via receptor-mediated endocytosis

and subsequent intracellular liberation of the potent drug. As with the mAb immunoconjugates the efficacy of these HA bioconjugates depend on the amount of loading of the cytotoxic agent. Cytotoxicity of highly loaded drugs on the HA conjugates has been found to be weaker than that of the drug alone.[73] Several tumor-targeting drug delivery systems such as HA-containing liposomes with entrapped doxorubicin[74] (DOX) and N-(2-hydroxypropyl) methacrylamide (HPMA) copolymer-hyaluronan-doxorubicin[38] (HPMA-HA-DOX) bioconjugates have been reported. The degree of HA-liposome uptake by murine melanoma tumor cell line (B16F10) was proportional to the loading of HA in the 0 - 3 mol % range. Even loading as low as 0.1 mol % HA showed selective tumor-targeting. The HA-containing DOX liposomes showed almost one order of magnitude better cytotoxicity than the drug alone and more than two orders of magnitude better activity than non-targeting liposomes against B16F10 cells. Additionally, the HA-containing DOX liposomes were not cytotoxic to CV-1 cells with a low level of CD44 expression. HPMA-HA-DOX bioconjugate demonstrated better internalization and cytotoxicity as compared to non-targeting HPMA-DOX conjugate against human breast cancer (HBL-100), ovarian cancer (SKOV-3), and colon cancer (HCT-116) cells. The IC_{50} value of HPMA-HA-DOX against HBL-100 (breast) cell line was 0.52 μM for 36 wt % loading of HA, which is more than one order of magnitude better than that of non-targeting HPMA-DOX (18.7 μM). It was also found that the systemic toxicity of HPMA-HA-DOX to the primary cells of murine fibroblast was low (IC_{50} =21.2 μM).

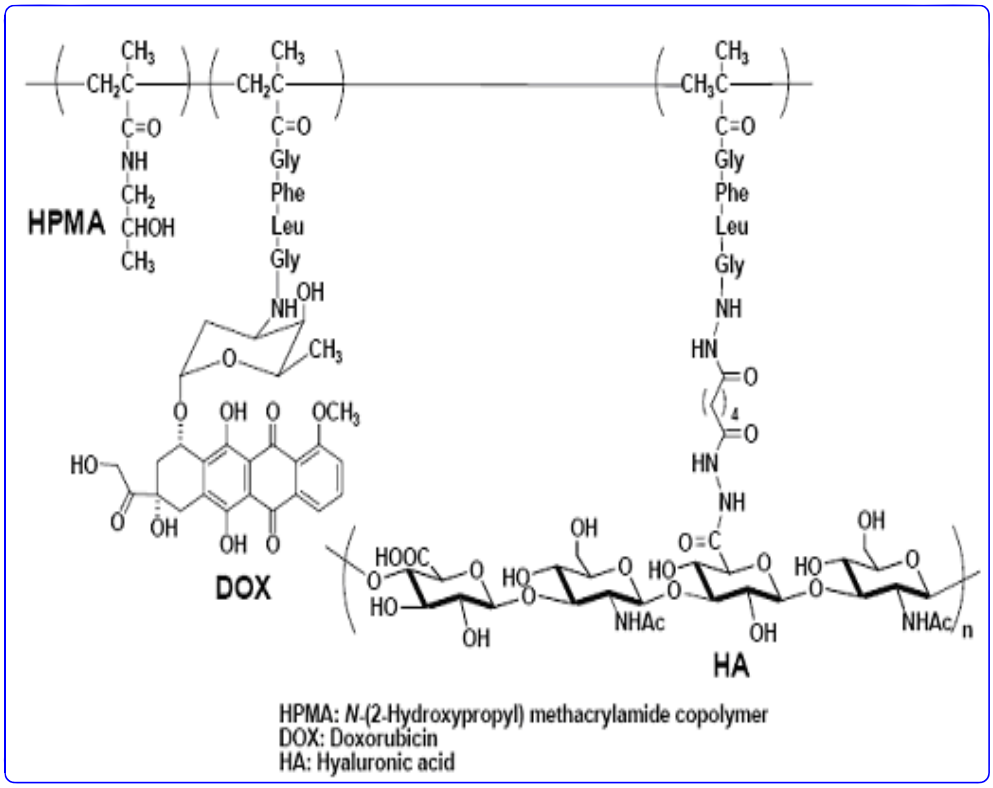

Figure 4-6. Structure of HPMA-HA-Dox[38]

Aptamers, discovered in 1990, are short strands of DNA or RNA with molecular weight in 5-15 kDa range.[75, 76] Aptamers are engineered through repeated rounds of *in vitro* selection or a systematic evolution of ligands in an exponential process of enrichment (SELEX). They can bind to various molecular targets such as proteins, small organic compounds, nucleic acids, and even entire cells, tissues and organisms with high binding affinity and specificity. They have an unusual tertiary structure which allows them to fold into stable scaffolds for molecular recognition. They can be engineered with various site-directed modifications for specific applications. Thus they are attractive candidates in biotechnology as diagnostic tools and target specific therapeutic agents.[77-80] Aptamers are similar to antibodies and can be specially engineered to bind to tumor-specific receptors specifically so that they can be used as tumor-targeting modules to deliver cytotoxic drug payloads inside the cancer cells.[35] They have many potential advantages over antibodies – a) aptamers elicit little to no immunogenicity in therapeutic applications, b) aptamers are robust with desirable storage properties and can be easily synthesized, c) their relatively small size allows them to penetrate tumors better and d) their half-life can be easily tuned to optimize the therapeutic index.

Archemix, an aptamer therapeutics company is leading the development of this new class of targeted therapeutics for prevention and treatment chronic and acute diseases and is currently in Phase 2 clinical trials for ARC1779 – its first-in-class antagonist of von Willebrand Factor.[81] The US FDA has already approved its first aptamer-based drug, Macugen, for the treatment of age-related macular degeneration (AMD).[82] However, developing tumor-targeted aptamer therapeutics is still in research phase. Doxorubicin conjugated to a A10 RNA aptamer that binds to the prostate-specific membrane antigen (PSMA) has been reported. PSMA can be used as an excellent disease marker as it is a tumor-associated antigen expressed specifically on cell surface of androgen independent prostate tumors. This aptamer-doxorubicin conjugate could bind efficiently to PSMA expressing cell lines, get internalized and release the drug inside the cell.[83]

Peptide based targeting is another attractive strategy in tumor-targeted drug delivery because high affinity peptide sequences and their truncated analogs with appropriate tumor recognition properties can be generated. Somatostatin (SST) is a hormonal neuropeptide and possesses high binding affinity to SSTR1-5 membrane receptors, which are overexpressed at significantly elevated levels in tumor cells.[84] Thus, somatostatin is a good candidate for cytotoxic drug delivery. However, the one of the active forms of SST has a short plasma half life which prompted the development of more stable synthetic analogs. Octapeptides RC-160 and RC-121 (Figure 4-4) were found to be more potent than SST with significantly improved metabolic stability.[85] Several conjugates of RC-160 and RC-121 with glutarate linked doxorubicin and 2-pyrrolino-doxorubicin(500-1000 times more cytotoxic than DOX) have been reported by Nagy *et al.*[37, 86]

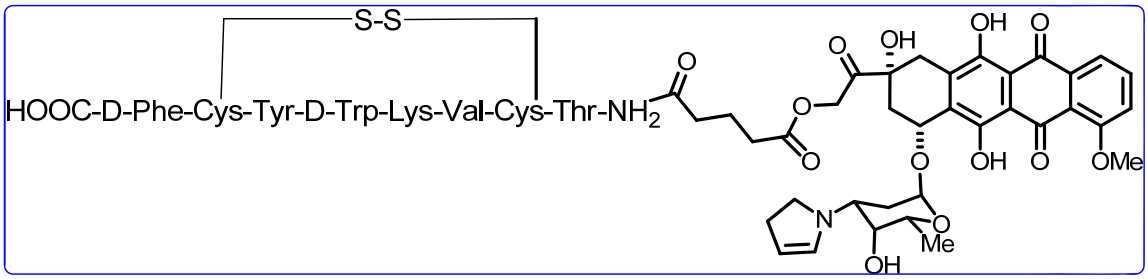

Figure 4-7. Structure of AN-238[37]

The *in vivo* antitumor activity assays against MXT murine mammary carcinoma in female BDF mice indicated that inhibition of tumor growth by AN-238, which is a conjugate of RC-121 and glutarate linked 2-pyrrolino-doxorubicin (Figure 4-7), was dose dependent with no systemic toxicity. In contrast, 2-pyrrolino-doxorubicin alone at the same dose was highly toxic and did not show any antitumor activity.[37] Studies showed that AN-238 inhibited growth of small cell lung cancer and non-small cell lung cancer cell lines in nude mice.[87]

The antitumor activity of paclitaxel (PTX) conjugated with a bicyclic peptide E[c(RGDyK)] (RGD) was evaluated in a metastatic breast cancer cell line (MDA-MB-435). The RGD peptide selectively binds to alpha(v) integrin receptors that are overexpressed in metastatic cancer cells and inhibits cell cycle proliferation by arresting cell growth in G0/G1 phase *in vitro*. The RGD-PTX (Figure 4-8) conjugate inhibited cell proliferation with activity comparable to that of paclitaxel and mediated cell cycle arrest at the G2/M phase followed by apoptosis. Although the RGD-PTX conjugate showed slightly decreased integrin binding affinity than the unconjugated peptide, it indicated integrin specific accumulation *in vivo*.[88]

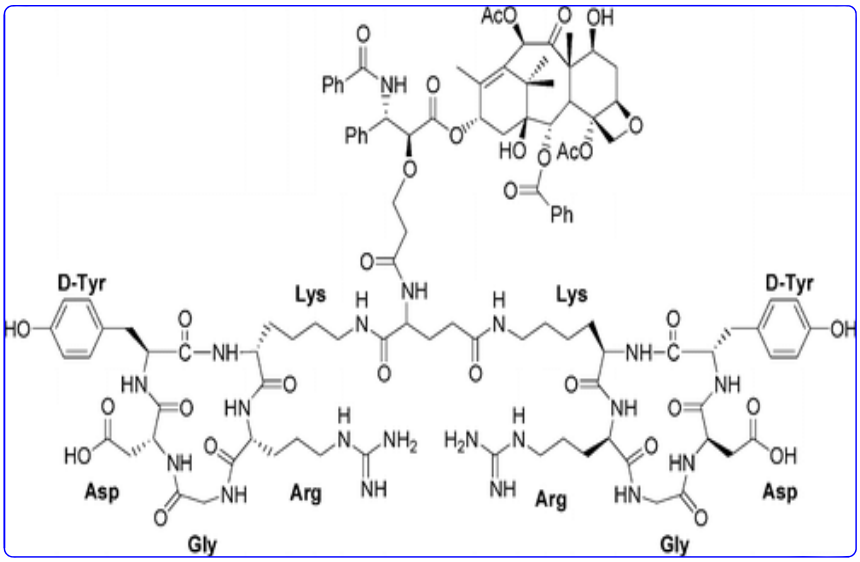

Figure 4-8. Structure of PTX-RGD[88]

Polyunsaturated fatty acids (PUFAs) (Figure 4-4) are essential fatty acids which are obtained from diet alone. There are several PUFAs which have exhibited antitumor activity against certain cancer cell lines. They are taken up greedily by the rapidly growing tumor cells presumably to meet their increased nutritional and energy demand and thus are attractive candidates for tumor-specific drug delivery though their tumor-specific mechanism is not clear (for details please refer to Chapter 6).

Cancer cells are also known to overexpress certain vitamin receptors which can bind the respective vitamins with high specificity. Thus the innocuous vitamins such as folic acid (for details please refer to later part of this chapter) and biotin are promising candidates for tumor-targeted drug delivery as well as diagnostic agents.

4.1.3 Linker

In the early stages of tumor-targeting drug conjugates it was believed that the specificity of these conjugates could be enhanced by merely linking these drugs to the targeting moieties directly. Thus several potent anticancer drugs[28, 51, 89] such as vinca alkaloids, methotrexate, mitomycin C, etc were linked via non-cleavable bonds to several murine mAbs. However, these conjugates lacked potency and were much less potent than the unconjugated drugs. Linking a large number of drug molecules to mAb directly or through macromolecular carrier resulted in impaired binding affinity *in vitro* and unfavorable pharmacokinetics *in vivo*.[90, 91] To realize the full potency of these potent drugs, focus shifted towards the development of linkers that could be cleaved inside the cancer cells and release the drug. The tumor-targeting conjugates thus comprise of a tumor-specific moiety conjugated either directly or via a linker to the anticancer drug(s) to increase their efficacy. Thus the linker moiety plays a critical role in the efficacy of these tumor-targeting conjugates. An ideal linker should maintain the stability of the conjugate while in circulation and be efficiently cleaved inside the cells to release the drug cargo. There is no universal linker and the selection of a suitable linker depends on the type of cancer, targeting moiety, drug and pharmacokinetic requirements. Different types of linkers are discussed in Chapter 3.

4.1.4 Cytotoxic Warheads

The success of a tumor-targeting drug delivery system depends on the cytotoxic drug to a great extent. There are several criteria such as potency, stability, chemically amenable functional groups, insensitivity towards multidrug resistance and lack of immunogenicity that have to be considered while selecting an appropriate drug for the tumor-targeting conjugate. Studies have shown that the promising efficacy of conjugates in animal tumor models is not translated in patients because of lack of potency. While animals could be dosed at 10-20 fold higher doses than tolerated by humans a lower dose in humans was not sufficient to achieve desired efficacy. Since only a limited number of cytotoxic molecules can be loaded onto the tumor recognition module without affecting its binding affinity to the receptor it is desirable to select a highly potent cytotoxic drug. Data from clinical trials showed peak circulating concentration of conjugates of doxorubicin and vinblastine with mAbs was in the range of 10^{-6} to 10^{-7} M[59, 92] which

could eliminate at best 50% of cells. Since calculation shows that maximum concentration of the drug that can be delivered inside cancer cells via receptor-mediated endocytosis would probably not exceed 10^{-7} M the toxicity of the drug should be in the subnanomolar range to be effective in humans.[50] Also tumor cells express only a limited number of antigens in most cases and to maximize the amount of drug and maintain its desired concentration it is essential to have a drug with high potency. The cytotoxic agent should also be stable in the proteolytic and acidic conditions of lysosomes where the cytotoxic agent is released. This is important because degradation of the agent in this environment can result in loss of potency or other undesirable effects. The presence of chemically amenable functional groups such as carboxyl, hydroxyl, amino, carbonyl and sulfhydryl groups are essential for ease of modification and conjugation to a linker. The cytotoxic agent should also be insensitive towards multi-drug resistant (MDR) cancers or cancers bearing MDR-reversal activity to prevent extensive leakage of the drug or its active metabolite from the cell by efflux or diffusion. Cytotoxic agents should have a desirable size because a large size contributes to a large conjugate which will result in poor penetration inside the tumor because of hampered binding to the receptor. Cytotoxic agents like plant toxins can be destroyed by the host immune system and thus lack of immunogenicity is another important criterion to consider while selecting an appropriate cytotoxic agent. Some representative cytotoxic agents commonly used in tumor-targeted drug delivery are summarized in Figure 4-9.

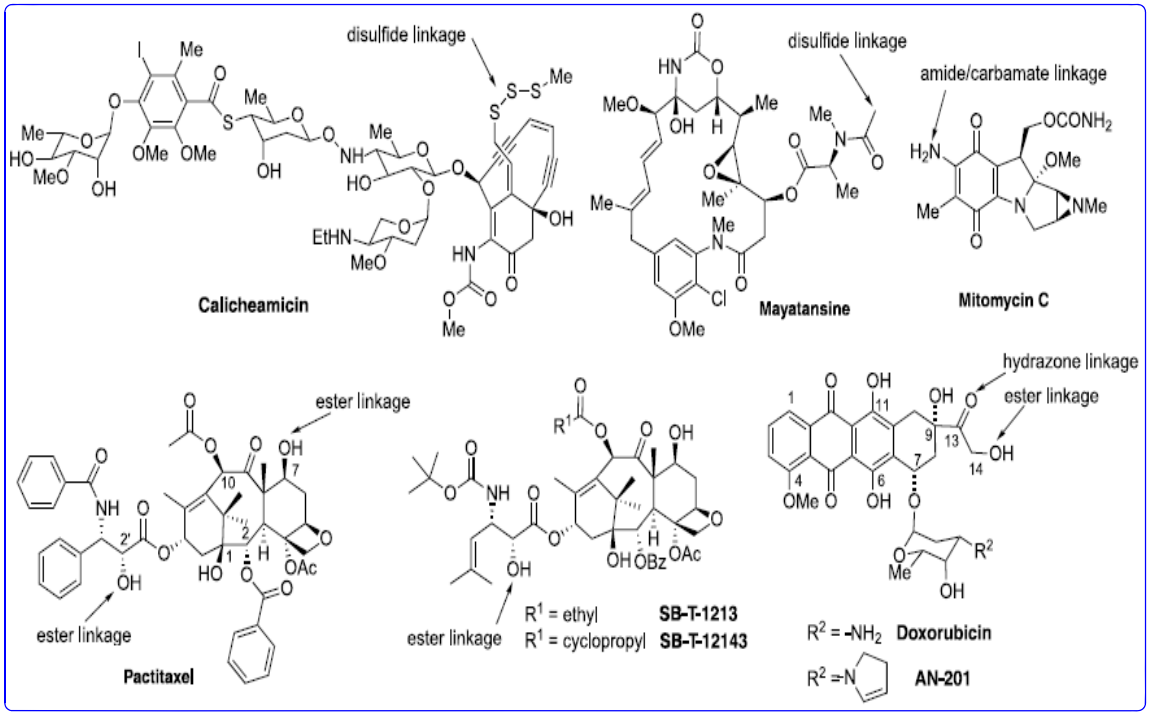

Figure 4-9. Representative cytotoxic warheads for tumor-targeted drug delivery

Calicheamicin is produced by *Micromonospora echinospora calichensis* and is a class of enediyne class of antibiotics containing an enediyne, an iodine atom and an

unusual trisulfide moiety. It binds to the minor groove of DNA and produces sequence specific DNA breaks.[93] Calicheamicin exhibits remarkable potency against various tumors and is ~ 4000-fold more active than doxorubicin, with an optimal dose of 0.5-1.5 μg/kg.[94, 95] It has a very narrow therapeutic window and thus has limited use as a single agent chemotherapeutic. However, its unique mechanism of action and high potency make it a good candidate for immunoconjugates.

Mayatansine is a chlorine-containing macrolactam with an epoxide ring and was isolated from the *Maytenus ovatus* plant.[96] It is an inhibitor of microtubule assembly and initial *in vitro* studies showed median effective (EC_{50}) values in the range of 0.6-2 nM.[97] Its synthetic analog methyldithio-maytansinoid (DM1), showed 100- to 1000-fold higher cytotoxicity than doxorubicin, methotrexate and vinca alkaloids, with a median inhibitory concentration (IC_{50}) in the picomolar level and has been explored as a potential mAb-based tumor-targeting therapeutic by Immunogen.[56]

Mitomycin A, B and C form a specific class of antitumor antibiotics and act as DNA alkylating agents.[98, 99] They were isolated from the soil bacteria *Streptomyces verticillatus*.[100] Mitomycin C was investigated as tumor-targeting immunoconjugate against human gastric cancer and biliary tract carcinoma xenografts in mice.[53, 101, 102]

Paclitaxel (please refer to chapter 1 for details) is a cytotoxic drug that has been used in developing mAb immunoconjugates. The observed inefficacy of mAb-paclitaxel conjugates can be ascribed to insufficient potency, insufficient intracellular release of the drug or unfavourable effects on the mAb function due to the high hydrophobicity of the drug as well as its susceptibility to drug-resistant cancer cells expressing MDR phenotypes.[103-105]

In sharp contrast most of the taxoids developed by Ojima *et al.*[106-110] exhibit one order of magnitude higher potency than that of paclitaxel against drug-sensitive cancer cell lines and two to three orders of magnitude higher potency than that of paclitaxel against MDR-expressing cell lines. Thus immunoconjugates of 2nd-generation taxoids such as SB-T-1213 and SB-T-1214 with mAbs have been studied and they show high potency and exceptional tumor-targeting specificity.[26, 27, 111]

Doxorubicin and daunorubicin belong to the anthracyclin group of cytotoxic agents and was isolated from cultures of *Streptomyces peucetius*.[112] Numerous immunoconjugates of mAb-doxorubicin have been investigated because of the potent broad-spectrum antitumor activity of doxorubicin notably BR96-Dox.[113]

4.2 Rational Design of Tumor-targeting Drug Delivery System

4.2.1 Previous Achievement with mAb-taxoid Conjugates

Cancer cells overexpress certain antigens on the cell surface and these tumor-specific antigens serve as a biomarker to differentiate tumor tissues from normal tissues. Therefore, certain antibodies can be used to recognize these tumor-specific antigens selectively. Monoclonal antibodies (mAbs) were chosen as tumor-targeting molecule because it was anticipated that their high binding specificity to tumor-specific antigens would enable mAbs to be used as a suitable drug delivery vehicles to carry a payload of cytotoxic agents specifically to the tumor site. The mAb-drug conjugate is internalized upon binding to the tumor-specific antigen *via* receptor-mediated endocytosis (RME) and

the payload is released inside the cancer cells. This process has been discussed earlier in this chapter. The cytotoxic drug gets liberated inside the cancer cells by various mechanisms such as proteolysis, acid-catalyzed hydrolysis or disulfide exchange depending on the linker used to connect the drug to the mAb. Thus the efficacy of the mAb-drug immunoconjugates depends not only on the specificity of the mAb and the potency of the cytotoxic drug, but also on the linker which connects the mAb to the drug. Monoclonal antibodies have been widely investigated in the past decades as a tumor-targeting molecule for efficient drug delivery and numerous review articles have been reported in the literature regarding mAb-mediated drug delivery. [18, 22, 24]

Paclitaxel and docetaxel are currently considered to be the two most widely used drugs in cancer chemotherapy. However, they suffer from lack of tumor specificity and multidrug resistance. Immunoconjugates of mAb-paclitaxel have recently been reported as potential tumor-targeted anticancer agents. Current studies indicate that the cytotoxicity of the drug that can be effectively used in immunoconjugates must be at IC_{50} level of $10^{-10\sim-11}$M. The IC_{50} values of paclitaxel and docetaxel are in the 10^{-9} M range, obviously not sufficient as the cytotoxic component of the conjugate for human clinical use. Besides, these conjugates are predicted to be inactive against tumors expressing MDR phenotype.[104, 114] Our group developed highly potent second-generation taxoids with 2-3 orders of magnitude higher potency than those of paclitaxel and docetaxel against drug-resistant cell lines expressing MDR phenotypes and one order of magnitude higher potency than that of paclitaxel against drug-sensitive cancer cell lines. Thus these novel taxoids could serve as highly promising drug candidates in mAb-cytotoxic agent conjugates.

Recently, our group successfully developed mAb-taxoid conjugates bearing disulfide linkers.[27] Disulfide linkers were chosen as they have superior efficacy compared to other linkers because of their favorable characteristics (for details please refer to chapter 3). A model mAb-taxoid conjugate is shown in Figure 4-10.

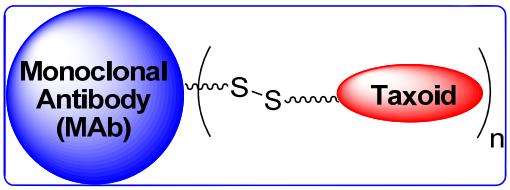

Figure 4-10. Schematic of mAb-linker-taxoid

Our group chose two of the second-generation taxoids which possess the required cytotoxicity, SB-T-1213 and SB-T-12162 with modification at C-10 position with methyldisulfanylalkanoyl (MDS-alkanoyl) as the cytotoxic drugs for these immunoconjugates. Various immunoglobin G (IgG) class mAbs recognizing the human epidermal growth factor receptor (EGFR) were linked to the taxoids via the disulfide linkage. The epidermal growth factor receptor (EGFR) was selected as the model antigen for mAb because it is known to be over-expressed in several human squamous cancers such as head, neck, lung, and breast cancers which have been extensively studied. The preparation of mAb-taxoid conjugates is illustrated in Scheme 4-1.

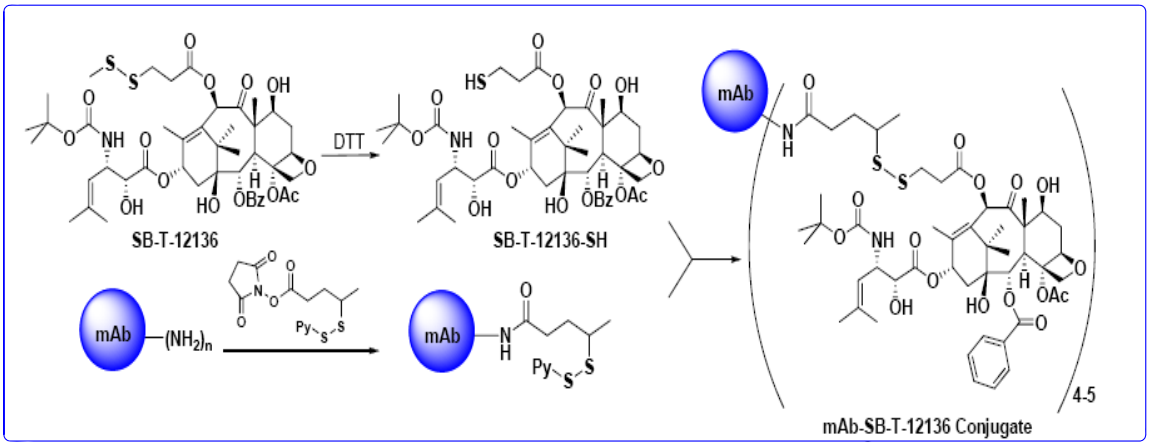

Scheme 4-1. Preparation of mAb-taxoid conjugate[27] (Adapted from Ref. 27)

Structure-activity relationship (SAR) studies demonstrated that cytotoxicity was retained when a 3-MDS-alkanoyl group was attached to the C-10 position of the taxoid. The novel taxoid SB-T-12136, the 10-MDS- propanoyl analog of SB-T-1213, was treated with dithiothreitol (DTT) to generate SB-T-12136-SH bearing free thiol functional group. The mAbs, KS61 (IgG2a), KS77 (IgG1) and KS78 (IgG2a), which specifically bind to EGFR, were also modified with *N*-succinimidyl-4-(2-pyridyldithio) pentanoate (SPP) to attach 4-pyridyldithio (PDT)-pentanoyl groups. The modified mAbs were subsequently conjugated with SB-T-12136-SH and purified by gel filtration to yield the immunoconjugates. Preliminary matrix-assisted laser desorption ionization time-of-flight (MALDI–TOF) analysis of the KS77-taxoid conjugate indicated that ~ 4-5 taxoids were loaded per mAb molecule. These three immunoconjugates showed quite impressive and promising results with cytotoxicities at 10^{-9} M level specifically against A-431 cancer cells expressing EGFR.

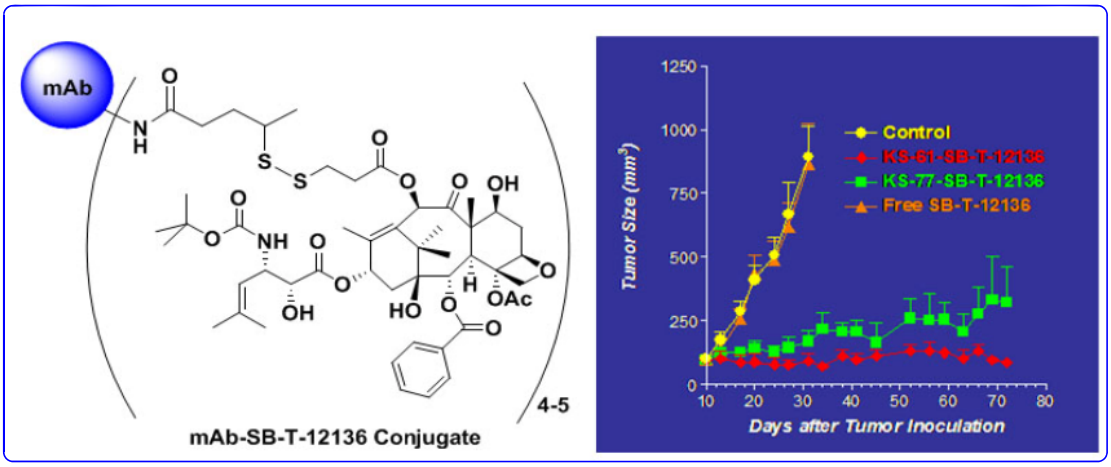

Figure 4-11. Antitumor activity of anti-EGFR mAb-taxoid conjugates against A-431 xenografts in SCID mice[27] (Adapted from Ref. 27)

However, non-binding immunoconjugate, mN901-SB-T-12136 exhibited no cytotoxicity against the A431 cell line. *In vivo* antitumor activities of two conjugates, KS61-SB-T-12136 and KS77-SB-T-12136, were evaluated against human squamous cancer (A431) xenografts in SCID mice. Both of them showed remarkable antitumor activity with complete inhibition of tumor growth in all the treated animals for the duration of the experiment. The free taxoid SB-T-12136 showed no therapeutic effect at the same dose (Figure 4-11). Moreover, the immunoconjugates were totally non-toxic to the mice as demonstrated by the absence of any weight loss. These promising results indicate excellent tumor target specificity of the immunoconjugates.[27]

4.2.2 Novel Disulfide Linker

Regardless of the success of the 1st-generation mAb-taxoid conjugate the taxoid, SB-T-12136-SH, released through the cleavage of the 1st-generation disulfide linker inside the cancer cell was modified at the C-10 position. This modification at C10, required to introduce the disulfide linker moiety, resulted in 8-10 times reduced potency compared to the parent taxoid SB-T-1213. Thus, it was not potent enough for clinical use in humans (IC_{50} 0.5-0.8 nM against A431 and MCF7).[27] Therefore it was essential to design and develop a novel disulfide linker which would readily cleave inside the cancer cell and liberate the taxoid without any loss in its potency. Several novel mechanism-based self-immolative disulfide linkers were designed and studied (for details please refer to chapter 3). This novel class of disulfide linkers is bifunctional and can be connected to various cytotoxic warheads on one end and to TTMs on the other end. Upon internalization of the tumor-activated prodrug conjugate, the glutathione-triggered cascade takes place to generate the original anticancer agent as shown in Figure 4-12.[21, 24]

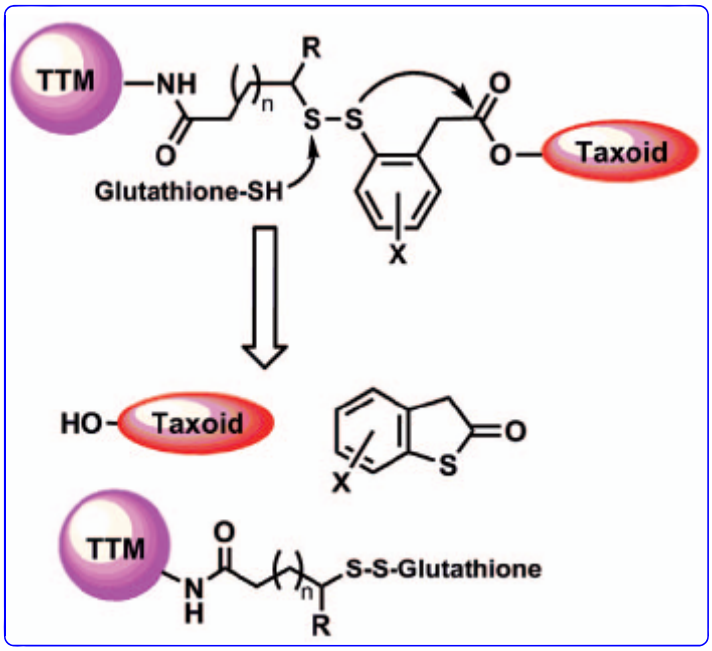

Figure 4-12. Mechanism of drug release of self-immolative disulfide linker[24]

4.2.3 Coupling Ready Warhead

As discussed in chapter 3 efforts on the construction of a versatile and efficient tumor-targeting drug delivery system by fine tuning the structure of the novel mechanism-based bifunctional disulfide linker are ongoing. The two carboxylic acid

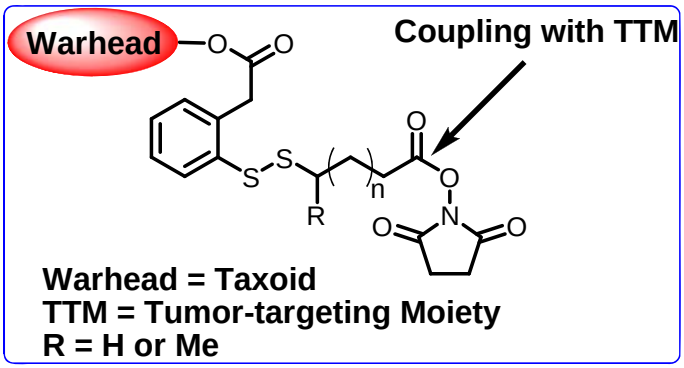

Figure 4-13. Coupling ready warhead construct

functional groups on the disulfide linker can be orthogonally protected. The unprotected carboxylic acid terminus can be coupled to the potent warhead which has a free hydroxyl group such as the novel 2nd-generation taxoids SB-T-1214, SB-T-1213, etc. The carboxylic acid group at the other terminus could then be converted to an active ester

moiety, *i.e.* hydroxysuccinimide to generate the 'coupling ready warhead' construct (Figure 4-13). Subsequently, any tumor-targeting moiety bearing amine residues can then be readily coupled to the active ester of the 'coupling ready warhead' under standard peptide coupling protocol. For this project we chose folic acid as the tumor-targeting moiety.

4.2.4 Folic Acid as the Tumor-targeting Moiety

Gene therapy vectors, liposome encapsulated drugs, protein therapeutics, biodegradable polymers with drugs, aptamers, etc show great potential for cancer targeted therapy because of their improved specificity, better potency compared to chemotherapeutic drugs and prolonged delivery. However, these macromolecular drugs often encounter major obstacles that limit their potential. Although the EPR effect allows the accumulation of these macromolecules inside the tumor cells,[6] the cell membrane still poses a significant barrier for those macromolecules that must traverse this membrane and enter the cancer cell to exert their effect. Also the delivery of these macromolecules to sites deep within the tumor mass gets compromised because the poor lymphatic drainage system increases the intratumor pressure.[115] Therefore, cancer cell specific ligands have been employed for improved delivery and retention of drugs inside the cancer cells.

Folic acid or vitamin B9 is an essential vitamin and functions as a cofactor in one-carbon transfer reactions in de novo nucleotide biosynthesis and plays a critical role in various metabolic pathways involved in DNA and RNA synthesis, epigenetic processes, cellular proliferation and survival.[116] Thus, folic acid is consumed in elevated quantities by rapidly proliferating cells to meet their rising need for nutrients. The major form of the vitamin that circulates in the serum is 5-methyltetrahydrofolate which is present at 5 - 30 nM concentration. According to various studies, folate deficiency is the cause of several conditions such as fetal nerve development disorders and cardiovascular disease besides its profound effect on DNA replication and repair and on gene expression.[117] At physiological pH, folates have an anionic and hydrophilic nature which prevents them from entering the cell by passive diffusion through the plasma membrane. Therefore cellular folate uptake in normal cells is mediated by transporters like the reduced folate carrier (RFC) and folate receptor (FR). The RFC is found in virtually all cells and is the major pathway for the uptake of physiological folates. FR is found mainly on polarized epithelial cells and activated macrophages.[118] Recently, a proton-coupled high-affinity folate transporter has been reported which is believed to be the major transporter of folate in low pH environments. It seems to be the primary transporter in the intestinal absorption of folates.[119]

The RFC is unable to bind folic acid which is the oxidized form of the vitamin and is the principal folate transporter. It is expressed virtually in all cells throughout development and in normal adult tissues.[120] The RFC is a transmembrane protein that transports folate via anion exchange and although it has a high dissociation constant for 5-methyltetrahydrofolate (micromolar range) the transport is rapid and normally adequate to meet the cellular needs. RFC can shuttle only folate molecules inside the cells and folate-drug conjugates are not substrates of RFC.[32]

Folate receptor (FR) is a cell surface glycosyl phosphatidylinositol (GPI)-anchored glycopolypeptide that binds folic acid as well as 5-methyltetrahydrofolate with a low dissociation constant (subnanomolar range) and transports them by a receptor-mediated endocytosis mechanism (RME).[121, 122] There are three well characterized isoforms of human FR with an average molecular weight in ~ 38 kDa range – FR-α, FR-β and FR-γ/γ' that are ~ 70-80% identical in amino acid sequence but differ in their expression patterns.[123, 124, 125] FR-α and FR-β are both membrane associated proteins by virtue of their attachment to the GPI anchor.[125] Figure 4-14 illustrates the special class of GPI-anchored proteins – (A) shows the core structure of a GPI-anchor and (B) shows how GPI-anchoring replaces C-terminal GPI-signal via a transamidation reaction involving the ethanolamine amine of the pre-formed GPI-anchor glycolipid and the GPI-attachment site carboxyl group in the lumen of the ER.[124] FR-α however binds folic acid and physiologic folates with a higher affinity (K_D ~ 0.1 nM) than FR-β (K_D ~ 1 nM).[126, 127] This high affinity of FR- α for folic acid has been the focus of development of FR-targeted therapeutic and diagnostic agents. FR-γ and a truncated form of the protein FR-γ' are not attached to the GPI anchor and are secreted in barely detectable amounts.[125] There are reports of another isoform FR-δ which was not found in detectable quantities in human tissues.

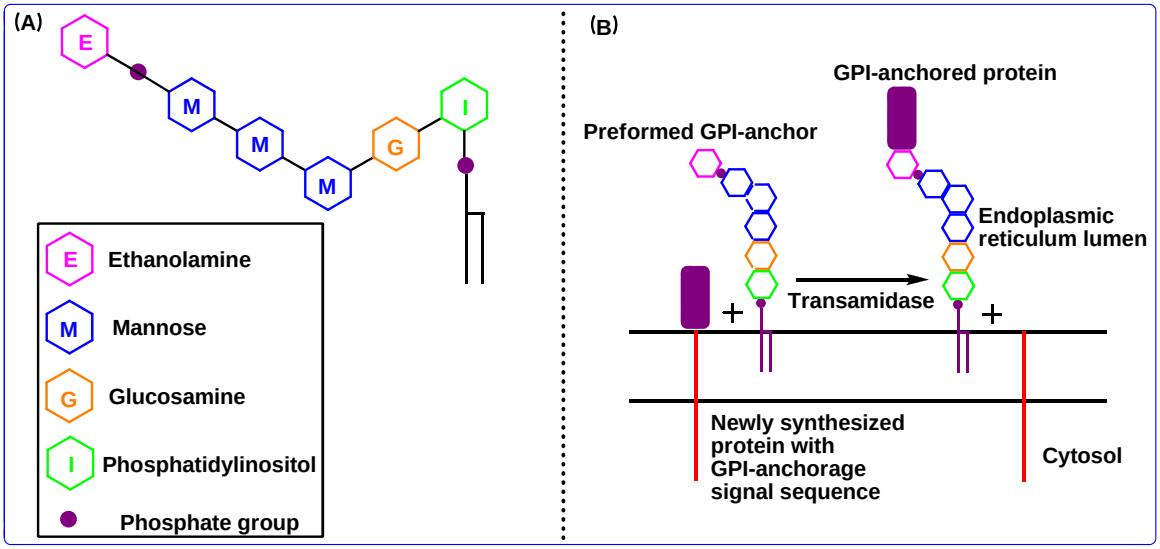

Figure 4-14. Illustration of GPI-anchored protein[124] (Adapted from Ref. 124)

The expression of these FR isoforms is tissue-specific and depends on differentiation.[128] FR-α is present at low levels in normal epithelial cells with the exception of some normal tissues like kidney, choroid plexus and placenta but is often present in elevated levels in epithelial malignant tissues especially ovary, uterus, kidney, head and neck, brain, endometrium, etc.[129-132] The upregulation of FR-α in malignant tissues can be two orders of magnitude higher than in normal tissues which is quite an impressive difference.[130] Although low concentrations of RFC are probably sufficient to meet folate requirements of most normal cells, the overexpression of FR in malignant cells is required to enable these cells to compete successfully for their elevated need for

folates when supplies are limited. Studies have shown that the level of FR-α expression can be correlated with higher histologic grade and more advanced stage of cancer suggesting the possible need of more folates in the more rapidly proliferating tumors. Also it has been found that there are usually higher levels of FR in tumors that have survived chemotherapy.[129, 133] Therefore, it is conceivable that the tumors that are more advanced and more resistant to standard chemotherapy can be most readily targeted by folate-conjugated drugs. FR-β is normally expressed in hematopoietic and non-epithelial cells[130] and is elevated in some malignancies of non-epithelial origin.[125, 134] Importantly, the FR-β detected on hematopoietic stem/precursor cells is expressed in an inactive conformation that shows no affinity for folates.[135]

Since there are relatively high levels of FR found in the choroid plexus of the brain and the proximal tubules of the kidney, there had been logical concern that FR targeted therapeutics could prove to be toxic to these tissues.[136] However, immunohistochemical studies and studies with radiolabeled folate demonstrate that there is a highly polarized pattern of distribution of FR on these normal epithelial cells. FR is found only on the apical or luminal surface i.e. urine facing surface of the proximal tubules of the kidney where it probably helps in the reabsorption of the folates from the urine. Thus folate-drug conjugates will not encounter kidney FR except in patients with certain kidney dysfunctions. FR in the brain also seems to be localized on the brain side of the blood-brain barrier where they probably assist in retaining the vitamin in the cerebrospinal fluid and thus folate-drug conjugates are not accessible by the brain FR.[136-138] Thus, FR further qualifies as a tumor-specific target because normal cell FR cannot access the blood borne folate-drug conjugates as FR generally becomes available to intravenous drugs after cells have undergone malignant transformation. When normal epithelial cells undergo malignant transformation the cell polarity is lost and FR becomes available to folate-drug conjugates in circulation. This dual mechanism for tumor specificity – overexpression and specific orientation on malignant cells besides its high affinity for folic acid makes FR an attractive target for folate-mediated selective drug delivery and diagnostic agents. FR seems to meet several of the desirable characteristics of an ideal cell surface molecule such as well defined structure expressed mainly on tumor tissues, binds targeting molecule with high affinity and limited distribution and accessibility on normal tissues.[18]

Folic acid in addition to its high affinity for FR, has several other advantages namely small size, amenable to chemical modifications, compatible with many aqueous and organic solvents, low immunogenicity, low cost and ready availability. Folic acid (Figure 4-15) has a pteroic acid moiety and a glutamic acid moiety. Studies show that the glutamic acid (Glu) residue of folic acid is not essential for the recognition of FR[139, 140] and thus modifications can be typically made to the Glu residue. Folate targeting was invented soon after it was reported that the folates entered cells via a receptor-mediated endocytosis process[141] and the physiological process of folate-drug delivery is identical to that of free folic acid.[142, 143]

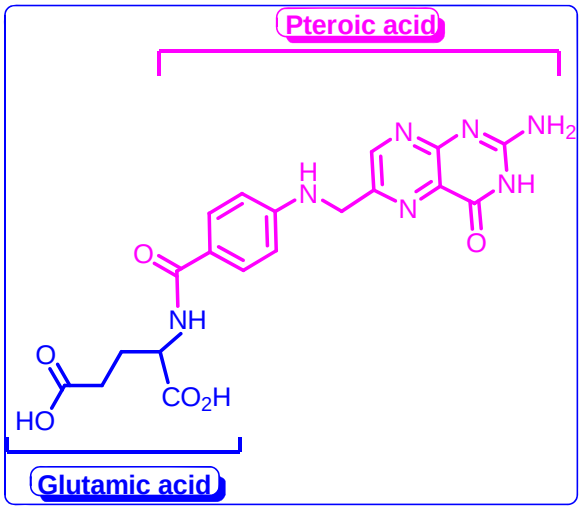

Figure 4-15. Structure of Folic acid

FR mediated transport of folic acid inside the cells is a highly specific receptor-mediated endocytosis pathway[31, 121] where folate (key) is inserted into the FR (lock) as illustrated in Figure 4-16. The exogenous folate-linker-drug binds to the FR which is externally oriented on the cell surface.

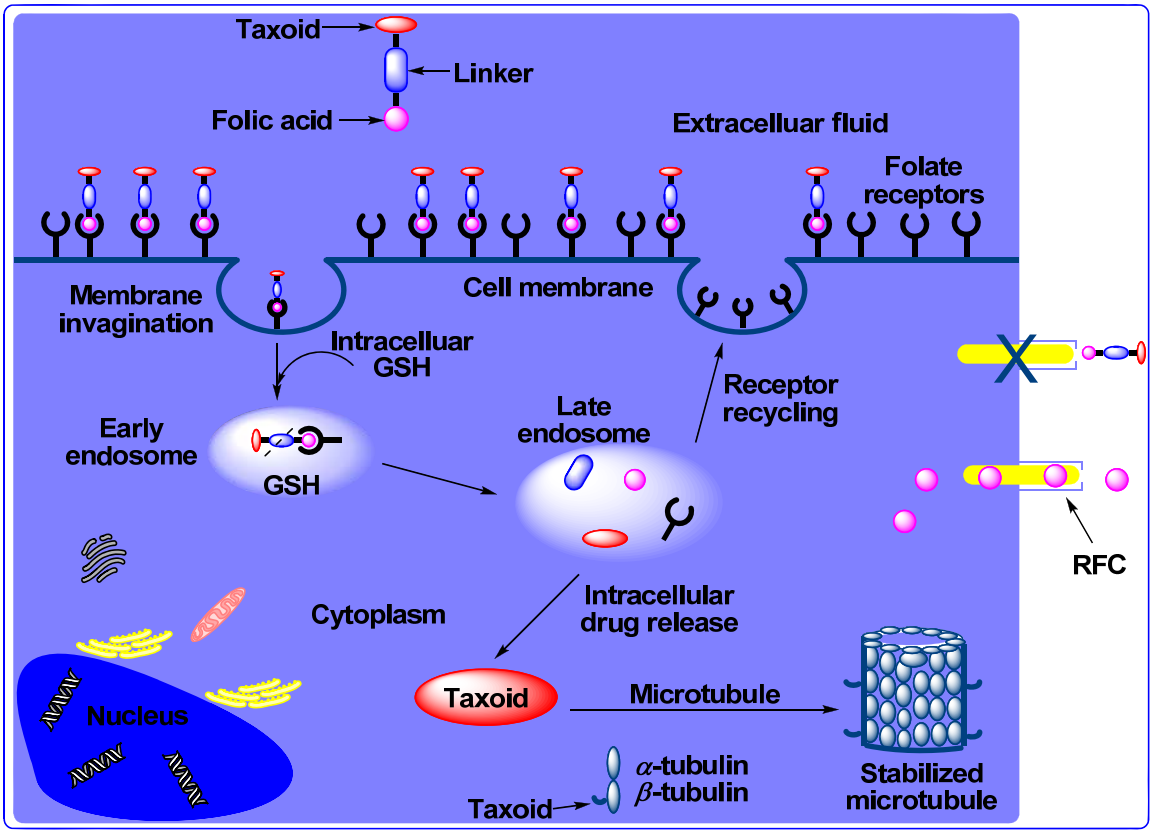

Figure 4-16. Receptor mediated endocytosis

Soon after binding to the FR, the membrane around the FR-folate-conjugate complex begins to invaginate to form a distinct internal vesicle known as the 'early endosome'. Irrespective of the size of the folate-drug conjugates, they internalize and traffic to these intracellular compartments or endosomes.[144] The pH of the vesicle lumen then drops to ~ 5 by the action of proton pumps that are co-localized in the membrane of the endosome in a process called endosome acidification.[145] The binding of folic acid to FR is pH dependant and hence this drop in pH values presumably protonates the numerous carboxyl groups on the FR and causes a change in conformation that releases the folate-drug molecule inside the cell. Upon its release, the parent drug is liberated by various mechanisms (discussed earlier in this chapter and in chapter 3) from the linker in its potent form. In the illustration in Figure 4-16, the drug (taxoid) is released from the novel disulfide linker (discussed earlier in this chapter and in chapter 3) by the action of intracellular glutathione (GSH) or other thiols in its potent form which then binds to microtubules and stabilizes them causing apoptosis of the cell (for details please refer to chapter 1). The RFC present in normal cells cannot internalize the folate-drug conjugate as mentioned earlier in this chapter. After releasing the drug cargo the FR recycles back to the cell surface and studies indicate that the total number of folate conjugates internalized is approximately proportional to the number of FR expressed on the cell surface and an average FR expressing cancer cell may internalize folate-drug conjugates at the rate of ~ 1-2 x 10^5 molecules/cell/h.[128] Consequently, all these exciting and promising research and discovery prompted us to design and develop FR targeted drug delivery system using folic acid as the tumor-targeting moiety in a molecular Trojan horse approach (discussed in more detail later in this chapter).

4.2.5 Design of fluorescent probes for internalization studies

Fluorescence microscopy has been extensively used to study cellular mechanisms of microtubule assembly and stabilization by paclitaxel using fluorescent paclitaxel derivatives.[146-148] Figure 4-17 shows the fluorescence microscopy images of permealized and fixed H-460 cells at interphase by FITC-labeled (A) and rhodamine-labeled (B) paclitaxel.[146]

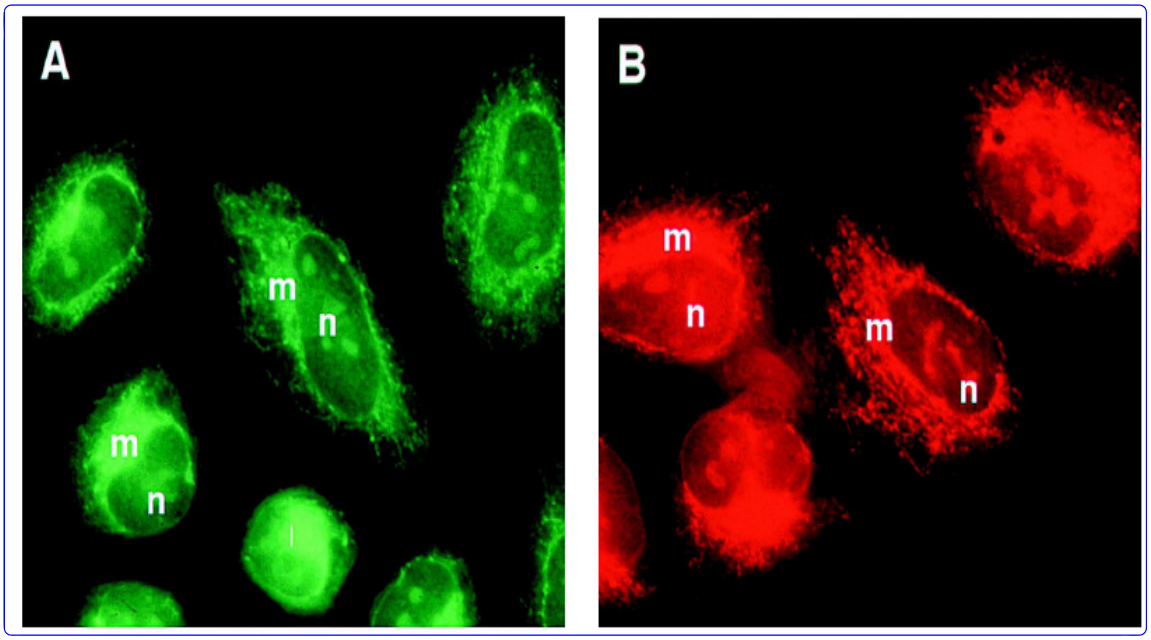

Figure 4-17. Fluorescence microscopy images of interphase stage of permealized and fixed H-460 cells by FITC-labeled (A) and rhodamine-labeled (B) paclitaxel[146] (m = microtubule organizing center; n = nucleolus) (Adapted from Ref. 146)

Fluorescent molecules such as fluorescein, fluorescein isothiocyanate, rhodamine, etc shown in Figure 4-18 are receptive to the intracellular environment of cells and are indispensable for the rapid detection of essential cellular functions in biology.[147, 149-154] Thus they are extensively used in biotechnology for target validation, drug discovery, drug delivery, etc using flow cytometry, fluorescence microscopy and instruments.

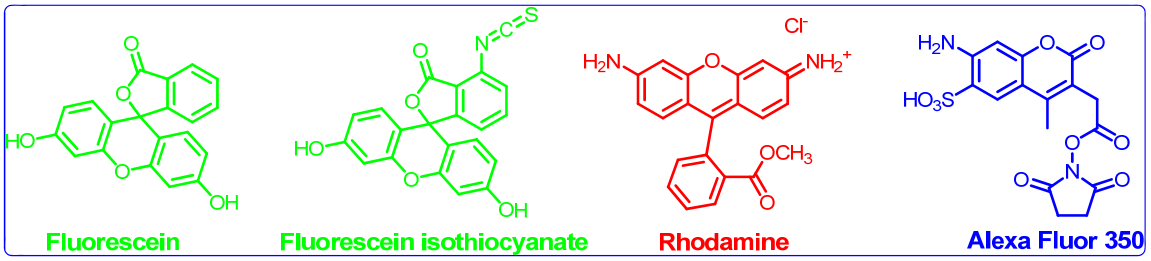

Figure 4-18. Structures of some commonly used fluorescent dyes

Figure 4-19 illustrates the use of fluorescent staining in cells to identify structures like actin, nucleus, microtubules, etc. Identifying these structures is critical in studying cellular processes.

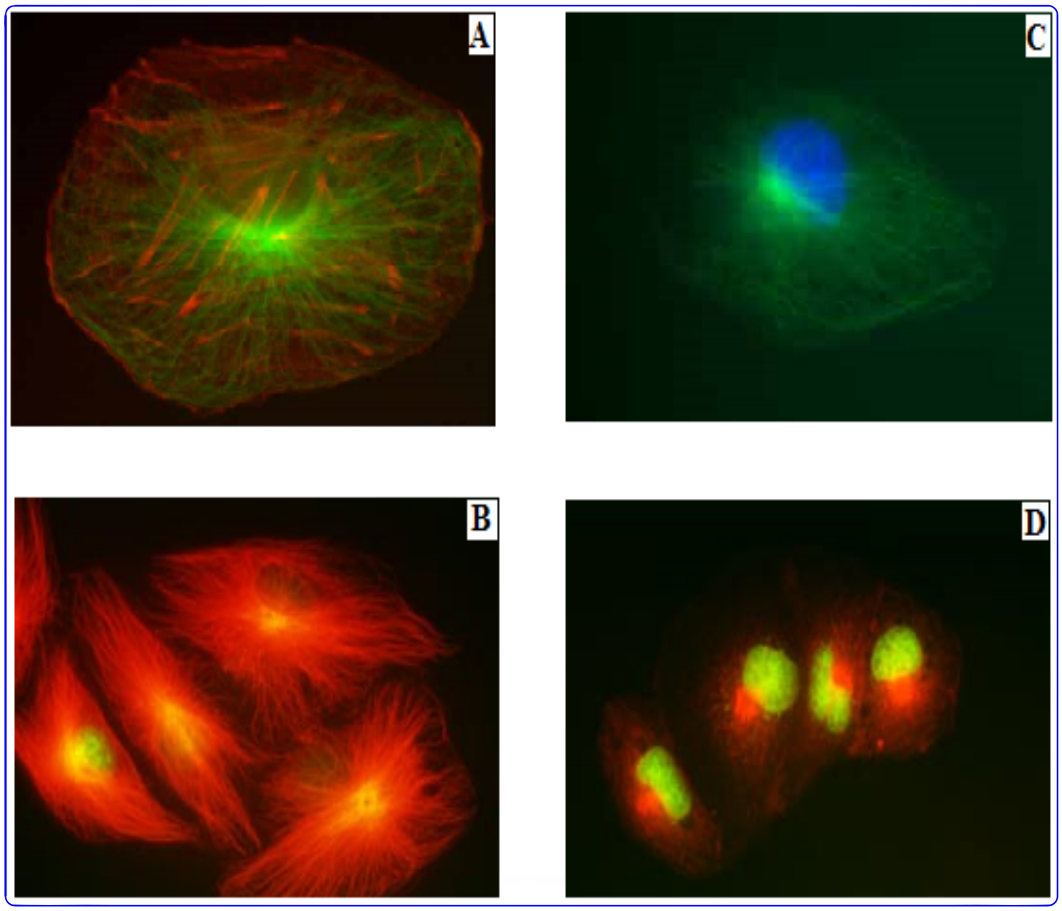

Figure 4-19. Fluorescently stained cellular structures[155] (Figure was adapted from http://www.itg.uiuc.edu/technology/atlas/structures/actin/images/actin_microtubules.jpg&imgrefurl)

In Figure 4-19 cultures epithelial cell are stained – (**A)** visualizes actin (red) cytoskeleton using rhodamine-conjugated phalloidin and microtubules (green) using fluorescein-conjugated antibodies to tubulin, **(B)** visualizes nucleus (green) using sytox green and microtubules (red) using rhodamine-conjugated antibodies to tubulin, **(C)** visualizes microtubules (green) using fluorescein-conjugated antibodies to tubulin and nucleus (blue) using chromamycin stain specific for DNA and **(D)** visualizes nucleus (green) using sytox green, a DNA specific dye and golgi apparatus (red) using rhodamine-conjugated antibodies to wheat germ agglutin.

Thus with so many readily available fluorophore dyes capable of detecting cellular organic biomolecules, we focused on fluorescein and fluorescein isothiocyanate (FITC) due to their high quantum yields, water solubility and ease of chemical modification without losing their fluorescent capability. A set of fluorescent probes – (a) Folate-4-carbon linker-FITC, (b) Folate-PEG-FITC and (c) Folate-PEG-linker-paclitaxel-fluorescein conjugate were synthesized and their structures are shown in Figure 4-20. These fluorescent probes were successfully used to study the effective internalization of

the tumor-targeting conjugates inside the cancer cells overexpressing folate receptors, effective cleavage of the disulfide linkers regenerating the potent taxane and the drug's binding to the microtubule.

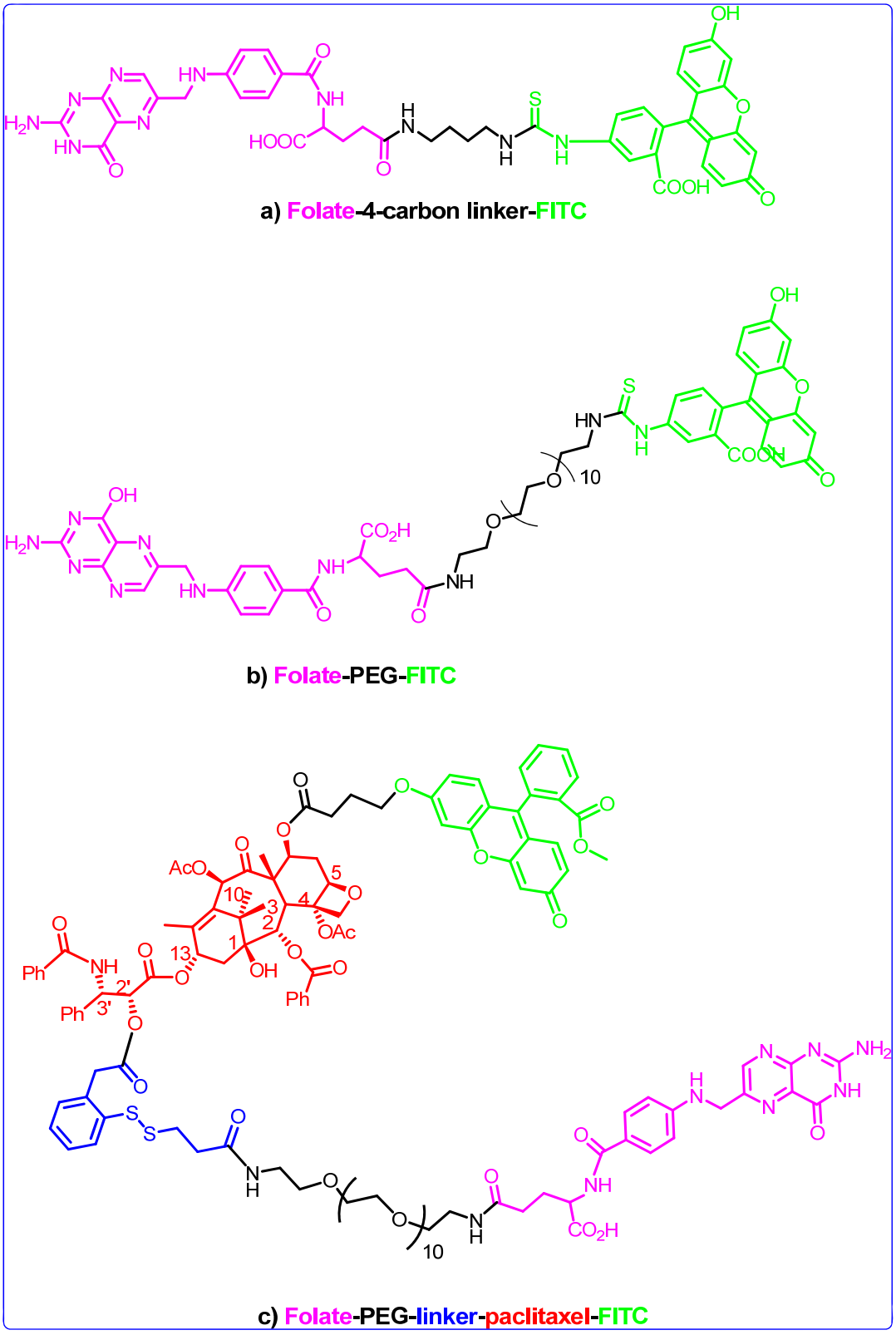

Figure 4-20. Structures of fluorescent probes

4.3 Results and Discussion

4.3.1 Design of Folate Receptor Targeted Drug Conjugate

A tumor-targeting drug delivery conjugate was designed to target cancer cells specifically using folic acid as the tumor-targeting moiety, taxane as the cytotoxic warhead and the novel mechanism-based self-immolative disulfide linker to connect the TTM to the cytotoxic drug as shown in Figure 4-21.

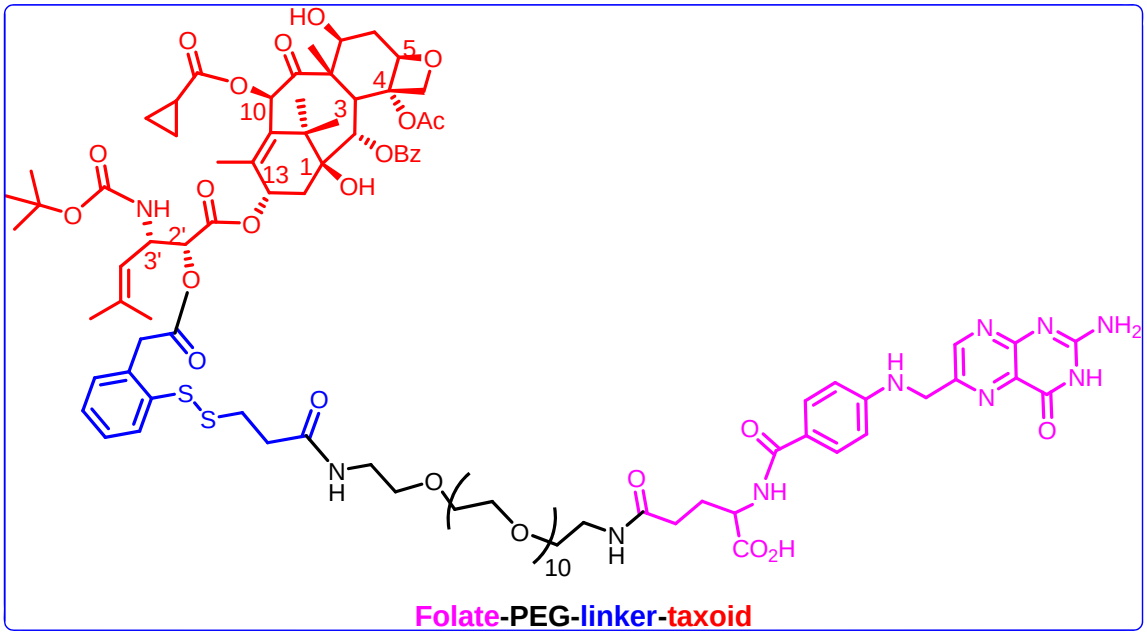

Figure 4-21. Structure of tumor-targeting drug delivery conjugate

A short heterofunctional polyethylene glycol (PEG) was introduced in the design to lend water solubility to the folate moiety. PEG is one of the most widely used biocompatible polymers in medicine and other industrial applications. It has excellent solubility in aqueous and most organic solvents. PEG has low toxicity and does not induce immunogenic response. It has favorable pharmacokinetics and tissue distribution. PEG has been approved by FDA for use *in vivo*. PEG modification of therapeutics has been clinically proven to have a) increased *in vivo* half-life because of decreased enzymatic degradation and decreased kidney excretion b) enhanced drug performance with reduced immunogenicity, antigenicity and toxicity c) improved physicochemical properties due to improved solubility and stability. Inside the blood stream, the PEG chain is heavily hydrated and is in rapid motion which causes the PEG to sweep out a large volume and prevent interference from other molecules. Therefore, PEG protects the drug molecules from immune responses and other clearance mechanisms. The short PEG moiety which was chosen had amine functional group at one terminus and azide functional group at the other terminus. The azide group can be converted to amine with relative ease for further conjugation and is versatile enough to be used for other reactions such as 'click chemistry' without compromising the integrity of the folate-PEG moiety. At an early

stage of design and planning it was realized that purification and isolation of these conjugates would require extensive reverse phase preparative HPLC and could not be performed using conventional flash chromatography. Thus to keep the purification process to a minimum the PEG moiety was first attached to the folate and the free azide group was reduced and then subjected to coupling with the coupling-ready warhead conjugate to obtain the final conjugate.

A model reaction with folic acid was carried out to determine reaction conditions and monitor progress of reaction using proton NMR. Folic acid was reacted with *N*-hydroxysuccinimide (NHS) in anhydrous dimethylsulfoxide (DMSO) at room temperature and then reacted with benzyl amine as shown in Scheme 4-2. This reaction was performed in an NMR vial and the progress was determined by the shift of the methylene protons in benzyl amine and the shift of the protons on the two methylene groups in NHS. Dicyclohexyl carbodiimide (DCC) and diisopropyl carbodiimide (DIC) were both tried. Anhydrous dimethylformamide (DMF) was also tried as a solvent but results with DMSO were consistent. Benzyl amine was chosen for the model reaction because it has less peaks interfering with FA, NHS, DCC and the intermediates formed during the reaction and the benzyl –CH_2– would give an identifiable and distinguishable peak. Both DIC and DCC were tried as coupling reagents to form the N-hydroxysuccinimide (NHS) activated ester. It was found during NMR monitor of the reaction that FA-NHS formation was slower with DIC than with DCC.

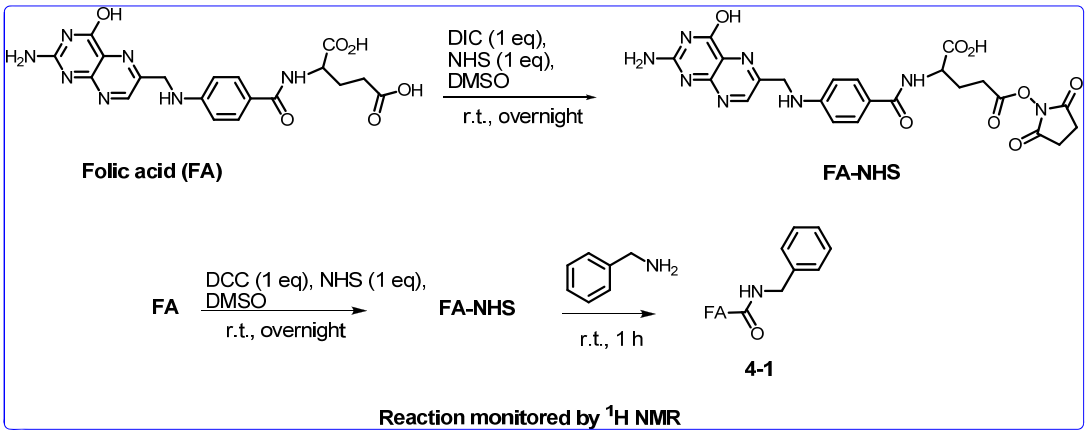

Scheme 4-2. Model reaction with folic acid monitored by NMR

Model reactions were performed using folic acid and benzyl amine to determine reaction conditions for scale up of the synthesis of folic acid PEG conjugate which would give pure products without requiring preparative HPLC purification (Scheme 4-3). Polymer supported carbodiimide (PS-DCC) was used in place of DCC to activate the folic acid for coupling with benzyl amine. This process also ensures that the urea byproduct formed would be easily removed and the product will be pure. In one instance HOBt was used to make the activated ester intermediate before coupling with benzyl amine to determine if there is any difference in the formation of the product. From the various reaction conditions used and MS monitoring (FIA and LC-MS) it seems that the

desired product is also associated with unreacted folic acid and the bis-substituted folic acid-benzyl amine.

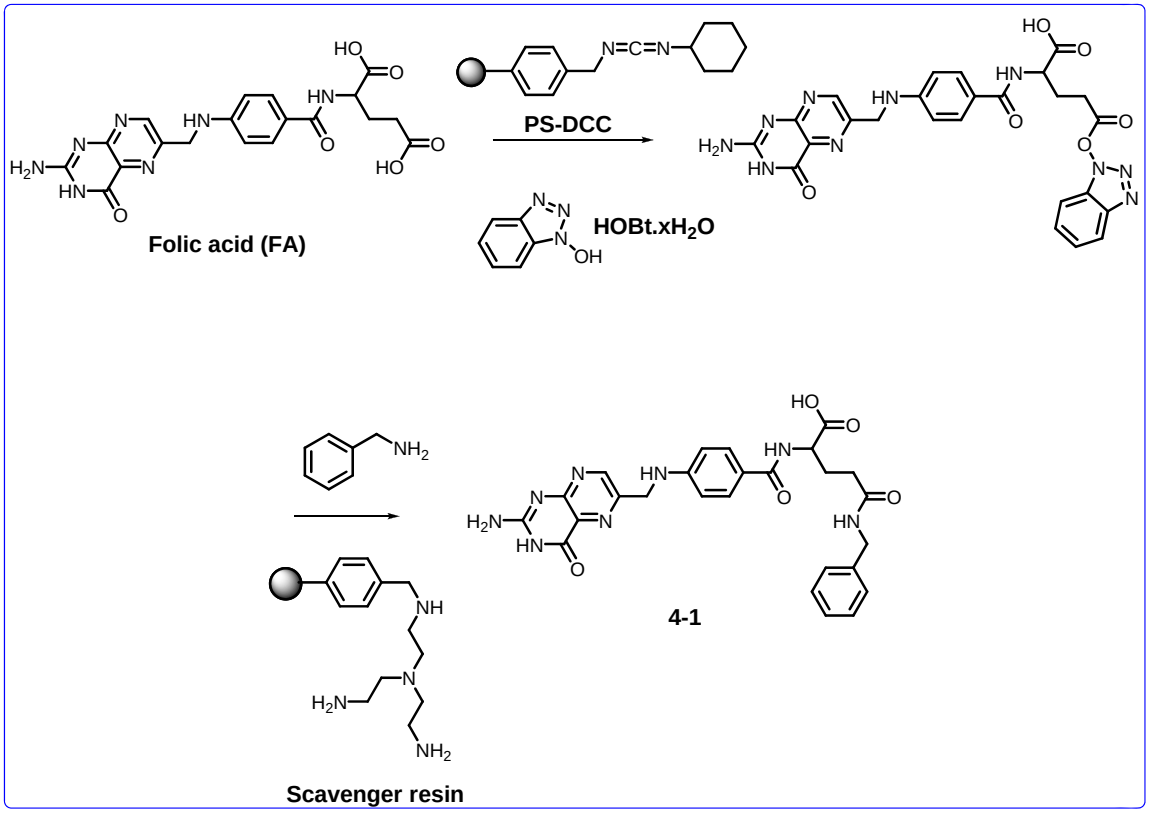

Scheme 4-3. Model reaction with folic acid using PS-DCC

The reaction conditions and results are tabulated in Table 4-1. In all the reactions listed below folic acid used was 50 mg (0.113 mmol) and the reactions were carried out at room temperature. The reactions were monitored by mass spec (FIA analysis) in ESI mode and the approximate yields are calculated based on MS data and benzyl amine as the limiting reagent. Reaction 7 has the desired mono-substituted product with very little contamination from starting material (FA) and may be used for scale-up.

	PS-DCC/ Time	HOBt/ scavenging resin	Benzyl amine/ Time	DMF	Pyridine	Yield (%)	Ratio of mono: bis: FA
1	1 eq/ 1 h	-	0.8 eq, 10 µL/ overnight	3 ml	0.1 ml	15 mg (~ 15 %)	1:0.1:2
2	3 eq/ 1 h	-	0.8 eq, 10 µL/ overnight	3 ml	0.1 ml	31 mg (~ 30 %)	1:0.25:0.9
3	5 eq/ 1 h	1.1 eq/10	0.8 eq, 10	3 ml	0.15 ml	36.9	1:1:1

		eq	µL/ 3 d			mg (~ 26 %)	
4	10 eq/ 1 h	-	0.8 eq, 10 µL/ 3 d	3 ml	0.15 ml	20 mg (~ 14 %)	1:2:0
5	10 eq/ 3 h	-	0.8 eq, 10 µL/ overnight	10 ml	0.1 ml	45 mg (~ 67 %)	1:0.25:0.15
6	10 eq/ 3 h	-	0.8 eq, 10 µL/ overnight	10 ml	0.5 ml	40 mg (~ 60 %)	1:0.25:0.15
7	0.5 eq/ overnight	-	0.25 eq, 3 µL/ overnight	6 ml	-	3 mg (~ 20 %)	1:0:0.07

Table 4-1. Reaction conditions using PS-DCC

(Mono – mono-substituted FA, bis – bis-substituted FA and FA – folic acid).

The coupling reaction between FA and PEG was also tried with hexamethylphosphoramide (HMPA) as solvent to eliminate the need for reverse phase preparative HPLC purification. The desired product was obtained as determined by mass spectroscopy but the conversion of azide to amine did not yield much of the desired product possibly because of residual HMPA.

4.3.2 Synthesis of fluorescent probe

A set of fluorescent probes were synthesized to monitor the internalization of folate conjugates inside cancer cells as shown in Scheme 4-4 and Scheme 4-5.

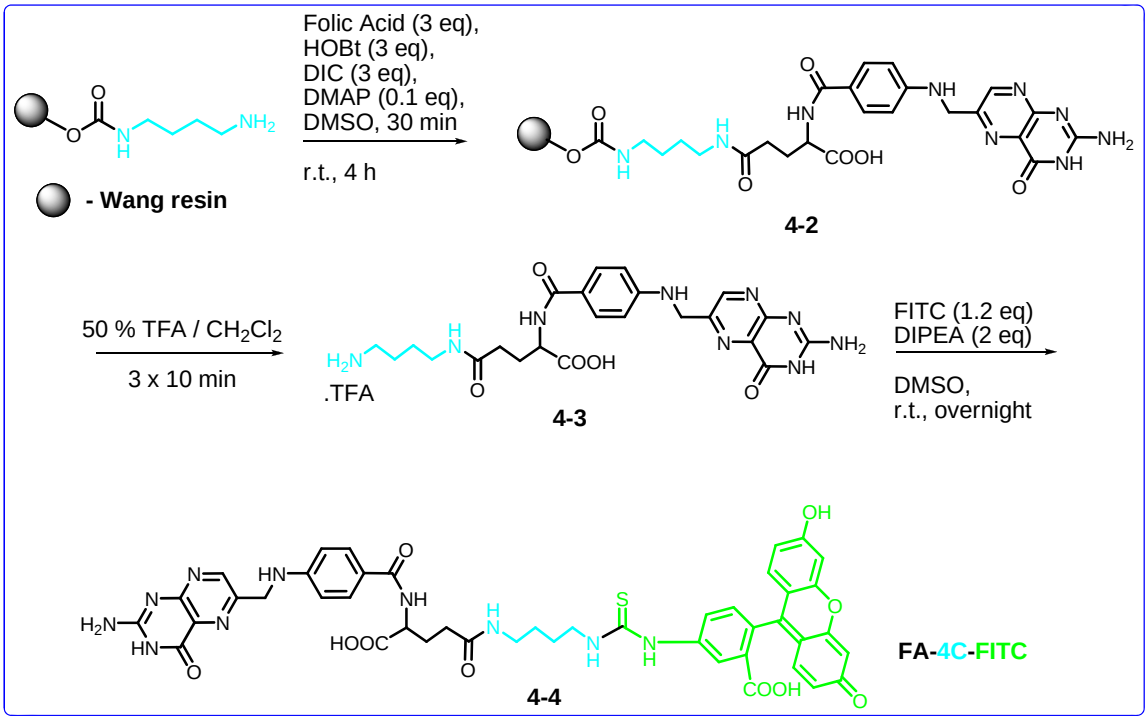

Scheme 4-4. Synthesis of FA-4C-FITC

A folate conjugate, FA-4C-FITC (**4-4**) was synthesized as an internalization standard to determine the specific internalization of folate conjugates inside cancer cell lines overexpressing folate receptor. This compound also provided a comparison parameter with the folate-PEG-FITC (**4-7**) conjugate and there was no determinable difference in efficacy of internalization between the two compounds. Thus introducing the short PEG chain in the compound **4-7** did not affect the efficacy or specificity of internalization.

Scheme 4-4 shows the solid phase synthetic scheme for the synthesis of FA-4C-FITC (**4-4**). An activated ester of FA was synthesized with *N*-hydroxybenzotriazole (HOBt) in presence of DIC using DMAP as catalyst and DMSO as solvent. This was then reacted with the 1,4-butane diamine attached to the Wang resin to form compound **4-2** which after TFA/DCM mediated cleavage from the resin yielded the TFA salt of folate-4C-NH_2 (**4-3**). Compound **4-3** was then coupled to fluorescein isothiocyanate (FITC) in presence of base and DMSO as solvent to obtain final internalization standard FA-4C-FITC (**4-4**).

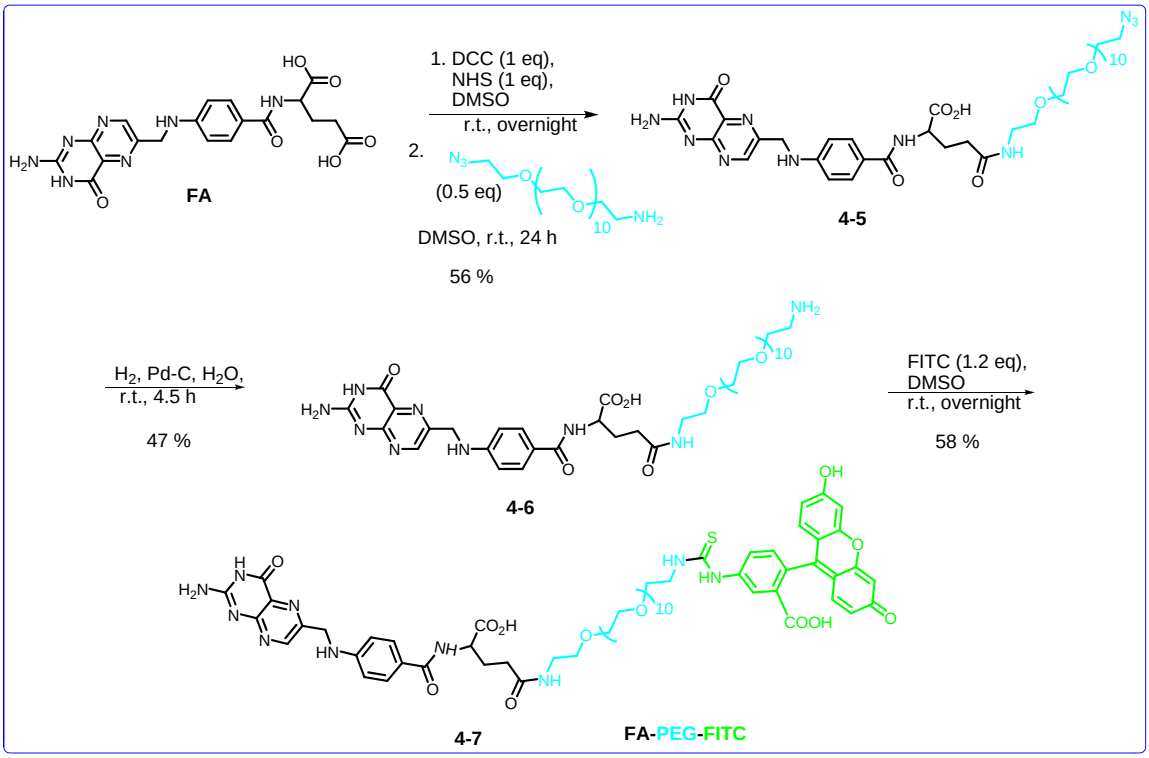

Scheme 4-5. Synthesis of FA-PEG-FITC conjugate

FA was converted to the active ester with *N*-hydroxysuccinimide (NHS) and reacted with azido-PEG-amine (10-mer) to form the desired azide terminated conjugate **4-5** as shown in Scheme 4-5. The γ-carboxylic acid group has higher reactivity than α-carboxylic acid group of the glutamic acid moiety of FA and therefore the γ-substituted product is the major product. The azide terminated conjugate **4-5** was soluble in water and was reduced to the amine **4-6** in presence of hydrogen gas using palladium-carbon (Pd/C) as catalyst. The compound **4-6** was then coupled with FITC in presence of base to form the desired FA-PEG-FITC conjugate (**4-7**). The α-substituted and the γ-substituted products were separated on preparative HPLC and no difference in their internalization ability was observed.[30, 156]

4.3.3 Synthesis of Novel Disulfide Linker

As discussed in chapter 3 novel mechanism-based disulfide linkers were synthesized and various studies were performed to determine the mode of cleavage and stability. The synthesis of the bifunctional disulfide linker used in the design of the tumor-targeting folate conjugate is shown in Scheme 4-6.

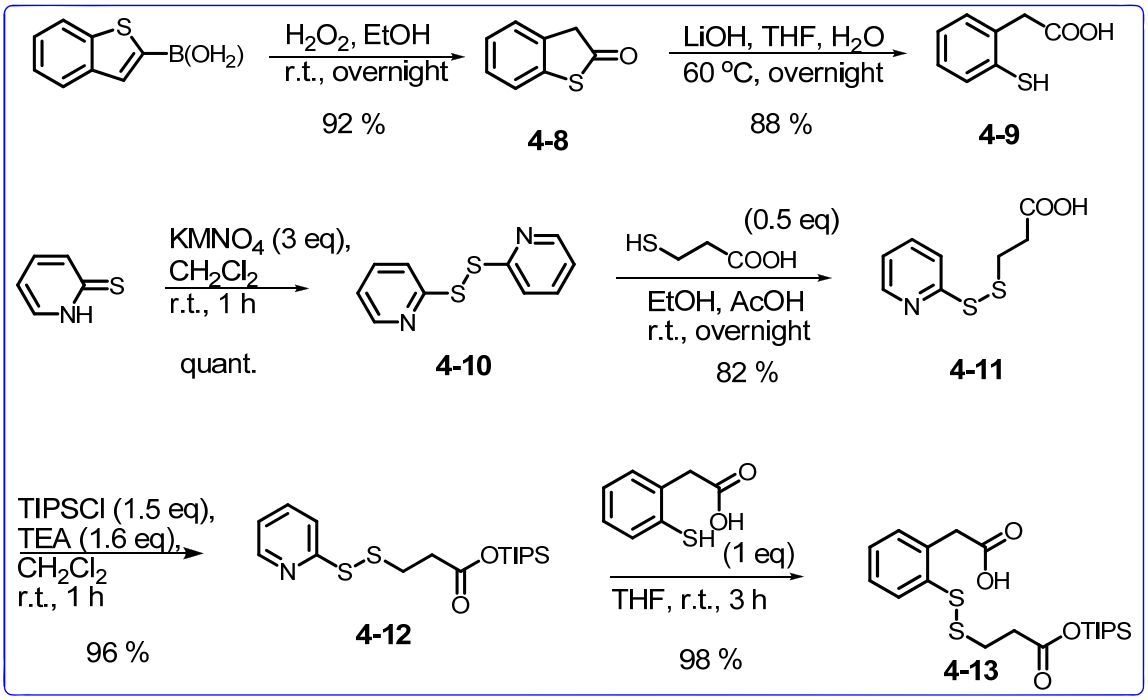

Scheme 4-6. Synthesis of novel disulfide linker

Thianaphthene-2-boronic acid was oxidized to the thiolactone **4-8** with hydrogen peroxide which was then hydrolyzed to (2-mercaptophenyl) acetic acid (**4-9**) using LiOH as base. Pyridine-2-thione was oxidized with potassium permanganate to yield 2, 2'-dithiodipyridine (**4-10**) which was then reacted with 3-mercapto propanoic acid to form 3-(2-pyridyldisulfanyl) propanoic acid (**4-11**). The compound **4-11** was protected with TIPS to generate **4-12** which was then reacted with **4-9** to form **4-13**. Another method was attempted to synthesize **4-10** but the method shown in Scheme 4-6 gave excellent yield of pure compound with no purification. The TIPS protected compound was used to connect the TTM with the cytotoxic warhead.

4.3.4 Synthesis of Fluorescent Probe to Study Drug Release

A fluorescent probe was designed and synthesized to visualize the drug release and binding to the microtubules. A fluorescein tag was attached to the taxane molecule to visualize its binding to the microtubules after its release from the folate prodrug conjugate. The synthetic steps are illustrated in Schemes 4-7, 4-8 and 4-9. Commercially available mono-*t*-boc protected succinic acid ester was reduced with borane dimethylsulfide to form the corresponding alcohol 4-hydroxy-butyric acid *t*-butyl ester **4-14**. This compound was used as a spacer to connect the fluorescein to the taxane molecule. Fluorescein was first converted to its methyl ester (**4-15**), followed by Mitsunobu coupling with 4-hydroxy-butyric acid tertbutyl ester (**4-14**), to give the protected fluorescein derivative (**4-16**). Deprotection of the tert-butyl group afforded 2-[6-(3-carboxy-propoxy)-3-oxo-3H-xanthen-9-yl]benzoic acid methyl ester (**4-17**).

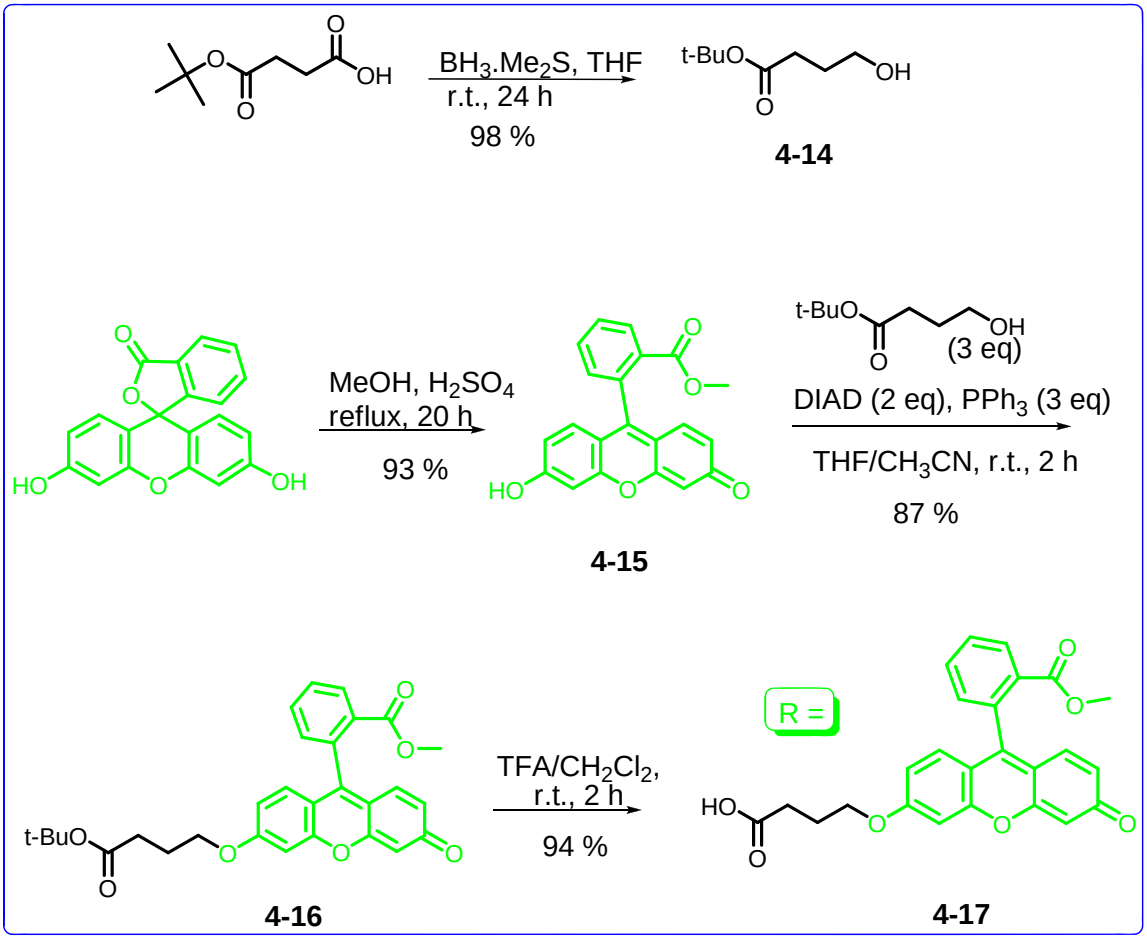

Scheme 4-7. Synthesis of modified fluorescein

Schemes 4-8 and 4-9 illustrate the installation of fluorescein-spacer unit (**4-17**) onto the paclitaxel. The free C-2' hydroxy group of paclitaxel was first protected by tert-butyldimethylsilyl (TBDMS) group to obtain (**4-18**), followed by C-7 modification with carboxylic acid tethered fluorescein unit (**4-17**) to give the protected fluorescein-paclitaxel conjugate (**4-19**). Deprotection of TBDMS, provided the desired fluorescein-paclitaxel conjugate (**4-20**). Subsequently, the resulting fluorescein-paclitaxel conjugate (**4-20**) was coupled with mono-TIPS ester of the disulfide linker carboxylic acid (**4-13**) to afford a TIPS-protected linker-paclitaxel-flurorescein conjugate (**4-21**). The TIPS protecting group was then removed by HF-pyridine to give the linker-paclitaxel-flurorescein conjugate (**4-22**). The resulting carboxylic acid group in (**4-22**) was converted to the corresponding activated ester (**4-23**) using NHS/DIC, which was then reacted with folate-PEG-amine conjugate (**4-6**) to provide the folate-linker-paclitaxel-fluorescein conjugate (**4-24**) in reasonable overall yield.

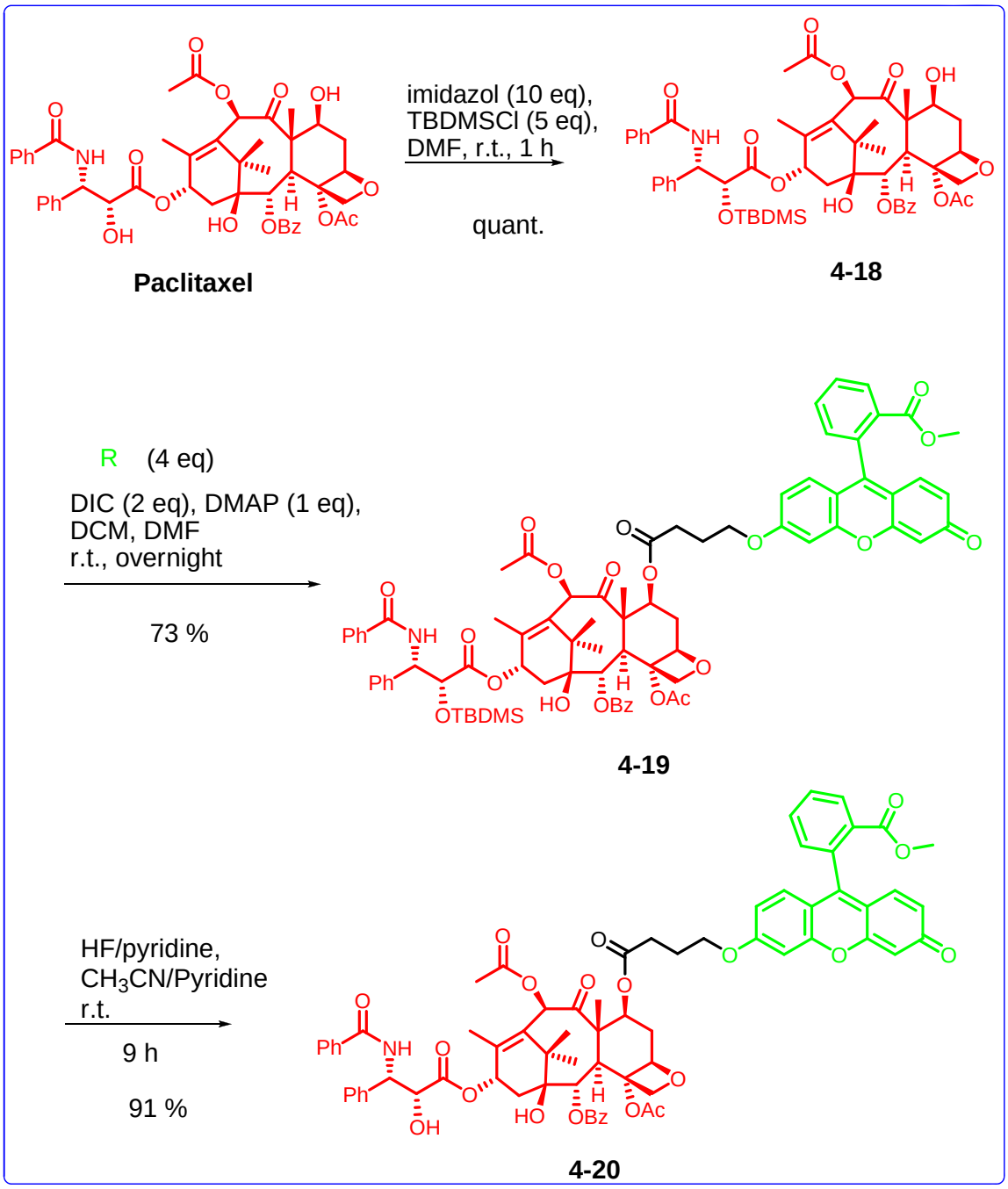

Scheme 4-8. Synthesis of fluorescein tagged paclitaxel

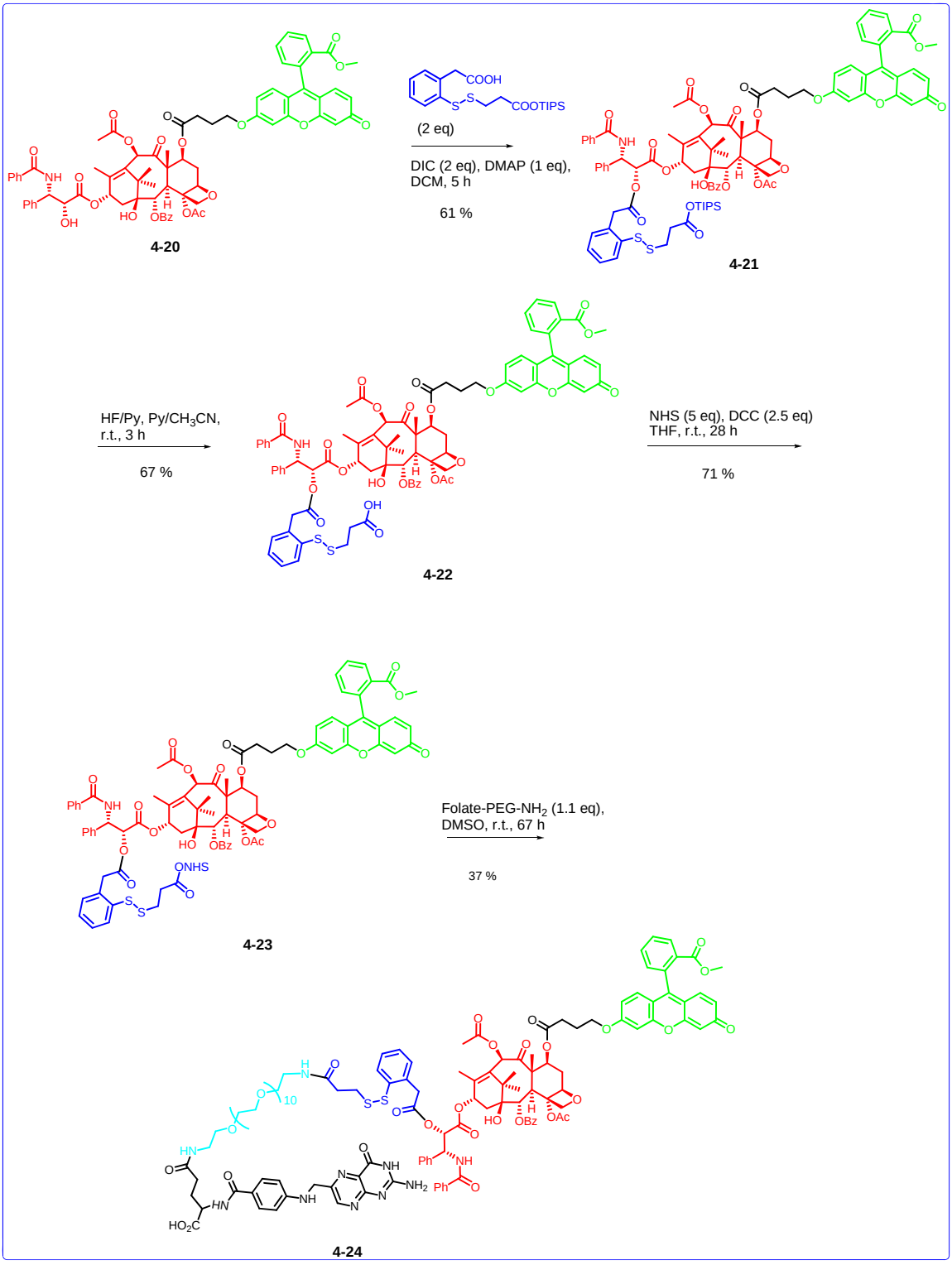

Scheme 4-9. Synthesis of fluorescein tagged tumor-targeting prodrug conjugate

4.3.5 Synthesis of Tumor-targeting Prodrug Conjugate

The tumor-targeting prodrug conjugate with folate as the TTM and novel second-generation taxoid as the cytotoxic warhead was synthesized as shown in Scheme 4-10.

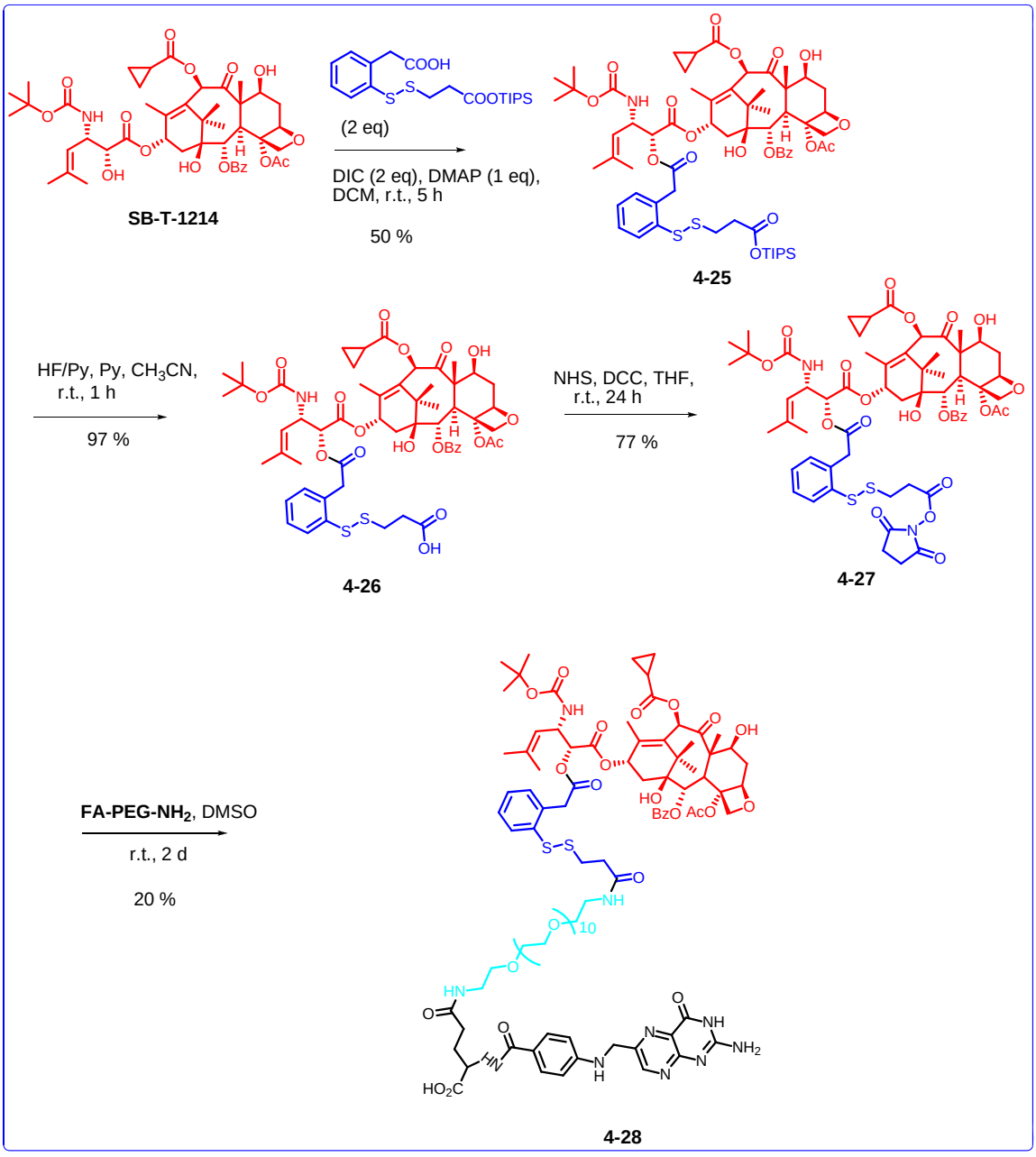

Scheme 4-10. Synthesis of folate-taxoid conjugate

Second-generation taxoid SB-T-1214 was prepared as described in chapter 1 and was used for the synthesis of the folate-taxoid conjugate. The linker **4-13** was coupled to the C-2' of SB-T-1214 to form conjugate **4-25** followed by deprotection of TIPS group using HF-pyridine to form the free acid terminated conjugate **4-26**. This compound was then

converted to the activated ester using NHS/DCC to form compound **4-27** which was then coupled to FA-PEG-NH_2 (**4-6**) conjugate to obtain desired conjugate **4-28**.

4.3.6 *In Vitro* Biological Evaluation

The cellular uptake of the tumor recognition moiety, i.e. folic acid, was assayed *in vitro* with leukemia cancer cells (L1210FR and L1210) using CFM under various conditions. Initially, certain parameters such as effect of conjugation to FA with small and long chained linkers, conjugate concentration and incubation time were examined. The results of the concentration dependent internalization studies using FA-4C-FITC (**4-4**) are shown in Figure 4-22. Studies were performed using **4-4** from concentrations ranging from 10 μM to 10 pM at ten times serial dilution.

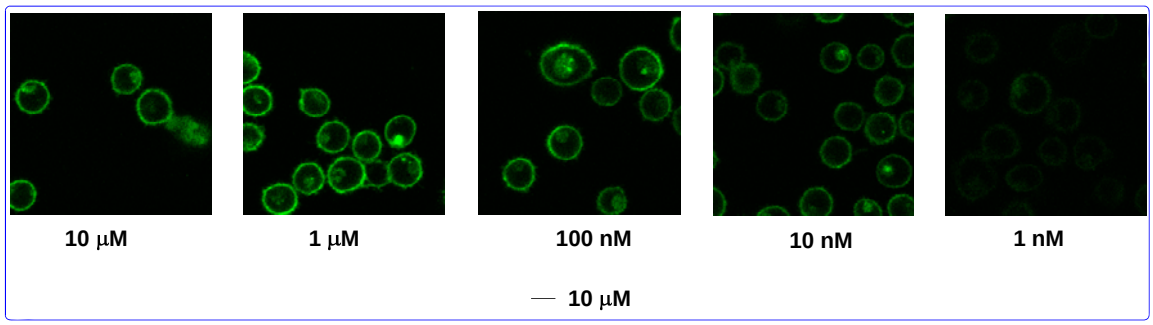

Figure 4-22. Concentration dependent CFM images of 4-4 with L1210FR leukemia cells

The results of the concentration dependent internalization studies using FA-PEG-FITC (**4-7**) are shown in Figure 4-23. Studies were performed using **4-7** from concentrations ranging from 10 μM to 10 pM at ten times serial dilution. There is no observed difference in internalization ability between **4-4** and **4-7**. All incubations were performed at 37 ^{o}C and for 3 h. The results clearly indicate that even at 10 nM concentration there is effective internalization. In both cases the fluorescence intensity decreased significantly at concentrations lower than 10 nM.

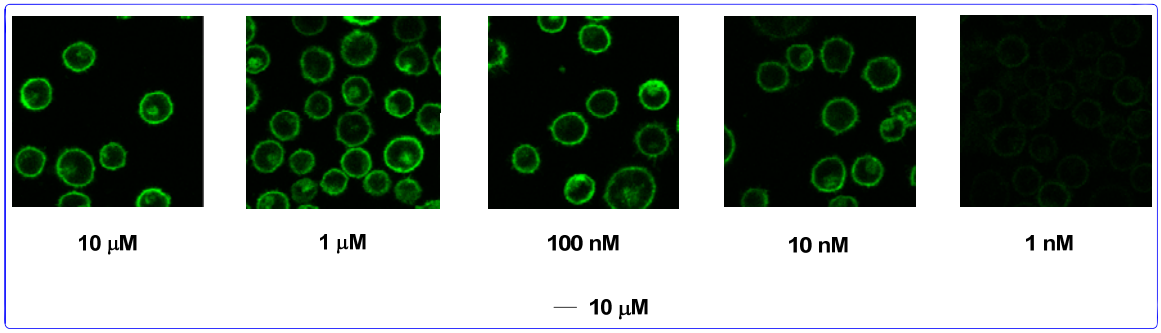

Figure 4-23. Concentration dependent CFM images of **4-7** with L1210FR leukemia cells

The two isomers of **4-7** were isolated and incubated at 100 nM concentration in L1210FR cells at 37 ^{o}C for 3 h and no difference in internalization ability were observed between the two isomers as shown in Figure 4-24.

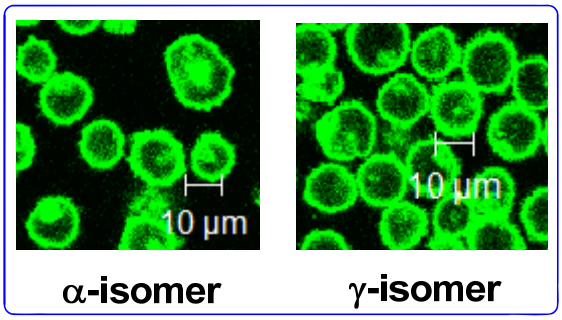

Figure 4-24. CFM images of both isomers of **4-7**

When **4-7** was incubated with L1210FR cells at 37 ^{o}C for various lengths of time such as 5 min, 10 min, 30 min and 60 min it effectively internalized inside the cells. Even at 5 min **4-7** binds to the L1210FR cells as shown in Figure 4-25.

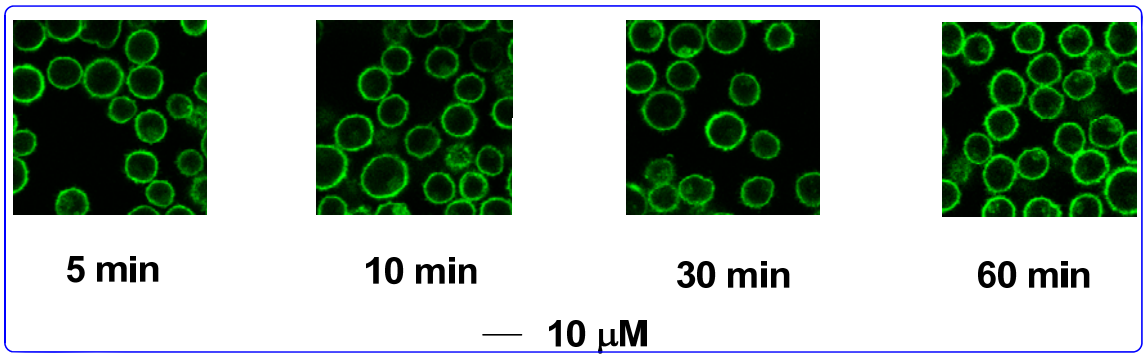

Figure 4-25. Time dependence CFM images of **4-7** incubated with L1210FR cells at 37 ^{o}C

Internalization of **4-7** (100 nM) was studied in presence of FA and compared with the control (no FA was added) as shown in Figure 4-26. Incubation was carried out at 37 ^{o}C for 3 h and even in the presence of 50 nM FA some internalization was observed. The physiological concentration of FA is typically between 5-20 nM.

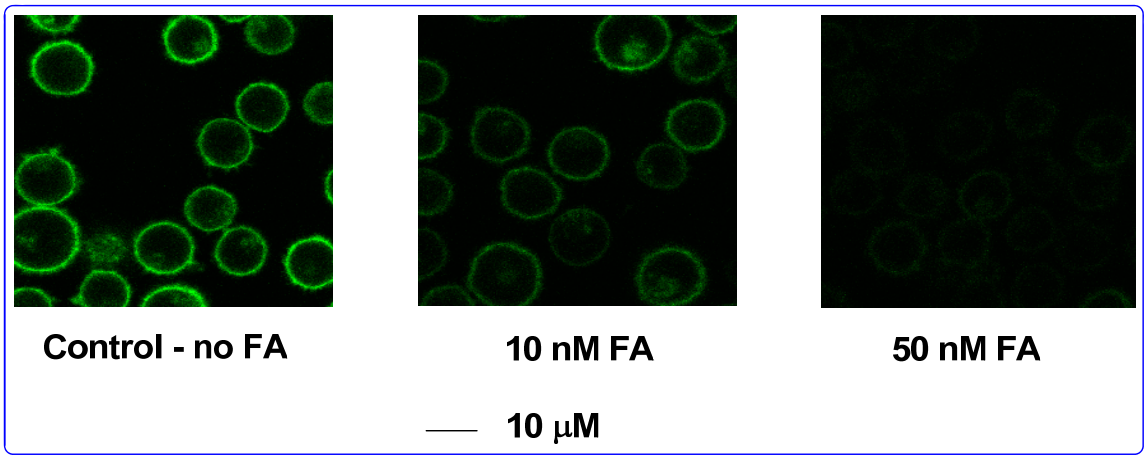

Figure 4-26. CFM images of 4-7 incubated with L1210FR in presence of 0, 10, 50 nM FA

Based on the above observations it can be concluded that 100 nM of the conjugate incubated for 1-3 h is suitable for further studies.

Figure 4-27 shows the various levels of folate receptor expression studied in different cell lines. It was determined that the level of FR expression can be categorized as –

(a) > 6 pmol/mg protein – high positive
(b) 2.5 – 6 pmol/mg protein – low positive
(c) < 2.5 pmol/mg protein – negligible

A549 human lung cancer cell lines has no FR expression while L1210 leukemia cell lines, KB human nasopharynx carcinoma, M109 lung cancer, HeLa human cervical cancer expresses FR at a high level.[157] Accordingly, A549 cell line was used as the control.

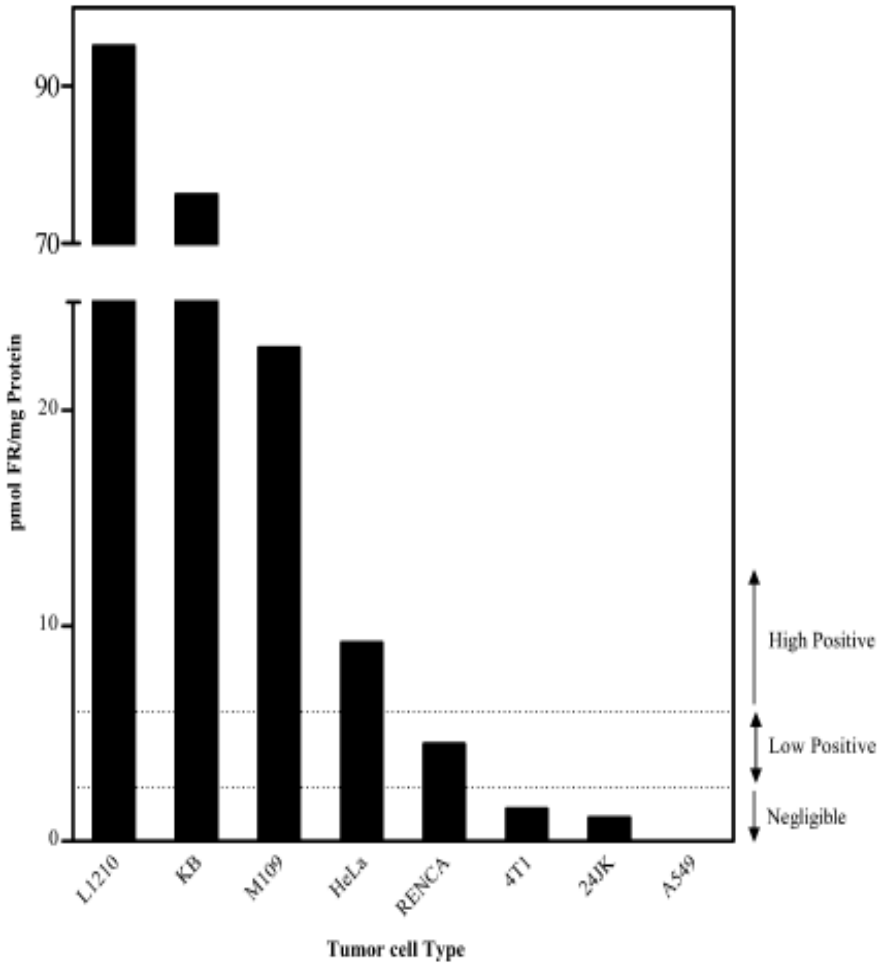

Figure 4-27. Folate receptor expression in various cells[157] (Figure adapted from Ref. 157)

Figure 4-28 shows the internalization specificity of **4-7** in various cell lines with different levels of folate receptor expression. The difference in fluorescence intensity in the CFM images clearly indicates that there is no internalization of the fluorescent probe in FR(-) A549 whereas the intensity difference clearly shows that ID8 which has a lower expression of FR compared to L1210 and L1210FR has a lesser internalization of **4-7**. The data clearly demonstrates the specificity of this conjugate which clearly correlates with the FACS analysis using flow cytometry.

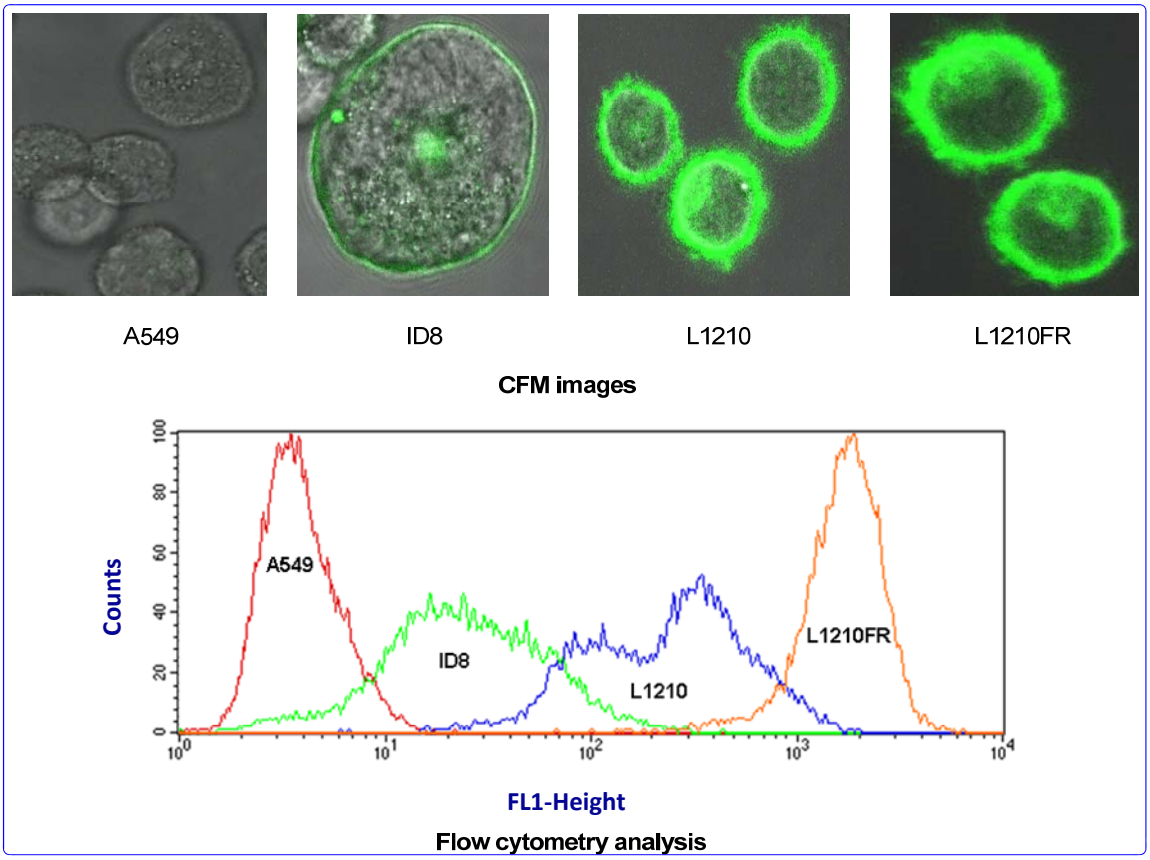

Figure 4-28. CFM images of **4-7** incubated with different cell lines along with FACS analysis

Figure 4-29 shows the internalization of fluorescent conjugate **4-24** in L1210FR cell lines in the absence and presence of glutathione. The CFM image A in Figure 4-29 clearly sows the internalization of the conjugate inside the cell while CFM image B shows that in the presence of glutathione there is release of the fluorescent labeled drug which is bound to the microtubules. To further study the internalization and visualize the release of the drug from the mechanism-based linker an immunofluorescent assay was performed with fluorescent conjugate **4-24** and the results are shown in Figure 4-30.

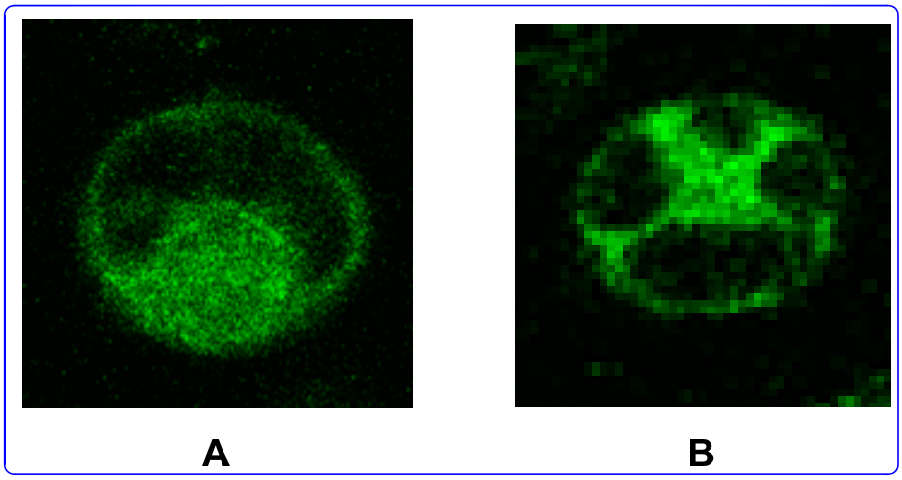

Figure 4-29. CFM images of 100 nM of **4-24** using L1210FR cell lines A) without glutathione B) with glutathione

Figure 4-30 shows the CFM images of indirect immunofluorescent assay. Figure 4-30 A shows that the microtubules in L1210FR have been stained, B shows that when **4-7** was incubated with L1210FR cells it internalized as can be seen from the red and green fluorescent colors and C shows that when **4-24** is incubated with L1210FR cell it internalizes and when glutathione is added to enhance the cleavage of the conjugate the drug gets released successfully and binds to the microtubules as can be seen from the yellow color. The yellow color is because of the overlap of green fluorescent label of the drug with the red stained microtubule.

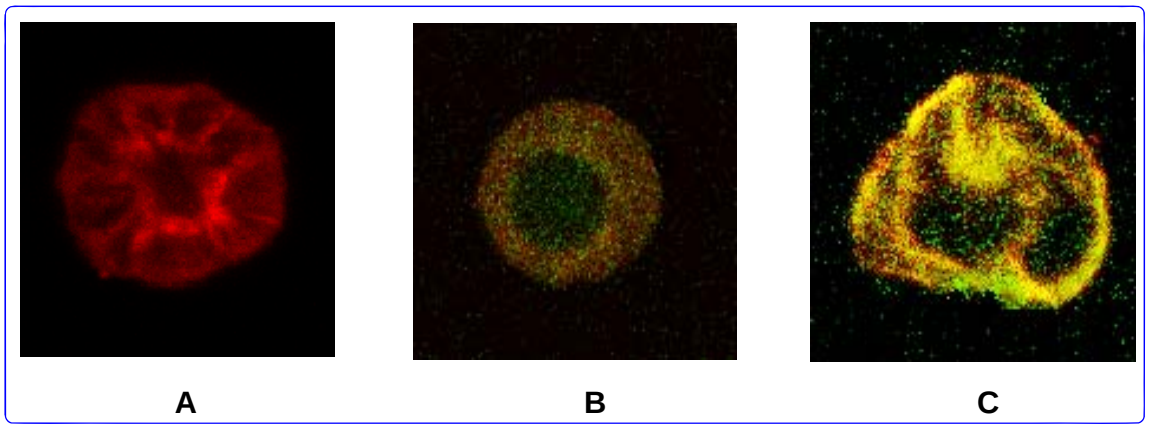

Figure 4-30. CFM images A) stained microtubule B) **4-7** incubated with L1210FR C) **4-24** incubated with L1210FR

These studies clearly indicate that the tumor-targeting DDS efficiently and specifically internalizes inside cancer cells *in vitro* and are worthy of further development.

In vitro cytotoxicity assays (IC_{50}, nM) performed in various cell lines clearly indicate the effectiveness and specificity of conjugate **4-28** as shown in Table 4-2.

Cell line	SB-T-1214	4-28	Paclitaxel
L1210FR	11.5	3	200
L1210	17.0	13	180
A549	1.4	>1000	7.3
ID8	7.6	<1	36.4

Table 4-2. *In vitro* cytotoxicity assay in various cell lines (IC_{50}, nM)

4.4 Experimental Section

General Methods: ^{1}H, ^{13}C and ^{19}F NMR spectra were measured on a Bruker AC-250 NMR spectrometer or a Varian 300, 400, 500, or 600 MHz NMR spectrometer. The melting points were measured on a "Uni-melt" capillary melting point apparatus from Arthur H. Thomas Company, Inc. Optical rotations were measured on a Perkin-Elmer Model 241 polarimeter. High-resolution mass spectrametric analyses were conducted at the Mass Spectrometry Laboratory, University of Illinois at Urbana-Champaign, Urbana, IL. GC-MS analyses were performed on an Agilent 6890 Series GC system equipped with the HP-5HS capillary column, (50 m X 0.25 mm, 0.25 μm) and with the Agilent 5973 network mass selective detector. LC-MS analyses were carried out on an Agilent 1100 Series Liquid Chromatograph Mass Spectrometer. IR spectra were measured on a Shimadzu FTIR-8400s spectrophotometer. TLC analyses were performed on Merck DC-alufolien with Kieselgel 60F-254 and were visualized with UV light, iodine chamber, 10 % sulfuric acid and 10% PMA solution. Column chromatography was carried out on silica gel 60 (Merck; 230-400 mesh ASTM). Chemical purity was determined with a Waters HPLC assembly consisting of dual Waters 515 HPLC pumps, a PC workstation running Millennium 32, and a Waters 996 PDA detector, using a Phenomenex Curosil-B column, employing CH_3CN/water as the solvent system with a flow rate of 1 mL/min, or shimazu HPLC. Chiral HPLC analysis for the determination of enantiomeric excess was carried out with a Waters HPLC assembly, comprising Waters M45 solvent delivery system, Waters Model 680 gradient controller, Water M440 detector (at 254 nm) equipped with a Spectra Physics Model SP4270 integrator. The system uses a DAICEL-CHIRACEL OD chiral column (25 x 0.46 cm i.d.), employing hexan/2-propanol as the solvent system with a flow rate of 1.0 mL/min.

Materials: The chemicals were purchased from Sigma Aldrich Company or Acros Organic Fischer Company. 10-Deacetyl baccatin III (DAB) was donated by Indena, SpA, Italy. Dichloromethane and methanol were dried before use by distillation over calcium

hydride under nitrogen or argon. Ether and THF were dried before use by distillation over sodium-benzophenone ketyl under nitrogen or argon. Toluene and benzene were dried by distillation over sodium metal under nitrogen or argon before use. Dry DMF was purchased from EMD chemical company, and used without further purification. PURE SOLV^{TM}, Innovative technology Inc, provided an alternative source of dry toluene, THF, ether, and dichloromethane. The glasses were dried in a 110 ^{o}C oven and allowed to cool to room temperature in a desiccator over "*Drierite*" (calcium sulfate) and assembled under inert gas nitrogen or argon atmosphere.

Model reactions with Folic acid

FA-benzylamine conjugate (4-1): Model reaction 1

In a NMR tube folic acid (22.6 mg, 0.05 mmol) dissolved in DMSO-d6 (c 0.05M) was added. ^{1}H NMR was recorded, NHS (1 eq) was added and ^{1}H NMR was recorded again. Next, dicyclohexylcarbodiimide (DCC, 1 eq) was added and NMR was monitored. After overnight reaction benzyl amine (1 eq) was added and the amide bond formation was monitored by ^{1}H NMR.

Also, DMF was tried as solvent instead of DMSO and DMSO proved more efficient and easier to work with.

FA-benzylamine conjugate (4-1): Model reaction 2

Model reactions were performed using folic acid and benzyl amine to determine reaction conditions for scale up of the synthesis of folic acid PEG conjugate which would give pure products without requiring preparative HPLC purification. Polymer supported carbodiimide (PS-DCC) was used in place of DCC to activate the folic acid for coupling with benzyl amine. This also ensures that the urea byproduct formed would be easily removed and the product will be pure. In one instance HOBt was used to make the activated ester intermediate before coupling with benzyl amine to determine if there is any difference in the formation of the product. A scavenging resin was added and reaction stirred overnight to remove impurities. From the various reaction conditions used and MS monitoring (FIA and LC-MS) it seems that the desired product is also associated with unreacted folic acid and the bis substituted folic acid-benzyl amine. The reaction conditions and results are tabulated in Table 4-1. Reaction 7 has the desired product with minimum impurities and could be optimized further.

Synthesis of fluorescent probes

FA-4C-resin (4-2):

To a solution of folic acid (3 eq), *N*-hydroxybenzotriazol (3 eq), *i*Pr$_2$EtN (3 eq) and DMAP (0.1 eq) in DMSO (0.1 M for folic acid) was added *N*, *N*'-diisopropylcarbodiimide (3 eq). After reacting for 45 minutes at room temperature, the solution was loaded into the plastic syringe (equipped with polypropylene filter) with the Wang resin attached to 1, 4-butane diamine (1 eq). The syringe was plugged and the reaction mixture was agitated for 4 hours on shaker. The solution was drained and the resin was thoroughly washed (3x DMF, 3x CH_2Cl_2, 2x MeOH, 2x CH_2Cl_2, 2x MeOH)

and dried under vacuum to remove MeOH and obtain **4-2**. The resin color changed to orange. The Kaiser test was negative indicating no free primary amine.

FA-4C-NH_2 (4-3):
The plastic syringe (with the filter) containing resin **4-2** was loaded with 50 % solution of TFA in CH_2Cl_2 (2-3 mL) and the syringe was agitated for 10 minutes. The solution was drained and collected. The procedure was repeated 2 more times and the combined solutions were evaporated. The crude product **4-3** was subjected to coupling with FITC.

FA-4C-FITC (4-4):
DIPEA (2 eq) was added to a solution of **4-3** in DMSO (c 0.07M). Fluorescein isothiocyanate (FITC, 1.2 eq) was dissolved in DMSO and added to the reaction flask. The reaction was stirred for 24 hrs at room temperature. The pure compound **4-4** was obtained by preparative HPLC using Shimadzu HPLC and Jupiter Proteo RP C18 (250 x 4.6 mm, 10 μ) column. The desired pure product 7 mg was collected at 11 min (flow rate 15 mL/min, H_2O/0.1% formic acid : Acetonitrile 90:10). HRMS: (Q-TOF TOF MS ES+) *m/z* Calculated for $C_{44}H_{41}O_{10}N_{10}S^+$: 901.2728 Found: 901.2731 (Δ = 0.3 ppm).

FA-PEG-N_3 conjugate (4-5):
Folic acid (34 mg, 0.076 mmol) was dissolved in DMSO-d6 (c 0.05M) and added to a NMR tube followed by NHS (1 eq) in DMSO-d6, DCC (1 eq). The reaction was allowed to progress overnight and then dry pyridine (24 eq) and azido-PEG-amine (0.5 eq) was added and the reaction proceeded for 5 h. FA-PEG conjugate formation was confirmed by MS. Analytical HPLC was performed to determine a suitable method to purify the product using preparative HPLC. LC-MS was performed to determine the retention time of the desired product. The reaction mixture was ultracentrifuged to remove precipitated dicyclohexylurea (DCU) and the clear supernatant liquid was subjected to reverse phase preparative HPLC using a mobile phase of acetonitrile/water (8 min at 5/95, gradient through 50 min at 90/10) flow rate of 1 mL/min (analytical) and 20 mL/min (preparative). Column used was Jupiter reverse phase 10 μ C18 Phenomenex 300 Å, 250 X 4.60 mm. The wavelengths monitored were 220 and 280 nm. Two peaks at 20 min and 22 min had the same desired mass. This is possibly due to the amide bond formation at the γ - COOH and α – COOH of the glutamic acid moiety of FA. The different fractions were collected, the solvents removed and lyophilized. The pure products were yellow solids. The fraction collected at 19-22 min was probably the γ – amide (**4-5-G**, 60 mg, 49 % yield) and the fraction collected at 23 min was probably the α – amide (**4-5-A,** 10 mg, 8 %).
Folic acid (113 mg, 0.25 mmol) was dissolved in DMSO (c 0.05M) followed by NHS (1 eq) and DCC (1 eq) in DMSO. The reaction was allowed to progress overnight and then dry pyridine (24 eq) and azido-PEG-amine (0.5 eq) was added and the reaction proceeded for 24 h. FA-PEG conjugate formation was confirmed by MS. LC-MS was performed to determine the retention time of the desired product. The reaction mixture was centrifuged to remove precipitated dicyclohexylurea (DCU) and the clear supernatant liquid was subjected to preparative HPLC using a mobile phase of acetonitrile/water-0.1 % formic acid (8 min at 5/95, gradient through 50 min at 90/10) flow rate of 0.75 mL/min (LC-MS) and 20 mL/min (preparative). Column used was Jupiter proteo reverse phase 10 μ 90 Å,

250 X 4.60 mm. The wavelengths monitored were 214 and 280 nm. Two peaks at 20 min and 22 min had the same desired mass. The pure product **4-5** was obtained as a yellow solid (220 mg, 97 %). HRMS: (Q-TOF TOF MS ES+) *m/z* Calculated for $C_{41}H_{64}O_{11}N_{15}^{+}$: 950.4583 Found: 950.4565 (Δ = -1.9 ppm).

Alternate method used to synthesize **4-5** for scale up – HMPA was used as the solvent in place of DMSO and the rest of the conditions were the same as above. After the formation of product was determined using MS the reaction was transferred in centrifuge tubes and washed thoroughly with methanol, DCM, ether to remove impurities including the solvent HMPA. Then the precipitate was dissolved in water and **4-5** dissolved in water while unreacted FA did not. However, when the **4-5** was further reacted to form **4-6** the hydrogenation reaction was hampered because of trace amounts of HMPA.

FA-PEG-NH_2 conjugate (4-6):
FA-PEG-N_3 (**4-5**, 24 mg, 0.025 mmol) was taken in a flask and 10.8 mg of Pd/C was added to it and the flask was inerted. Then 4.6 mL of distilled water was added to dissolve 1-1b and H_2 was passed into the flask overnight and the reaction mixture was kept at room temperature. The product formation was confirmed by mass and the Pd/C was removed by centrifugation and the product was purified by preparative HPLC using Waters 996 photodiode array detector, Waters 515 HPLC pump and Jupiter Proteo RP C18 (250 x 4.6 mm, 10 μ) column. The desired pure product **4-6** was collected at 8.4 min (flow rate 16 mL/min, H_2O/0.1% formic acid : Acetonitrile 87:13) in 86 % yield (20 mg). ^{1}H NMR (400 MHz, D_2O): δ 1.92-2.38 (m, 4 H), 3.13-3.62 (m, 46 H), 4.36 (d, 3 H), 6.57 (s, 2 H), 7.47 (s, 2 H), 8.5 (s, 1 H), ^{13}C NMR (400 MHz, D_2O): δ 39.40, 49.19, 66.62, 66.96, 69.82, 70.26, 121.28, 129.53, 163.11, 165.92, HRMS: (Q-TOF TOF MS ES+) *m/z* Calculated for $C_{41}H_{66}O_{15}N_9^{+}$: 924.4678 Found: 924.4668 (Δ = - 1.1 ppm).

FA-PEG-FITC conjugate (4-7):
A flask containing **4-6** (9.4 mg, 0.01 mmol) and fluorescein isothiocyanate (1.2 eq) was inerted and dry DMSO (c 0.05 M) was added to the flask followed by diisopropylethylamine (DIPEA, 2 eq). The reaction was stirred at room temperature for 24 h and purified by reverse phase preparative HPLC (Jupiter Proteo RP C18 (250 x 4.6 mm, 10 μ) column, H_2O/0.1% formic acid : Acetonitrile) to obtain **4-7** as a yellow solid (7.5 mg) in 58 % yield. HRMS: (Q-TOF TOF MS ES+) *m/z* Calculated for $C_{62}H_{77}O_{20}N_{10}S^{+}$: 1313.5036 Found: 1313.5043 (Δ = 0.5 ppm).

Synthesis of disulfide linker

Benzo[b]thiophen-2(3H)-one (4-8):[158, 159]
Thianaphthene-2-boronic acid (1.81 g, 10 mmol) was dissolved in EtOH (17.5 mL) and hydrogen peroxide (30%, 3.3 mL) was added dropwise. The reaction mixture color changed from pink to reddish pink within 1 hr. The reaction mixture was stirred overnight at room temperature. TLC (eluant hexane/ethyl acetate 5:1) was performed. The reaction mixture was evaporated *in vacuo*. The reddish white crude residue was dissolved in saturated NaCl solution and extracted with chloroform (x3). The combined organic layer was dried over anhydrous $MgSO_4$ and concentrated *in vacuo*. The pure

compound 4-8 was obtained as white solid by flash chromatography on silica gel (40:1 hexane/ethyl acetate) in 92 % yield (1.38 g). ^{1}H NMR (300 MHz, $CDCl_3$): δ 3.98 (s, 2 H), 7.2-7.4 (m, 4 H).

(2-Mercaptophenyl)acetic acid (4-9):
Benzo[b]thiophen-2(3H)-one (**4-8)** (483 mg, 3.21 mmol) was added in a flask which was inerted (vaccum/nitrogen) and dissolved with dry THF (c 0.2 M). Distilled water (6.3 mL) was added to the flask. (Both THF and water was degassed before addition). Lithium hydroxide monohydrate (6 eq) was dissolved in 25 mL distilled water and syringed into the flask. The reaction mixture was heated to 60 ^{o}C using an oil bath for 14 h (overnight). The reaction was checked by TLC (eluant hexane/ethyl acetate 2:1) the next day and stopped. The flask was cooled to room temperature and the reaction mixture was diluted with water (20 mL) and diethyl ether (45 mL). The organic and aqueous layer was separated and the yellow aqueous layer was acidified with 6N aqueous HCl to pH ~2. The aqueous layer became white on acidification and was extracted with diethyl ether (x 3). The combined organic layer was then washed with brine, dried over anhydrous $MgSO_4$ and concentrated *in vacuo*. The pure compound **4-9** was obtained by flash chromatography on silica gel (10:1 hexane/ethylacetate) in 88 % yield (477 mg). ^{1}H NMR (300 MHz, $CDCl_3$): δ 3.49 (s, 1 H, S-H), 3.83 (s, 2 H on methylene carbon), 7.18-7.29 (m, 3 H), 7.41 (m, 1 H), 10.10 (b, 1 H), ^{13}C NMR (400 MHz, CDCl3): δ 39.85, 126.94, 128.25, 130.74, 131.00, 132.41, 133.33, 176.16

2, 2'-Dithiodipyridine (4-10):[160]
Pyridine-2-thione (114 mg, 1 mmol) was dissolved in DCM (c 0.08 M) in a flask. Potassium permanganate (3.2 mmol) was ground into fine powder using mortar and pestle and added in small portions over 15 – 20 min while vigorously stirring the reaction mixture at room temperature. TLC monitor (1:1 hexane/ethyl acetate) after 30 min indicated no starting material. The reaction mixture was filtered using frit funnel lined with celite and washed with DCM. The solution was concentrated *in vacuo* and dried to give **4-10** as yellow solid in quantitative yield (118 mg) with melting point of 55-58 ^{o}C. ^{1}H NMR (300 MHz, $CDCl_3$): δ 7.1 (m, 2 H), 7.6 (m, 4 H), 8.4 (m, 2 H).

2, 2'-Dithiodipyridine (4-10):[161] Alternate method
Pyridine-2-thione (208 mg, 1.87 mmol) was taken in a flask which was inerted and dissolved in DCM (c 0.25 M). Sulfuryl chloride (2.2 eq) was dissolved in DCM and added dropwise over 5-7 min using a dropping funnel. TLC monitor (1:1 hexane/ethyl acetate) after 30 min indicated no starting material. The yellow reaction mixture was concentrated *in vacuo* which resulted in a white powder with a melting point of 123-126 ^{o}C and insoluble in most organic solvents but soluble in water. This is probably the protonated form of 2-1. The previous procedure is more efficient and was used for synthesis of this compound.

3-(2-Pyridyldisulfanyl) propanoic acid (4-11):
A flask containing **4-10** (1.9 g, 8.6 mmol) was inerted. Degassed ethanol (200 proof, 7.6 mL) and glacial acetic acid (0.2 mL) was added. Degassed ethanol (200 proof, 1.4 mL) was used to dissolve and transfer 3-mercaptopropanoic acid (0.5 eq) dropwise into the

reaction mixture. The reaction mixture was stirred overnight at room temperature. The reaction mixture was concentrated *in vacuo* and the oily residue was dissolved in DCM and purified by flash chromatography using neutral alumina (DCM/methanol/acetic acid). The white product **4-11** was collected and dried under high vacuum to remove acetic acid (759 mg) in 82 % yield. ^{1}H NMR (400 MHz, $CDCl_3$): δ 2.79 (t, J = 6.8 Hz, 2 H), 3.06 (t, J = 6.8 Hz, 2 H), 7.14 (m, 2 H), 7.66 (m, 1 H), 8.48 (dd, J = 3.3, 1.2 Hz, 1 H), ^{13}C NMR (400 MHz, $CDCl_3$): δ 33.9, 34.1, 120.5, 121.2, 137.4, 149.4, 159.2, 175.6.

3-(2-Pyridyldisulfanyl)propanoic acid TIPS ester (4-12):
A flask containing **4-11** (124 mg, 0.57 mmol) was inerted and dry DCM (c 0.24M) was added to dissolve the solid. The reaction was cooled to 0 ^{o}C. Triethylamine (1.6 eq) was then added followed by triisopropylsilylchloride (TIPSCl, 1.5 eq). The reaction was then brought to room temperature and allowed to stir for 30 min. The reaction was monitored by TLC (5:1 hexane/ethyl acetate), concentrated *in vacuo* and purified using silica gel (30:1 hexane/ethyl acetate) to yield colorless viscous oil **4-12** (205 mg, 96 % yield). ^{1}H NMR (400 MHz, $CDCl_3$): δ 1.03 (d, J = 7.2 Hz, 23 H), 1.24 (m, 3 H), 2.8 (t, J = 6.9 Hz, 2 H), 3.04 (t, J = 6.9 Hz, 2 H), 7.09 (m, 2 H), 7.67 (m, 1 H), 8.47 (dd, J = 3.3, 1.2 Hz, 1 H), ^{13}C NMR (400 MHz, $CDCl_3$): δ 11.7, 12.2, 17.6, 33.7, 35.2, 119.6, 120.6, 136.9, 159.8, 171.3.

2-(*O*-TIPSO-carbonylethyldisulfanyl)phenyl acetic acid (4-13):
A flask containing **4-12** (106 mg, 0.28 mmol) was inerted and dissolved in dry THF (c 0.2M). A solution of **4-9** (1 eq) in dry THF (c 0.4M) was added at 0 ^{o}C and the reaction mixture was allowed to come to room temperature. The reaction was stirred for 3 h and monitored by TLC (2:1 hexane/ethyl acetate), concentrated *in vacuo* and purified using silica gel chromatography (8:1 hexane/ethyl acetate) to yield **4-13** as a viscous liquid (120 mg, 98 %). ^{1}H NMR (300 MHz, $CDCl_3$): δ 1.04 (m, 18 H), 1.27 (m, 3 H), 2.7 (t, 2 H), 2.9 (t, 2 H), 3.8 (s, 2 H), 7.27 (m, 2 H), 7.77 (m, 2 H).

Synthesis of drug –TTM fluorescent probe

***tert*-Butyl 4-hydroxybutanoate (4-14):**
4-*tert*-Butoxy-4-oxobutanoic acid (1 g, 5.7 mmol) (543.8 mg, 3.12 mmol) was taken in a flask and inerted. Dry THF (10 mL) was added to dissolve the solid and the flask was cooled to 0 ^{o}C using ice bath. $BH_3.Me_2S$ 2M solution in THF (3 mL) was added dropwise to the reaction mixture. The reaction was allowed to stir at room temperature for 24 h. The reaction mixture was cooled to room temperature and the THF was removed by rotary evaporation. Saturated potassium carbonate was added to the reaction mixture and it was extracted with ether. The organic layer was washed with brine, dried with anhydrous magnesium sulfate and concentrated *in vacuo* to give **4-14** as a colorless liquid (894 mg) in 98 % yield. ^{1}H NMR (400 MHz, $CDCl_3$): δ 1.43 (s, 9H), 1.83 (m, 2H), 1.97 (br, 1H), 2.34 (t, 2H, *J* = 6 Hz), 3.66 (t, 2H, *J* = 6 Hz), ^{13}C NMR (400 MHz, $CDCl_3$): δ 27.78, 27.98, 32.31, 61.97, 80.43, 173.41.

Fluorescein methyl ester (4-15):

Fluorescein (2 g, 6 mmol) was dissolved in methanol (c 0.05 M) and sulfuric acid (3.75 mL) and refluxed for 20 h. The methanol was removed by rotary evaporation and the reaction mixture was dissolved in large volume of chloroform and washed repeatedly with water to remove any remaining acid. The organic layer was washed with brine, dried with anhydrous magnesium sulfate and concentrated to obtain **4-15** as a dark orange powder (1.94 g) in 93 % yield. ^{1}H NMR (400 MHz, DMSO-d_6): δ 3.56 (s, 3H), 7.02 (m, 2H), 7.13 (m, 1H), 7.24 (m, 3H), 7.52 (m, 1H), 7.90 (m, 2H), 8.27 (m, 1H)

Methyl 2-[3-(4-*tert*-butoxy-4-oxobutoxy)-6-oxo-6H-xanthen-9-yl]benzoate (4-16):
The dye **4-15** (105.3 mg, 0.3 mmol), **4-14** (0.9 mmol, 3 eq) and Ph_3P (0.9 mmol, 3 eq) was taken in a flask and inerted. DIAD (0.6 mmol, 2 eq) was added to it and THF/CH_3CN (1 mL each) was added to dissolve them. The reaction was stirred for 2 h at room temperature and stopped. TLC monitor (10 % MeOH in DCM) indicated no starting material. The reaction mixture was subjected to rotary evaporation to remove solvents and **4-16** was obtained by flash chromatography on silica gel (2 % MeOH in DCM) as an orange solid in 87 % yield. ^{1}H NMR (400 MHz, $CDCl_3$): δ 1.45 (s, 9H), 2.10 (m, 2H), 2.42 (t, 2H, *J* = 6 Hz), 3.62 (s, 3H), 4.10 (t, 2H, *J* = 6 Hz), 6.53 (m, 2H), 6.72 (m, 1H), 6.89 (m, 3H), 7.30 (m, 1H), 7.71 (m, 2H), 8.24 (m, 1H), ^{13}C NMR (400 MHz, $CDCl_3$): δ 24.70, 28.42, 32.04, 52.68, 68.04, 80.91, 101.15, 106.04, 113.96, 115.09, 117.84, 129.13, 130.47, 130.59, 130.85, 131.41, 132.30, 132.43, 132.98, 134.92, 150.43, 154.52, 159.22, 163.63, 165.88, 172.44, 185.92.

4-[9-(2-Methoxycarbonylphenyl)-6-oxo-6H-xanthen-3-yloxy]butanoic acid (4-17):
The compound **4-16** (146.4 mg, 0.3 mmol) was taken in a flask and inerted. Dry DCM (0.2M) was added to dissolve it. TFA (c 0.2 M) was added dropwise and the reaction was allowed to stir at room temperature for 2 h. TLC monitor (10 % MeOH in DCM) indicated product. The reaction mixture was rotary evaporated and **4-17** was obtained by flash chromatography on silica gel (3 % MeOH in DCM) as an orange solid (121 mg) in 94 % yield. ^{1}H NMR (400 MHz, $CDCl_3$): δ 2.26 (m, 2H), 2.67 (t, 2H), 3.64 (s, 3H), 4.38 (t, 2H), 7.14 (m, 1H), 7.41 (m, 4H), 7.84 (m, 3H), 8.35 (m, 1H)

Paclitaxel-2'-TBDMS (4-18):
Paclitaxel (200 mg, 0.23 mmol), imidazol (10 eq), TBDMSCl (5 eq) was dissolved in dry DMF (c 0.75 M) and stirred at room temperature for 1 h. TLC monitor (1:1 hexane/ethyl acetate) indicated no starting material. The reaction mixture was diluted with ethyl acetate and washed with water, brine, dried with anhydrous magnesium sulfate and concentrated *in vacuo*. The desired product **4-18** was obtained as white solid in quantitative yield by flash chromatography on silica gel (1:1 hexane/ethyl acetate). ^{1}H NMR (300 MHz, $CDCl_3$): δ -0.3 (s, 3H) (TBDMS Me), -0.04 (s, 3H) (TBDMS Me), 0.79 (s, 9H) (TBDMS t-Bu), 1.13 (s, 3H), 1.24 (s, 3H), 1.68 (s, 4H), 1.9 (d, 4H), 2.12 (m, 1H), 2.27 (s, 3H), 2.41 (m, 2H), 2.54 (m, 4H), 3.8 (d, 1H), 4.27 (dd, 2H), 4.42 (m, 1H), 4.66 (d, 1H), 4.9 (m, 1H), 5.7 (m, 2H), 6.3 (m, 2H), 7.0 (d, 1H), 7.7 (m, 2H), 7.6 (m, 1H), 7.5 (m, 3H), 7.4 (m, 4H), 7.3 (m, 3H), 8.1 (d, 2H).

SB-T-1214-2'-TBDMS (4-18a):

White solid, 89 % yield. ^{1}H NMR (300 MHz, $CDCl_3$) δ 0.09 (s, 3 H) (TBDMS Me), 0.12 (s, 3 H) (TBDMS Me), 0.94 (s, 9 H) (TBDMS t-Bu), 0.98 (m, 2 H) (C-10 CH_2), 1.10 (m, 2 H) (C-10 CH_2), 1.15 (s, 3 H) (C-16 Me), 1.27 (s, 3 H) (C-17 Me), 1.35 (s, 9 H) (Boc), 1.67 (s, 3 H) (C-19 Me), 1.75 (s, 3 H) (isobutenyl Me), 1.78 (s, 3 H) (isobutenyl), 1.82 (m, 1 H) (C-6 1 H), 1.88 (s, 3 H) (C-18 Me), 2.27 (m, 1 H) (C-10 1 H), 2.40 (m, 1 H) (C-6 1 H), 2.42 (s, 3 H) (OAc), 2.55 (m, 2 H) (C-14), 3.81 (d, *J* = 7.2 Hz, 1 H) (C-3), 4.20 (d, *J* = 8.1 Hz, 1 H) (C-20), 4.25 (d, *J* = 3.0 Hz, 2H) (C-2'), 4.31 (d, *J* = 8.1 Hz, 1 H) (C-20), 4.43 (m, 1 H) (C-7), 4.77 (m, 2 H) (C-3', C-4'), 4.98 (d, *J* = 9.3 Hz, 1 H) (C-5), 5.25 (d, *J* = 8.1 Hz, 1 H) (NH), 5.68 (d, *J* = 7.2 Hz, 1 H) (C-2), 6.19 (t, J=7.6, 1H) (C-13), 6.29 (s, 1H) (C-10), 7.49 (t, *J* = 8.1 Hz, 2 H), 7.61 (t, J=7.2, 1 H), 8.11 (d, *J* = 8.4 Hz, 2 H).

Paclitaxel-7-fluorescein-2'-TBDMS (4-19):
Paclitaxel-2'-TBDMS (**4-18**) (45 mg, 0.046 mmol), **4-17** (4 eq) and DMAP (1 eq) was taken in a flask and inerted. Dry DCM (c 0.02 M) and dry DMF (c 0.06 M) was added to dissolve the solids, the flask cooled to 0 ^oC and DIC (2 eq) was added to the reaction mixture. The reaction was stirred overnight at room temperature. TLC monitor (10 % MeOH in DCM) indicated starting material and product. The solvents were removed and **7-2** was obtained as an orange solid (53 mg) in 73 % yield after flash chromatography (2 % MeOH in DCM). ^{1}H NMR (400 MHz, $CDCl_3$): δ –0.3 (s, 3H) (TBDMS Me), -0.03 (s, 3H) (TBDMS Me), 0.79 (s, 9H) (TBDMS t-Bu), 1.2 (t, 9H), 1.87 (m, 5H), 1.9 (s, 4H), 2.13 (m, 4H), 2.5 (m, 8H), 3.6 (s, 3H), 3.96 (d, 1H), 4.19 (m, 4H), 4.34 (d, 1H), 4.67 (d, 1H) 4.98 (d, 1H), 5.67 (m, 4H), 6.2 (m, 2H), 6.64 (m, 2H), 6.78 (m, 2H), 6.89 (m, 3H), 7.00 (m, 1H), 7.10 (d, 1H), 7.3 (m, 5H), 7.38 (m, 4H), 7.5 (m, 3H), 7.6 (t, 1H), 7.67 (t, 1H), 7.73 (m, 3H), 8.12 (d, 2H), 8.25 (d, 1H), ^{13}C NMR (400 MHz, $CDCl_3$): δ 10.85, 14.57, 18.06, 20.65, 20.67, 21.36, 22.94, 23.66, 25.47, 26.31, 30.20, 33.38, 35.56, 43.30, 46.79, 52.39, 55.64, 55.99, 68.03, 71.24, 71.45, 74.45, 75.05, 75.17, 76.34, 78.57, 80.87, 83.86, 100.71, 100.73, 105.39, 114.88, 117.34, 126.37, 126.95, 127.92, 128.69, 128.73, 129.03, 129.77, 130.15, 130.23, 130.35, 130.40, 131.12, 131.76, 132.57, 132.66, 133.67, 134.06, 134.39, 138.21, 140.90, 159.06, 165.44, 165.46, 166.84, 166.97, 168.98, 169.92, 171.40, 171.92, 171.94, 201.99, 201.01.

SB-T-1214-7-fluorescein-2'-TBDMS (4-19a):
Orange solid, 82 % yield. ^{1}H NMR (300 MHz, $CDCl_3$) δ 0.07 (s, 3 H) (TBDMS Me), 0.10 (s, 3 H) (TBDMS Me), 0.92 (s, 9 H) (TBMDS t-Bu), 0.99 (m, 2 H) (H10), 1.06 (m, 2 H) (H10), 1.16 (s, 3 H) (H16 Me), 1.22 (s, 3 H) (C17 Me), 1.34 (s, 9 H) (Boc), 1.66 (m, 1 H) (H10), 1.73 (s, 3 H) (H19 Me), 1.77 (s, 3 H) (isobutenyl Me), 1.79 (s, 3 H) (isobutenyl Me), 1.93 (s, 3 H) (H18 Me), 2.09 (m, 2 H) (fluorescein CH_2), 2.15 (m, 1 H) (H6 1 H), 2.29 (m, 1 H) (H6 1 H), 2.40 (s, 3 H) (OAc), 2.46 (m, 2 H) (fluorescein CH_2), 2.57 (m, 2 H) (H14), 3.61 (s, 3 H) (fluorescein Me), 3.69 (s, 1 H) (OH), 3.95 (d, J = 6.8 Hz, 1 H) (H3), 4.10 (m, 2 H) (fluorescein CH_2), 4.17 (d, J = 8.4 Hz, 1 H) (H20), 4.23 (d, J = 3.2 Hz, 1 H) (H2'), 4.30 (d, J = 8.4 Hz, 1 H) (H20), 4.74 (m, 1 H) (H4'), 4.80 (m, 1 H) (H3'), 4.93 (d, J = 8.8 Hz, 1 H) (H5), 5.22 (d, J = 8.0 Hz, 1 H) (NH), 5.60 (dd, J = 10.8, 7.2 Hz, 1 H) (H7), 5.66 (d, J = 6.8 Hz, 1 H) (H2), 6.13 (t, J = 8.8 Hz, 1 H) (H13), 6.29 (s, 1 H) (H10), 6.49 (s, 1 H), 6.54 (d, J = 10 Hz, 1 H), 6.73 (m, 1 H), 6.86 (m, 2 H), 6.96 (t,

J = 2.4 Hz, 1 H), 7.28 (d, J = 7.2 Hz, 1 H), 7.46 (t, J = 8.0 Hz, 2 H), 7.64 (m, 3 H), 8.08 (d, J = 8.8 Hz, 2 H), 8.22 (m, 1 H).

Paclitaxel-7-fluorescein-2'-OH (4-20):
Paclitaxel-7-fluorescein-2'-TBDMS (**4-19**) (14 mg, 0.01 mmol) was dissolved in acetonitrile/pyridine (0.26 mL each). The flask was cooled to 0 ^{o}C and HF/pyridine (65-70 %, 0.13 mL) was added dropwise. The mixture was stirred at room temperature for 9 h. The reaction was neutralized with $NaHCO_3$ solution, pyridine was removed by evaporation, and the solid was dissolved with ethyl acetate. The organic layer was washed with water (x3), NaCl (x1) and dried over anhydrous $MgSO_4$ and concentrated *in vacuo*. The crude product was purified on a silica gel column (2 % methanol in dichloromethane) to afford **4-20** as an orange solid (11.6 mg, 91 % yield)
^{1}H NMR (400 MHz, $CDCl_3$): δ 1.19 (m), 1.81 (m), 2.27 (m), 2.5 (m), 3.7 (m), 3.98 (t), 4.18 (d), 4.31 (d), 4.89 (s), 4.98 (d), 5.6 (d), 5.7 (m), 6.1 (m), 6.2 (s), 6.9 (m), 7.0 (m), 7.6 (m), 7.77 (m), 7.90 (d), 8.1 (d), 8.3 (d), ^{13}C NMR (400 MHz, $CDCl_3$): δ 10.85, 14.57, 14.63, 20.83, 20.94, 22.52, 22.63, 26.35, 28.88, 29.00, 29.67, 30.01, 33.46, 35.47, 43.12, 47.11, 52.76, 52.79, 56.07, 56.36, 69.21, 70.79, 71.86, 73.48, 73.57, 74.36, 75.49, 76.34, 78.63, 78.67, 80.50, 83.96, 100.64, 103.75, 116.37, 116.85, 127.18, 127.21, 127.50, 127.58, 127.73, 128.32, 128.35, 128.57, 128.70, 128.86, 129.11, 129.74, 129.84, 130.13, 130.65, 131.02, 131.36, 131.47,131.60, 132.01, 132.07, 133.04, 133.25, 133.77, 133.96, 139.02, 141.54, 141.63, 159.70, 159.77, 164.99, 166.87, 167.27, 169.11, 170.34, 172.21, 172.25, 202.31.

SB-T-1214-7-fluorescein-2'-OH (4-20a):[162]
Orange solid, 72 % yield. ^{1}H NMR (300 MHz, $CDCl_3$) δ 0.93 (m, 2 H) (H10), 1.08 (m, 2 H) (H10), 1.18 (s, 3 H) (H16 Me), 1.24 (s, 3 H) (C17 Me), 1.35 (s, 9 H) (Boc), 1.68 (m, 1 H) (H10), 1.73 (s, 3 H) (H19 Me), 1.77 (s, 3 H) (isobutenyl Me), 1.81 (s, 3 H) (isobutenyl Me), 2.02 (s, 3 H) (H18 Me), 2.10 (m, 2 H) (fluorescene CH_2), 2.20 (m, 1 H) (H6 1 H), 2.33 (m, 1 H) (H6 1 H), 2.38 (s, 3 H) (OAc), 2.42 (m, 2 H) (fluorescene CH_2), 2.57 (m, 2 H) (H14), 3.62 (s, 3 H) (fluorescene Me), 3.97 (d, J = 6.8 Hz, 1 H) (H3), 4.13 (m, 2 H) (fluorescene CH_2), 4.17 (d, J = 8.4 Hz, 1 H) (H20), 4.27 (d, J = 3.2 Hz, 1 H) (H2'), 4.31 (d, J = 8.4 Hz, 1 H) (H20), 4.77 (m, 1 H) (H4'), 4.95 (m, 2 H) (H3', H5), 5.35 (d, J = 8.0 Hz, 1 H) (NH), 5.67 (m, 2 H) (H7, H2), 6.13 (t, J = 8.8 Hz, 1 H) (H13), 6.32 (s, 1 H) (H10), 6.56 (s, 1 H), 6.60 (d, J = 10 Hz, 1 H), 6.74 (m, 1 H), 6.89 (m, 2 H), 7.15 (t, J = 2.4 Hz, 1 H), 7.29 (d, J = 7.2 Hz, 1 H), 7.48 (t, J = 8.0 Hz, 2 H), 7.64 (m, 3 H), 8.09 (d, J = 8.8 Hz, 2 H), 8.24 (m, 1 H).

Paclitaxel-7-fluorescein-2-linker-OTIPS (4-21):
A flask containing **4-20** (38 mg, 0.011 mmol), DMAP (1 eq) and linker (2 eq) was inerted and dichloromethane (1.5 mL) was added to dissolve the solids. The flask was cooled to 0 ^{o}C and DIC (2 eq) was then added dropwise. The solution was stirred for 5 h at room temperature and the crude product was purified on a silica gel column (1:2 hexane:ethyl acetate) to afford **4-21** (30.6 mg, 61 % yield) as an orange solid.
^{1}H NMR (400 MHz, $CDCl_3$): δ 1.14 (d, 6H), 1.37 (m), 1.8 (s), 2.0 (m), 2.1 (m), 2.4 (d), 2.7 (m), 2.8 (m), 3.6 (s), 3.9 (m), 4.1 (m), 4.3 (m), 4.9 (d), 5.4 (m), 5.6 (m), 5.8 (m), 6.2 (m), 6.8 (m), 6.9 (m), 7.1 (m), 7.3 (m), 7.4 (m), 7.5 (m), 7.6 (m), 7.7 (m), 8.1 (t), 8.3 (d),

^{13}C NMR (400 MHz, $CDCl_3$): δ 6.75, 10.86, 11.83, 12.24, 14.15, 14.50, 17.72, 20.54, 20.69, 21.00, 21.26, 22.65, 23.60, 26.37, 29.65, 29.81, 30.11, 33.34, 33.70, 35.22, 38.90, 43.23, 46.86, 52.49, 52.77, 53.12, 55.98, 60.36, 68.41, 71.55, 74.49, 75.25, 76.31, 76.68, 76.99, 77.31, 78.55, 80.75, 80.89, 83.89, 100.72, 104.94, 117.17, 126.53, 126.75, 127.19, 127.92, 128.08, 128.32, 128.70, 128.90, 129.11, 129.43, 130.14, 130.84, 131.02, 131.22, 131.89, 132.36, 132.76, 133.06, 133.24, 133.55, 133.68, 134.08, 136.33, 136.88, 141.29, 141.45, 159.37, 159.51, 165.33, 166.84, 167.15, 167.30, 167.78, 168.13, 168.95, 169.30, 169.62, 170.25, 171.30, 171.73, 171.99, 173.95, 174.87, 202.15.

SB-T-1214-7-fluorescein-2-linker-OTIPS (4-21a):[162]
Orange solid, 63 % yield. ^{1}H NMR (300 MHz, $CDCl_3$): δ 0.98-1.05 (m, 2 H), 1.07 (d, J = 6.9 Hz, 18 H), 1.13-1.21 (m, 2 H), 1.15 (s, 3 H), 1.26 (s, 3 H), 1.29 (m, 3 H), 1.35 (s, 9 H), 1.62 (m, 2 H), 1.65 (s, 3 H), 1.67 (s, 3H), 1.72 (m, 1 H), 1.75 (s, 3 H), 1.92 (s, 3 H), 2.12 (m, 2 H), 2.24 (m, 2 H), 2.32 (s, 3 H), 2.41 (m, 2 H), 2.52 (m, 1 H), 2.72 (t, J = 6.6 Hz, 2 H), 2.91 (t, J = 6.6 Hz, 2 H), 3.58 (d, J = 0.9 Hz, 3 H), 3.87 (m, 2 H), 4.02-4.14 (m, 4 H), 4.26 (d, J = 8.4 Hz, 1 H), 4.7-4.9 (m, 4H), 5.04 (d, J = 8.4 Hz, 1 H), 5.55 (dd, J = 10.5, 6.9 Hz, 1 H), 5.63 (d, J = 6.9 Hz, 1 H), 6.11 (t, J = 7.2 Hz, 1 H), 6.25 (s, 1 H), 6.41 (s, 1 H), 6.47 (d, J = 9.9 Hz, 1 H), 6.68 (dd, J = 9.0, 2.1 Hz, 1 H), 6.80 (m, 2 H), 6.92 (t, J = 2.1 Hz, 1 H), 7.27 (m, 4 H), 7.43 (t, J = 7.8 Hz, 2 H), 7.54-7.73 (m, 4 H), 8.06 (d, J = 8.4 Hz, 2 H), 8.19 (dd, J = 8.1, 1.5 Hz, 1 H).

Paclitaxel-7-fluorescein-2-linker-COOH (4-22):
A flask containing **4-21** (29 mg, 0.0228 mmol) was inerted and 0.6 mL of dry pyridine/acetonitrile (1:1) was added to dissolve it. The flask was cooled to 0 ^{o}C and HF/pyridine (70:30, 0.08 mL) was added dropwise at 0 ^{o}C. The mixture was stirred at room temperature for 5 h. The reaction was quenched with aqueous saturated sodium carbonate solution and the pyridine evaporated. The solid was then dissolved in ethyl acetate, washed with $NaHCO_3$ (x 3), water, brine and dried over anhydrous magnesium sulfate and purified by flash chromatography (5 % MeOH in DCM) to afford **4-22** as an orange solid in 67 % yield. ^{1}H NMR (400 MHz, $CDCl_3$): δ 1.25 (m), 1.79 (s), 2.06 (m), 2.2 (m), 2.5 (m), 2.8 (m), 3.6 (s), 3.9 (m), 4.0 (m), 4.1 (m), 4.3 (m), 4.9 (m), 5.5 (m), 5.6 (m), 5.8 (m), 6.1 (m), 6.2 (s), 7.0 (m), 7.1 (m), 7.3 (m), 7.4 (m), 7.5 (m), 7.6 (m), 7.7 (m), 8.1 (d), 8.2 (d). ^{13}C NMR (400 MHz, $CDCl_3$): δ 10.85, 14.17, 14.67, 20.39, 20.62, 21.02, 21.15, 22.65, 23.54, 26.39, 26.67, 33.34, 33.81, 35.21, 38.84, 43.19, 47.01, 52.55, 53.18, 55.96, 60.37, 68.54, 71.65, 74.52, 75.27, 76.28, 77.31, 78.54, 80.76, 80.93, 83.80, 100.54, 100.69, 104.72, 117.00, 126.80, 126.86, 127.24, 127.28, 127.92, 128.35, 128.63, 128.73, 128.92, 129.07, 130.15, 130.94, 131.19, 131.27, 131.92, 132.29, 132.80, 133.05, 133.55, 133.77, 136.66, 136.91, 141.51, 159.57, 165.28, 166.84, 167.25, 168.19, 168.29, 168.98, 169.64, 172.05, 173.63, 202.15.

SB-T-1214-7-fluorescein-2-linker-COOH (4-22a):[162]
Orange solid, 95 % yield. ^{1}H NMR (300 MHz, $CDCl_3$): δ 0.98-1.05 (m, 2 H), 1.13-1.21 (m, 8 H), 1.35 (s, 9 H), 1.62 (m, 2 H), 1.72-1.78 (m, 10 H), 1.97 (s, 3 H), 2.12 (m, 2 H), 2.3-2.6 (m, 8 H), 2.68 (t, J = 6.9 Hz, 2 H), 2.95 (m, 2 H), 3.62 (d, J = 0.9 Hz, 3 H), 3.94 (m, 2 H), 4.02-4.25 (m, 4 H), 4.33 (d, J = 8.7 Hz, 1 H), 4.90-4.97 (m, 4 H), 5.12 (d, J = 8.4 Hz, 1 H), 5.58 (dd, J = 10.5, 6.9 Hz, 1 H), 5.69 (d, J = 6.9 Hz, 1 H), 6.17 (t, J = 7.2

Hz, 1 H), 6.28 (s, 1 H), 6.58-6.62 (m, 2 H), 6.74 (dd, J = 9.0, 2.1 Hz, 1 H), 6.88 (m, 2 H), 7.03 (t, J = 1.8 Hz, 1 H), 7.27 (m, 4 H), 7.43 (t, J = 7.8 Hz, 2 H), 7.54-7.73 (m, 4 H), 8.06 (d, J = 8.4 Hz, 2 H), 8.19 (dd, J = 8.1, 1.5 Hz, 1 H).

Paclitaxel-7-fluorescein-2-linker-OSu (4-23):
A flask containing **4-22** (17 mg, 0.011 mmol), *N*-hydroxysuccinimide (5 eq), DCC (2.5 eq) was inerted and dry THF (0.05 M) was added to dissolve the solids. The flask was cooled to 0 ^{o}C. The reaction was then stirred for 28 h at room temperature till TLC indicated conversion to product (**4-23**) and MALDI indicated no starting material. The solvent was removed and the product was obtained by flash chromatography (2 % MeOH in DCM) in 71 % yield as an orange solid (13 mg). The product was verified by MALDI and used immediately for the next reaction.

Paclitaxel-7-fluorescein-2-linker-PEG-Folic acid (4-24):
A flask containing **4-23** (13 mg, 0.0086 mmol) was inerted and DMSO (0.5 mL) was added to dissolve it. FA-PEG-NH_2 (**4-6**) (1 eq) was dissolved in DMSO and added. The reaction was stirred at room temperature for 67 h with a further addition of 0.1 eq of FA-PEG-NH_2. MALDI indicated no starting material. The reaction was stopped and the product **4-24** purified by HPLC (Acetonitrile: water/0.1 % formic acid 70:30) and obtained as a yellow solid (7.6 mg, 37 % yield, mixture of α and γ isomers). HRMS: (Q-TOF TOF MS ES+) *m/z* Calculated for $C_{124}H_{142}O_{37}N_{10}S_2^+$ ($M^+/2$): 1214.4568 Found: 1214.4525 (Δ = - 3.5 ppm).

Synthesis of tumor-targeting drug conjugate

SB-T-1214-2'-linker-OTIPS (4-25):[162]
A flask containing **SB-T-1214** (70 mg, 0.08 mmol), DMAP (0.5 eq) and TIPS protected linker **4-13** (1.2 eq) was inerted and dichloromethane (1.5 mL) was added to dissolve the solids. The flask was cooled to 0 ^{o}C and DIC (2 eq) was then added dropwise. The solution was stirred for 5 h at room temperature and the crude product was purified on a silica gel column (1:1 hexane:ethyl acetate) to afford **4-25** (50 mg, 50 % yield) as an white solid. ^{1}H NMR (300 MHz, $CDCl_3$): δ 1.13 (s, 3 H), 1.14 (s, 3 H), 1.25 (s, 4 H), 1.22 (d, *J* = 7.2 Hz, 18 H), 1.31 (m, 3H), 1.34 (s, 9 H), 1.66 (s, 3 H), 1.71 (s, 1 H), 1.75 (s, 6 H), 1.82 (s, 1 H), 1.86(m, 1 H), 1.91 (s, 3 H), 2.31 (s, 1 H), 2.33 (s, 1 H), 2.37 (s, 3 H), 2.60 (m, 2 H), 2.87 (d, *J* = 6 Hz, 2 H), 2.97 (d, *J* = 6 Hz, 2 H), 3.80 (d, *J* = 7.2 Hz, 1 H), 4.17 (s, 2 H), 4.19 (d, *J* = 8.7 Hz, 1 H), , 4.30 (d, *J* = 8.7 Hz, 1 H), 4.43 (dd, *J* = 10.6, 6.6 Hz, 1 H), 4.9-5.0 (m, 4 H), 5.19 (s, 1 H), 5.66 (d, *J* = 7.2 Hz, 1 H), 6.17 (t, *J* = 8.7 Hz, 1 H), 6.29 (s, 1 H), 7.34 (m, 3 H), 7.47 (t, *J* = 7.5 Hz, 2 H), 7.60 (t, *J* = 7.3 Hz, 1 H), 7.80 (d, *J* = 7.2 Hz, 1 H), 8.10 (d, *J* = 7.4 Hz, 2 H), ^{13}C NMR (100 MHz, $CDCl_3$): δ 1.22, 9.32, 9.53, 9.75, 13.21, 13.90, 15.00, 18.75, 19.32, 22.42, 22.63, 23.69, 25.80, 25.94, 26.91, 28.44, 29.90, 30.86, 32.84, 33.54, 35.67, 35.95, 43.40, 45.84, 49.20, 58.71, 64.56, 72.05, 72.37, 75.05, 75.45, 75.66, 76.62, 79.51, 80.07, 81.22, 84.70, 120.15, 128.57, 128.85, 129.20, 129.51, 130.38, 131.03, 131.27, 132.12, 132.76, 133.82, 136.70, 138.16, 143.58, 155.13, 166.58, 167.21, 168.39, 169.20, 169.86, 171.19, 175.30, 204.30.

SB-T-1214-2'-linker-COOH (4-26):[162]

A flask containing **4-25** (50 mg, 0.04 mmol) was inerted and 1 mL each of dry pyridine/acetonitrile (1:1) was added to dissolve it. The flask was cooled to 0 ^{o}C and HF/pyridine (70:30, 0.5 mL) was added dropwise at 0 ^{o}C. The mixture was stirred at room temperature for 1 h. The reaction was quenched with aqueous saturated sodium carbonate solution and the pyridine evaporated. The solid was then dissolved in ethyl acetate, washed with $NaHCO_3$ (x 3), water, brine and dried over anhydrous magnesium sulfate and purified by flash chromatography (5 % MeOH in DCM) to afford **4-26** as a white solid in 97 % yield. ^{1}H NMR (300 MHz, $CDCl_3$): δ 1.13 (s, 3 H), 1.14 (s, 3 H), 1.25 (s, 4 H), 1.34 (s, 9 H), 1.66 (s, 3 H), 1.71 (s, 1 H), 1.75 (s, 6 H), 1.82 (s, 1 H), 1.86(m, 1 H), 1.91 (s, 3 H), 2.31 (s, 1 H), 2.33 (s, 1 H), 2.37 (s, 3 H), 2.60 (m, 2 H), 2.87 (d, *J* = 6 Hz, 2 H), 2.97 (d, *J* = 6 Hz, 2 H), 3.80 (d, *J* = 7.2 Hz, 1 H), 4.17 (s, 2 H), 4.19 (d, *J* = 8.7 Hz, 1 H), , 4.30 (d, *J* = 8.7 Hz, 1 H), 4.43 (dd, *J* = 10.6, 6.6 Hz, 1 H), 4.9-5.0 (m, 4 H), 5.19 (s, 1 H), 5.66 (d, *J* = 7.2 Hz, 1 H), 6.17 (t, *J* = 8.7 Hz, 1 H), 6.29 (s, 1 H), 7.34 (m, 3 H), 7.47 (t, *J* = 7.5 Hz, 2 H), 7.60 (t, *J* = 7.3 Hz, 1 H), 7.80 (d, *J* = 7.2 Hz, 1 H), 8.10 (d, *J* = 7.4 Hz, 2 H)

SB-T-1214-2'-linker-OSu (4-27):[162]

A flask containing **4-26** (40 mg, 0.036 mmol), *N*-hydroxysuccinimide (5 eq), D1C (2.5 eq) was inerted and dry THF (c 0.05 M) was added to dissolve the solids. The flask was cooled to 0 ^{o}C. The reaction was then stirred for 24 h at room temperature till TLC indicated conversion to product (**4-27**) and MALDI analysis indicated no starting material. The solvent was removed and the product was obtained by flash chromatography (1:1 hexane:ethyl acetate) in 77 % yield as a white solid (33 mg). The product was verified by MALDI and used for the next reaction. ^{1}H NMR (400 MHz, $CDCl_3$): δ 1.13 (s, 3 H) (H16), 1.14 (s, 3 H) (H17), 1.25 (s, 4 H) (H10 cyclopropane), 1.34 (s, 9 H) (Boc), 1.66 (s, 3 H) (H19), 1.71 (s, 1 H) (cyclopropane), 1.75 (s, 6 H) (isobutenyl), 1.82 (s, 1 H) (OH), 1.86(m, 1 H) (H6a), 1.91 (s, 3 H) (H18), 2.31 (s, 1 H) (H 6), 2.33 (s, 1 H) (OH), 2.37 (s, 3 H) (OAc), 2.60 (m, 2 H) (H 14), 2.83 (s, 4 H) (OSu), 2.87 (d, J =6 Hz, 2 H) (CH_2-CO_2Su), 2.97 (d, J =6 Hz, 2 H) (S-CH_2), 3.80 (d, J = 7.2 Hz, 1 H) (H3), 4.17 (s, 2 H) (Ph-CH_2-CO_2), 4.19 (d, J = 8.7 Hz, 1 H) (H20a), , 4.30 (d, J = 8.7 Hz, 1 H) (H20b), 4.43 (dd, J = 10.6, 6.6 Hz, 1 H) (H7), 4.9-5.0 (m, 4 H) (H3', H4'isoButenyl, H5, H2'), 5.19 (s, 1 H) (NH), 5.66 (d, J = 7.2 Hz, 1 H) (H2), 6.17 (t, J = 8.7 Hz, 1 H) (H13), 6.29 (s, 1 H) (H10), 7.34 (m, 3 H) (Ph linker), 7.47 (t, J = 7.5 Hz, 2 H) (Bz), 7.60 (t, J = 7.3 Hz, 1 H) (Bz), 7.80 (d, J = 7.2 Hz, 1 H) (Ph linker), 8.10 (d, J = 7.4 Hz, 2 H) (Bz), ^{13}C NMR (400 MHz, $CDCl_3$): δ 1.22, 9.32, 9.53, 9.75, 13.21, 13.90, 15.00, 18.75, 19.32, 22.42, 22.63, 23.69, 25.80, 25.94, 26.91, 28.44, 29.90, 30.86, 32.84, 33.54, 35.67, 35.95, 43.40, 45.84, 49.20, 58.71, 64.56, 72.05, 72.37, 75.05, 75.45, 75.66, 76.62, 79.51, 80.07, 81.22, 84.70, 120.15, 128.57, 128.85, 129.20, 129.51, 130.38, 131.03, 131.27, 132.12, 132.76, 133.82, 136.70, 138.16, 143.58, 155.13, 166.58, 167.21, 168.39, 169.20, 169.86, 171.19, 175.30, 204.30.

SB-T-1214-2'-linker-PEG-folate (4-28):

A flask containing **4-27** was inerted and anhydrous DMSO was added to dissolve it. Then FA-PEG-NH_2 **4-6** (1.1 eq) was dissolved in anhydrous DMSO and added to the flask. The reaction was carried out at room temperature for 3 days. LC/MS was performed to determine conditions for purification and the compound was purified using preparative

HPLC (water/acetonitrile) and obtained as a light yellow solid. The product was verified by MALDI MS. HRMS: (Q-TOF TOF MS ES+) *m/z* Calculated for $C_{97}H_{133}N_{10}O_{32}S_2^+$: 2013.8529 Found: 2013.8521 (Δ = - 0.4 ppm).

Biological assays:

Cell culture: L1210FR cell line was received as a gift from Dr. Gregory Russell-Jones (Access Pharmaceuticals Australia Pty Ltd., Targeted Delivery, Unit 5, 15-17 Gibbes St, Chatswood, NSW, Sydney 2067, Australia). L1210, A549, ID8 were purchased from ATCC. The cells were grown in RPMI-1640 cell culture medium (Invitrogen) in the absence of folate receptor (FR) supplemented with 10 % fetal bovine serum (FBS). Prior to incubation, the cells were collected by centrifugation at 1000 rpm for 6 min and resuspended in RPMI medium without FR at a cell density of 5×10^5 cells/mL.

Incubation of cells with the folate-4C-FITC (4-4) folate-PEG-FITC conjugate (4-7):
The cell suspension (1 mL each) was added to separate microtubes. The folate-FITC conjugates (**4-4** and **4-7**) (10 μL) in DMSO was added to the microtube at a final concentration of 100 nM and incubated at 37 ^oC for 3 h. After incubation, the cells were washed with phosphate buffered saline (PBS) and collected by centrifugation twice, and resuspended in 100 μL phosphate buffered saline (PBS) for imaging.

Low temperature incubation of cells with the folate-PEG-FITC conjugate (4-7):
The incubation of L1210FR with the folate-PEG-FITC conjugate (**4-7**) was carried out in the cold room at ~ 4 ^oC. The isolation and washing of the cells were achieved as described above.

Blocking the receptors on L1210FR cells with excess folic acid:
Before incubation with the folate-PEG-FITC conjugate (**4-7**), the cells were treated with folic acid at a several concentrations for 1 h.

Incubation of cells with the folate-PEG-linker-paclitaxel-fluorescein conjugate (4-24):
The cell suspension (1 mL) was added to microtube. The conjugates (10 μL) in DMSO were added to the microtube at a final concentration of 20 μM. After incubation at 37 ^oC for 2 h, the cells were washed twice with phosphate buffered saline (PBS) to remove excess conjugates and resuspended in the medium. DMSO (10 μL) was then added to the suspension as a control and incubated for another 1 h. After incubation, the cells were washed with phosphate buffered saline (PBS) and collected by centrifugation twice, and resuspended in 100 μL phosphate buffered saline (PBS) for imaging.

Release of the taxane in cells:
The conjugates (10 μL) in DMSO were added to 1 mL of cells in the microtube at a final concentration of 20 μM. After incubation at 37 ^oC for 2 h, the cells were washed twice with phosphate buffered saline (PBS) to remove excess conjugates and resuspended in the medium. Glutathione monoester (GSH-OEt) (10 μL) was then added to the suspension at a final concentration of 2 mM and incubated for another 1 h. The excess

GSH-OEt was removed by washing twice with phosphate buffered saline (PBS) and the cells were resuspended in 100 μL phosphate buffered saline (PBS) before imaging.

Immunofluorescent assay in L1210FR cells:
Indirect immunofluorescent assay using folate-PEG-linker-paclitaxel-fluorescein conjugate (**4-24**) following standard protocol. Cells were first incubated with **4-24** at 100 nM cell concentration for 3 h at 37 ^{o}C and excess conjugate was removed in the usual way. GSH-OEt was then added as described in the previous procedure to enhance the release of the taxane. The microtubules were stabilized using PIPES buffer and incubated with the primary goat antibody and the cells were permeabilized. The cells were then incubated with antigoat antimouse antibody, washed in the usual way described above and resuspended in 100 μL PBS for CFM imaging.

Confocal microscopy imaging of the treated cells:
All the confocal images were taken immediately after the incubation and washing steps. 100 μL of the cell suspension was transferred to the bottom-glass dish using micropipette and imaged by a Zeiss LSM 510 confocal microscope.

Flow cytometry fluorescent measurements of the cells:
Flow cytometry analysis was performed immediately after the incubation and washing steps. Cells were resuspended in 0.5 mL of PBS and analyzed using a flow cytometer, FACSCalibur, operating at a 488 nm excitation wavelength and detecting emission wavelengths with a 530/30 nm bandpass filter. At least 10,000 cells were counted for each experiment using CellQuest 3.3 software (Becton Dickinson) and the distribution of FITC fluorescence was analyzed using WinMDI 2.8 freeware (Joseph Trotter, Scripps Research Institute).

***In vitro* cytotoxicity assay:**
The cytotoxicity of folate-PEG-linker-SB-T-1214 (**4-28**) was quantitatively evaluated *in vitro* on FR(+)leukemia mouse cell lines L1210FR, L1210, FR(-) lung cancer cell line A549, FR(+) ovarian cancer cell line ID8 and the measurement was performed with the well-established MTT (3-(4,5-dimethylthiazolyl)-2,5-diphenyl-2H-tetrazolium bromide) cell proliferation assay. Paclitaxel and second-generation taxoid, SB-T-1214 were also assayed as control. The cell suspension was cultured and incubated at a concentration of ~ 2×10^4 in each well of a 96-well plate. For the adhesive cell type, the cells were allowed to reseed to the bottom of the plates overnight and fresh medium was added to each well upon removal of the old medium. Cells were subsequently treated with 10 μL of the folate-PEG-linker-SB-T-1214 (**4-28**) dissolved in medium at different final concentrations ranging from 0.01 to 1000 nM for 72 h. The cells were then centrifuged down, old medium was removed and fresh medium containing MTT (e.g. 100 μL of 0.5 mg/mL) was added and incubated at 37 ^{o}C for 4 h. The medium was then removed and the insoluble violet formazan crystals, which were the product of the mitochondrial reduction of MTT by succinic dehydrogenase, were further dissolved using 0.1 N HCl in isopropanol which formed a violet solution. The absorbance measurement of each well in the 96-well plate was performed at 570 nm and gave a direct estimate of cell viability and activity. The viability of the cells was plotted as a function of concentration and the

cytotoxicity of folate-PEG-linker-SB-T-1214 (**4-28**) was also determined by the IC_{50} value, which was defined as the drug concentration inducing 50 % of the cells death. Finally, the IC_{50} value from the viability-concentration curve was calculated with the Sigma Plot.

Chapter 5
Functionalized SWNT (*f*-SWNT) as a Versatile Platform for Tumor-targeted Drug Delivery and Dual Therapy

5.1 Introduction

5.1.1 Nanotechnology – Opportunities in Diagnostic and Therapeutic Nanomedicine

Nanotechnology encompasses a vast and diverse array of devices or nanovectors from multidisciplinary fields of chemistry, physics, biology and engineering which can be applied for diagnosis and treatment of diseases. Nanomedicine or the medical applications of nanotechnology include nanomaterials, nanoelectronic biosensors and molecular nanotechnology.[1] The last few years have witnessed a surge in the discovery and development of novel nanomaterials which consist of inorganic and organic matter as is evidenced by the allocation of $144 million in 2004 by the National Cancer Institute (NCI), $54 million by the National Heart, Lung and Blood Institute in U.S.A. for research in nanomedicine, sharp increase of patent filings in this area[2] as well as funding by European Commission. Nanotechnology typically refers to man-made devices that are in the 1-100 nm range at least in one dimension.[3] To put things in perspective a DNA double helix has a diameter of 2 nm and the smallest cellular life form is around 200 nm in length. Thus nanoparticles are in the same dimension range as antibodies, nucleic acids, receptors, proteins and other biomolecules. The basic nanotechnology approaches for medical application can be traced back a few decades but the recent success of nanomedicine has fueled interest in research as well as funding. The first example of lipid vesicles or liposomes was reported in 1965,[4] the first controlled release polymer system was reported in 1976,[5] first long circulating stealth polymeric nanoparticle was reported in 1994,[6] the first quantum dot bioconjugate was reported in 1998[7, 8] and the first nanowire nanosensor was reported in 2001.[9] Structures of some organic nanoparticles are shown in Figure 5-1 and inorganic nanoparticles are shown in Figure 5-2.[10]

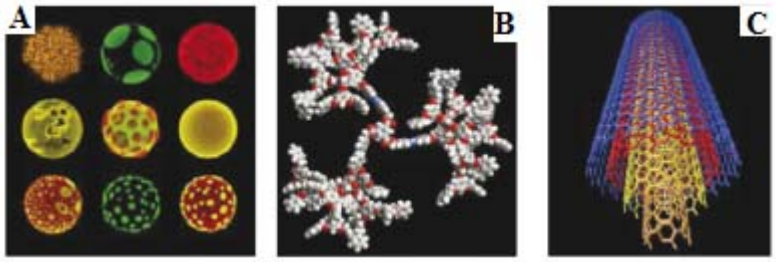

Figure 5-1. Structures of organic nanoparticles A) liposomes, B) dendrimers and C) carbon nanotubes[10] (Figure adapted from Ref. 10)

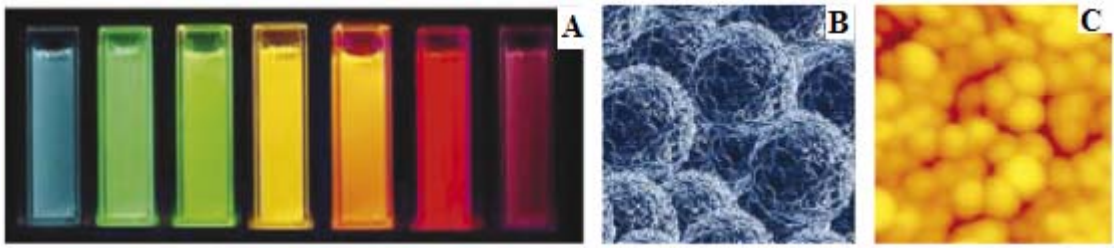

Figure 5-2. Structures of inorganic nanoparticles A) quantum dots, B) magnetic nanoparticles and C) gold nanoparticles[10] (Figure adapted from Ref. 10)

Currently, research in nanotechnology include developing novel nanomaterials for applications in –
1) nanomedicine for the purpose of a) disease diagnosis, b) disease imaging and c) drug delivery;
2) arranging small components into complex ones such as DNA nanotechnology
3) biomimetics; besides many others.
Some of the applications of nanomaterials in medicine are summarized in Table 5-1.[11]

Nanomaterials	Size	Toxicity	Status	Application
Gold nanoparticle	2-4 nm	Low	Commercial	Delivery/Treatment
Quantum dot	2-10 nm	Toxic	Commercial	Delivery/Imaging
Liposome	100-200 nm	Low	Clinical use	Delivery
Polymer	~ 200 KDa	Low	Clinical use	Delivery
Dendrimer	2-6 nm	Variable	Phase I	Delivery
Virus	30-100 nm	High	Phase II	Delivery
Single-walled carbon nanotube	1-2 nm diameter Variable length	Variable	Research	Delivery

Multi-walled carbon nanotube	20-25 nm diameter Variable length	Variable	Research	Delivery
Magnetic nanoparticle	~ 100 nm	Low	Research	Delivery/Imaging
Nanowire	Variable length/diameter	N/A	Research	Sensing

Table 5-1. Summary of application of some nanomaterials[11] (Table adapted from Ref.11)

Several excellent reviews on nanoparticles and their applications have been reported in literature.[1, 3, 12, 13] Many multifunctional nanoparticles are in various stages of preclinical and clinical development. Abraxane® (ABI-007), a novel cremophor free formulation of anticancer agent paclitaxel, was approved by the FDA in 2005 as a second line treatment for breast cancer.[14] The traditional excipients, polyoxyethylated castor oil and alcohol such as Cremophor was replaced with human serum albumin (HSA) to minimize side effects such as hypersensitivity associated with Cremophor.[15] Abraxane® is a 130 nm particle obtained as a colloidal suspension derived from the lyophilized formulation of paclitaxel and human serum albumin diluted in saline solution (0.9% NaCl). A high pressure homogenization of paclitaxel in the presence of HSA resulted in the nanoparticle colloidal suspension. The ultrasonic irradiation process created tremendous local heat and pressure, which resulted in the formation of superoxide ions that cross-linked the HSA by oxidizing the sulfhydryl residues. Paclitaxel was then encapsulated into the albumin-containing aqueous solution. The HSA serves to stabilize the drug and prevents the risk of capillary obstruction and does not require any premedication before the drug administration.[16] In this nanoparticle formulation the concentration of paclitaxel was increased to 2-10 mg/mL in normal saline and clinical studies showed that the therapeutic response rate was doubled, the time to disease progression was prolonged and overall survival rate of breast cancer patients increased.[14, 17] It has been suggested that an albumin-binding protein, known as "albondin" or "gp60" found on endothelial cells within the microvasculature of tissue may be responsible for rapid binding and transportation of albumin-bound paclitaxel from the bloodstream, across the blood vessel and into the underlying tumor tissue space.[18] Then the HSA-drug complex binds to SPARC (secreted protein, acidic and rich in cysteine) and rapidly internalizes into the tumor cells *via* a non-lysosomal pathway. This transendothelial transportation mechanism may in part be responsible for the efficient delivery and accumulation of paclitaxel besides the passive enhanced permeability and retention (EPR) effect.[19]

Examples of some commercial applications of nanoparticles are summarized in Table 5-2.[10]

Nanoparticle component	**Application**	**Indication**
Liposomes	Drug delivery	Cancer, Vaccines: influenza, hepatitis A, Fungal infection

Dendrimers	Therapeutics	HIV, cancer, ophthalmology, inflammation
Carbon nanotubes	In vitro diagnostics	Respiratory function monitoring
	Imaging	Atomic-force microscopy probe tip
Quantum dots	In vitro diagnostics, imaging	Labelling reagents: Western blotting, flow cytometry, biodetection
Magnetic nanoparticles	In vitro diagnostics	Cancer
	Imaging, therapeutics	Liver tumours, cardiovascular disease, anaemia
	Therapeutics	Cancer
Gold nanoparticles	In vitro diagnostics	HIV
	In vitro diagnostics, imaging	Labelling reagents (PCR, RNA, Western blotting), angiography and kidney

Table 5-2. Summary of application of some nanomaterials[10] (Table adapted from Ref. 10)

5.1.2 Nanovector Toolbox

Though there has been outstanding progress in the understanding of cancer biology it has not translated in comparable advances in the clinic largely because of inability to deliver therapeutic agents to target sites selectively without little to none collateral damage.[12, 20] The efficacy of the therapeutic or imaging agent can be enhanced by increasing its target selectivity and ensuring that it can overcome the barriers that prevent it from reaching its target.[21, 22] Thus nanomaterials with their biomimetic features, high surface to volume ratio and prospect of modulating their properties provide great promise in revolutionizing medical treatment in areas of therapy, drug delivery, imaging, faster diagnosis, etc.[23, 24] Nanoparticles are generally hollow or solid materials with more than two dimensions in the size range of 1-100 nm and exhibit unique size dependent physical and chemical properties. Their specific properties are also dependent on their shape and chemical composition. Thus these nanovectors can be filled with or suitably modified on their surface with drugs, imaging/detection agents, targeting moieties, etc and used in targeted drug delivery, imaging, disease diagnosis and medical devices.

5.1.2.1. Liposomes

Liposomes are the typical form of nanovectors which have been reported as early as 1965.[4] They are phospholipid vesicles with a bilayer membrane structure similar to that of biological membranes with an internal aqueous phase. They are classified according to their size and number of layers – unilamellar liposomes are spherical concentric structures with one bilayer and multilamellar liposomes are spherically concentric structures with many bilayers as depicted in Figure 5-3. The amphiphilic

nature of liposomes allows them to transport hydrophilic drugs trapped in their aqueous interior and hydrophobic drugs dissolved in their membrane. Liposomes have excellent circulation, penetration and diffusion properties because of their physical and chemical characteristics and are amenable to surface modification to increase targeted drug delivery.[25] Liposomes use the overexpression of fenestrations in the tumor vasculature to increase the drug concentration at the tumor site. Formulations of doxorubicin encapsulated in liposomes have been approved for the treatment of Kaposi's sarcoma and are now being used for the treatment of breast cancer and refractory ovarian cancer (Doxil®). Liposome-encapsulated doxorubicin is less cardiotoxic than unencapsulated doxorubicin.[26, 27, 28] Myocet, a non-pegylated form of liposomal doxorubicin is used for the treatment of metastatic breast cancer in Europe and Canada.[29] Liposomes are being modified and applied to more cancer indications.[21, 30] There is a growing number of liposomal nanovectors under development for novel and more effective drug delivery.[12, 20, 31, 32]

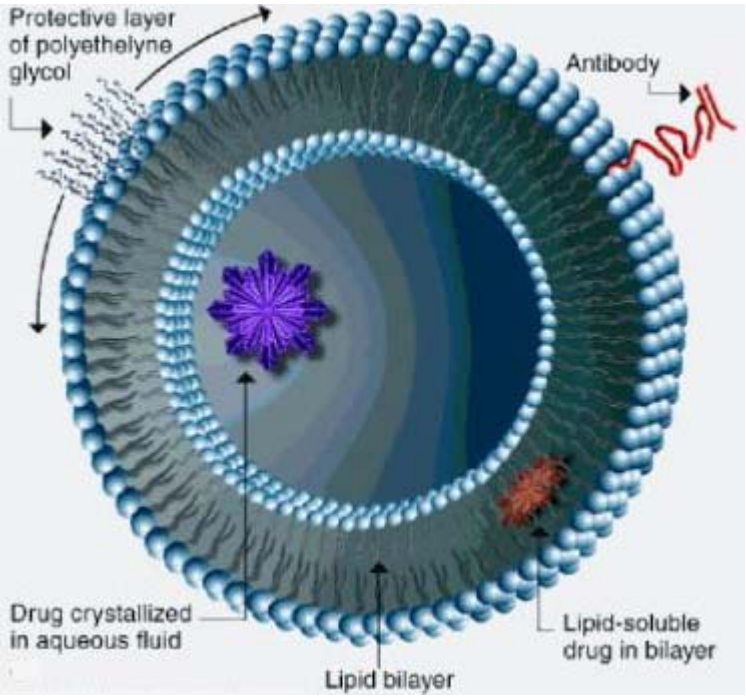

Figure 5-3. Illustration of liposomal structure for drug delivery[33] (Adapted from http://www.nanopharmaceuticals.org/sitebuilder/images/liposome-379x402.jpg)

5.1.2.2. Dendrimers

Dendrimers are highly branched synthetic polymers with a central core, an internal region and many terminal groups that determine the characteristics of the dendrimer. Dendrimers can be synthesized to make it more soluble and more biocompatible. They are excellent vehicles for drugs, imaging agents through modification of their numerous terminal groups.[34]

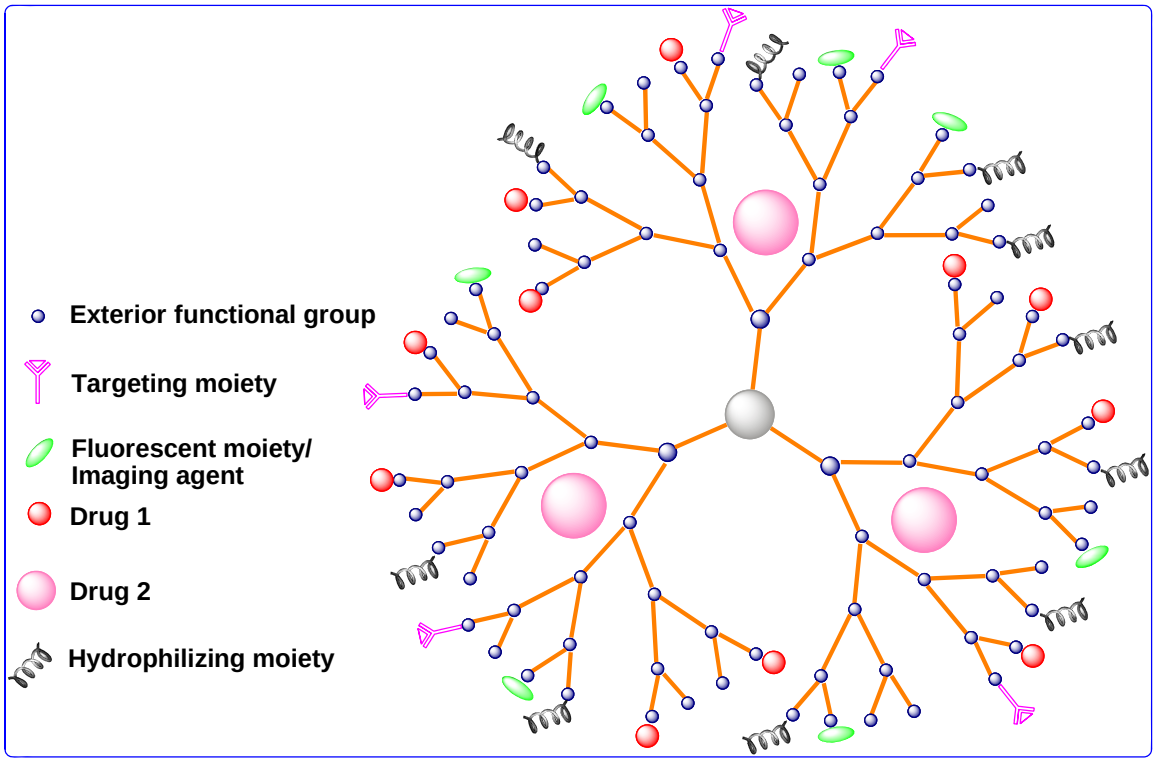

Figure 5-4. Schematic of a dendrimer vehicle

Since dendrimers are produced by multistep organic synthesis they are structurally well defined and monodispersed[35] unlike linear polymers. Dendrimers can be manipulated for precise control of size, shape and placement of functional groups that is desirable for drug delivery and imaging agents. Depending on the generation the hyperbranched structure of the dendrimer can lead to a densely packed, globular structure with unique, well-defined outer and inner structure depending on the monomer used. At lower generations the dendrimer branch may fold back on itself depending on the pH, solvent polarities and surface group.[36, 37] A G-4 polyamidoamine (PAMAM) dendrimer have 64 surface amine groups and can be used for multivalent interactions for installing more than one drug, imaging or contrast agents, targeting moieties, groups for biocompatibility, etc simultaneously to create a polyfunctional nanomaterial which can be fine tuned for the individual patient with potential to revolutionize personalized medicine. Dendrimers can be used for both covalent and non-covalent interactions with drugs.[38]

Dendrimers contain a hydrophobic core and a polar surface with numerous functional groups which are ionizable and can be used to form complexes with drugs. Dendrimers can be loaded with drugs *via* non-covalent interactions and the host-guest interactions are determined by the hydrophilic and hydrophobic properties of the dendrimer, along with its branching and rotational angles and the length of the repeat units.[39] Cytotoxicity, immunogenicity, hemocompatibility, and organ accumulation are some of the critical factors that have to be considered for *in vivo* use of dendrimers. Studies indicate that the cytotoxicity of dendrimers is dependent on their generation, concentration and the chemistry of terminal groups. The cell permeability and

cytotoxicity of dendrimers rise with increasing generation and concentration.[40] It has been reported that cationic PAMAM dendrimers show higher toxicity than anionic dendrimers.[41, 42] Cationic dendrimers with positively charged surface groups are prone to destabilize cell membranes and cause cell lysis. Amino-terminated PAMAM dendrimers showed significant cytotoxicity on human intestinal adenocarcinoma Caco-2 cells in *in vitro* studies and the cytotoxicity increased with higher generation of dendrimers.[43-45]

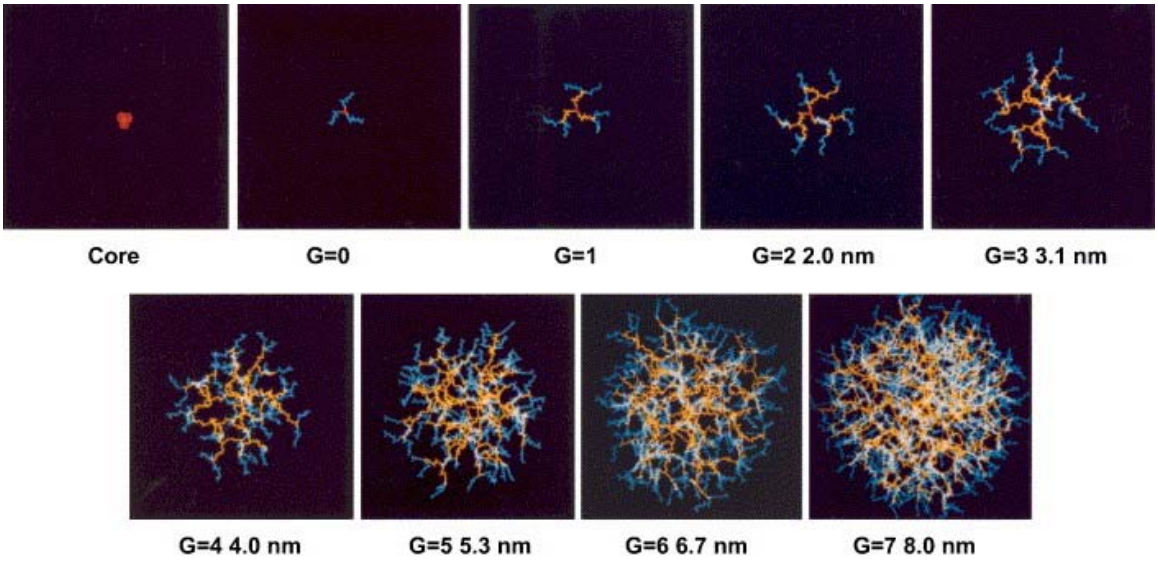

Figure 5-5. Illustration of dendrimer generation (G) from core to G7[40] (Figure adapted from Ref. 40)

An anionic PAMAM dendrimer developed for gene silencing in cancer cells showed no cytotoxic effects, and had greater membrane transport than cationic PAMAM dendrimers.[46] This opens up new possibilities for non-cytotoxic gene transfer vectors for the treatment of cancer.

Often polyethyleneglycol (PEG) is conjugated to the surface of dendrimers to create a hydrophilic shell around the hydrophobic core of the dendrimer to form a unimolecular micelle to solubilize hydrophilic drugs in the PEG layer or hydrophobic drugs in the interior of the dendrimer.[47-50] The anticancer drug 5-fluorouracil[50] and the blood schizonticide chloroquine phosphate[51] have been encapsulated in PEGylated dendrimers which resulted in increased drug entrapment and increase in molecular weight of PEG[51] as compared to non-PEGylated dendrimers.[50] They also exhibited decreased cytotoxicity and hemolytic activity. PAMAM dendrimers with varying lengths of PEG were also studied for the encapsulation of methotrexate (MTX) and adriamycin and it was found that the encapsulation ability increased with increasing generation of the dendrimer and with increasing PEG length. A G4 dendrimer coated with PEG2000 encapsulated the highest number of drug molecules – 26 MTX and 6.5 adriamycin molecules per molecule of dendrimer. The MTX molecules were released slowly in aqueous solutions of low ionic strength but rapidly in isotonic solutions.[48] Similar results were observed in the release of MTX from non-PEGylated PAMAM dendrimers conjugated with folate.[52] Paclitaxel, a poorly water soluble antitumor drug (for details

please refer to Chapter 1) was solubilized hydrotropically in polyglycerol dendrimers which resulted in a 10,000-fold increase in solubilization at an aqueous concentration of 80 wt% of dendrimer.[47] This increase in solubilization was due to the high density of ethylene glycol units in the dendrimer. The anticancer drug 10-hydroxycamptothecin (10-HCPT) was encapsulated within a carboxylated poly(glycerol succinic acid) dendrimer[53] and also within a triblock macromolecule composed of two poly(glycerol succinic acid) dendrons linked by PEG3400.[49] There was a 20-fold increase in water solubility of 10-HCPT with the triblock polymer. The anticancer drug cisplatin was encapsulated within PAMAM dendrimers to form conjugates that exhibited slower release, higher accumulation in solid tumors, and lower toxicity compared to free cisplatin.[54]

The dendrimer surface with its numerous terminal groups provides an excellent platform for covalent modifications to attach cell-specific ligands, imaging agents, therapeutic agents, solubility modifiers, etc. This characteristic of dendrimer to allow attachment of well-defined molecules in a controlled manner on a robust surface differentiates them from other nanovectors such as liposomes. Folate-dendrimer conjugates have been shown to be well-suited for cancer-specific targeted drug delivery of cytotoxic agents.[55-57] Folate-PAMAM dendrimers have been successfully used as carriers of boron isotopes in boron neutron-capture treatment of cancer.[58] Carbohydrates are another class of biological recognition molecules and to achieve high binding affinity they have to be present in clusters. The dendrimer platform offers excellent opportunity for such an orientation. The Thomsen-Friedenreich carbohydrate antigen (T-antigen), β-Gal-(1-3)-α-GalNAc, is an important antigen for the detection and immunotherapy of carcinomas such as breast cancer and has been attached to the surface of PAMAM and other dendrimers and an enhanced binding was observed.[59-61] These conjugates could potentially block metastatic sites of tumor cells. The effect of glycodendrimer on binding affinity and other properties were studied and the effect of complex formation on biological recogmition with anticancer drug docetaxel was investigated.[62] Studies revealed an increase in binding affinity between the glycodendrimers and the cell surface with increasing sugar moieties.[63] Attachment of PEG molecules to the surface of dendrimers could reduce cytotoxicity besides improving solubility. Modifications to the dendrimer surface using techniques such as 'click' reaction open up more possibilities to modulate the dendrimer's properties to make them more biocompatible and less toxic.

5.1.2.3. Gold nanoparticles

Gold nanoparticles (AuNPs) can be prepared with different shapes such as nanoshells, nanocages, nanorods or nanospheres. AuNPs have unique physicochemical properties, such as ultra small size, large surface area to mass ratio, and high surface reactivity, presence of surface plasmon resonance (SPR) bands, biocompatibility and ease of surface functionalization which may be used for targeted drug delivery[64, 65] and in diagnostics. When these particles are irradiated with light, photons are emitted with the same frequency in all directions thereby exhibiting localized surface plamon resonant properties. These particles are excellent labels for biosensors because they can be detected by fluorescence, optical absorption, electrical conductivity, etc.[66] Gold nanoshell which comprises of a precisely tunable gold layer over a silica core can be selectively activated through tissue radiation with near infra-red light to perform localized thermal ablation of target cells and it has been used to eradicate tumors in mice.[67]

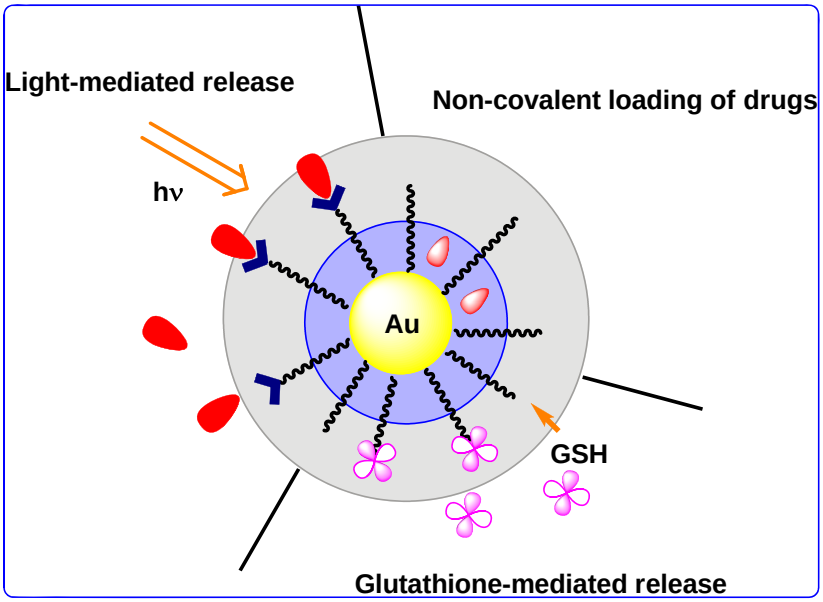

Figure 5-6. Schematic of AuNP as multimodal drug delivery system[65]

The AuNPs can be fabricated with a wide variety of core sizes with relative ease and in a scalable fashion. The use of the place-exchange reaction is the most commonly used method for creation of mixed monolayer-protected AuNPs.[68] In this protocol, external thiols replace the existing ligands on AuNPs in an equilibrium process. The ligand structure can be controlled to make the AuNPs more suitable for delivery applications such as through use of biocompatible polyethylene glycol (PEG) and oligoethylene glycol (OEG) moieties.[69, 70, 71]

Core size (d)	Synthetic methods	Capping agents
1–2 nm	Reduction of $AuCl(PPh_3)$ with diborane or sodium borohydride	Phosphine
1.5–5 nm	Biphasic reduction of $HAuCl_4$ by sodium borohydride in the presence of thiol capping agents	Alkanethiol
3.5–10 nm	Heat-induced size ripening method	Alkanethiol
10–150 nm	Reduction of $HAuCl_4$ with sodium citrate in water	Citrate

Table 5-3. Different synthetic methods employed for synthesis of AuNP[65]

The surface functionality, size[72] and charge[73, 74] are important factors in determining the cellular uptake and intracellular fate of the AuNPs. The cellular uptake of AuNPs is dependent on their size as has been demonstrated by Chan et al.[75] ErbB2 receptor mediated internalization in breast cells were studied using AuNPs (2–100 nm) coated with Herceptin. AuNPs with 20–50 nm size exhibited the most efficient cellular uptake and apoptosis or programmed cell death was enhanced by AuNPs in the 40–50 nm range. Passive targeting of AuNPs in the 10–100 nm size range was also investigated and it was found that the larger AuNPs remained near the vasculature whereas the smaller nanoparticles rapidly diffused from blood vessels to the tumor matrix.[76] It has been shown that the cellular uptake is dependent on both charge and hydrophobicity[68] as well as ligand shell morphology.[77] AuNPs with a structured ligand shell are capable of passing directly through the cell's plasma membrane without making pores on the cell membrane which can result in cytotoxicity. Targeting moieties can be attached on the surface of the AuNPs for target specific delivery of therapeutic or diagnostic agents. It has been shown that by modifying the surface of the AuNPs with cell penetrating peptides [e.g. the oligopeptides TAT (AGRKKRRQRRR) and Pntn (GRQIKIWFQNRRMKWKK)] and the nuclear localization sequence (NLS: GGFSTSLRARKA) specific cellular components such as nucleus and other organelles can be targeted. The particles appeared to enter the cytosol either directly through the cell membrane or by endosomal escape.[78] The modified AuNPs appeared to be capable of disrupting the endosomal morphology and dissolving the endosomal membrane resulting in the release of its content. The nuclear targeting has been reported by other studies as well.[79, 80]

As with other nanovectors, both the transport and drug release play critical roles in efficient and specific delivery. Active drugs can be loaded *via* non-covalent interactions on the surface of the nanoparticle and covalent conjugation to the nanoparticle generally requires cellular processing of the prodrug to release the active drug.[81] Drug delivery systems (DDS) based on glutathione (GSH)-mediated release of active drug are designed to exploit the higher intracellular GSH concentration compared to the extracellular level of the thiol[82] (for details please refer to chapters 3 and 5). This elevated level of GSH can be used to release prodrugs on AuNPs *via* disulfide exchange or place-exchange reactions at the core. The monolayer of nanoparticles can provide steric protection against disulfide exchange with surface cysteines of proteins in the blood stream,[83, 84] increasing their potential *in vivo* use. The cationic surface of the nanoparticles facilitated their penetration through cell membranes and the prodrug release was triggered by intracellular GSH.

Light-mediated drug release of caged drugs has also been reported where the activity of the drug was suppressed by attaching it to a blocking element *via* a photolabile protecting group.[85] This concept has been applied to AuNP delivery vehicles using a photocleavable *o*-nitrobenzyl ester moiety that dissociated upon light irradiation to change the surface potential from positive to negative and releasing adsorbed DNA.[86] Light-controlled release of anticancer drug 5-fluorouracil from AuNPs has also been demonstrated using a *o*-nitrobenzyl linkage.[87] Other delivery strategies have also been explored using AuNP platforms. It has been shown that nitric oxide (NO) can be efficiently released at acidic pH from AuNPs,[88] providing a potential means of controlling multiple cellular processes including angiogenesis, vasodilation and immune

response.[89, 90] A phosphate linker was used to conjugate paclitaxel to AuNP and Fe_3O_4 particles. The drug could be released from the particles using phosphodiesterase.[91]

5.1.2.4. Quantum dots

Quantum dots (QDs) are colloidal fluorescent semiconductor nanocrystals consisting of a central core made up of elements from groups II-VI such as CdS, CdSe, ZnS and ZnSe or from groups III-V such as InS, InP, GaS and GaP with an outer coating of a layer of ZnS. QDs are photostable, exhibit size and composition dependent emission spectra[92] and have high quantum yield. QDs are resistant to photobleaching and chemical degradation.[93] Figure 5-7 shows ten distinguishable emission colors of CdSe QDs capped with ZnS after excitation with a near-UV lamp. The emission spectra are located at 443, 473, 481, 500, 518, 543, 565, 587, 610, and 655 nm respectively from blue to red (left to right).[92] QDs have the potential to be used as a sensitive probe for screening cancer markers, specific label for classifying biopsied tissue and as a high resolution contrast agent for detecting tumors. QDs have a high surface-to-volume ratio which makes them suitable for a multifunctional nanoplatform where the QDs can be a nanoscaffold for therapeutic and diagnostic (theranostic) modalities besides being imaging agents.

Figure 5-7. Ten distinguishable emission colors of CdSe QDs capped with ZnS[92] (Figure adapted from Ref. 92)

QDs have a 10-100 times stronger fluorescence and have 100-1000 times stronger fluorescence stability against photobleaching than organic fluorophores and fluorescent proteins which make them suitable for long-term monitoring of inter- and intra-molecular processes in live cells and organisms.[94, 95] One of the predominant ways to prepare a QD is to coat a CdSe core with a ZnS layer to obtain the best crystalline quality and monodispersity. The ZnS layer protects the core from oxidation, reduces toxicity by preventing the CdSe from leaching out to the surrounding solutions and enhances the photoluminescence yield. However, QDs coated with ZnS are soluble in nonpolar organic solvents only and require an alteration in their surface properties from hydrophobic to hydrophilic to be suitable for use in the aqueous biological environment.[94, 96, 97] Also QDs have no innate biological specificity and rely on conjugation with antibodies,[98] peptides,[99-102] aptamers,[103] folate[104] and small molecule ligands to gain biological affinity.[105] Figure 5-8 shows the structure of a multifunctional QD probe where the

polymer coating can be conjugated with PEG to make the QD more biocompatible and the affinity ligands can suitably chosen to lend specificity to the QD.

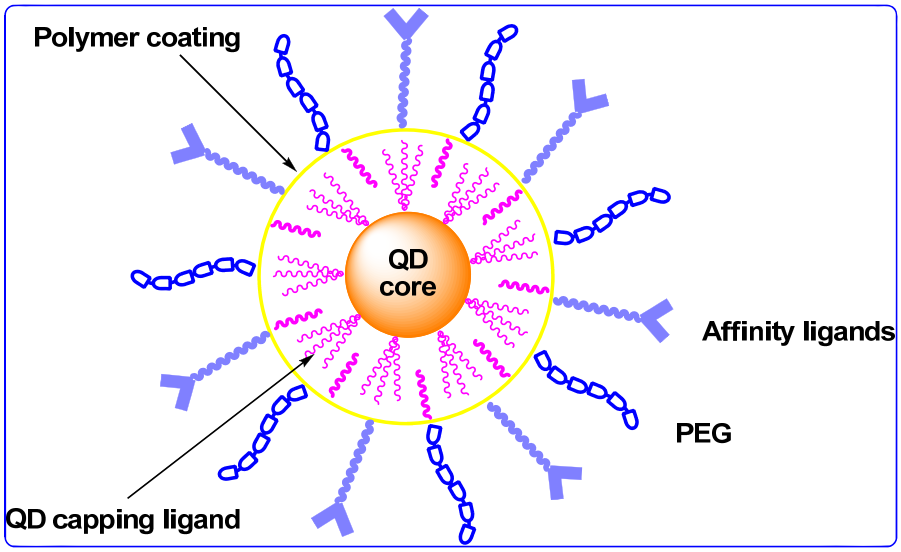

Figure 5-8. Structure of a QD probe

Figure 5-9 shows the possibilities of an idealized multiply functionalized QD probe which consists of an integrated nanoplatform which can target tumor cells specifically, transport and liberate the drug payload and image the therapeutic response simultaneously.[106]

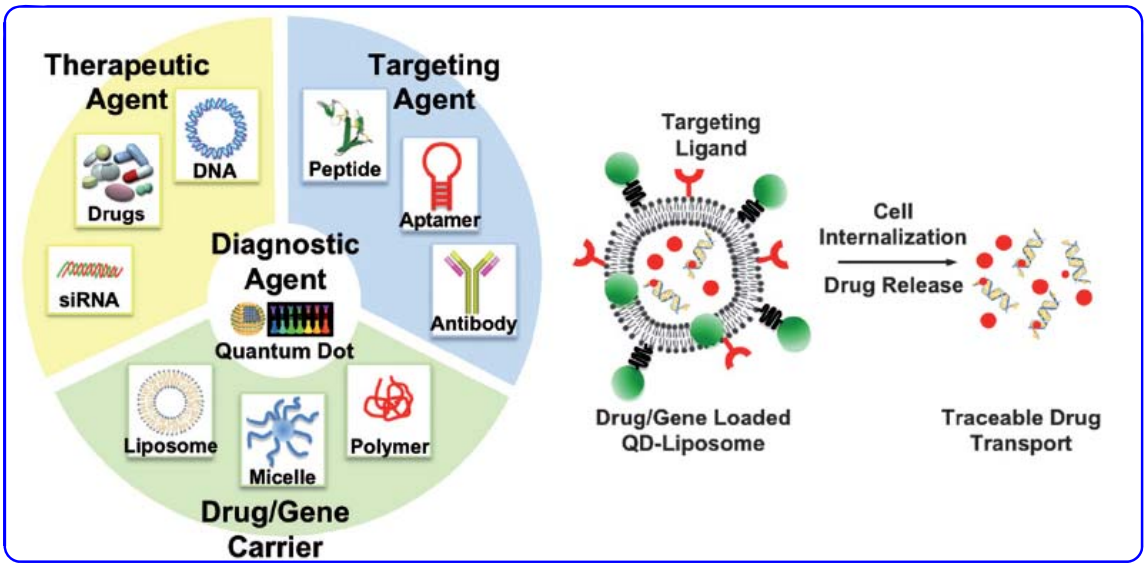

Figure 5-9. Structure of an idealized QD nanoplatform[106] (Figure adapted from Ref. 106)

Nie and coworkers reported the development of a novel series of multifunctional QD probes for cancer targeting and *in vivo* imaging in animals. The luminescent QDs were encapsulated with a triblock copolymer and linked to tumor-targeting ligands and drug-delivery functionalities. The QDs were then injected into nude mice bearing human prostate cancer xenografts and studies indicated that the QDs accumulated at tumor sites both by enhanced permeability and retention (EPR) effect (for details please refer to Chapter 4) and by PSMA (prostate specific membrane antigen) targeting monoclonal antibody binding to tumor-specific cell surface biomarkers. Figure 5-10 shows the results of the sensitivity and multicolor capability of *in vivo* QD imaging. Figure 5-10 A) shows the *in vivo* imaging of multicolor QD-encoded microbeads. The right hand figure in A) shows the QD-encoded microbeads (0.5 μm diameter) emitting green, yellow or red light. Approximately 1–2 million beads in each color were injected subcutaneously at three adjacent locations on a host animal. Figure 5-10 B) shows the whole animal and the tumor where the QD probes are clearly seen against a black background with little or no interference from the mouse autofluorescence.[98]

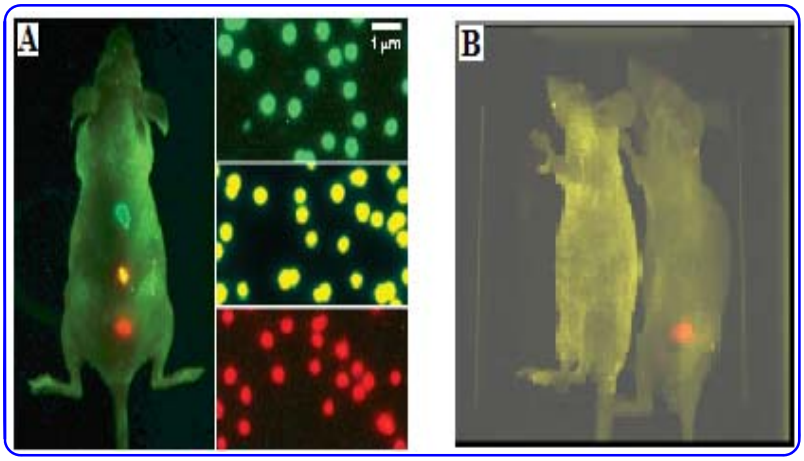

Figure 5-10. A) *in vivo* simultaneous imaging of multicolor QD-encoded microbeads and B) *in vivo* image of QD-PSMA Ab with tumor xenograft[98] (Figure adapted from Ref. 98)

QDs have the promising potential of detection of cancer eliminating the need for biopsy. When different sized quantum dots are combined within a single bead, probes that release distinct colors and intensities of light can be created which upon stimulation by UV light will emit light that serves as a sort of spectral bar code, identifying a particular region. The QD particles used for drug delivery can be injected in the blood stream to bind to specific antigens to detect cancer cells. The QDs radiate photons when infra-red light is shone on the cancer site which can simultaneously release the anticancer drug as well as pinpoint the location of the cancer.[11, 107] A QD-aptamer-doxorubicin (QD-Apt-Dox) conjugate has been reported for simultaneous cancer-targeted imaging, therapy and sensing system. The surface of the fluorescent QD was functionalized with A10 RNA aptamer which recognized the extracellular domain of the PSMA. This multifunctional QD could deliver Dox to the targeted prostate cancer cells and sensed the delivery of Dox by activating the fluorescence of QD, which imaged the cancer cells simultaneously.[107]

However, the significant concern for the use of QDs is their inherent cytotoxicity from surface oxidation and leaching-out of heavy metal ions from the core of the QD. [108, 109] The cytotoxicity depends on the physicochemical properties of QDs, such as size, surface charge and coating materials, besides the dosage of QDs and the duration of exposure.[110] Table 5-4 shows the animal biodistribution of QDs with various core and surface modifications and size.[111]

QD Core	QD Shell	QD Surface	Emission Peak of QD	QD Size	Animal Model	Principal Organ Accumulation
CdSe	ZnS	lysine-modified BSA	ND	25 nm	sprague-dawley rats	Liver
			ND	80 nm		Liver
$Cd^{125m}Te$	ZnS	mAb to mouse lung	ND	ND	female Balb/c mice	Lung
		control mAb				Liver
CdSe	CdS	PEG	621 nm	37 nm	SKH-1 mice	Liver
CdTe	ZnS	PEG	705 nm	13 nm	male ICR mice	Liver
CdSe	ZnS	cystein-^{99m}Tc	515 nm	4 nm	CD-1 mice	Bladder
		cystein-^{99m}Tc	575 nm	9 nm		Liver
CdSe	ZnS	NH_2-PEG-^{64}Cu	525 nm	12 nm	nude mice	Liver
		COOH-^{64}Cu	525 nm	12 nm		
		NH_2-PEG-^{64}Cu	800 nm	21 nm		
		COOH-^{64}Cu	800 nm	21 nm		
CdSeTe	ZnS	NH_2 NH_2-EGF	800 nm 800 nm	21 nm 26 nm	male nude mice	Liver
CdSe	ZnS	COOH	655 nm	16 nm	female nude mice	Auxiliary lymph node
CdSeS	SiO_2	OH	570 nm	22 nm	male ICR mice	Liver
CdSe	ZnS	nothing	596 nm	4 nm	wistar rats	Digestive system

Table 5-4. Biodistribution studies of QDs[111] (Table adapted from Ref. 111) (ND – no data)

QDs hold significant and exciting promise in personalized nanomedicine with the potential for tunable functionalization for simultaneous imaging, diagnosis and treatment.

5.1.2.5. Magnetic nanoparticles

Magnetic nanoparticles (MNPs) are spherical nanocrystals with a Fe^{2+} and Fe^{3+} core coated with a shell of PEG or dextran molecules and are amenable to functionalization on the surface for active *in vitro* and *in vivo* targeting. Targeting ligands and additional imaging modalities are attached to the shell and therapeutic agents can be embedded in the shell structure or chemically bonded to its surface. The magnetic properties of these nanoparticles make them excellent labeling agents in bioassays as well as MRI contrast agents.[112] Thus fascinating opportunities exist in the cell-specific targeting, drug delivery and multi-modal imaging by MNPs by modulating and utilizing their physicochemical properties. A few MNPs are commercially available or under clinical trials such as Ferimoxides (Endorem®/Feridex®) and Ferumoxtran-10.[113]

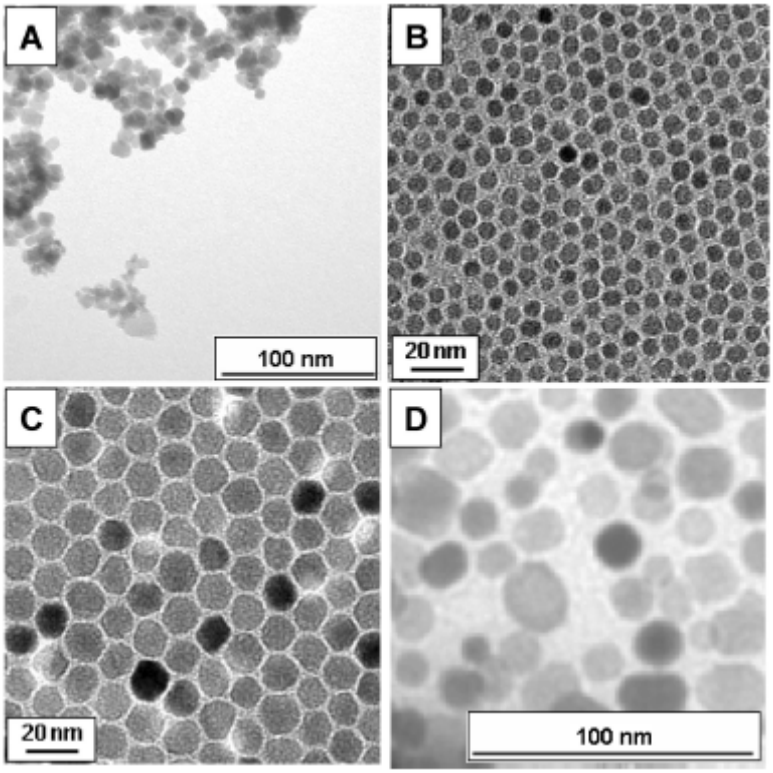

Figure 5-11. TEM images of MNPs prepared using different synthetic routes[114] (Figure adapted from Ref. 114)

MNPs have to overcome considerable physiological barriers to be a successful therapeutic and diagnostic vehicle. The body's intrinsic defense mechanism can restrict the function of the MNPs by blocking their movement, causing physical changes to them or by eliciting a negative biochemical host response.[115] Additionally, upon administration

in the body MNPs will encounter blood, plasma proteins, etc which can cause agglomeration, alter their magnetic properties and cause particle sequestration, nonspecific interaction with proteins, cell surfaces, etc. This would result in premature binding or uptake by cells before reaching the target tissue.[116] The MNPs also have to overcome size restrictions which may prevent them from accessing the target tissue.[3, 117] The *in vivo* pharmacokinetics and cellular uptake of MNPs are dependent on their physicochemical properties such as morphology, hydrodynamic size, charge, etc.[118] MNPs are referred to as SPION (superparamagnetic iron oxide nanoparticle) or USPION (ultrasmall superparamagnetic iron oxide nanoparticle) depending on their hydrodynamic diameter.

MNPs can be designed for both passive (utilizing EPR effect) and active targeting and MNPs are being designed with targeting molecules which have specific affinity to biomarkers on the diseased tissue. SPION systems have utilized various targeting ligands such as small organic molecules,[119, 120] peptides,[121, 122] aptamers,[123] antibodies,[124, 125] etc. The density and molecular organization of the bound ligands influence the binding of the MNPs to the target cells because of the multivalent binding which is the enhanced binding observed when multiple ligands bind with multiple receptors.[126, 127] When MNPS were conjugated with RGD peptides (4.1, 20, and 52 peptides per MNP) simultaneous ligand binding increased with increasing RGD peptides upto a certain density after which steric hindrance affected the multivalent interactions.[128] The size of the MNPs also affected multivalency. Studies showed that when MNPs ranging from 2-100 nm were attached to herceptin targeting antibodies, MNPs less than 25 nm in size did not exhibit multivalency unlike the larger MNPs while the larger MNPs were not endocytosed by cells effectively.[129] The shape of the MNPs also influence their targeting abilities, rod shaped "nanoworm" MNPs exhibited enhanced cell binding compared to peptide modified spherical MNPs in several studies[121, 130-132] as shown in the schematic in Figure 5-12.

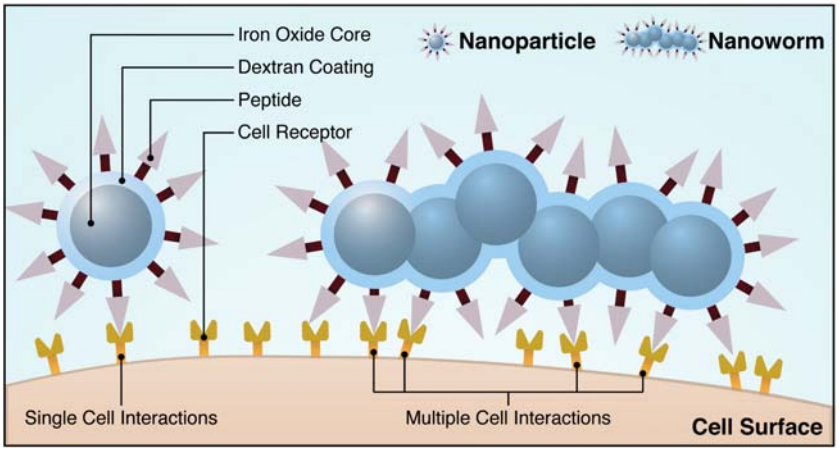

Figure 5-12. Schematic of multivalent interactions of MNPs[133] (Figure adapted from Ref. 133)

Yang et al. studied simultaneous targeted drug delivery and MR imaging of breast cancer tumors through the use multifunctional magneto-polymeric nanohybrids (MMPNs) composed of magnetic nanocrystals and doxorubicin which were simultaneously encapsulated within an amphiphilic block copolymer shell and the surface of these nanoparticles were functionalized with breast cancer targeting anti-Herceptin antibody. *In vivo* studies performed in nude mice bearing NIH3T6.7 breast cancer tumors showed that MNPs functionalized with targeting ligands and loaded with doxorubicin were most effective in inhibiting tumor growth.[134] MNPs hold exciting potential in simultaneous targeted therapy and imaging as well as diagnosis.

5.1.2.6. Fullerenes

Fullerenes were discovered in 1985[135] and their unique physical and chemical properties make them an important member of the nanomaterial family. Buckminsterfullerene (C_{60}) is a truncated icosahedron with a diameter of ~ 0.7 nm and contains 60 carbon atoms with C5–C6 double bonds forming hexagons and C5–C5 single bonds forming pentagons.[135] They have poor aqueous solubility and form aggregates in aqueous solutions and hence not attractive as such for applications in nanomedicine. However, appropriate functionalization of fullerenes can overcome the problems posed by fullerenes.[136, 137] Fullerenes can have multimodal applications such as in drug delivery,[138] as MRI contrast agents[139, 140] and targeted imaging[140] and are being investigated for diagnosis and treatment of diseases like cancer,[141] lung, heart[142] and blood diseases. Figure 5-13 shows the chemical structure of an amphiphilic fullerene.[143]

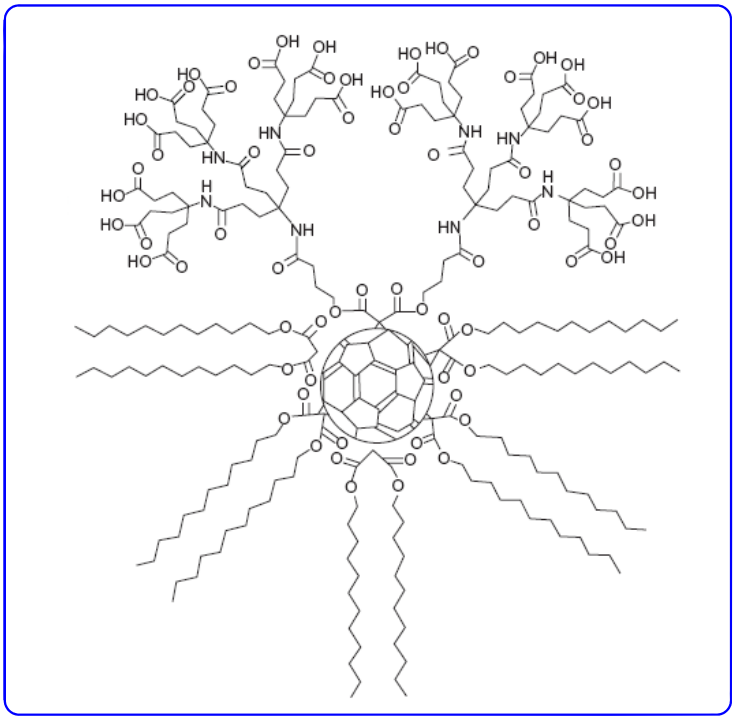

Figure 5-13. Structure of an amphiphilic fullerene monomer[143] (Figure adapted from Ref. 143)

Fullerenes can be modified to produce a lipophilic slow release system and their three-dimensional scaffolding can be used to covalently attach multiple drugs to create a single-dose 'drug-cocktail'. A fullerene-paclitaxel conjugate has been reported which was designed to release the drug slowly for aerosol liposome delivery of paclitaxel for lung cancer therapy.[144] The size range of the aggregates was in the 120-145 nm range and did not vary with concentration. Paclitaxel was released *via* enzymatic hydrolysis and the release half-life was 80 min in bovine plasma. In another study, amphiphilic fullerene embedded with paclitaxel in its hydrophobic pockets was used to enhance water solubility of paclitaxel eliminating the need for non-aqueous solvents. A higher concentration of paclitaxel could be delivered using this method as compared to Abraxane® which could potentially increase tumor uptake and reduce the infusion time.[145] Fullerene based nanovectors can also be used for passive targeting by utilizing the EPR effect exhibited by tumor cells. A tissue vectored bisphosphonate fullerene was reported to have successfully targeted bone tissue *in vitro*. The amide bisphosphonate functionalization along with multiple hydroxyl groups conferred a strong affinity for the calcium phosphate mineral hydroxyapatite of bone.[146] The fullerene cage can encapsulate metals and protect them from chemical and enzymatic attack as well as prevent them from unwarranted release. Proper functionalization of the fullerenes can make them biocompatible and target-specific. In fact gadolinium encapsulated fullerenes have been reported where the metal is shielded within the fullerene cage allowing for applications that require longer residency times. Also, gadofullerenes enhances the quality of the MRI.[147, 148] Carbon nanotubes are elongated members of the family of fullerenes and have promising applications in nanomedicine as discussed later in this chapter. Figure 5-14 shows a brief summary of the nanovector arsenal and their exciting potential multimodal applications in nanomedicine.

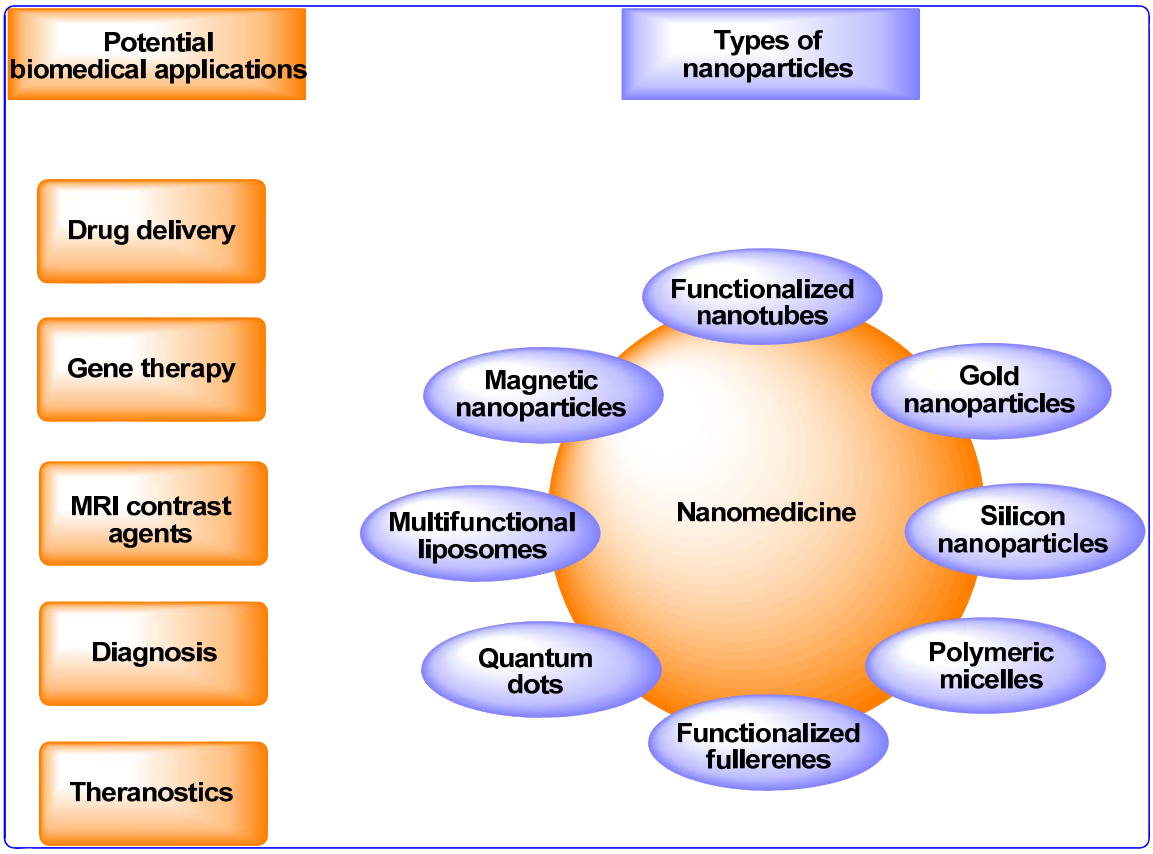

Figure 5-14. Summary of potential applications of nanotechnology in medicine

5.1.3 Carbon Nanotubes (CNTs) – Versatile Nanovector

Carbon nanotubes (CNTs) first discovered by Iijima and coworkers in 1991[149] is an allotrope of carbon along with graphite and diamond with a cylindrical nanostructure and belongs to the family of fullerenes. This novel nanomaterial has unique electronic, structural and mechanical properties that make it a promising candidate in potential applications in nanomedicine and material science. CNTs have various structures (Figure 5-15 and Figure 5-16) and are classified into two broad categories – single-walled (SWNT) which consist of one layer of cylinder graphene and multi-walled (MWNT) which consist of several concentric sheets of graphene. SWNTs have diameters from 0.4-2.0 nm and lengths from 20-1000 nm while MWNT are bigger and have diameters from 1.4-100 nm and lengths from 1 to several μm.

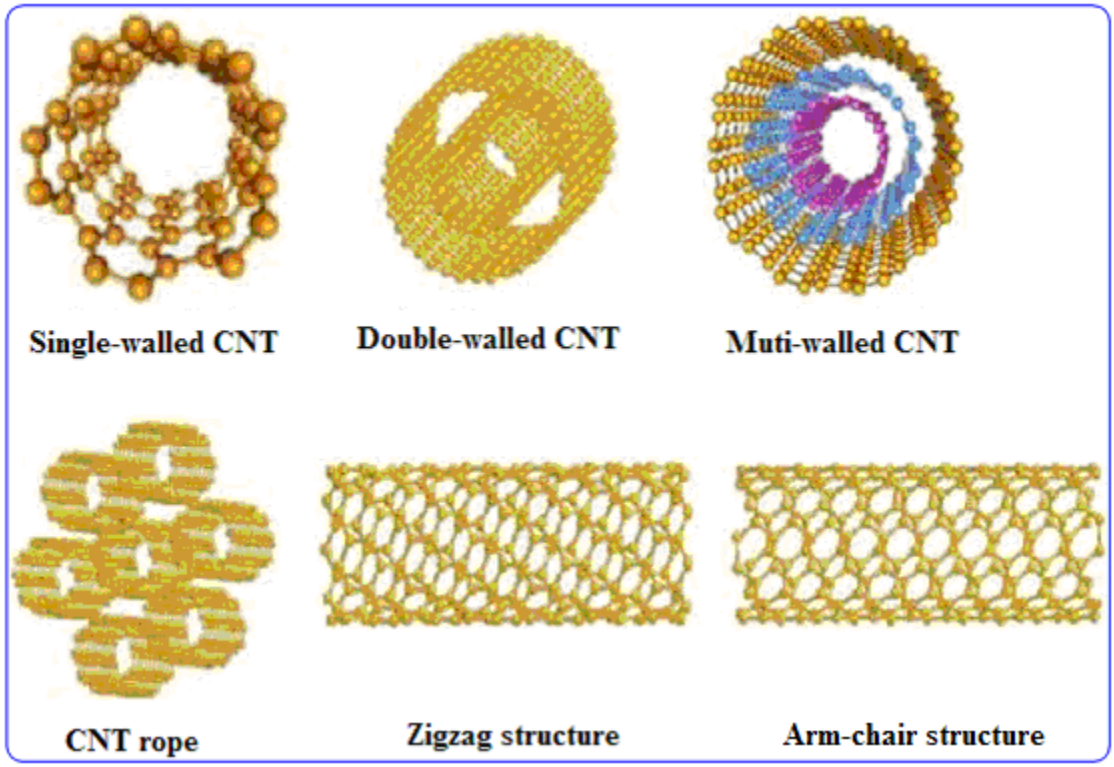

Figure 5-15. Structures of carbon nanotubes (Figure is adapted from http://nanotube.korea.ac.kr/images/introd2.jpg)

CNTs are made commercially by various methods such as chemical vapor deposition (CVD),[150] high pressure carbon monoxide (HiPCO),[151] arc discharge,[152] and laser ablation.[153, 154] CNTs possess remarkable physicochemical properties such as ordered structure with high aspect ratio, high mechanical strength, high electrical conductivity, high thermal conductivity, high surface area, ultra-light weight, and metallic or semi-metallic behavior[155, 156] which have potential use in diverse applications such as biosensors, gas storage, fillers in polymer matrixes, field-emission devices, molecular electronics, catalyst supports, probes for scanning probe microscopy and others.[157-159] There is a burgeoning interest in exploring CNTs in nanomedicine and there are extensive reviews reported in literature.[160, 161] The state-of-the-art application of this nano platform ranges from detection at molecular level to diagnosis of genetic or biological diseases and delivery of various therapeutic agents.[162-164]

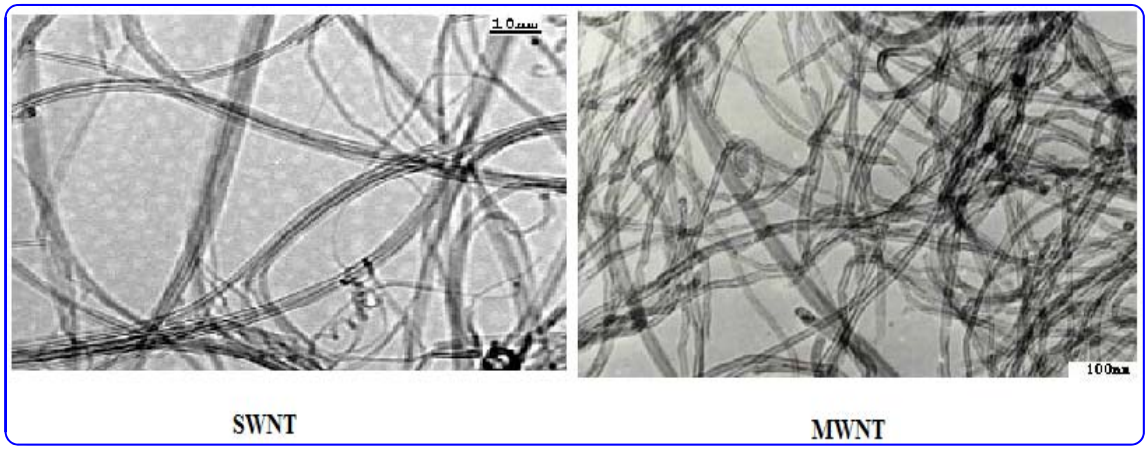

Figure 5-16. TEM images of SWNT and MWNT (Figure is adapted from http://www.cheaptubes.com/images/tem)

5.1.3.1. Toxicological and pharmacological profile of CNTs

Despite the promising potential that CNTs hold as efficient carriers for drugs, antigens and genes that will facilitate specific transport into targeted tissues, cells and cellular compartments that would minimize deleterious side effects, the path to such a 'smart' nanomedicine is fraught with obstacles and results from numerous biological studies are still controversial.[165] Some of the potential challenges faced by the CNTs after administration to the body are summarized in Figure 5-17. The difficulties arise mainly because of the problems in controlling and manipulating CNTs. Pristine non-functionalized CNTs are inherently hydrophobic and have very low solubility in all organic and aqueous solvents which is a problem in biology and medicinal chemistry. CNTs form bundles or aggregates which can be composed of several hundred single nanotubes which entangle together in the solid state through van der Waals forces forming a highly complex network. These bundles can be temporarily dispersed in solvents by sonication but precipitates as soon as the sonication is stopped. It is challenging to produce chemically and structurally reproducible batches of CNTs with identical characteristics, minimal impurities and high quality control.[1, 160]

There are several factors that are responsible for the harmful effects of CNTs amongst which the high surface area and the intrinsic surface toxicity are the most important.[166, 167] The CNTs with their small size can be potentially more toxic to the lung which is the portal of entry, can escape from the body's phagocytic defenses, can relocate from their site of deposition or can modify the protein structures,[166] all of which can induce unexpected toxicological effects in biological systems. The structural characteristics of CNTs such as the fiber shape, length and aggregation affect the local deposition and immunological response.[168] Even in a few milligrams of CNTs there are a large number of cylindrical, fiber-like particles of CNTs which results in a very high total surface area because of their nanoscale dimensions. The total surface area also varies with the degree of aggregation or bundling in solution. Besides, the large surface area, the intrinsic toxicity of CNTs also varies with the degree of surface functionalization and the varying toxicities of the functional groups.[169] After synthesis, batches of pristine CNTs

can contain impurities such as amorphous carbon and metallic particles from metal catalysts used which cause severe toxicity.

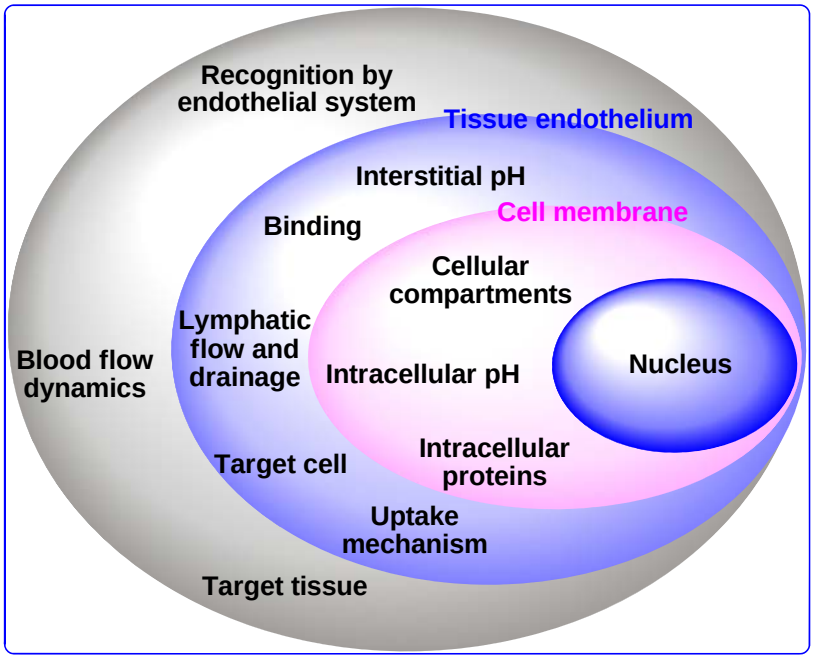

Figure 5-17. Some obstacles that affect the fate of CNTs in the body

Bioavailability of CNTs in the body is another important factor to consider and the mechanism of CNT accumulation, metabolism, degradation and clearance from the body needs to be explored. Acute pulmonary toxicity in mice was reported when SWNT dispersed in phosphate buffer saline (PBS) with 1% Tween 80 was administered to mice causing 15% mortality. Agglomeration of the CNTs in the major airways was attributed to the major cause of death.[170] Mice exposed to pharyngeal aspiration of pristine SWNTs in PBS showed acute inflammation, granuloma formation and progressive fibrosis.[171] Studies also showed that the length of CNTs modulates the immune response, bioavailability and clearance kinetics regardless of whether the CNTs are pristine or functionalized.[172, 173] A summary of *in vivo* pharmacological and toxicological investigations using CNTs reported in the literature is presented in Table 5-5 and Table 5-6 respectively.[1]

CNT	Amount	Model	Toxicity	Ref.
^{125}I-SWNT (OH)	1.5 μg/ mouse	Male KM mice	Distribute in the entire body quickly except for the brain. Accumulate in the bone. Excreted *via* urine.	174
[^{111}In] DTPA-CNT	60 and 400 μg/ mouse	Female BALB/c mice	Not retained in any of the reticuloendothelial system organs. Rapidly cleared from systemic blood circulation *via* renal excretion. No accumulation was observed. Without any toxic side effects or mortality.	175

Table 5-5. *In vivo* pharmacological studies performed with CNTs

CNT	Amount	Model	Toxicity	Ref.
Pristine Arc-CNT	25 mg/ Kg	Male dunkin Hartley guiea pigs	Not induce any abnormalities of pulmonary function or measurable inflammation	176
Pristine Laser SWNT	1 and 5 mg/Kg	Male Crl:CD® (SD)IGS BR Rats	Exposure to the high dose produced mortality within 24 h post-instillation. Pulmonary inflammation with non-dose-dependent granulomas.	170
Raw and purified HiPCO CNT and Arc-CNT	0.1 and 0.5 mg/mouse	Male mice B6C3F1	Induced dose-dependent epithelioid granulomas. Mortality was observed with the high dose.	177
MWNT	0.5, 2 and 5 mg/rat	Female Sprague-Dawley rats	Not ground MWNT accumulate in the airways. Ground MWNTs were cleared more rapidly. Both MWNT have induced inflammatory and fibrotic reactions. Also both have caused pulmonary lesions at 2 months.	178
Metal-free HiPCO SWNT	0-40 μg/mouse	Female C57BL/6 mice	Rapid progressive fibrosis and granulomas. Dose-dependent increase in expiratory time. Increased pulmonary resistance.	171

Purified open SWNT and MWNT	50 μg/mL	Wistar-Kyoto rats	Accelerated time and the rate of development of carotid artery thrombosis.	179

Table 5-6. *In vivo* toxicological studies performed with CNTs

More research in *in vivo* evaluations is being conducted with aim in therapeutic, imaging and other biomedical applications. Systematic studies in mice with water soluble ^{125}Iodine-labeled multiple hydroxylated SWNTs (^{125}I-SWNTs-OH) functionalized by oxidation of the CNTs showed that biodistribution was not significantly influenced by the route of administration and ^{125}I-SWNTs-OH distributed quickly throughout the whole body. Accumulation was observed in stomach, kidney and bone and 94% of the CNTs were excreted into the urine and 6% in feces. Interestingly, no tissue damage or distress was observed.[174] Another *in vivo* study in mice using water soluble CNTs modified *via* 1, 3-dipolar cycloaddition reaction and functionalized with chelating ligand diethylentriaminepentaacetic acid (DTPA) and radio-labeled with ^{111}Indium (^{111}In-DTPA-CNT) showed an affinity to kidneys, muscle, skin, bone and blood half an hour after administration. The maximum blood circulation half time was 3.5 h and these CNTs were quickly cleared from all tissues. These CNTs were excreted through the renal route into the bladder and urine and were intact upon excretion.[175] More studies remain to be carried out to get a better and reliable toxicological and pharmacological profile of the CNTs.

5.1.3.2. Surface modifications of CNTs

The application of CNTs as delivery vehicle relies on the successful surface modifications which can render the CNTs more compatible with biological systems. Since pristine CNTs are insoluble in organic and aqueous solvents they cause a high degree of aggregation in biological environment and hinder their integration into biological systems resulting in some health concerns. Therefore, it is critical to develop efficient and practical approaches for the preparation of water soluble CNTs, which can be used in biological applications, especially drug delivery.[13] CNTs can be functionalized by non-covalent and covalent modifications of the surface of the CNT as shown on Figure 5-18. The surface chemistry of CNTs have been explored and there are several reviews in literature.[161, 180] Non covalent complexes of CNTs with peptides,[181, 182] oligonucleotides,[183, 184] proteins,[185] polysaccharides,[186] different types of polymers,[187, 188] etc have been realized and these macromolecules were able to wrap around the tubes and increase their solubility.

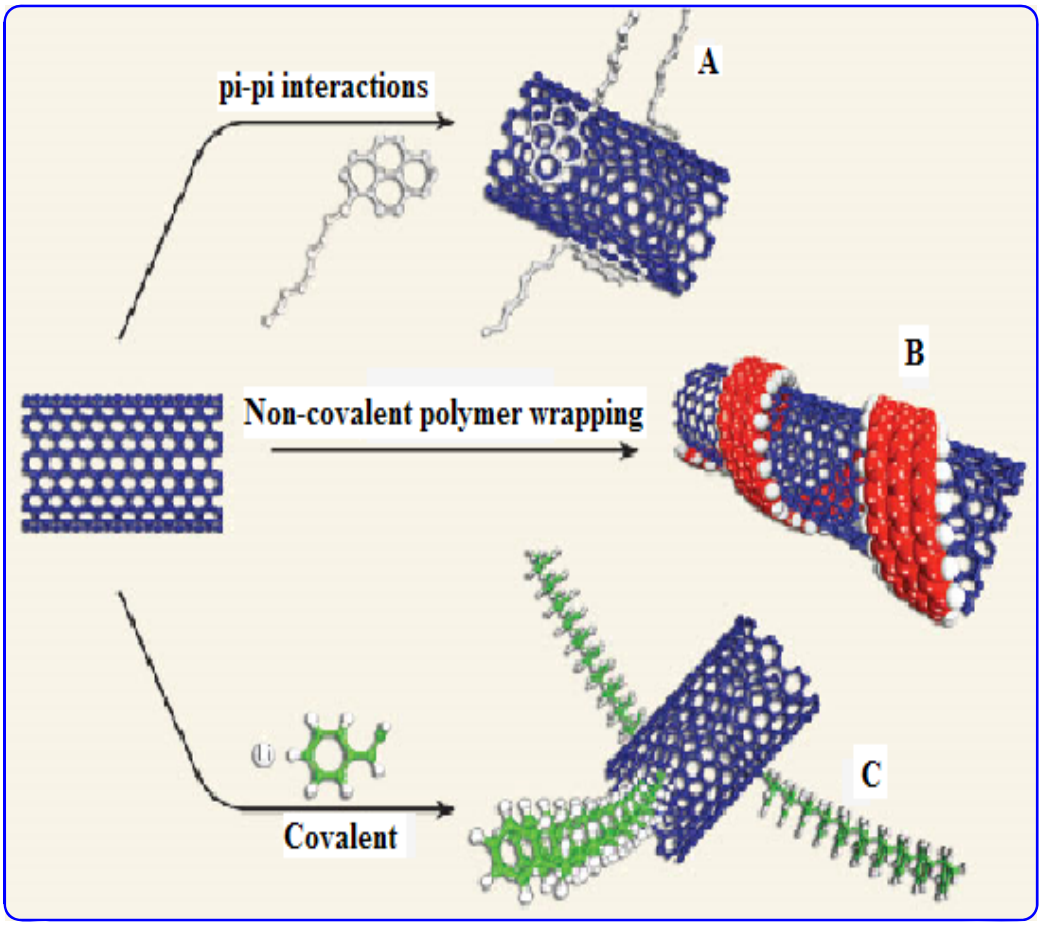

Figure 5-18. Possible modifications of CNTs[189] (Figure is adapted from Ref. 189)

Covalent chemical modifications to the surface of the CNTs on their sidewalls and end or tip parts have been explored. A study found that when SWNT was covalently modified with phenyl-SO_3H or phenyl-$(COOH)_2$ groups they produced less toxicity compared to pristine SWNTs dispersed in aqueous solution with surfactant. Also, the increase in sidewall functionalization decreased cytotoxicity.[169] Various covalent modifications such as acid oxidation,[190, 191] 1,3-dipolar cycloaddtion,[192, 193] nitrene cycloaddition,[194] Bingel reaction,[195, 196] nucleophilic addition,[155, 197] dichlorocarbene addition,[198] ozonization,[199, 200] diazotization,[201] radical addition,[202] fluorination,[203] alkylation,[204] hydrogenation,[205] etc have been attempted. Several surface functionalization reactions of CNTs are summarized in Figures 5-19 and 5-20.[160]

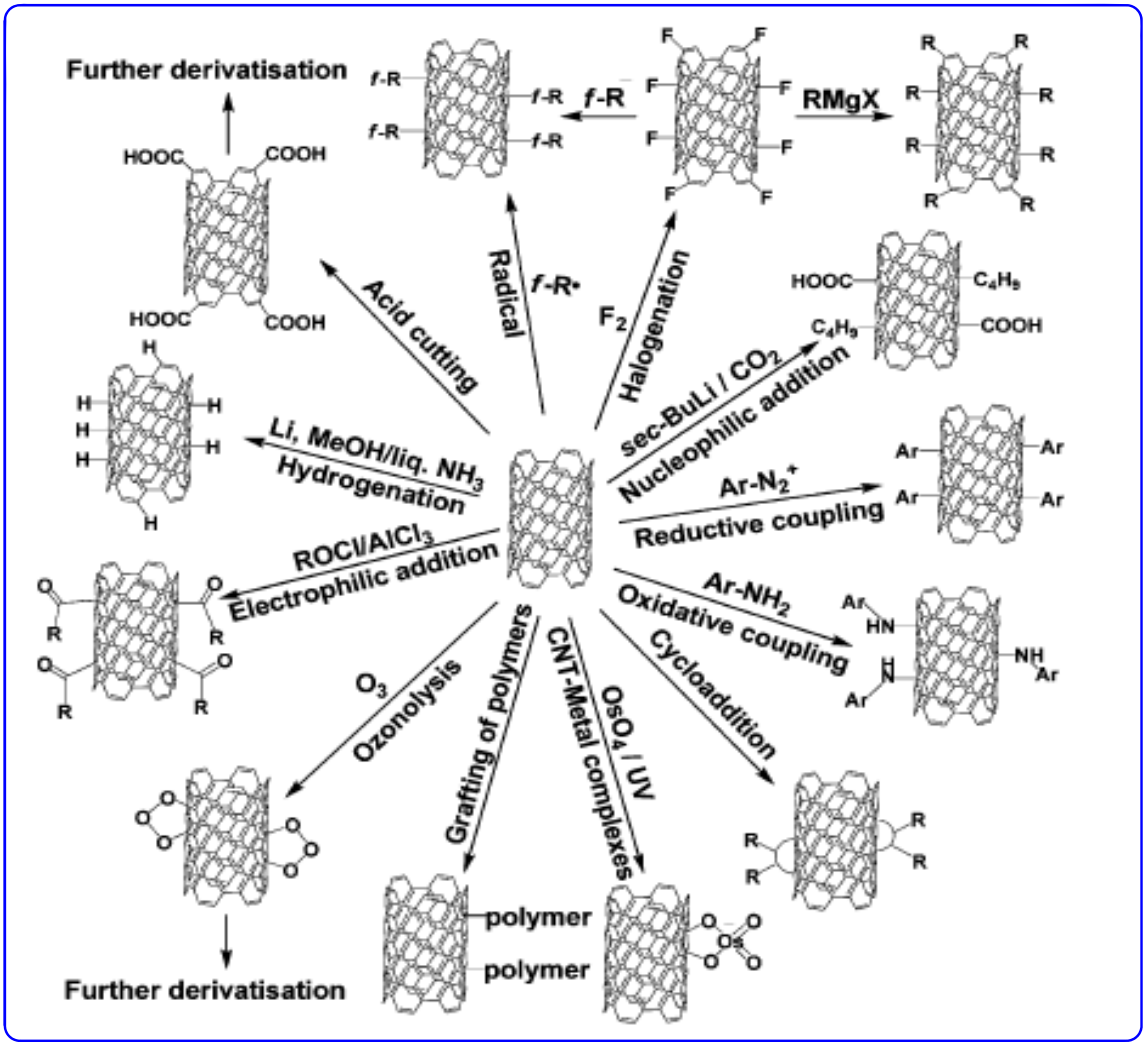

Figure 5-19. Various surface modification reactions on CNTs[160] (Figure is adapted from Ref. 160)

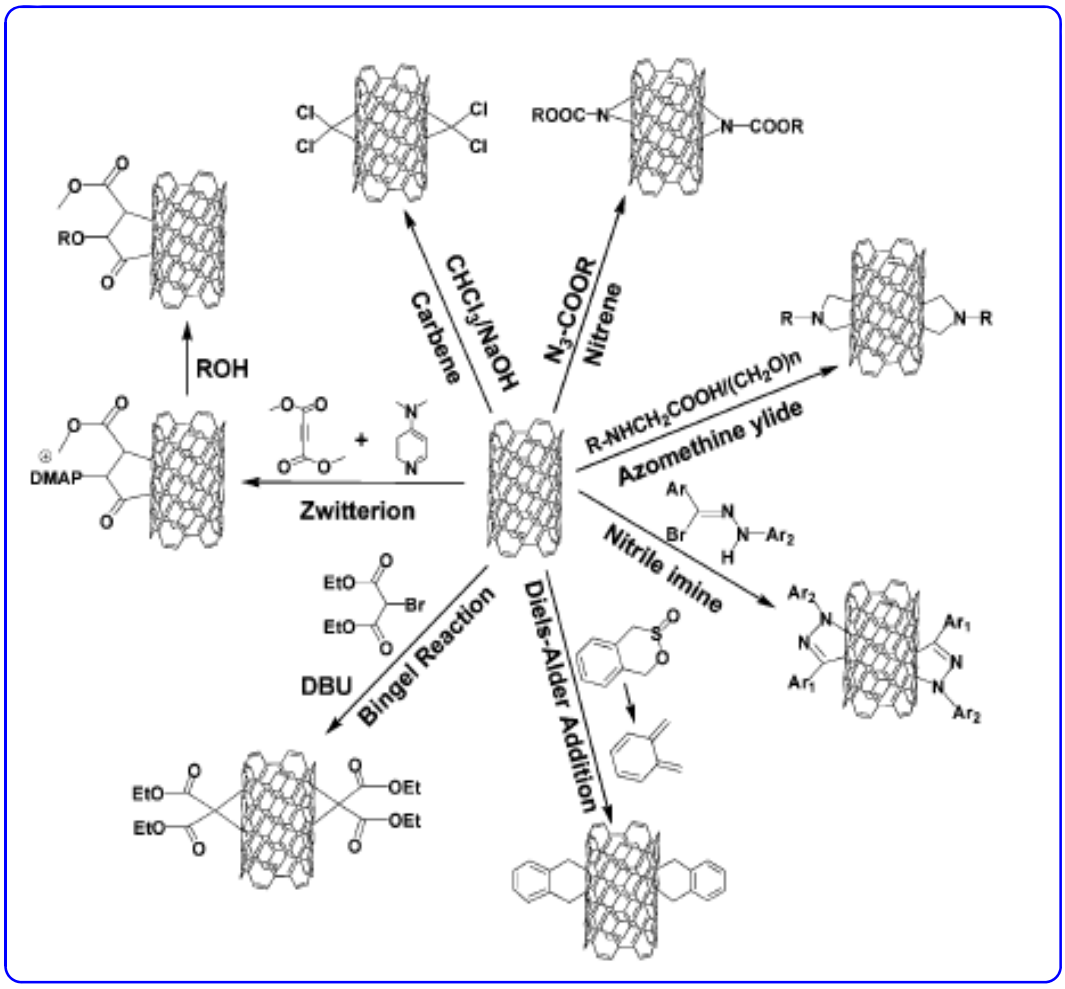

Figure 5-20. Various cycloaddition reactions on the surface of CNTs[160] (Figure is adapted from Ref. 160)

The surface of CNTs can be modified in two zones – tips and sidewalls. The reactivity of the sidewalls is considerably lower than the tips and most reactions are expected to occur first on the tips and then on the sidewalls specially where defects are present.[206] Acid oxidation and 1,3-dipolar cycloaddtion are the two most valuable methodologies to obtain CNTs that are soluble in water or organic solvent. Originally, acid oxidation was applied for the purification of as-produced or raw CNTs which generally contained impurities. The treatment of CNTs with strong oxidative acid (combination of HNO_3 and H_2SO_4) induces opening of the tips as well as formation of holes on the sidewalls of CNTs, producing CNT fragments modified with carboxylic acid groups.[207] Consequently, amidation or esterification of oxidized CNTs terminated with carboxylic acids, is a convenient way to produce either lipophilic[198] or hydrophilic[208] carbon nanotubes. 1,3-Dipolar cycloaddition developed by Prato and Bianco, is another way for efficient functionalization of CNTs.[192, 193] During the reaction azomethine ylides, that are generated *in situ* by the condensation reaction between glycine derivatives and aldehydes, undergo 1,3-dipolar cycloaddition on the graphitic surface of the CNTs

forming pyrrolidine rings. The resulting amine-functionalized CNTs are particularly useful for the covalent attachment of molecules, such as amino acids,[209] peptides,[210] nucleic acids[211] and therapeutic agents.[212] Encouraging results have been obtained from rational functionalization of CNTs, however, more research is required in manipulating the properties of these unique nanovectors in a more predictive manner which can have a desirable impact on solubility, biocompatibility, toxicity and other parameters.

5.1.3.3. Thermal properties of CNTs

Nanostructures possess unique photophysical properties such as photothermal and photoacoustic properties which have been explored as promising techniques to destroy cancer cells.[213, 214] SWNTs can exhibit either metallic or semiconducting behavior depending on diameter and chirality[215] and are very suitable for these techniques due to their strong optical absorbance in the near infra-red (NIR) region (700–1100 nm).[216] This intrinsic property arises from the electronic band structure of CNTs. The electronic transitions from the first or second van Hove singularities give rise to the strong optical absorbance. When the Van Hove-like singularity in the density of states (DOS) moves towards the top of the valance band it enhances the effective DOS near the Fermi energy which results in an increase in the electron-phonon interaction and a consequent increase in the temperature of the CNTs.[217] CNTs have therefore been explored as photothermal agents for killing cancer cells by heating the CNTs *via* continuous laser irradiation at high power density (3.5–35W/cm^2) for a long time (3–4 min).[214, 218, 219] Besides laser induced thermal ablation there are several thermal delivery methods such as microwave and radiofrequency (RF) ablation,[220] magnetic thermal ablation,[213] and focused ultrasound[221, 222] that warrant investigation for local tissue ablation.

Biological systems are transparent to NIR light and the strong optical absorbance of SWNTs in this spectral window can be effectively used for optically stimulating the CNTs inside the cancer cells and causing irreversible death of the cells. When CNTs enter cells *via* nanoneedle mechanism[206] or by active targeting with tumor targeting moieties[214] then the CNTs can thermally destroy the specific cells upon exposure to laser irradiation or other forms of radiation. This ability of CNTs to convert NIR light to heat has been explored for cancer phototherapy. When CNTs generate heat after laser or other forms of irradiation they cause hyperthermia in cells. Hyperthermia has been used clinically for solid tumor management in combination with other forms of therapy. Hyperthermia also has an added advantage – it causes an increase in the permeability of tumor vasculature compared to normal vasculature which can enhance drug delivery into tumors.[219] When an anti-CD22-targeted mAb non-covalently bound to CNT was studied *in vitro* in human Burkitt's lymphoma cells it selectively bound to the tumor cells and caused NIR-induced thermal ablation of the targeted tumor cells.[219] Other studies have shown that mAbs non-covalently attached to CNTs could be used in photothermal therapy.[223] Studies have shown that folic acid-coated CNTs could target folate receptor (FR)-positive cells and that NIR light killed the cells.[214] Non-covalent attachment of targeting moieties to CNTs carry the risk of dissociation of the targeting moiety from the CNTs *in vivo*. Studies performed with mAbs covalently linked to CNTs successfully targeted human B lymphoma cells *in vitro* and caused their NIR photothermal ablation. The study showed that mAbs were stably attached to CNTs chemically, bound to target cells specifically and remained specific even after incubation in mouse serum and only

the specifically targeted cells were thermally ablated upon irradiation with NIR light.[218] Similar studies was also performed using anti-HER2 IgY antibody-functionalized SWNTs. In this study the dual functionality of SWNT, namely strong Raman signal for cancer cell detection and NIR mediated selective photothermal ablation of tumors, were successfully exploited for both detection and selective destruction of cancer cells in an *in vitro* model consisting of HER2-expressing SK-BR-3 and HER2-negative MCF-7 cancer cells.[224] Figure 5-21 shows selective destruction of targeted cancer cells with folate coupled SWNTs utilizing the unique ablation ability of SWNTs.[222]

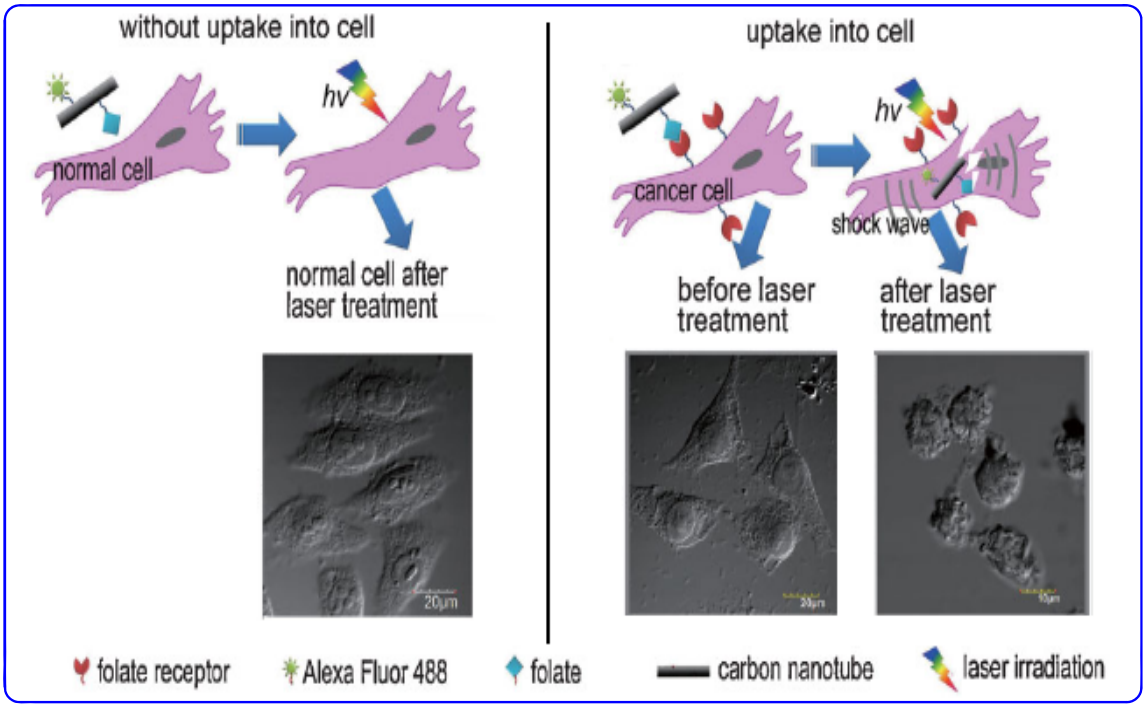

Figure 5-21. Targeted destruction of cancer cells[222] (Figure is adapted from Ref. 222)

Thus the unique laser induced properties of SWNTs can be used for targeted drug delivery, detection and diagnosis by themselves or in combination with other forms of therapy.

5.1.3.4. Functionalized CNTs – a desirable delivery platform

Functionalized CNTs (*f*-CNTs) are promising tools for the efficient delivery of diverse imaging agents, therapeutic agents, radionuclides, etc for disease detection, diagnosis and therapy. As discussed earlier in this chapter CNTs have been shown to effectively deliver their cargo across cell membranes. SWNTs with non-covalently and covalently linked mAbs, proteins, oligonucleotides, etc as well as therapeutic agents have been explored.[212, 224-228] Studies have shown that CNTs can passively cross cell membranes *via* a translocation mechanism or 'nanoneedle' mechanism[206] or *f*-CNTs can actively enter cells *via* endocytosis. Figure 5-22 shows a cationic glycopolymers

functionalized SWNT used as an *in vitro* gene transfer agent. This *f*-CNT was found to be biocompatible.[229]

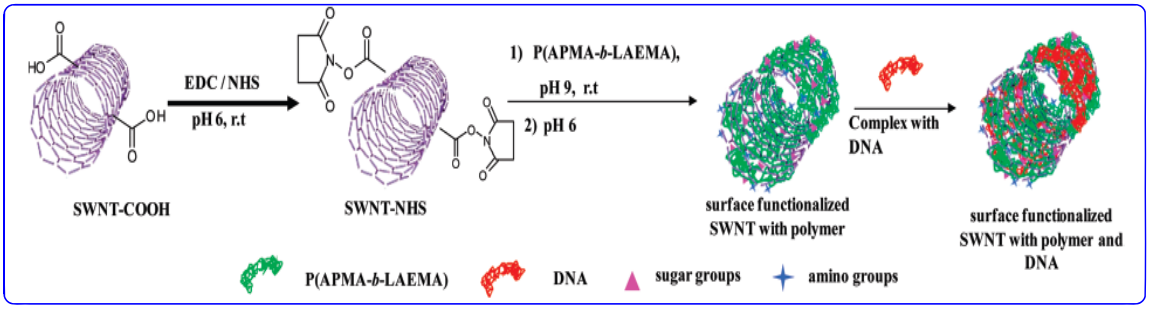

Figure 5-22. SWNT functionalized on the surface with polymers[229] (Figure is adapted from Ref. 229)

The transportation mechanism of SWNTs has been explored using fluorescein-labeled SWNTs (SWNT-biotin-SA, structure shown on the left in Figure 5-23) in human promyelocytic leukemia (HL60) cells and human T cells (Jurkat) using the endosome marker FM 4-64 (red fluorescence), which was reported to specifically stain the endosomes *via* the endocytosis pathway. The authors claimed that red fluorescence caused by FM 4-64 and the green fluorescence by nanotube conjugates in the endosome regions completely overlapped with each other, which provided the direct evidence for the endocytosis cellular uptake pathway of protein-SWNT conjugates.[225]

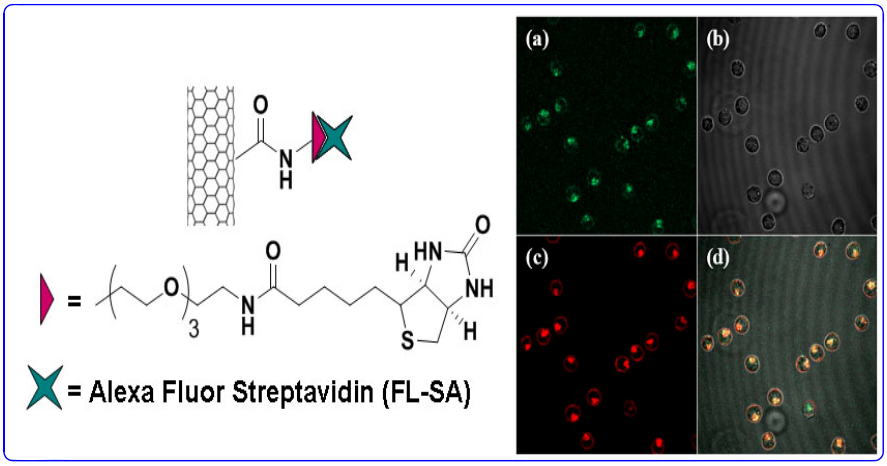

Figure 5-23. Confocal fluorescent microscopy images of dual staining of endosomes in HL60 cells shows endocytosis mechanism of fluorescein-labeled SWNTs (SWNT-biotin-SA, on the left) (a) Green fluorescent SWNT-biotin-SA (0.05 mg/mL, 37 ^{o}C, 1 h) inside cells; (b) bright- field image of cells; (c) red endosomes inside cells stained by red endosome marker FM 4-64; and (d) overlap of (a)-(c)[225] (Figure is adapted from Ref. 225)

SWNT derivatized with carboxylate groups and coated with a polysaccharide material, was loaded with the anticancer drug doxorubicin (Dox) to design a targeted drug delivery system. Changes in pH, for example, lysosomal pH and the pH characteristics of certain tumor environments triggered the release of the drug. Folic acid was additionally tethered to this *f*-CNT to selectively deliver this drug inside the lysosome of HeLa cells which showed higher efficiency of nuclear damage leading to inhibition of cell proliferation as compared to free Dox.[230] Platinum(IV) complexes attached to amine-functionalized SWNTs modified with phospholipids and PEG to make them water soluble have been used to deliver the Pt-based anticancer agents inside tumor cells. Pt(IV) complexes, *c*,*c*,*t*-[$Pt(NH_3)_2Cl_2(OEt)(O_2CCH_2CH_2CO_2H)$] served as prodrugs with almost no toxicity to cells. Once the water soluble CNT prodrug conjugates were internalized inside the cancer cells through endocytosis, the active drug was dissociated *via* reduction in pH environment in cancer cells and showed a significantly enhanced cytotoxicity as compared with the untethered complex.[231]

Non-endocytosis mechanism of *f*-CNT uptake and internalization by cells has also been reported. This uptake mechanism is different from *f*-CNTs coated with polymers or biomacromolecules. Jurkat cells were incubated with *f*-CNTs in the presence of sodium azide (NaN_3) at 4 ^oC, which is commonly used to inhibit endocytosis process. The authors claimed that there was no significant change between the cells with and without NaN_3 treatment, which clearly indicated that energy-independent intercession took place during the cellular uptake of *f*-CNTs.[232] The structures of *f*-CNTs obtained *via* 1,3-dipolar cycloaddition and their uptake in cells are shown in Figure 5-24.

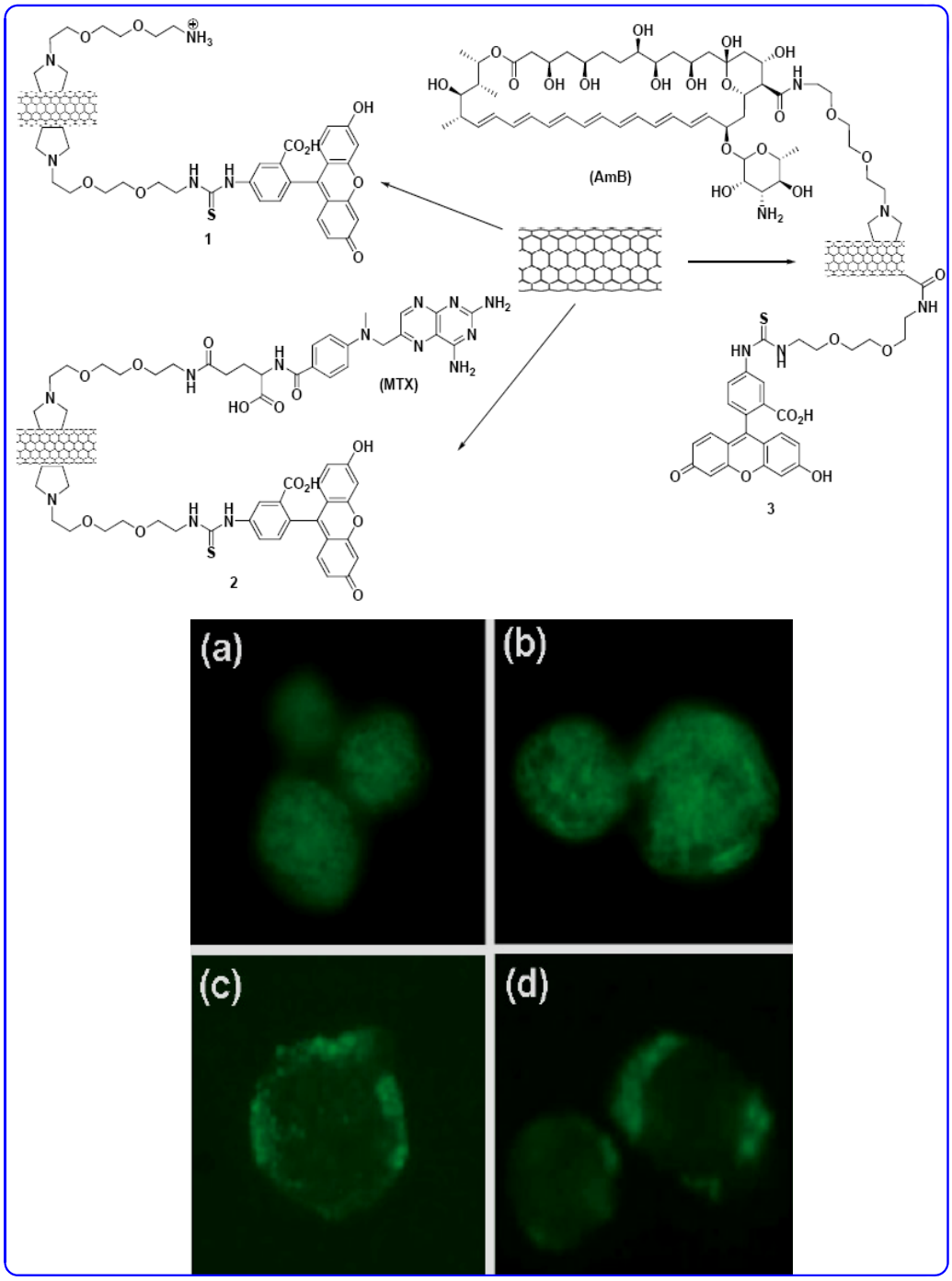

Figure 5-24. Epifluorescence images of Jurkat cells incubated with *f*-CNTs: (a) *f*-CNT **1** (0.5 μg/mL), 37 °C, 16 h, in the presence of NaN_3; (b) *f*-CNT **2** (5 μg/mL), 37 °C, 16 h, in the presence of NaN_3; (c) *f*-CNT **3** (20 μg/mL), 4 °C, 1 h; and (d) *f*-CNT **3** (20 μg/mL), 37 °C, 1 h, in the presence of NaN_3 [232] (Figure is adapted from Ref. 232)

Ojima group has successfully proved that SWNTs covalently functionalized with biotin as TTM and novel disulfide linker-taxoid conjugate can specifically deliver the

drug inside cancer cells overexpressing biotin receptor (Figure 5-25) and release the taxoid by an intracellular thiolactonization process triggered by excess glutathione or similar thiol present in tumor cells. The conjugate was shown to be internalized by a receptor-mediated endocytosis process.[212]

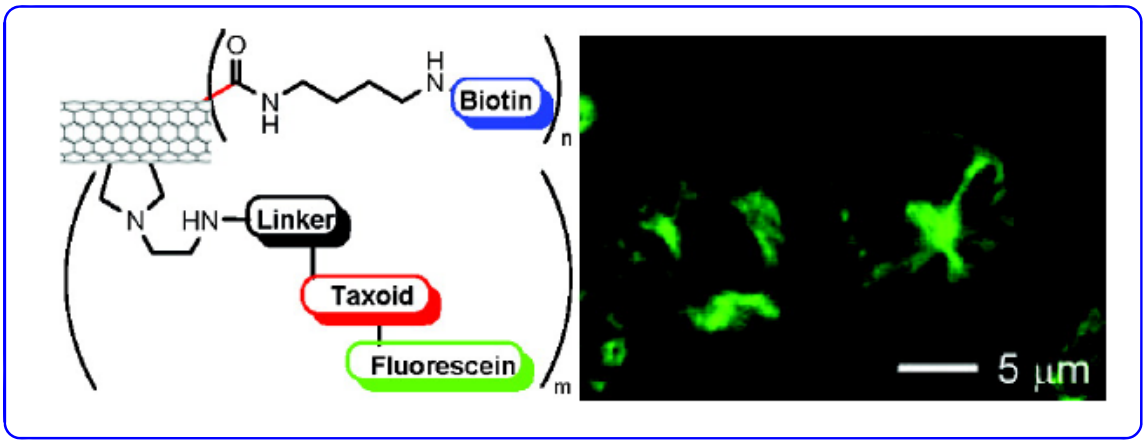

Figure 5-25. Functionalized SWNT and it's internalization in L1210FR leukemia cells[212] (Figure is adapted from Ref. 212)

Thus besides the ability of *f*-CNTs to cross cellular membranes and deliver peptides, radionuclides, nucleic acids, proteins, etc they can also be used to deliver therapeutic agents or imaging agents in a highly specific targeted manner by covalently functionalizing them with TTM like biotin, folic acid, mAbs, etc which would specifically bind to tumor specific biomarkers. Such a targeted delivery system would minimize systemic toxicity associated with chemotherapeutic agents (as discussed in earlier chapters). Excitingly, the unique thermal properties of CNTs can also be used in conjunction with targeted delivery of agents to induce a synergistic dual therapy namely targeted and specific killing of tumor cells employing thermal ablation and cytotoxicity. A rationally designed SWNT provides a versatile platform for simultaneously accommodating TTM (like folic acid, biotin, mAb, etc), imaging agents (like gadolinium, technetium, fluorescein, etc) and multiple therapeutic drugs while enhancing biocompatibility and creating a unique multimodal nanovector. Thus among the various approaches to designing nanomedicine SWNT was chosen for this project because of its unique physical and thermal properties and its amenability to chemical modifications which impart tumor specificity to the SWNT.

5.2 Results and Discussion

5.2.1 Design of a CNT-Drug Delivery Vehicle

Ojima group has successfully designed a CNT-drug delivery vehicle with biotin as the TTM and second-generation taxoid connected to the CNT platform through a novel

disulfide linker as described earlier. A novel CNT-drug delivery vehicle was designed and synthesized to study the synergistic effect of thermal ablation induced by CNT on exposure to laser at NIR range and the cytotoxic effect of the potent taxoid. The versatile design also accommodates modification on the CNT platform to enable imaging simultaneously with targeted drug delivery which would enable us to get further insight into the efficacy of CNT-mediated targeted drug delivery system. The design of this CNT nanovector allows the incorporation of multiple different TTMs, drugs with different mechanism of action and linkers with different cleavage mechanisms. This multi-component multimodal system is a promising targeted pharmaceutical system that can give us an insight to the challenges that exist in the development of personalized medicine. The conventional tumor-targeting DDS was a prodrug conjugate formed *via* connecting a TTM to a cytotoxic warhead directly or through suitable linker as described in Chapter 4 which would result in monovalent binding of the TTM to the receptor. Unlike traditional DDS, the chemical functionalization of TTMs at the end tips and side walls of SWNTs may potentially exhibit polyvalent effects in addition to the EPR effect. Multiple TTMs would increase the binding ability of the conjugate to the target receptor and multiple drug molecules would increase the efficacy of the whole conjugate. Besides, the unique one-dimensional structure may facilitate SWNTs leaking out from blood microvessels to reach cancer cells through vascular and interstitial barriers.

Scheme 5-1 shows the synthesis of the spacers (A, B and C) with various protecting groups that were used for the attachment to the CNT platform.

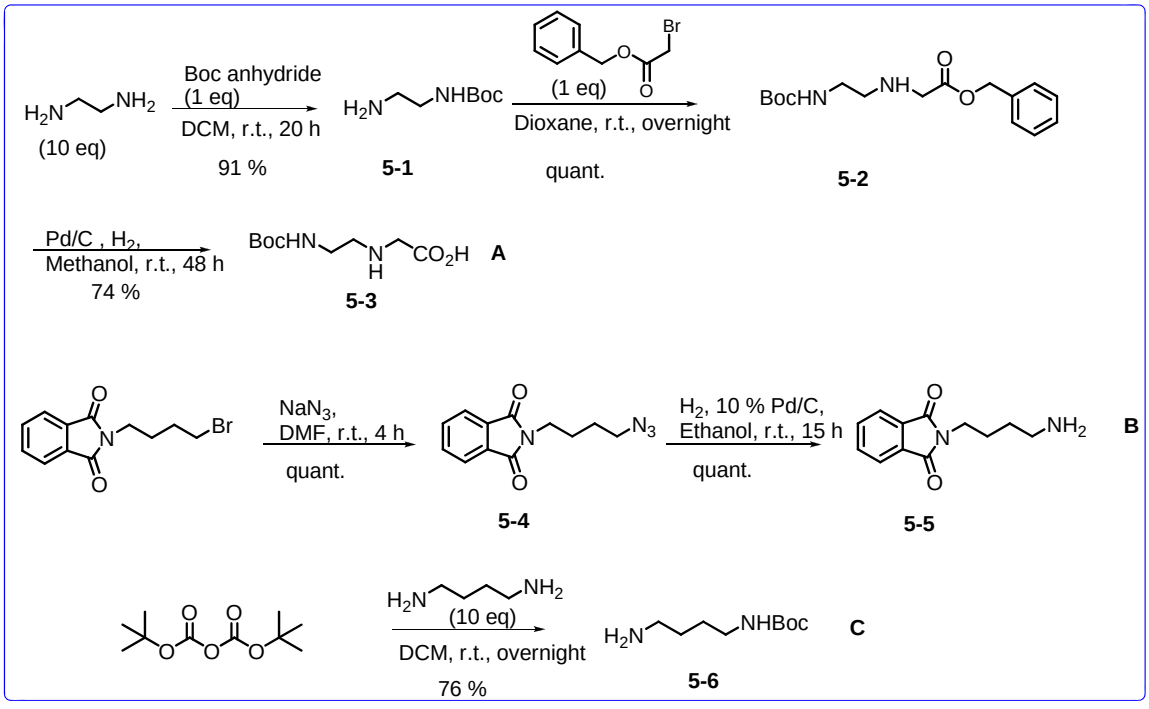

Scheme 5-1. Synthesis of different spacers

Ethylene diamine was mono *t*-boc protected using Boc anhydride as the limiting reagent to obtain **5-1** and then reacted with benzyl-2-bromoacetate to obtain **5-2** which was then subjected to hydrogenolysis to obtain the substituted glycine **5-3**. The compound **5-4** was obtained by substituting the bromine group in the phthalimide terminated bromo butane. Subsequently, the azide in **5-4** was reduced to the amine to obtain **5-5**. Butylene diamine was also mono *t*-boc protected using Boc anhydride as the limiting reagent to obtain **5-6**.

The CNT-drug delivery vehicle was synthesized as shown in Scheme 5-2. A fluorescein tag was attached to the CNT platform *via* a linker to monitor the fate of the CNT using fluorescent microscope.

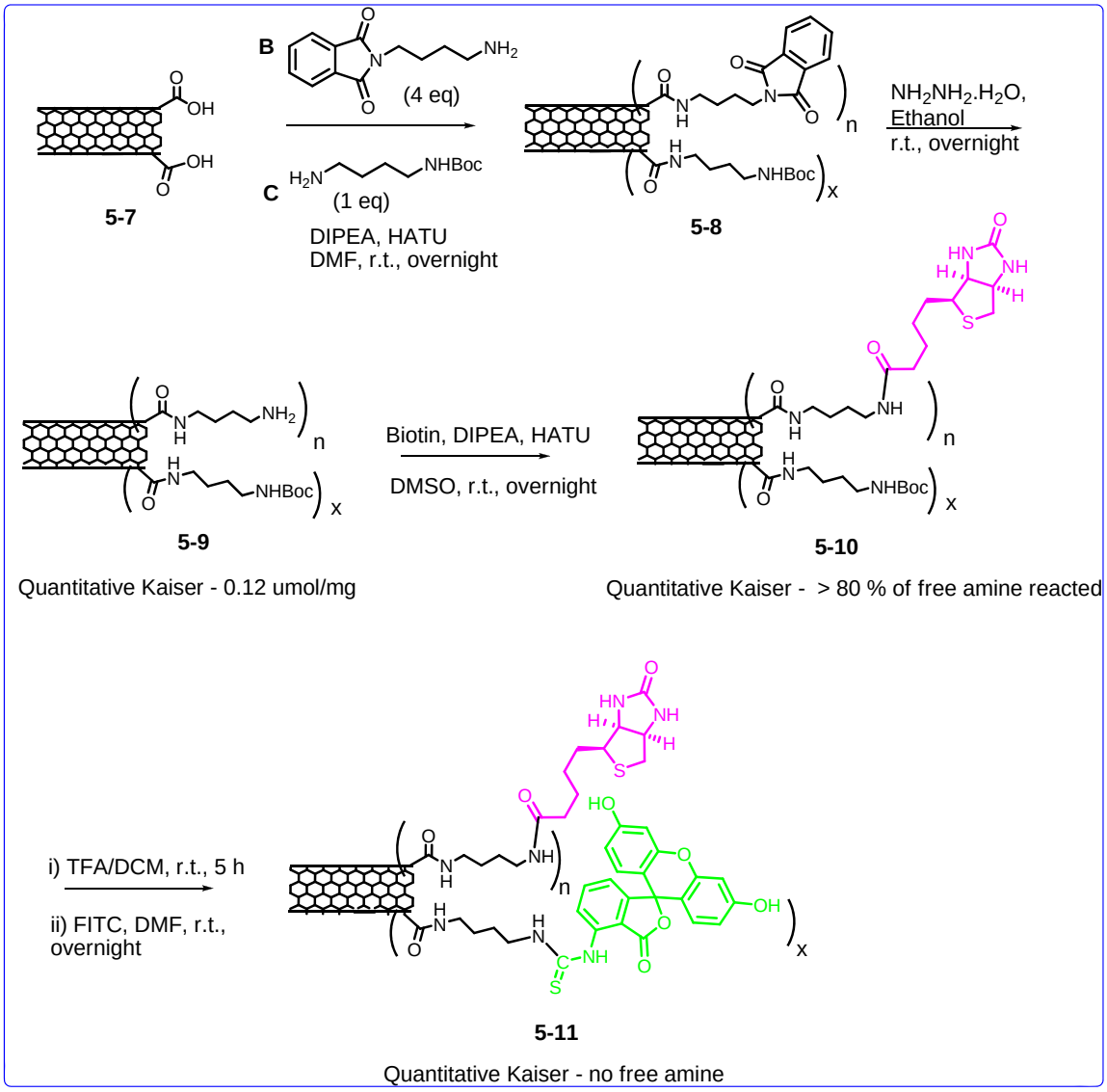

Scheme 5-2. Synthesis of fluorescein tagged CNT nanovector

Pristine SWNTs were oxidized to yield the functionalized SWNT (**5-7**) using 3:1 (v/v) concentrated H_2SO_4 and HNO_3 solution by sonicating at 40 ^oC for 2 h, followed by

heating at 70 ^{o}C for 30 min. The reaction mixture was diluted with water and filtered through a 0.2 μm polycarbonate membrane. The product (**5-7**) was then washed extensively with water until the pH reached neutral conditions and further oven dried at 120 ^{o}C under vacuum.[212, 233] This compound was prepared by a graduate student from Wong group as well as a senior post-doc from the Ojima group. Oxidized SWNT **5-7** was used to attach spacers **B** and **C** to obtain **5-8**. The phthalimide group was then selectively removed using hydrazine to obtain the free amine terminated CNT **5-9** which was then reacted with biotin using HATU to obtain biotin coupled CNT **5-10**. The *t*-boc group was then removed using TFA/DCM and the free amine thus generated was reacted with FITC to generate CNT **5-11**. Another protocol was also developed to synthesize **5-11** wherein only spacer **B** was used to obtain **5-12** which was then reacted with a limited concentration of biotin to synthesize **5-13**. The free amine in **5-13** was then reacted with FITC to obtain compound **5-11** as shown in Scheme 5-3. The CNT nanovectors can be modified by varying the type of the spacers and the protecting groups with which appropriate protection and deprotection can be used to generate the free amine or carboxylic groups for further reactions to synthesize a multimodal DDS.

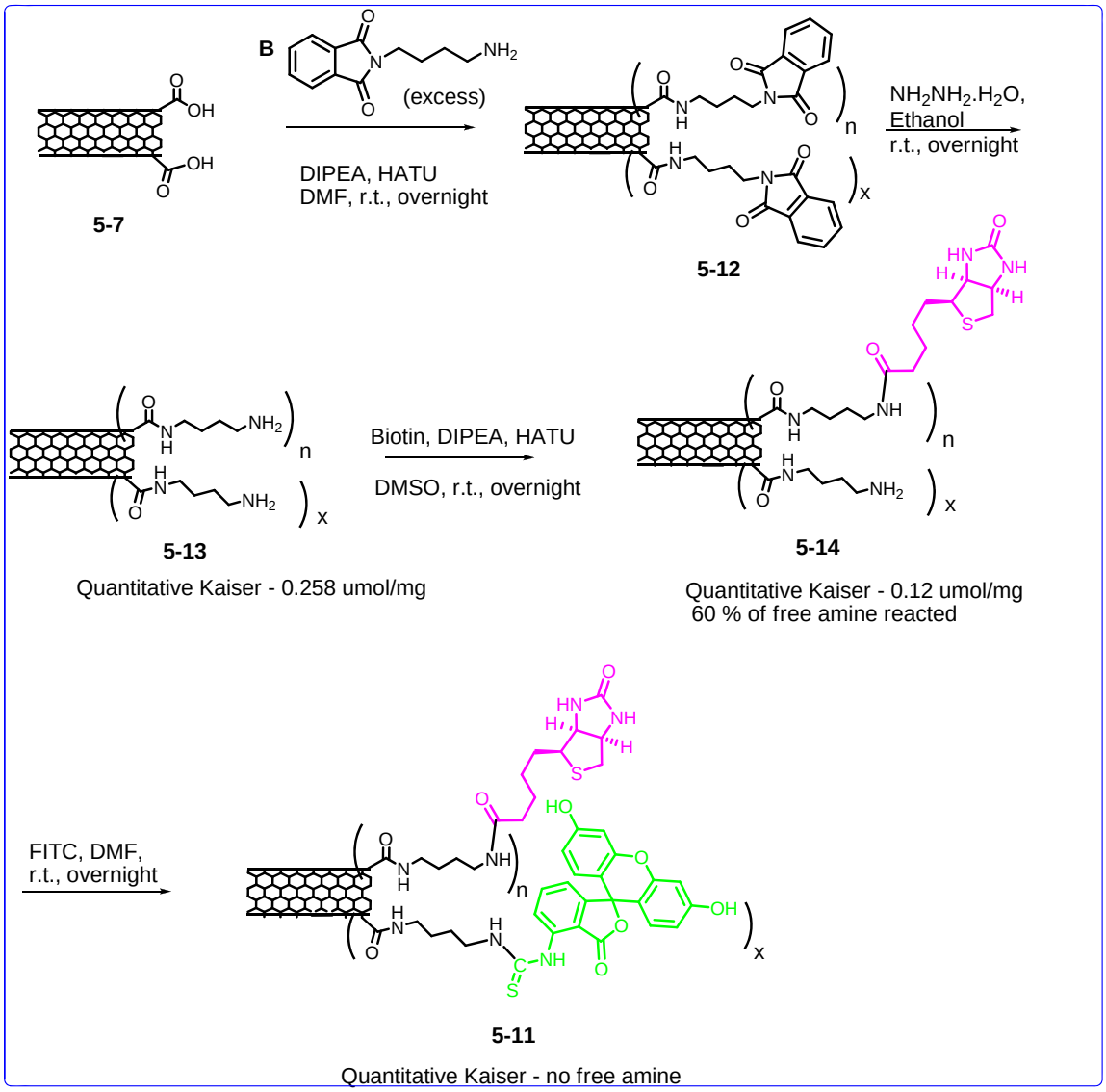

Scheme 5-3. Another protocol for the synthesis of fluorescein tagged CNT nanovector

The CNT **5-15** was synthesized *via* a 1,3-dipolar cycloaddition reaction as shown in Scheme 5-4 and the final CNT **5-16** was synthesized by Dr. Larisa Kuznetsova for biological studies towards thermal ablation.

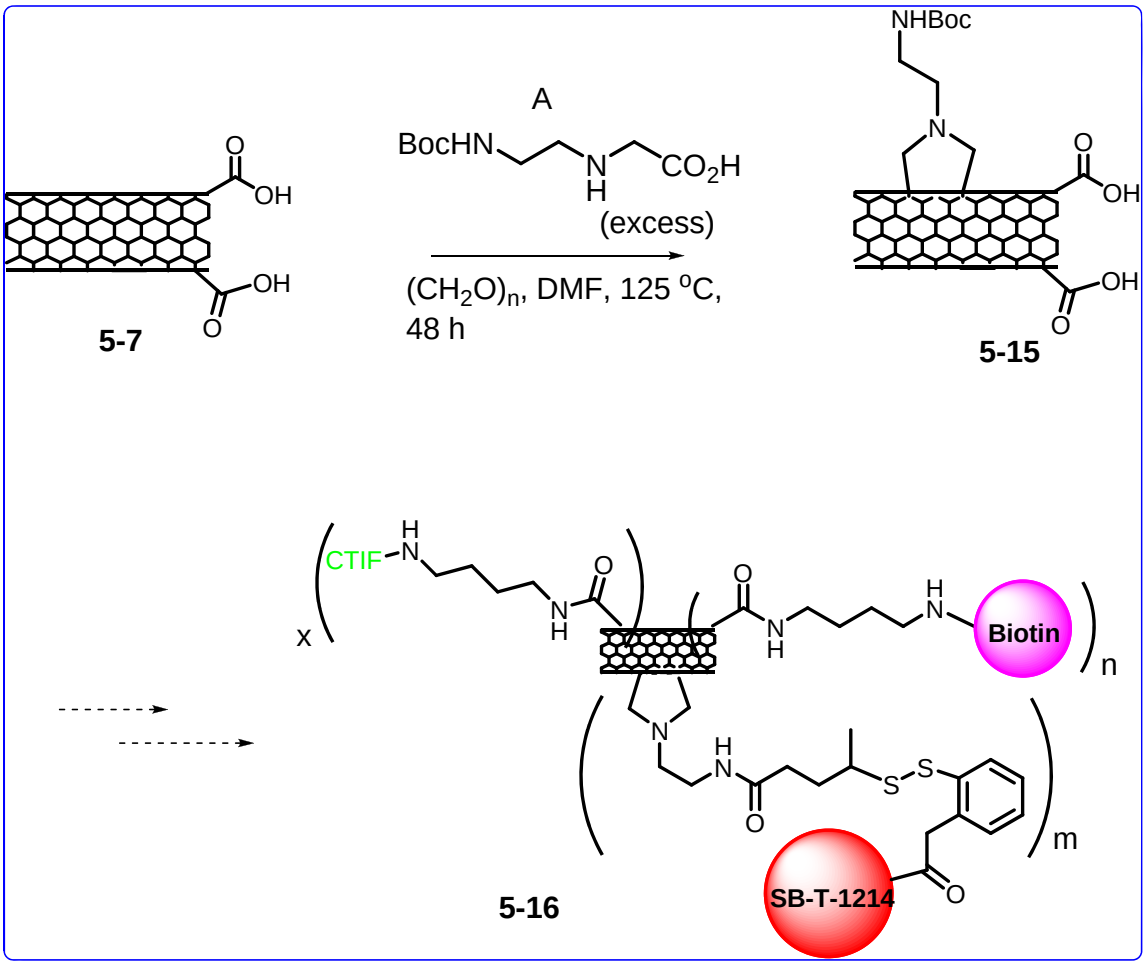

Scheme 5-4. Synthesis of final CNT conjugate

5.2.2 *In Vitro* Biological Evaluation of Thermal Ablation

The fluorescent labeled SWNT conjugate **5-11** and **5-16** were used to study the selective biotin-receptor mediated internalization into cancer cells as well as the effect of thermal ablation. As discussed earlier in this chapter SWNTs have an intrinsic property where they can convert light from NIR source to heat. When SWNTs are delivered selectively inside the cells and exposed to NIR light they can function as 'nano heaters' to generate hyperthermia which can destroy the cells. The SWNT-biotin-FITC conjugate **5-11** was incubated with L1210 and L1210FR leukemia cells and selectively internalized in L1210FR which overexpresses biotin receptors.[234, 235]

The mechanism of internalization of SWNTs into cells has not been fully established. It has been proposed that SWNTs wrapped with proteins or genes can be internalized into cells *via* endocytosis,[236] whereas SWNTs functionalized with small molecules tended to act as nanoneedles that can pierce cell membranes, thereby allowing for their diffusion into cells.[232] Endocytosis is known to be energy dependent and can be blocked at low temperature or in the presence of the metabolism inhibitor, such as

NaN_3.[236] It was demonstrated from previous work in our group that the FITC-labeled SWNT was able to traverse the cell membrane at low temperature or in the presence of 0.05% NaN_3 after 3 h incubation. It was determined that the internalization of SWNT itself into the cells was temperature-related, but energy independent.[212] The SWNT-FITC conjugate used in the internalization study and the results of the experiments are shown in Figure 5-26.

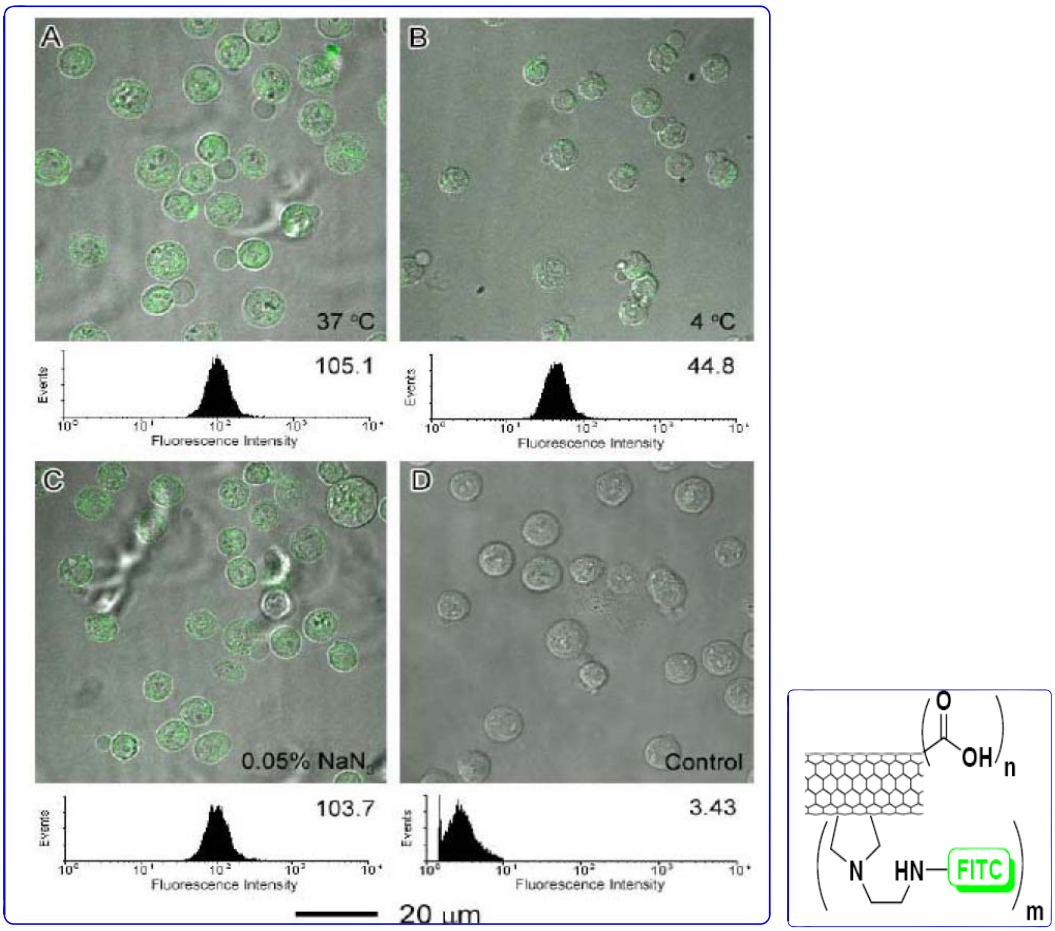

Figure 5-26. CFM images and the flow cytometry analysis of L1210FR cells after incubation with SWNT-FITC conjugate at the final concentration of 10 μg/mL under different conditions for 3 h: (A) at 37 °C for 3 h; (B) at 4 °C; and (C) at 37 °C in the presence of 0.05 % NaN_3 (D) CFM images and flow cytometry data of L1210FR cells after treatment with oxidized SWNT at the same concentration at 37 °C for 3 h as the control experiment.[212]

The internalization of biotin and FITC labeled SWNT conjugate yielded far more intense fluorescence than SWNT-FITC conjugate which can be attributed to the remarkably increased permeability of the biotin and FITC labeled SWNT conjugate into the cancer cells because of the highly effective interaction of biotin and its receptors on the leukemia cells. Also studies with DMSO and oxidized SWNT (**5-7**) showed no

internalization. It was also shown that the biotin and FITC labeled conjugates selectively internalized into L1210FR and not into the L1210 leukemia and WI38 noncancerous human embryonic lung fibroblast cells.[212]

The conjugate **5-11** was used to study the specific internalization and thermal ablation of cells using confocal fluorescent microscopy (CFM). Figure 5-27 shows the internalization of conjugate **5-11** specifically inside the L1210FR cells (shown on the left) using CFM.

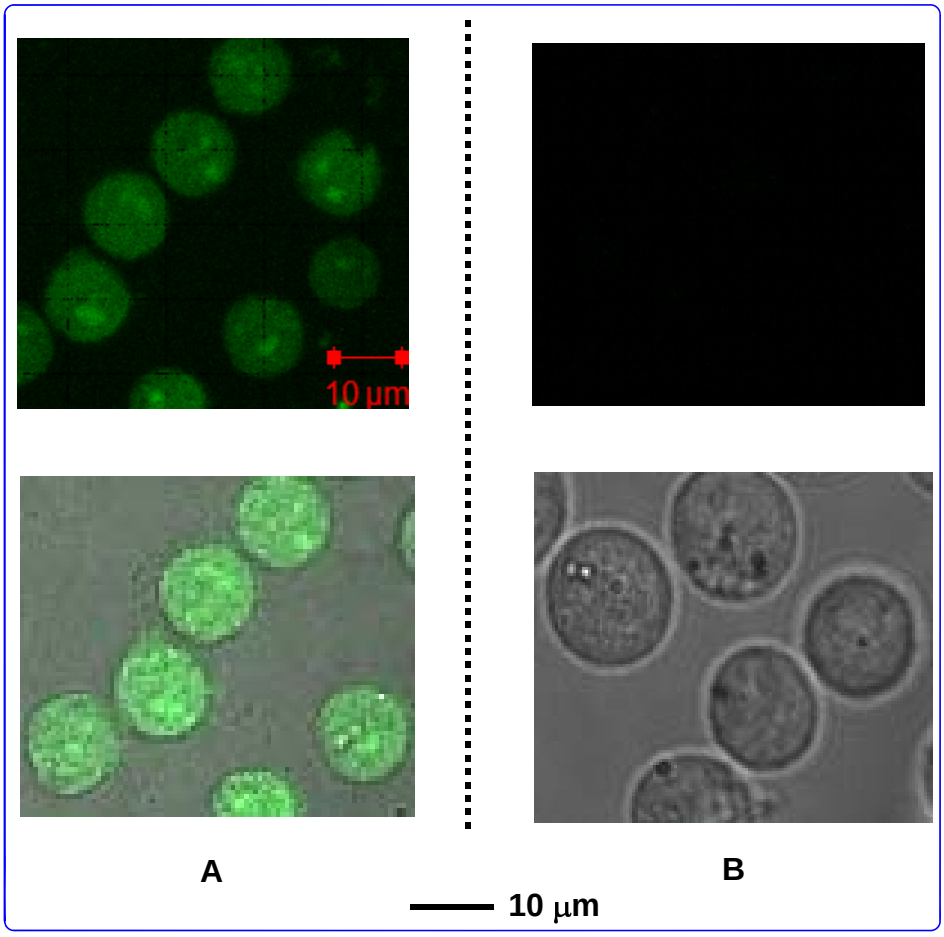

Figure 5-27. CFM of 10 µg/mL of **5-11** incubated with A) L1210FR and B) L1210 cell lines at 37 ^{o}C for 3 h shows internalization in biotin receptor overexpressing L1210FR while there is no internalization in L1210 which does not overexpress biotin receptor

The pictures in the top row show the color mode while the pictures in the bottom row show the overlap of the color and gray modes of the image. It is clearly demonstrated from the results that there was no internalization in the L1210 cell lines while there was internalization in the L1210FR cell lines which overexpress biotin receptor.

The CFM images in Figure 5-28 clearly demonstrates that upon exposure to laser at NIR range the L1210FR cells have been disrupted as is seen from the change of morphology of the cells in (C). In pictures (A) and (B) in Figure 5-28 the L1210FR cells

are healthy as can be seen from the round, even shape of the cells. Laser exposure alone without any internalized SWNT as is seen in (A) did not cause any change of morphology of the L1210FR cells while L1210FR cells with internalized SWNT which were not exposed to laser are also healthy as is seen in (B).

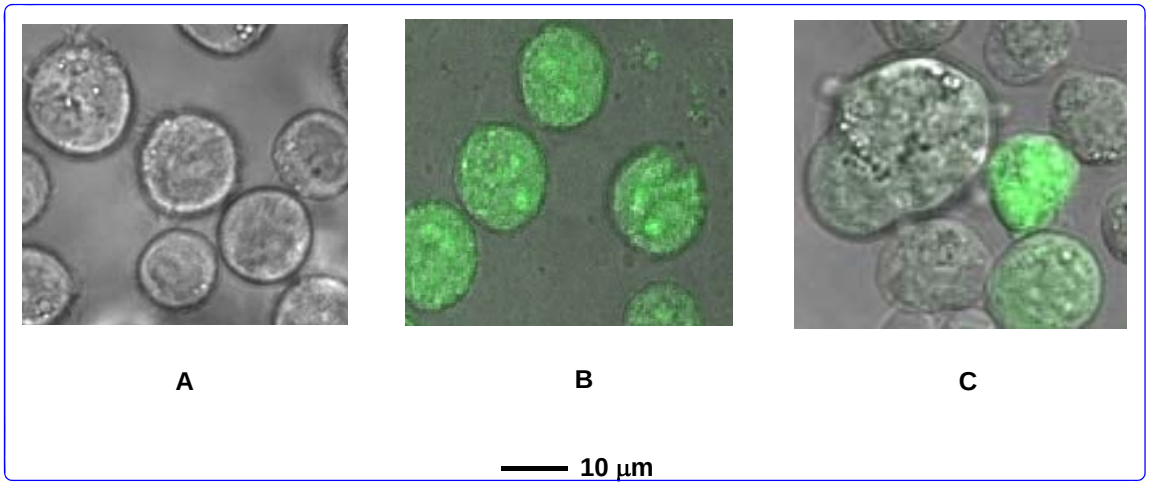

Figure 5-28. CFM of L1210FR cells incubated at 37 ^{o}C for 3 h with A) no SWNT and laser exposure B) 10 μg/mL of **5-11** and no laser exposure C) 10 μg/mL of **5-11** and 2 min laser exposure

Thus, it can be concluded that the SWNT upon internalization thermally ablates the cancer cells upon laser exposure and does not affect the cells which are not exposed to the laser. Moreover, it is clear that the laser alone is not responsible for causing any damage to the cells.

CFM images in Figure 5-29 clearly demonstrates that upon laser exposure for 7 min the L1210FR cells show a distinct change in morphology while the under the same conditions L1210 cells which had no internalized SWNT are perfectly healthy.

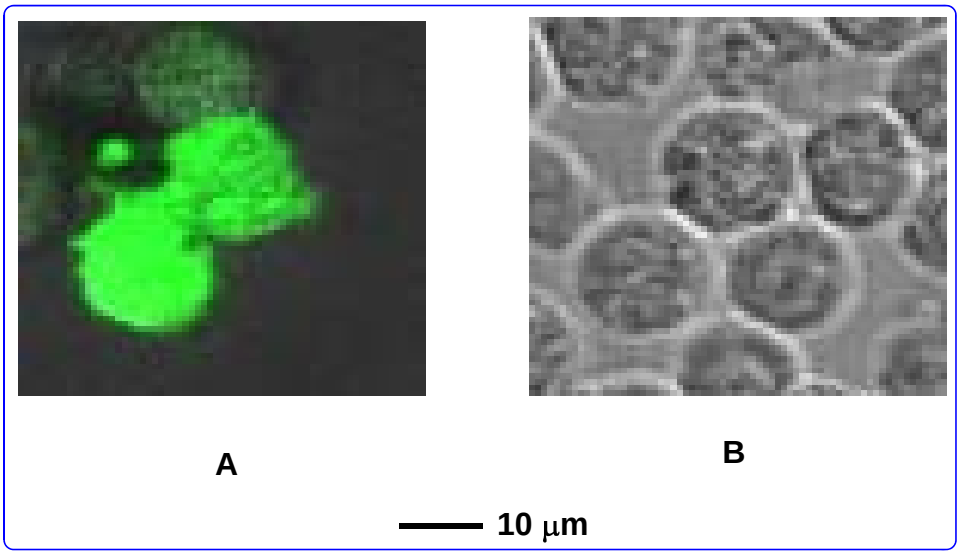

Figure 5-29. CFM of 10 μg/mL of **5-11** incubated at 37 °C A) L1210FR with 7 min laser exposure B) L1210 with 7 min laser exposure

CFM images shown in Figure 5-30 (overlap of color and gray modes) indicate that when L1210FR cells with internalized conjugates **5-11** (Figure 5-30 A) and **5-16** (Figure 5-30 B**)** are exposed to NIR light for 5 min the cells are damaged as can be seen from the distinct change in morphology.

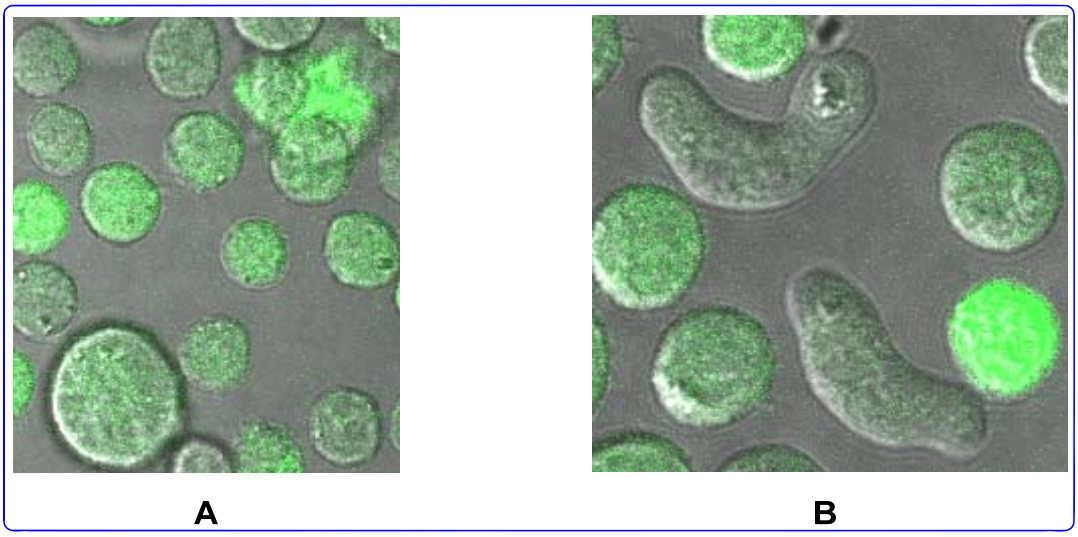

Figure 5-30. CFM of L1210FR A) incubated with 10 μg/mL of **5-11** B) incubated with 10 μg/mL of **5-16**

All the above experiments were performed using continuous wave (CW) mode laser. CFM images shown in Figure 5-31 shows that using pulsed mode laser in NIR range also

has similar effect. When L1210FR cells were exposed to pulsed mode NIR laser for 5 min the cells are not damaged as can be seen from Figure 5-31 (A) while there is some cell damage when L1210FR is incubated with **5-16** and not exposed to laser presumably because of the cytotoxic drug as seen from Figure 5-31 (B). Cell damage can be clearly visible from the CFM images of L1210FR incubated with **5-11** as shown in Figure 5-31 (C) and CFM images of L1210FR incubated with **5-16** as shown in Figure 5-31 (D).

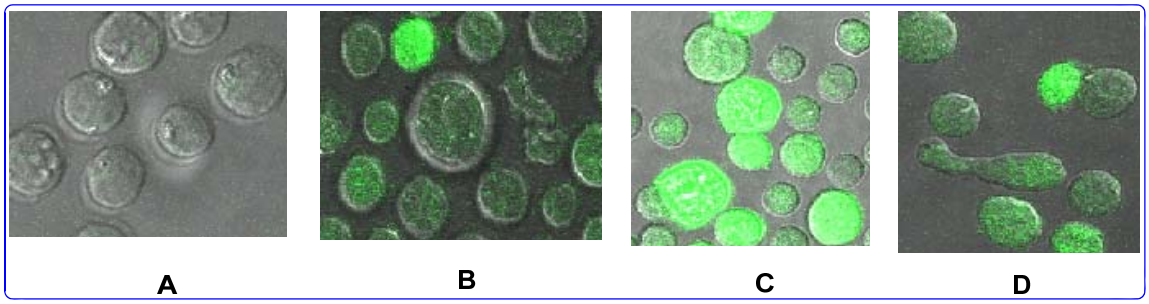

Figure 5-31. CFM of L1210FR A) with no internalized conjugate B) incubated with **5-16** (not exposed to laser) C) incubated with **5-11** D) incubated with **5-16**

Thus, attaching TTM such as biotin to SWNT ensures the specific and selective delivery of these nanovectors inside targeted cells allowing NIR light induced thermal ablation of the targeted cells.

5.3 Experimental Section

General Methods: ^{1}H and ^{13}C NMR spectra were measured on a Varian 300, 400, 500, or 600 MHz NMR spectrometer. High-resolution mass spectrometric analyses were conducted at the Mass Spectrometry Laboratory, University of Illinois at Urbana-Champaign, Urbana, IL. GC-MS analyses were performed on an Agilent 6890 Series GC system equipped with the HP-5HS capillary column, (50 m X 0.25 mm, 0.25 um) and with the Agilent 5973 network mass selective detector. LC-MS analyses were carried out on an Agilent 1100 Series Liquid Chromatograph Mass Spectrometer. Infrared spectra were obtained on a Nexus 670 (Thermo Nicolet) equipped with a single reflectance ZnSe ATR accessory, a KBr beam splitter, and a DTGS KBr detector. UV-vis spectra were recorded on a UV1 (Thermo Spectronic) spectrometer. TLC analyses were performed on Merck DC-alufolien with Kieselgel 60F-254 and were visualized with UV light, iodine chamber, 10 % sulfuric acid-EtOH or 10 % PMA-EtOH solution. The staining agent on TLC for biotin derivatives was 4-*N*,*N*-Dimethylamino-cinnamaldehyde ethanol solution. Column chromatography was carried out on silica gel 60 (Merck; 230-400 mesh ASTM). Chemical purity was determined with a Waters HPLC or Shimadzu HPLC, using a Phenomenex Curosil-B column, employing CH_3CN/water as the solvent system with a flow rate of 1 mL/min. Dark room, aluminum foil, and inert nitrogen atmosphere were applied when necessary.

Materials: The chemicals were purchased from Sigma Aldrich Company, Fischer Company or Acros Organic Company. Dichloromethane and methanol were dried before use by distillation over calcium hydride under nitrogen or argon. Ether and THF were dried before use by distillation over sodium-benzophenone kept under nitrogen or argon. Toluene and benzene were dried by distillation over sodium metal under nitrogen or argon before use. Dry DMF was purchased from EMD chemical company, and used without further purification. PURE SOLV™, Innovative Technology Inc, provided an alternative source of dry toluene, THF, ether, and dichloromethane. The reaction flasks were dried in a 110 ^{o}C oven and allowed to cool to room temperature in a desiccator over "Drierite" (calcium sulfate) and assembled under inert gas nitrogen or argon atmosphere.

5.3.1 Synthesis of SWNT Conjugates

tert-Butyl 2-aminoethylcarbamate (5-1):[237]
A solution of di-*tert* butyldicarbonate (2 g, 9.16 mmol, 1 eq) in DCM (18 mL) was added dropwise to a solution of ethylenediamine (6 mL, 91.6 mmol, 10 eq) in DCM at 0 ^{o}C. The resulting reaction mixture was then stirred at room temperature for 20 h. The DCM was then removed *in vacuo*. The residue was taken up in EtOAc, washed with a saturated solution of Na_2CO_3, dried over $MgSO_4$, and concentrated *in vacuo* to obtain the desired product **5-1** (1.33 g) as a white solid in 91 % yield. ^{1}H NMR (300 MHz, $CDCl_3$): δ 1.34 (s, 9H), 2.69 (t, *J* 5.7 Hz, J_2 6.0 Hz, 2H), 3.04-3.09 (m, 2H), 5.22 (bs, 1H, NH_2). ^{13}C NMR (400 MHz, $CDCl_3$): δ 28.2, 41.6, 43.1, 78.8, 156.1.

Benzyl 2-[2-(_tert_-butoxycarbonylamino)ethylamino]acetate (5-2):[237]
A solution of benzyl-2-bromoacetate (1 eq, 1.36 mmol) in 4 mL dioxane was added to a solution of **5-1** (654 mg, 3 eq, 4 mmol) in 2.7 mL dioxane and the reaction was stirred overnight at room temperature. The solvent was evaporated under reduced pressure, and the residue was dissolved in water and extracted with ethyl acetate. The combined organic phase was dried over Na_2SO_4, and the solvent was removed under vacuum. The crude residue was purified by chromatography (1/1 EtOAc/hexane followed by pure EtOAc) to afford the desired compound **5-2** (419 mg) as colorless oil in quantitative yield. ^{1}H NMR (300 MHz, $CDCl_3$): δ 1.43 (s, 9H), 2.3 (bs, 1H), 2.75 (m, 2H), 3.22 (m, 2H), 3.46 (s, 2H), 5.12 (bs, 1H), 5.16 (s, 2 H), 7.35 (m, 5H). ^{13}C NMR (400 MHz, $CDCl_3$): δ 28.7, 40.4, 49.0, 50.7, 66.9, 86.2, 128.7, 128.8, 128.9, 135.9, 156.5, 172.6.

***N*-(2-*N*-Boc-aminoethyl)glycine (5-3):**[237]
The compound **5-2** (650 mg, 2.1 mmol) and Pd/C (10 wt %, 65 mg) were dissolved in methanol and H_2 gas was passed through the reaction mixture for 48 h till TLC indicated no starting material remained. The reaction mixture was then filtered through celite to remove the Pd/C catalyst and the solvent removed. The pure product **5-3** (337 mg) was obtained as a white solid in 74 % yield. ^{1}H NMR (300 MHz, D_2O): δ 1.42 (s, 9H), 3.15 (t, *J* 5.7 Hz 2H), 3.41 (t, 2H, *J* 5.7 Hz, J_2 5.4 Hz,), 3.60 (s, 2H), ^{13}C NMR (400 MHz, D_2O): δ 27.79, 36.85, 47.49, 49.06, 49.43, 81.69, 158.37, 171.17.

***N*-(4-Azidobutyl)phthalimide (5-4):**[238]

Sodium azide (290 mg, 4.4 mmol) was added to a solution of *N*-(4-(bromobutyl) phthalimide (1.0 g, 3.5 mmol) in 10 mL of DMF. The reaction mixture was then allowed to stir for 4 h under nitrogen at room temperature. The solvent was removed *in vacuo* to yield a white semisolid, which was further dissolved in water and extracted with three 50 mL portions of ethyl acetate. The combined organic layers were dried over anhydrous magnesium sulfate and filtered, and the solvent was removed to obtain **5-4** as a white amorphous powder (854 mg) in quantitative yield. ^{1}H NMR (300 MHz, $CDCl_3$) δ 1.47-1.54 (m, 2 H), 1.58-1.66 (m, 2 H), 3.19 (t, J = 7.2 Hz, 2 H), 3.56 (t, J = 7.2 Hz, 2 H), 7.60 (m, 2 H), 7.64 (m, 2 H), ^{13}C NMR (400 MHz, $CDCl_3$): δ 25.37, 25.77, 36.76, 50.39, 122.69, 131.55, 133.51, 167.77.

***N*-(4-Aminobutyl)phthalimide (5-5):**[238]
N-(4-azidobutyl)phthalimide (**5-4**) (854 mg, 3.5 mmol) was dissolved in 50 mL of ethanol along with 100 mg of 10% Pd/C and H_2 gas was passed through the reaction mixture for 12 h. The reaction mixture was then filtered through celite and the filtrate was concentrated *in vacuo* to yield *N*-(4-aminobutyl)phthalimide (**5-5**) as an amorphous white solid (764 mg) in quantitative yield. ^{1}H NMR (500 MHz, DMSO) δ 1.08 (t, 2 H), 1.57 (m, 2 H), 3.22 (t, 2 H), 3.35 (t, 2 H), 7.40 (m, 2 H), 7.85 (m, 2 H), ^{13}C NMR (500 MHz, DMSO): δ 55.98, 26.30, 18.51, 122.95, 127.57, 129.10, 134.31, 136.33, 168.09.

***tert*-Butyl 4-aminobutylcarbamate (5-6):**[237]
A solution of di-*tert* butyldicarbonate (2 g, 9.16 mmol, 1 eq) in DCM (18 mL) was added dropwise to a solution of 1,4-butanediamine (9.2 mL, 91.6 mmol, 10 eq) in DCM at 0 ^{o}C. The resulting reaction mixture was then stirred at room temperature for 20 h. The DCM was then removed *in vacuo*. The residue was taken up in EtOAc, washed with a saturated solution of Na_2CO_3, dried over $MgSO_4$, and concentrated *in vacuo* to obtain the desired product **5-6** (1.31 g) as a white solid in 76 % yield. ^{1}H NMR (300 MHz, $CDC1_3$): δ 0.99 (m, 2 H), 1.21 (s, 9 H), 1.27 (m, 4 H), 2.48 (m, 2 H), 2.88 (m, 2 H), 5.18 (br, 1 H), ^{13}C NMR (300 MHz, $CDC1_3$): 27.00, 27.98, 30.46, 39.90, 41.35, 78.19, 155.71.

SWNT-conjugate (5-8):
Functionalized SWNT **5-7** (10 mg), *N*-(4-aminobutyl)phthalimide, *N*-benzylbutane-1,4-diamine (amines in 4:1 ratio, excess) DIPEA and HATU was suspended in anhydrous DMF and stirred at room temperature overnight. The black residue was washed 5 times with methanol/ether (4/1, 12 mL/3 mL) to remove an excess of amines and dried under vacuum to afford modified SWNT **5-8**.

SWNT-conjugate (5-9):
A mixture of SWNT **5-8** and hydrazine hydrate (25%) in ethanol was stirred overnight at room temperature in a nitrogen atmosphere. The resulting product **5-9** was obtained by centrifugation/precipitation as described above. The loading of amine groups per gram was estimated using the quantitative Kaiser test (0.12 μmol/mg).

SWNT-conjugate (5-10):
Amine-functionalized **SWNT 5-9**, biotin, DIPEA and HATU were suspended in anhydrous DMF. The resulting suspension was stirred overnight at room temperature.

Excess reagents were removed by filtration. The resulting residue was purified by centrifugation-precipitation, using methanol/ether 5 times (12 mL x 4 and 3 mL x 1) to thoroughly remove organic reactants and dried under vacuum to obtain SWNT **5-10**. Quantitative Kaiser test indicated very little free amine.
This reaction was tried with biotin-NHS activated ester under the same reaction conditions except the reaction was stirred for total of 48 h but the reaction did not proceed as well as the process described above.

Biotin-SWNT-FITC conjugate (5-11):
The SWNT **5-10** was suspended in TFA/DCM (1:1) and stirred vigorously overnight at room temperature to remove the *t*-boc protecting group. The resulting residue was isolated by the usual centrifugation-precipitation process and used for the next reaction after quantitative Kaiser test.
A solution of FITC and DIPEA in DMF was added to a suspension/solution of SWNT (obtained above) in DMF. The mixture was stirred overnight at room temperature. The resulting crude was washed 5 times through centrifugation-precipitation process, using methanol/ether (12 mL x 4 and 3 mL x 1) to thoroughly remove free FITC. The absence of free FITC was confirmed by TLC analysis and the product was dried under vacuum to give SWNT **5-11**. Quantitative Kaiser test indicated absence of free amine. This conjugate was used for the *in vitro* biological experiments.

SWNT-linker (5-15)
Oxidized SWNT **5-7** (11 mg) was suspended in DMF (5 mL) and *N*-(2-*N*-Boc-aminoethyl)glycine (**5-3**) (70 mg, 0.32 mmol) and paraformaldehyde (47 mg, 1.57 mmol) were added to it. The reaction mixture was subsequently heated overnight at 125 °C under a N_2 atmosphere. Excess amino acid **5-3** and paraformaldehyde were removed by filtration. The resulting residue was purified by centrifugation-precipitation, using methanol/ether 5 times (12 mL x 4 and 3 mL x 1) to thoroughly remove organic reactants and dried under vacuum to give **5-15**.

Quantitative Kaiser test:
The quantitative Kaiser test was performed using the modified procedure as described in the literature.[212] The reagents A and B for the Kaiser test were prepared as follows: For reagent A, 40 g of phenol dissolved in 10 mL of ethanol were mixed with 2 mL of 10 mM KCN aqueous solution in 100 mL pyridine. For reagent B, 2.5 g of ninhydrin were dissolved in 50 mL of ethanol and stored in the dark under nitrogen. Functionalized SWNT (~1 mg) were added to a 10 × 75-mm test tube, followed by addition of 100 μL of reagent A and 25 μL of reagent B. The same amount of reagent A and B were added to another test tube in the absence of the SWNT sample as a control. The solution was shaken well and both test tubes were heated in an oil bath at 100 ^{o}C for 10 min, and then placed in cold water. Then 1 mL of 60% ethanol in water was added to each test tube and mixed thoroughly. The solution in each test tube was filtered through a Pasteur pipette containing a tight plug of glass wool. The glass wool was rinsed twice with 0.5 mL of 60% ethanol. The filtrate solution was diluted with 60% ethanol and measured the absorbance (< 1 a.u.) at 570 nm against the blank reagent. The concentration of free amine was calculated by using $c = a/(\varepsilon \times b)$, where c is the concentration (M), a is the

absorbance, ε is the effective extinction coefficient (1.5×10^4 M^{-1} cm^{-1})[212], and b is the optical path length of the cuvette (1 cm). The primary amine content (mol) per sample was calculated using concentration multiplied by the volume of solution. Finally, the number of amine in the functionalized SWNT sample was indicated as mmol/g. Three parallel tests were done for each sample and the standard deviation value was obtained using Microsoft Excel.

5.3.2 Biological Assays

Cell culture: The L1210FR cell line was received as a gift from Dr. Gregory Russell-Jones (Access Pharmaceuticals Australia Pty Ltd., Targeted Delivery, Unit 5, 15-17 Gibbes St, Chatswood, NSW, Sydney 2067, Australia). L1210FR cells were grown in a RPMI-1640 cell culture medium (Gibco) in the absence of folic acid (FA) supplemented with 10 % fetal bovine serum (FBS) and 1 % Penicillin and Streptomycin. Prior to incubation, the cells were collected by centrifugation at 1000 rpm for 6 min and resuspended in RPMI medium without FBS at a cell density of 5×10^5 cells/mL. Similar procedure was followed for the L1210 cells purchased from ATCC (American Type Culture Collection P.O. Box 1549 Manassas, VA 20108 USA).

Incubation of cells with biotin-SWNT-FITC (5-11) and biotin-SWNT-FITC-Linker-SB-T-1214 (5-16):
The cell suspension (1 mL) was initially added to a microtube. The nanotube conjugates (10 μL) in DMSO were then added to the microtube for a final concentration of 10 μg/mL and the resultant suspension was incubated at 37 ^oC for 3 h. After incubation, the cells were washed with phosphate buffer saline solution (PBS), collected by centrifugation twice and resuspended in culture media at the desired concentration for further analysis. The same protocol was followed for the controls except conjugate **5-11** or **5-16** were not used.

Laser exposure of cells incubated with biotin-SWNT-FITC (5-11) and biotin-SWNT-FITC-Linker-SB-T-1214 (5-16):
The cells after being treated with or without **5-11** or **5-16** were plated in a flat-bottomed 96-well plate and exposed to laser at NIR range (800 nm) for 0 min (control), 2 min, 5 min, 7 min and 10 min and then incubated at 37 ^oC for 24 h. After incubation, the cells were washed with PBS, collected by centrifugation and resuspended in 100 μL media/PBS prior to imaging. (Note: there was no difference in images of cells when suspended in media or PBS)
A Spectra-Physics MaiTai Ti:sapphire laser was used as the laser source. The laser had a nominal wavelength of 800 nm and could be run in either continuous-wave (CW) or pulsed mode. In CW mode, the laser could deliver up to 1.20 W at its output. In pulsed mode, the laser produced pulses approximately 80 fs in duration at a rate of 80 MHz and with a total power output of approximate 1.15W. This corresponded to pulse energy of approximately 14 nJ per pulse. The beam exited the laser at a height of 10 cm from the optical table and with a beam diameter of roughly 2.5 mm. The beam was horizontally polarized with a very nearly TEM_{00} modeshape. The beam was routed through several dielectric folding mirrors to avoid other components on the optical table and was finally

brought into an opaque enclosure approximately 55 cm (w) x 43 cm (d) x 30 cm (h) high that contained the cell plate and support fixture. The beam entered the enclosure and was sent to a 25 mm diameter diverging lens with focal length f = –50 mm. The diverging lens served to expand the beam, thus providing the ability to illuminate the entire bottom aperture of the cell well. A dielectric mirror located 80 mm from the lens was used to re-orient the beam vertically upward, allowing the beam to enter the cell well vertically from the bottom and pass through the culture media (Figure 5-32). The enclosure serves as a beam block to contain scattered and residual laser light from escaping during the experiment. A 96-well cell Microtiter plate was used to contain the cell media. Each well was 6.5 mm in diameter, 9 mm high and spaced 9 mm apart from its nearest neighbor. The cell plate was positioned approximately 25 mm above the mirror. The total distance from the diverging lens to the bottom of the cell well was approximately 105 mm, which resulted in a beam diameter of roughly 7-8 mm at the well, as estimated using a thick paper card at the plane of the cell well. The laser beam struck the card and was scattered forming an illuminated circular disk that was then imaged using an ElectroPhysics ElectroViewer 7215 intensified imager and a transparent ruler. The beam size was selected so as to slightly overfill the cell well. As the beam had a TEM_{00} intensity profile, there would be some variation in the laser intensity as a function of radial distance from the beam (cell) centerline. By overfilling the well slightly, these effects were minimized.

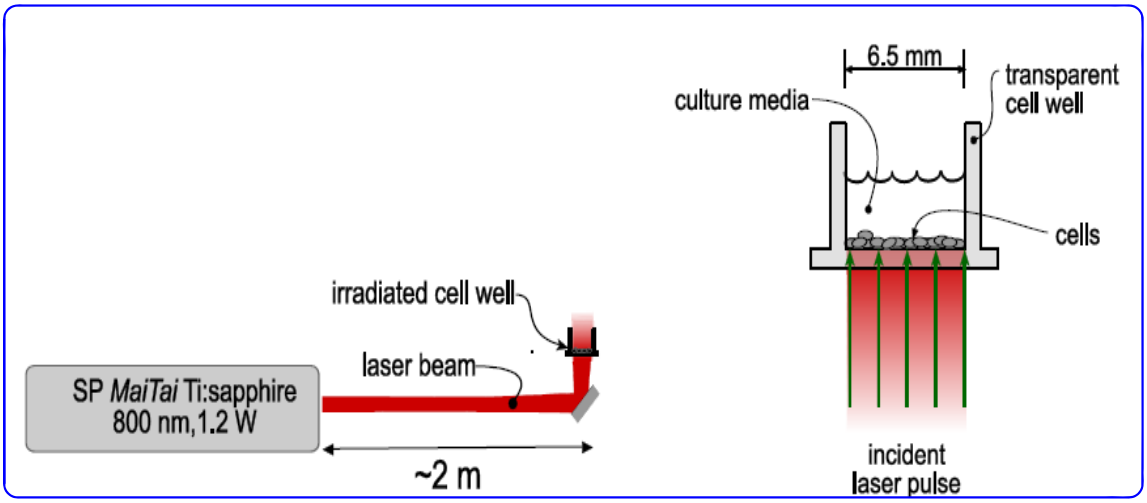

Figure 5-32. Schematic of experimental configuration (left) side-view of experiment, showing Spectra-Physics laser source, beam, vertical mirror and cell well, (right) detail of cell well and cells during laser irradiation (support stage not shown)

The experiments with laser were performed in collaboration with Prof. Jon Longtin of the Mechanical Engineering Department of Stony Brook University.

Chapter 6
Synthesis of novel taxoid for PET studies

6.1 Introduction

6.1.1 Principles of PET

In the past few decades Positron Emission Tomography (PET) has emerged as a powerful tool due to the advances made in radiotracer chemistry and instrumentation. PET has found increased application in the study and measurement of drug pharmacokinetics and drug pharmacodynamics using positron emitter labeled drug and/or tracer. Molecular imaging systems such as PET are important scientific tools which enable the investigations of molecular phenomena that are the cause of human disease and enable the development of effective treatments. Accordingly, PET has acquired an important role as a diagnostic tool for human cancers and is a popular modality in oncology.[1-3] PET provides functional data on the response to disease and therapy, identification of disease recurrence and therapy planning as well as clinical management of the disease.[4]

The PET procedure is based on the detection of photons released by the annihilation of positrons emitted by radiopharmaceuticals. Radionuclides that emit positrons are produced in a cyclotron by bombarding the target material with accelerated protons. These radionuclides are then used to synthesize radiopharmaceuticals which emit positrons inside the body and undergo annihilation by colliding with nearby electrons resulting in the release of two photons. These photons (511 keV) are released at an angle of 180 degrees and are detected by coincidence imaging as they strike scintillation crystals. A PET scanner consists of a ring of detectors surrounding the object to be imaged. The detectors are optimized to capture photons produced from beta decays. Photons acquired within 5 to 15 nanoseconds in a straight line are assumed to be released from the same positron-electron annihilation event. A PET scanner consists of a ring of detectors which surround the object to be imaged. These detectors are optimized to capture photons produced from beta decays and photons acquired within 5 to 15 nanoseconds in a straight line are assumed to be released from the same positron-electron annihilation event. These photon pairs or “coincidences” form the lines of response (LORs) and the location of the radiation source is determined by calculating the crossing of all the LORs. The algorithm takes into account dead time that arises from the inability of the system to capture all photons, scatter, and attenuation of true coincidence via the Compton process and tissue absorption while constructing the image.[5] The resulting data is recorded by a computer to show the distribution of the radiotracer within the body. Figure 6-1 shows a schematic of the basic principle of PET.

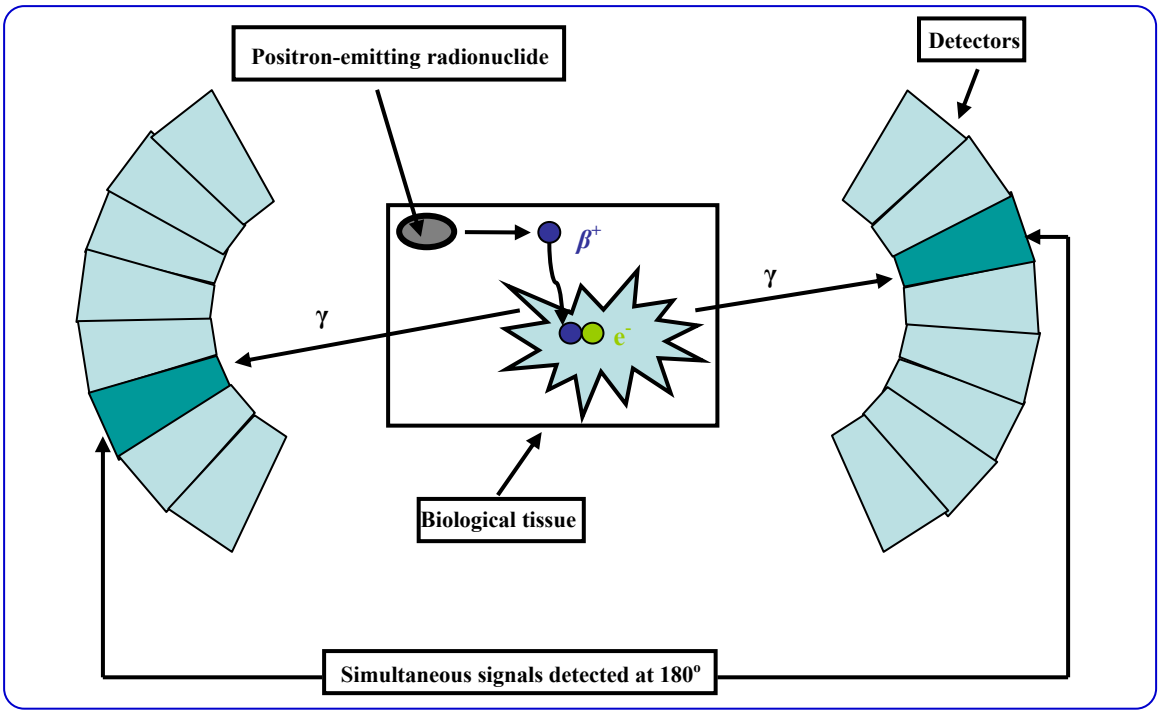

Figure 6-1. Schematic of the basic principles of PET

A major advantage of PET imaging is its versatility and numerous different positron emitters with varying characteristics are available which it makes it possible to synthesize a wide variety of radiopharmaceuticals.[6] Some of the more commonly used isotopes for PET are shown in Table 6-1.[1, 7]

Isotope	Half-life	β^+ yield (%)	Max. tissue range (mm)	Avg. β^+ Energy (MeV)
^{11}C	20.4 minutes	100	4.2	0.39
^{18}F	109.8 minutes	97	2.6	0.25
^{13}N	9.98 minutes	100	5.4	0.49
^{15}O	2.03 minutes	100	8.4	0.74
^{68}Ga	68.1 minutes	89	-	0.84

Table 6-1. Most commonly used isotopes for PET studies

These novel radiopharmaceuticals enable the visualization of tumor metabolism, specific cell surface receptors, angiogenesis, cellular proliferation and tumor hypoxia with high sensitivity. The most widely used PET tracer is FDA approved ^{18}F-fluorodeoxyglucose (^{18}F-FDG) which is a glucose analog[8, 9] that allows the mapping of glucose uptake by tumors because malignant tumors have an elevated glucose metabolism.[10] Another agent ^{18}F-fluoride is used as PET tracer for bone imaging to visualize areas of altered osteogenic activity.[11, 12] A normalized quantitative measure of

FDG accumulation in tissue or standardized uptake values (SUVs) is obtained by normalizing the tissue radioactivity measured with PET to the injected dose and the body weight of the patient.[13] The SUVs provide extremely reproducible parameters of tumor glucose uptake which allows comparison of PET studies performed in different patients or in the same patient at different time points when strict PET protocols are followed.[14] Dynamic scans provide tracer distribution information over time and the first such study with FDG was performed in the 1980s[15] and since then many dynamic PET studies have been performed with various tracers.[16, 17]

Valuable pharmacokinetics information can be obtained from PET imaging when the drug is radiolabeled and this allows for the assessment of drug metabolism, drug action and toxicity. PET imaging is highly sensitive, minimal amount of radiolabeled drugs (nano- to picomolar range) which is several orders of magnitude below expected toxicity levels can be used. This enables the investigation of PK information before human clinical trials and the information thus obtained can be directly transferred to clinical trials. This is an advantage over the current practice of predicting PK data for human clinical trials from animal models which do not always correlate with human results. Radiolabeled drugs can be used to obtain information about two key parameters – a) pharmacokinetics (PK) *i.e.* how the drug distributes in the body and b) pharmacodynamics (PD) *i.e.* what the drug does to the organism. Table 6-2 shows the results of pharmacokinetic (PK) studies performed with some radiolabeled drugs.[18]

Radiolabeled Drug	Mechanism of Action	Pharmacokinetic Information
[^{11}C]-Temozolomide	DNA alkylating drug	Biodistribution in tumor and normal tissue, mechanism of action, Phases 1 and 2 trials[19]
[^{11}C]-N-[2(Dimethylamino) ethyl]acridine-4 carboxamide ([^{11}C]-DACA)	Topoisomerase I/II inhibitor	Biodistribution in tumor and normal tissue, metabolism, potential cardiotoxicity was identified, Prephase 1 study[19]
[^{18}F]-5-Fluorouracil	Antimetabolite that inhibits thymidylate synthase	Biodistribution in tumor and normal tissue, mechanism of action, biomodulation using eniluracil to improve efficacy[19, 20]

Radiolabeled Drug	Mechanism of Action	Pharmacokinetic Information
[^{13}N]-Cisplatin	Cisplatin is a platinum compound chemotherapy drug that acts like an alkylating agent.	Biodistribution in tumor and normal tissue, blood clearance, metabolism comparison intra-arterial *vs*. intravenous administration[21]
[^{11}C]-BCNU	Single chemotherapeutic agent for primary brain tumors	Biodistribution in tumor and normal tissue, comparison of intra-arterial *vs*. intravenous administration[22]
[^{18}F]-Tamoxifen	Down regulates estrogen receptors for breast cancer	Biodistribution in tumor and normal tissue, predicting effect of tamoxifen therapy on patients with estrogen-receptor-positive breast cancer[23]
[^{18}F]-Paclitaxel	Prevents cell division by promoting disassembly of microtubules	Biodistribution, radiation dose estimates, and *in vivo* P-glycoprotein (Pgp) modulation studies[24]
[^{18}F]-ZD1839 (IRESSA)	Epidermal growth factor receptor (EGFR) inhibitor	Molecule has been labeled with ^{18}F. Potential to predict which patients will respond to IRESSA treatment[25, 26]

Table 6-2. Pharmacokinetic studies on some radiolabeled drugs[18]

Table 6-3 shows some of the tracer dose required in various subjects.[27] The development of small animal PET scanners has enabled the whole body, functional and non-invasive imaging strategy for animal studies which give crucial information about the pathology of the disease such as receptor overexpression on tumor cells which can be used to plan targeted therapies.[28]

Subject	Tracer dose (mCi)
Mice	0.05-0.2
Rats	0.5-2
Non-human primates	2-8
Humans	2-20

Table 6-3. Typical dose required for PET imaging[27]

6.1.2 DHA a Tumor-targeting Moiety

The lack of tumor specificity in traditional chemotherapeutic drugs used for cancer treatment is a serious drawback and results in severe undesirable side effects. In order to solve this problem, tumor-targeting prodrugs, based on a conjugate of a cytotoxic drug to a tumor-specific molecule can be designed. The basic premise of a 'tumor-targeting prodrug' is that the drug is inactive until it is delivered to the target tumor cells by the tumor-specific molecule. At the target tumor cell the drug is internalized and released from the carrier to restore its original activity. Polyunsaturated fatty acids (PUFAs) are ideal candidates as tumor-specific molecules. Representative naturally occurring PUFAs possess 18, 20, and 22 carbons, and 2–6 unconjugated cis-double bonds separated by one methylene, such as linolenic acid (LNA), linoleic acid (LA), arachidonic acid (AA), eicosapentaenoic acid (EPA), and docosahexaenoic acid (DHA).[29-34] PUFAs are found in vegetable oils, cold-water fish, and meat and are classified as a nutritional additive by the FDA in the US. Thus, DHA and its metabolites are considered to be safe to humans.[32, 35, 36] Taxoprexin® (DHA-paclitaxel) was successfully developed by coupling DHA to the C-2' position of paclitaxel.[37] This conjugate exhibited substantially increased antitumor activity and reduced systemic toxicity against the M109 lung tumor xenograft in mice compared to paclitaxel itself. This conjugate was found to be stable in blood plasma and had a prolonged half life (85 h)[38] with sustained levels of DHA-paclitaxel in the blood. High concentration of this conjugate was maintained in tumor cells for a long period of time which released paclitaxel slowly approximating continuous infusion of paclitaxel. The slowly released paclitaxel killed the slowly cycling or residual tumor cells and thus reduces side effects.[39] Taxoprexin® was selected as a fast-track drug development candidate by FDA and has advanced to human phase III clinical trials.

Ojima *et al*. have further explored a family of Taxoprexin® analogs (Figure 6-2) comprising our cytotoxic warheads, *i.e.* 2nd-generation taxoids and DHA as promising drug candidates. These 2nd-generation taxoids alone exhibited 2-3 orders of magnitude higher activity against drug-resistant cancer cells and tumor xenografts in mice, expressing MDR phenotypes[40-42] and thus they would be better than paclitaxel in several drug resistant cancer cells. The antitumor bioactivities of these tumor-targeting drug conjugates were evaluated against the drug-sensitive A121 human ovarian tumor xenograft (Figure 6-3) and the drug-resistant DLD-1 human colon tumor xenograft (Figure 6-4) in SCID mice.[43] DHA-taxoid conjugates showed excellent antitumor

activities against the drug-sensitive A121 ovarian tumor xenograft. The conjugates also exhibited complete regression of the tumor (administration on days 5, 8, and 11) over the duration of experiment for 201 days against the drug-resistant DLD-1 human colon tumor xenograft in all treated animals.[44]

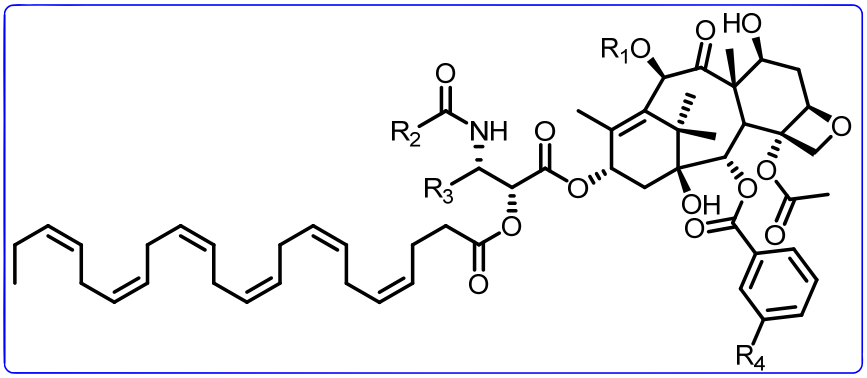

Figure 6-2. DHA-taxoid conjugate

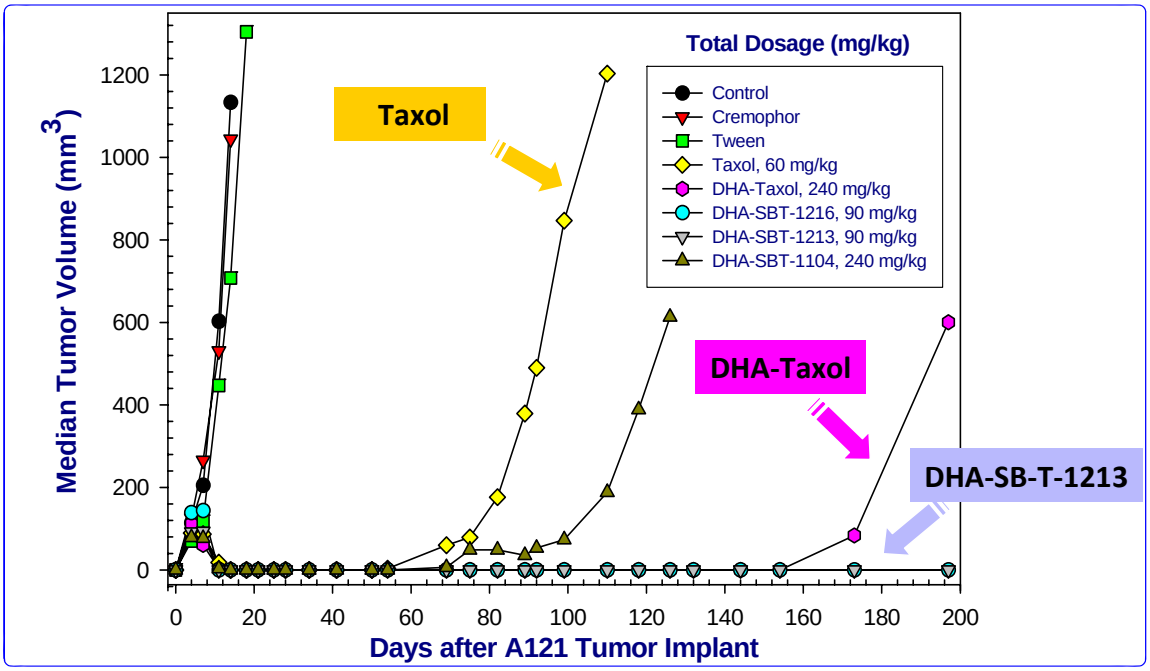

Figure 6-3. Effect of DHA-conjugates on human ovarian tumor xenograft (Pgp-) A121[43]

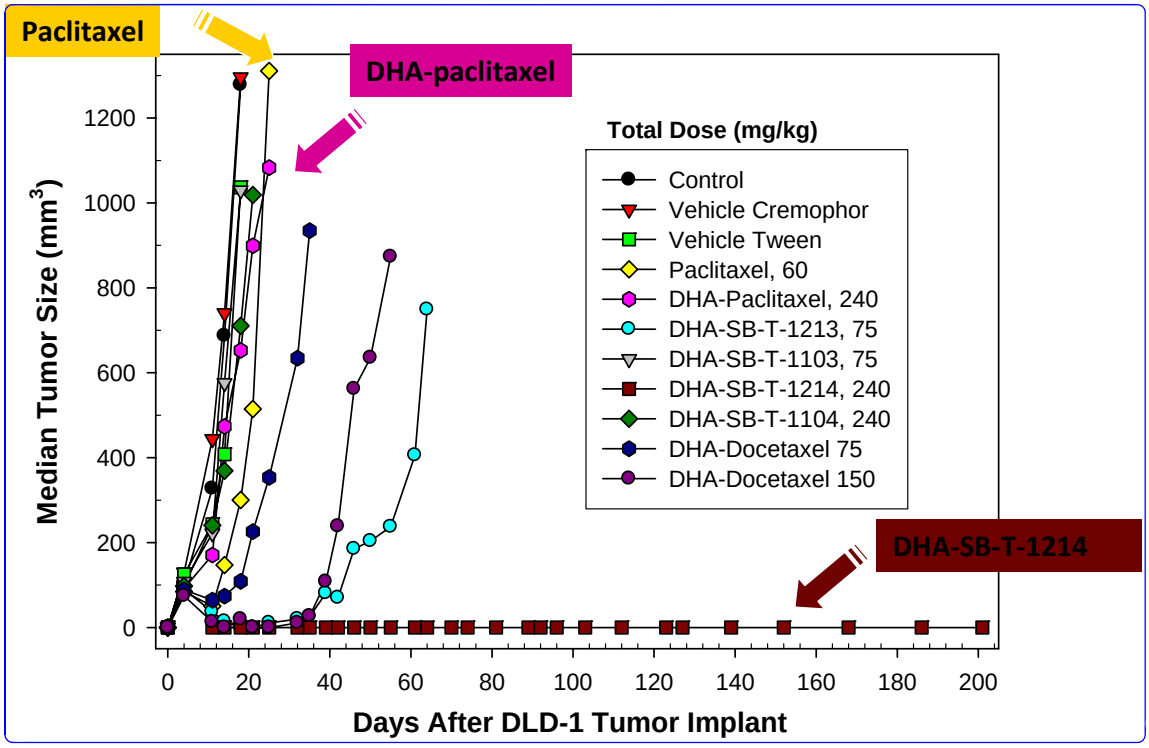

Figure 6-4. Effect of DHA-conjugates on human colon tumor xenograft (Pgp+) DLD-1[43]

Figure 6-3 shows that with Pgp(-) A121 tumor xenografts the effect of DHA-paclitaxel and DHA-taxoids are far superior than paclitaxel alone. As expected DHA-taxoids showed superior potency in Pgp(+) DLD-1 tumor xenografts where paclitaxel alone and DHA-paclitaxel had almost no effect as shown in Figure 6-4. These and other promising results led us to design a novel second-generation (SB-T-121402) DHA conjugate which could be labeled with carbon-11. The labeled SB-T-121402 and its labeled conjugate would be used for small animal PET studies to study the PK and PD of these drugs and to determine the specific accumulation of the DHA-taxoid conjugate inside the tumors.

6.1.3 Labeled Pharmaceuticals used for PET Studies

PET can be used to monitor various disease targets including genes, antigens, ligand-receptor interactions and pathways involved in signal transduction, cell cycle, cell death, drug resistance and angiogenesis. The synthetic pyrimidine, 5-fluorouracil (5-FU) which is an analog of the pyrimidine uracil is a common anticancer agent used for the treatment of gastrointestinal malignancies.[45] Substitution of hydrogen with fluorine at the 5-position transforms uracil into a cytotoxic compound. The drug exerts its effects through its metabolites which inhibit DNA synthesis.[45] Studies have shown that the antitumor activity of 5-FU is limited and it has not consistently improved survival when administered alone or in combination with other anti-neoplastic agents.[46] The pharmacokinetics of 5-FU has been studied with radiolabeled 5-FU. The favorable half-

life of [18]F and the ease of chemical synthesis of 5-[18F]FU have made it the most often monitored anticancer drug using PET. Figure 6-5 shows the synthesis of [18F]FU.[47]

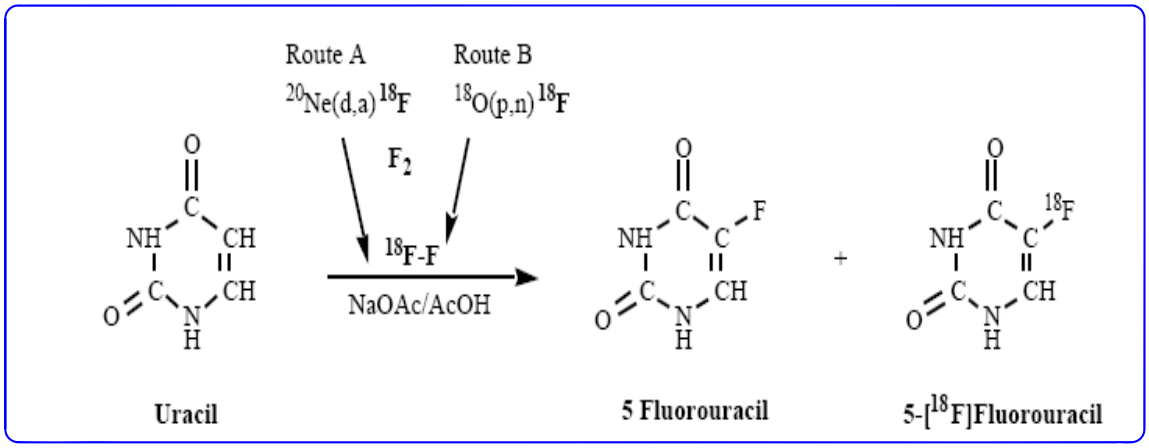

Figure 6-5. Radiochemical synthesis of 5-FU using ^{18}F[47]

PET studies with radiolabeled 5-FU is used to determine aspects of its PK such as its localization in liver, gall bladder and its clearance rate from these organs. Biodistribution studies with 5-[18F]-FU in rodents indicated a direct relationship between the tumor response and tumor levels of 5-[18F]-FU in different lines of tumors in mice and rats was found.[48]

Paclitaxel (PAC) is a FDA approved anticancer drug with potent antitumor activity as discussed in Chapter 1. However, paclitaxel's effectiveness in multidrug resistant tumors is greatly reduced.[49] The MDR is mainly caused by the enhanced expression of P-glycoprotein which acts as an efflux pump and removes a number of cytotoxic drugs leading to MDR.[50] Accordingly, radiolabeled analogs of paclitaxel have been synthesized to evaluate the expression of Pgp in certain tumor types. Biodistribution studies of halogenated (^{18}F, ^{76}Br, ^{124}I) paclitaxel were performed to determine their potential utility in PET. The uptake of [18F]FPAC and [76Br]BrPAC increased significantly in rat kidney upon preinjection with PAC. However, this increased uptake could not be attributed to inhibition of P-gp-mediated transport as determined from studies in knockout mice. All three radiolabeled PAC analogs exhibited increased uptakes in lung with a predose of PAC, which suggested a P-gp-mediated transport.[51]

[18F]-FDG has been by far the most extensively used radiopharmaceutical for oncologic nuclear imaging with PET. The development of several new radiopharmaceutical agents has made it possible to monitor a variety of biological processes related to the diagnosis and treatment of cancer.

6.2 Results and Discussion

6.2.1 Synthesis of Tributyl Tin Substituted Benzoic Acid

PET imaging can be used to study the drug delivery process and accordingly novel second generation taxoids with C-11 labels were proposed as shown in Scheme 6-1.

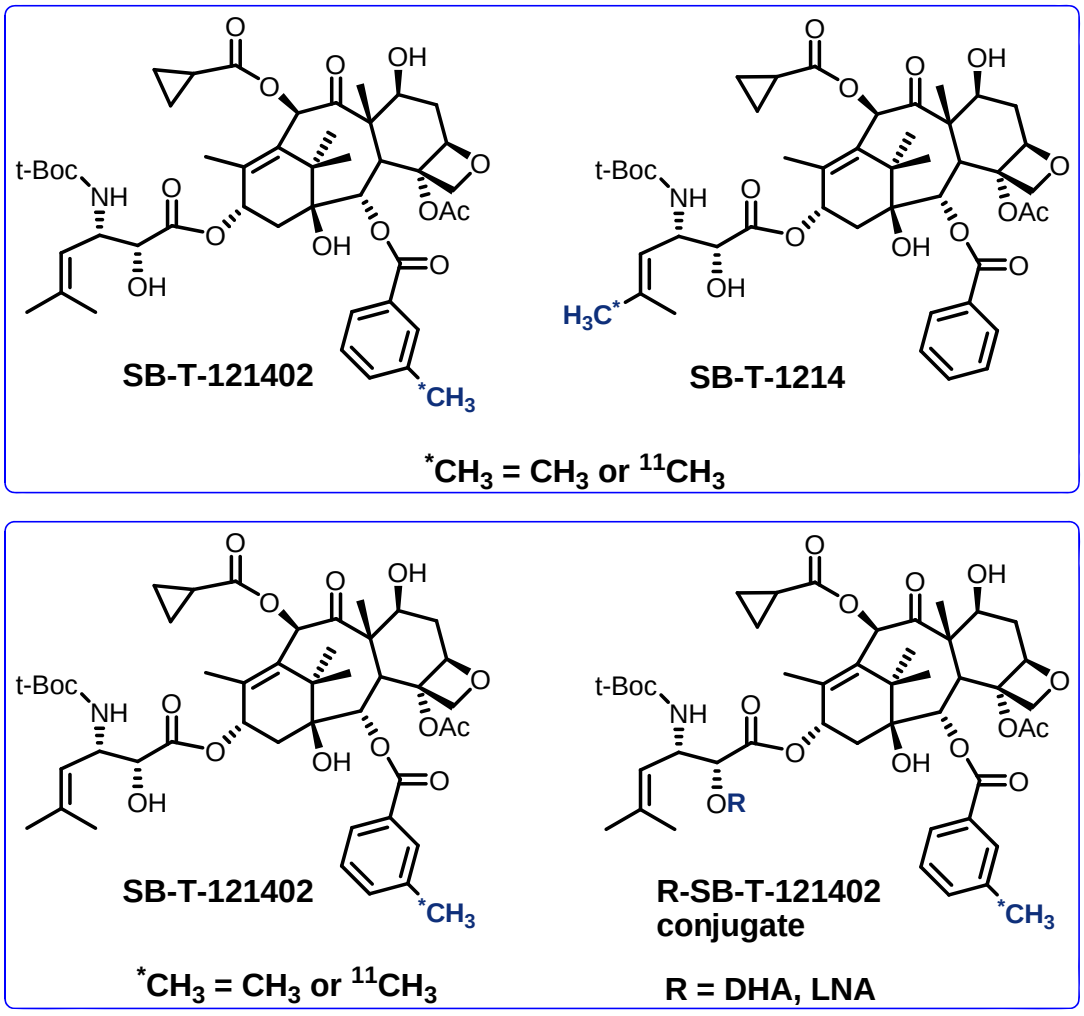

Scheme 6-1. Carbon-11 labeled taxoids

The $^{11}CH_3$ label can be introduced in the meta-position of the C-2 benzoyl group of SB-T-121402 or in the methyl of the isobutenyl group in SB-T-1214. The novel taxoid SB-T-121402 was chosen for the development of the carbon-11 labeled drug using cold material. This novel taxoid structurally belongs to the second- and advanced second-generation taxoids which are not only very potent but also can modulate Pgp thereby bypassing MDR in cancer cells as discussed in Chapter 1. Carbon-11 was chosen as the label because it can replace a carbon in the novel potent taxoid and therefore will not

affect its potency. Also, methyl group is least bulky and non-polar and will not alter the biological efficacy significantly. The short half-life of C-11 also makes many experiments possible per day without any special precautions. The C-CH_3 derivatives are more tolerant to metabolic processes compared to O-CH_3 and N-CH_3 derivatives. Besides, various synthetically well-established precursors, such as $^{11}CH_3I$, ^{11}CO and $^{11}CO_2$, are readily available.[52] However, there is a temporal restriction when employing carbon-11 to synthesize radiopharmaceuticals or radiotracers. The short half-life of 20.3 min makes it very challenging to design an experiment because typically the total time allowed for synthesis of a PET tracer should be within two to three radionuclide half-lives. This means that the complete synthesis of an ^{11}C-labeled compound must be accomplished within 40 to 60 min. The time allowed for the reaction in tracer synthesis is only about 5 to 10 min taking into account the time for reaction, purification and injection and thus a rapid reaction is crucial.

Rapid methylation using Stille type cross-coupling has been used to install the methyl group using methyl iodide and appropriate stannanes. Organostannane precursors provide certain advantages such as high tolerance to various chemical reactions and chromatographic purification conditions which makes it easier to incorporate the radioisotope in the final step as well as extremely low polarity which makes it easier to separate it from the desired product. Accordingly, a 3-tributylstannyl benzoic methyl ester compound was synthesized which could be incorporated in the baccatin. The synthetic scheme is shown in Scheme 6-2.

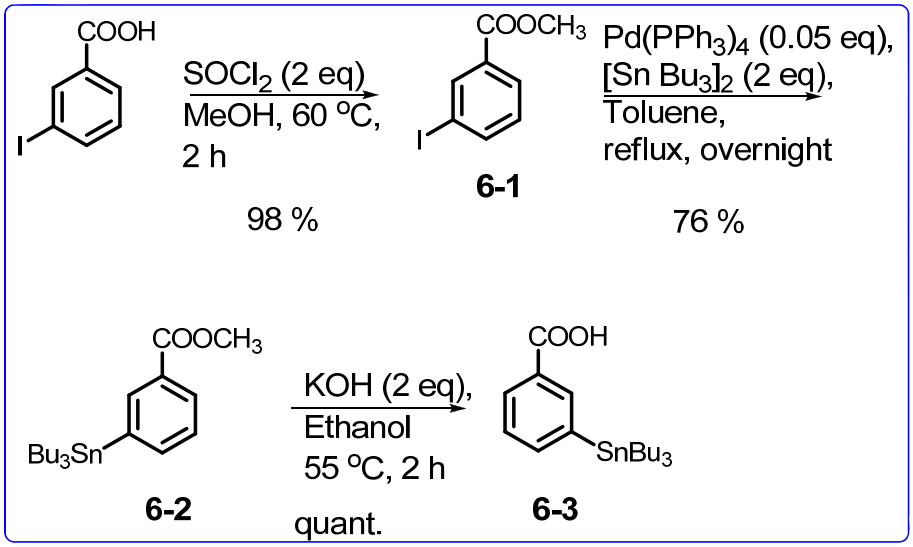

Scheme 6-2. Synthesis of tributyl tin substituted benzoic acid

The commercially available 3-iodo benzoic acid was used to esterify the free acid to form the methyl 3-iodobenzoate **6-1** using thionyl chloride in methanol. This ester was then reacted with tetrakis(triphenylphosphine) palladium and hexabutyl distannane to synthesize the methyl-3-(tributylstannyl) benzoate **6-2**. This was followed by hydrolysis to synthesize 3-(tributylstannyl) benzoic acid **6-3** which was used to couple with TES protected modified baccatin to synthesize the desired modified baccatin.

6.2.2 Synthesis of SB-T-121402

The 10-DAB-III was first suitably modified as shown in Scheme 6-3 for the synthesis of SB-T-121402. The 10-DAB-III was first protected with TES at C-7, 10 and 13 positions to obtain **6-4** followed by reduction with Red Al to remove the C-2 benzoyl group to obtain **6-5**. The modified baccatin **6-5** was then coupled with *m*-toluic acid to obtain compound **6-6**. The silyl protecting groups were then removed to obtain baccatin **6-7** with the C-2 *m*-methyl benzoyl group installed in place C-2 benzoyl group.

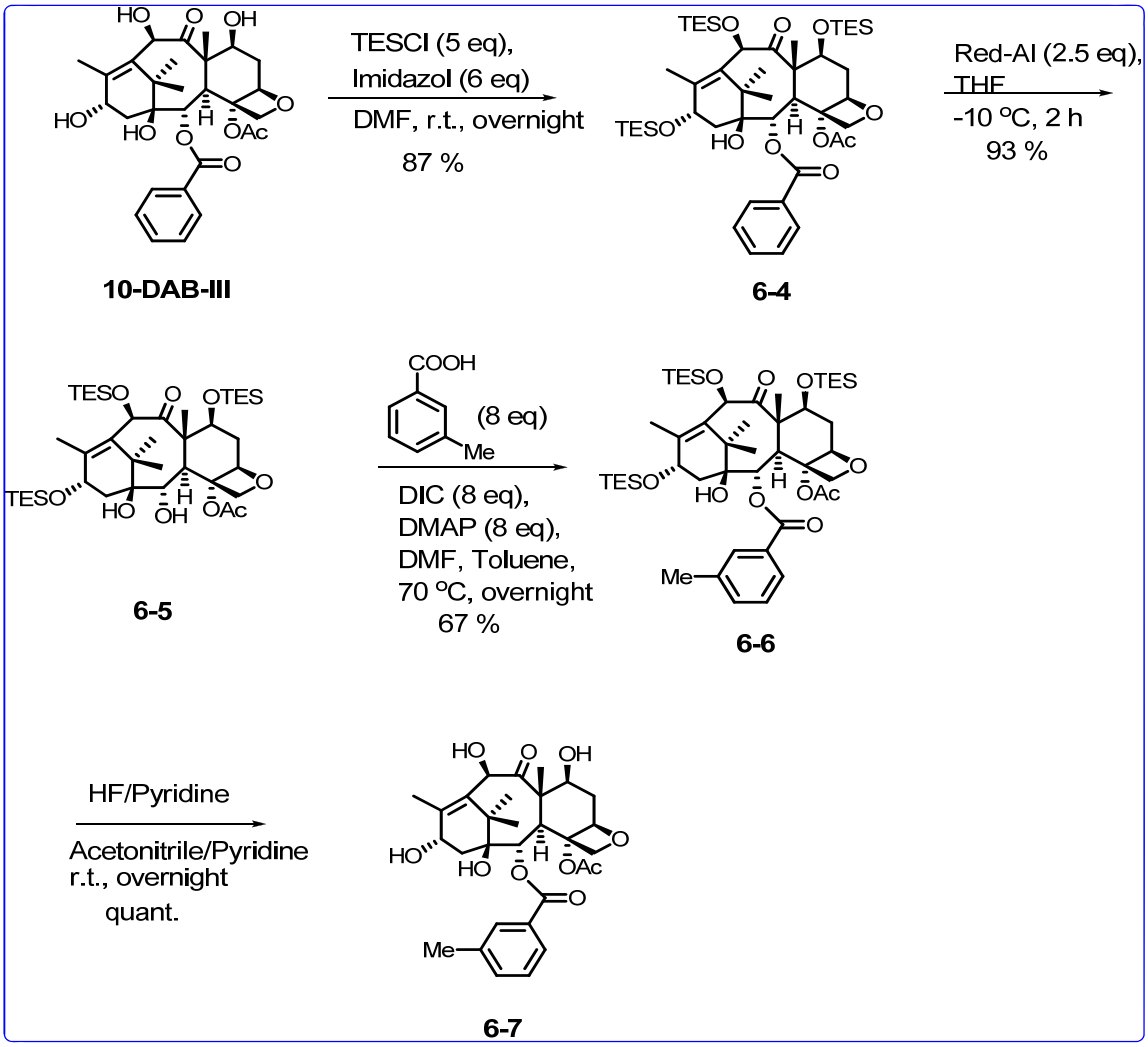

Scheme 6-3. Modification of baccatin core

The desired novel second-generation taxoid SB-T-121402 was synthesized from modified baccatin core **6-7** as shown in Scheme 6-4. The baccatin **6-7** was first protected with TES at the C-7 position to form **6-8** which was then cyclopropanoylated at the C-10 position to obtain **6-9**. The baccatin **6-9** was then coupled with *β*-lactam to form **6-10** following the Ojima coupling protocol and the silyl groups were subsequently

deprotected to form desired novel taxoid SB-T-121402. This taxoid will be coupled to DHA and other suitable polyunsaturated fatty acids to synthesize the corresponding tumor-specific conjugate.

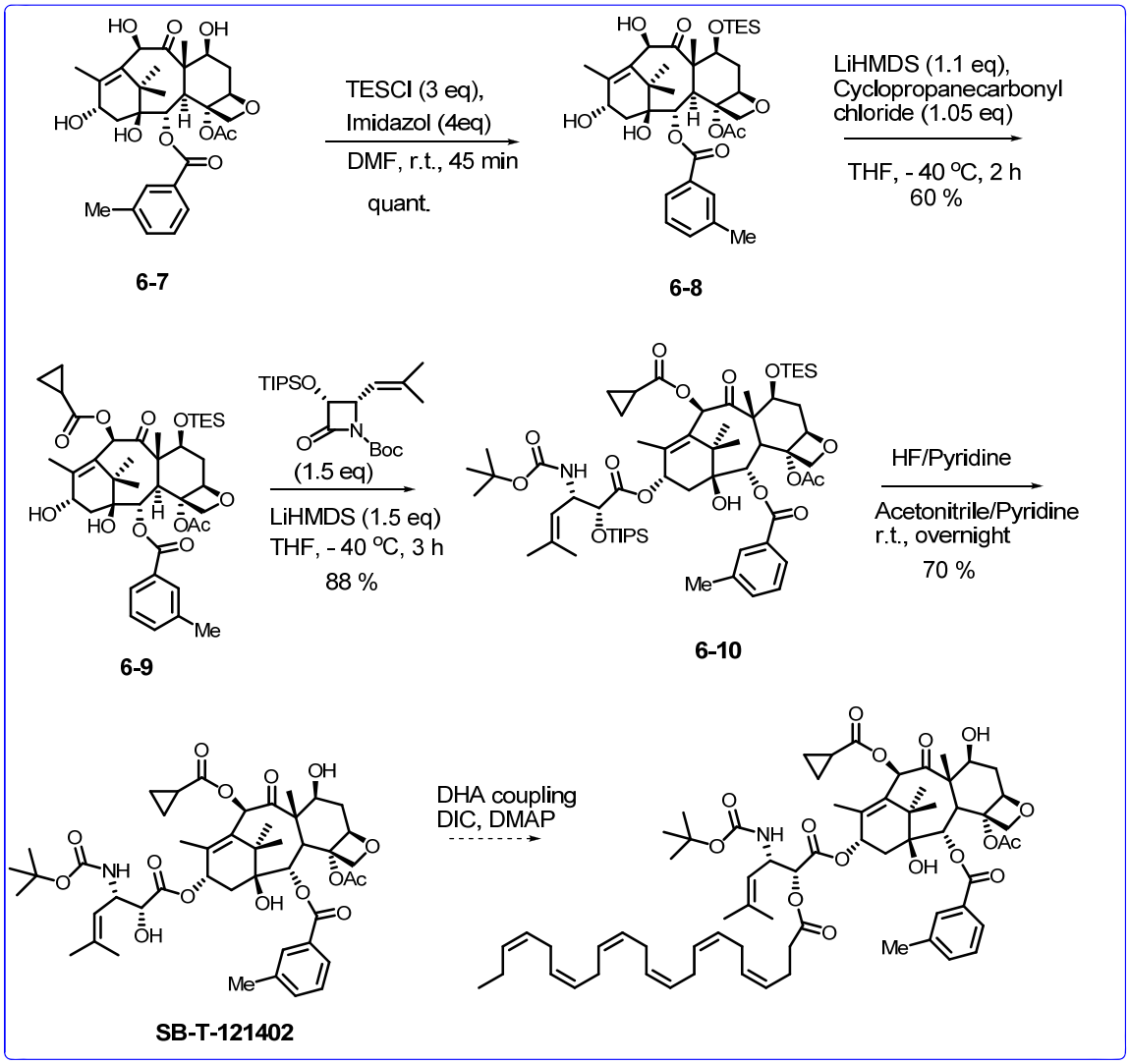

Scheme 6-4. Synthesis of SB-T-121402

6.2.3 Synthesis of Tributyl Tin Substituted SB-T-121402 and Labeled SB-T-121402 using Cold Material

The synthesis of the tin precursor for the modified Stille coupling is shown in Scheme 6-5. The compound **6-5** was coupled with 3-(tributylstannyl) benzoic acid **6-3** to obtain **6-11** which was then deprotected to obtain the tributyltin substituted baccatin **6-12.** This modified baccatin was TES protected at the C-7 position to form **6-13** which was then cyclopropanoylated at the C-10 position to obtain **6-14**. The baccatin **6-14** was then coupled with *β*-lactam to form **6-15** following the Ojima coupling protocol and the silyl

groups were subsequently deprotected to form desired novel tin precursor taxoid **6-16**. This was subjected to rapid methylation to form SB-T-121402 and the reaction conditions were developed. This taxoid will be coupled to DHA and other suitable polyunsaturated fatty acids to synthesize the corresponding tumor-specific conjugate.

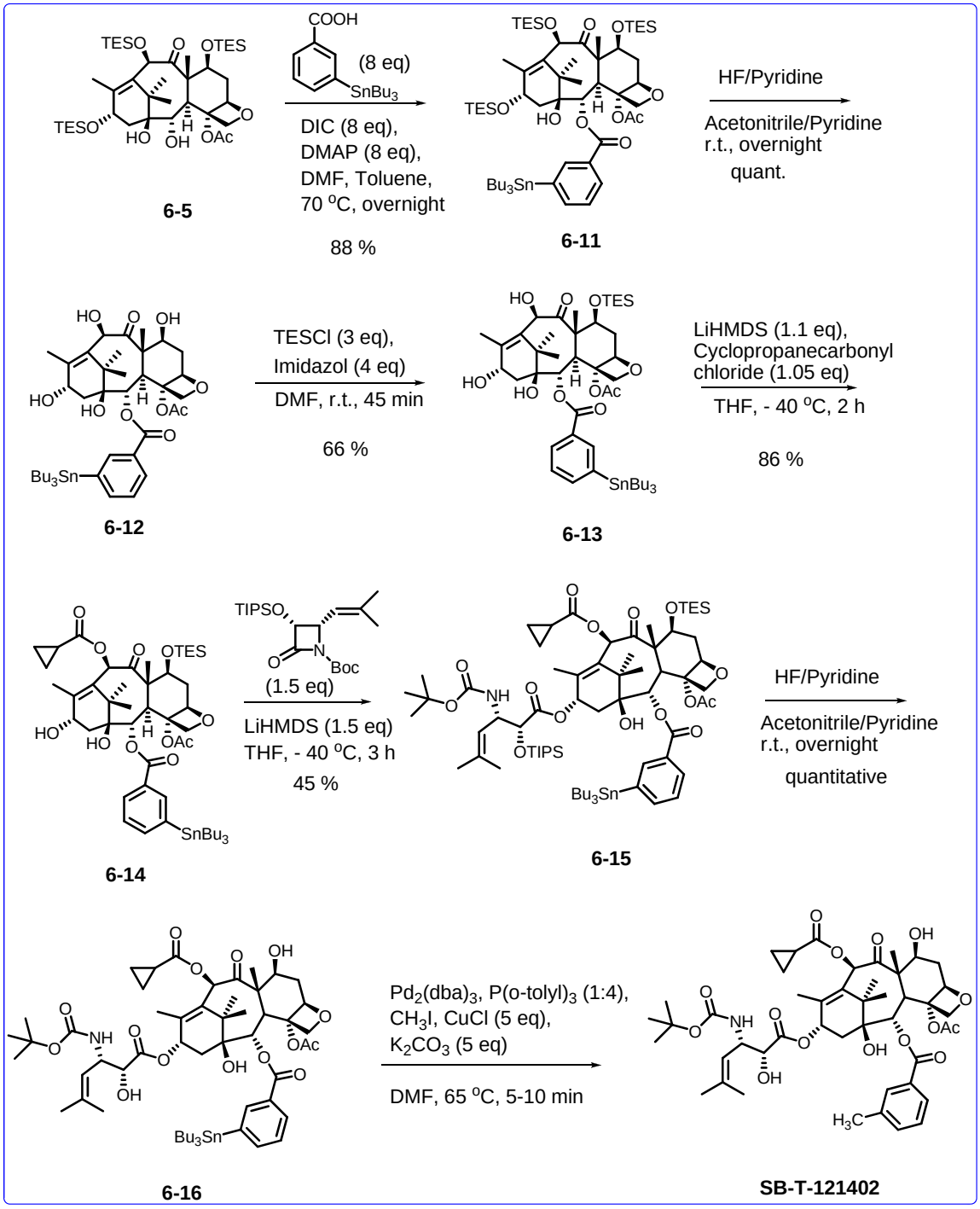

Scheme 6-5. Synthesis of tin taxoid precursor and cold SB-T-121402

Initially model Stille reactions were performed using **6-11** and **6-14** which indicated the formation of the desired product with CH_3 substituted for $SnBu_3$. The copper(I) salt and the solvent have a special role. When model reactions with **6-2** were performed the desired CH_3 substituted compound was formed within 5 min in the presence of copper(I) salt. Studies have shown that the modified Stille coupling between the sp^3-sp^2 carbons can be enhanced with a combination of Cu(I) salt/F^- system and phosphines.[53] The favorable role of Cu(I) salts in Stille coupling is well known and its role in the catalytic cycle is solvent dependent.[54-57] In solvents such as dioxane and THF the role of Cu is that of a scavenger for the free neutral ligand which is responsible for the autoretardation of the associative transmetalation which is the rate determining step.[55, 57] However, in very polar solvents such as DMF and *N*-methylpyrrolidone (NMP) the Cu(I) salt accelerates the rate of the reaction by a preliminary transmetalation reaction from organostannane to a more reactive organocopper intermediate which takes part in the catalytic cycle.[56, 57] It has been shown that the F^- increases the rate of the palladium-catalyzed coupling reaction between vinyl triflates and organostannanes[58] and also efficiently transforms the Bu_3Sn-halide by-product into insoluble Bu_3SnF which can be easily filtered out. Thus the high efficiency of the combined use of Cu(I)X and CsF is attributed to the synergic effect of the generation of a more reactive organocopper intermediate through Sn/Cu transmetallation18,19 and the removal of Bu_3SnX (X = Cl, Br or I) by the formation of insoluble Bu_3SnF to shift the equilibrium to the organocopper species.[53, 55] The efficiency of the reaction could also be enhanced by using K_2CO_3 which also had a similar synergic effect of Sn/Cu transmetalation and formation of the stable bis(tributylstannyl)carbonate, $[Bu_3SnO]_2CO$.[59] This is summarized in Scheme 6-6.

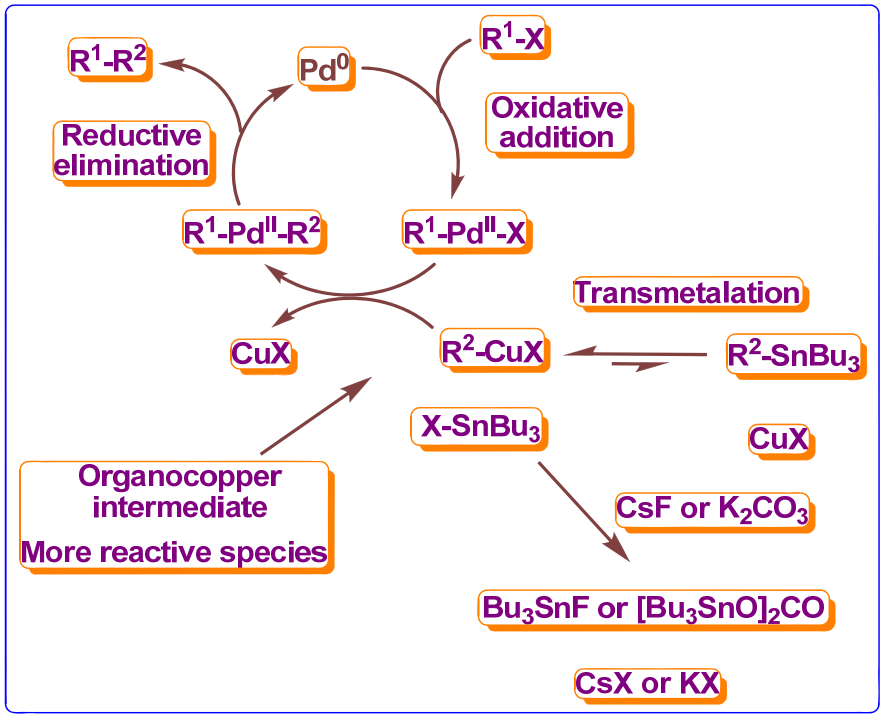

Scheme 6-6. Possible role of Cu(I) and F^- or CO_3^{2-} in the catalytic cycle

The role of the phosphine P(*o*-tolyl)$_3$ is also crucial. Trialkylphosphines have a higher nucleophilic character than triarylphosphines which leads to undesirable side products and prevents the use of a large quantity of phosphines. Using P(*o*-tolyl)$_3$ is also more convenient because it is an air stable crystalline compound. The use of a coordinatively unsaturated Pd(0) complex, such as Pd[P(*o*-tolyl)$_3$] and consequently, sterically bulky phosphines (e.g., cone angle 194^o (P(*o*-tolyl)$_3$) vs. 145^o (PPh$_3$)), enhances the sp^3–sp^2 coupling efficiency. The concept of synergic effect and the use of a bulky triarylphosphine allowed an efficient rapid sp^3–sp^2 Stille coupling reaction potentially useful for synthesis of PET tracers.[52]

6.2.4 Biological evaluation

Cytotoxicity assays were performed to determine the potency of the novel second generation taxoid as well as the DHA-SB-T-1214 against various cancer cell lines. MTT assays were performed in all cases and the results are shown in Table 6-4.

Cell line	SB-T-1214	SB-T-121402	DHA-SB-T-1214	Paclitaxel
MCF7-R	4.0	< 1	-	300
Panc-1	5.0	< 1	50	26
DLD-1	4.5	< 1	114	-
LCC6 MDR	8.4	< 1	52	346
A549	1.4	< 1	-	7.3
ID8	7.6	< 1	-	36.4

Table 6-4. *In vitro* cytotoxicity assay (IC_{50}, nM)

The cell line used were MCF-7-R – human breast cancer (drug resistant), Panc-1 – human pancreatic cancer, DLD-1 – human colon cancer, LCC6 MDR – human breast cancer (multidrug resistant), A549 – human lung cancer, ID8 – mouse ovarian cancer. The novel taxoid SB-T-121402 was found to be very potent.

6.3 Experimental Section

General Methods: ^{1}H and ^{13}C NMR spectra were measured on a Bruker AC-250 NMR spectrometer or a Varian 300, 400, 500, or 600 MHz NMR spectrometer. The melting

points were measured on a "Uni-melt" capillary melting point apparatus from Arthur H. Thomas Company, Inc. Optical rotations were measured on a Perkin-Elmer Model 241 polarimeter. High-resolution mass spectrometric analyses were conducted at the Mass Spectrometry Laboratory, University of Illinois at Urbana-Champaign, Urbana, IL. GC-MS analyses were performed on an Agilent 6890 Series GC system equipped with the HP-5HS capillary column, (50 m X 0.25 mm, 0.25 um) and with the Agilent 5973 network mass selective detector. LC-MS analyses were carried out on an Agilent 1100 Series Liquid Chromatograph Mass Spectrometer. IR spectra were measured on a Shimadzu FTIR-8400s spectrophotometer. TLC analyses were performed on Merck DC-alufolien with Kieselgel 60F-254 and were visualized with UV light, iodine chamber, 10 % sulfuric acid and 10% PMA solution. Column chromatography was carried out on silica gel 60 (Merck; 230-400 mesh ASTM). Chemical purity was determined with a Waters HPLC assembly consisting of dual Waters 515 HPLC pumps, a PC workstation running Millennium 32, and a Waters 996 PDA detector, using a Phenomenex Curosil-B column, employing CH_3CN/water as the solvent system with a flow rate of 1 mL/min, or Shimadzu HPLC.

Materials: The chemicals were purchased from Sigma Aldrich Company or Acros Organic Fischer Company. 10-Deacetyl baccatin III (DAB) was donated by Indena, SpA, Italy. Dichloromethane and methanol were dried before use by distillation over calcium hydride under nitrogen or argon. Ether and THF were dried before use by distillation over sodium-benzophenone and kept under nitrogen or argon. Toluene and benzene were dried by distillation over sodium metal under nitrogen or argon before use. Dry DMF was purchased from EMD chemical company, and used without further purification. PURE SOLV™, Innovative Technology Inc, provided an alternative source of dry toluene, THF, ether, and dichloromethane. The glasses were dried in a 110 ^oC oven and allowed to cool to room temperature in a desiccator over "*Drierite*" (calcium sulfate) and assembled under inert gas nitrogen or argon atmosphere.

Methyl 3-iodobenzoate (6-1):
3-Iodobenzoic acid (4 g, 16 mmol) was dissolved in 40 mL of methanol in a round bottom flask, followed by the addition of thionyl chloride ($SOCl_2$, 2 eq) drop wise. The reaction was heated to 60 ^oC and was monitored using TLC (5:1 hexane/ethyl acetate). After the reagents were consumed after two hours, the reaction was cooled to room temperature. Then, the solvent was removed using rotary evaporation and was neutralized using saturated sodium bicarbonate solution. Subsequently, the aqueous layer was washed with DCM (50 mL X 3) and the organic layers were combined and dried with anhydrous magnesium sulfate. Afterwards, magnesium sulfate was filtered off and DCM was removed using rotary evaporation. Finally, the solvent was removed under reduced pressure to give the desired compound (**6-1)** as a white solid (4.14 g) in 98 % yield: ^1H NMR (300 MHz, $CDCl_3$): δ 3.92 (s, 3H), 7.19 (m, 1H), 7.89 (m, 1H), 8 (m, 1H), 8.38 (m, 1H).

Methyl 3-(tributylstannyl)benzoate (6-2):[60]
Methyl 3-iodobenzoate **(6-1)** (300mg, 1.14mmol) and tetrakis(triphenylphosphine) palladium (0.05 eq) were dissolved in 6 mL of toluene in a round bottom flask and

maintained under an inert atmosphere. Hexabutyl distannane (2 eq) was added drop wise to the flask and the reaction was refluxed overnight. After all the starting materials were consumed, the reaction was cooled to room temperature, filtered through celite and subjected to flash chromatography (2 % DCM in hexane) to obtain the pure compound (**6-2)** as a clear transparent oil (367 mg) in 76 % yield: ^{1}H NMR (300 MHz, $CDCl_3$): δ 0.9 (m, 9H), 1.09 (m, 6H), 1.3 (m, 6H), 1.55 (m, 6H), 3.92 (s, 3H), 7.38 (m, 1H), 7.63 (m, 1H), 7.95 (m, 1H), 8.13 (m, 1H); ^{13}C NMR (400 MHz, $CDCl_3$): δ 9.60, 13.60, 27.28, 28.99, 51.97, 127.67, 129.10, 129.35, 137.26, 140.94, 142.49, 167.61.

3-(Tributylstannyl)benzoic acid (6-3):
Methyl 3-(tributylstannyl)benzoate **(6-2)** (316 mg, 0.74 mmol) was dissolved in 4 mL of ethanol in a round bottom flask. Then, 1M KOH (2 eq) was added and the flask was heated to 55 ^{o}C. After all the reagents were consumed, the reaction was cooled to room temperature and the solvent was removed using rotary evaporation. Subsequently, the reaction mixture was neutralized with 2N HCl until there was no white precipitate. Then, the aqueous layer was washed with DCM (20 mL X 3) and the combined organic layer was washed with water and was dried using anhydrous magnesium sulfate. Finally, the product was dried under reduced pressure to obtain the desired compound (**6-3)** as an oil in quantitative yield: ^{1}H NMR (300 MHz, $CDCl_3$): δ 0.89 (m, 9H), 1.1 (m, 6H), 1.35 (m, 6H), 1.55 (m, 6H), 7.42 (m, 1H), 7.69 (m, 1H), 8.02 (m, 1H), 8.20 (m, 1H); ^{13}C NMR (300 MHz, $CDCl_3$): δ 9.65, 13.63, 27.30, 29.01, 127.82, 128.51, 129.77, 137.91, 141.87, 142.77, 172.78.

7,10,13-Tris(triethylsilyl)-DAB III (6-4):[41]
10-DAB III (51 mg, 0.09 mmol) and imidazole (6 eq) were dissolved in 0.5 mL of DMF in around bottom flask. Then, triethylsilyl chloride (TESCL) (5 eq) was added drop wise and the reaction mixture was stirred overnight at room temperature. After all the starting materials were consumed, the mixture was diluted with ethyl acetate. Then, the mixture was washed with a saturated aqueous solution of ammonium chloride, water, and brine, dried over anhydrous $MgSO_4$ and concentrated *in vacuo*. Finally, the crude product was purified by column chromatography on silica gel (hexanes:EtOAc = 10:1) to give **6-4** as a white solid (36 mg) in 87 % yield: ^{1}H NMR (300 MHz, $CDCl_3$): δ 0.65 (m, 18 H), 0.99 (m, 27 H), 1.11 (s, 3 H), 1.18 (s, 3 H), 1.64 (s, 3 H), 1.87 (m, 1 H), 1.97 (s, 3 H), 2.08 (dd, J = 15.2, 8.8 Hz, 1 H), 2.21 (dd, J = 15.1, 8.2 Hz, 1 H), 2.27 (s, 3 H), 2.51 (m, 1 H), 3.84 (d, J = 7.0 Hz, 1 H), 4.13 (d, J = 8.3 Hz, 1 H), 4.27 (d, J = 8.3 Hz, 1 H), 4.40 (dd, J = 10.5, 6.6 Hz, 1 H), 4.92 (m, 2 H), 5.18 (s, 1 H), 5.61 (d, J = 7.1 Hz, 1 H), 7.44 (t, J = 7.3 Hz, 2 H), 7.57 (t, J = 7.3 Hz, 1 H), 8.07 (d, J = 7.4 Hz, 1 H); ^{13}C NMR (400 MHz, $CDCl_3$): δ 4.7, 5.2, 5.9, 6.9, 10.4, 14.8, 20.5, 22.4, 26.3, 37.3, 19.8, 42.4, 46.8, 58.2, 68.3, 72.6, 75.4, 75.7, 76.6, 79.5, 80.7, 83.9, 128.5, 129.6, 130.0, 133.4, 135.7, 139.3, 167.1, 169.7, 205.6.

2-Debenzoyl-7,10,13-tris(triethylsilyl)-DAB III (6-5):[41]
7,10,13-tris(triethylsilyl)-10-deacetyl baccatin III **(6-4)** (346mg, 0.39 mmol) was dissolved in 6 mL of anhydrous THF in a round bottom flask. A solution of Red-Al in toluene (65% wt, 2.5 eq) was added drop wise at -15 ºC and the reaction mixture was stirred for 4 hours at -15 ºC. After all the starting materials were consumed, the reaction

was quenched with aqueous saturated ammonium chloride solution. Then, the aqueous layer was extracted using ethyl acetate and the combined extracts were dried over anhydrous $MgSO_4$ and concentrated *in vacuo.* Finally, the crude product was purified by column chromatography on silica gel (hexanes:EtOAc = 4:1) to give **6-5** as a white solid (283 mg) in 93 % yield: ^{1}H NMR (300 MHz, $CDCl_3$): δ 0.57 (m, 18 H), 0.94 (m, 27 H), 1.11 (s, 3 H), 1.55 (s, 3 H), 1.87 (m, 1 H), 1.88 (s, 3 H), 1.94 (m, 1 H), 2.00 (m, 1 H), 2.12 (s, 3 H), 2.47 (m, 1 H), 3.42 (d, J = 6.6 Hz, 1 H), 3.80 (d, J = 6.6 Hz, 1 H), 4.31 (dd, J = 10.4, 6.5 Hz, 1 H), 4.50 (d, J = 9.0 Hz, 1 H), 4.57 (d, J = 9.1 Hz, 1 H), 4.63 (s, 1 H), 4.89 (d, J = 8.3 Hz, 1 H), 4.91 (m, 1 H), 5.08 (s, 1 H); ^{13}C NMR (400 MHz, $CDCl_3$): δ 4.7, 5.1, 5.8, 6.7, 6.8, 10.5, 14.4, 20.5, 22.3, 37.3, 40.3, 42.5, 58.1, 65.0, 66.3, 72.6, 74.6, 75.7, 77.9, 78.5, 81.9, 83.7, 126.8, 127.4, 128.4, 135.9, 138.9, 169.6, 206.3.

2-(3-Methylbenzoyl)-7,10,13-tris(triethylsilyl)-DAB III (6-6):
2-debenzoyl-7,10,13-tris(triethylsilyl)-10-deacetylbaccatin III **(6-5)** (102 mg, 0.13 mmol), *m*-toluic acid (8 eq) and DMAP (8 eq) were dissolved in 0.32 mL of toluene and 0.52 mL of DMF in a round bottom flask. Then 1,3-diisopropylcarbodiimide (DIC, 8 eq) was added drop wise and the reaction mixture was stirred at 70 ^{o}C overnight. After completion of the reaction, the precipitate was filtered off and washed with DCM. Then, the filtrate was washed with a saturated sodium bicarbonate solution, water and brine and dried over $MgSO_4$, and concentrated *in vacuo*. Finally, the crude was purified by column chromatography on silica gel (hexanes/EtOAc) to give **6-6** as a white solid (79 mg) in 67 % yield: ^{1}H NMR (400 MHz,$CDCl_3$): δ 0.6 (m, 19 H), 0.9 (m, 30 H), 1.09 (s, 3 H), 1.18 (s, 3 H), 1.33 (s, 3 H), 1.39 (s, 1 H), 1.90 (m, 4 H), 2.15 (s, 3 H), 3.64 (d, 1 H), 3.85 (m, 1 H), 4.00 (d, 1 H), 4.11 (d, 1 H), 4.55 (m, 1 H), 4.97 (m, 1 H), 5.07 (s, 1 H), 5.70 (m, 1 H), 7.57 (t, 1 H), 7.8 (m, 1 H), 7.95 (m, 1 H), 8.15 (m, 1 H),

2-(3-Methylbenzoyl)-DAB III (6-7):
The compound **6-6** (153 mg, 0.17 mmol) was taken in a flask which was inerted and cooled to 0 °C. Acetonitrile and dry pyridine (4 mL each, 1:1) was added to dissolve the solid compound. Then HF/Pyridine was added (2 mL) dropwise, the reaction was allowed to warm to room temperature and stirred overnight. TLC (1:1 hexane:ethyl acetate) indicated complete conversion and the reaction was quenched with saturated $NaHCO_3$ slowly and stirred. The reaction mixture was diluted with ethyl acetate and the organic layer was washed with saturated $NaHCO_3$ several times to remove unreacted HF. The combined organic layers were then washed with copper sulphate solution to remove pyridine till no color change was observed. The organic layer was then washed with distilled water to remove copper sulphate, dried over brine and anhydrous magnesium sulphate and concentrated *in vacuo*. The pure product was obtained by performing flash chromatography (5:1, 1:1 hexane:ethyl acetate) as a white solid in quantitative (95 mg) yield. ^{1}H NMR (CDCl3, 400 MHz): δ 1.00 (s, 6 H), 1.4 (s, 3 H), 1.6 (m, 1 H), 1.88 (s, 1 H), 2.04 (s, 1 H), 2.12 (s, 3 H), 2.28 (s, 3 H), 2.40 (s, 3 H), 2.88 (m, 2 H), 3.87 (m, 1 H), 4.01 (d, 1 H), 4.13 (m, 1 H), 4.47 (m, 1 H), 4.91 (t, 1 H), 5.10 (s, 1 H), 5.76 (m, 1 H), 7.39 (m, 2 H), 7.74 (m, 2 H), ^{13}C NMR (300 MHz, $CDC1_3$): 14.29, 15.08, 20.26, 21.20, 22.49, 25.60, 36.03, 39.40, 42.48, 49.41, 55.19, 67.96, 69.83, 71.65, 73.13, 76.11, 86.28, 90.01, 126.65, 128.53, 129.19, 130.09, 134.33, 136.60, 138.52, 143.17, 165.21, 171.62,

214.21. HRMS: (Q-TOF TOF MS ES+) m/z Calculated for $C_{30}H_{38}O_{10}Na$ 581.2363 Found: 581.2361 (Δ = - 0.3 ppm).

2-(3-Methylbenzoyl)-7-triethylsilyl-DAB III (6-8):
A flask containing **6-7** (48 mg, 0.086 mmol) and imidazole (4 eq) was inerted. Anhydrous DMF (c 0.04 M) was added via syringe to dissolve the solids in the flask. The temperature of the flask was maintained at 0 ˚C. Triethylsilylchloride (3 eq) was then added dropwise via syringe in the flask. The reaction was monitored by TLC (1:1 hexane:ethyl acetate) and quenched with saturated ammonium chloride solution after 45 min. The reaction mixture was diluted with ethyl actetate and the organic and aqueous layer was separated. The organic layer was washed with brine, dried over anhydrous magnesium sulphate and concentrated *in vacuo*. The pure product **6-8** was obtained by performing flash chromatography (4:1, 1:1 hexane:ethyl acetate) as a white solid in quantitative (58 mg) yield. ^{1}H NMR (300 MHz, $CDC1_3$): δ 0.55 (m, 7 H), 0.92 (m, 10 H), 1.6 (s, 2 H), 1.7 (s, 3 H), 2.07 (m, 5 H), 2.26 (m, 5 H), 2.4 (s, 3 H), 2.86 (m, 2 H), 3.95 (d, 1 H), 4.13 (m, 1 H), 4.47 (m, 1 H), 4.91 (t, 1 H), 5.16 (s, 1 H), 5.58 (d, 1 H), 7.37 (m, 2 H), 7.90 (m, 2 H)

2-(3-Methylbenzoyl)-7-triethylsilyl-10-cyclopropanecarbonyl-DAB III (6-9):
A flask containing **6-8** (67 mg, 0.09 mmol) was inerted and dry THF (c 0.06 M) was added to dissolve it. The flask was cooled to -40 ^{o}C. LiHMDS 1.0 M in THF (1.1 eq) was added dropwise *via* syringe. The mixture was stirred at -40 ^{o}C for 5 min, and then cyclopropanecarbonyl chloride (1.05 eq) was added dropwise. After 2 h, the reaction was quenched with aqueous saturated NH_4Cl (10 mL), extracted with CH_2Cl_2 (x 3), and the combined organic layers were dried over anhydrous $MgSO_4$ and concentrated *in vacuo*. The crude product was purified on a silica gel column (hexane : ethylacetate = 4 : 1 followed by 2 : 1 and then 1 : 1) to afford **6-9** as a white solid (44 mg, 60 % yield).
^{1}H NMR (400 MHz, $CDC1_3$): δ 0.529 (m, 7 H), 0.88 (m, 12 H), 0.99 (m, 4 H), 1.14 (m, 4 H), 1.64 (s, 1H), 1.73 (s, 3H), 1.87 (m, 1 H), 2.16 (s, 3H), 2.24 (s, 6 H), 2.38 (s, 3H), 2.48 (m, 1 H), 3.83 (d, 1 H), 4.09 (d, 1 H), 4.27 (d, J = 4.8 Hz, 1 H), 4.45 (m, 1 H), 4.79 (m, 1 H), 4.92 (d, J = 8.0 Hz, 1 H), 5.58 (d, J = 7.2 Hz, 1 H), 6.43 (s, 1 H), 7.34 (m, 2 H), 7.88 (m, 2 H), ^{13}C NMR ($CDCl_3$, 400 MHz) δ 5.2, 6.7, 8.49, 8.61, 9.92, 12.99, 14.87, 20.14, 21.35, 22.59, 26.80, 37.23, 38.27, 42.76, 47.26, 58.60, 67.97, 72.35, 74.6, 75.54, 78.77, 80.91, 84.21, 127.22, 128.45, 129.32, 130.73, 132.78, 134.31, 138.28, 143.85, 167.21, 170.65, 173.14, 202.29.

3'-(2-Methyl-1-propenyl)-2-(3-methylbenzoyl)-7-triethylsilyl-10-cyclopropanecarbonyl-DAB III (6-10):
A flask containing **6-9** (69 mg, 0.09 mmol) was inerted and dry THF (7 mL) was added to dissolve it. *β*-lactam (1.5 eq) was dissolved in 2 mL of dry THF and added to the reaction flask. The flask was cooled to -40 ^{o}C and LiHMDS (1 M in THF solution, 1.5 eq) was added dropwise via syringe and the reaction was monitored by TLC (2:1 hexane:ethyl acetate). The reaction was quenched after 3 h with saturated ammonium chloride solution and extracted with dichloromethane three times. The combined organic layers was dried with brine and anhydrous magnesium sulphate and concentrated *in vacuo*. The pure product **6-10** was obtained by performing flash chromatography (20:1,

4:1 hexane:ethyl acetate) as a white solid in 88 % (90 mg) yield. ^{1}H NMR (400 MHz, $CDC1_3$): δ 0.56 (m, 8 H), 0.91 (m, 18 H), 1.1 (m, 24 H), 1.2-1.3 (m, 22 H), 2.00 (s, 3 H), 2.36 (s, 3 H), 2.41 (s, 3 H), 3.83 (d, 1 H), 4.19 (d, 1 H), 4.31 (d, 1 H), 4.43 (m, 1 H), 4.84 (d, 1 H), 4.95 (d, 1 H), 5.33 (d, 1 H), 5.67 (d, 1 H), 6.08 (m, 1 H), 6.48 (s, 1 H), 7.37 (m, 2 H), 7.91 (m, 2 H), ^{13}C NMR (400 MHz, $CDC1_3$): δ 5.31, 6.74, 8.60, 8.70, 10.06, 12.55, 12.96, 14.09, 14.31, 17.96, 18.02, 18.58, 21.33, 22.51, 22.67, 25.65, 26.30, 28.25, 29.33, 31.91, 35.48, 37.19, 43.23, 46.75, 58.33, 71.91, 72.22, 74.80, 74.90, 75.32, 78.85, 79.43, 81.10, 84.29, 122.19, 127.33, 128.43, 129.34, 130.75, 133.39, 134.29, 138.22, 140.88, 155.14, 167.01, 169.71, 171.88, 173.04, 202.06.

SB-T-121402:

A flask containing **6-10** (51 mg, 0.044 mmol) was inerted and 2 mL of dry pyridine/acetonitrile (1:1) was added to dissolve it. The flask was cooled to 0 ^{o}C and HF/pyridine (70:30, 0.5 mL) was added dropwise at 0 ^{o}C. The mixture was stirred at room temperature overnight. The reaction was quenched with aqueous saturated sodium carbonate solution, diluted with ethyl acetate, washed with aqueous saturated copper sulfate solution (x 3) and water, dried over anhydrous magnesium sulfate and concentrated *in vacuo* to afford **SB-T-121402** as a white solid in 73 % yield (28 mg). ^{1}H NMR (400 MHz, $CDC1_3$): δ 0.99 (m, 2 H), 1.14 (m, 5 H), 1.34 (s, 9 H), 1.66 (s, 3 H), 1.76 (d, 8 H), 1.89 (s, 3 H), 2.35 (s, 3 H), 2.42 (s, 3 H), 3.80 (d, 1 H), 4.18 (m, 2 H), 4.30 (d, 1 H), 4.41 (m, 1 H), 4.76 (m, 2 H), 4.96 (d, 1 H), 5.32 (d, 1 H), 5.64 (d, 1 H), 6.17 (t, 1 H), 6.30 (s, 1 H), 7.37 (m, 2 H), 7.90 (m, 2 H), ^{13}C NMR (400 MHz, $CDC1_3$): δ 9.14, 9.38, 9.48, 13.01, 14.96, 18.54, 21.32, 21.93, 22.33, 25.68, 26.68, 28.20, 29.67, 35.51, 35.57, 43.17, 45.65, 51.54, 58.56, 72.23, 72.39, 73.72, 74.94, 75.43, 76.47, 79.18, 79.92, 81.10, 84.43, 120.67, 127.30, 128.51, 129.13, 130.79, 132.94, 134.42, 138.33, 142.63, 155.39, 167.07, 169.97, 175.11, 203.91, HRMS: (Q-TOF TOF MS ES+) *m/z* Calculated for $C_{46}H_{62}O_{15}N^{+}$: 868.4119 Found: 868.4106 (Δ = -1.5 ppm).

2-(3-Tributylstannylbenzoyl)-7,10,13-tris(triethylsilyl)-DAB III (6-11):

2-Debenzoyl-7,10,13-tris(triethylsilyl)-10-deacetylbaccatin III **(6-5)** (116 mg, 0.15 mmol), 3-tributylstannylbenzoic acid (**6-3**, 8 eq) and DMAP (8 eq) were dissolved in 0.37 mL of toluene and 0.6 mL of DMF in a round bottom flask. Then DIC (8 eq) was added drop wise and the reaction mixture was stirred at 70 ^{o}C overnight. After completion, the precipitate was filtered and washed with DCM. Then, the filtrate was washed with a saturated sodium bicarbonate solution, dried over $MgSO_4$, and concentrated *in vacuo*. Finally, the residue was purified by column chromatography on silica gel (hexanes/EtOAc) to give **6-11** as a white solid (154 mg) in 88 % yield: ^{1}H NMR (400 MHz, $CDCl_3$): δ 0.65 (m, 17 H), 0.87 (t, 9 H), 0.99 (m, 26 H), 1.30 (m, 11 H), 1.90 (s, 3 H), 2.14 (s, 3 H), 2.85 (m, 1 H), 3.60 (d, 1 H), 3.82 (d, 1 H), 3.96 (d, 1 H), 4.08 (d, 1 H), 4.55 (m, 1 H), 4.97 (m, 1 H), 5.07 (s, 1 H), 5.66 (m, 1 H), 7.40 (t, 1 H), 7.67 (d, 1 H), 7.85 (d, 1 H), 8.05 (m, 1 H), ^{13}C NMR (400 MHz, $CDCl_3$): δ 4.82, 5.21, 5.55, 6.61, 6.86, 6.89, 9.67, 13.61, 13.90, 14.33, 20.89, 22.29, 25.17, 27.29, 28.89, 29.00, 29.10, 37.96, 40.65, 42.88, 50.78, 55.59, 68.53, 70.83, 71.92, 72 89, 86.34, 90.15, 127.95, 128.58, 129.08, 137.24, 137.67, 139.24, 141.54, 143.07, 165.53, 170.98, 206.44. HRMS: (Q-TOF TOF MS ES+) m/z Calculated for $C_{59}H_{105}O_{10}Si_3{}^{120}Sn$ 1177.6038 Found: 1177.6044 (Δ = 0.5 ppm).

2-(3-Tributylstannylbenzoyl)-DAB III (6-12):
The compound **6-11** (225 mg, 0.19 mmol) was taken in a flask which was inerted and cooled to 0 °C. Acetonitrile and dry pyridine (4 mL each, 1:1) was added to dissolve the solid compound. Then HF/Pyridine was added (70:30, 2 mL) dropwise, the reaction was allowed to warm to room temperature and stirred overnight. TLC (1:1 hexane:ethyl acetate) indicated complete conversion and the reaction was quenched with saturated $NaHCO_3$ slowly and stirred. The reaction mixture was diluted with ethyl acetate and the organic layer was washed with saturated $NaHCO_3$ several times to remove unreacted HF. The combined organic layers were then washed with copper sulphate solution to remove pyridine till no color change was observed. The organic layer was then washed with distilled water to remove copper sulphate, dried over brine and anhydrous magnesium sulphate and concentrated *in vacuo*. The pure product **6-12** was obtained by performing flash chromatography (5:1, 1:1 hexane:ethyl acetate) as a white solid in quantitative (159 mg) yield. ^{1}H NMR (400 MHz, $CDCl_3$): δ 0.85 (t, 9 H), 1.0 (m, 3 H), 1.05 (m, 6 H), 1.12 (m, 3 H), 1.29 (m, 8 H), 1.32 (s, 9 H), 1.40 (s, 3 H), 1.48 (m , 5 H), 1.91 (s, 3 H), 2.08 (s, 3 H), 3.83 (m, 2 H), 4.01 (d, 1 H), 4.11 (d, 1 H), 4.45 (m, 1 H), 4.89 (m. 1 H), 5.08 (s, 1 H), 5.73 (m, 1 H), 7.40 (m, 1 H), 7.68 (d, 1 H), 7.82 (d, 1 H), 8.02 (d, 1 H), ^{13}C NMR (400 MHz, $CDCl_3$): δ 6.54, 9.68, 13.56, 13.62, 14.02, 15.07, 17.50, 20.23, 22.46, 25.59, 26.81, 27.29, 28.89, 29.10, 36.26, 39.39, 42.48, 49.50, 55.18, 67.94, 69.90, 71.63, 73.15, 86.24, 90.03, 127.97, 128.64, 129.04, 136.57, 137.25, 141.64, 143.16, 165.51, 171.63, 214.02.

2-(3-Tributylstannylbenzoyl)-7-triethylsilyl-DAB III (6-13):
A flask containing **6-12** (197 mg, 0.23 mmol) and imidazole (4 eq) was inerted. Anhydrous DMF (c 0.04 M) was added via syringe to dissolve the solids in the flask. The temperature of the flask was maintained at 0 ˚C. Triethylsilylchloride (3 eq) was then added dropwise via syringe in the flask. The reaction was monitored by TLC (1:1 hexane:ethyl acetate) and quenched with saturated ammonium chloride solution after 45 min. The reaction mixture was diluted with ethyl actetate and the organic and aqueous layer was separated. The organic layer was washed with brine, dried over anhydrous magnesium sulphate and concentrated *in vacuo*. The pure product **6-13** was obtained by performing flash chromatography (hexane:ethyl acetate) as a white solid in 66 % (148 mg) yield. ^{1}H NMR (300 MHz, $CDC1_3$): δ 0.56 (m, 6 H), 0.93 (m, 23 H), 1.09 (m, 5 H), 1.38 (m, 3 H), 1.54 (m, 14 H), 2.01 (s, 3 H), 2.13 (s, 3 H), 2.29 (m, 2 H), 2.45 (m, 1 H), 2.85 (m, 1 H), 3.75 (d, 1 H), 3.86 (d, 1 H), 4.00 (d, 1 H), 4.07 (d, 1 H), 4.27 (s, 1 H), 4.61 (m, 1 H), 4.9 (m, 1 H), 5.07 (s, 1 H), 5.64 (m, 1 H), 7.41 (t, 1 H), 7.69 (d, 1 H), 7.87 (m, 1 H), 8.06 (m, 1 H)

2-(3-Tributylstannylbenzoyl)-7-triethylsilyl-10-cyclopropanecarbonyl-DAB III (6-14):
A flask containing **6-13** (148 mg, 0.156 mmol) was inerted and dry THF (c 0.06 M) was added to dissolve it. The flask was cooled to -40 ^{o}C. LiHMDS 1.0 M in THF (1.1 eq) was added dropwise *via* syringe. The mixture was stirred at -40 ^{o}C for 5 min, and then cyclopropanecarbonyl chloride (1.05 eq) was added dropwise. After 2 h, the reaction was

quenched with aqueous saturated NH_4Cl (10 mL), extracted with CH_2Cl_2 (x 3), and the combined organic layers were dried over anhydrous $MgSO_4$ and concentrated *in vacuo*. The crude product was purified on a silica gel column (hexane:ethylacetate) to afford **6-14** as a white solid (136 mg, 86 % yield). ^{1}H NMR (300 MHz, $CDC1_3$): δ 0.60 (m, 5 H), 0.95 (m, 17 H), 1.16 (m, 10 H), 1.27 (t, 3 H), 1.39 (m, 8 H), 1.59 (m, 8 H), 1.73 (m, 1 H), 2.04 (s, 2 H), 2.06 (s, 3 H), 2.12 (s, 3 H), 2.32 (d, 2 H), 2.52 (m, 1 H), 2.87 (m, 1 H), 3.67 (d, 1 H), 3.85 (d, 1 H), 3.99 (d, 1 H), 4.12 (m, 2 H), 4.64 (m, 1 H), 4.88 (m, 1 H), 5.65 (m, 1 H), 6.41 (s, 1 H), 7.40 (m, 1 H), 7.66 (m, 1 H), 7.85 (m, 1 H), 8.05 (m, 1 H)
^{13}C NMR (400 MHz, $CDC1_3$): δ 5.04, 6.74, 8.42, 8.63, 9.68, 12.96, 13.33, 13.62, 14.17, 14.83, 20.45, 22.43, 25.62, 27.30, 28.90, 29.01, 29.10, 38.22, 39.03, 42.63, 50.75, 56.11, 60.37, 68.03, 70.52, 72.03, 73.16, 75.98, 76.08, 85.78, 90.16, 127.97, 128.55, 129.08, 134.58, 137.24, 141.57, 143.09, 143.88, 165.48, 171.31, 172.99, 202.72.

3'-(2-Methyl-1-propenyl)-2'-triisopropylsilyl-2-(3-tributylstannylbenzoyl)-7-triethylsilyl-10-cyclopropanecarbonyl-DAB III (6-15):
A flask containing **6-14** (136 mg, 0.13 mmol) was inerted and dry THF (10 mL) was added to dissolve it. *β*-lactam (1.5 eq) was dissolved in 3 mL of dry THF and added to the reaction flask. The flask was cooled to -40 ^{o}C and LiHMDS (1 M in THF solution, 1.5 eq) was added dropwise via syringe and the reaction was monitored by TLC (2:1 hexane:ethyl acetate). The reaction was quenched after 3 h with saturated ammonium chloride solution and extracted with dichloromethane three times. The combined organic layers was dried with brine and anhydrous magnesium sulphate and concentrated *in vacuo*. The pure product **6-15** was obtained by performing flash chromatography (20:1, 4:1 hexane:ethyl acetate) as a white solid in 45 % (85 mg) yield. ^{1}H NMR (300 MHz, $CDC1_3$): δ 0.56 (m, 8 H), 0.96 (m, 25 H), 1.05 (m, 27 H), 1.25 (m, 18 H), 1.40 (m, 10 H), 1.53 (m, 7 H), 1.59 (m, 7 H), 1.73 (m, 7 H), 1.86 (s, 3 H), 2.03 (s, 2 H), 2.15 (s, 3 H), 2.36 (m, 2 H), 3.58 (d, 1 H), 3.83 (d, 1 H), 4.0 (d, 1 H), 4.10 (m, 2 H), 4.36 (m, 1 H), 4.60 (m, 1 H), 5.28 (m, 1 H), 5.67 (m, 1 H), 6.12 (m, 1 H), 6.39 (s, 1 H), 7.39 (m, 1 H), 7.68 (m, 1 H), 7.85 (m, 1 H), 8.05 (m, 1 H), ^{13}C NMR (300 MHz, $CDC1_3$): δ 5.04, 5.79, 6.56, 6.74, 8.54, 8.71, 9.70, 11.41, 12.53, 12.89, 13.63, 14.18, 14.26, 17.51, 17.93, 17.99, 18.59, 21.53, 22.34, 25.19, 25.61, 26.83, 27.03, 27.31, 27.60, 27.83, 28.28, 28.91, 29.02, 29.12, 29.68, 35.69, 37.72, 43.10, 50.42, 52.15, 55.63, 56.66, 60.38, 70.28, 71.76, 72.10, 72.97, 75.08, 75.26, 79.57, 86.14, 90.49, 127.99, 128.45, 129.09, 135.75, 137.26, 140.60, 141.65, 143.14, 155.10, 165.54, 170.54, 171.13, 171.86, 172.95, 202.42.

2-(3-Tributylstannylbenzoyl)-SB-T-1214 (6-16):
A flask containing **6-15** (76 mg, 0.05 mmol) was inerted and 2 mL of dry pyridine/acetonitrile (1:1) was added to dissolve it. The flask was cooled to 0 ^{o}C and HF/pyridine (70:30, 0.5 mL) was added dropwise at 0 ^{o}C. The mixture was stirred at room temperature overnight. The reaction was quenched with aqueous saturated sodium carbonate solution, diluted with ethyl acetate, washed with aqueous saturated copper sulfate solution (x3) and water, dried over anhydrous magnesium sulfate and concentrated *in vacuo* to afford **6-16** as a white solid in quantitative yield (57 mg). ^{1}H NMR (300 MHz, $CDC1_3$): δ 0.87 (t, 9 H), 0.96 (m, 3 H), 1.08 (m, 10 H), 1.2-1.4 (m, 20 H), 1.21 (m, 1 H), 1.54 (m, 6 H), 1.68 (s, 3 H), 1.71 (s, 3 H), 1.77 (s, 3 H), 2.14 (s, 2 H), 2.4 (m, 2 H), 2.82 (m, 1 H), 3.58 (d, 1 H), 3.80 (d, 1 H), 4.09 (m, 3 H), 4.52 (m, 1 H),

4.67 (m, 1 H), 5.24 (d, 1 H), 5.72 (m, 1 H), 6.15 (m, 1 H), 6.28 (s, 1 H), 7.37 (t, 1 H), 7.6 (d, 1 H), 7.81 (d, 1 H), 8.02 (m, 1 H), ^{13}C NMR (300 MHz, $CDC1_3$): δ 8.92, 9.11, 9.68, 12.96, 13.43, 13.63, 14.75, 17.50, 18.61, 22.07, 22.35, 25.48, 25.64, 26.82, 27.02, 27.30, 27.58, 27.82, 28.24, 28.90, 29.01, 29.10, 35.37, 35.83, 43.07, 49.30, 51.57, 55.50, 69.83, 71.57, 72.89, 73.11, 73.51, 75.77, 76.35, 79.96, 86.29, 90.43, 120.50, 127.97, 128.41, 129.07, 135.30, 137.25, 137.85, 141.63, 142.11, 143.11, 155.33, 165.49, 170.77, 173.36, 174.12, 205.58, HRMS: (Q-TOF TOF MS ES+) *m/z* Calculated for $C_{57}H_{86}O_{15}NSn^+$: 1144.5034 Found: 1144.5050 (Δ = - 1.39 ppm).

SB-T-121402 (Stille coupling):

A small vial containing $Pd_2(dba)_3$ (0.6 mg), P(*o*-tolyl)$_3$ (0.78 mg) (1:4) was inerted and 200 μL of anhydrous DMF was added to it and stirred for 30 min till yellow color was observed. Then methyl iodide (0.04 μL, 0.6 μmol, 1 eq) was added to it and the whole reaction mixture was transferred to another small vial containing compound **6-16** (3.4 mg, 0.003 μmol, 5 eq), CuCl (5 eq) and K_2CO_3 (5 eq) in 30 μL anhydrous DMF under inert atmosphere. The vial was heated to 65 ^{o}C and the reaction was monitored after 5 min and stopped after 10 min. The formation of the desired SB-T-121402 was confirmed from TLC comparison as well as from HPLC. The product and the tin precursor were well separated in HPLC column and the desired compound elutes out first in a reverse phase Luna PFP column.

References

References for Chapter 1:

1. Jemal, A.; Siegel, R.; Ward, E.; Hao, Y.; Xu, J.; Thun, M. J., Cancer Statistics, 2009. *CA Cancer J Clin* **2009,** 59, (4), 225-249.
2. http://www.iarc.fr/en/media-centre/iarcnews/2010/GLOBOCAN2008.pdf.
3. http://64.202.120.86/upload/image/articles/2008/smart-bombing-cancer/cell-grow.jpg.
4. Goodman, J., Walsh, Vivien, *The Story of Taxol: Nature and Politics in the Pursuit of an Anti-Cancer Drug*. Cambridge Univ. Press: 2001.
5. Georg, G. I.; Chen, T. T.; Ojima, I.; Vyas, D. M., *Taxane Anticancer Agents: Basic Science and Current Status*. American Chemical Society: Washington, D. C., 1995.
6. Wani, M. C.; Taylor, H. L.; Wall, M. E.; Coggon, P.; McPhail, A. T., Plant antitumor agents. VI. The isolation and structure of taxol, a novel antileukemic and antitumor agent from Taxus brevifolia. *J. Am. Chem. Soc.* **1971,** 93, (9), 2325-7.
7. Kumar, N., Taxol-Induced Polymerization of Purified Tubulin. *J. Biol. Chem.* **1981,** 256, (20), 10435-10441.
8. Schiff, P. B.; Fant, J.; Horwitz, S. B., Promotion of Microbubule Assembly *in vitro* by Taxol. *Nature* **1979,** 277, 665-667.
9. Schiff, P. B.; Horwitz, S. B., Taxol stabilizes microtubules in mouse fibroblast cells. *Proc. Natl. Acad. Sci. USA* **1980,** 77, (3), 1561-1565.
10. Schiff, P. B.; Horwitz, S. B., Taxol Assembles Tubulin in the Absence of Exogenous Guanosine 5'-Triphosphate or Microtubule-Associated Proteins. *Biochemistry* **1981,** 20, 3247-3252.
11. Abal, M.; Andreu, J. M.; Barasoain, I., Taxanes: microtubule and centrosome targets, and cell cycle dependent mechanisms of action. *Curr. Cancer Drug Targets* **2003,** 3, (3), 193-203.
12. Wilson, L. J., M.A., *Microtubules*. John Wiley and Sons, Inc.: New York, 1994.
13. Campbell, N. A., *Biology*. Benjamin/Cummings Publishing Co.: Menlo Park, CA, 1987.
14. http://kirschner.med.harvard.edu/files/images/cell_cycle.jpg
15. www.itg.uiuc.edu/technology/atlas/structures/actin/images/actin_microtubules.jpg &imgrefurl.
16. Wu, X. D., Synthesis and biological evaluation of tumor-targeting taxane based anticancer agents and mdr modulators. In *Ph.D. Dissertation*, State University of New York at Stony Brook: 2003.
17. Caplow, M.; Ruhlen, R.; Shanks, J.; Walker, R. A.; Salmon, E. D., Stabilization of microtubules by tubulin-GDP-inorganic phosphate subunits. *Biochemistry* **1989,** 28, (20), 8136-8141.

18. Jose Fernando Dfaz, J. M. A., Assembly of purified GDP-tubulin into microtubules induced by Taxol and Taxotere: Reversibility, ligand stoichiometry, and competition. *Biochemistry* **1993,** 32, 2141-2155.
19. Abal, M. S., A. A.; Amat-Guerri, F.; Acuna, A. U.; Andreu, J. M.; Barasoain, I Centrosome and spindle pole microtubules are main targets of a fluorescent taxoid inducing cell death. *Cell Motil. Cytoskeleton* **2001,** 49, 1-15.
20. Jordan, M. A. W., K.; Gardiner, S.; Derry, W. B, Mitotic block induced in Hela cells by low concentrations of paclitaxel (Taxol) results in abnormal mitotic exit and apoptotic cell death. *Cancer Res.* **1996,** 56, 816-825.
21. Lin, H. L. C., Y. F.; Liu, T. Y.; Wu, C. W.; Chi, C. W., Submicromolar Paclitaxel induces apoptosis in human gastric cancer cells at early G1 phase. *Anticancer Res.* **1998,** 18, 3443-3449.
22. Woods, C. M. Z., J.; McQueney, P. A.; Bollag, D.; Lazarides, E, Taxol-induced mitotic block triggers rapid onset of a p53-independent apoptotic pathway. *Mol. Med.* **1995,** 1, 506-526.
23. Donaldson, K. L. G., G.; Kiener, P. A.; Wahl, A. F., Activation of p34cdc2 coincident with taxol-induced apoptosis. *Cell Growth Differ.* **1994,** 5, 1041-1050.
24. Huang, T. S. S., C. H.; Yang, W. K.; Whang Peng, J., Activation of CDC 25 phosphatase and CDC 2 kinase involved in GL331-induced apoptosis. *Cancer Res.* **1997,** 57, 2974-2978.
25. Ibrado, A. M. K., C. N.; Bhalla, K., Temporal relationship of CDK1 activation and mitotic arrest to cytosolic accumulation of cytochrome C and caspase-3 activity during taxol-induced apoptosis of human AML (acute myeloid leukemia) HL-60 cells. *Leukemia* **1998,** 12, 1930-1936.
26. Shen, S. C. H., T. S.; Jee, S. H.; Kuo, M. L, Taxol-induced p34cdc2 kinase activation and apoptosis inhibited by 12-O-tetradecanoylphorbol-13-acetate in human breast MCF-7 carcinoma cells. *Cell Growth Differ.* **1998,** 9, 23-29.
27. Blagosklonny, M. V. G., P.; El-Deiry, W. S.; Kingston, D. G. I.; Higgs, P. I.; Neckers, L.; Fojo, T, Raf-1/bcl-2 phosphorylation: a step from microtubule damage to cell death. *Cancer Res.* **1997,** 57, 130-135.
28. Haldar, S. J., N.; Croce, C. M., Inactivation of Bcl-2 by phosphorylation. . *Proc. Natl. Acad. Sci. USA* **1995,** 92, 4507-4511.
29. Haldar, S. B., A.; Croce, C. M., Serine-70 is one of the critical sites for drug-induced Bcl2 phosphorylation in cancer cells. *Cancer Res.* **1998,** 58, 1609-1615.
30. Roth, W. W., B.; Grimmel, C.; Dichgans, J.; Weller, M. . Br. J., Taxol-mediated augmentation of CD95 ligand-induced apoptosis of human malignant glioma cells: association with bcl-2 phosphorylation but neither activation of p53 nor G2/M cell cycle arrest. *Cancer* **1998,** 77, 404-411.
31. Milas, L. H., N. R.; Kurdoglu, B.; Mason, K. A.; Meyn, R. E.; Stephens, L. C.; Peters, L. J, Kinetics of mitotic arrest and apoptosis in murine mammary and ovarian tumors treated with Taxol. *Cancer Chemother. Pharmacol.* **1995,** 35, 297-303.
32. Milross, C. G. M., K. A.; Hunter, N. R.; Chung, W. K.; Peters, L. J.; Milas, L, Relationship of mitotic arrest and apoptosis to antitumor effect of Paclitaxel. *J. Natl. Cancer Inst.* **1996,** 88, 1308-1314.

33. Sorger PK, D. M., Tournebize R, Hyman AA, Coupling cell division and cell death to microtubule dynamics. *Curr. Opin. Cell Biol.* **1997,** 9, 807-814.
34. Cassimeris, L., Accessory protein regulation of microtubule dynamics throughout the cell cycle. *Curr. Opin. Cell Biol.* **1999,** 11, 134-141.
35. Fussenegger, M., Bailey, JE, Molecular regulation of cell-cycle progression and apoptosis in mammalian cells: implications for biotechnology. *Biotechnol. Prog.* **1998,** 14, 807-833.
36. Wang, T. H. W., H. S.; Soong, Y. K. , Paclitaxel-induced cell death: where the cell cycle and apoptosis come together. *Cancer* **2000,** 88, 2619-2628.
37. Nicolaou, K. C.; Dai, W.-M.; Guy, R. K., Chemistry and Biology of Taxol. *Angew. Chem. Int. Ed. Engl.* **1994,** 33, 15-44.
38. Brieva, R.; Crich, J. Z.; Sih, C. J., Chemoenzymatic Synthesis of the C-13 Side Chain of Taxol: Optically-Active 3-Hydroxy-4-phenyl β-Lactam Derivatives. *J. Org. Chem.* **1993,** 58, 1068-1075.
39. Nicolaou, K. C.; Yang, Z.; Liu, J. J.; Ueno, H.; Nantermet, P. G.; Guy, R. K.; Claiborne, C. F.; Renaud, J.; Couladouros, E. A.; Paulvannan, K.; Sorensen, E. J., Total Synthesis of Taxol. *Nature* **1994,** 367, 630-634.
40. Nicolaou, K. C.; Nantermet, P. G.; Ueno, H.; Guy, R. K.; Couladouros, E. A.; Sorensen, E. J., Total Synthesis of Taxol. 1. Retrosynthesis, Degradation, and Reconstitution. *J. Am. Chem. Soc.* **1995,** 117, 624-633.
41. Nicolaou, K. C.; Liu, J.-J.; Yang, Z.; Ueno, H.; Sorensen, E. J.; Claiborne, C. F.; Guy, R. K.; Hwang, C.-K.; Nakada, M.; Nantermet, P. G., Total Synthesis of Taxol. 2. Construction of A and C Ring Intermediates and Initial Attempts to Construct the ABC Ring System. *J. Am. Chem. Soc.* **1995,** 117, 634-644.
42. Nicolaou, K. C.; Yang, Z.; Liu, J.-J.; Nantermet, P. G.; Claiborne, C. F.; Renaud, J.; Guy, R. K.; Shibayama, K., Total Synthesis of Taxol. 3. Formation of Taxol's ABC Ring Skeleton. *J. Am. Chem. Soc.* **1995,** 117, 645-652.
43. Nicolaou, K. C.; Ueno, H.; Liu, J.-J.; Nantermet, P. G.; Yang, Z.; Renaud, J.; Paulvannan, K.; Chadha, R., Total Synthesis of Taxol. 4. The Final Stages and Completion of the Synthesis. *J. Am. Chem. Soc.* **1995,** 117, 653-659.
44. Holton, R. A.; Somoza, C.; Kim, H.-B.; Liang, F.; Biediger, R. J.; Boatman, P. D.; Shindo, M.; Smith, C. C.; Kim, S.; Nadizadeh, H.; Suzuki, Y.; Tao, C.; Vu, P.; Tang, S.; Zhang, P.; Murthi, K. K.; Gentile, L. N.; Liu, J. H., First Total Synthesis of Taxol. 1. Functionalization of the B Ring. *J. Am. Chem. Soc.* **1994,** 116, 1597-1598.
45. Holton, R. A.; Kim, H.-B.; Somoza, C.; Liang, F.; Biediger, R. J.; Boatman, P. D.; Shindo, M.; Smith, C. C.; Kim, S.; Nadizadeh, H.; Suzuki, Y.; Tao, C.; Vu, P.; Tang, S.; Zhang, P.; Murthi, K. K.; Gentile, L. N.; Liu, J. H., First Total Synthesis of Taxol. 2. Completion of the C and D Rings. *J. Am. Chem. Soc.* **1994,** 116, 1599-1600.
46. Wender, P. A.; Mucciaro, T. P., A New and Practical Approach to the Synthesis of Taxol and Taxol Analogues: The Pinene Path. *J. Am. Chem. Soc.* **1992,** 114, 5878-5879.
47. Wender, P. A.; Badham, N. F.; Conway, S. P.; Floreancig, P. E.; Glass, T. E.; Houze, J. B.; Krauss, N. E.; Lee, D.; Marquess, D. G.; McGrane, P. L.; Meng, W.; Natchus, M. G.; Shuker, A. J.; Sutton, J. C.; Taylor, R. E., The Pinene Path to

Taxanes. 6. A Concise Stereocontrolled Synthesis of Taxol. *J . Am. Chem. Soc.* **1997,** 119, 2757-2758.
48. Morihira, K.; Hara, R.; Kawahara, S.; Nishimori, T.; Nakamura, N.; Kusama, H.; Kuwajima, I., Enantioselective total synthesis of taxol. *J. Am. Chem. Soc.* **1998,** 120, 12980-12981.
49. Mukaiyama, T.; Shiina, I.; Sakata, K.; Emura, T.; Seto, K.; Saitoh, M., A Novel Approach to the Synthesis of Taxol. A Synthesis of Optically Active 3,7-Dibenzyloxy-4,8-di-*t*-butyl-dimethylsiloxy-5,5-dimethyl-6-*p*-methoxybenzyloxy-2-ocatnone by Way of Stereoselective Aldol Reactions. *Chem. Lett.* **1995,** 3, 179-180.
50. Mukaiyama, T.; Shiina, I.; Kimura, K.; Akiyama, Y.; Iwadare, H., Synthesis of AB Ring Model System of Taxol *via* Allylation of 8-Membered Ring Compound and Intramolecular Aldol Condensation. *Chem. Lett.* **1995,** 3, 229-230.
51. Mukaiyama, T.; Shiina, I.; Iwadare, H.; Saitoh, M.; Nishimura, T.; Ohkawa, N.; Sakoh, H.; Nishimura, K.; Tani, Y.; Hasegawa, M.; Yamada, K.; Saitoh, K., Asymmetric total synthesis of Taxol (R). *Chem-Eur. J.* **1999,** 5, 121-161.
52. Gibson, D. M.; Ketchum, R. E. B.; Vance, N. C.; Christen, A. A., Initiation and growth of cell-lines of *Taxus brevifolia* (pacific yew). *Plant Cell Rep.* **1993,** 12, (9), 479-482.
53. Edgington, S. M., Taxol: Out of the woods. *Biotechnology* **1991,** 9, 933-938.
54. Christen, A. A. B., J.; Gibson, DM., Cell cultures as a means to produce Taxol. *Proc. Am. Assoc. Cancer Res.* **1989,** 30, 566-570.
55. Michael, C. N. S., C.R., Cell cycle analysis of *Taxus* suspension cultures at the single cell level as an indicator of culture heterogeneity. *Biotech. Bioeng.* **2005**, (90), 491-500.
56. Yuan, Y. J. L., C.; Hu, Z.D.; Wu, J.C., A double oxidative burst for taxol production in suspension cultures of Taxus chinensis var. mairei induced by oligosaccharide from Fusarium oxysprum. *Enzyme Microb. Tech.* **2002,** 30, 774-778.
57. Huang, Y. F. L., W.Z.; Chen, C.; Yu, L.J., The role of lipoxygenase in elicitor-induced taxol production in *Taxus* chinensis cell cultures. *Process Biochem.* **2005,** 40, 2793-2797.
58. Hajnos, M. L. Z., A.M.; lowniak, KG. , The influence of ultraviolet radiation on the content of pharmacologically active taxoids in yew tissues. *Phytomedicine* **2001,** 8, 139-143.
59. Furmanowa, M. S.-B., K. , Hairy root cultures of Taxus x media var. Hicksii Rehd. as a new source of paclitaxel and 10-deacetylbaccatin 111. *Biotechnol. Lett.* **2000,** 22, 683-686.
60. Dejong, J. M. L., Y.; Bollon, A.P.; Long, R.M.; Jennewein, S.; Williams, D.; Croteau, R.B., , Genetic engineering of taxol biosynthetic genes in Saccharomyces cerevisiae. *Biotechnol. Bioeng.* **2006,** 93, 212-224.
61. Wang, Y. D. Y., Y.J.; Wu, J.C., Induction studies of methyl jasmonate and salicylic acid on taxane production in suspension cultures of Taxus chinensis var. mairei. *Biochem. Engineer. J.* **2004,** 19, 259-265.
62. Stierle, A. S., G.; Stierle, D., Taxol and taxane production by *Taxomyces andreanae* an endophytic fungus of Pacific yew. *Science* **1993,** 260, 214-216.

63. Strobel, G. Y., X.S.; Sears, J.; Kramer R.; Sidhu, R.S.; Hess, W.M., Taxol from Pestalotiopsis microspora, an endophytic fungus of *Taxus wallachiana*. *Microbiology* **1996,** 142, 435-440.
64. Wang, J. L., G.L.; Lu, H.Y.; Zheng, Z.H.; Huang, Y.J.; Su, W.J., Taxol from Tubercularia sp. strain TF5, an endophytic fungus of *Taxus mairei*. *FEMS Microbiol. Lett.* **2000,** 193, 249-253.
65. Denis, J.-N.; Greene, A. E.; Guénard, D.; Guéritte-Voegelein, F.; Mangatal, L.; Potier, P. A., Highly Efficient, Practical Approach to Natural Taxol. *J. Am. Chem. Soc.* **1988,** 110, 5917-5919.
66. Gueitte-Voegelein, F. S., V.; David, B.; Gueard, D.; Potier, P., Chemical studies of 10-deacetyl Baccatin III. Hemisynthesis of Taxol derivatives. *Tetrahedron* **1986,** 42, 4451-4460.
67. Denis, J.-N.; Correa, A.; Greene, A. E., An Improved Synthesis of the Taxol Side Chain and of RP 56976. *J. Org. Chem.* **1990,** 55, 1957-1959.
68. Denis, J.-N.; Correa, A.; Greene*, A. E., Direct, Highly Efficient Synthesis from (*S*)-(+)-Phenylglycine of the Taxol and Taxotere Side Chains. *J. Org. Chem.* **1991,** 56, 6939-6942.
69. Denis, J.-N.; Greene, A. E.; Serra, A. A.; Luche, M.-J., An Efficient, Enantioselective Synthesis of the Taxol Side Chain. *J. Org. Chem.* **1986,** 51, 46-50.
70. Deng, L.; Jacobsen, E. N., A Practical, Highly Enatioselective Synthesis of the Taxol Side Chain via Asymmetric Catalysis. *J. Org. Chem.* **1992,** 57, 4320-4323.
71. Wang, Z.; Kolb, H. C.; Sharpless, K. B., Large-Scale and Highly Enatioselective Synthesis of the Taxol C-13 Side Chain through Asymmetric Dihydroxylation. *J. Org. Chem.* **1994,** 59, 5104-5105.
72. Li, G.; Sharpless, K. B., Catalytic Asymmetric Amionohydroxylation Provides a Short Taxol Side-chain Synthesis. *Acta. Chem. Scand.* **1996,** 50, 649-651.
73. Mukai, C.; Kim, I. J.; Furu, E.; Hanaoka, M., Highly Stereocontrolled Asymmetric Syntheses of Taxol and Taxotère C-13 Side Chain Analogues. *Tetrahedron* **1993,** 49, (37), 8323-8336.
74. Gou, D.-M.; Liu, Y.-C.; Chen, C.-S., A Practical Chemoenzymatic Synthesis of the Taxol C-13 Side Chain *N*-Benzoyl-(2*R*,3*S*)-3-phenylisoserine. *J. Org. Chem.* **1993,** 58, 1287.
75. Kobayashi, S.; Ishitani, H.; Ueno, M., Catalytic Asymmetric Synthesis of Both Syn- and Anti-beta-Amino Alcohols. *J. Am. Chem. Soc.* **1998,** 120, 431-432.
76. Commerçon, A.; Bourzat, J. D.; Didier, E.; Lavelle, F., Practical Semisynthesis and Antimitotic Activity of Decetaxel and Side-Chain Analogues. In *Taxane Anticancer Agents: Basic Science and Current Status*, Georg, G. I.; Chan, T. T.; Ojima, I.; Vyas, D. M., Eds. American Chemical Society: Washington, D. C., 1995; pp 233-246.
77. Ojima, I.; Habus, I.; Zhao, M.; Zucco, M.; Park, Y. H.; Sun, C. M.; Brigaud, T., New and Efficient Approaches to the Semisynthesis of Taxol and Its C-13 Side-Chain Analogs by Means of Beta-Lactam Synthon Method. *Tetrahedron* **1992,** 48, (34), 6985-7012.

78. Ojima, I.; Sun, C. M.; Zucco, M.; Park, Y. H.; Duclos, O.; Kuduk, S. D., A Highly Efficient Route to Taxotère by the b-Lactam Synthon Method. *Tetrahedron Lett.* **1993,** 34, 4149-4152.
79. Holton, R. A.; Biediger, R. J.; Boatman, P. D., Semisynthesis of Taxol and Taxotere. In *Taxol®: Science and Applications*, Suffness, M., Ed. CRC Press: New York, 1995; pp 97-121.
80. Holton, R. A., Method for Preparation of Taxol Using Oxazinone. *U.S. Patent* **1991**, 5,175,315.
81. Kingston, D. G. I.; Chaudhary, A. G.; Gunatilaka, A. A. L.; Middleton, M. L., Synthesis of Taxol from Baccatin III via an Oxazoline Intermediate. *Tetrahedron Lett.* **1994,** 35, 4486-4489.
82. Ojima, I., β-Lactam Synthon Method - Enantiomerically Pure β–Lactams as Synthetic Intermediates. In *The Organic Chemistry of β–Lactam Antibiotics*, Georg, G. I., Ed. VCH Publishers: New York, 1992; pp 197-255.
83. Ojima, I., Recent Advances in β-Lactam Synthon Method. *Acc. Chem. Res.* **1995,** 28, 383-389.
84. Ojima, I.; Park, Y. H.; Sun, C. M.; Brigaud, T.; Zhao, M., New and Efficient Routes to Norstatine and Its Analogs with High Enantiomeric Purity by β-Lactam Synthon Method. *Tetrahedron Lett.* **1992,** 33, (39), 5737-5740.
85. Ojima, I.; Zucco, M.; Duclos, O.; Kuduk, S. D.; Sun, C.-M.; Park, Y. H., *N*-Acyl-3-hydroxy-β-lactams as Key Intermediates for Taxotère and Its Analogs. *Bioorg. Med. Chem. Lett.* **1993,** 3, (11), 2479-2482.
86. Gueard, D. G.-V., F.; Potier, P., Taxol and Taxotere: Discovery, chemistry, and structure-activity relationships. *Acc. Chem. Res.* **1993,** 26, 160-167.
87. Gueitte-Voegelein, F. M., L.; Gueard, D.; Potier, P.; Guilhem, J.; Cesario, M.; Pascard, C., Structure of a synthetic Taxol precursor: N-*tert*-Butoxycarbonyl-10-deacetyl-N-debenzoyltaxol. *Acta Crystallogr.* **1990,** C46, 781-784.
88. Colin, M.; Guénard, D.; Guéritte-Voegelein, F.; Potier, P., Taxotere, European Patent Application. *Eur. Pat. Appl.* **1988**, EP 253,738: *Chem. Abstr.* **1988**, *109*, 22762w.
89. Seidman, A. D., Clinical Results of Taxol in the Treatment of Advanced Breast Cancer: Single Agent Trials. In *Stony Brook Symposium on Taxol and Taxotère*, Stony Brook, NY, May 14-15, 1993; pp Abstracts 14-16.
90. Boge, T. C.; Georg, G. I., The Medicinal Chemistry of b-Amino Acids: Paclitaxel As an Illustrative Example. In *Enantioselective Synthesis of β-Amino Acids*, Juaristi, E., Ed. Wiley-VCH: New York, 1997; pp 1-43.
91. Ojima, I.; Lin, S.; Wang, T., The Recent Advances in the Medicinal Chemistry of Taxoids with Novel β-Amino Acid Side Chains." In "The Chemistry and Biology of β-Amino Acids." *Curr. Med. Chem.* **1999,** 6, 927-954.
92. Ojima, I.; Kuduk, S. D.; Chakravarty, S., Recent Advances in the Medicinal Chemistry of Taxoid Anticancer Agents. In *Advanced Medicinal Chemistry*, Maryanoff, B. E.; Reitz, A. B., Eds. JAI Press: Greenwich, CT, 1998; Vol. 4, pp 69-124.
93. Kingston, D. G. I., Recent Advances in the Chemistry and Structure-Activity Relationships of Paclitaxel. In *Taxane Anticancer Agents: Basic Science and*

Current Status; ACS Symp. Ser. 583, Georg, G. I.; Chen, T. T.; Ojima, I.; Vyas, D. M., Eds. American Chemical Society: Washington, D. C., 1995; pp 203-216.

94. Kingston, D. G. I. J., P. G.; Yuan, H.; Samala, L., The chemistry of taxol and related taxoids. *Prog. Chem. Org. Nat. Prod.* **2002,** 84, 53-225.
95. Georg, G. I.; Boge, T. C.; Cheruvallath, Z. S.; Clowers, J. S.; Harriman, G. C. B.; Hepperle, M.; Park, H., The medicinal chemistry of taxol. *Taxol: Science and Applications* **1995**, 317-75.
96. Geney, R. S., C.; Ojima, I., Computational analysis of the paclitaxel binding site in b-tubulin. In *222nd ACS National Meeting, Abstracts of Papers, MEDI-065*, Chicago, IL, 2001.
97. Kant, J.; Huang, S.; Wong, H.; Fairchild, C.; Vyas, D.; Farina, V., Studies toward structure-activity relationships of taxol(R): synthesis and cytotoxicity of taxol(R) analogues with C-2' modified phenylisoserine side chains. *Bioorg. Med. Chem. Lett.* **1993,** 3, (11), 2471-2474.
98. Ueda, Y.; Mikkilineni, A. B.; Knipe, J. O.; Rose, W. C.; Casazza, A. M.; Vyas, D. M., Novel Water Soluble Phosphate Prodrugs of Taxol Possessing in Vivo Antitumor Activity. *BioMed. Chem. Lett.* **1993,** 3, (8), 1761-1766.
99. Ueda, Y.; Wong, H.; Matiskella, J. D.; Mikkilineni, A. B.; Farina, V.; Fairchild, C.; Rose, W. C.; Mamber, S. W.; Long, B. H.; Kerns, E. H.; Casazza, A. M.; Vyas, D. M., Synthesis and Antitumor Evaluation of 2'-Oxycarbonylpaclitaxels (Paclitaxel-2'-carbonates). *BioMed. Chem. Lett.* **1994,** 4, (16), 1861-1864.
100. Ueda, Y.; Matiskella, J. D.; Mikkilineni, A. B.; Farina, V.; Knipe, J. O.; Rose, W. C.; Casazza, A. M.; Vyas, D. M., Novel, Water-Soluble Phosphate Derivatives of 2'-Ethoxycarbonylpaclitaxel as Potential Prodrugs of Paclitaxel: Synthesis and Antitumor Evaluation. *BioMed. Chem. Lett.* **1995,** 5, 247-252.
101. Ojima, I.; Slater, J. S.; Kuduk, S. D.; Takeuchi, C. S.; Gimi, R. H.; Sun, C.-M.; Park, Y. H.; Pera, P.; Veith, J. M.; Bernacki, R. J., Syntheses and Structure-Activity Relationships of Taxoids Derived from 14β-Hydroxy-10-deacetylbaccatin III. *J. Med. Chem.* **1997,** 40, 267-278.
102. Ojima, I.; Slater, J. C.; Michaud, E.; Kuduk, S. D.; Bounaud, P.-Y.; Vrignaud, P.; Bissery, M.-C.; Veith, J.; Pera, P.; Bernacki, R. J., Syntheses and Structure-Activity Relationships of the Second Generation Antitumor Taxoids. Exceptional Activity against Drug-Resistant Cancer Cells. *J. Med. Chem.* **1996,** 39, 3889-3896.
103. Ojima, I.; Lin, S., Efficient Asymmetric Syntheses of β-Lactams Bearing a Cyclopropane or an Epoxide Moiety and Their Application to the Syntheses of Novel Isoserines and Taxoids. *J. Org. Chem.* **1998,** 63, 224-225.
104. Georg, G. I.; Harriman, G. C. B.; Hepperle, M.; Clowers, J. S.; Vander Velde, D. G.; Hines, R. H., Synthesis, Conformational Analysis, and Biological Evaluation of Heteroaromatic Taxanes. *J. Org. Chem.* **1996,** 61, 2664-2676.
105. Roh, E. J.; Song, C. E.; Kim, D.; Pae, H. O.; Cung, H. T.; Lee, K. S.; Chai, K.; Lee, C. O.; Chi, S. U., Synthesis and Biology of 3'-*N*-Acyl-*N*-debezoylpaclitaxel Analogues. *Bioorg. Med. Chem.* **1999,** 7, 2115-2119.
106. Ojima, I.; Fenoglio, I.; Park, Y. H.; Pera, P.; Bernacki, R. J., Synthesis and biological activity of 14-hydroxydocetaxel. *Bioorg. Med. Chem. Lett.* **1994,** 4, (13), 1571-1576.

107. Ojima, I.; Duclos, O.; Zucco, M.; Bissery, M.-C.; Combeau, C.; Vrignaud, P.; Riou, J. F.; Lavelle, F., Synthesis and Structure-Activity Relationships of New Antitumor Taxoids. Effects of Cyclohexyl Substitution at the C-3' and/or C-2 of Taxotère (Docetaxel). *J. Med. Chem.* **1994,** 37, (16), 2602-2608.
108. Kingston, D. G. I.; Samaramayake, G.; Ivey, C. A., The Chemistry of Taxol, a Clinically Useful Anticancer Agent. *J. Nat. Prod.* **1990,** 53, (1), 1-12.
109. Kingston, D. G. I., The Chemistry of Taxol. *Pharmacol. Ther.* **1991,** 52, 1-34 and references cited therein.
110. Kingston, D. G. I.; Molinero, A. A.; Rimoldi, J. M., The Taxane Diterpenoids. *Prog. Chem. Org. Nat. Prod.* **1993,** 61, 1-192.
111. Samaranayake, G.; Magri, N. F.; Jitrangsri, C.; Kingston, D. G. I., Modified Taxols. 5. Reaction of Taxol with Electrophilic Reagents and Preparation of a Rearranged Taxol Derivatives with Tubulin Assembly Activity. *J. Org. Chem.* **1991,** 56, 5114-5119.
112. Wahl, A.; Guéritte-Voegelein, F.; Guénard, D.; Le Goff, M.-T.; Potier, P., Rearrangement Reactions of Taxanes: Structural Modifications of 10-Deacetylbaccatin III. *Tetrahedron* **1992,** 48, 6965-6974.
113. Ojima, I.; Fenoglio, I.; Park, Y. H.; Sun, C.-M.; Appendino, G.; Pera, P.; Bernacki, R. J., Synthesis and Structure-Activity Relationships of Novel Nor-Seco Analogs of Taxol and Taxotère. *J. Org. Chem.* **1994,** 59, 515-517.
114. Ojima, I.; Lin, S.; Chakravarty, S.; Fenoglio, I.; Park, Y. H.; Sun, C.-M.; Appendino, G.; Pera, P.; Veith, J. M.; Bernacki, R. J., Synthesis and Structure-Activity Relationships of Novel Nor-seco Taxoids. *J. Org. Chem.* **1998,** 63, 1637-1645.
115. Klein, L. L.; Maring, C. J.; Li, L.; Yeung, C. M.; Thomas, S. A.; Grampovnik, D. J.; Plattner, J. J.; Henry, R. F., Synthesis of Ring B-Rearranged Taxane Analogs. *J. Org. Chem.* **1994,** 59, 2370-2373.
116. Liang, X.; Kingston, D. G. I.; Lin, C. M.; Hamel, E., Synthesis and biological evaluation of paclitaxel analogs modified in ring C. *Tetrahedron Lett.* **1995,** 36, 2901-2904.
117. Liang, X.; Kingston, D. G. I.; Long, B. H.; Fairchild, C. A.; Johnston, K. A., Synthesis, structure elucidation and biological evaluation of C-norpaclitaxel. *Tetrahedron Lett.* **1995,** 36, 7795-7798.
118. Chen, S.-H.; Fairchild, C.; Long, B. H., Synthesis and Biological Evaluation of Novel C-4 Aziridine-Bearing Paclitaxel (Taxol®) Analogs. *J. Med. Chem.* **1995,** 38, (12), 2263-2267.
119. Marder-Karsenti, R.; Dubois, J.; Bricard, L.; Guénard, D.; Guéritte-Voegelein, F., Synthesis and Biological Evaluation of D-Ring-Modified Taxanes:1 5(20)-Azadocetaxel Analogs. *J. Org. Chem.* **1997,** 62, 6631-6637.
120. Gunatilaka, L. A. A.; Ramdayal, F. D.; Sarragiotto, M. H.; Kingston , D. I.; Sackett, D. L.; Hamel, E., Synthesis and Biological Evaluation of Novel Paclitaxel (Taxol) D-Ring Modified Analogues. *J. Org. Chem.* **1999,** 64, (8), 2694-2703.
121. Dubois, J.; Thoret, S.; Guéritte, F.; Guénard, D., Synthesis of 5(20)deoxydocetaxel, a new active docetaxel analogue. *Tetrahedron Lett.* **2000,** 41, 3331-3334.

122. Chordia, M. D.; Kingston, D. G. I., Synthesis and Biological Evaluation of 2-epi-Paclitaxel. *J. Org. Chem.* **1996,** 61, 799-801.
123. Monsarrat, B.; Mariel, E.; Cros, S.; Garès, M.; Guénard, D.; Guéritte-Voegelein, F.; Wright, M., Taxol Metabolism. Isolation and Identification of Three Major Metabolites of Taxol in Rat Bile. *Drug Metab. Dispos.* **1990,** 18, 895-901.
124. Ojima, I.; Inoue, T.; Slater, J. C.; Lin, S.; Kuduk, S. C.; Chakravarty, S.; Walsh, J. J.; Gilchrist, L.; McDermott, A. E.; Cresteil, T.; Monsarrat, B.; Pera, P.; Bernacki, R. J., Synthesis of Enatiopure F-Containing Taxoids and Their Use as Anticancer Agents as well as Probes for Biomedical Problems. In *Asymmetric Fluoroorganic Chemistry: Synthesis, Application, and Future Directions; ACS Symposium Series 746*, Ramachandran, P. V., Ed. American Chemical Society: Washington, D. C., 1999; pp 158-181.
125. Chaudhary, A. G.; Gharpure, M. M.; Rimoldi, J. M.; Chordia, M. D.; Gunatilaka, A. A. L.; Kingston, D. G. I.; Grover, S.; Lin, C. M.; Hamel, E., Unexpectedly Facile Hydrolysis of the 2-Benzoate Group of Taxol and Syntheses of Analogs with Increased Activities. *J. Am. Chem. Soc.* **1994,** 116, (9), 4097-4098.
126. Ojima, I.; Kuduk, S. D.; Pera, P.; Veith, J. M.; Bernacki, R. J., Synthesis of and Structure-Activity Relationships of Non-Aromatic Taxoids. Effects of Alkyl and Alkenyl Ester Groups on Cytotoxicity. *J. Med. Chem.* **1997,** 40, 279-285.
127. Chen, S.-H.; Wei, J.-M.; Long, B. H.; Fairchild, C. A.; Carboni, J.; Mamber, S. W.; Rose, W. C.; Johnston, K.; Casazza, A. M.; Kadow, J. F.; Farina, V.; Vyas, D. M.; Doyle, T. W., Novel C-4 Paclitaxel (Taxol) Analogs: Potent Antitumor Agents. *Bioorg. Med. Chem. Lett.* **1995,** 5, (22), 2741-2746.
128. Chen, S.-H.; Kadow, J. F.; Farina, V.; Fairchild, C. R.; Johnston, K. A., First Syntheses of Novel Paclitaxel (Taxol) Analogs Modified at the C-4 Position. *J. Org. Chem.* **1994,** 59, (21), 6156-6158.
129. Georg, G. I.; Ali, S. M.; Boge, T. C.; Datta, A.; Falborg, L.; Himes, R. H., Selective C-2 and C-4 Deacylation and Acylation of Taxol: The First Synthesis of a C-4 Substituted Taxol Analogue. *Tetrahedron Lett.* **1994,** 35, 8931-8934.
130. Chen, S. H.; Kant, J.; Mamber, S. W.; Roth, G. P.; Wei, J.; Marshall, D.; Vyas, D.; Farina, V., Taxol Structure Activity Relationships: Synthesis and Biological Activity of Taxol and Analogs Modified at C-7. *Bioorg. Med. Chem. Lett.* **1994,** 4, 2223-2228.
131. Chaudhary, A. G.; Rimoldi, J. M.; Kingston, D. G. I., Modified Taxols. 10. Preparation of 7-Deoxytaxol, a Highly Bioactive Taxol Derivative, and Interconversion of Taxol and 7-*epi*-Taxol. *J. Org. Chem.* **1993,** 58, (15), 3798-3799.
132. Chen, S.-H.; Wei, J.-M.; Vyas, D. M.; Soyle, T. W.; Farina, V., A Facile Synthesis of 7,10-Dideoxy Taxol and 7-*epi*-10-Deoxy Taxol. *Tetrahedron Lett.* **1993,** 34, 6845-6848.
133. Klein, L. L., Synthesis of 9-Dihydrotaxol: A Novel Bioactive Taxane. *Tetrahedron Lett.* **1993,** 34, (13), 2047-2050.
134. Pulicani, J.-P.; Bourzat, J.-D.; Bouchard, H.; Commerçon, A., Electrochemical Reduction of Taxiods: Selective Preparation of 9-dihydro-, 10-deoxy and 10-deacetoxy-Taxoids. *Tetrahedron Lett.* **1994,** 35, 4999-5002.

135. Datta, A.; Aubé, J.; Georg, G. I.; Mitscher, L. A.; Jayasinghe, L. R., The First Synthesis of a C-9 Carbonyl Modified Baccatin III Derivative and Its Conversion to Novel Taxol and Taxotère Analogues. *BioMed. Chem. Lett.* **1994,** 4, (16), 1831-1834.
136. Datta, A.; Vander Velde, D. G.; Georg, G. I.; Himes, R. H., Syntheses of Novel C-9 and C-10 Modified Bioactive Taxanes. *Tetrahedron Lett.* **1995,** 36, 1985-1988.
137. Georg, G. I.; Cheruvallath, Z. S.; Vander Velde, D. G.; Himes, R. H., Stereoselective Synthesis of 9β-Hydroxytaxanes via Reduction with Samarium Diiodide. *Tetrahedron Lett.* **1995,** 36, 1783-1786.
138. Chaudhary, A. G.; Kingston, D. G. I., Synthesis of 10-Deacetoxytaxol and 10-Deoxytaxotere. *Tetrahedron Lett.* **1993,** 34, 4921-4924.
139. Kant, J.; O'Keeffe, W. S.; Chen, S.-H.; Farina, V.; Fairchild, C.; Johnston, K.; Kadow, J. F.; Long, B. H.; Vyas, D., A Chemoselective Approach to Functionalize the C-10 Position of 10-Deacetylbaccatin III. Synthesis and Biological Properties of Novel C-10 Taxol Analogues. *Tetrahedron Lett.* **1994,** 35, 5543-5546.
140. Ojima, I.; Wang, T.; Miller, M. L.; Lin, S.; Borella, C.; Geng, X.; Pera, P.; Bernacki, R. J., Syntheses and Structure-Activity Relationships of New Second-Generation Taxoids. *Bioorg. Med. Chem. Lett.* **1999,** 9, 3423-3428.
141. Georg, G. I.; Ravikumar, V. T., *The Organic Chemistry of β-Lactams*. VCH: New York, 1992; p 295 and references cited therein.
142. Duerckheimer, W.; Blumbach, J.; Lattrell, R.; Scheunemann, K. H., New developments in.beta.-lactam antibiotics. *Angew. Chem., Int. Ed. Engl.* **1985,** 97, 183-205.
143. Southgate, R., The synthesis of natural β-lactam antibiotics. *Contemp. Org. Synth.* **1994,** 1, 417-431.
144. Ojima, I.; Delaloge, F., Asymmetric Synthesis of Building-Blocks for Peptides and Peptidomimetics by Means of β-Lactam Synthon Method. *Chem. Soc. Rev.* **1997,** 26, 377-386.
145. Ojima, I., Asymmetric Syntheses by Means of β-Lactam Synthon Method. In *Advances in Asymmetric Synthesis*, Hassner, A., Ed. JAI Press: Greenwich, 1995; Vol. 1, pp 95-146.
146. Holton, R. A.; Biediger, R. J.; Boatman, P. D., Semisynthesis of Taxol and Taxotere. In *Taxol: Science and Applications*, Suffness, M., Ed. CRC Press: New York, 1995; pp 97-121.
147. Guénard, D.; Guéritte-Vogelein, F.; Potier, P., Taxol and Taxotere: Discovery, Chemistry, and Structure-Activity Relationships. *Acc. Chem. Res.* **1993,** 26, 160-167.
148. Georg, G. I.; Harriman, G. C. B.; Vander Velde, D. G.; Boge, T. C.; Cheruvallath, Z. S.; Datta, A.; Hepperle, M.; Park, H.; Himes, R. H.; Jayasinghe, L., Medicinal Chemistry of Paclitaxel: Chemistry, Structure-Activity Relationships, and Conformational Analysis. In *Taxane Anticancer Agents: Basic Science and Current Status*, Georg, G. I.; Chen, T. T.; Ojima, I.; Vyas, D. M., Eds. American Chemical Society: Washington D.C., 1995; pp 217-232.

149. Danishefsky, S.; Masters, J.; Young, W.; Link, J.; Snyder, L.; Magee, T.; Jung, D.; Isaacs, R.; Bornmann, W.; Alaimo, C.; Coburn, C.; Di Grandi, M., Total Synthesis of Baccatin III and Taxol. *J. Am. Chem. Soc.* **1996,** 118, 2843-2859.
150. Ojima, I.; Habus, I.; Zhao, M.; Zucco, M.; Park, Y. H.; Sun, C.-M.; Brigaud, T., New and Efficient Approaches to the Semisynthesis of Taxol and Its C-13 Side Chain Analogs by Means of β-Lactam Synthon Method. *Tetrahedron* **1992,** 48, 6985-7012.
151. Ojima, I.; Delaloge, F., Syntheses of norstatine, its analogs, and dipeptide isosteres by means of b-lactam synthon method. *Methods Mol. Med.* **1999,** 23, (Peptidomimetics Protocols), 137-160.
152. Koppel, G. A., The synthesis of the b-lactam function. *Chem. Heterocycl. Comp.* **1983,** 42, 219-441.
153. De Kimpe, N., Azetidines, Azetines, and Azetes: monocyclic. In *Comprehensive Heterocyclic Chemistry II*, Padwa, A., Ed. Elsevier: Oxford, UK, 1996; pp 507-589.
154. Palomo, C.; Aizpurua, J. M.; Ganboa, I.; Oiarbide, M., Asymmetric synthesis of b-lactams by Staudinger ketene-imine cycloaddition reaction. *Eur. J. Org. Chem.* **1999**, 3223-3235.
155. Hart, D. J.; Ha, D.-C., The Ester Enolate-Imine Condensation Route to β-Lactams. *Chem. Rev.* **1989,** 89, 1447-1465.
156. Brown, M. J., Literature review of the ester enolate imine condensation. *Heterocycles* **1989,** 29, 2225-2244.
157. Fujisawa, T.; Shimizu, M., Switching of stereochemistry using different metal enolate species for construction of b-lactam skeletons. *Rev. Heteroatom Chem.* **1996,** 15, 203-225.
158. Cainelli, G.; Panunzio, M.; Andreoli, P.; Martelli, G.; Spunta, G.; Giacomini, D.; Bandini, E., Metallo-imines: useful reagents in organic synthesis. *Pure Appl. Chem.* **1990,** 62, 605-612.
159. Cainelli, G.; Panunzio, M.; Giacomini, D.; Martelli, G.; Spunta, G.; Bandini, E., Addition of enolates and metalloalkyls to imines. Stereospecific synthesis of b-lactams, amines, aziridines and aminols. In *NATO ASI Series, Series E: Applied Sciences*, Kluwer: Bologna, Italy, 1996; pp 25-60.
160. Miller, M. J., Hydroxamate approach to the synthesis of b-lactam antibiotics. *Acc. Chem. Res.* **1986,** 19, 49-56.
161. Chmielewski, M.; Kaluza, Z.; Furman, B., Stereocontrolled synthesis of 1-oxabicyclic b-lactam antibiotics via [2+2]cycloaddition of isocyanates to sugar vinyl ethers. *Chem. Commun.* **1996**, 2689-2696.
162. Hegedus, L. S., Synthesis of Amino Acids and Peptides Using Chromium Carbene Complex Photochemistry. *Acc. Chem. Res.* **1995,** 28, 299-305.
163. Staudinger, H., Ketenes. 1. Diphenylketene. *Justus Liebigs Ann. Chem.* **1907,** 356, 51-123.
164. Whitesell, J. K.; Lawrence, R. M., Practical Enzymatic Resolution of Chiral Auxiliaries - Enantiomerically Pure *trans*-2-Phenylcyclohexanol and *trans*-2-(α-Cumyl)cyclohexanol. *Chimia* **1986,** 40, 318-321.
165. Schwartz, A.; Madan, P.; Whitesell, J. K.; Lawrence, R. M., Whitesell Chiral Auxilliary. *Org. Syn.* **1990,** 69, 1-9.

166. Oppolzer, W.; Chapuis, C.; Bernardinelli, G., Asymmetric Diels-Alder Reactions: Facile Preparation and Structure of Sulfonamido-Isobornyl Acrylates. *Tetrahedron Lett.* **1984,** 25, 5885-5888.
167. Oppolzer, W.; Dudfield, P.; Stevenson, T.; Godel, T., Oppolzer's Chiral Auxilliary, Helv. Chim. Acta 1985, 68, 212. *Helv. Chim. Acta* **1985,** 68, 212.
168. Ojima, I.; Kuduk, S. D.; Slater, J. C.; Gimi, R. H.; Sun, C. M., Syntheses of new fluorine-containing taxoids by means of β-lactam synthon method. *Tetrahedron* **1996,** 52, (1), 209-24.
169. Ojima, I.; Geng, X.; Lin, S.; Pera, P.; Bernacki, R. J., Design, synthesis and biological activity of novel C2-C3' N-Linked macrocyclic taxoids. *Bioorg. Med. Chem. Lett.* **2002,** 12, (3), 349-352.
170. Whitesell, J. K.; Chen, H.-H.; Lawrence, R. M., trans-2-phenylcyclohexanol. A Powerful and Readily Available Chiral Auxiliary. *J. Org. Chem.* **1985,** 50, 4663-4664.
171. Ojima, I.; Lin, S.; Inoue, T.; Miller, M. L.; Borella, C. P.; Geng, X.; Walsh, J. J., Macrocycle Formation by Ring-Closing Metathesis (RCM). Application to the Syntheses of Novel Macrocyclic Taxoids. *J. Am. Chem. Soc.* **2000,** 122, 5343-5353.
172. Thomas, R. C., Synthetic aspects of monocyclic b-lactam antibiotics. *Recent Prog. Chem. Synth. Antibiot.* **1990**, 533-564.
173. Ternansky, R. J.; Morin, J. M., Jr., Novel methods for the construction of the b-lactam ring. *Org. Chem.* **1993**, 257-293.
174. Lynch, J. E.; Riseman, S. M.; Laswell, W. L.; Volante, R. P.; Smith, G. B.; Shinkai, I.; Tschaen, D. M., Mechanism of an acid chloride-imine reaction by low-temperature FT-IR: b-lactam formation occurs exclusively through a ketene intermediate. *J. Org. Chem.* **1989,** 54, 3792-3796.
175. Georg, G. I.; Ravikumar, V. T., Stereocontrolled ketene-imine cycloaddition reactions. In *Organic Chemistry b-Lactams*, Georg, G. I., Ed. VCH: New York, 1993; pp 295-368.
176. Hegedus, L. S.; Montgomery, J.; Narukawa, Y.; Snustad, D. C., A contribution to the confusion surrounding the reaction of ketenes with imines to produce b-lactams. A comparison of stereoselectivity dependence on the method of ketene generation: acid chloride/triethylamine vs photolysis of chromium carbene complexes. *J. Am. Chem. Soc.* **1991,** 113, 5784-5791.
177. Dumas, S.; Hegedus, L. S., Electronic Effects on the Stereochemical Outcome of the Photochemical Reaction of Chromium Carbene Complexes with Imines to Form b-Lactams. *J. Org. Chem.* **1994,** 59, 4967-4971.
178. Cossio, F. P.; Ugalde, J. M.; Lopez, X.; Lecea, B.; Palomo, C., A semiempirical theoretical study on the formation of b-lactams from ketenes and imines. *J. Am. Chem. Soc.* **1993,** 115, 995-1004.
179. Lopez, R.; Sordo, T. L.; Sordo, J. A.; Gonzalez, J., Torquoelectronic effect in the control of the stereoselectivity of ketene-imine cycloaddition reactions. *J. Org. Chem.* **1993,** 58, 7036-7037.
180. Cossio, F. P.; Arrieta, A.; Lecea, B.; Ugalde, J. M., Chiral Control in the Staudinger Reaction between Ketenes and Imines. A Theoretical SCF-MO Study on Asymmetric Torquoselectivity. *J. Am. Chem. Soc.* **1994,** 116, 2085-2093.

181. Banik, B. K.; Manhas, M. S.; Bose, A. K., Stereospecific Glycosylation via Ferrier Rearrangement for Optical Resolution. *J. Org. Chem.* **1994,** 59, 4714-4716.
182. Verweij, J.; Clavel, M.; Chevalier, B., Paclitaxel (Taxol) and Docetaxel (Taxotere): Not Simply Two of a Kind. *Ann. Oncol.* **1994,** 5, 495-505.
183. Ojima, I., Chemistry of Taxoid Antitumor Agents at the Biomedical Interface. *7th International Kyoto Conference on Organic Chemistry, Kyoto, Japan, November 10-14*, **1997,** Abstracts, IL-19.
184. Ojima, I., Science of Taxol. *Farumashia* **2003,** 39, 49-53.
185. Ojima, I.; Bounaud, P.-Y.; Takeuchi, C. S.; Pera, P.; Bernacki, R. J., New Taxanes as Highly Efficient Reversal Agents for Multi-Drug Resistance in Cancer Cells. *Bioorg. Med. Chem. Lett.* **1998,** 8, 189-194.
186. Ojima, I.; Geney, R.; Ungureanu, I. M.; Li, D., Medicinal chemistry and chemical biology of new generation taxane antitumor agents. *IUBMB Life* **2002,** 53, 269-274.
187. Ojima, I.; Kuduk, S. D.; Slater, J. C.; Gimi, R. H.; Sun, C. M.; Chakravarty, S.; Ourevich, M.; Abouabdellah, A.; Bonnet-Delpon, D.; Bégué, J.-P.; Veith, J. M.; Pera, P.; Bernacki, R. J., Synthesis, Biological Activity, and Conformational Analysis of Fluorine-Containing Taxoids. In *"Biomedical Frontiers of Fluorine Chemistry" ACS Symp. Ser. 639*, Ojima, I.; McCarthy, J. R.; Welch, J. T., Eds. American Chemical Society: Washington, D. C., 1996; pp 228-243.
188. Ojima, I.; Chen, J.; Sun, L.; Borella, C. P.; Wang, T.; Miller, M. L.; Lin, S.; Geng, X.; Kuznetsova, L. V.; Qu, C.; Gallager, D.; Zhao, X.; Zanardi, I.; Xia, S.; Horwtiz, S. B.; Mallen-St. Clair, J.; Guerriero, J. L.; Bar-Sagi, D.; Veith, J. M.; Pera, P.; Bernacki, R. J., Design, Synthesis and Biological Evaluation of New Second-Generation Taxoids. *J. Med. Chem.* **2008,** 51, 3203-3221.
189. Ojima, I.; Das, M., Recent Advances in the Chemistry and Biology of New Generation Taxoids. *J. Nat. Prod.* **2009,** 72, (3), 554-565.
190. Appendino, G.; Gariboldi, P.; Gabetta, B.; Pace, R.; Bombardelli, E.; Viterbo, D., 14β-Hydroxy-10-deacetylbaccatin III, a New Taxane from Himalayan Yew (*Taxus Wallichiana Zucc.*). *J. Chem. Soc., Perkins Trans 1* **1992**, 2925-2929.
191. Horwitz, S. B. In *Taxol: Mechanism of Action and Resistance*, Stony Brook Symposium on Taxol and Taxotère, Stony Brook , NY, May 14-15, 1993; Stony Brook , NY, May 14-15, 1993; pp Abstracts 23-24.
192. Nicoletti, M. I.; Colombo, T.; Rossi, C.; Monardo, C.; Stura, S.; Zucchetti, M.; Riva, A.; Morazzoni, P.; Donati, M. B.; Bombardelli, E.; D'Incalici, M.; Giavazzi, R., IDN5109, a Taxane with Oral Bioavailability, and Potent Antitumor Activity. *Cancer Res.* **2000,** 60, 842-846.
193. Polizzi, D.; Pratesi, G.; Monestiroli, S.; Tortoreto, M.; Zunino, F.; Bombardelli, E.; Riva, A.; Morazzoni, P.; Colombo, T.; D'Incalici, M.; Zucchetti, M., Oral Efficacy and Bioavailability of a Novel Taxane. *Clin. Cancer Res.* **2000,** 6, 2070-2074.
194. Beer, M.; Lenaz, L.; Amadori, D.; Ortataxel Study Group., Phase II study of ortataxel in taxane-resistant breast cancer. *J. Clin. Oncol. (Meeting Abstracts) 2008 ASCO Annual Meeting Proceedings (Post-Meeting Edition)* **2008,** 26, (15_suppl), 1066-1066.

195. Kingston, D. G. I.; Chaudhary, A. g.; Chordia, M. D.; Gharpure, M.; Gunatilaka, A. A. L.; Higgs, P. I.; Rimoldi, J. M.; Samala, L.; Jagtap, P. G.; Giannakakou, P.; Jiang, Y. Q.; Lin, C. M.; Hamel, E.; Long, B. H.; Fairchild, C. R.; Johnston, K. A., Synthesis and Biological Evaluation of 2-Acyl Analogues of Paclitaxel (Taxol). *J. Med. Chem.* **1998,** 41, 3715-3726.
196. Slater, J. C., *Ph.D. Dissertation*. SUNY at Stony Brook: Stony Brook, 1997; p Chapter 1.
197. Wang, T., *Ph. D. Dissertation*. SUNY at Stony Brook: Stony Brook, 1999; p Chapter 2.

References for Chapter 2:

1. Begue, J.-P.; Bonnet-Delpon, D., Recent advances (1995-2005) in fluorinated pharmaceuticals based on natural products. *J. Fluorine Chem.* **2006,** 127, (8), 992-1012.
2. Isanbor, C.; O'Hagan, D., Fluorine in medicinal chemistry: A review of anti-cancer agents. *J. Fluorine Chem.* **2006,** 127, (3), 303-319.
3. O'Hagan, D.; Harper, D. B., Fluorine-containing natural products. *J. Fluorine Chem.* **1999,** 100, 127-133.
4. Pollina Cormier, E.; Das, M.; Ojima, I., Approved active pharmaceutical ingredients containing fluorine. In *Fluorine in medicinal chemistry and chemical biology*, Ojima, I., Ed. Wiley-Blackwell: 2009; pp 525-604.
5. Cottet, F.; Marull, M.; Lefebvre, O.; Schlosser, M., Recommendable Routes to Trifluoromethyl-Substituted Pyridine- and Quinolinecarboxylic Acids. *Eur. J. Org. Chem.* **2003**, (8), 1559-1568.
6. Bondi, A., van der Waals volumes and radii. *J. Phys. Chem.* **1964,** 68, (3), 441-51.
7. Bohm, H.-J.; Banner, D.; Bendels, S.; Kansy, M.; Kuhn, B.; Muller, K.; Obst-Sander, U.; Stahl, M., Fluorine in medicinal chemistry. *Chembiochem* **2004,** 5, (5), 637-643.
8. Ojima, I.; McCarthy, J. M.; Welch, J. T., *Biomedical Frontiers of Fluorine Chemistry*. American Chemical Society: Washington, D. C., 1996.
9. Kukhar, V. P.; Soloshonok, V. A., *Fluorine-containing Amino Acids: Synthesis and Properties*. John Wiley & Sons: Chichester, 1995.
10. Kirk, K. L., Fluorine in medicinal chemistry: Recent therapeutic applications of fluorinated small molecules. *J. Fluorine Chem.* **2006,** 127, 1013-1029.
11. Müller, K.; Faeh, C.; Diederich, F., Fluorine in pharmaceuticals: looking beyond intuition. *Science* **2007,** 317, (5846), 1881-1886.
12. Gerhard, U.; Thomas, S.; Mortishire-Smith, R., Accelerated metabolite identification by "extraction-NMR". *J. Pharm. Biol. Analysis* **2003**, 531-538.
13. O'Hagan, D.; Schaffrath, C.; Cobb, S. L.; Hamilton, J. T. G.; Murphy, C. D., Biochemistry: Biosynthesis of an organofluorine molecule. *Nature* **2002,** 416, (6878), 279-280.
14. Martino, R.; Malet-Martino, M.; Gilard, V., Fluorine Nuclear Magnetic Resonance, a Privileged Tool for Metabolic Studies of Fluoropyrimidine Drugs. *Curr. Drug Metab.* **2000,** 1, (3), 271-303.
15. Khalafallah, A. K.; Hassan, M. E.; Soleman, H. A., Synthesis and biological studies on some spiro Schiff base derivatives. *J. Ind. Chem. Soc.* **1992,** 69, (6), 318-320.
16. Page, M. I., The mechanisms of reactions of β-lactam antibiotics. *Acc. Chem. Res.* **1984,** 17, (4), 144-151.
17. Lukic, I. Preparation of novel derivatives of 3-bromo and 3,3-dibromo-4-oxo-1-azetidines for their use in antibacterial or antitumor therapy. Eur. Pat. Appl. 791580, 1997.
18. Borthwick, A. D.; Weingarten, G.; Haley, T. M.; Tomaszewski, M.; Wang, W.; Hu, Z.; Bedard, J.; Jin, H.; Yuen, L.; Mansour, T. S., Design and synthesis of

monocyclic b-lactams as mechanism-based inhibitors of human cytomegalovirus protease. *Bioorg. Med. Chem. Lett.* **1998,** 8, (4), 365-370.

19. Ogilvie, W.; Bailey, M.; Poupart, M.-A.; Abraham, A.; Bhavsar, A.; Bonneau, P.; Bordeleau, J.; Bousquet, Y.; Chabot, C.; Duceppe, J.-S.; Fazal, G.; Goulet, S. G.-M., C.; Guse, I.; Halmos, T.; Lavallee, P.; Leach, M.; Malenfant, E.; O'Meara, J.; Plante, R.; Plouffe, C.; Poirier, M.; Soucy, F.; Yoakim, C.; Deziel, R., Peptidomimetic Inhibitors of the Human Cytomegalovirus Protease. *J. Med. Chem.* **1997,** 40, (25), 4113-4135.
20. Ojima, I.; Lin, S.; Wang, T., The Recent Advances in the Medicinal Chemistry of Taxoids with Novel β-Amino Acid Side Chains." In "The Chemistry and Biology of β-Amino Acids." *Curr. Med. Chem.* **1999,** 6, 927-954.
21. Ojima, I.; Kuduk, S. D.; Chakravarty, S., Recent Advances in the Medicinal Chemistry of Taxoid Anticancer Agents. In *Advanced Medicinal Chemistry*, Maryanoff, B. E.; Reitz, A. B., Eds. JAI Press: Greenwich, CT, 1998; Vol. 4, pp 69-124.
22. Ojima, I.; Delaloge, F., Asymmetric Synthesis of Building-Blocks for Peptides and Peptidomimetics by Means of β-Lactam Synthon Method. *Chem. Soc. Rev.* **1997,** 26, 377-386.
23. Ojima, I., Recent Advances in β-Lactam Synthon Method. *Acc. Chem. Res.* **1995,** 28, 383-389.
24. Ojima, I., Asymmetric syntheses by means of the β-lactam synthon method. *Adv. Asymmetric Synth.* **1995,** 1, 95-146.
25. Ojima, I.; Delaloge, F., Syntheses of norstatine, its analogs, and dipeptide isosteres by means of b-lactam synthon method. *Methods Mol. Med.* **1999,** 23, (Peptidomimetics Protocols), 137-160.
26. Kuznetsova, L.; Ungureanu, I. M.; Pepe, A.; Zanardi, I.; Wu, X.; Ojima, I., Trifluoromethyl- and difluoromethyl-β-lactams as useful building blocks for the synthesis of fluorinated amino acids, dipeptides, and fluoro-taxoids. *J. Fluorine Chem.* **2004,** 125, (4), 487-500.
27. Vuilhorgne, M.; Gaillard, C.; Sanderlink, G. J.; Royer, I.; Monsarrat, B.; Dubois, J.; Wright, M., Metabolism of Taxoid Drugs. In *Taxane Anticancer Agents: Basic Science and Current Status, ACS Symp. Ser. 583*, Georg, G. I.; Chen, T. T.; Ojima, I.; Vyas, D. M., Eds. American Chemical Society: Washington, D. C., 1995; pp 98-110.
28. Gut, I.; Ojima, I.; Vaclavikova, R.; Simek, P.; Horsky, S.; Soucek, P.; Kondrova, E.; Kuznetsova, L. V.; Chen, J., Metabolism of New Generation Taxanes in Human, Pig, Minipig and Rat Liver Microsomes. *Xenobiotica* **2006,** 36, 772-792.
29. Ojima, I.; Das, M., Recent Advances in the Chemistry and Biology of New Generation Taxoids. *J. Nat. Prod.* **2009,** 72, (3), 554-565.
30. Yamazaki, T.; Hiraoka, S.; Sakamoto, J.; Kitazume, T., Mesyloxy-group migration as the stereoselective preparation method of various functionalized olefins and its reaction mechanism. *Org. Lett.* **2001,** 3, 743-746.
31. Lim, M. H.; Kim, H. O.; Moon, H. R.; Chun, M. W.; Jeong, L. S., Synthesis of Novel D-2'-Deoxy-2'-C-difluoromethylene-4'-thiocytidine as a Potential Antitumor Agent. *Org. Lett.* **2002,** 4, 529-531.

32. Bhadury, P. S.; Palit, M.; Sharma, M.; Raza, S. K.; Jaiswal, D. K., Fluorinated phosphonium ylides: versatile in situ Wittig intermediates in the synthesis of hydrofluorocarbons. *J. Fluorine Chem.* **2002,** 116, 75-80.
33. Ojima, I.; Slater, J. C.; Pera, P.; Veith, J. M.; Abouabdellah, A.; Begue, J.-P.; Bernacki, R. J., Synthesis and biological activity of novel 3'-trifluoromethyl taxoids. *Bioorg. Med. Chem. Lett.* **1997,** 7, (2), 133-138.
34. Ojima, I.; Lin, S.; Slater, J. C.; Wang, T.; Pera, P.; Bernacki, R. J.; Ferlini, C.; Scambia, G., Syntheses and biological activity of C-3'-difluoromethyl-taxoids. *Bioorg. Med. Chem.* **2000,** 8, (7), 1619-1628.
35. Skehan, P.; Streng, R.; Scudierok, D.; Monks, A.; McMahon, J.; Vistica, D.; Warren, J. T.; Bokesch, H.; Kenney, S.; Boyd, M. R., New colorimetric cytotoxicity assay for anticancer-drug screening. *J. Nat. Cancer Inst.* **1990,** 82, 1107-1112.
36. Ojima, I.; Slater, J. S.; Kuduk, S. D.; Takeuchi, C. S.; Gimi, R. H.; Sun, C.-M.; Park, Y. H.; Pera, P.; Veith, J. M.; Bernacki, R. J., Syntheses and Structure-Activity Relationships of Taxoids Derived from 14β-Hydroxy-10-deacetylbaccatin III. *J. Med. Chem.* **1997,** 40, 267-278.

References for Chapter 3:

1. Frei, E.; Elias, A.; Wheeler, C.; Richardson, P.; Hryniuk, W., The relationship between high-dose treatment and combination chemotherapy: The concept of summation dose intensity. *Clin. Cancer Res.* **1998,** 4, 2027-2037.
2. Sawyers, C. L., Disabling Abl--Perspectives on Abl kinase regulation and cancer therapeutics. *Cancer Cell* **2002,** 1, (1), 13-15.
3. Shah, N. P.; Sawyers, C. L., Mechanisms of resistance to STI571 in Philadelphia chromosome-associated leukemias. *Oncogene* **2003,** 22, (47), 7389-7395.
4. Sawyers, C. L., Opportunities and challenges in the development of kinase inhibitor therapy for cancer. *Genes Dev.* **2003,** 17, (24), 2998-3010.
5. Druker, B. J.; Talpaz, M.; Resta, D. J.; Peng, B.; Buchdunger, E.; Ford, J. M.; Lydon, N. B.; Kantarjian, H.; Capdeville, R.; Ohno-Jones, S.; Sawyers, C. L., Efficacy and Safety of a Specific Inhibitor of the BCR-ABL Tyrosine Kinase in Chronic Myeloid Leukemia. *N. Engl. J. Med.* **2001,** 344, (14), 1031-1037.
6. Sawyers, C. L.; Hochhaus, A.; Feldman, E.; Goldman, J. M.; Miller, C. B.; Ottmann, O. G.; Schiffer, C. A.; Talpaz, M.; Guilhot, F.; Deininger, M. W. N.; Fischer, T.; O'Brien, S. G.; Stone, R. M.; Gambacorti-Passerini, C. B.; Russell, N. H.; Reiffers, J. J.; Shea, T. C.; Chapuis, B.; Coutre, S.; Tura, S.; Morra, E.; Larson, R. A.; Saven, A.; Peschel, C.; Gratwohl, A.; Mandelli, F.; Ben-Am, M.; Gathmann, I.; Capdeville, R.; Paquette, R. L.; Druker, B. J., Imatinib induces hematologic and cytogenetic responses in patients with chronic myelogenous leukemia in myeloid blast crisis: results of a phase II study. *Blood* **2002,** 99, (10), 3530-3539.
7. Shah, N. P.; Nicoll, J. M.; Nagar, B.; Gorre, M. E.; Paquette, R. L.; Kuriyan, J.; Sawyers, C. L., Multiple BCR-ABL kinase domain mutations confer polyclonal resistance to the tyrosine kinase inhibitor imatinib (STI571) in chronic phase and blast crisis chronic myeloid leukemia. *Cancer Cell* **2002,** 2, (2), 117-125.
8. Branford, S.; Rudzki, Z.; Walsh, S.; Parkinson, I.; Grigg, A.; Szer, J.; Taylor, K.; Herrmann, R.; Seymour, J. F.; Arthur, C.; Joske, D.; Lynch, K.; Hughes, T., Detection of BCR-ABL mutations in patients with CML treated with imatinib is virtually always accompanied by clinical resistance, and mutations in the ATP phosphate-binding loop (P-loop) are associated with a poor prognosis. *Blood* **2003,** 102, (1), 276-283.
9. Hamann, P. R.; Hinman, L. M.; Hollander, I.; Beyer, C. F.; Lindh, D.; Holcomb, R.; Hallett, W.; Tsou, H.-R.; Upeslacis, J.; Shochat, D.; Mountain, A.; Flowers, D. A.; Bernstein, I., Gemtuzumab Ozogamicin, A Potent and Selective Anti-CD33 Antibody-Calicheamicin Conjugate for Treatment of Acute Myeloid Leukemia. *Bioconjugate Chem.* **2002,** 13, (1), 47-58.
10. Chari, R. V. J., Targeted delivery of chemotherapeutics: Tumor Activated Prodrug (TAP) therapy. *Adv. Drug Delivery Rev.* **1998,** 31, 89-104.
11. Chen, J.; Jaracz, S.; Zhao, X.; Chen, S.; Ojima, I., Antibody-based toxin conjugates for cancer therapy. *Exp. Opin. Drug Delivery* **2005,** 2, 873-890.
12. Shen, W. C.; Ryser, H. J. P., Cis-Aconityl Spacer between Daunomycin and Macromolecular Carriers - a Model of Ph-Sensitive Linkage Releasing Drug from

a Lysosomotropic Conjugate. *Biochem. Biophys. Res. Commun.* **1981,** 102, 1048-1054.

13. Yang, H. M.; Reisfeld, R. A., Pharmacokinetics and Mechanism of Action of a Doxorubicin- Monoclonal Antibody 9.2.27 Conjugate Directed to a Human-Melanoma Proteoglycan. *J. Nat. Cancer Inst.* **1988,** 80, 1154-1159.
14. Dillman, R. O.; Johnson, D. E.; Shawler, D. L.; Koziol, J. A., Superiority of an Acid-Labile Daunorubicin Monoclonal Antibody Immunoconjugate Compared to Free Drug. *Cancer Res.* **1988,** 48, 6097-6102.
15. Trail, P. A.; Willner, D.; Lasch, S. J.; Henderson, A. J.; Hofstead, S.; Casazza, A. M.; Firestone, R. A.; Hellstrom, I.; Hellstrom, K. E., Cure of Xenografted Human Carcinomas by BR96-Doxorubicin Immunoconjugates. *Science* **1993,** 261, (5118), 212-215.
16. Kaneko, T.; Willner, D.; Monkovic, I.; Knipe, J. O.; Braslawsky, G. R.; Greenfield, R. S.; Vyas, D. M., New hydrazone derivatives of Adriamycin and their immunoconjugates - a correlation between acid stability and cytotoxicity. *Bioconjugate Chem.* **1991,** 2, (3), 133-141.
17. Griffiths, G. L.; Hansen, H. J.; Goldenberg, D. M.; Lundberg, B. B. Anti-CD74 immunoconjugates and their therapeutic and diagnostic uses. (Immunomedics, Inc., USA). 2004.
18. Hamaan, P. R.; Hinman, L. M.; Hollander, I.; Beyer, C. F.; Lindh, D.; Holcomb, R.; Hallett, W.; Tsou, H.-H.; Upeslacis, J.; Shochat, D.; Mountain, A.; Flowers, D. A.; Bernstein, I., Gemtuzumab Ozogamicin, a potent and selective anti-CD33 antibody-calicheamicin conjugate for treatment of acute myeloid leukemia. *Bioconjugate Chem.* **2002,** 13, 47-58.
19. Apelgren, L. D.; Zimmerman, D. L.; Briggs, S. L.; Bumol, T. F., Antitumor Activity of the Monoclonal Antibody-Vinca Alkaloid Immunoconjugate LY203725 (KS1/4-4-Desacetylvinblastine-3-carboxhydrazide) in a Nude Mouse Model of Human Ovarian Cancer. *Cancer Res.* **1990,** 50, (12), 3540-3544.
20. Greenfield, R. S.; Kaneko, T.; Daues, A.; Edson, M. A.; Fitzgerald, K. A.; Olech, L. J.; Grattan, J. A.; Spitalny, G. L.; Braslawsky, G. R., Evaluation in Vitro of Adriamycin Immunoconjugates Synthesized Using an Acid-sensitive Hydrazone Linker. *Cancer Res.* **1990,** 50, (20), 6600-6607.
21. Willner, D.; Trail, P. A.; Hofstead, S. J.; King, H. D.; Lasch, S. J.; Braslawsky, G. R.; Greenfield, R. S.; Kaneko, T.; Firestone, R. A., (6-Maleimidocaproyl)hydrazone of doxorubicin. A new derivative for the preparation of immunoconjugates of doxorubicin. *Bioconjugate Chem.* **1993,** 4, (6), 521-527.
22. Wahl, A., F. ; Donaldson, K., L. ; Mixan, B., J. ; Trail, P., A. ; Siegall, C., B. , Selective tumor sensitization to taxanes with the mAb-drug conjugate cBR96-doxorubicin. *Int. J. Cancer* **2001,** 93, (4), 590-600.
23. Hamann, P. R.; Hinman, L. M.; Beyer, C. F.; Lindh, D.; Upeslacis, J.; Flowers, D. A.; Bernstein, I., An Anti-CD33 Antibody-Calicheamicin Conjugate for Treatment of Acute Myeloid Leukemia. Choice of Linker. *Bioconjugate Chem.* **2001,** 13, (1), 40-46.
24. www.fda.gov/Safety/MedWatch/SafetyInformation/SafetyAlertsforHumanMedicalProducts/ucm216458.htm.

25. Dyba, M.; Tarasova, N. I.; Michejda, C. J., Small molecule toxins targeting tumor receptors. *Curr. Pharm. Des.* **2004,** 10, (19), 2311-2334.
26. Dubowchik, G. M.; Radia, S.; Mastalerz, H.; Walker, M. A.; Firestone, R. A.; Dalton King, H.; Hofstead, S. J.; Willner, D.; Lasch, S. J.; Trail, P. A., Doxorubicin immunoconjugates containing bivalent, lysosomally-cleavable dipeptide linkages. *Bioorg. Med. Chem. Lett.* **2002,** 12, 1529-1532.
27. Rejmanova, P.; Kopecek, J.; Duncan, R.; Lloyd, J. B., Stability in Rat Plasma and Serum of Lysosomally Degradable Oligopeptide Sequences in N-(2-Hydroxypropyl) Methacrylamide Copolymers. *Biomaterials* **1985,** 6, 45-48.
28. Sinha, A. A.; Jamuar, M. P.; Wilson, M. J.; Rozhin, J.; Sloane, B. F., Plasma membrane association of cathepsin B in human prostate cancer: biochemical and immunogold electron microscopic analysis. *Prostate* **2001,** 49, (3), 172-184.
29. Doronina, S. O.; Toki, B. E.; Torgov, M. Y.; Mendelsohn, B. A.; Cerveny, C. G.; Chace, D. F.; DeBlanc, R. L.; Gearing, R. P.; Bovee, T. D.; Siegall, C. B.; Francisco, J. A.; Wahl, A. F.; Meyer, D. L.; Senter, P. D., Development of potent monoclonal antibody auristatin conjugates for cancer therapy. *Nat. Biotechnol.* **2003,** 21, (7), 778-784.
30. Safavy, A.; Bonner, J. A.; Waksal, H. W.; Buchsbaum, D. J.; Gillespie, G. Y.; Arani, R.; Chen, D.-T.; Carpenter, M.; Raisch, K. P., Synthesis and Biological Evaluation of Paclitaxel-C225 Conjugate as a Model for Targeted Drug Delivery. *Bioconjugate Chem.* **2003,** 14, (2), 302-310.
31. Safavy, A.; Georg, G. I.; Velde, D. V.; Raisch, K. P.; Safavy, K.; Carpenter, M.; Wang, W.; Bonner, J. A.; Khazaeli, M. B.; Buchsbaum, D. J., Site-Specifically Traced Drug Release and Biodistribution of a Paclitaxel-Antibody Conjugate toward Improvement of the Linker Structure1. *Bioconjugate Chem.* **2004,** 15, (6), 1264-1274.
32. Zheng, Z.-B.; Zhu, G.; Tak, H.; Joseph, E.; Eiseman, J. L.; Creighton, D. J., N-(2-Hydroxypropyl)methacrylamide copolymers of a glutathione (GSH)-activated glyoxalase I inhibitor and DNA alkylating agent: synthesis, reaction kinetics with GSH, and in vitro antitumor activities. *Bioconjugate Chem.* **2005,** 16, 598-607.
33. Liu, C.; Tadayoni, B. M.; Bourret, L. A.; Mattocks, K. M.; Derr, S. M.; Widdison, W. C.; Kedersha, N. L.; Ariniello, P. D.; Goldmacher, V. S.; Lambert, J. M.; Blättler, W.; Chari, R. V. J., Eradication of large colon tumor xenografts by trageted delivery of maytansinoids. *Proc. Natl. Acad. Sci. U.S.A.* **1996,** 93, 8618-8623.
34. Lam, L.; Lam, C.; Li, W.; Cao, Y., Recent advances in drug-antibody immunoconjugates for the treatment of cancer. *Drugs of the Future* **2003,** 28, (9), 905-910.
35. Tolcher, A. W.; Ochoa, L.; Hammond, L. A.; Patnaik, A.; Edwards, T.; Takimoto, C.; Smith, L.; de Bono, J.; Schwartz, G.; Mays, T.; Jonak, Z. L.; Johnson, R.; DeWitte, M.; Martino, H.; Audette, C.; Maes, K.; Chari, R. V. J.; Lambert, J. M.; Rowinsky, E. K., Cantuzumab mertansine, a maytansinoid immunoconjugate directed to the CanAg antigen: A phase I, pharmacokinetic, and biologic correlative study. *J. Clin. Oncol.* **2003,** 21, 211-222.
36. Widdison, W. C.; Wilhelm, S. D.; Cavanagh, E. E.; Whiteman, K. R.; Leece, B. A.; Kovtun, Y.; Goldmacher, V. S.; Xie, H.; Steeves, R. M.; Lutz, R. J.; Zhao, R.;

Wang, L.; Blättler, W. A.; Chari, R. V. J., Semisynthetic maytansine analogues for the targeted treatment of cancer. *J. Med. Chem.* **2006,** 49, 4392-4408.
37. Chari, R. V. J., Targeted Cancer Therapy: Conferring Specificity to Cytotoxic Drugs. *Acc. Chem. Res.* **2008,** 41, (1), 98-107.
38. Ojima, I.; Geng, X.; Wu, X.; Qu, C.; Borella, C. P.; Xie, H.; Wilhelm, S. D.; Leece, B. A.; Bartle, L. M.; Goldmacher, V. S.; Chari, R. V. J., Tumor-Specific Novel Taxoid-Monoclonal Antibody Conjugates. *J. Med. Chem.* **2002,** 45, (26), 5620-5623.
39. Ojima, I.; Das, M.; Zuniga, E., Novel Taxoid Based Tumor-Targeting Drug Conjugates. *Chemistry Today/Chimica Oggi* **2009,** 27, (6), 54-56.
40. Cook, J. A.; Pass, H. I.; Iype, S. N.; Friedman, N.; DeGraff, W.; Russo, A.; Mitchell, J. B., Cellular glutathione and thiol measurements from surgically resected human lung tumor and normal lung tissue. *Cancer Res.* **1991,** 51, 4287-4294.
41. Blair, S. L.; Heerdt, P.; Sachar, S.; Abolhoda, A.; Hochwald, S.; Cheng, H.; Burt, M., Glutathione metabolism in patients with non-small cell lung cancers. *Cancer Res.* **1997,** 57, 152-155.
42. Kosower, N. S., The glutathione status of cells. *Int. Rev. Cytol.* **1978,** 54, 109-160.
43. Britten, R. A.; Green, J. A.; Warenius, H. M., Cellular glutathione (GSH) and glutathione S-transferase (GST) activity in human ovarian tumor biopsies following exposure to alkylating agents. *Int. J. Radiat. Oncol., Biol., Phys.* **1992,** 24, 527-531.
44. Ojima, I., Use of fluorine in the medicinal chemistry and chemical biology of bioactive compounds - a case study on fluorinated taxane anticancer agents. *ChemBioChem* **2004,** 5, (5), 628-635.
45. Ojima, I., Guided Molecular Missiles for Tumor-Targeting Chemotherapy: Case Studies Using the 2nd-Generation Taxoids as Warheads. *Acc. Chem. Res.* **2008,** 41, 108-119.
46. Singh, R.; Whitesides, G. M., Comparisons of rate constants for thiolate-disulfide interchange in water and in polar aprotic solvents using dynamic proton NMR line shape analysis. *J. Am. Chem. Soc.* **1990,** 112, (3), 1190-1197.
47. DeCollo, T. V.; Lees, W. J., Effects of Aromatic Thiols on Thiol-Disulfide Interchange Reactions That Occur during Protein Folding. *J. Org. Chem.* **2001,** 66, (12), 4244-4249.
48. Hayes, J. M.; Bachrach, S. M., Effect of Micro and Bulk Solvation on the Mechanism of Nucleophilic Substitution at Sulfur in Disulfides. *J. Phys. Chem. A* **2003,** 107, (39), 7952-7961.
49. Fernandes, P. A.; Ramos, M. J., Theoretical Insights into the Mechanism for Thiol/Disulfide Exchange. *Chem. - Eur. J.* **2004,** 10, (1), 257-266.
50. Ingold, C. K., The conditions underlying the formation of unsaturated and of cyclic compounds from halogenated open-chain derivatives. I. Products derived from α-halogenated glutaric acids. *J. Chem. Soc., Trans.* **1921,** 119, 305-329.
51. Ingold, C. K.; Sako, S.; Thorpe, J. F., Influence of substituents on the formation and stability of heterocyclic compounds. I. Hydantoins. *J. Chem. Soc., Trans.* **1922,** 121, 1177-1198.

52. Allinger, N. L.; Zalkow, V., Conformational analysis. IX. gem-Dimethyl effect. *J. Org. Chem.* **1960,** 25, 701-704.
53. Blagoeva, I.; Kurtev, B.; Pozharliev, I., β-Ureido acids and dihydrouracils. II. Linear free energy-steric strain energy relations for the gem-dimethyl effect. Acid-catalyzed ring closure of methyl-substituted 3-ureidopropionic acids. *J. Chem. Soc., Perkin Trans. 2: Phys. Org. Chem.* **1979**, 1115-1122.
54. Litvinenko, L. M.; Dadali, V. A.; Savelova, V. A.; Krichevtsova, T. I., A New Method for the Synthesis of Arylsulfonyl Bromides and Iodides. *J. Gen. Chem. USSR (Engl. Transl.)* **1964,** 34, (11), 3780-3783.
55. Ranasinghe, M. G.; Fuchs., P. L., A Facile Synthesis of Unsymmetrical Thiosulfonates via Sulfonylation of Mercaptans. *Syn. Comm.* **1988,** 18, (3), 227-232.

References for Chapter 4:

1. Frei, E., III, Combination Cancer Therapy: Presidential Address. *Cancer Res.* **1972,** 32, (12), 2593-2607.
2. Frei, E., III; Freireich, E. J. , Progress and Perspectives in the Chemotherapy of Acute Leukemia. *Advan. Chemotherapy* **1965,** 2, 269-278.
3. Thomas, G. D., *Drug Targeting Strategies, Principles, and Applications*. Humana Press: 2000; p 97-114.
4. Jain, R. K., Transport of Molecules in the Tumor Interstitium: A Review. *Cancer Res.* **1987,** 47, (12), 3039-3051.
5. Maeda, H. F. J. I., T.; Kitamoto, Y., Vascular permeability enhancement in solid tumor: various factors, mechanisms involved and its implications. *Int. Immunopharmacol.* **2003,** 3, 319-328.
6. Maeda, H.; Matsumura, Y.; Oda, T.; Sasamoto, K., In *Protein Tailoring for Food and Medical Uses*, Feeny, R. E. W., J. R., Ed. Marcel Dekker: New York, 1986; pp 353-382.
7. Maeda, H.; Bharate, G. Y.; Daruwalla, J., Polymeric drugs for efficient tumor-targeted drug delivery based on EPR-effect. *Eur. J. Pharm. Biopharm.* **2009,** 71, (3), 409-419.
8. Rainer, H. F., Kratz., Polymer Therapeutics: Concepts and Applications. *Angew. Chem. Int.* **2006,** 45, (8), 1198-1215.
9. Maeda, H. M., Y., Tumoritropic and lymphotropic principles of macromolecular drugs. *Crit. Rev. Ther. Drug Carrier Syst.* **1989,** 6, 193-210.
10. Maeda, H., SMANCS and polymer-conjugated macromolecular drugs: advantages in cancer chemotherapy. *Adv. Drug Deliv. Rev.* **1991,** 6, 181 - 202.
11. Maeda, H. S., L.; Miyamoto, Y., Conjugation of anticancer agents and polymers: advantages of macromolecular therapeutics in vivo. *Bioconjugate Chem.* **1992,** 3, 351- 362.
12. Muggia, F. M., Doxorubicin-polymer conjugates: further demonstration of the concept of enhanced permeability and retention. *Clin. Cancer Res.* **1999,** 5, 7-8.
13. Suzuki, M. H., K.; Abe, Z.; Asito, S.; Sato, H. , A new approach to cancer chemotherapy: selective enhancement of tumor blood flow with angiotensin II. *J. Natl. Cancer Inst.* **1981,** 67, 663- 669.
14. Hori, K. S., S.; Takahashi, H.; Sato, H.; Maeda, H.; Sato, Y., Tumor-selective blood flow decrease induced by an angiotensin converting enzyme inhibitor, temocapril hydrochloride. *Jpn J Cancer Res* **2000,** 91, (261-269).
15. Hori, K. S., M.; Tanda, S.; Saito, S.; Shinozaki, M.; Zhang, Q.H., Fluctuations in tumor blood flow under normotension and the effect of angiotensin II-induced hypertension. *Jpn. J. Cancer Res.* **1991,** 82, 1309-1316.
16. Matsumura, Y. M., H., A new concept for macromolecular therapeutics in cancer chemotherapy: mechanism of tumoritropic accumulation of proteins and the antitumor agent SMANCS. *Cancer Res.* **1986,** 46, 6387- 6392.
17. Noguchi, Y. W., J.; Duncan, R.; Strohalm, J.; Ulbrich, K.; Akaike, T.; et. al., Early phase tumor accumulation of macromolecules: a great difference in clearance rate between tumor and normal tissues. *Jpn. J. Cancer Res.* **1998,** 89, 307-314.

18. Chari, R. V. J., Targeted delivery of chemotherapeutics: tumor-activated prodrug therapy. *Adv. Drug Delivery Rev.* **1998,** 31, (1,2), 89-104.
19. Griffiths, J. R., Are cancer cells acidic? *Br. J. Cancer* **1991,** 64, (3), 425-427.
20. Schornack, P. A. G., R. J., Contributions of Cell Metabolism and H+ Diffusion to the Acidic pH of Tumors. *Neoplasia* **2003,** 5, (2), 135-145.
21. Ojima, I., Guided Molecular Missiles for Tumor-Targeting Chemotherapy: Case Studies Using the 2nd-Generation Taxoids as Warheads. *Acc. Chem. Res.* **2008,** 41, 108-119.
22. Chen, J.; Jaracz, S.; Zhao, X.; Chen, S.; Ojima, I., Antibody-based toxin conjugates for cancer therapy. *Exp. Opin. Drug Delivery* **2005,** 2, 873-890.
23. Jaracz, S.; Chen, J.; Kuznetsova, L. V.; Ojima, I., Recent Advances in Tumor-targeting Anticancer Drug Conjugates. *Bioorg. Med. Chem.* **2005,** 13, 5043-5054.
24. Ojima, I.; Das, M.; Zuniga, E., Novel Taxoid Based Tumor-Targeting Drug Conjugates. *Chemistry Today/Chimica Oggi* **2009,** 27, (6), 54-56.
25. Hamaan, P. R.; Hinman, L. M.; Hollander, I.; Beyer, C. F.; Lindh, D.; Holcomb, R.; Hallett, W.; Tsou, H.-H.; Upeslacis, J.; Shochat, D.; Mountain, A.; Flowers, D. A.; Bernstein, I., Gemtuzumab Ozogamicin, a potent and selective anti-CD33 antibody-calicheamicin conjugate for treatment of acute myeloid leukemia. *Bioconjugate Chem.* **2002,** 13, 47-58.
26. Wu, X.; Ojima, I., Tumor specific novel taxoid-monoclonal antibody conjugates. *Curr. Med. Chem.* **2004,** 11, 429-438.
27. Ojima, I.; Geng, X.; Wu, X.; Qu, C.; Borella, C. P.; Xie, H.; Wilhelm, S. D.; Leece, B. A.; Bartle, L. M.; Goldmacher, V. S.; Chari, R. V. J., Tumor-Specific Novel Taxoid-Monoclonal Antibody Conjugates. *J. Med. Chem.* **2002,** 45, (26), 5620-5623.
28. Endo, N.; Takeda, Y.; Kishida, K.; Kato, Y.; Saito, M.; Umemoto, N.; Hara, T., Target-selective cytotoxicity of methotrexate conjugated with monoclonal anti-MM46 antibody. *Cancer Immunol. Immunother.* **1987,** 25, 1-6.
29. Pietersz, G. A.; Krauer, K., Antibody-targeted drugs for the therapy of cancer. *J. Drug Targeting* **1994,** 2, 183-215.
30. Lee, J. W.; Lu, J. Y.; Low, P. S.; Fuchs, P. L., Synthesis and Evaluation of Taxol-Folic Acid Conjugates as Targeted Antineoplastics. *Bioorg. Med. Chem.* **2002,** 10, (7), 2397-2414.
31. Low, P. S.; Henne, W. A.; Doorneweerd, D. D., Discovery and Development of Folic-Acid-Based Receptor Targeting for Imaging and Therapy of Cancer and Inflammatory Diseases. *Acc. Chem. Res.* **2008,** 41, (1), 120-129.
32. Leamon, C. P.; Reddy, J. A., Folate-targeted chemotherapy. *Adv. Drug Delivery Rev.* **2004,** 56, 1127-1141.
33. Chen, J.; Chen, S.; Zhao, X.; Kuznetsova, L. V.; Wong, S. S.; Ojima, I., Functionalized Single-Walled Carbon Nanotubes as Rationally Designed Vehicles for Tumor-Targeted Drug Delivery. *J. Am. Chem. Soc.* **2008,** 130, (49), 16778-16785.
34. Chen, S.; Zhao, X.; Chen, J.; Chen, J.; Kuznetsova, L. V.; Wong, S. S.; Ojima, I., Mechanism-Based Tumor-Targeting Drug Delivery System. Validation of Efficient Vitamin Receptor-Mediated Endocytosis and Drug Release. *Bioconjugate Chem.* **2010,** 21, (5), 979-987.

35. Hicke, B. J.; Stephens, A. W., Escort aptamers: a delivery service for diagnosis and therapy. *J. Clin. Invest.* **2000,** 106, (8), 923-928.
36. Chu, T. C.; Marks, J. W. I.; Lavery, L. A.; Faulkner, S.; Rosenblum, M. G.; Ellington, A. D.; Levy, M., Aptamer:toxin conjugates that specifically target prostate tumor cells. *Cancer Res.* **2006,** 66, 5989-5992.
37. Nagy, A.; Schally, A. V.; Halmos, G.; Armatis, P.; Cai, R.-Z.; Csernus, V.; Kovacs, M.; Koppan, M.; Szepeshazi, K.; Kahan, Z., Synthesis and biological evaluation of cytotoxic analogs of somatostatin containing doxorubicin or its intensely potent derivative, 2-pyrrolinodoxorubicin. *Proc. Natl. Acad. Sci. U. S. A.* **1998,** 95, (4), 1794-1799.
38. Luo, Y.; Bernshaw, N. J.; Lu, Z.-R.; Kopecek, J.; Prestwich, G. D., Targeted Delivery of Doxorubicin by HPMA Copolymer-Hyaluronan Bioconjugates. *Pharm. Res.* **2002,** 19, 396-402.
39. Luo, Y.; Ziebell, M. R.; Prestwich, G. D., A hyaluronic acid taxol antitumor bioconjugate targeted to cancer cells. *Biomacromolecules* **2000,** 1, 208–218.
40. Bradley, M. O.; Webb, N. L.; Anthony, F. H.; Devanesan, P.; Witman, P. A.; Hemamalini, S.; Chander, M. C.; Baker, S. D.; He, L.; Horowitz, S. B.; Swindell, C. S., Tumor Targeting by Covalent Conjugation of a Natural Fatty Acid to Taxol. *Clin. Cancer Res.* **2001,** 7, 3229-3238.
41. Kuznetsova, L. V.; Chen, J.; Sun, L.; Wu, X.; Pepe, A.; Veith, J. M.; Pera, P.; Bernacki, R. J.; Ojima, I., Syntheses and Evaluation of Novel Fatty Acid-2nd-generation Taxoid Conjugates as Promising Anticancer Agents. *Bioorg. Med. Chem. Lett.* **2006,** 16, 974-977
42. Ehrlich, P., A general review of the recent work in immunity. In *Collected papers of Paul Ehrlich*, 1956; Vol. 2, pp 442-447.
43. Kohler, G.; Milstein, C., Continuous cultures of fused cells secreting antibody of predefined specificity. *Nature* **1975,** 256, (5517), 495-497.
44. Carter, P., Improving the efficacy of antibody-based cancer therapies. *Nat. Rev. Cancer* **2001,** 1, (2), 118-129.
45. Yokota, T.; Milenic, D. E.; Whitlow, M.; Schlom, J., Rapid tumor penetration of a single-chain Fv and comparison with other immunoglobulin forms. *Cancer Res.* **1992,** 52, 3402-3408.
46. Yokota, T.; Milenic, D. E.; Whitlow, M.; Wood, J. F.; Hubert, S. L.; Schlom, J., Microautoradiographic analysis of the normal organ distribution of radioiodinated single-chain Fv and other immunoglobulin forms *Cancer Res.* **1993,** 53 3776-3783.
47. King, D. J.; Turner, A.; Farnsworth, A. P. H.; Adair, J. R.; Owens, R. J.; Pedley, R. B.; Baldock, D.; Proudfoot, K. A.; Lawson, A. D. G.; Beeley, N. R. A.; Millar, K.; Millican, T. A.; Boyce, B. A.; Antoniw, P.; Mountain, A.; Begent, R. H. J.; Shochat, D.; Yarranton, Y. T., Improved tumor targeting with chemically cross-linked recombinant antibody fragments. *Cancer Res.* **1994,** 54 6176–6185.
48. Otsuji, E.; Yamaguchi, T.; Tsuruta, H.; Yata, Y.; Nishi, H.; Okamoto, K.; Taniguchi, K.; Kato, M.; Kotani, T.; Kitamura, K.; Takahashi, T., Effects of neocarzinostatin-chimeric Fab conjugates on the growth of human pancreatic carcinoma xenografts. *Br. J. Cancer* **1996,** 73, (10), 1178-1182.

49. Roguska, M. A.; Pedersen, J. T.; Henry, A. H., A comparison of two murine monoclonal antibodies humanized by CDR-grafting and variable domain resurfacing. *Protein Eng.* **1996,** 9, (10), 895-904.
50. Moody, T. W.; Czerwinski, G.; Tarasova, N. I.; Michejda, C. J., Pellipticine derivatives inhibit the growth of breast cancer cells. *Life Sci.* **2002,** 71, (9), 1005-1014.
51. Spearman, M. E.; Goodwin, R. M.; Apelgren, L. D.; Bumol, T. F., Disposition of the monoclonal antibody-vinca alkaloid conjugate KS1/4-DAVLB (LY256787) and free 4-desacetylvinblastine in tumor-bearing nude mice. *J. Pharmacol. Exp. Ther.* **1987,** 241, (2), 695-703.
52. Apelgren, L. D.; Zimmerman, D. L.; Briggs, S. L.; Bumol, T. F., Antitumor Activity of the Monoclonal Antibody-Vinca Alkaloid Immunoconjugate LY203725 (KS1/4-4-Desacetylvinblastine-3-carboxhydrazide) in a Nude Mouse Model of Human Ovarian Cancer. *Cancer Res.* **1990,** 50, (12), 3540-3544.
53. Manabe, Y.; Tsubota, T.; Haruta, Y.; Kataoka, K.; Okazaki, M.; Haisa, S.; Nakamura, K.; Kimura, I., Production of a monoclonal antibody-mitomycin C conjugate, utilizing dextran T-40, and its biological activity. *Biochem. Pharmacol.* **1985,** 34, (2), 289-291.
54. Hamann, P. R.; Hinman, L. M.; Hollander, I.; Beyer, C. F.; Lindh, D.; Holcomb, R.; Hallett, W.; Tsou, H.-R.; Upeslacis, J.; Shochat, D.; Mountain, A.; Flowers, D. A.; Bernstein, I., Gemtuzumab Ozogamicin, A Potent and Selective Anti-CD33 Antibody-Calicheamicin Conjugate for Treatment of Acute Myeloid Leukemia. *Bioconjugate Chem.* **2002,** 13, (1), 47-58.
55. Doronina, S. O.; Toki, B. E.; Torgov, M. Y.; Mendelsohn, B. A.; Cerveny, C. G.; Chace, D. F.; DeBlanc, R. L.; Gearing, R. P.; Bovee, T. D.; Siegall, C. B.; Francisco, J. A.; Wahl, A. F.; Meyer, D. L.; Senter, P. D., Development of potent monoclonal antibody auristatin conjugates for cancer therapy. *Nat. Biotechnol.* **2003,** 21, (7), 778-784.
56. Liu, C.; Tadayoni, B. M.; Bourret, L. A.; Mattocks, K. M.; Derr, S. M.; Widdison, W. C.; Kedersha, N. L.; Ariniello, P. D.; Goldmacher, V. S.; Lambert, J. M.; Blättler, W.; Chari, R. V. J., Eradication of large colon tumor xenografts by trageted delivery of maytansinoids. *Proc. Natl. Acad. Sci. U.S.A.* **1996,** 93, 8618-8623.
57. Chari, R. V. J.; Jackel, K. A.; Bourret, L. A.; Derr, S. M.; Tadayoni, B. M.; Mattocks, K. M.; Shah, S. A.; Liu, C.; Blattler, W. A.; Goldmacher, V. S., Enhancement of the selectivity and antitumor efficacy of a CC-1065 analog through immunoconjugate formation. *Cancer Res.* **1995,** 55, (18), 4079-84.
58. Lam, L.; Lam, C.; Li, W.; Cao, Y., Recent advances in drug-antibody immunoconjugates for the treatment of cancer. *Drugs of the Future* **2003,** 28, (9), 905-910.
59. Saleh, M. N.; LoBuglio, A. F.; Trail, P. A., Monoclonal antibody-based immunoconjugate therapy of cancer: studies with BR96-doxorubicin. *Basic Clin. Oncol.* **1998,** 15, 397-416.
60. Gillespie, A. M.; Broadhead, T. J.; Chan, S. Y.; Owen, J.; Farnsworth, A. P.; Sopwith, M.; Coleman, R. E., Phase I open study of the effects of ascending doses

of the cytotoxic immunoconjugate CMB-401 (hCTMO1-calicheamicin) in patients with epithelial ovarian cancer. *Ann. Oncol.* **2000,** 11, (6), 735-741.
61. Toole, B., In *Cell Biology of the Extracellular Matrix*, Hay, E., Ed. Plenum Press: New York, 1982; pp 259–294.
62. Huang, L.; Grammatikakis, N.; Yoneda, M.; Banerjee, S. D.; Toole, B. P., Molecular Characterization of a Novel Intracellular Hyaluronan-binding Protein. *J. Biol. Chem.* **2000,** 275, (38), 29829-29839.
63. Ponta, H.; Sherman, L.; Herrlich, P. A., CD44: From adhesion molecules to signalling regulators. *Nat. Rev. Mol. Cell Biol.* **2003,** 4, (1), 33-45.
64. Toole, B. P.; Wight, T. N.; Tammi, M. I., Hyaluronan-Cell Interactions in Cancer and Vascular Disease. *J. Biol. Chem.* **2002,** 277, (7), 4593-4596.
65. Yang, B.; Zhang, L.; Turley, E. A., Identification of two hyaluronan-binding domains in the hyaluronan receptor RHAMM. *J. Biol. Chem.* **1993,** 268, (12), 8617-8623.
66. Day, A. J.; Prestwich, G. D., Hyaluronan-binding Proteins: Tying Up the Giant. *J. Biol. Chem.* **2002,** 277, (7), 4585-4588.
67. Turley, E. A.; Belch, A. J.; Poppema, S.; Pilarski, L. M., Expression and function of a receptor for hyaluronan-mediated motility on normal and malignant B lymphocytes. *Blood* **1993,** 81, (2), 446-453.
68. Hua, Q.; Knudson, C. B.; Knudson, W., Internalization of hyaluronan by chondrocytes occurs via receptor-mediated endocytosis. *J. Cell Sci.* **1993,** 106, (1), 365-375.
69. Kosaki, R.; Watanabe, K.; Yamaguchi, Y., Overproduction of Hyaluronan by Expression of the Hyaluronan Synthase Has2 Enhances Anchorage-independent Growth and Tumorigenicity. *Cancer Res.* **1999,** 59, (5), 1141-1145.
70. Liu, N.; Gao, F.; Han, Z.; Xu, X.; Underhill, C. B.; Zhang, L., Hyaluronan Synthase 3 Overexpression Promotes the Growth of TSU Prostate Cancer Cells. *Cancer Res.* **2001,** 61, (13), 5207-5214.
71. Lesley, J.; Hascall, V. C.; Tammi, M.; Hyman, R., Hyaluronan Binding by Cell Surface CD44. *J. Biol. Chem.* **2000,** 275, (35), 26967-26975.
72. Day, A. J.; Prestwich, G. D., Hyaluronan-binding Proteins: Tying Up the Giant. *J. Biol. Chem.* **2002,** 277, 4585–4588.
73. Danila, C.; Cinzia, P.; Giuliana, M.; Maria Grazia, D.; Alberto, P., Hyaluronic acid as drug delivery for sodium butyrate: Improvement of the anti-proliferative activity on a breast-cancer cell line. *Int. J. Cancer* **1999,** 81, (3), 411-416.
74. Eliaz, R. E.; Szoka, F. C., Liposome-encapsulated Doxorubicin Targeted to CD44. *Cancer Res.* **2001,** 61, (6), 2592-2601.
75. Tuerk, C.; Gold, L., Systematic Evolution of Ligands by Exponential Enrichment: RNA Ligands to Bacteriophage T4 DNA Polymerase. *Science* **1990,** 249, (4968), 505-510.
76. Ellington, A. D.; Szostak, J. W., In vitro selection of RNA molecules that bind specific ligands. *Nature* **1990,** 346, (6287), 818-822.
77. Feigon, J.; Dieckmann, T.; Smith, F. W., Aptamer structures from A to Z. *Chem. Biol.* **1996,** 3, (8), 611-617.
78. Gold, L., Oligonucleotides as Research, Diagnostic, and Therapeutic Agents. *J. Biol. Chem.* **1995,** 270, (23), 13581-13584.

79. White, R. R.; Sullenger, B. A.; Rusconi, C. P., Developing aptamers into therapeutics. *J. Clin. Invest.* **2000,** 106, 929-934.
80. Blank, M.; Blind, M., Aptamers as tools for target validation. *Curr. Opin. Chem. Biol.* **2005,** 9, (4), 336-342.
81. Gilbert, J. C.; DeFeo-Fraulini, T.; Hutabarat, R. M.; Horvath, C. J.; Merlino, P. G.; Marsh, H. N.; Healy, J. M.; BouFakhreddine, S.; Holohan, T. V.; Schaub, R. G., First-in-Human Evaluation of Anti von Willebrand Factor Therapeutic Aptamer ARC1779 in Healthy Volunteers. *Circulation* **2007,** 116, (23), 2678-2686.
82. Melnikova, I., RNA-based therapies. *Nat. Rev. Drug Discovery* **2007,** 6, (11), 863-864.
83. Vaishali, B.; Omid, C. F.; Robert, L.; Sangyong, J., An Aptamer-Doxorubicin Physical Conjugate as a Novel Targeted Drug-Delivery Platform. *Angew. Chem. Int. Ed. Engl.* **2006,** 45, (48), 8149-8152.
84. Orlando, C.; Raggi, C. C.; Bianchi, S.; Distante, V.; Simi, L.; Vezzosi, V.; Gelmini, S.; Pinzani, P.; Smith, M. C.; Buonamano, A.; Lazzeri, E.; Pazzagli, M.; Cataliotti, L.; Maggi, M.; Serio, M., Measurement of somatostatin receptor subtype 2 mRNA in breast cancer and corresponding normal tissue. *Endocr. Relat. Cancer* **2004,** 11, 323-332.
85. Weckbecker, G.; Raulf, F.; Stolz, B.; Bruns, C., Somatostatin analogs for diagnosis and treatment of cancer. *Pharmacol. Ther.* **1993,** 60, 245-264.
86. Szepeshazi, K.; Schally, A. V.; Halmos, G.; Sun, B.; Hebert, F.; Csernus, B.; Nagy, A., Targeting of Cytotoxic Somatostatin Analog AN-238 to Somatostatin Receptor Subtypes 5 and/or 3 in Experimental Pancreatic Cancers. *Clin. Cancer Res.* **2001,** 7, (9), 2854-2861.
87. Kiaris, H.; Schally, A. V.; Nagy, A.; Szepeshazi, K.; Hebert, F.; Halmos, G., A targeted cytotoxic somatostatin (SST) analogue, AN-238, inhibits the growth of H-69 small-cell lung carcinoma (SCLC) and H-157 non-SCLC in nude mice. *Eur. J. Cancer* **2001,** 37, (5), 620-628.
88. Chen, X.; Plasencia, C.; Hou, Y.; Neamati, N., Synthesis and biological evaluation of dimeric RGD peptide-paclitaxel conjugate as a model for integrin-targeted drug delivery. *J. Med. Chem.* **2005,** 48, (4), 1098-1106.
89. Smyth, M. J.; Pietersz, G. A.; McKenzie, I. F. C., Selective enhancement of anti-tumor activity of N-acetyl melphalan upon conjugation to monoclonal antibodies. *Cancer Res.* **1987,** 47, 62-69.
90. Hurwitz, E.; Wilchek, M.; Pitha, J., Soluble macromolecules as carriers for daunorubicin. *J. Appl. Biochem.* **1980,** 2, 25-35.
91. Endo, N.; Takeda, Y.; Umemoto, N.; Kishida, K.; Watanabe, K.; Saito, M.; Kato, Y.; Hara, T., Nature of linkage and mode of action of methotrexate conjugated with antitumor antibodies: implications for future preparation of conjugates. *Cancer Res.* **1988,** 48, 3330-3335.
92. Schneck, D.; Butler, F.; Dugan, W.; Littrell, D.; Petersen, B.; Bowsher, R.; DeLong, A.; Dorrbecker, S., Disposition of a murine monoclonal antibody-Vinca conjugate (KS1/4-DAVLB) in patients with adenocarcinoma. *Clin. Pharmacol. Ther.* **1990,** 47, 36-41.

93. Nicolaou, K. C.; Ogawa, Y.; Zuccarello, G.; Kataoka, H., DNA cleavage by a synthetic mimic of the calicheamicin-esperamicin class of antibiotics. *J. Am. Chem. Soc.* **1988,** 110, 7247-7248.
94. Lee, M. D.; Dunne, T. S.; Siegel, M. M.; Chang, C. C.; Morton, G. O.; Borders, D. B., Calichemicins, a novel family of antitumor antibiotics. 1. Chemistry and partial structure of calichemicin g1I. *J. Am. Chem. Soc.* **1987,** 109, 3464-3466.
95. Lee, M. D.; Dunne, T. S.; Chang, C. C.; Ellestad, G. A.; Siegel, M. M.; Morton, G. O.; McGahren, W. J.; Borders, D. B., Calichemicins, a novel family of antitumor antibiotics. 2. Chemistry and structure of calichemicin g1I. *J. Am. Chem. Soc.* **1987,** 109, 3466-3468.
96. Kupchan, S. M.; Komoda, Y.; Thomas, G. J.; Smith, R. M.; Bryan, R. F.; Haltiwanger, R. C.; Karim, A.; Court, W. A.; Gilmore, C. J., Tumor Inhibitors .73. Maytansine, a Novel Antileukemic Ansa Macrolide from Maytenus-Ovatus. *J. Am. Chem. Soc.* **1972,** 94, 1354-1356.
97. Wolpert-DeFilippes, M. K.; Adamson, R. H.; Cysyk, R. L.; Johns, D. G., Initial Studies on Cytotoxic Action of Maytansine, a Novel Ansa Macrolide. *Biochem. Pharmacol.* **1975,** 24, 751-754.
98. Keyes, S. R.; Heimbrook, D. C.; Fracasso, P. M.; Rockwell, S.; Sligar, S. G.; Sartorelli, A. C., Chemotherapeutic attack of hypoxic tumor cells by the bioreductive alkylating agent mitomycin C. *Adv. Enzyme Regul.* **1985,** 23, 291-307.
99. Li, V.-S.; Choi, D.; Tang, M.-S.; Kohn, H., Concerning In Vitro Mitomycin-DNA Alkylation. *J. Am. Chem. Soc.* **1996,** 118, 3765-3766.
100. Hata, T.; Sano, Y.; Sugawara, R.; Matsumae, A.; Kanamori, K.; Shima, T.; Hoshi, T., Mitomycin, a new antibiotic from Streptomyces. I. *J. Antibiot.* **1956,** 9, 141-146.
101. Tanaka, J.-I.; Sato, E.; Saito, Y.; Kusano, T.; Koyama, K., Preparation of a conjugate of mitomycin C and anti-neural cell adhesion molecule monoclonal antibody for specific chemotherapy against biliary tract carcinoma. *Surg. Today* **1998,** 28, 1217-1220.
102. Li, S.; Zhang, X.; Zhang, S.; Chen, X.; Chen, L.; Shu, Y.; Zhang, J.; Fan, D., Preparation of antigastric cancer monoclonal antibody MGb2-mitomycin C conjugate with improved antitumor activity. *Bioconjugate Chem.* **1990,** 1, 245-250.
103. Ojima, I., Science of Taxol. *Farumashia* **2003,** 39, 49-53.
104. Guillemard, V.; Saragovi, H. U., Taxane-antibody conjugates afford potent cytotoxicity, enhanced solubility, and tumor target selectivity. *Cancer Res.* **2001,** 61, 694-699.
105. Safavy, A.; Bonner, J. A.; Waksal, H. W.; Buchsbaum, D. J.; Gillespie, G. Y.; Arani, R.; Chen, D.-T.; Carpenter, M.; Raisch, K. P., Synthesis and Biological Evaluation of Paclitaxel-C225 Conjugate as a Model for Targeted Drug Delivery. *Bioconjugate Chem.* **2003,** 14, (2), 302-310.
106. Ojima, I.; Slater, J. C.; Michaud, E.; Kuduk, S. D.; Bounaud, P.-Y.; Vrignaud, P.; Bissery, M.-C.; Veith, J.; Pera, P.; Bernacki, R. J., Syntheses and Structure-Activity Relationships of the Second Generation Antitumor Taxoids. Exceptional

Activity against Drug-Resistant Cancer Cells. *J. Med. Chem.* **1996,** 39, 3889-3896.

107. Ojima, I.; Slater, J. S.; Kuduk, S. D.; Takeuchi, C. S.; Gimi, R. H.; Sun, C.-M.; Park, Y. H.; Pera, P.; Veith, J. M.; Bernacki, R. J., Syntheses and Structure-Activity Relationships of Taxoids Derived from 14β-Hydroxy-10-deacetylbaccatin III. *J. Med. Chem.* **1997,** 40, 267-278.
108. Ojima, I.; Kuduk, S. D.; Pera, P.; Veith, J. M.; Bernacki, R. J., Synthesis of and Structure-Activity Relationships of Non-Aromatic Taxoids. Effects of Alkyl and Alkenyl Ester Groups on Cytotoxicity. *J. Med. Chem.* **1997,** 40, 279-285.
109. Ojima, I.; Lin, S., Efficient Asymmetric Syntheses of β-Lactams Bearing a Cyclopropane or an Epoxide Moiety and Their Application to the Syntheses of Novel Isoserines and Taxoids. *J. Org. Chem.* **1998,** 63, 224-225.
110. Ojima, I.; Wang, T.; Miller, M. L.; Lin, S.; Borella, C.; Geng, X.; Pera, P.; Bernacki, R. J., Syntheses and Structure-Activity Relationships of New Second-Generation Taxoids. *Bioorg. Med. Chem. Lett.* **1999,** 9, 3423-3428.
111. Ojima, I.; Geney, R.; Ungureanu, I. M.; Li, D., Medicinal chemistry and chemical biology of new generation taxane antitumor agents. *IUBMB Life* **2002,** 53, 269-274.
112. Dimarco, A.; Valentine, L.; Scarpina, B. M.; Dasdia, T.; Soldati, M.; Gaetani, M.; Orezzi, P.; Silvestrini, R., Daunomycin New Antibiotic of Rhodomycin Group. *Nature* **1964,** 201, 706-707.
113. Wahl, A. F.; Donaldson, K. L.; Mixan, B. J.; Trail, P. A.; Siegall, C. B., Selective tumor sensitization to taxanes with the mAb-drug conjugate cBR96-doxorubicin. *Int. J. Cancer* **2001,** 93, (4), 590-600.
114. Jaime, J.; Page, M., Paclitaxel immunoconjugate for the specific treatment of ovarian cancer in vitro. *Anticancer Res.* **2001,** 21, 1119-1128.
115. Netti, P. A.; Baxter, L. T.; Boucher, Y.; Skalak, R.; Jain, R. K., Time-dependent behavior of interstitial fluid pressure in solid tumors: implications for drug delivery. *Cancer Res.* **1995,** 55, 5451-5458.
116. Stover, P. J., Physiology of Folate and Vitamin B12 in Health and Disease. *Nutr. Rev.* **2004,** 62, (6), S3-12 discussion S13.
117. Salazar, M.; Ratnam, M., The folate receptor: What does it promise in tissue-targeted therapeutics? *Cancer Metastasis Rev.* **2007,** 26, (1), 141-152.
118. Nakashima-Matsushita, N.; Homma, T.; Yu, S.; Matsuda, T.; Sunahara, N.; Nakamura, T.; Tsukano, M.; Ratnam, M.; Matsuyama, T., Selective expression of folate receptor beta and its possible role in methotrexate transport in synovial macrophages from patients with rheumatoid arthritis. *Arthritis Rheum.* **1999,** 42, (8), 1609-1616.
119. Qiu, A.; Jansen, M.; Sakaris, A.; Min, S. H.; Chattopadhyay, S.; Tsai, E.; Sandoval, C.; Zhao, R.; Akabas, M. H.; Goldman, I. D., Identification of an Intestinal Folate Transporter and the Molecular Basis for Hereditary Folate Malabsorption. *Cell* **2006,** 127, (5), 917-928.
120. Matherly, L. H.; Goldman, D. I., Membrane transport of folates. *Vitam. Horm.* **2003,** 66, 403-456.
121. Antony, A. C., The biological chemistry of folate receptors. *Blood* **1992,** 79, (11), 2807-2820.

122. Kamen, B. A.; Smith, A. K., A review of folate receptor alpha cycling and 5-methyltetrahydrofolate accumulation with an emphasis on cell models in vitro. *Adv. Drug Deliv. Rev.* **2004,** 56, (8), 1085-1097.
123. Antony, A. C., Folate Receptors. *Annu. Rev. Nutr.* **1996,** 16, (1), 501-521.
124. Sabharanjak, S.; Mayor, S., Folate receptor endocytosis and trafficking. *Adv. Drug Deliv. Rev.* **2004,** 56, (8), 1099-1109.
125. Shen, F.; Ross, J. F.; Wang, X.; Ratnam, M., Identification of a novel folate receptor, a truncated receptor, and receptor type beta in hematopoietic cells: cDNA cloning, expression, immunoreactivity, and tissue specificity. *Biochemistry* **1994,** 33, 1209-1215.
126. Kamen, B. A.; Caston, J. D., Properties of a folate binding protein (FBP) isolated from porcine kidney. *Biochem. Pharmacol.* **1986,** 35, 2323-2329.
127. da Costa, M.; Rothenberg, S. P., Purification and characterization of folate binding proteins from rat placenta. *Biochim. Biophys. Acta* **1996,** 1292, 23-30.
128. Yingjuan, L.; Low, P. S., Folate-mediated delivery of macromolecular anticancer therapeutic agents. *Adv. Drug Deliv. Rev.* **2002,** 54, 675-693.
129. Toffoli, G.; Cernigoi, C.; Russo, A.; Gallo, A.; Bagnoli, M.; Boiocchi, M., Overexpression of folate binding protein in ovarian cancers. *Int. J. Cancer* **1997,** 74, 193-198.
130. Ross, J. F.; Chaudhuri, P. K.; Ratnam, M., Differential regulation of folate receptor isoforms in normal and malignant tissues in vivo and in established cell lines. Physiologic and clinical implications. *Cancer* **1994,** 73, 2432-2443.
131. Wu, M.; Gunning, W.; Ratnam, M., Expression of folate receptor type alpha in relation to cell type, malignancy, and differentiation in ovary, uterus, and cervix. *Cancer Epidemiol. Biomarkers Prev.* **1999,** 8 775-782.
132. Weitman, S. D.; Frazier, K. M.; Kamen, B. A., The folate receptor in central nervous system malignancies of childhood. *Arthritis J. Neurooncol.* **1994,** 21, 107-112.
133. Toffoli, G.; Russo, A.; Gallo, A.; Cernigoi, C.; Miotti, S.; Sorio, R.; Tumolo, S.; Boiocchi, M., Expression of folate binding protein as a prognostic factor for response to platinum containing chemotherapy and survival in human ovarian cancer. *Int. J. Cancer* **1998,** 79, 121-126.
134. Ross, J. F.; Wang, H.; Behm, F. G.; Mathew, P.; Wu, M.; Booth, R.; Ratnam, M., Folate receptor type beta is a neutrophilic lineage marker and is differentially expressed in myeloid leukemia. *Cancer* **1999,** 85, 348-357.
135. Reddy, J. A.; Haneline, L. S.; Srour, E. F.; Antony, A. C.; Clapp, D. W.; Low, P. S., Expression and functional characterization of the beta-isoform of the folate receptor on CD34(1) cells. *Blood* **1999,** 93, 3940-3948.
136. Weitman, S. D.; Weinberg, A. G.; Coney, L. R.; Zurawski, V. R.; Jennings, D. S.; Kamen, B. A., Cellular localization of the folate receptor: potential role in drug toxicity and folate homeostasis. *Cancer Res.* **1992,** 52, 6708-6711.
137. Patrick, T. A.; Kranz, D. M.; van Dyke, T. A.; Roy, E. J., Folate receptors as potential therapeutic targets in choroid plexus tumors of SV40 transgenic mice. *J. Neurooncol.* **1997,** 32, 111-123.

138. Birn, H.; Nielsen, S.; Christensen, E. I., Internalization and apical-to-basolateral transport of folate in rat kidney proximal tubule. *Am. J. Physiol.* **1997,** 272, F70-78.
139. Leamon, C. P.; DePrince, R. B.; Hendren, R. W., Folate-mediated drug delivery: effect of alternative conjugation chemistry. *J. Drug Targeting* **1999,** 7, 157-169.
140. Leamon, C. P.; Cooper, S. R.; Hardee, G. E., Folate-liposome-mediated antisense oligodeoxynucleotide targeting to cancer cells: evaluation *in vitro* and *in vivo*. *Bioconjug. Chem.* **2003,** 14, 738-747.
141. Kamen, B. A.; Capdevila, A., Receptor-mediated folate accumulation is regulated by the cellular folate content. *Proc. Natl. Acad. Sci. U.S.A.* **1986,** 83, 5983-5987.
142. Leamon, C. P.; Low, P. S., Delivery of macromolecules into living cells: a method that exploits folate receptor endocytosis. *Proc. Natl. Acad. Sci. U. S. A.* **1991,** 88, 5572- 5576.
143. Leamon, C. P.; Low, P. S., Membrane folate-binding proteins are responsible for folate- protein conjugate endocytosis into cultured cells. *Biochem. J.* **1993,** 291, 855- 860.
144. Turek, J. J.; Leamon, C. P.; Low, P. S., Endocytosis of folate-protein conjugates: ultrastructural localization in KB cells. *J. Cell. Sci.* **1993,** 106, 423-430.
145. Lee, R. J.; Wang, S.; Low, P. S., Measurement of endosome pH following folate receptor-mediated endocytosis. *Biochim. Biophys. Acta* **1996,** 1312, 237-242.
146. Rao, C. S.; Chu, J.-J.; Liu, R.-S.; Lai, Y.-K., Synthesis and evaluation of [14C]-Labelled and fluorescent-Tagged paclitaxel derivatives as new biological probes. *Bioorg. Med. Chem.* **1998,** 6, (11), 2193-2204.
147. Evangelio, J. A.; Abal, M.; Barasoain, I.; Souto, A. A.; Lillo, M. P.; Acuna, A. U.; Amat-Guerri, F.; Andreu, J. M., Fluorescent taxoids as probes of the microtubule cytoskeleton. *Cell Motil. Cytoskeleton* **1998,** 39, 73-90.
148. Guy, R. K.; Scott, Z. A.; Sloboda, R. D.; Nicolaou, K. C., Fluorescent taxoids. *Chem. Biol.* **1996,** 3, (12), 1021-1031.
149. Errington, R. J.; Ameer-Beg, S. M.; Vojnovic, B.; Patterson, L. H.; Zloh, M.; Smith, P. J., Advanced microscopy solutions for monitoring the kinetics and dynamics of drug-DNA targeting in living cells. *Adv. Drug Deliv. Rev.* **2004,** 57, 153-167.
150. Diaz, J. F.; Strobe, R.; Engelborghs, Y.; Souto, A. A.; Andreu, J. M., Molecular Recognition of Taxol by Microtubules. *J. Biol. Chem.* **2000,** 275, (34), 26265-26276.
151. Edler, M. C.; Buey, R. n. M.; Gussio, R.; Marcus, A. I.; Vanderwal, C. D.; Sorensen, E. J.; DÃ-az, J. F.; Giannakakou, P.; Hamel, E., Cyclostreptin (FR182877), an Antitumor Tubulin-Polymerizing Agent Deficient in Enhancing Tubulin Assembly Despite Its High Affinity for the Taxoid Site. *Biochemistry* **2005,** 44, (34), 11525-11538.
152. Hsu, H.-J.; Liang, M.-R.; Chen, C.-T.; Chung, B.-c., Pregnenolone stabilizes microtubules and promotes zebrafish embryonic cell movement. *Nature* **2006,** 439, (7075), 480-483.
153. Watson, P.; Jones, A. T.; Stephens, D. J., Intracellular trafficking pathways and drug delivery: fluorescence imaging of living and fixed cells. *Adv. Drug Deliv. Rev.* **2004,** 57, 43-61.

154. Gumbleton, M.; Stephens, D. J., Coming out of the dark: the evolving role of fluorescence imaging in drug delivery research. *Adv. Drug Deliv. Rev.* **2004,** 57, 5-15.
155. www.itg.uiuc.edu/technology/atlas/structures/actin/images/actin_microtubules.jpg &imgrefurl.
156. Hwa Kim, S.; Hoon Jeong, J.; Joe, C. O.; Gwan Park, T., Folate receptor mediated intracellular protein delivery using PLL-PEG-FOL conjugate. *J. Controlled Release* **2005,** 103, (3), 625-634.
157. Parker, N.; Turk, M. J.; Westrick, E.; Lewis, J. D.; Low, P. S.; Leamon, C. P., Folate receptor expression in carcinomas and normal tissues determined by a quantitative radioligand binding assay. *Anal. Biochem.* **2005,** 338, (2), 284-293.
158. Bordwell, F. G. F., H. E., Heterocyclic aromatic anions with 4n + 2.pi.-electrons. *J. Org. Chem.* **1991,** 56, 4218-4223.
159. Lumma, W. C., Jr.; Dutra, G. A.; Voeker, C. A. , Synthesis of two benzothiacyclanones via a novel two-carbon ring expansion of thiolactones with vinyllithium. *J. Org. Chem.* **1970,** 35, 3442-3444.
160. Shaabani, A., Tavasoli-Rad, F., Potassium Permanganate Oxidation of Organic Compounds. *Syn. Comm.* **2005,** 35, 571-580.
161. Leino, R., Lonnqvist, J-E., A very simple method for the preparation of symmetrical disulfides. *Tet. Lett.* **2004,** 45, 8489-8491.
162. Chen, S.; Zhao, X.; Chen, J.; Chen, J.; Kuznetsova, L.; Wong, S. S.; Ojima, I., Mechanism-Based Tumor-Targeting Drug Delivery System. Validation of Efficient Vitamin Receptor-Mediated Endocytosis and Drug Release. *Bioconjug. Chem.* **2010,** 21, (5), 979-987.

References for Chapter 5:

1. Lacerda, L.; Bianco, A.; Prato, M.; Kostarelos, K., Carbon nanotubes as nanomedicines: From toxicology to pharmacology. *Adv. Drug Deliv. Rev.* **2006,** 58, (14), 1460-1470.
2. Farokhzad, O. C.; Langer, R., Nanomedicine: Developing smarter therapeutic and diagnostic modalities. *Adv. Drug Deliv. Rev.* **2006,** 58, (14), 1456-1459.
3. Ferrari, M., Cancer nanotechnology: opportunities and challenges. *Nat. Rev. Cancer* **2005,** 5, (3), 161-171.
4. Bangham, A. D.; Standish, M. M.; Watkins, J. C., Diffusion of univalent ions across the lamellae of swollen phospholipids. *J. Mol. Biol.* **1965,** 13, 238-252.
5. Langer, R.; Folkman, J., Polymers for the sustained release of proteins and other macromolecules. *Nature* **1976,** 263, 797-800.
6. Gref, R.; Minamitake, Y.; Peracchia, M. T.; Trubetskoy, V.; Torchilin, V.; Langer, R., Biodegradable long-circulating polymeric nanospheres. *Science* **1994,** 263, 1600-1603.
7. Bruchez Jr., M.; Moronne, M.; Gin, P.; Weiss, S.; Alivisatos, A. P., Semiconductor nanocrystals as fluorescent biological labels. *Science* **1998,** 281, 2013-2016.
8. Chan, W. C.; Nie, S., Quantum dot bioconjugates for ultrasensitive nonisotopic detection. *Science* **1998,** 281, 2016-2018.
9. Cui, Y.; Wei, Q.; Park, H.; Lieber, C. M., Nanowire nanosensors for highly sensitive and selective detection of biological and chemical species. *Science* **2001,** 293, 1289-1292.
10. Sanvicens, N.; Marco, M. P., Multifunctional nanoparticles - properties and prospects for their use in human medicine. *Trends Biotechnol.* **2008,** 26, (8), 425-433.
11. Pathak, P.; Katiyar, V. K., Multi-functional nanoparticles and their role in cancer drug delivery - a review. *Online J. Nanotechnol.* **2007,** 3, No pp given.
12. Langer, R., Drug delivery and targeting. *Nature* **1998,** 392, 5-10.
13. Bianco, A.; Hoebeke, J.; Kostarelos, K.; Prato, M.; Partidos, C. D., Carbon nanotubes: On the road to deliver. *Curr. Drug Deliv.* **2005,** 2, 253-259.
14. Harries, M.; Ellis, P.; Harper, P., Nanoparticle albumin-bound paclitaxel for metastatic breast cancer. *J. Clin. Oncol.* **2005,** 23, 7768-7771.
15. Damascelli, B.; Cantu, G.; Mattavelli, F.; Tamplenizza, P.; Bidoli, P.; Leo, E.; Dosio, F.; Cerrotta, A. M.; Di Tolla, G.; Frigerio, L. F.; Garbagnati, F.; Lanocita, R.; Marchiano, A.; Patelli, G.; Spreafico, C.; Ticha, V.; Vespro, V.; Zunino, F., Intraarterial chemotherapy with polyoxyethylated castor oil free paclitaxel, incorporated in albumin nanoparticles (ABI-007): Phase I study of patients with squamous cell carcinoma of the head and neck and anal canal: preliminary evidence of clinical activity. *Cancer* **2001,** 92, 2592-2602.
16. Desai, N.; Trieu, V.; Yao, Z.; Louie, L.; Ci, S.; Yang, A.; Tao, C.; De, T.; Beals, B.; Dykes, D.; Noker, P.; Yao, R.; Labao, E.; Hawkins, M.; Soon-Shiong, P., Increased antitumor activity, intratumor paclitaxel concentrations, and endothelial cell transport of cremophor-free, albumin-bound paclitaxel, ABI-007, compared with cremophor-based paclitaxel. *Clin. Cancer Res.* **2006,** 12, (4), 1317-1324.

17. Ibrahim, N. K.; Desai, N.; Legha, S.; Soon-Shiong, P.; Theriault, R. L.; Rivera, E.; Esmaeli, B.; Ring, S. E.; Bedikian, A.; Hortobagyi, G. N.; Ellerhorst, J. A., Phase I and pharmacokinetic study of ABI-007, a cremophor-free, protein-stabilized, nanoparticle formulation of paclitaxel. *Clin. Cancer Res.* **2002,** 8, 1038-1044.
18. John, T. A.; Vogel, S. M.; Tiruppathi, C.; Malik, A. B.; Minshall, R. D., Quantitative analysis of albumin uptake and transport in the rat microvessel endothelial monolayer. *Am. J. Physiol.* **2003,** 284, 187-196.
19. Miele, E.; Spinelli, G. P.; Miele, E.; Tomao, F.; Tomao, S., Albumin-bound formulation of paclitaxel (Abraxane® ABI-007) in the treatment of breast cancer. *Int. J. Nanomedicine* **2009,** 4, 99-105.
20. Duncan, R., The dawning era of polymer therapeutics. *Nature Rev. Drug Discov.* **2003,** 2, 347-360.
21. Allen, T. M., Ligand-targeted therapeutics in anticancer therapy. *Nature Rev. Drug Discov.* **2002,** 2, 750-763.
22. Jain, R. K., The next frontier of molecular medicine: delivery of therapeutics. *Nature Med.* **1998,** 4, 655-657.
23. Yezhelyev, M. V. e. a., Emerging use of nanoparticles in diagnosis and treatment of breast cancer. *Lancet Oncol.* **2006,** 7, 657-667.
24. Pison, U. e. a., Nanomedicine for respiratory diseases. *Eur. J. Pharmacol. Rev.* **2006,** 533, 341-350.
25. Torchilin, V. P., Recent advances with liposomes as pharmaceutical carriers. *Nat. Rev. Drug Discov.* **2005,** 4, 145-160.
26. Gabizon, A.; Shmeeda, H.; Barenholz, Y., Pharmacokinetics of Pegylated Liposomal Doxorubicin: Review of Animal and Human Studies. *Clin. Pharmacokinet.* **2003,** 42, 419-436.
27. Cattel, L., From conventional to stealth liposomes: a new frontier in cancer chemotherapy. *Tumori* **2003,** 89, (3), 237-249.
28. Markman, M., New, expanded, and modified use of approved antineoplastic agents in ovarian cancer. *Oncologist* **2007,** 12, (2), 186-190.
29. Del Barco, S.; Colomer, R.; Calvo, L.; Tusquets, I.; Adrover, E.; Sánchez, P.; Rifà, J.; De la Haba, J.; Virizuela, J., Non-pegylated liposomal doxorubicin combined with gemcitabine as first-line treatment for metastatic or locally advanced breast cancer. Final results of a phase I/II trial. *Breast Cancer Research & Treatment* **2009,** 116, (2), 351-358.
30. Park, J. W., Liposome-based drug delivery in breast cancer treatment. *Breast Cancer Res.* **2002,** 4, (3), 95 - 99.
31. Wang, T.; Yang, S.; Petrenko, V. A.; Torchilin, V. P., Cytoplasmic Delivery of Liposomes into MCF-7 Breast Cancer Cells Mediated by Cell-Specific Phage Fusion Coat Protein. *Mol. Pharmaceutics* **2010**, ASAP.
32. Gilles, E. M.; Frechet, J. M. J., Designing macromolecules for therapeutic applications: Polyester dendrimerpolyethylene oxide 'bow-tie' hybrids with tunable molecular weights and architecture. *J. Am. Chem. Soc.* **2002,** 124, 14137-14146.
33. http://www.nanopharmaceuticals.org/sitebuilder/images/liposome-379x402.jpg.

34. Lee, C. C., Designing dendrimers for biological applications. *Nat. Biotechnol.* **2005,** 23, 1517-1526.
35. Tomalia, D. A., Birth of a new macromolecular architecture: dendrimers as quantized building blocks for nanoscale synthetic organic chemistry. *Aldrichimica Acta* **2004,** 37, 39-57.
36. Bosman, A. W.; Janssen, H. M.; Meijer, E. W., About Dendrimers: Structure, Physical Properties, and Applications. *Chem. Rev.* **1999,** 99, (7), 1665-1688.
37. Lee, I.; Athey, B. D.; Wetzel, A. W.; Meixner, W.; Baker, J. R., Structural Molecular Dynamics Studies on Polyamidoamine Dendrimers for a Therapeutic Application: Effects of pH and Generation. *Macromolecules* **2002,** 35, (11), 4510-4520.
38. Crampton, H. L.; Simanek, E. E., Dendrimers as drug delivery vehicles: non-covalent interactions of bioactive compounds with dendrimers. *Polym. Int.* **2007,** 56, (4), 489-496.
39. Esfand, R.; Tomalia, D. A., Poly(amidoamine) (PAMAM) dendrimers: from biomimicry to drug delivery and biomedical applications. *Drug Discovery Today* **2001,** 6, (8), 427-436.
40. Svenson, S.; Tomalia, D. A., Dendrimers in biomedical applications--reflections on the field. *Adv. Drug Deliv. Rev.* **2005,** 57, (15), 2106-2129.
41. Malik, N.; Wiwattanapatapee, R.; Klopsch, R.; Lorenz, K.; Frey, H.; Weener, J. W.; Meijer, E. W.; Paulus, W.; Duncan, R., Dendrimers:: Relationship between structure and biocompatibility in vitro, and preliminary studies on the biodistribution of 125I-labelled polyamidoamine dendrimers in vivo. *J. Controlled Release* **2000,** 65, (1-2), 133-148.
42. Chen, H.-T.; Neerman, M. F.; Parrish, A. R.; Simanek, E. E., Cytotoxicity, Hemolysis, and Acute in Vivo Toxicity of Dendrimers Based on Melamine, Candidate Vehicles for Drug Delivery. *J. Am. Chem. Soc.* **2004,** 126, (32), 10044-10048.
43. Jevprasesphant, R.; Penny, J.; Jalal, R.; Attwood, D.; McKeown, N. B.; D'Emanuele, A., The influence of surface modification on the cytotoxicity of PAMAM dendrimers. *Int. J. Pharm.* **2003,** 252, 263-266.
44. El-Sayed, M.; Ginski, M.; Rhodes, C.; Ghandehari, H., Transepithelial transport of poly(amidoamine) dendrimers across Caco-2 cell monolayers. *J. Controlled Release* **2002,** 81, 355-365.
45. Fischer, D.; Li, Y.; Ahlemeyer, B.; Krieglstein, J.; Kissel, T., In vitro cytotoxicity testing of polycations: influence of polymer structure on cell viability and hemolysis. *Biomaterials* **2003,** 24, 1121-1131.
46. Hussain, M.; Shchepinov, M.; Sohail, M.; Benter, I. F.; Hollins, A. J.; Southern, E. M.; Akhtar, S., A novel anionic dendrimer for improved cellular delivery of antisense oligonucleotides. *J. Controlled Release* **2004,** 99, (1), 139-155.
47. Ooya, T.; Lee, J.; Park, K., Effects of ethylene glycol-based graft, star-shaped, and dendritic polymers on solubilization and controlled release of paclitaxel. *J. Controlled Release* **2003,** 93, (2), 121-127.
48. Kojima, C.; Kono, K.; Maruyama, K.; Takagishi, T., Synthesis of Polyamidoamine Dendrimers Having Poly(ethylene glycol) Grafts and Their

Ability To Encapsulate Anticancer Drugs. *Bioconjugate Chem.* **2000,** 11, (6), 910-917.

49. Morgan, M. T.; Carnahan, M. A.; Finkelstein, S.; Prata, C. A. H.; Degoricija, L.; Lee, S. J.; Grinstaff, M. W., Dendritic supramolecular assemblies for drug delivery. *Chem. Commun.* **2005**, 4309-4311.
50. Bhadra, D.; Bhadra, S.; Jain, S.; Jain, N. K., A PEGylated dendritic nanoparticulate carrier of fluorouracil. *Int. J. Pharm.* **2003,** 257, (1-2), 111-124.
51. Bhadra, D.; Bhadra, S.; Jain, N., PEGylated Peptide Dendrimeric Carriers for the Delivery of Antimalarial Drug Chloroquine Phosphate. *Pharm. Res.* **2006,** 23, (3), 623-633.
52. Patri, A. K.; Kukowska-Latallo, J. F.; Baker, J. R. J., Targeted drug delivery with dendrimers: Comparison of the release kinetics of covalently conjugated drug and non-covalent drug inclusion complex. *Adv. Drug Deliv. Rev.* **2005,** 57, (15), 2203-2214.
53. Morgan, M. T.; Carnahan, M. A.; Immoos, C. E.; Ribeiro, A. A.; Finkelstein, S.; Lee, S. J.; Grinstaff, M. W., Dendritic Molecular Capsules for Hydrophobic Compounds. *J. Am. Chem. Soc.* **2003,** 125, (50), 15485-15489.
54. Malik, N.; Evagorou, E. G.; Duncan, R., Dendrimer-platinate: a novel approach to cancer chemotherapy. *Anti-cancer Drugs* **1999,** 10, 767-776.
55. Kono, K.; Liu, M.; Fréchet, J. M. J., Design of dendritic macromolecules containing folate or methotrexate residues. *Bioconjugate Chem.* **1999,** 10, 1115-1121.
56. Quintana, A.; Raczka, E.; Piehler, L.; Lee, I.; Myc, A.; Majoros, I.; Patri, A. K.; Thomas, T.; Mule, J.; Baker, J. R. J., Design and function of a dendrimer-based therapeutic nanodevice targeted to tumor cells through the folate receptor. *Pharm. Res.* **2002,** 19, 1310-1316.
57. Ross, J. F.; Chaudhuri, P. K.; Ratnam, M., Differential regulation of folate receptor isoforms in normal and malignant tissues in vivo and established cell lines. Physiologic and clinical implications. *Cancer* **1994,** 73, 2432-2443.
58. Shukla, S.; Wu, G.; Chatterjee, M.; Yang, W.; Sekido, M.; Diop, L. A.; Muller, R.; Sudimack, J. J.; Lee, R. J.; Barth, R. F.; Tjarks, W., Synthesis and biological evaluation of folate receptor-targeted boronated PAMAM dendrimers as potential agents for neutron capture therapy. *Bioconjugate Chem.* **2003,** 14, 158-167.
59. Baek, M. G.; Roy, R., Synthesis and protein binding properties of T-antigen containing GlycoPAMAM dendrimers. *Bioorg. Med. Chem.* **2002,** 10 11-17.
60. Roy, R.; Baek, M. G.; Rittenhouse-Olson, K., Synthesis of N,N′-bis(acrylamido)acetic acid-based T-antigen glycodendrimers and their mouse monoclonal IgG antibody binding properties. *J. Am. Chem. Soc.* **2001,** 123, 1809-1816.
61. Roy, R.; Baek, M. G., Glycodendrimers: novel glycotope isosteres unmasking sugar coating. Case study with T-antigen markers from breast cancer MUC1 glycoprotein. *Rev. Mol. Biotechnol.* **2002,** 90, 291-309.
62. Benito, J. M.; Gomez-Garcia, M.; Mellet, C. O.; Baussanne, I.; Defaye, J.; Fernandez, J. M. G., Optimizing saccharide-directed molecular delivery to biological receptors: design, synthesis, and biological evaluation of

glycodendrimer-cyclodextrin conjugates. *J. Am. Chem. Soc.* **2004,** 126, 10355-10363.
63. Hansen, H. C.; Haataja, S.; Finne, J.; Magnusson, G., Di-, tri-, and tetravalent dendritic galabiosides that inhibit hemagglutination by Streptococcus suis at nanomolar concentration. *J. Am. Chem. Soc.* **1997,** 119, 6974-6979.
64. Patra, C. R.; Bhattacharya, R.; Mukhopadhyay, D.; Mukherjee, P., Fabrication of gold nanoparticles for targeted therapy in pancreatic cancer. *Adv. Drug Deliv. Rev.* **2010,** 62, (3), 346-361.
65. Kim, C.-K.; Ghosh, P.; Rotello, V. M., Multimodal drug delivery using gold nanoparticles. *Nanoscale* **2009,** 1, 61-67.
66. Huang, X. e. a., Gold nanoparticles: interesting optical properties and recent applications in cancer diagnostics and therapy. *Nanomedicine* **2007,** 2, 681-693.
67. Hirsch, L. R.; Halas, N. J.; West, J. L., Nanoshell-mediated near-infrared thermal therapy of tumors under magnetic resonance guidance. *Proc. Natl. Acad. Sci. U.S.A.* **2003,** 100.
68. Templeton, A. C.; Wuelfing, W. P.; Murray, R. W., Monolayer-Protected Cluster Molecules. *Acc. Chem. Res.* **1999,** 33, (1), 27-36.
69. Otsuka, H.; Nagasaki, Y.; Kataoka, K., PEGylated nanoparticles for biological and pharmaceutical applications. *Adv. Drug Delivery Rev.* **2003,** 55, 403-419.
70. Takae, S.; Akiyama, Y.; Otsuka, H.; Nakamura, T.; Nagasaki, Y.; Kataoka, K., Ligand Density Effect on Biorecognition by PEGylated Gold Nanoparticles: Regulated Interaction of RCA120 Lectin with Lactose Installed to the Distal End of Tethered PEG Strands on Gold Surface. *Biomacromolecules* **2005,** 6, 818-824.
71. Khalil, H.; Mahajan, D.; Rafailovich, M.; Gelfer, M.; Pandya, K., Synthesis of Zerovalent Nanophase Metal Particles Stabilized with Poly(ethylene glycol). *Langmuir* **2004,** 20, (16), 6896-6903.
72. Ferrari, M., Nanogeometry: Beyond drug delivery. *Nat. Nanotechnol.* **2008,** 3, (3), 131-132.
73. Cho, E. C.; Xie, J.; Wurm, P. A.; Xia, Y., Understanding the Role of Surface Charges in Cellular Adsorption versus Internalization by Selectively Removing Gold Nanoparticles on the Cell Surface with a I2/KI Etchant. *Nano Lett.* **2009,** 9, (3), 1080-1084.
74. Zhu, Z.-J.; Ghosh, P. S.; Miranda, O. R.; Vachet, R. W.; Rotello, V. M., Multiplexed Screening of Cellular Uptake of Gold Nanoparticles Using Laser Desorption/Ionization Mass Spectrometry. *J. Am. Chem. Soc.* **2008,** 130, (43), 14139-14143.
75. Wen, J.; Kim, B. Y. S.; Rutka, J. T.; Chan, W. C. W., Nanoparticle-mediated cellular response is size-dependent. *Nat. Nanotechnol.* **2008,** 3, (3), 145-150.
76. Perrault, S. D.; Walkey, C.; Jennings, T.; Fischer, H. C.; Chan, W. C. W., Mediating Tumor Targeting Efficiency of Nanoparticles Through Design. *Nano Lett.* **2009,** 9, (5), 1909-1915.
77. Verma, A.; Uzun, O.; Hu, Y.; Hu, Y.; Han, H.-S.; Watson, N.; Chen, S.; Irvine, D. J.; Stellacci, F., Surface-structure-regulated cell-membrane penetration by monolayer-protected nanoparticles. *Nat. Mater.* **2008,** 7, (7), 588-595.
78. Nativo, P.; Prior, I. A.; Brust, M., Uptake and Intracellular Fate of Surface-Modified Gold Nanoparticles. *ACS Nano* **2008,** 2, (8), 1639-1644.

79. Tkachenko, A. G.; Xie, H.; Coleman, D.; Glomm, W.; Ryan, J. L.; Anderson, M. F.; Franzen, S.; Feldheim, D. L., Multifunctional Gold Nanoparticle-Peptide Complexes for Nuclear Targeting. *J. Am. Chem. Soc.* **2003,** 125, 4700-4701.
80. Oyelere, A. K.; Chen, P. C.; Huang, X.; El-Sayed, I. H.; El-Sayed, M. A., Peptide-Conjugated Gold Nanorods for Nuclear Targeting. *Bioconjugate Chem.* **2007,** 18, 1490-1497.
81. Morgan, M. T.; Nakanishi, Y.; Kroll, D. J.; Griset, A. P.; Carnahan, M. A.; Wathier, M.; Oberlies, N. H.; Manikumar, G.; Wani, M. C.; Grinstaff, M. W., Dendrimer-Encapsulated Camptothecins: Increased Solubility, Cellular Uptake, and Cellular Retention Affords Enhanced Anticancer Activity In vitro. *Cancer Res.* **2006,** 66, (24), 11913-11921.
82. Jones, D. P.; Carlson, J. L.; Mody, V. C.; Cai, J.; Lynn, M. J.; Sternberg, P., Redox state of glutathione in human plasma. *Free Radical Biol. Med.* **2000,** 28, (4), 625-635.
83. Ghosh, P.; Han, G.; De, M.; Kim, C. K.; Rotello, V. M., Gold nanoparticles in delivery applications. *Adv. Drug Deliv. Rev.* **2008,** 60, (11), 1307-1315.
84. Verma, A.; Simard, J. M.; Worrall, J. W. E.; Rotello, V. M., Tunable Reactivation of Nanoparticle-Inhibited β-Galactosidase by Glutathione at Intracellular Concentrations. *J. Am. Chem. Soc.* **2004,** 126, (43), 13987-13991.
85. McCoy, C. P.; Rooney, C.; Edwards, C. R.; Jones, D. S.; Gorman, S. P., Light-Triggered Molecule-Scale Drug Dosing Devices. *J. Am. Chem. Soc.* **2007,** 129, (31), 9572-9573.
86. Han, G.; You, C.-C.; Kim, B.-j.; Turingan, R. S.; Forbes, N. S.; Martin, C. T.; Rotello, V. M., Light-Regulated Release of DNA and Its Delivery to Nuclei by Means of Photolabile Gold Nanoparticles13. *Angew. Chem., Int. Ed. Engl.* **2006,** 45, (19), 3165-3169.
87. Agasti, S. S.; Chompoosor, A.; You, C.-C.; Ghosh, P.; Kim, C. K.; Rotello, V. M., Photoregulated Release of Caged Anticancer Drugs from Gold Nanoparticles. *J . Am. Chem. Soc.* **2009,** 131, (16), 5728-5729.
88. Polizzi, M. A.; Stasko, N. A.; Schoenfisch, M. H., Water-Soluble Nitric Oxide-Releasing Gold Nanoparticles. *Langmuir* **2007,** 23, (9), 4938-4943.
89. Yang, Q.; Wang, S.; Fan, P.; Wang, L.; Di, Y.; Lin, K.; Xiao, F.-S., pH-Responsive Carrier System Based on Carboxylic Acid Modified Mesoporous Silica and Polyelectrolyte for Drug Delivery. *Chem. Mater.* **2005,** 17, (24), 5999-6003.
90. Mocellin, S.; Bronte, V.; Nitti, D., Nitric oxide, a double edged sword in cancer biology: Searching for therapeutic opportunities. *Med. Res. Rev.* **2007,** 27, (3), 317-352.
91. Hwu, J. R.; Lin, Y. S.; Josephrajan, T.; Hsu, M.-H.; Cheng, F.-Y.; Yeh, C.-S.; Su, W.-C.; Shieh, D.-B., Targeted Paclitaxel by Conjugation to Iron Oxide and Gold Nanoparticles. *J . Am. Chem. Soc.* **2008,** 131, (1), 66-68.
92. Han, M.; Gao, X.; Su, J. Z.; Nie, S., Quantum-dot-tagged microbeads for multiplexed optical coding of biomolecules. *Nat. Biotechnol.* **2001,** 19, (7), 631-635.

93. Medintz, I. L.; Uyeda, H. T.; Goldman, E. R.; Mattoussi, H., Quantum dot bioconjugates for imaging, labelling and sensing. *Nat. Mater.* **2005,** 4, (6), 435-446.
94. Correa-Duarte, M. A.; Giersig, M.; Liz-Marzán, L. M., Stabilization of CdS semiconductor nanoparticles against photodegradation by a silica coating procedure. *Chem. Phys. Lett.* **1998,** 286, (5-6), 497-501.
95. Resch-Genger, U.; Grabolle, M.; Cavaliere-Jaricot, S.; Nitschke, R.; Nann, T., Quantum dots versus organic dyes as fluorescent labels. *Nat. Methods* **2008,** 5, (9), 763-775.
96. Rogach, A. L.; Nagesha, D.; Ostrander, J. W.; Giersig, M.; Kotov, N. A., "Raisin Bun"-Type Composite Spheres of Silica and Semiconductor Nanocrystals. *Chem. Mater.* **2000,** 12, (9), 2676-2685.
97. Gaponik, N.; Talapin, D. V.; Rogach, A. L.; Hoppe, K.; Shevchenko, E. V.; Kornowski, A.; Eychmuller, A.; Weller, H., Thiol-Capping of CdTe Nanocrystals: An Alternative to Organometallic Synthetic Routes. *J. Phys. Chem. B* **2002,** 106, (29), 7177-7185.
98. Gao, X.; Cui, Y.; Levenson, R. M.; Chung, L. W. K.; Nie, S., In vivo cancer targeting and imaging with semiconductor quantum dots. *Nat. Biotechnol.* **2004,** 22, (8), 969-976.
99. Akerman, M. E.; Chan, W. C. W.; Laakkonen, P.; Bhatia, S. N.; Ruoslahti, E., Nanocrystal targeting in vivo. *Proc. Natl. Acad. Sci. U. S. A.* **2002,** 99, (20), 12617-12621.
100. Cai, W.; Shin, D.-W.; Chen, K.; Gheysens, O.; Cao, Q.; Wang, S. X.; Gambhir, S. S.; Chen, X., Peptide-Labeled Near-Infrared Quantum Dots for Imaging Tumor Vasculature in Living Subjects. *Nano Lett.* **2006,** 6, (4), 669-676.
101. Pinaud, F.; King, D. J.; Moore, H.-P.; Weiss, S., Bioactivation and Cell Targeting of Semiconductor CdSe/ZnS Nanocrystals with Phytochelatin-Related Peptides. *J . Am. Chem. Soc.* **2004,** 126, (19), 6115-6123.
102. Boeneman, K.; Delehanty, J. B.; Susumu, K.; Stewart, M. H.; Medintz, I. L., Intracellular Bioconjugation of Targeted Proteins with Semiconductor Quantum Dots. *J . Am. Chem. Soc.* **2010,** 132, (17), 5975-5977.
103. Chu, T. C.; Shieh, F.; Lavery, L. A.; Levy, M.; Richards-Kortum, R.; Korgel, B. A.; Ellington, A. D., Labeling tumor cells with fluorescent nanocrystal-aptamer bioconjugates. *Biosens. Bioelectron.* **2006,** 21, (10), 1859-1866.
104. Bharali, D. J.; Lucey, D. W.; Jayakumar, H.; Pudavar, H. E.; Prasad, P. N., Folate-Receptor-Mediated Delivery of InP Quantum Dots for Bioimaging Using Confocal and Two-Photon Microscopy. *J . Am. Chem. Soc.* **2005,** 127, (32), 11364-11371.
105. Lidke, D. S.; Nagy, P.; Heintzmann, R.; Arndt-Jovin, D. J.; Post, J. N.; Grecco, H. E.; Jares-Erijman, E. A.; Jovin, T. M., Quantum dot ligands provide new insights into erbB/HER receptor-mediated signal transduction. *Nat. Biotechnol.* **2004,** 22, (2), 198-203.
106. Ho, Y.-P.; Leong, K. W., Quantum dot-based theranostics. *Nanoscale* **2010,** 2, 60-68.
107. Bagalkot, V.; Zhang, L.; Levy-Nissenbaum, E.; Jon, S.; Kantoff, P. W.; Langer, R.; Farokhzad, O. C., Quantum Dot-Aptamer Conjugates for Synchronous Cancer

Imaging, Therapy, and Sensing of Drug Delivery Based on Bi-Fluorescence Resonance Energy Transfer. *Nano Lett.* **2007,** 7, (10), 3065-3070.
108. Chang, E.; Thekkek, N.; Yu, W. W.; Colvin, V. L.; Drezek, R., Evaluation of Quantum Dot Cytotoxicity Based on Intracellular Uptake13. *Small* **2006,** 2, (12), 1412-1417.
109. Derfus, A. M.; Chan, W. C. W.; Bhatia, S. N., Probing the Cytotoxicity of Semiconductor Quantum Dots. *Nano Lett.* **2003,** 4, (1), 11-18.
110. Hoshino, A.; Manabe, N.; Fujioka, K.; Suzuki, K.; Yasuhara, M.; Yamamoto, K., Use of fluorescent quantum dot bioconjugates for cellular imaging of immune cells, cell organelle labeling, and nanomedicine: surface modification regulates biological function, including cytotoxicity. *J. Artif. Organs* **2007,** 10, (3), 149-157.
111. Pic, E.; Bezdetnaya, L.; Guillemin, F.; Marchal, F., Quantification Techniques and Biodistribution of Semiconductor Quantum Dots. *Anti-Cancer Agents Med. Chem.* **2009,** 9, 295-303.
112. Lu, A.-H.; Salabas, E. L.; Schüth, F., Magnetic Nanoparticles: Synthesis, Protection, Functionalization, and Application. *Angew. Chem., Int. Ed. Engl.* **2007,** 46, (8), 1222-1244.
113. Jung, C. W., Surface properties of superparamagnetic iron oxide MR contrast agents: Ferumoxides, ferumoxtran, ferumoxsil. *Magn. Reson. Imaging* **1995,** 13, (5), 675-691.
114. Majewski, P.; Thierry, B., Functionalized Magnetite Nanoparticles-Properties, and Bio-Applications. *Crit. Rev. Solid State Mater. Sci.* **2007,** 32, 203-215.
115. Belting, M.; Sandgren, S.; Wittrup, A., Nuclear delivery of macromolecules: barriers and carriers. *Adv. Drug Deliv. Rev.* **2005,** 57, 505-527.
116. Davis, M. E., Non-viral gene delivery systems. *Curr. Opin. Biotechnol.* **2002,** 13, 128-131.
117. Longmire, M.; Choyke, P. L.; Kobayashi, H., Clearance properties of nano-sized particles and molecules as imaging agents: considerations and caveats. *Nanomedicine* **2008,** 3, 703-717.
118. Dobrovolskaia, M. A.; Aggarwal, P.; Hall, J. B.; McNeil, S. E., Preclinical studies to understand nanoparticle interaction with the immune system and its potential effects on nanoparticle biodistribution. *Mol. Pharmaceutics* **2008,** 5, 487-495.
119. Zhang, Y.; Kohler, N.; Zhang, M. Q., Surface modification of superparamagnetic magnetite nanoparticles and their intracellular uptake. *Biomaterials* **2002,** 23, 1553-1561.
120. Kohler, N.; Sun, C.; Wang, J.; Zhang, M. Q., Methotrexate-modified superparamagnetic nanoparticles and their intracellular uptake into human cancer cells. *Langmuir* **2005,** 21, 8858-8864.
121. Park, J. H.; von Maltzahn, G.; Zhang, L. L.; Schwartz, M. P.; Ruoslahti, E.; Bhatia, S. N.; Sailor, M. J., Magnetic iron oxide nanoworms for tumor targeting and imaging. *Adv. Mater.* **2008,** 20, 1630-1635.
122. Veiseh, O.; Sun, C.; Gunn, J.; Kohler, N.; Gabikian, P.; Lee, D.; Bhattarai, N.; Ellenbogen, R.; Sze, R.; Hallahan, A.; Olson, J.; Zhang, M. Q., Optical and MRI multifunctional nanoprobe for targeting gliomas. *Nano Lett.* **2005,** 5, 1003-1008.

123. Yigit, M. V.; Mazumdar, D.; Kim, H. K.; Lee, J. H.; Dintsov, B.; Lu, Y., Smart "Turn-on" magnetic resonance contrast agents based on aptamer-functionalized superparamagnetic iron oxide nanoparticles. *ChemBioChem* **2007,** 8, 1675-1678.
124. Artemov, D.; Mori, N.; Okollie, B.; Bhujwalla, Z. M., MR molecular imaging of the Her-2/neu receptor in breast cancer cells using targeted iron oxide nanoparticles. *Magn. Reson. Med.* **2003,** 49, 403-408.
125. Huh, Y. M.; Jun, Y. W.; Song, H. T.; Kim, S.; Choi, J. S.; Lee, J. H.; Yoon, S.; Kim, K. S.; Shin, J. S.; Suh, J. S.; Cheon, J., In vivo magnetic resonance detection of cancer by using multifunctional magnetic nanocrystals. *J. Am. Chem. Soc.* **2005,** 127, 12387-12391.
126. Montet, X.; Montet-Abou, K.; Reynolds, F.; Weissleder, R.; Josephson, L., Nanoparticle imaging of integrins on tumor cells. *Neoplasia* **2006,** 8, 214-222.
127. Hong, S.; Leroueil, P. R.; Majoros, I. J.; Orr, B. G.; Baker, J. R.; Holl, M. M. B., The binding avidity of a nanoparticle-based multivalent targeted drug delivery platform. *Chem. Biol.* **2007,** 14, 105-113.
128. Montet, X.; Funovics, M.; Montet-Abou, K.; Weissleder, R.; Josephson, L., Multivalent effects of RGD peptides obtained by nanoparticle display. *J. Med. Chem.* **2006,** 49, 6087-6093.
129. Jiang, W.; Kim, B. Y. S.; Rutka, J. T.; Chan, W. C. W., Nanoparticle-mediated cellular response is size-dependent. *Nat. Nanotechnol.* **2008,** 3, 145-150.
130. Chithrani, B. D.; Ghazani, A. A.; Chan, W. C. W., Determining the size and shape dependence of gold nanoparticle uptake into mammalian cells. *Nano Lett.* **2006,** 6, 662-668.
131. Gratton, S. E. A.; Pohhaus, P. D.; Lee, J.; Guo, I.; Cho, M. J.; DeSimone, J. M., Nanofabricated particles for engineered drug therapies: A preliminary Biodistribution study of PRINT (TM) nanoparticles. *J. Controlled Release* **2007,** 121, 10-18.
132. Decuzzi, P.; Ferrari, M., The adhesive strength of non-spherical particles mediated by specific interactions. *Biomaterials* **2006,** 27, 5307-5314.
133. Veiseh, O.; Gunn, J. W.; Zhang, M., Design and fabrication of magnetic nanoparticles for targeted drug delivery and imaging. *Adv. Drug Deliv. Rev.* **2010,** 62, (3), 284-304.
134. Yang, J.; Lee, C. H.; Ko, H. J.; Suh, J. S.; Yoon, H. G.; Lee, K.; Huh, Y. M.; Haam, S., Multifunctional magneto-polymeric nanohybrids for targeted detection and synergistic therapeutic effects on breast cancer. *Angew. Chem., Int. Ed. Engl.* **2007,** 46, 8836-8839.
135. Kroto, H. W.; Heath, J. R.; O'Brien, S. C.; Curl, R. F.; Smalley, R. E., C60: Buckminsterfullerene. *Nature* **1985,** 318, 162-163.
136. Ruoff, R. S.; Tse, D. S.; Malhotra, R.; C., L. D., Solubility of fullerene (C60) in a variety of solvents. *J. Phys. Chem.* **1993,** 97, 3379-3383.
137. Sivaraman, N.; Dhamodaran, R.; Kaliappan, I.; Srinivassan, T. G.; Rao, P. R. V.; Mathews, C. K., Solubility of C60 in organic solvents. *J. Org. Chem.* **1992,** 57, 6077-6079.
138. Farokhzad, O. C.; Langer, R., Impact of nanotechnology on drug delivery. *ACS Nano* **2009,** 3, (1), 16-20.

139. Sitharaman, B.; Tran, L. A.; Pham, Q. P. e. a., Gadofullerenes as nanoscale magnetic labels for cellular MRI. *Contrast Media Mol. Imaging* **2007,** 2, (3), 139-146.
140. Lucignani, G., Nanoparticles for concurrent multimodality imaging and therapy: The dawn of new theragnostic synergies. *Eur. J. Nucl. Med. Mol. Imaging* **2009,** 36, (5), 869-874.
141. Larocque, J.; Bharali, D. J.; Mousa, S. A., Cancer detection and treatment: The role of nanomedicines. *Mol. Biotechnol.* **2009,** 42, (3), 358-366.
142. Schoenhagen, P.; Conyers, J. L., Nanotechnology and atherosclerosis imaging: emerging diagnostic and therapeutic applications. *Recent Pat. Cardiovasc. Drug Discov.* **2008,** 3, (2), 98-104.
143. Partha, R.; Conyers, J. L., Biomedical applications of functionalized fullerene-based nanomaterials. *Int. J. Nanomedicine* **2009,** 4, 261-275.
144. Zakharian, T. Y.; Seryshev, A.; Sitharaman, B.; Gilbert, B. E.; Knight, V.; Wilson, L. J., A fullerene-paclitaxel chemotherapeutic: synthesis, characterization, and study of biological activity in tissue culture. *J. Am. Chem. Soc.* **2005,** 127, (36), 12508-12509.
145. Partha, R.; Mitchell, L. R.; Lyon, J. L.; Joshi, P. P.; Conyers, J. L., Buckysomes: fullerene-based nanocarriers for hydrophobic molecule delivery. *ACS Nano* **2008,** 2, (9).
146. Gonzalez, K. A.; Wilson, L. J.; Wu, W.; Nancollas, G. H., Synthesis and in vitro characterization of a tissue-selective fullerene: vectoring C(60)(OH)(16)AMBP to mineralized bone. *Bioorg. Med. Chem.* **2002,** 10, (6), 1991-1997.
147. Bolskar, R. D.; Benedetto, A. F.; Husebo, L. O.; Price, R. E.; Jackson, E. F.; Wallace, S.; Wilson, L. J.; Alford, J. M., First Soluble M@C60 Derivatives Provide Enhanced Access to Metallofullerenes and Permit in Vivo Evaluation of Gd@C60[C(COOH)2]10 as a MRI Contrast Agent. *J . Am. Chem. Soc.* **2003,** 125, (18), 5471-5478.
148. Toth, E.; Bolskar, R. D.; Borel, A.; GonzÃ¡lez, G.; Helm, L.; Merbach, A. E.; Sitharaman, B.; Wilson, L. J., Water-Soluble Gadofullerenes: Toward High-Relaxivity, pH-Responsive MRI Contrast Agents. *J . Am. Chem. Soc.* **2004,** 127, (2), 799-805.
149. Iijima, S., Helical microtubules of graphitic carbon. *Nature* **1991,** 354, 56-58.
150. Jose-Yacaman, M.; Miki-Yoshida, M.; Rendon, L.; Santiesteban, J. G., Catalytic growth of carbon microtubules with fullerene structure. *Appl. Phys. Lett.* **1993,** 62, 657-659.
151. Chiang, I. W.; Brinson, B. E.; Huang, A. Y.; Willis, P. A.; Bronikowski, M. J.; Margrave, J. L.; Smalley, R. E.; Hauge, R. H., Purification and Characterization of Single-Wall Carbon Nanotubes (SWNTs) Obtained from the Gas-Phase Decomposition of CO (HiPco Process). *J. Phys. Chem. B* **2001,** 105, 8297-8301.
152. Ebbesen, T. W.; Ajayan, P. M., Large-scale synthesis of carbon nanotubes. *Nature* **1992,** 358, 220-222.
153. Guo, T.; Nikolaev, P.; Rinzler, A. G.; Tomanek, D.; Colbert, D. T.; Smalley, R. E., Self-Assembly of Tubular Fullerenes. *J. Phys. Chem.* **1995,** 99, 10694-10697.

154. Guo, T.; Nikolaev, P.; Thess, A.; Colbert, D. T.; Smalley, R. E., Catalytic growth of single-walled nanotubes by laser vaporization. *Chem. Phys. Lett.* **1995,** 243, 49-54.
155. Hirsch, A., Functionalization of single-walled carbon nanotubes. *Angew. Chem., Int. Ed. Engl.* **2002,** 41, 1853-1859.
156. Banerjee, S.; Kahn, M. G. C.; Wong, S. S., Rational chemical strategies for carbon nanotube functionalization. *Chem. Eur. J.* **2003,** 9, 1898-1908.
157. Baughman, R. H.; Zakhidov, A. A.; de Heer, W. A., Carbon nanotubes-the route toward applications. *Science* **2002,** 297, 787-792.
158. Dresselhaus, M. S.; Dresselhaus, G.; Avouris, P., Carbon Nanotubes Synthesis, Structure, Properties, and Applications. *Top. Appl. Phys.* **2001,** 80, 447.
159. Ajayan, P. M., Nanotubes from Carbon. *Chem. Rev.* **1999,** 99, 1787-1799.
160. Wu, H.-C.; Chang, X.; Liu, L.; Zhao, F.; Zhao, Y., Chemistry of carbon nanotubes in biomedical applications. *J. Mater. Chem.* **2010,** 20, 1036-1052.
161. Kam, N. W. S.; Dai, H., Single walled carbon nanotubes for transport and delivery of biological cargos. *Phys. Status Solidi B* **2006,** 243, (13), 3561-3566.
162. Bianco, A.; Kostarelos, K.; Prato, M., Applications of carbon nanotubes in drug delivery. *Curr. Opin. Chem. Biol.* **2005,** 9, 674-679.
163. Pastorin, G.; Kostarelos, K.; Prato, M.; Bianco, A., Functionalized carbon nanotubes: Towards the delivery of therapeutic molecules. *J. Biomed. Nanotechnol.* **2005,** 1, 133-142.
164. Bianco, A., Carbon nanotubes for the delivery of therapeutic molecules. *Expert Opin. Drug Deliv.* **2004,** 1, 57-65.
165. Lam, C.-w.; James, J. T.; McCluskey, R.; Arepalli, S.; Hunter, R. L., A Review of Carbon Nanotube Toxicity and Assessment of Potential Occupational and Environmental Health Risks. *Crit. Rev. Toxicol.* **2006,** 36, 189-217.
166. Donaldson, K.; Stone, V.; Tran, C. L.; Kreyling, W.; Borm, P. J. A., Nanotoxicology. *Occup. Environ. Med.* **2004,** 61, 727-728.
167. Jia, G.; Wang, H.; Yan, L.; Wang, X.; Pei, R.; Yan, T.; Zhao, Y.; Guo, X., Cytotoxicity of Carbon Nanomaterials: Single-Wall Nanotube, Multi-Wall Nanotube, and Fullerene. *Environ. Sci. Technol.* **2005,** 39, (5), 1378-1383.
168. Donaldson, K.; Aitken, R.; Tran, L.; Stone, V.; Duffin, R.; Forrest, G.; Alexander, A., Carbon nanotubes: a review of their properties in relation to pulmonary toxicology and workplace safety. *Toxicol. Sci.* **2006,** 92, 5-22.
169. Sayes, C. M.; Liang, F.; Hudson, J. L.; Mendez, J.; Guo, W.; Beach, J. M.; Moore, V. C.; Doyle, C. D.; West, J. L.; Billups, W. E.; Ausman, K. D.; Colvin, V. L., Functionalization density dependence of single-walled carbon nanotubes cytotoxicity in vitro. *Toxicol. Lett.* **2006,** 161, 135-142.
170. Warheit, D. B.; Laurence, B. R.; Reed, K. L.; Roach, D. H.; Reynolds, G. A. M.; Webb, T. R., Comparative Pulmonary Toxicity Assessment of Single-wall Carbon Nanotubes in Rats. *Toxicol. Sci.* **2004,** 77, 117-125.
171. Shvedova, A. A.; Kisin, E. R.; Mercer, R.; Murray, A. R.; Johnson, V. J.; Potapovich, A. I.; Tyurina, Y. Y.; Gorelik, O.; Arepalli, S.; Schwegler-Berry, D.; Hubbs, A. F.; Antonini, J.; Evans, D. E.; Ku, B. K.; Ramsey, D.; Maynard, A.; Kagan, V. E.; Castranova, V.; Baron, P., Unusual inflammatory and fibrogenic

pulmonary responses to single walled carbon nanotubes in mice. *Am. J. Physiol., Lung Cell. Mol. Physiol* **2005,** 289, L698-L708.
172. Sato, Y.; Yokoyama, A.; Shibata, K.-i.; Akimoto, Y.; Ogino, S.-i.; Nodasaka, Y.; Kohgo, T.; Tamura, K.; Akasaka, T.; Uo, M.; Motomiya, K.; Jeyadevan, B.; Ishiguro, M.; Hatakeyama, R.; Watari, F.; Tohji, K., Influence of length on cytotoxicity of multiwalled carbon nanotubes against human acute monocytic leukemia cell line THP-1 in vitro and subcutaneous tissue of rats in vivo. *Mol. BioSyst.* **2005,** 1, 176-182.
173. Muller, J.; Huaux, F.; Moreau, N.; Misson, P.; Heilier, J. F.; Delos, M.; Arras, M.; Fonseca, A.; Nagy, J. B.; Lison, D., Respiratory toxicity of multi-wall carbon nanotubes. *Toxicol. Appl. Pharmacol.* **2005,** 207, 221-231.
174. Wang, H. F.; Wang, J.; Deng, X. Y.; Sun, H. F.; Shi, Z. J.; Gu, Z. N.; Liu, Y. F.; Zhao, Y. L.; . Biodistribution of carbon single-wall carbon nanotubes in mice. *J. Nanosci. Nanotechnol.* **2004,** 4, 1019-1024.
175. Singh, R.; Pantarotto, D.; Lacerda, L.; Pastorin, G.; Klumpp, C.; Prato, M.; Bianco, A.; Kostarelos, K., Tissue biodistribution and blood clearance rates of intravenously administered carbon nanotube radiotracers. *Proc. Natl. Acad. Sci. U. S. A.* **2006,** 103, 3357-3362.
176. Huczko, A.; Lange, H.; Calko, E.; Grubek-Jaworska, H.; Droszcz, P., Physiological testing of carbon nanotubes: are they asbestos-like? *Fullerene Sci. Technol.* **2001,** 9, 251-254.
177. Lam, C.-W.; James, J. T.; McCluskey, R.; Hunter, R. L., Pulmonary Toxicity of Single-Wall Carbon Nanotubes in Mice 7 and 90 Days After Intratracheal Instillation. *Toxicol. Sci.* **2004,** 77, 126-134.
178. Muller, J.; Huaux, F.; Moreau, N.; Misson, P.; Heilier, J.-F.; Delos, M.; Arras, M.; Fonseca, A.; Nagy, J. B.; Lison, D., Respiratory toxicity of multi-wall carbon nanotubes. *Toxicol. Appl. Pharmacol.* **2005,** 207, 221-231.
179. Radomski, A.; Jurasz, P.; Alonso-Escolano, D.; Drews, M.; Morandi, M.; Malinski, T.; Radomski, M. W., Nanoparticle-induced platelet aggregation and vascular thrombosis. *Br. J. Pharmacol.* **2005,** 146, 882-893.
180. Prato, M.; Kostarelos, K.; Bianco, A., Functionalized Carbon Nanotubes in Drug Design and Discovery. *Acc. Chem. Res.* **2007,** 41, (1), 60-68.
181. Dieckmann, G. R.; Dalton, A. B.; Johnson, P. A.; Razal, J.; Chen, J.; Giordano, G. M.; Munoz, E.; Musselman, I. H.; Baughman, R. H.; Draper, R. K., Controlled Assembly of Carbon Nanotubes by Designed Amphiphilic Peptide Helices. *J. Am. Chem. Soc.* **2003,** 125, 1770-1777.
182. Wang, S.; Humphreys, E. S.; Chung, S.-Y.; Delduco, D. F.; Lustig, S. R.; Wang, H.; Parker, K. N.; Rizzo, N. W.; Subramoney, S.; Chiang, Y.-M.; Jagota, A., Peptides with selective affinity for carbon nanotubes. *Nat. Mater.* **2003,** 2, 196-200.
183. Zheng, M.; Jagota, A.; Semke, E. D.; Diner, B. A.; McLean, R. S.; Lustig, S. R.; Richardson, R. E.; Tassi, N. G., DNA-assisted dispersion and separation of carbon nanotubes. *Nat. Mater.* **2003,** 2, 338-342.
184. Zheng, M.; Jagota, A.; Strano, M. S.; Santos, A. P.; Barone, P.; Chou, S. G.; Diner, B. A.; Dresselhaus, M. S.; McLean, R. S.; Onoa, G. B.; Samsonidze, G. G.;

Semke, E. D.; Usrey, M.; Walls, D. J., Structure-Based Carbon Nanotube Sorting by Sequence-Dependent DNA Assembly. *Science* **2003,** 302, 1545-1548.
185. Chen, R. J.; Zhang, Y.; Wang, D.; Dai, H., Noncovalent sidewall functionalization of single-walled carbon nanotubes for protein immobilization. *J. Am. Chem. Soc.* **2001,** 123, 3838-3839.
186. Kim, O. K.; Je, J.; Baldwin, J. W.; Kooi, S.; Pehrsson, P. E.; Buckley, L. J., Solubilization of Single-Wall Carbon Nanotubes by Supramolecular Encapsulation of Helical Amylose. *J. Am. Chem. Soc.* **2003,** 125 4426-4427.
187. Wang, J.; Musameh, M.; Lin, Y., Solubilization of carbon nanotubes by nafion toward the preparation of amperometric biosensors. *J. Am. Chem. Soc.* **2003,** 125, 2408-2409.
188. O'Connell, M. J.; Boul, P.; Ericson, L. M.; Huffman, C.; Wang, Y.; Haroz, E.; Kuper, C.; Tour, J.; Ausman, K. D.; Smalley, R. E., Reversible water solubilization of single-walled carbon nanotubes by polymer wrapping. *Chem. Phys. Lett.* **2001,** 342, 265-271.
189. Ajayan, P. M.; Tour, J. M., Materials Science: Nanotube composites. *Nature* **2007,** 447, (7148), 1066-1068.
190. Sun, Y.-P.; Fu, K.; Lin, Y.; Huang, W., Functionalized Carbon Nanotubes: Properties and Applications. *Acc. Chem. Res.* **2002,** 35, (12), 1096-1104.
191. Ivanov, V.; Fonesca, A.; Nagy, J. B.; Lucas, A.; Lambin, P.; Bernaerts, D.; Zhang, X. B., Catalytic production and purification of nanotubules having fullerene-scale diameters. *Carbon* **1995,** 33, 1727-1738.
192. Georgakilas, V.; Kordatos, K.; Prato, M.; Guldi, D. M.; Holzinger, M.; Hirsch, A., Organic functionalization of carbon nanotubes. *J. Am. Chem. Soc.* **2002,** 124, 760-761.
193. Tagmatarchis, N.; Prato, M., Functionalization of carbon nanotubes via 1,3-dipolar cycloadditions. *J. Mater. Chem.* **2004,** 14, 437-439.
194. Holzinger, M.; Abraham, J.; Whelan, P.; Graupner, R.; Ley, L.; Hennrich, F.; Kappes, M.; Hirsch, A., Functionalization of Single-Walled Carbon Nanotubes with (R-)Oxycarbonyl Nitrenes. *J. Am. Chem. Soc.* **2003,** 125, 8566-8580.
195. Coleman, K. S.; Bailey, S. R.; Fogden, S.; Green, M. L. H., Functionalization of Single-Walled Carbon Nanotubes via the Bingel Reaction. *J. Am. Chem. Soc.* **2003,** 125, 8722-8723.
196. Worsley, K. A.; Moonoosawmy, K. R.; Kruse, P., Long-range periodicity in carbon nanotube sidewall functionalization. *Nano Lett.* **2004,** 4, 1541-1546.
197. Holzinger, M.; Vostrowsky, O.; Hirsch, A.; Hennrich, F.; Kappes, M.; Weiss, R.; Jellen, F., Sidewall functionalization of carbon nanotubes. *Angew. Chem., Int. Ed. Engl.* **2001,** 40, 4002-4005.
198. Chen, J.; Hamon, M. A.; Hu, H.; Chen, Y.; Rao, A. M.; Eklund, P. C.; Haddon, R. C., Solution properties of single-walled carbon nanotubes. *Science* **1998,** 282, 95-98.
199. Banerjee, S.; Wong, S. S., Rational Sidewall Functionalization and Purification of Single-Walled Carbon Nanotubes by Solution-Phase Ozonolysis. *J. Phys. Chem. B* **2002,** 106, 12144-12151.

200. Banerjee, S.; Hemraj-Benny, T.; Balasubramanian, M.; Fischer, D. A.; Misewich, J. A.; Wong, S. S., Ozonized single-walled carbon nanotubes investigated using NEXAFS spectroscopy. *Chem. Commun.* **2004**, 772-773.
201. Bahr, J. L.; Yang, J.; Kosynkin, D. V.; Bronikowski, M. J.; Smalley, R. E.; Tour, J. M., Functionalization of carbon nanotubes by electrochemical reduction of aryl diazonium salts: A bucky paper electrode. *J. Am. Chem. Soc.* **2001,** 123, 6536-6542.
202. Peng, H.; Alemany, L. B.; Margrave, J. L.; Khabashesku, V. N., Sidewall Carboxylic Acid Functionalization of Single-Walled Carbon Nanotubes. *J. Am. Chem. Soc.* **2003,** 125, 15174-15182.
203. Nakajima, T.; Kasamatsu, S.; Matsuo, Y., Synthesis and characterization of fluorinated carbon nanotube. *Eur. J. Solid State Inorg. Chem.* **1996,** 33, 831-840.
204. Liang, F.; Sadana, A. K.; Peera, A.; Chattopadhyay, J.; Gu, Z.; Hauge, R. H.; Billups, W. E., A Convenient Route to Functionalized Carbon Nanotubes. *Nano Lett.* **2004,** 4, 1257-1260.
205. Pekker, S.; Salvetat, J. P.; Jakab, E.; Bonard, J. M.; Forro, L., Hydrogenation of Carbon Nanotubes and Graphite in Liquid Ammonia. *J. Phys. Chem. B* **2001,** 105, 7938-7943.
206. Prato, M.; Kostarelos, K.; Bianco, A., Functionalized Carbon Nanotubes in Drug Design and Discovery. *Acc. Chem. Res.* **2008,** 41, (1), 60-68.
207. Bonifazi, D.; Nacci, C.; Marega, R.; Campidelli, S.; Ceballos, G.; Modesti, S.; Meneghetti, M.; Prato, M., Microscopic and spectroscopic characterization of paintbrush-like single-walled carbon nanotubes. *Nano Lett.* **2006,** 6, 1408-1414.
208. Sun, Y.-P.; Zhou, B.; Henbest, K.; Fu, K.; Huang, W.; Lin, Y.; Taylor, S.; Carroll, D. L., Luminescence anisotropy of functionalized carbon nanotubes in solution. *Chem. Phys. Lett.* **2002,** 351, 349-353.
209. Bianco, A.; Prato, M., Can carbon nanotubes be considered useful tools for biological applications? . *Adv. Mater.* **2003,** 15, 1765-1768.
210. Pantarotto, D.; Partidos, C. D.; Hoebeke, J.; Brown, F.; Kramer, E.; Briand, J.-P.; Muller, S.; Prato, M.; Bianco, A., Immunization with Peptide-Functionalized Carbon Nanotubes Enhances Virus-Specific Neutralizing Antibody Responses. *Chem. Biol.* **2003,** 10, 961-966.
211. Pantarotto, D.; Singh, R.; McCarthy, D.; Erhardt, M.; Briand, J.-P.; Prato, M.; Kostarelos, K.; Bianco, A., Functionalized carbon nanotubes for plasmid DNA gene delivery. *Angew. Chem., Int. Ed. Engl.* **2004,** 43, 5242-5246.
212. Chen, J.; Chen, S.; Zhao, X.; Kuznetsova, L. V.; Wong, S. S.; Ojima, I., Functionalized Single-Walled Carbon Nanotubes as Rationally Designed Vehicles for Tumor-Targeted Drug Delivery. *J. Am. Chem. Soc.* **2008,** 130, (49), 16778-16785.
213. Hirsch, L. R.; Stafford, R. J.; Bankson, J. A.; Sershen, S. R.; Rivera, B.; Price, R. E.; Hazle, J. D.; Halas, N. J.; West, J. L., Nanoshell-mediated near-infrared thermal therapy of tumors under magnetic resonance guidance. *Proc. Natl. Acad. Sci. U. S. A.* **2003,** 100, (23), 13549-13554.
214. Kam, N. W. S.; O'Connell, M.; Wisdom, J. A.; Dai, H., Carbon nanotubes as multifunctional biological transporters and near-infrared agents for selective cancer cell destruction. *Proc. Natl. Acad. Sci. USA* **2005,** 102, (33), 11600-11605.

215. Hamada, N.; Sawada, S.-i.; Oshiyama, A., New one-dimensional conductors: Graphitic microtubules. *Phys. Rev. Lett.* **1992,** 68, (10), 1579.
216. O'Connell, M. J.; Bachilo, S. M.; Huffman, C. B.; Moore, V. C.; Strano, M. S.; Haroz, E. H.; Rialon, K. L.; Boul, P. J.; Noon, W. H.; Kittrell, C.; Ma, J.; Hauge, H. R.; Weisman, B. R.; Smalley, R. E., Band Gap Fluorescence from Individual Single-Walled Carbon Nanotubes. *Science* **2002,** 297, (5581), 593-596.
217. Kim, P.; Odom, T. W.; Huang, J.-L.; Lieber, C. M., Electronic Density of States of Atomically Resolved Single-Walled Carbon Nanotubes: Van Hove Singularities and End States. *Phys. Rev. Lett.* **1999,** 82, (6), 1225.
218. Marches, R.; Chakravarty, P.; Musselman, I. H.; Bajaj, P.; Azad, R. N.; Pantano, P.; Draper, R. K.; Vitetta, E. S., Specific thermal ablation of tumor cells using single-walled carbon nanotubes targeted by covalently-coupled monoclonal antibodies. *Int. J. Cancer* **2009,** 125, (12), 2970-2977.
219. Chakravarty, P.; Marches, R.; Zimmerman, N. S.; Swafford, A. D. E.; Bajaj, P.; Musselman, I. H.; Pantano, P.; Draper, R. K.; Vitetta, E. S., Thermal ablation of tumor cells with antibody-functionalized single-walled carbon nanotubes. *Proc. Natl. Acad. Sci. U.S.A.* **2008,** 105, (25), 8697-8702.
220. Gannon, C. J.; Cherukuri, P.; Yakobson, B. I.; Cognet, L.; Kanzius, J. S.; Kittrell, C.; Weisman, R. B.; Pasquali, M.; Schmidt, H. K.; Smalley, R. E.; Curley, S. A., Carbon nanotube-enhanced thermal destruction of cancer cells in a noninvasive radiofrequency field. *Cancer* **2007,** 110, 2654-2665.
221. Green, D. E.; Longtin, J. P.; Sitharaman, B., The Effect of Nanoparticle-Enhanced Photoacoustic Stimulation on Multipotent Marrow Stromal Cells. *ACS Nano* **2009,** 3, (8), 2065-2072.
222. Kang, B.; Yu, D.; Dai, Y.; Chang, S.; Chen, D.; Ding, Y., Cancer-Cell Targeting and Photoacoustic Therapy Using Carbon Nanotubes as "Bomb" Agents. *Small* **2009,** 5, (11), 1292-1301.
223. Shao, N.; Lu, S.; Wickstrom, E.; Panchapakesan, B., Integrated molecular targeting of IGF1R and Her2 surface receptors and destruction of breast cancer cells using singlewall carbon nanotubes. *Nanotechnology* **2007,** 18, 315101-315109.
224. Xiao, Y.; Gao, X.; Taratula, O.; Treado, S.; Urbas, A.; Holbrook, D. R.; Cavicchi, R.; Avedisian, T. C.; Mitra, S.; Savla, R.; Wagner, P.; Srivastava, S.; He, H., Anti-HER2 IgY antibody-functionalized single-walled carbon nanotubes for detection and selective destruction of breast cancer cells. *BMC Cancer* **2009,** 9, (1), 351.
225. Kam, N. W. S.; Jessop, T. C.; Wender, P. A.; Dai, H., Nanotube Molecular Transporters: Internalization of Carbon Nanotube-Protein Conjugates into Mammalian Cells. *J . Am. Chem. Soc.* **2004,** 126, (22), 6850-6851.
226. Gao, L.; Nie, L.; Wang, T.; Qin, Y.; Guo, Z.; Yang, D.; Yan, X., Carbon nanotube delivery of the GFP gene into mammalian cells. *ChemBioChem* **2006,** 7, 239-242.
227. Singh, R.; Pantarotto, D.; McCarthy, D.; Chaloin, O.; Hoebeke, J.; Partidos, C. D.; Briand, J.-P.; Prato, M.; Bianco, A.; Kostarelos, K., Binding and Condensation of Plasmid DNA onto Functionalized Carbon Nanotubes: Toward the Construction of Nanotube-Based Gene Delivery Vectors. *J . Am. Chem. Soc.* **2005,** 127, (12), 4388-4396.

228. Pantarotto, D.; Singh, R.; McCarthy, D.; Erhardt, M.; Briand, J.-P.; Prato, M.; Kostarelos, K.; Bianco, A., Functionalized Carbon Nanotubes for Plasmid DNA Gene Delivery. *Angew. Chem., Int. Ed. Engl.* **2004,** 43, (39), 5242-5246.
229. Ahmed, M.; Jiang, X.; Deng, Z.; Narain, R., Cationic Glyco-Functionalized Single-Walled Carbon Nanotubes as Efficient Gene Delivery Vehicles. *Bioconjugate Chem.* **2009,** 20, (11), 2017-2022.
230. Zhang, X.; Meng, L.; Lu, Q.; Fei, Z.; Dyson, P. J., Targeted delivery and controlled release of doxorubicin to cancer cells using modified single wall carbon nanotubes. *Biomaterials* **2009,** 30, (30), 6041-6047.
231. Feazell, R. P.; Nakayama-Ratchford, N.; Dai, H.; Lippard, S. J., Soluble Single-Walled Carbon Nanotubes as Longboat Delivery Systems for Platinum(IV) Anticancer Drug Design. *J. Am. Chem. Soc.* **2007,** 129, 8438-8439.
232. Kostarelos, K.; Lacerda, L.; Pastorin, G.; Wu, W.; Wieckowski, S.; Luangsivilay, J.; Godefroy, S.; Pantarotto, D.; Briand, J.-P.; Muller, S.; Prato, M.; Bianco, A., Cellular uptake of functionalized carbon nanotubes is independent of functional group and cell type. *Nat. Nanotechnol.* **2007,** 2, 108-113.
233. Liu, J.; Rinzler, A. G.; Dai, H.; Hafner, J. H.; Bradley, R. K.; Boul, P. J.; Lu, A.; Iverson, T.; Shelimov, K.; Huffman, C. B.; Rodriguez-Macias, F.; Shon, Y.-S.; Lee, T. R.; Colbert, D. T.; Smalley, R. E., Fullerene pipes. *Science* **1998,** 280, 1253-1256.
234. Russell-Jones, G.; McTavish, K.; McEwan, J.; Rice, J.; Nowotnik, D., Vitamin mediated targeting as a potential mechanism to increase drug uptake by tumors. *J. Inorg. Biochem.* **2004,** 98, 1625-1633.
235. Russell-Jones, G.; McEwan, J. Amplification of biotin-mediated targeting. 2004045647, 20031121, 2004.
236. Kam, N. W. S.; Liu, Z.; Dai, H., Carbon nanotubes as intracellular transporters for proteins and DNA: an investigation of the uptake mechanism and pathway. *Angew. Chem. Int. Ed.* **2006,** 45, 577-581.
237. Kordatos, K.; Da Ros, T.; Bosi, S.; Vazquez, E.; Bergamin, M.; Cusan, C.; Pellarini, F.; Tomberli, V.; Baiti, B.; Pantarotto, D.; Georgakilas, V.; Spalluto, G.; Prato, M., Novel Versatile Fullerene Synthons. *J. Org. Chem.* **2001,** 66, 4915-4920.
238. Varghese, S.; Gupta, D.; Baran, T.; Jiemjit, A.; Gore, S. D.; Casero, R. A. J.; Woster, P. M., Alkyl-Substituted Polyaminohydroxamic Acids: A Novel Class of Targeted Histone Deacetylase Inhibitors. *J. Med. Chem.* **2005,** 48, 6350-6365.

References for Chapter 6:

1. Boss, D. S.; Olmos, R. V.; Sinaasappel, M.; Beijnen, J. H.; Schellens, J. H. M., Application of PET/CT in the Development of Novel Anticancer Drugs. *Oncologist* **2008,** 13, (1), 25-38.
2. Pantaleo, M. A.; Nannini, M.; Maleddu, A.; Fanti, S.; Ambrosini, V.; Nanni, C.; Boschi, S.; Biasco, G., Conventional and novel PET tracers for imaging in oncology in the era of molecular therapy. *Cancer Treat. Rev.* **2008,** 34, (2), 103-121.
3. Coleman, E. R., Value of FDG-PET scanning in management of lung cancer. *Lancet* **2002,** 359, (9315), 1361.
4. Ambrosini, V.; Tomassetti, P.; Rubello, D.; Campana, D.; Nanni, C.; Castellucci, P.; Farsad, M.; Montini, G.; Al-Nahhas, A.; Franchi, R.; Fanti, S., Role of 18F-dopa PET/CT imaging in the management of patients with 111In-pentetreotide negative GEP tumours. *Nucl. Med. Comm.* **2007,** 28, (6), 473-477.
5. Surti, S.; Karp, J. S.; Kinahan, P. E., Pet Instrumentation. *Radiol. Clin. North. Am.* **2004,** 42, (6), 1003-1016.
6. Pagani, M.; Stone-Elander, S.; Larsson, S. A., Alternative positron emission tomography with non-conventional positron emitters: Effects of their physical properties on image quality and potential clinical applications. *Eur. J. Nucl. Med.* **1997,** 24, 1301-1327.
7. Shukla, A.; Kumar, U., Positron emission tomography: An overview. *J. Med. Phys.* **2006,** 31, (1), 13-21.
8. Rohren, E. M.; Turkington, T. G.; Coleman, R. E., Clinical applications of PET in oncology. *Radiology* **2004,** 231, 305-332.
9. Juweid, M. E.; Cheson, B. D., Positron-emission tomography and assessment of cancer therapy. *N. Engl. J. Med.* **2006,** 354, 496 -507.
10. Warburg, O., On the origin of cancer cells. *Science* **1956,** 123, 309 -314.
11. Brenner, W.; Bohuslavizki, K. H.; Eary, J. F., PET imaging of osteosarcoma. *J. Nucl. Med.* **2003,** 44, 930 -942.
12. Even-Sapir, E., Imaging of malignant bone involvement by morphologic, scintigraphic, and hybrid modalities. *J. Nucl. Med.* **2005,** 46, 1356 -1367.
13. Zasadny, K. R.; Wahl, R. L., Standardized uptake values of normal tissues at PET with 2-[fluorine-18]-fluoro-2-deoxy-D-glucose: Variations with body weight and a method for correction. *Radiology* **1993,** 189, 847- 850.
14. Weber, W. A.; Ziegler, S. I.; Thodtmann, R.; Hanauske, A.-R.; Schwaiger, M., Reproducibility of Metabolic Measurements in Malignant Tumors Using FDG PET. *J. Nucl. Med.* **1999,** 40, (11), 1771-1777.
15. Herholz, K.; Ziffling, P.; Staffen, W.; et al, Uncoupling of hexose transport and phosphorylation in human gliomas demonstrated by PET. *Eur. J. Cancer Clin. Oncol.* **1988,** 24, 1139 -1150.
16. Zhang, X.; Xiong, Z.; Wu, Y.; Cai, W.; Tseng, J. R.; Gambhir, S. S.; Chen, X., Quantitative PET Imaging of Tumor Integrin {alpha}v{beta}3 Expression with ^{18}F-FRGD2. *J. Nucl. Med.* **2006,** 47, (1), 113-121.
17. Schiepers, C.; Chen, W.; Cloughesy, T.; Dahlbom, M.; Huang, S.-C., ^{18}F-FDOPA Kinetics in Brain Tumors. *J. Nucl. Med.* **2007,** 48, (10), 1651-1661.

18. Wang, J.; Maurer, L., Positron Emission Tomography: applications in drug discovery and drug development. *Curr. Top. Med. Chem.* **2005,** 5, (11), 1053-1075.
19. Gupta, N.; Price, P. M.; Aboagye, E. O., Pet for in vivo Pharmacokinetic and Pharmacodynamic Measurements. *Eur. J. Cancer* **2002,** 38, 2094-2107.
20. Saleem, A.; Yap, J.; Osman, S.; Brady, F.; Suttle, B.; Lucas, S. V.; Jones, T.; Price, P. M.; Aboagye, E. O., Modulation of Fluorouracil Tissue Pharmacokinetics by Eniluracil: In vivo Imaging of Drug Action. *Lancet* **2000,** 355, 2125-2131.
21. Ginos, J. Z.; Cooper, A. J.; Dhawan, V.; Lai, J. C.; Strother, S. C.; Alcock, N.; Rottenberg, D. A., [13n]Cisplatin Pet to Assess Pharmacokinetics of Intra-Arterial Versus Intravenous Chemotherapy for Malignant Brain Tumors. *J. Nucl. Med.* **1987,** 28, 1844-1852.
22. Tyler, J. L.; Yamamoto, Y. L.; Diksic, M.; Theron, J.; Villemure, J. G.; Worthington, C.; Evans, A. C.; Feindel, W., Pharmacokinetics of Superselective Intra-Arterial and Intravenous [11c]Bcnu Evaluated by Pet. *J. Nucl. Med.* **1986,** 27, 775-780.
23. Inoue, T.; Kim, E. E.; Wallace, S.; Yang, D. J.; Wong, F. C.; Bassa, P.; Cherif, A.; Delpassand, E.; Buzdar, A.; Podoloff, D. A., Positron Emission Tomography Using [18f]Fluorotamoxifen to Evaluate Therapeutic Responses in Patients with Breast Cancer: Preliminary Study. *Cancer. Biother. Radiopharm.* **1996,** 11, 235-245.
24. Kurdziel, K. A.; Kiesewetter, D. O.; Carson, R. E.; Eckelman, W. C.; Herscovitch, P., Biodistribution, Radiation Dose Estimates, and in. Vivo Pgp Modulation Studies of 18f-Paclitaxel in Nonhuman Primates. *J. Nucl. Med.* **2003,** 44, 1330-1339.
25. Aboagye, E. O., Positron Emission Tomography Imaging of Small Animals in Anticancer Drug Development. *Mol. Imaging Biol.* **2005,** 7, 53-58.
26. Hammond, L. A.; Cavanaugh, S. X.; Thomas, C. R., An Image Worth a Thousand Lives? . *Nat. Biotechnol.* **2004,** 22, 677-678.
27. Cherry, S. R.; Gambhir, S. S., Use of Positron Emission Tomography in Animal Research. *ILAR J.* **2001,** 42, 219-232.
28. Ambrosini, V.; Quarta, C.; Nanni, C.; Pettinato, C.; Franchi, R.; Grassetto, G.; Nahhas, A. A.; Fanti, S.; Rubello, D., Small animal PET in oncology: the road from bench to bedside.(positron emission tomography)(Report). *Cancer Biotherapy Radiopharm.* **2009,** 24, (2), 277(9).
29. Widmer, C., Jr.; Holman, R. T., Polyethenoid fatty acid metabolism. II. Deposition of polyunsaturated fatty acids in fat-deficient rats upon single fatty acid supplementation. *Arch. Biochem.* **1950,** 25, 1-12.
30. Hardman, W. E., Omega-3 Fatty Acids to Augment Cancer Therapy. *J. Nutrition* **2002,** 132, 3508S-3512S.
31. Tapiero, H.; Nguyen Ba, G.; Couvreur, P.; Tew, K. D., Polyunsaturated fatty acids (PUFA) and eicosanoids in human health and pathologies. *Biomed. Pharmacother.* **2002,** 56, 215-222.
32. Moser, U., N-3 and N-6 PUFAS in healthy and diseased skin. *J. Appl. Cosmet.* **2002,** 20, 137-142.

33. Huang, Y.-S.; Pereira, S. L.; Leonard, A. E., Enzymes for transgenic biosynthesis of long-chain polyunsaturated fatty acids. *Biochimie* **2004,** 86, 793-798.
34. Morimoto, K. C.; Van Eenennaam, A. L.; DePeters, E. J.; Medrano, J. F., Hot topic: endogenous production of n-3 and n-6 fatty acids in mammalian cells. *J. Dairy Sci.* **2005,** 88, 1142-1146.
35. Heird, W. C.; Lapillonne, A., The role of essential fatty acids in development. *Annu. Rev. Nutr.* **2005,** 25, 549-571.
36. Harris, W. S., Omega-3 fatty acids. In *Encyclopedia of Dietary Supplements*, Coates, P. M., Ed. Marcel Decker: New York, 2005; pp 493–504.
37. Bradley, M. O.; Webb, N. L.; Anthony, F. H.; Devanesan, P.; Witman, P. A.; Hemamalini, S.; Chander, M. C.; Baker, S. D.; He, L.; Horowitz, S. B.; Swindell, C. S., Tumor Targeting by Covalent Conjugation of a Natural Fatty Acid to Taxol. *Clin. Cancer Res.* **2001,** 7, 3229-3238.
38. Wolff, A. C.; Donehower, R. C.; Carducci, M. K.; Carducci, M. A.; Brahmer, J. R.; Zabelina, Y.; Bradley, M. O.; Anthony, F. H.; Swindell, C. S.; Witman, P. A.; Webb, N. L.; Baker, S. D., Phase I Study of Docosahexaenoic Acid-Paclitaxel. *Clin. Cancer Res.* **2003,** 9, (10), 3589-3597.
39. Fracasso, P.; Picus, J.; Wildi, J.; Goodner, S.; Creekmore, A.; Gao, F.; Govindan, R.; Ellis, M.; Tan, B.; Linette, G.; Fu, C.; Pentikis, H.; Zumbrun, S.; Egorin, M.; Bellet, R., Phase 1 and pharmacokinetic study of weekly docosahexaenoic acid-paclitaxel, Taxoprexin®, in resistant solid tumor malignancies. *Cancer Chemother. Pharmacol.* **2009,** 63, (3), 451-458.
40. Ojima, I.; Lin, S.; Wang, T., The Recent Advances in the Medicinal Chemistry of Taxoids with Novel β-Amino Acid Side Chains." In "The Chemistry and Biology of β-Amino Acids." *Curr. Med. Chem.* **1999,** 6, 927-954.
41. Ojima, I.; Wang, T.; Miller, M. L.; Lin, S.; Borella, C.; Geng, X.; Pera, P.; Bernacki, R. J., Syntheses and Structure-Activity Relationships of New Second-Generation Taxoids. *Bioorg. Med. Chem. Lett.* **1999,** 9, 3423-3428.
42. Lin, S.; Geng, X.; Qu, C.; Tynebor, R.; Gallagher, D. J.; Pollina, E.; Rutter, J.; Ojima, I., Synthesis of highly potent second-generation taxoids through effective kinetic resolution coupling of racemic .beta.-lactams with baccatins. *Chirality* **2000,** 12, (5/6), 431-441.
43. Kuznetsova, L. V.; Chen, J.; Sun, L.; Wu, X.; Pepe, A.; Veith, J. M.; Pera, P.; Bernacki, R. J.; Ojima, I., Syntheses and Evaluation of Novel Fatty Acid-2nd-generation Taxoid Conjugates as Promising Anticancer Agents. *Bioorg. Med. Chem. Lett.* **2006,** 16, 974-977
44. Geney, R.; Chen, J.; Ojima, I., Recent Advance in the New Generation Taxane Anticancer Agents. *Med. Chem.* **2005,** 1, 125-139.
45. Chen, A. P.; Grem, J. L., Antimetabolites. *Curr. Opin. Oncol.* **1992,** 4, (6), 1089-98.
46. Richards, F. D.; Case, L. D.; White, D. R.; Muss, H. B.; Spurr, C. L.; Jackson, D. V.; Cooper, M. R.; Zekan, P.; Cruz, J.; Stuart, J. J., Combination chemotherapy (5-fluorouracil, methyl-CCNU, mitomycin C) versus 5-fluorouracil alone for advanced previously untreated colorectal carcinoma. A phase III study of the Piedmont Oncology Association. *J. Clin. Oncol.* **1986,** 4, (4), 565-570.

47. Hutchinson, C. O.; Collingridge, D. R.; Barthel, H.; Price, P. M.; Aboagye, E. O., Pharmacokinetics of Radiolabelled Anticancer Drugs for Positron Emission Tomography. *Curr. Pharm. Des.* **2003,** 9, 917-929.
48. Shani, J.; Wolf, W., A model for prediction of chemotherapy response to 5-fluorouracil based on the differential distribution of 5-[18F]fluorouracil in sensitive versus resistant lymphocytic leukemia in mice. *Cancer Res.* **1977,** 37, 2306-2308.
49. Thiebaut, F.; Tsuruo, T.; Hamada, H.; Gottesman, M. M.; Pastan, I.; Willingham, M. C., Cellular-localization of the multidrug-resistance geneproduct P-glycoprotein in normal human tissues. *Proc. Natl. Acad. Sci. U.S.A.* **1987,** 84, 7735-7738.
50. Ambudkar, S. V.; Dey, S.; Hrycyna, C. A.; Ramachandra, M.; Pastan, I.; Gottesman, M. M., Biochemical, cellular, and pharmacological aspects of the multidrug transporter. *Annu. Rev. Pharmacol. Toxicol.* **1999,** 39, 361-398.
51. Kiesewetter, D. O.; Jagoda, E. M.; Kao, C.-H. K.; Ma, Y.; Ravasi, L.; Shimoji, K.; Szajek, L. P.; Eckelman, W. C., Fluoro-, bromo-, and iodopaclitaxel derivatives: synthesis and biological evaluation. *Nucl. Med. Biol.* **2003,** 30, 11-24.
52. Hosoya, T.; Sumi, K.; Doi, H.; Wakaoa, M.; Suzuki, M., Rapid methylation on carbon frameworks useful for the synthesis of $^{11}CH_3$-incorporated PET tracers: Pd(0)-mediated rapid coupling of methyl iodide with an alkenyltributylstannane leading to a 1-methylalkene. *Org. Biomol. Chem.* **2006,** 4, 410–415.
53. Mee, S. P. H.; Lee, V.; Baldwin, J. E., Stille Coupling Made Easier-The Synergic Effect of Copper(I) Salts and the Fluoride Ion. *Angew. Chem. Int. Ed.* **2004,** 43, 1132 -1136.
54. Liebeskind, L. S.; Fengl, R. W., 3-Stannylcyclobutenediones as nucleophilic cyclobutenedione equivalents. Synthesis of substituted cyclobutenediones and cyclobutenedione monoacetals and the beneficial effect of catalytic copper iodide on the Stille reaction. *J. Org. Chem.* **1990,** 55, (19), 5359-5364.
55. Farina, V.; Kapadia, S.; Krishnan, B.; Wang, C.; Liebeskind, L. S., On the Nature of the "Copper Effect" in the Stille Cross-Coupling. *J. Org. Chem.* **1994,** 59, (20), 5905-5911.
56. Han, X.; Stoltz, B. M.; Corey, E. J., Cuprous Chloride Accelerated Stille Reactions. A General and Effective Coupling System for Sterically Congested Substrates and for Enantioselective Synthesis. *J. Am. Chem. Soc.* **1999,** 121, (33), 7600-7605.
57. Casado, A. L.; Espinet, P., Quantitative Evaluation of the Factors Contributing to the "Copper Effect" in the Stille Reaction. *Organometallics* **2003,** 22, (6), 1305-1309.
58. Scott, W. J.; Stille, J. K., Palladium-catalyzed coupling of vinyl triflates with organostannanes. Synthetic and mechanistic studies. *J. Am. Chem. Soc.* **1986,** 108, (11), 3033-3040.
59. Gallagher, W. P.; Terstiege, I.; Maleczka, R. E., Stille Couplings Catalytic in Tin: The "Sn-O" Approach. *J. Am. Chem. Soc.* **2001,** 123, (14), 3194-3204.
60. Tu, Z.; Xu, J.; Jones, L. A.; Li, S.; Dumstorff, C.; Vangveravong, S.; Chen, D. L.; Wheeler, K. T.; Welch, M. J.; Mach, R. H., Fluorine-18-Labeled Benzamide

Analogues for Imaging the ó2 Receptor Status of Solid Tumors with Positron Emission Tomography. *J. Med. Chem.* **2007,** 50, 3194-3204.

Appendices

^{1}H NMR Spectrum of **1-8**

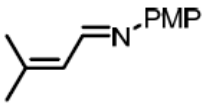

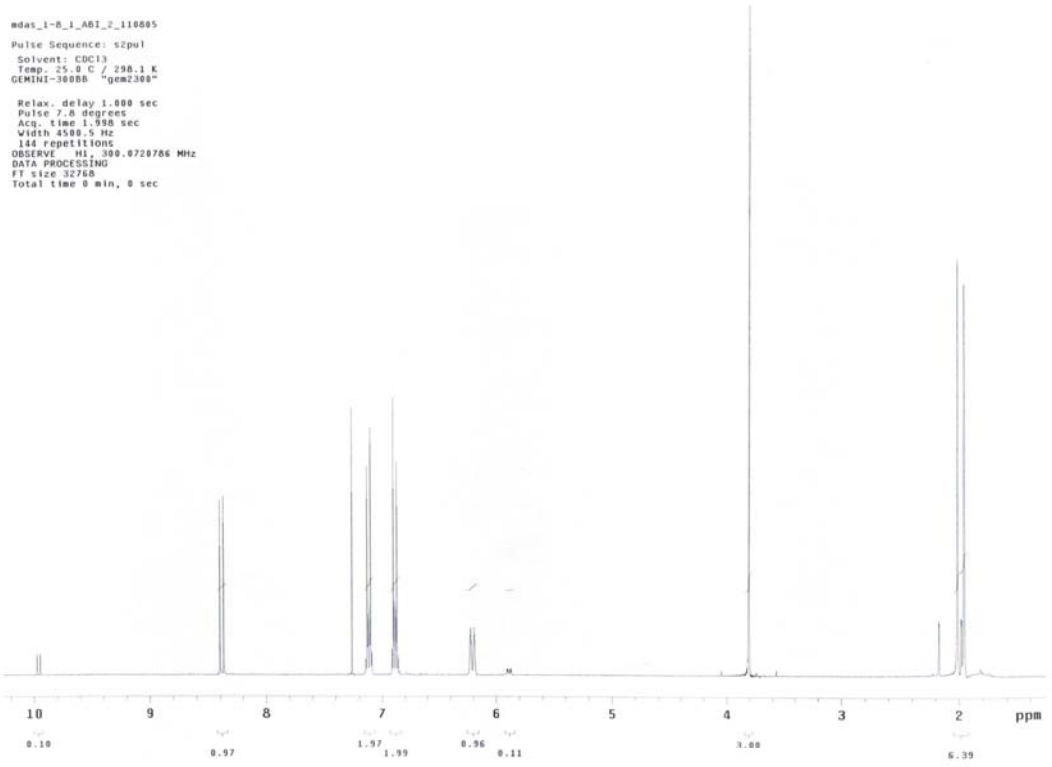

^{1}H NMR Spectrum of **1-9**

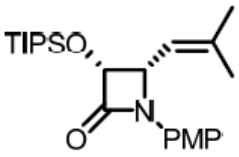

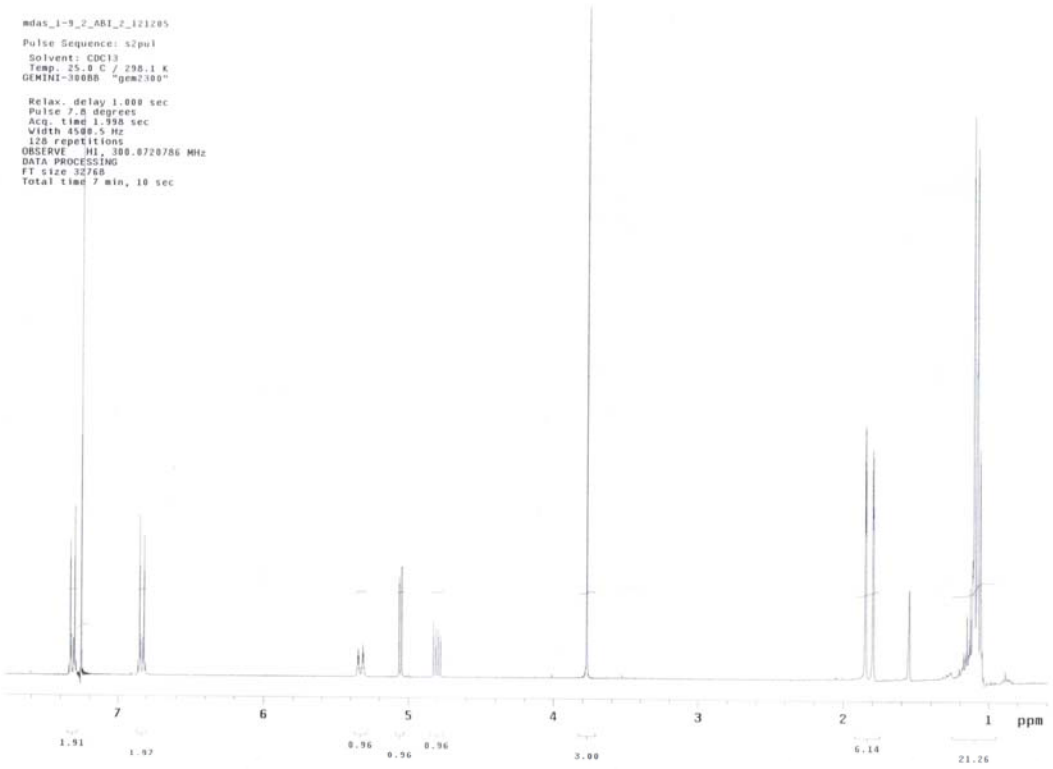

^{1}H NMR Spectrum of **SB-T-1214**

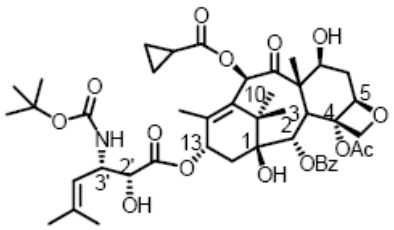

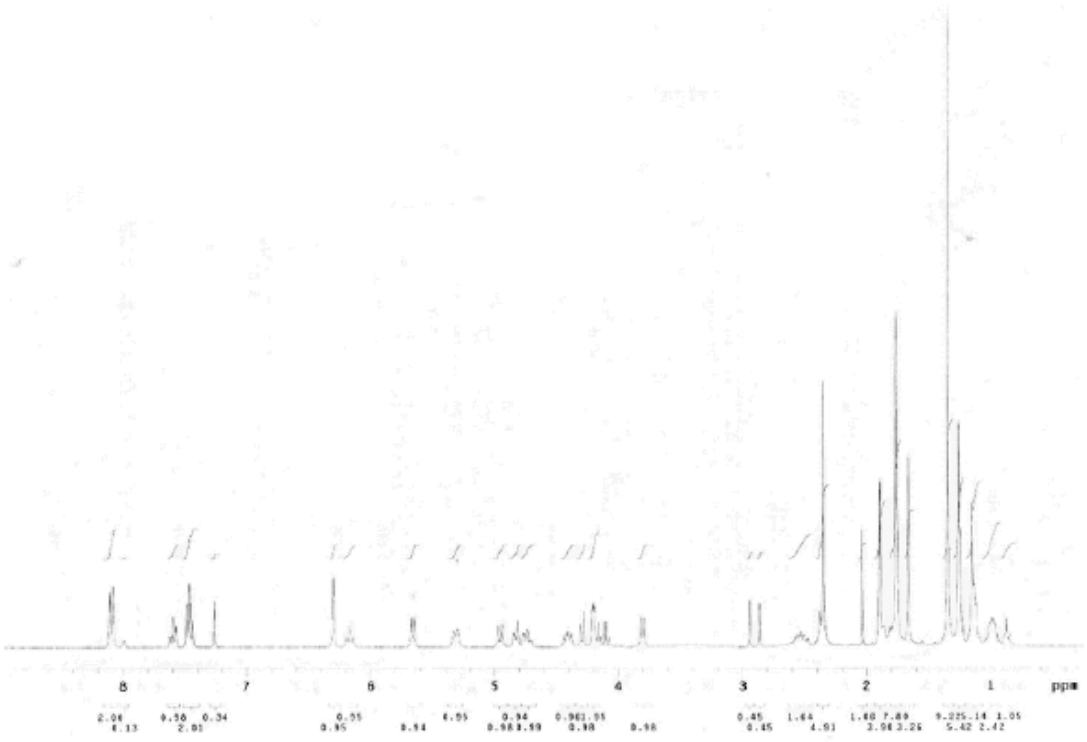

^{13}C NMR Spectrum of **SB-T-1214**

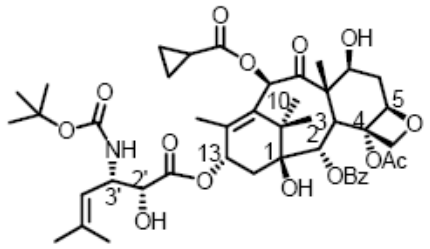

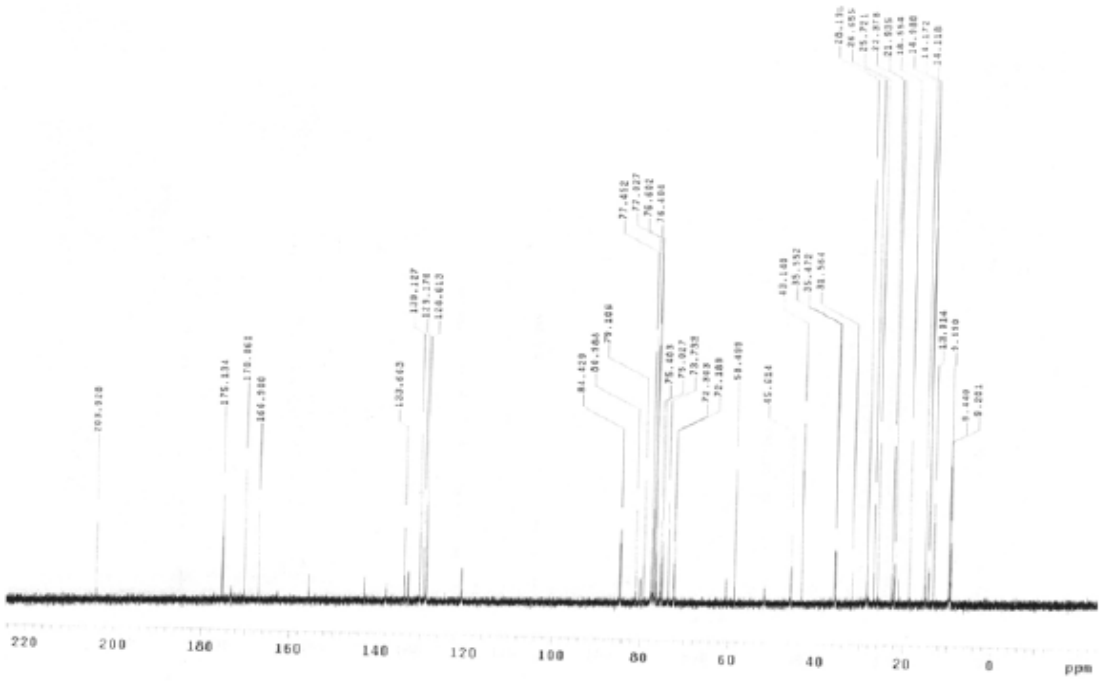

^{1}H NMR Spectrum of **2-1**

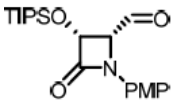

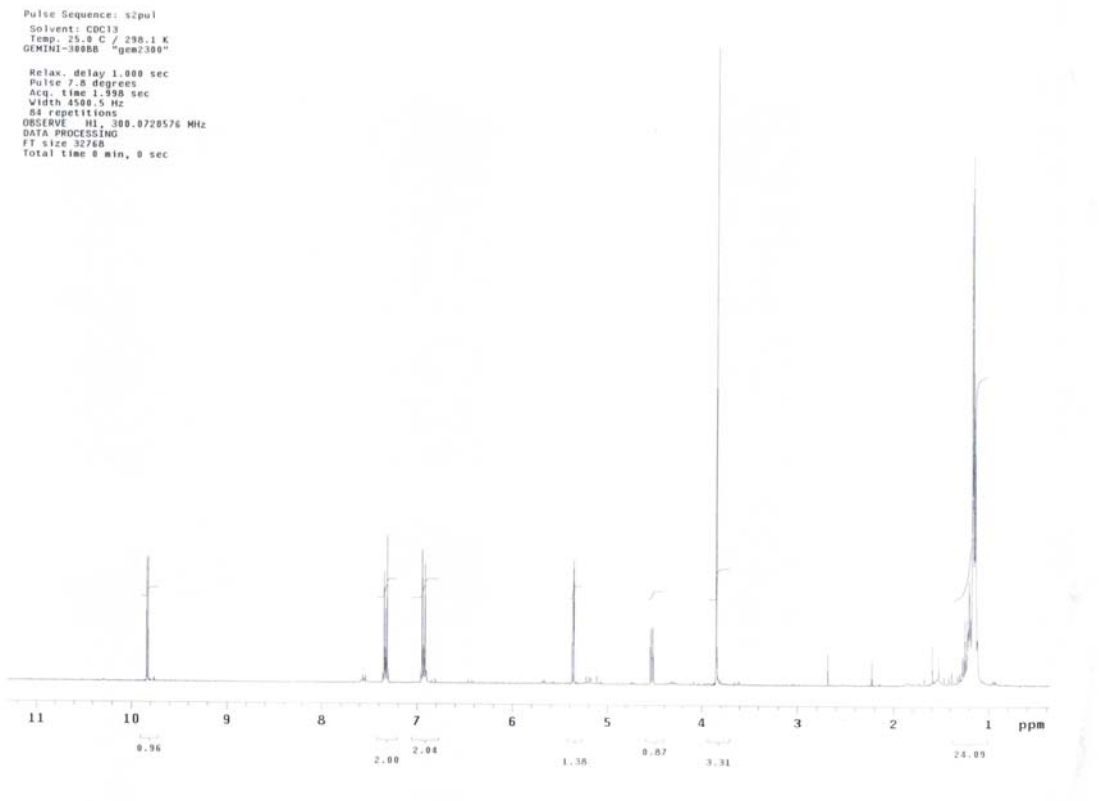

^{1}H NMR Spectrum of **2-2**

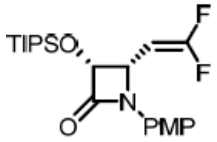

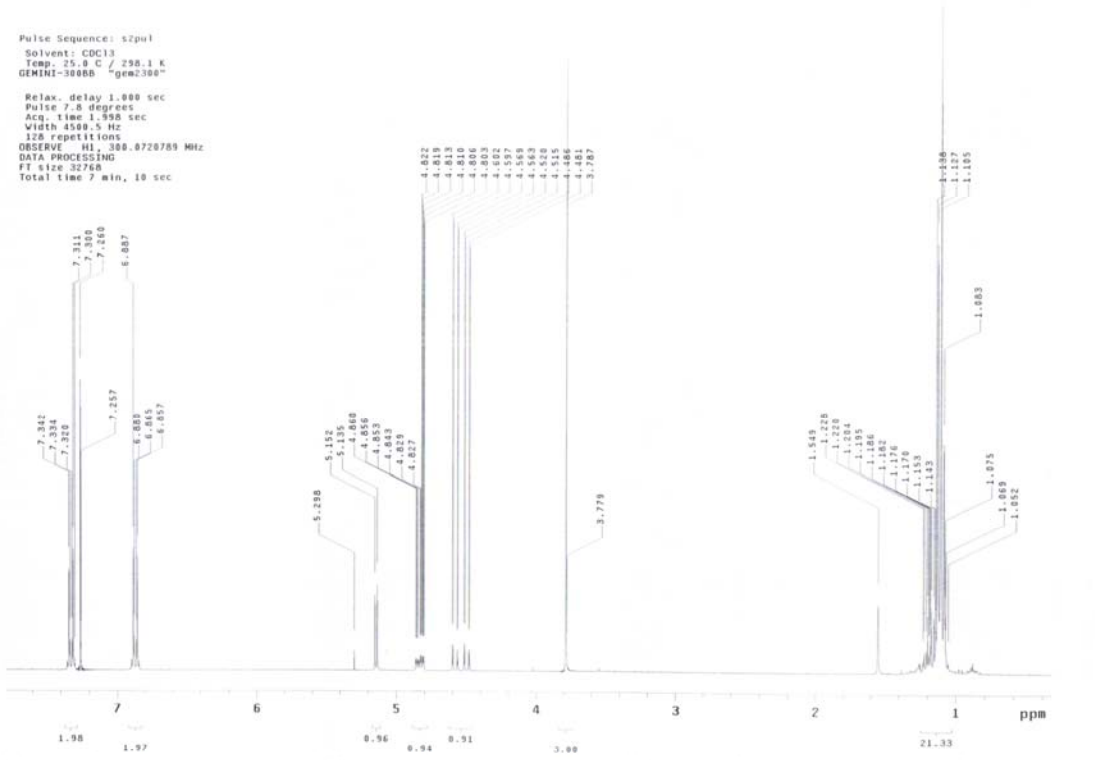

^{19}F NMR Spectrum of **2-2**

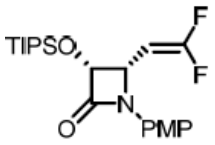

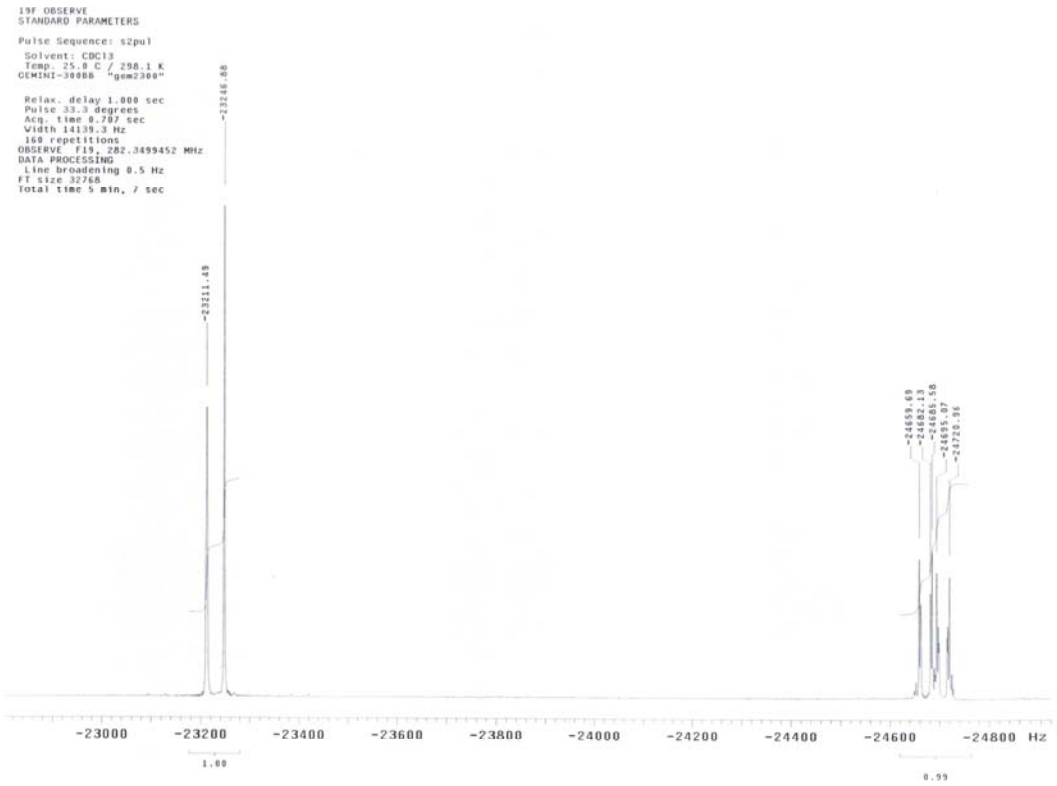

^{1}H NMR Spectrum of **2-3**

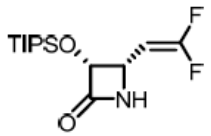

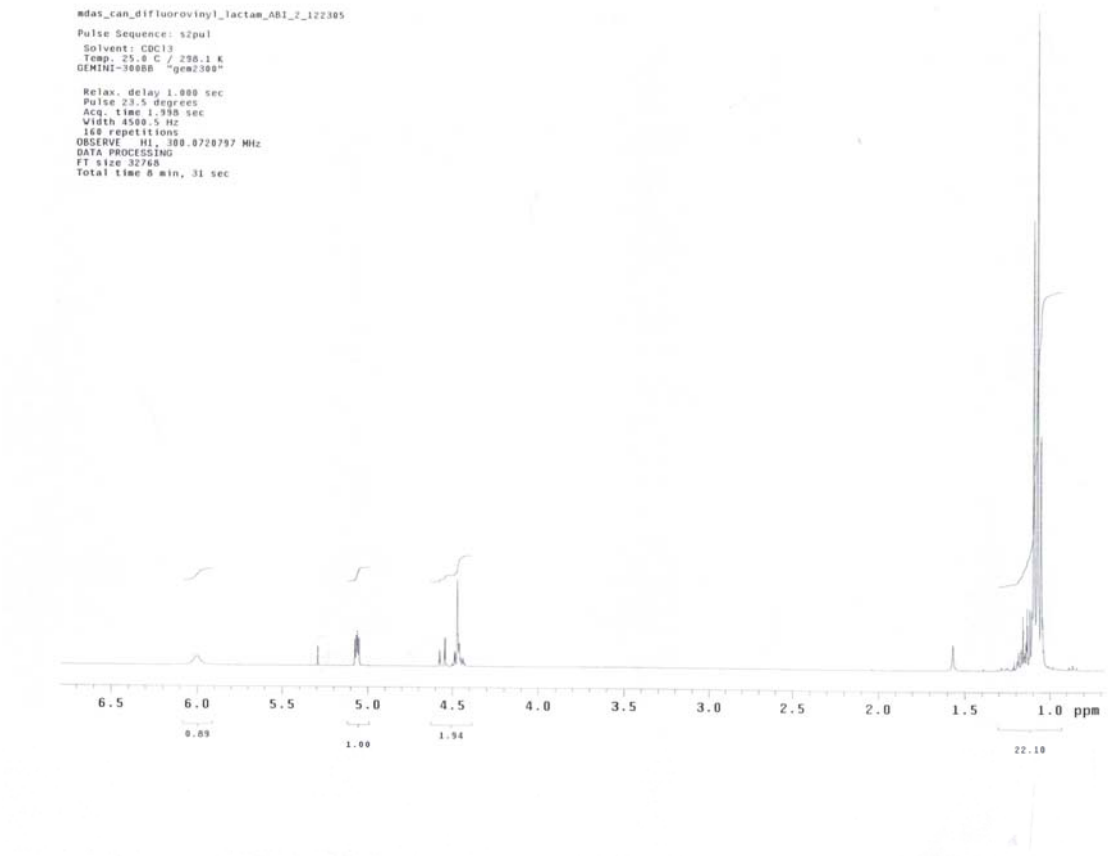

^{1}H NMR Spectrum of **2-4**

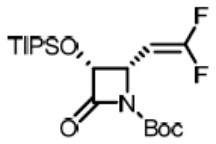

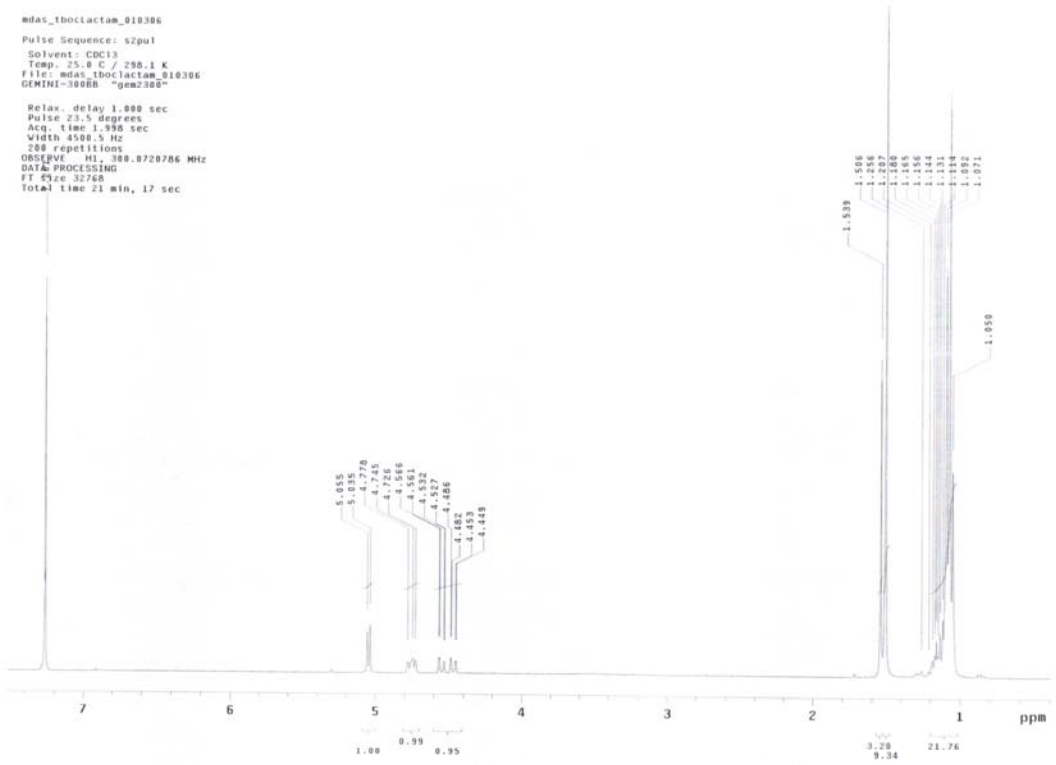

^{1}H NMR Spectrum of **2-5**

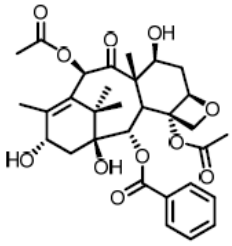

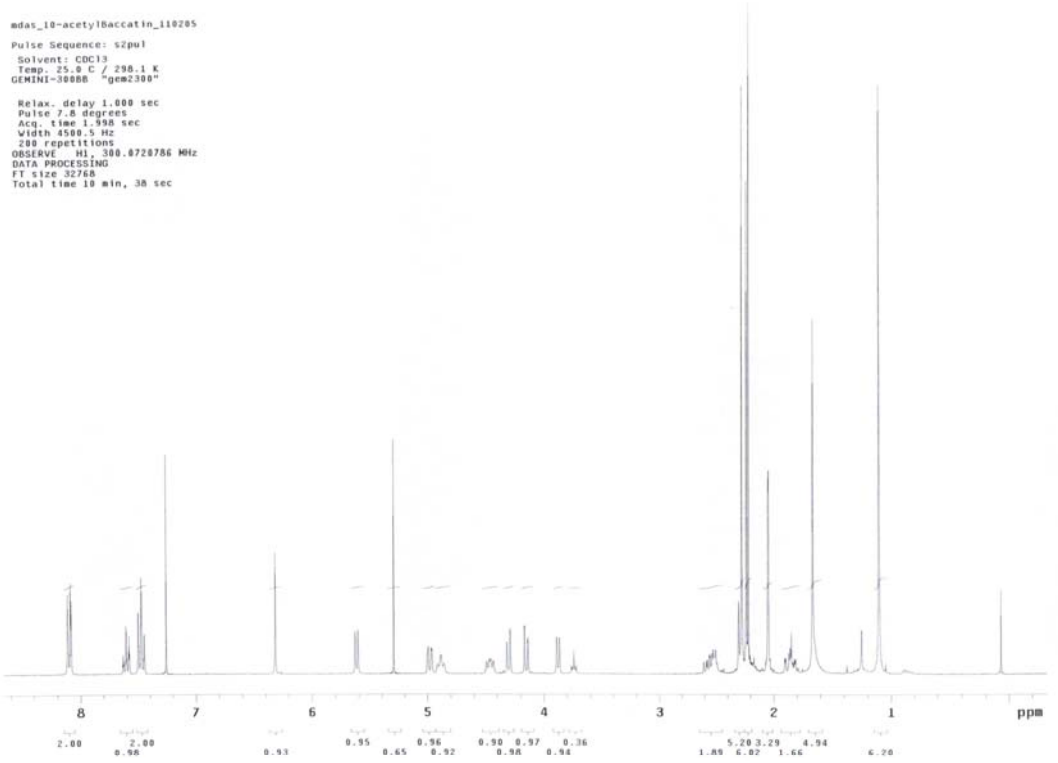

^{1}H NMR Spectrum of **2-6**

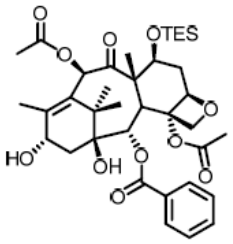

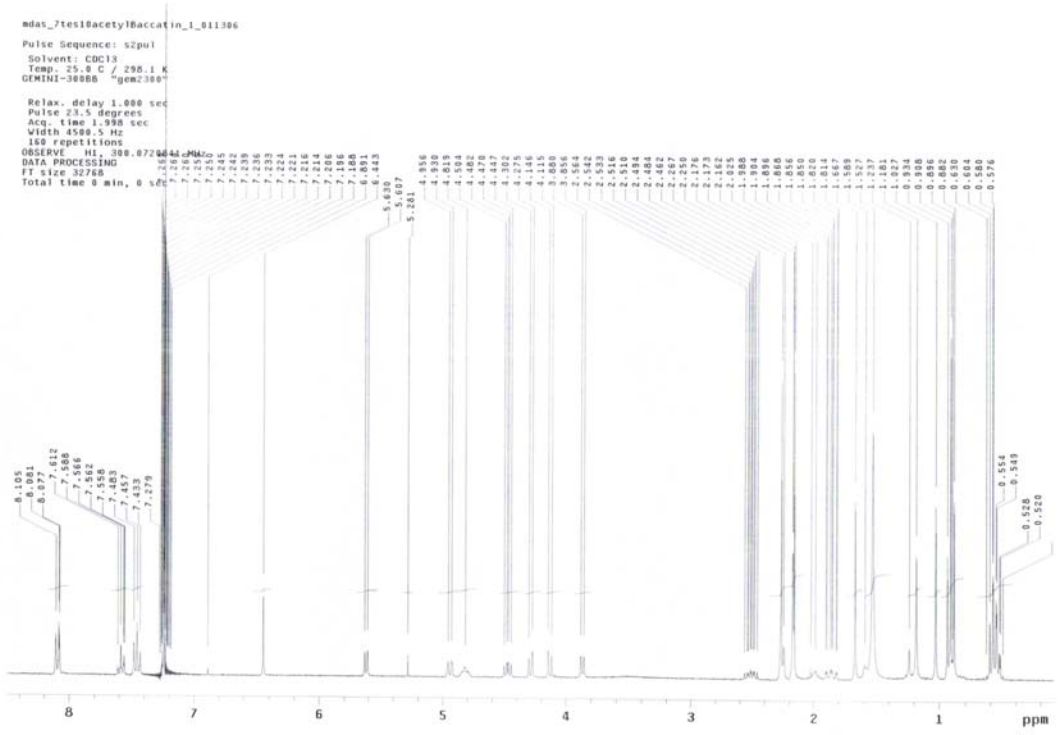

^{1}H NMR Spectrum of **2-7**

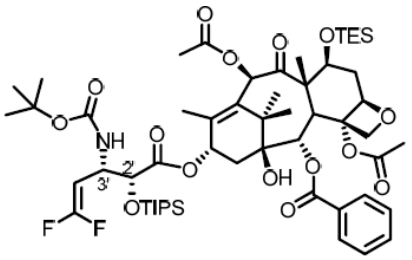

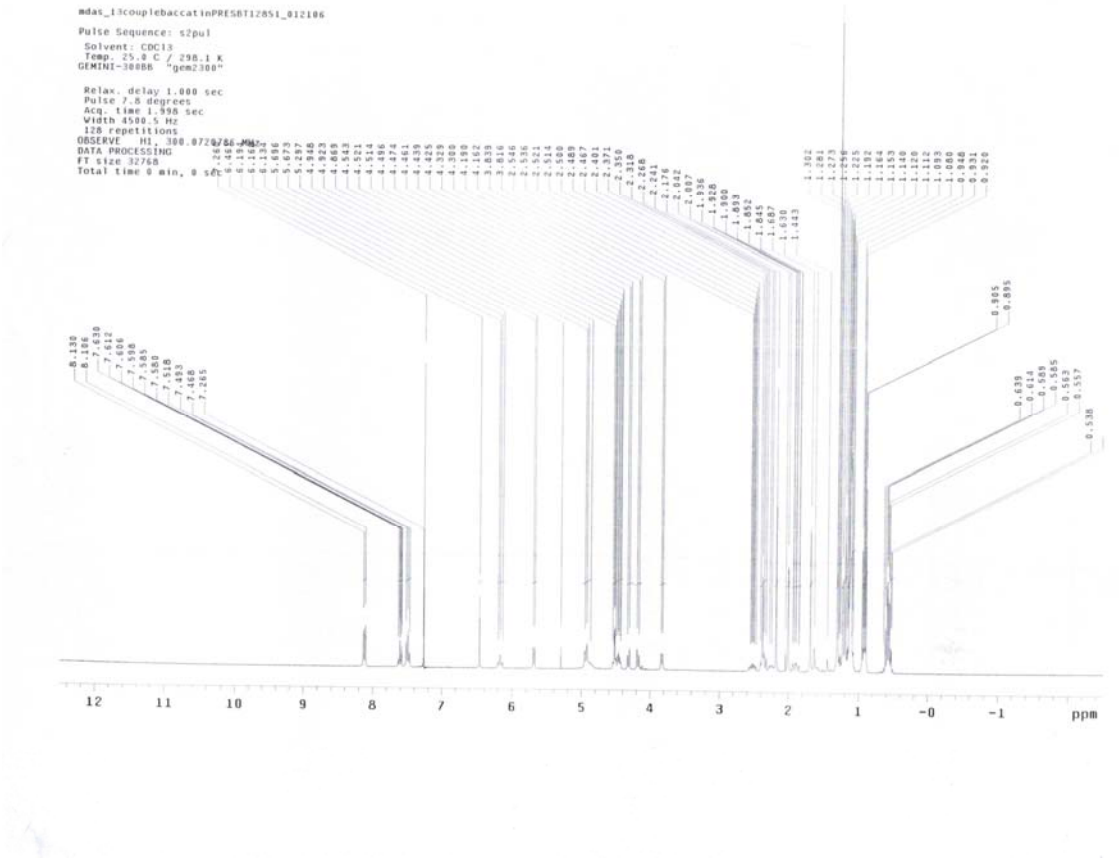

^{1}H NMR Spectrum of **SB-T-12851**

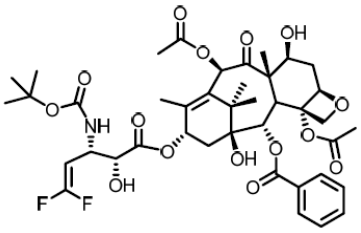

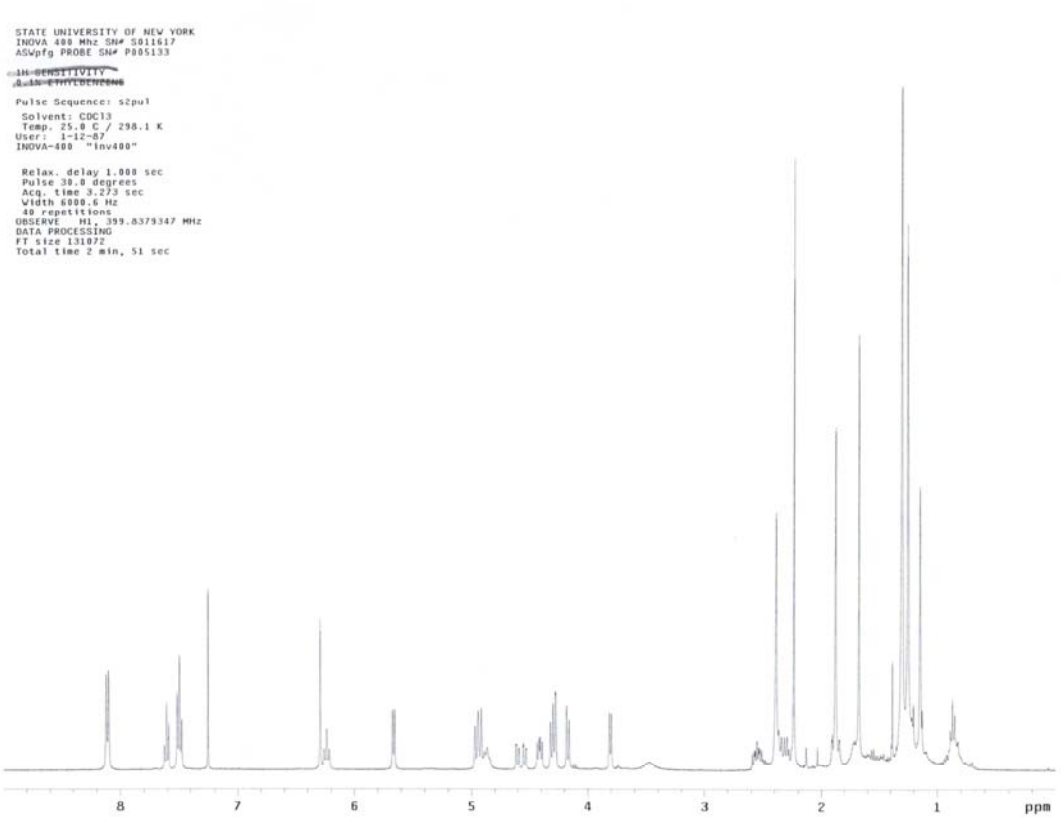

^{13}C NMR Spectrum of **SB-T-12851**

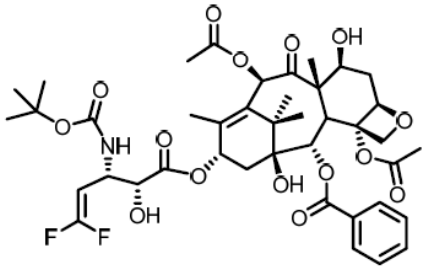

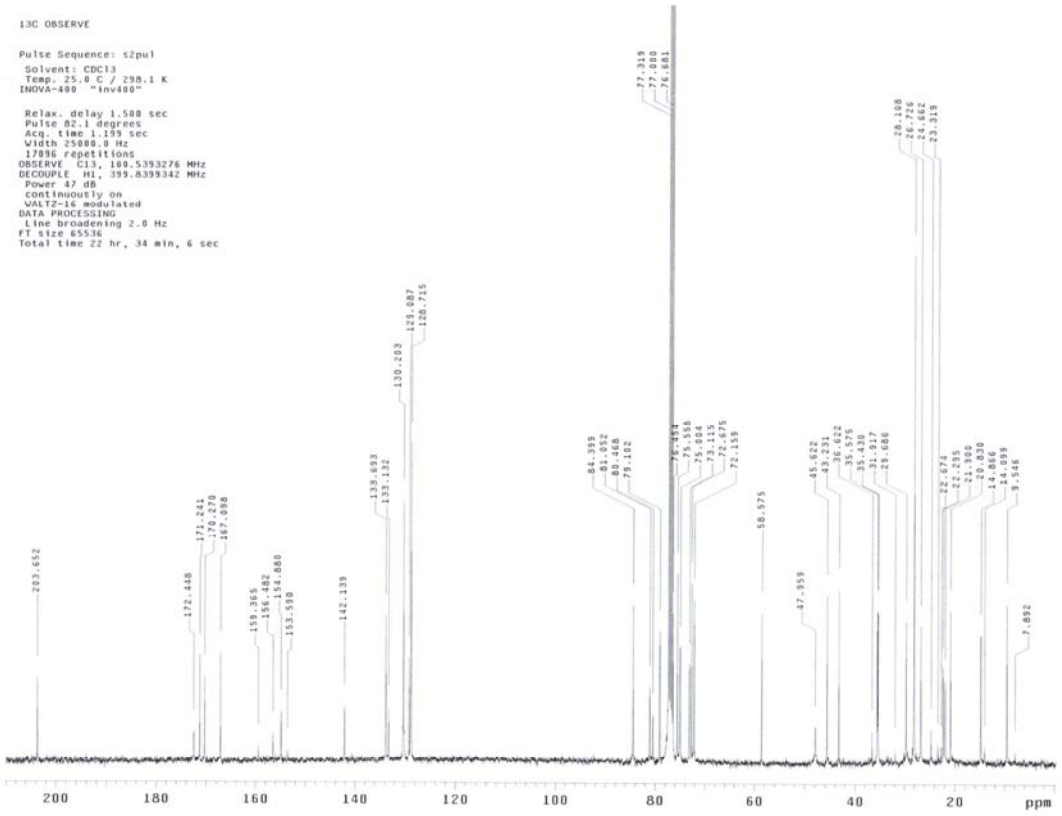

^{1}H NMR Spectrum of **3-1**

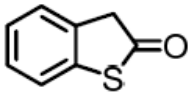

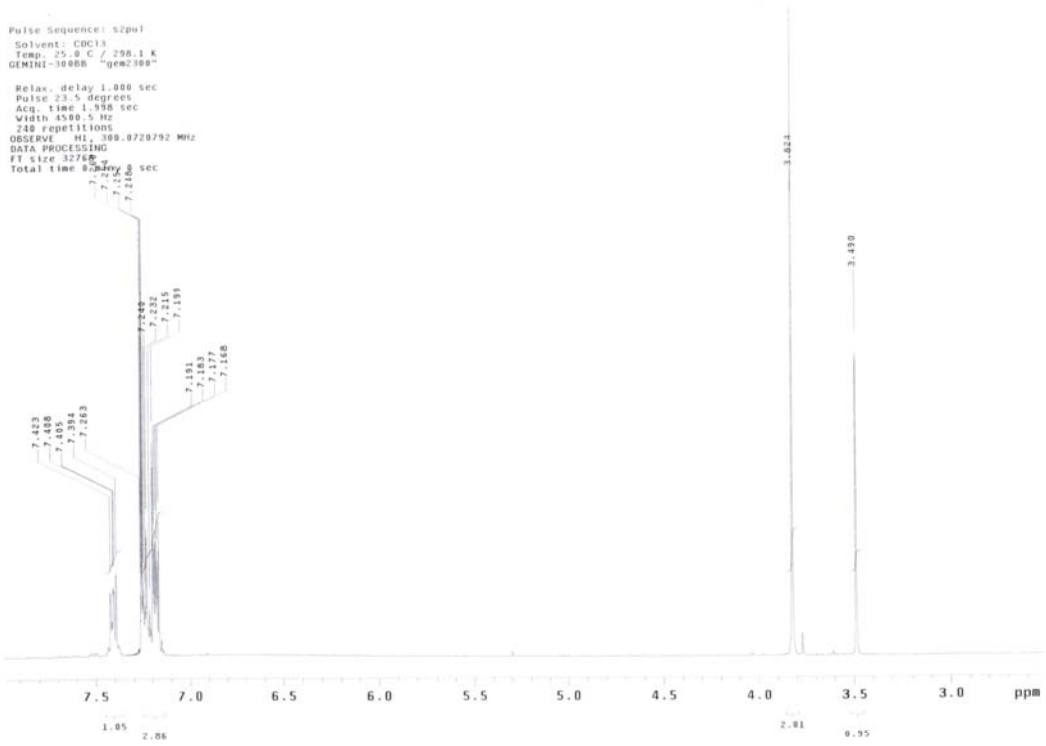

^{1}H NMR Spectrum of **3-2**

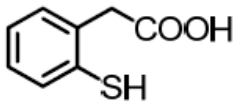

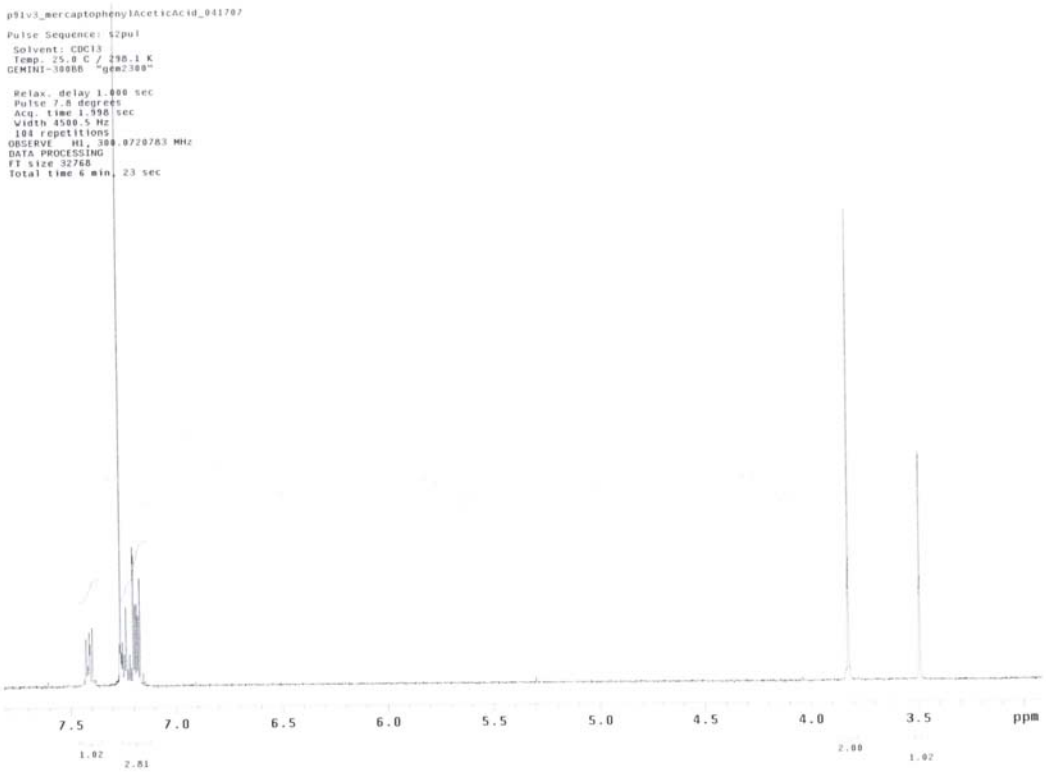

^{1}H NMR Spectrum of **3-3**

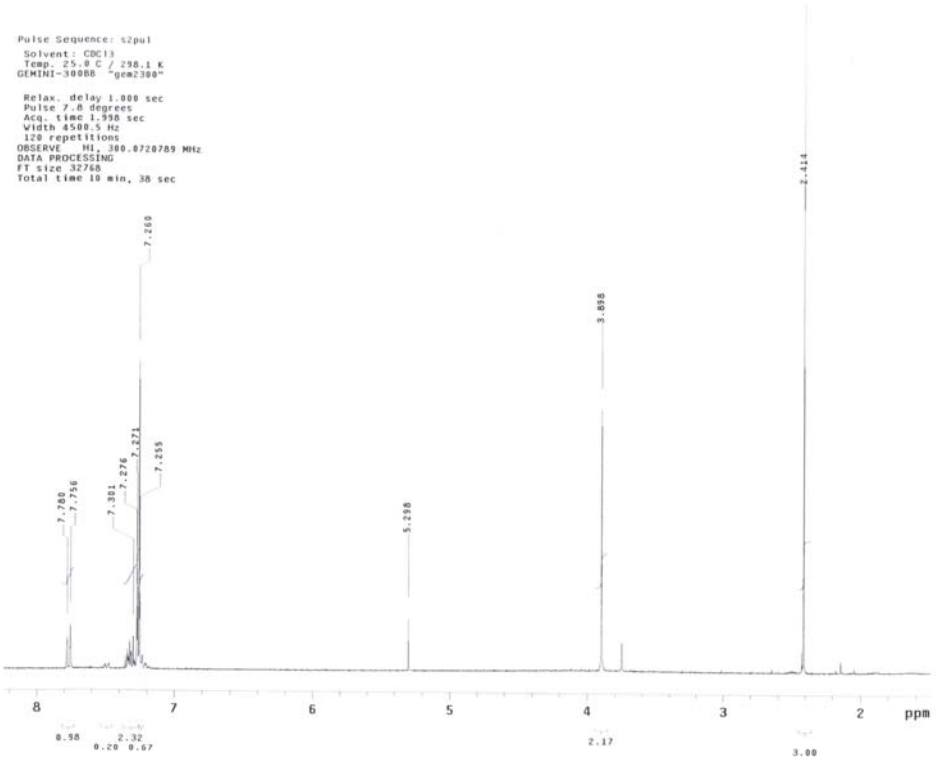

^{13}C NMR Spectrum of **3-3**

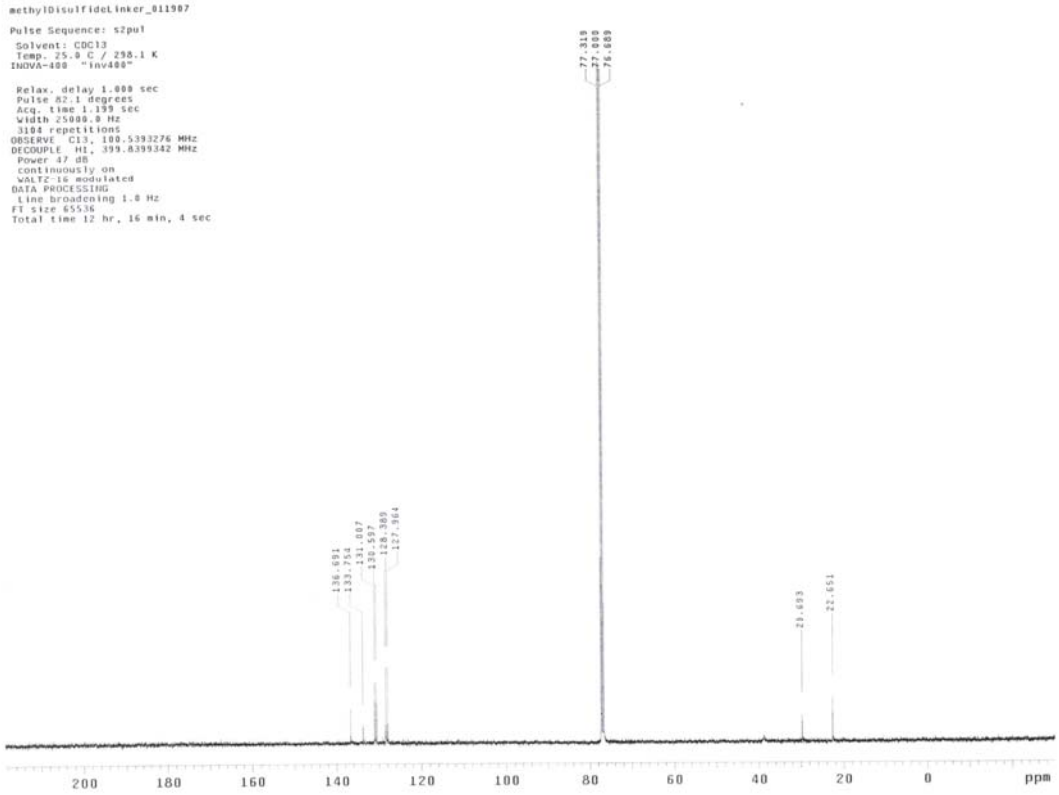

^{1}H NMR Spectrum of **3-4**

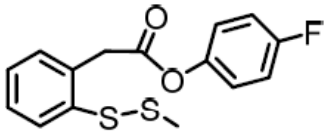

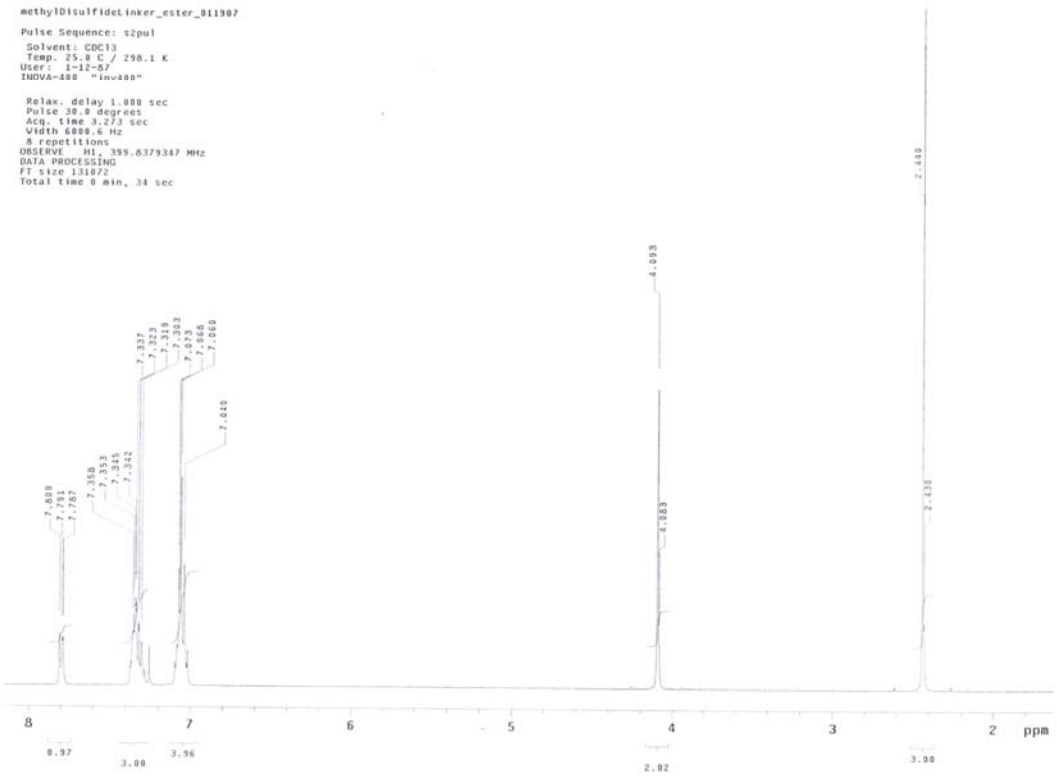

^{13}C NMR Spectrum of **3-4**

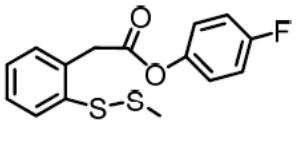

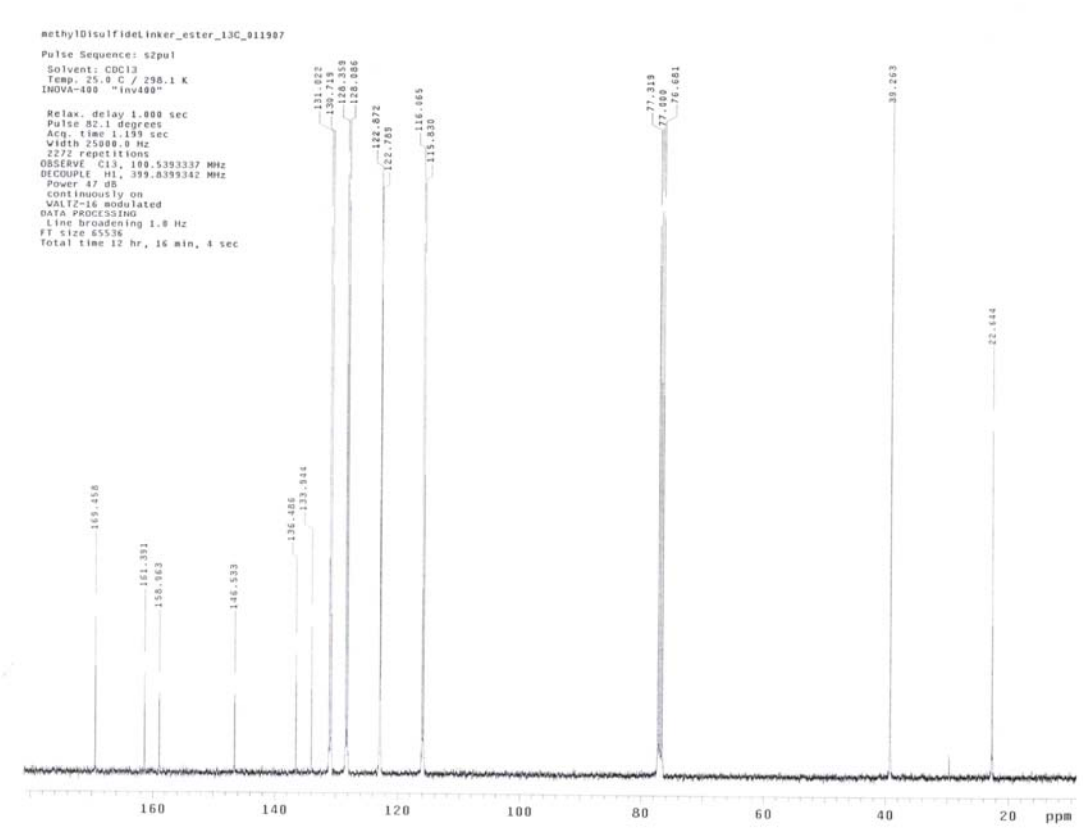

^{19}F NMR Spectrum of **3-4**

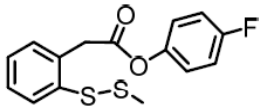

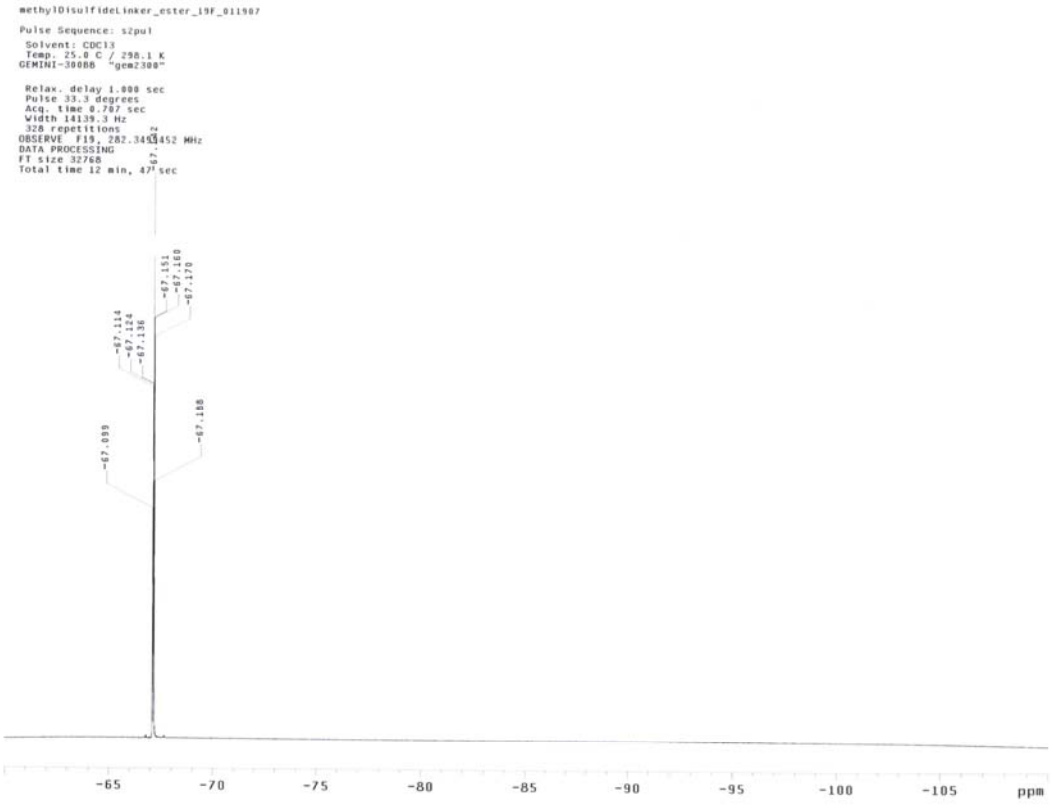

^{1}H NMR Spectrum of **3-5**

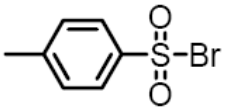

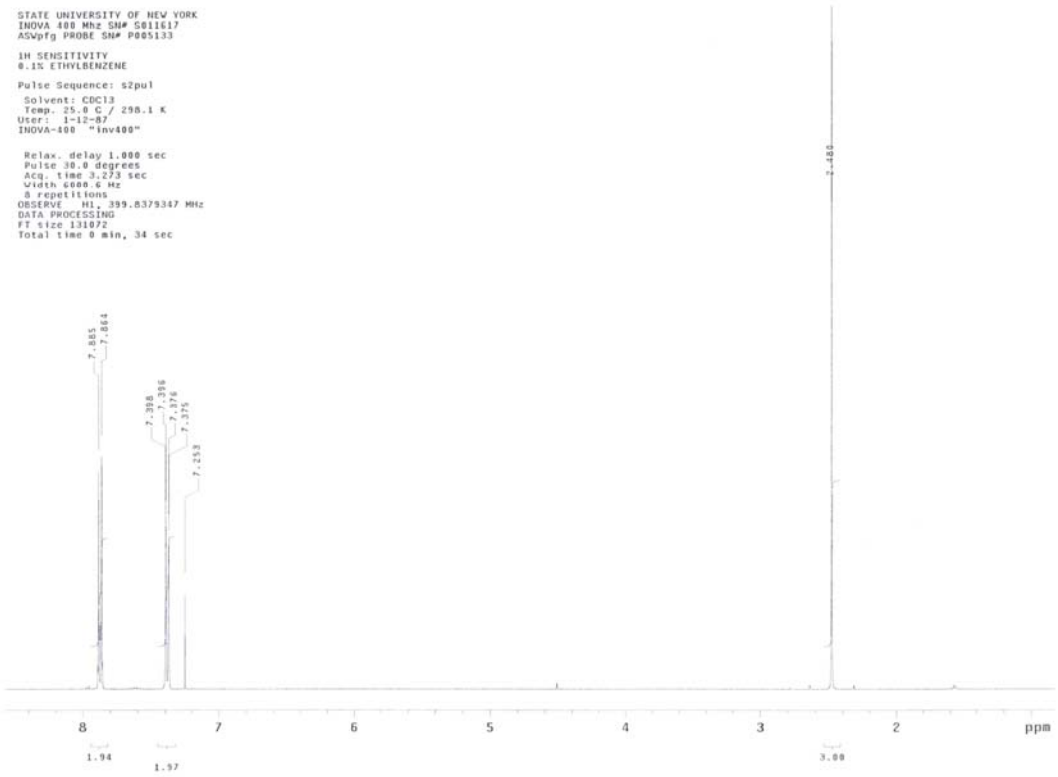

^{13}C NMR Spectrum of **3-5**

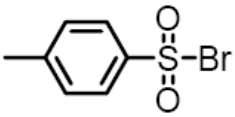

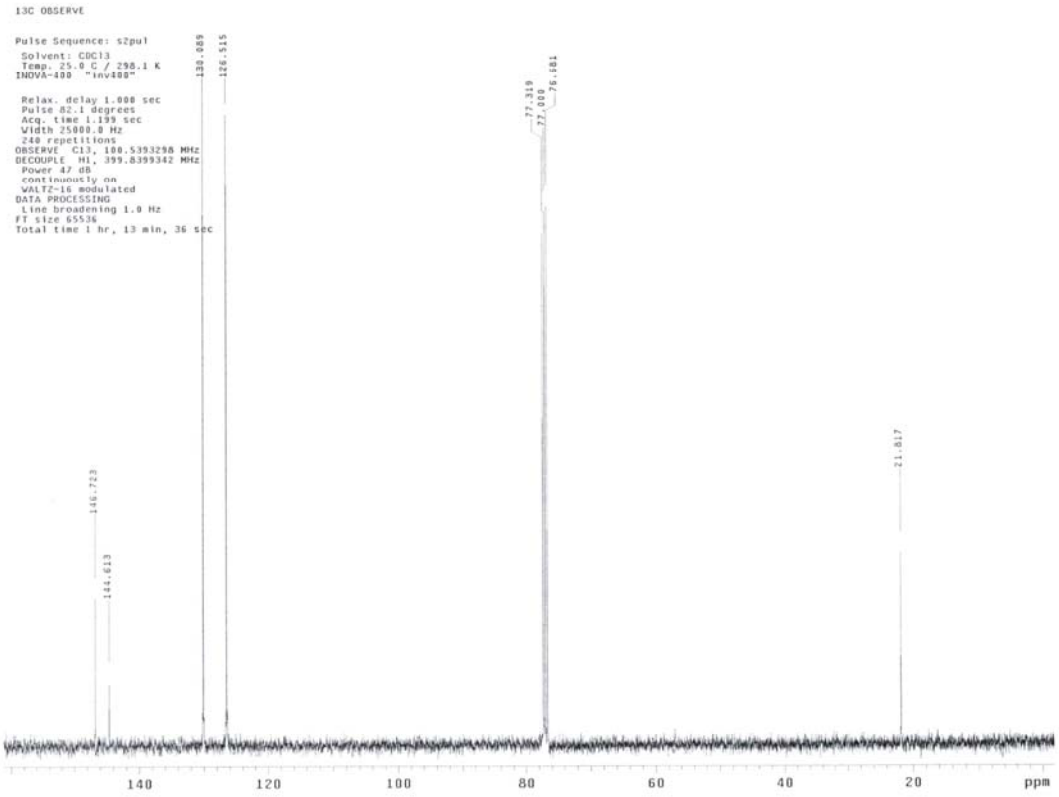

^{1}H NMR Spectrum of **3-6**

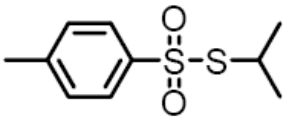

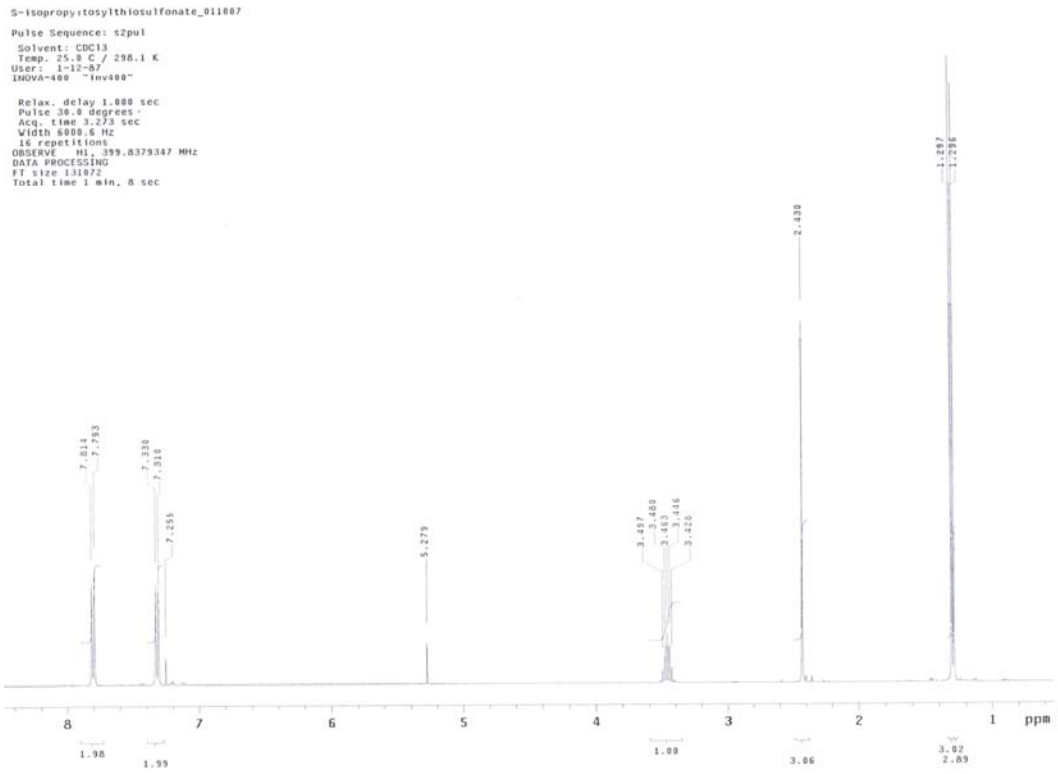

^{13}C NMR Spectrum of **3-6**

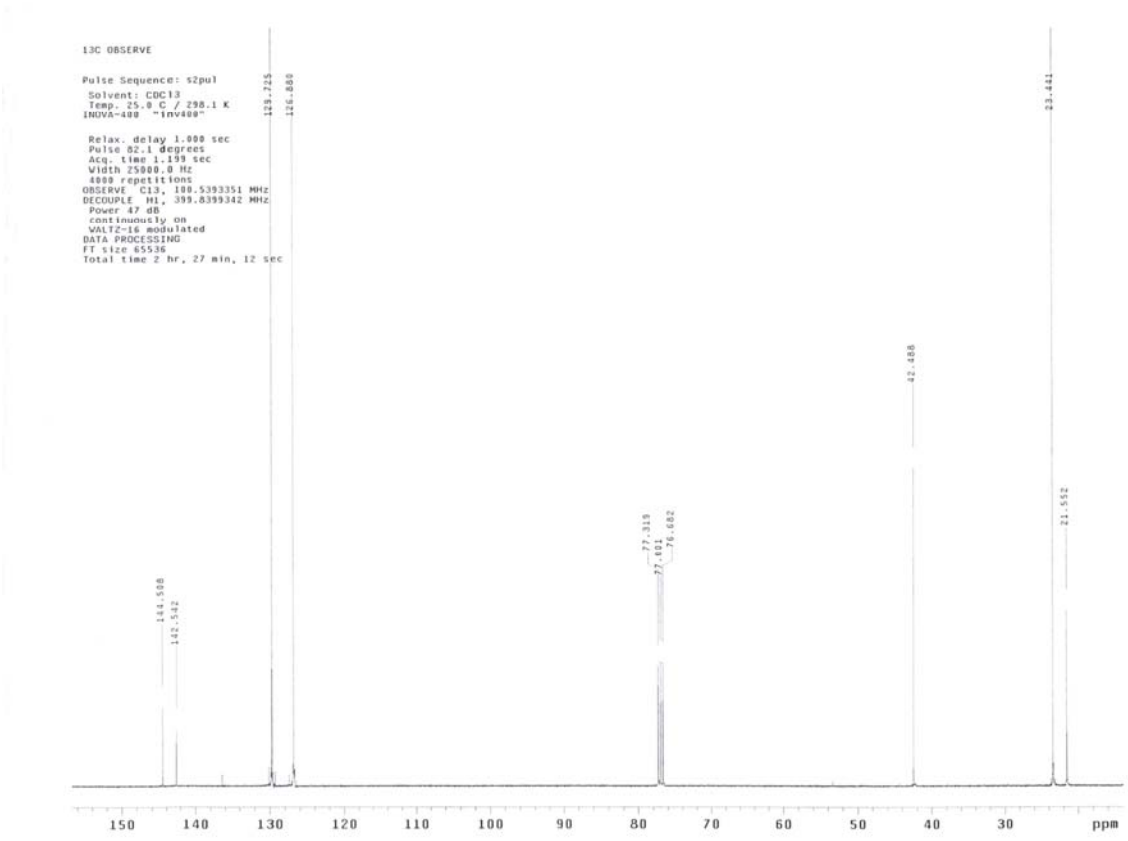

^{1}H NMR Spectrum of **3-7**

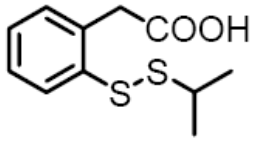

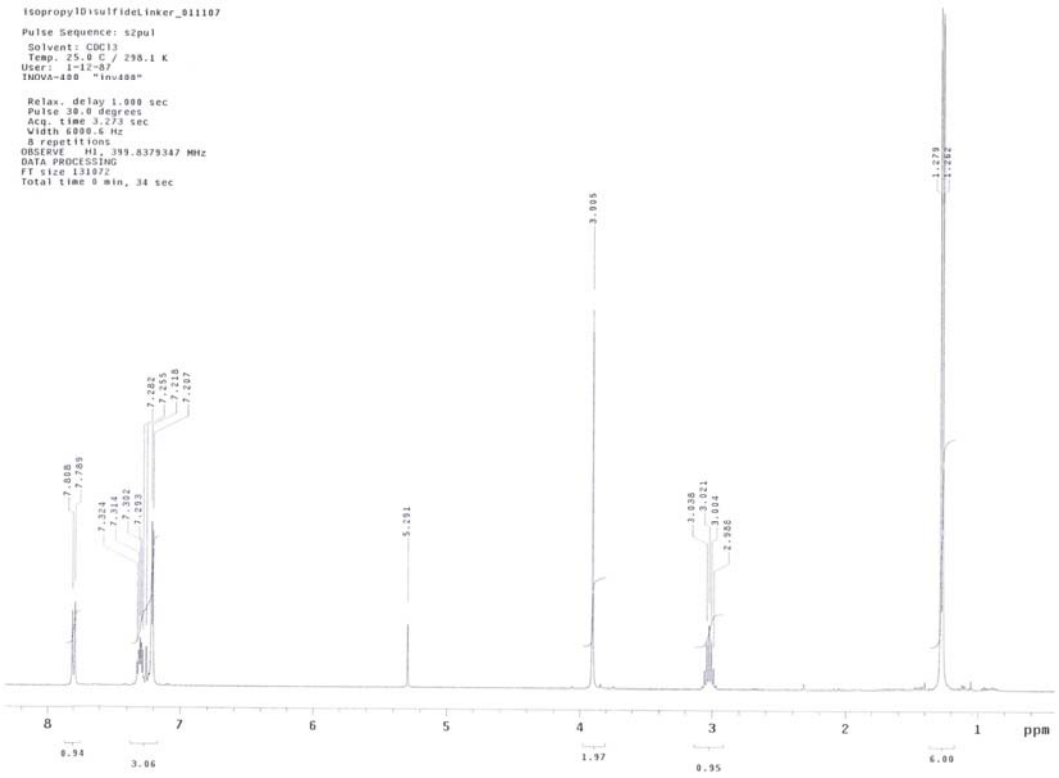

^{13}C NMR Spectrum of **3-7**

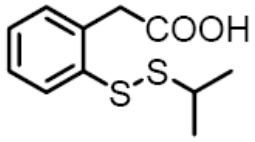

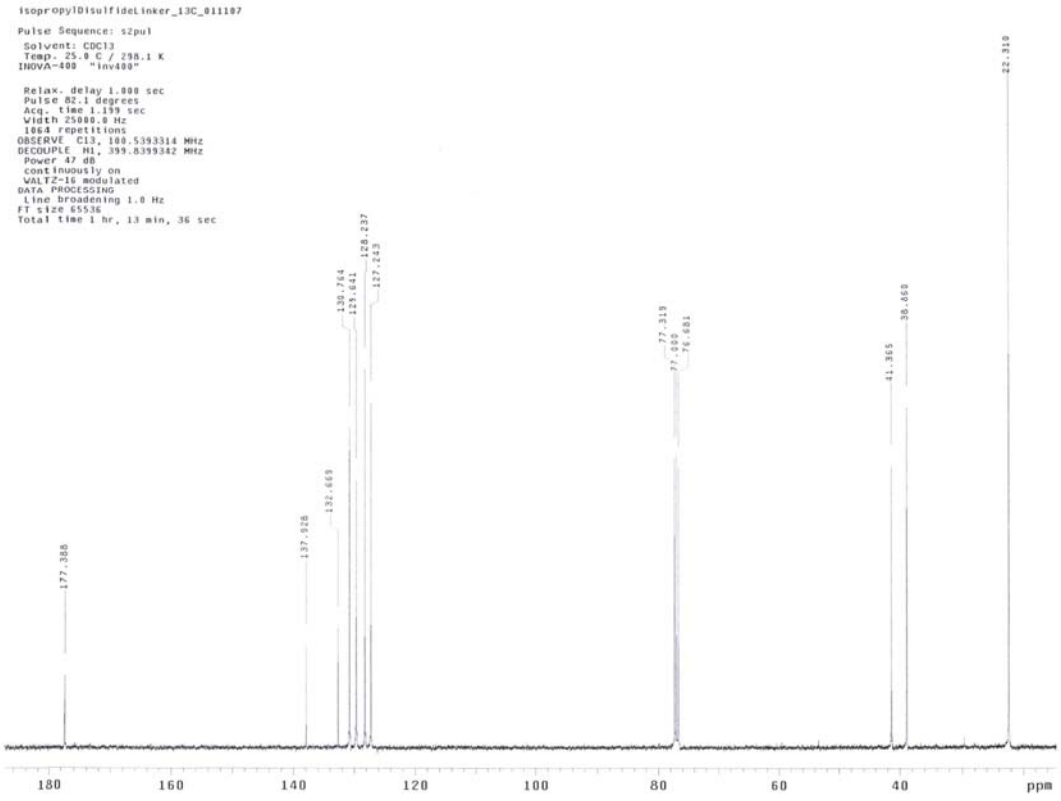

^{1}H NMR Spectrum of **3-8**

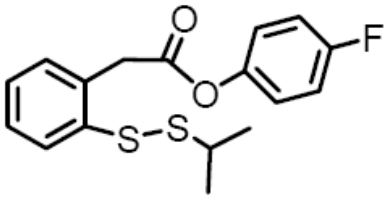

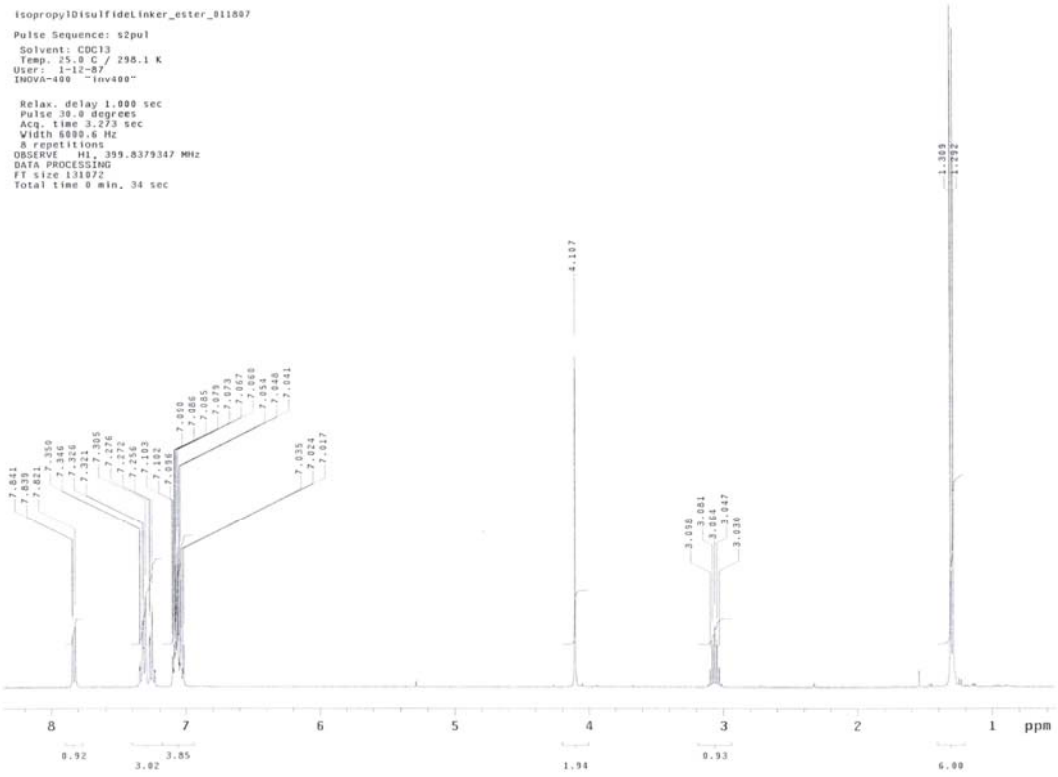

^{13}C NMR Spectrum of **3-8**

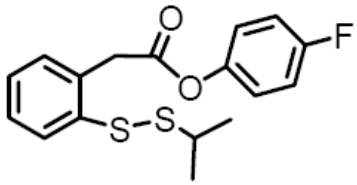

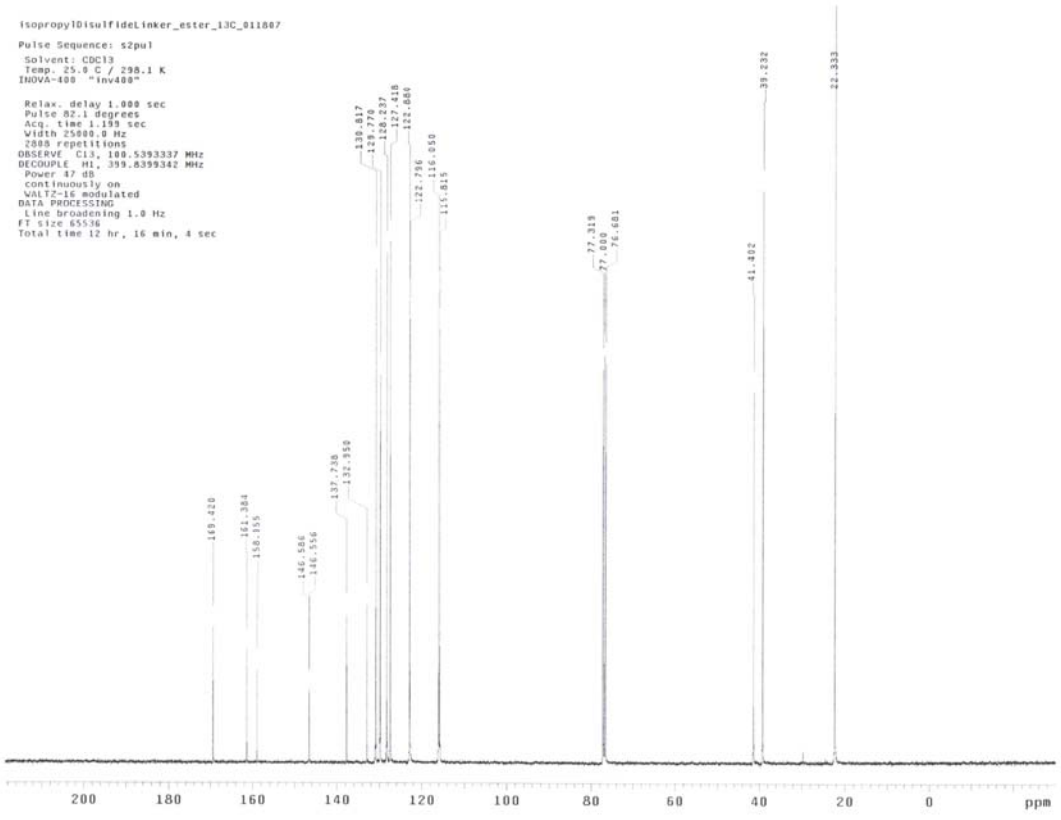

^{19}F NMR Spectrum of **3-8**

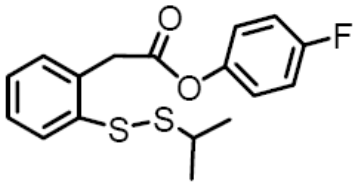

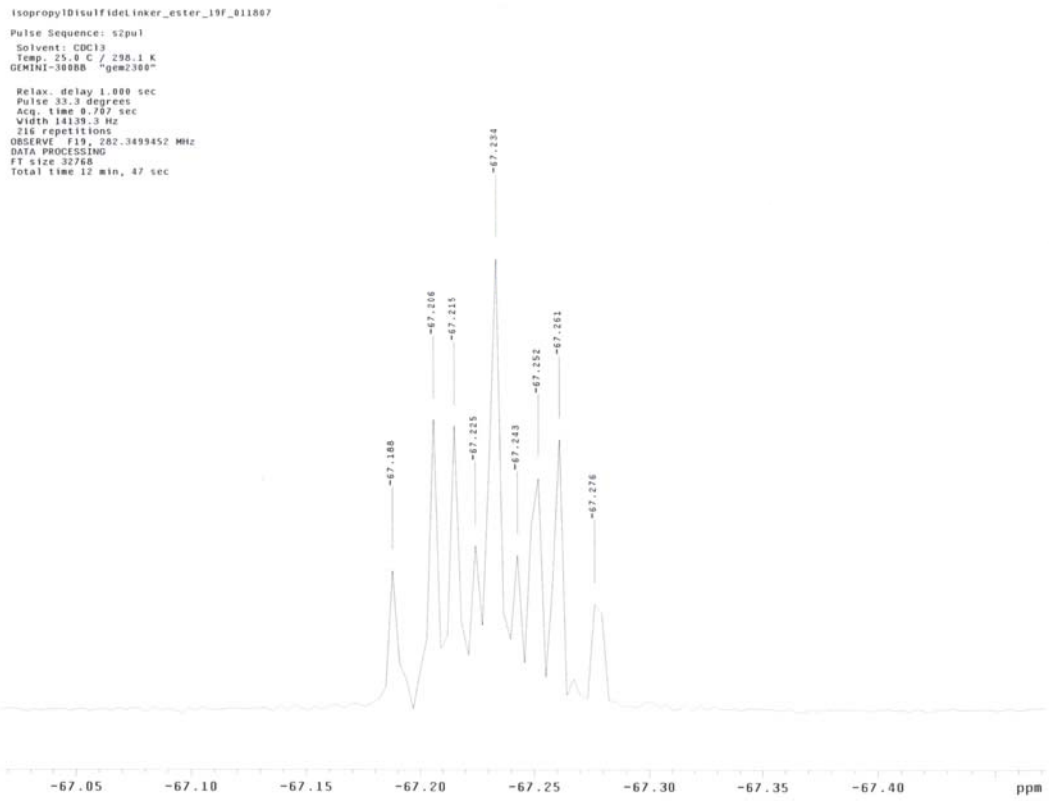

^{1}H NMR Spectrum of **3-9**

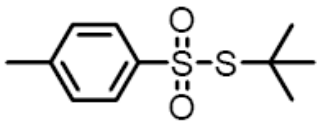

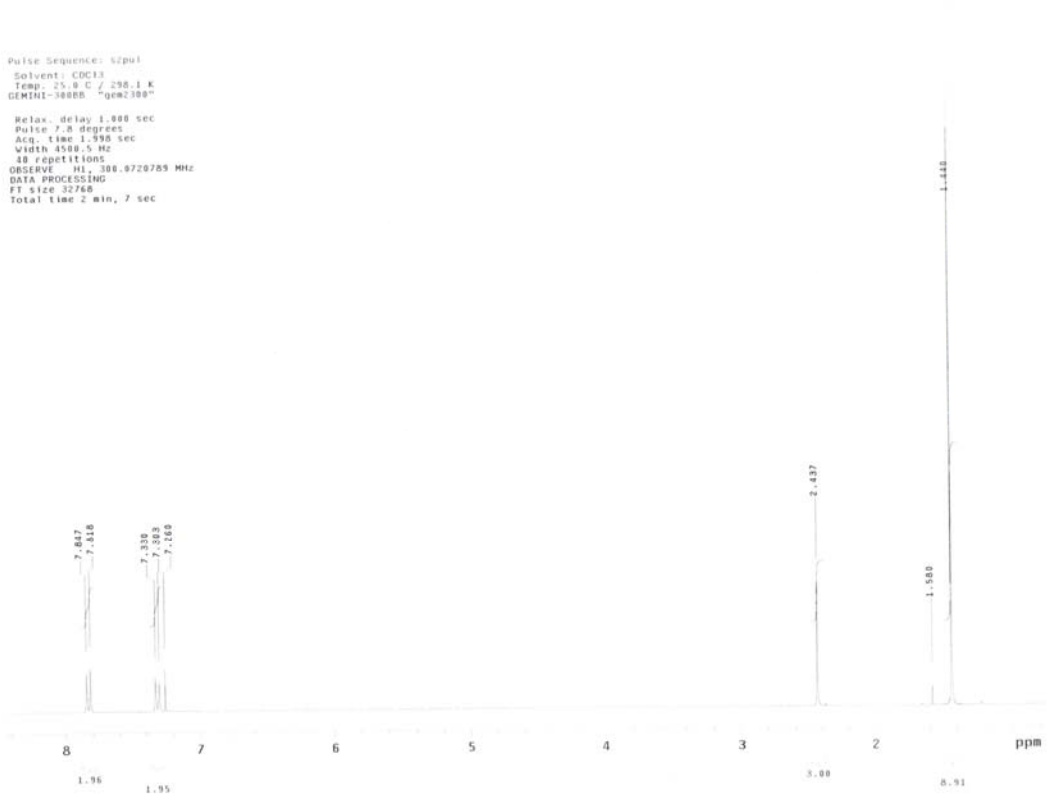

^{13}C NMR Spectrum of **3-9**

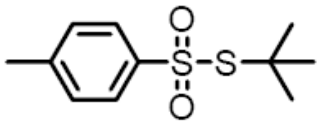

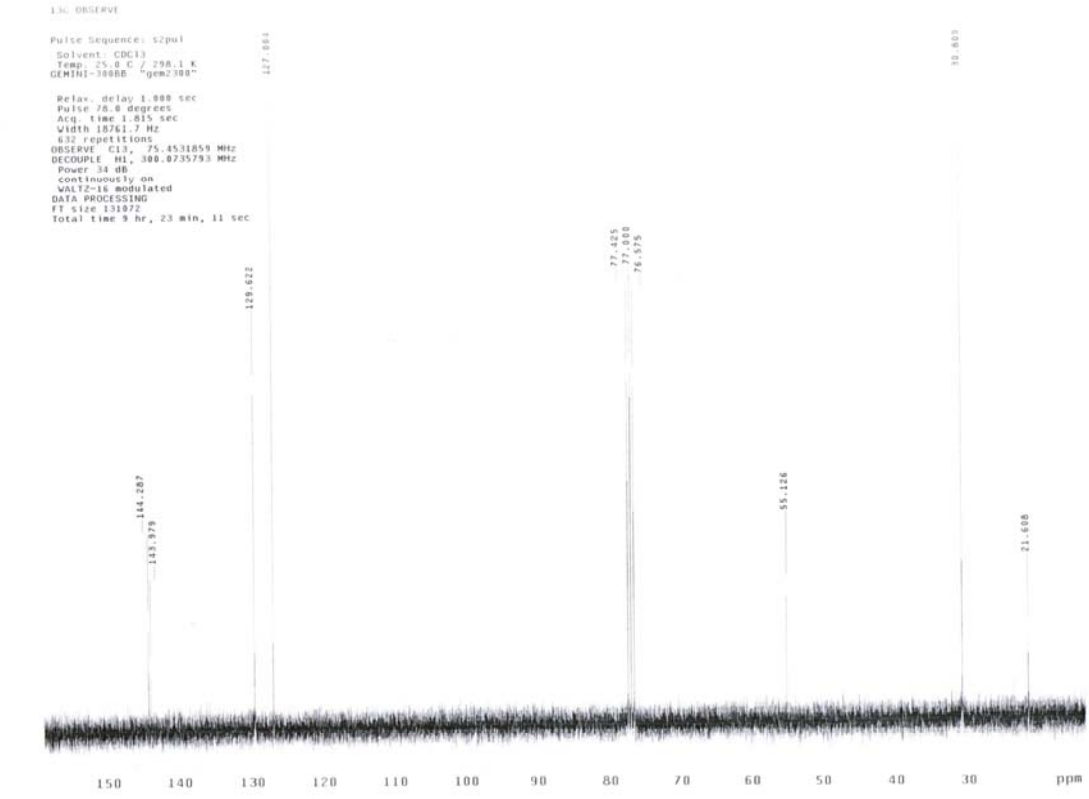

^{1}H NMR Spectrum of **3-10**

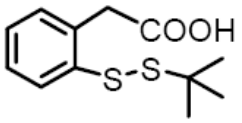

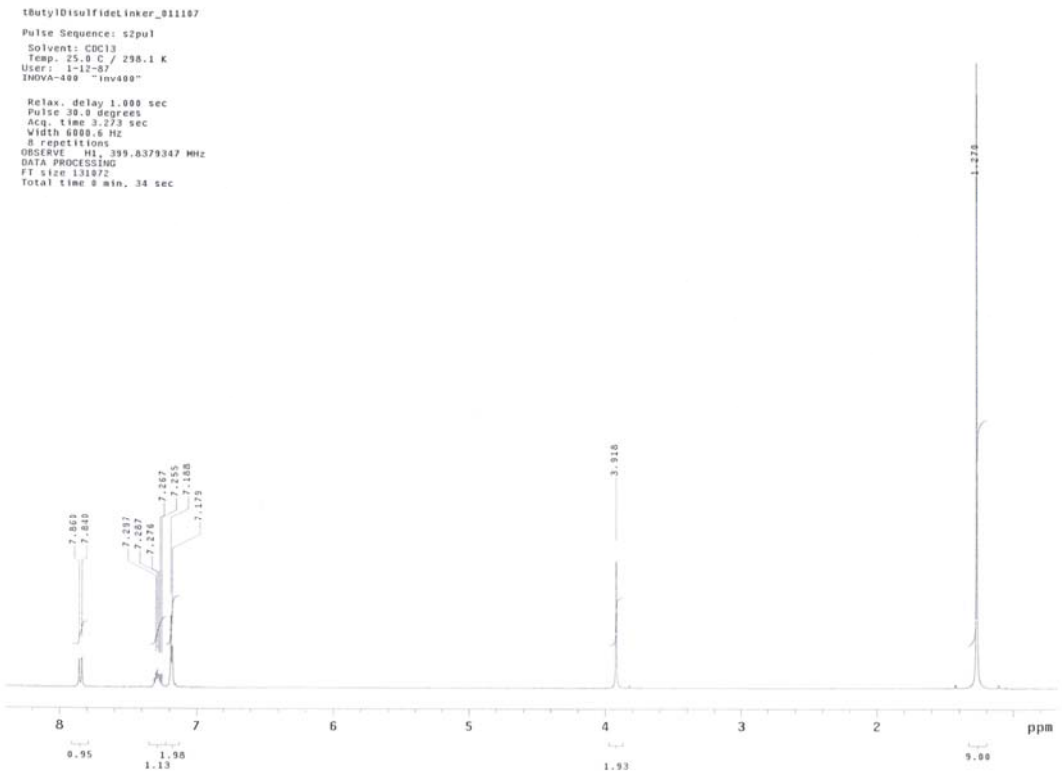

^{13}C NMR Spectrum of **3-10**

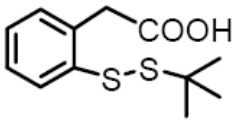

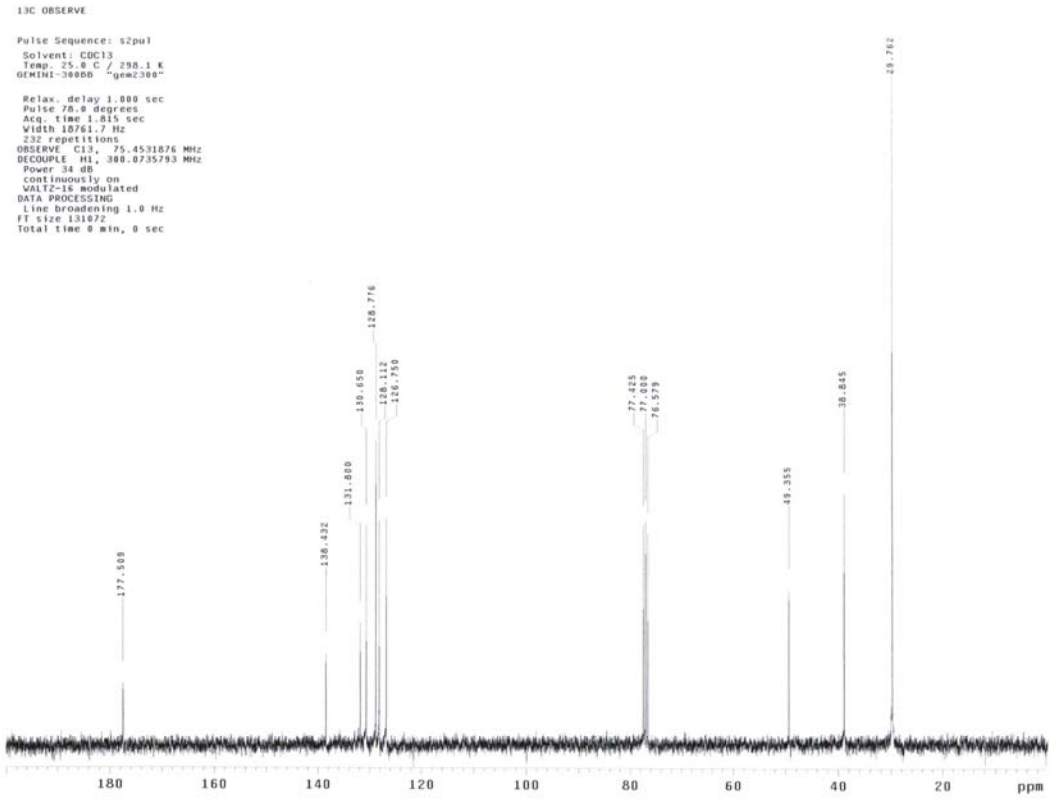

^{1}H NMR Spectrum of **3-11**

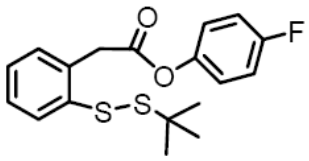

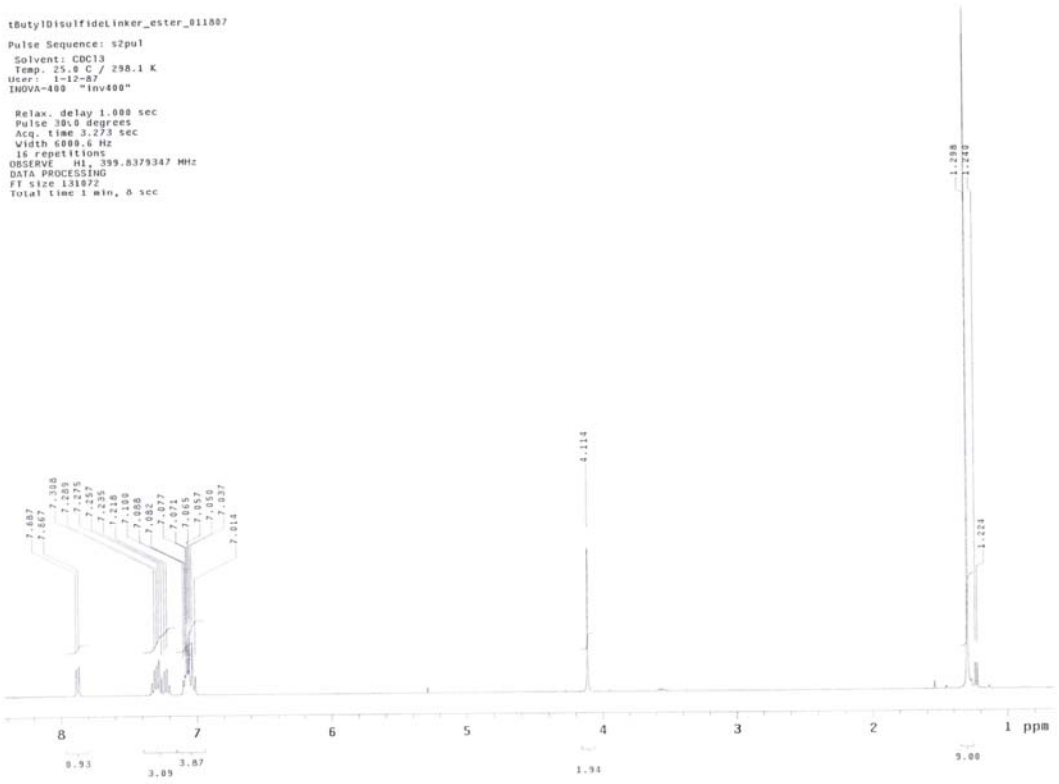

^{13}C NMR Spectrum of **3-11**

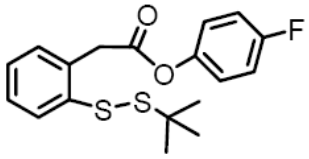

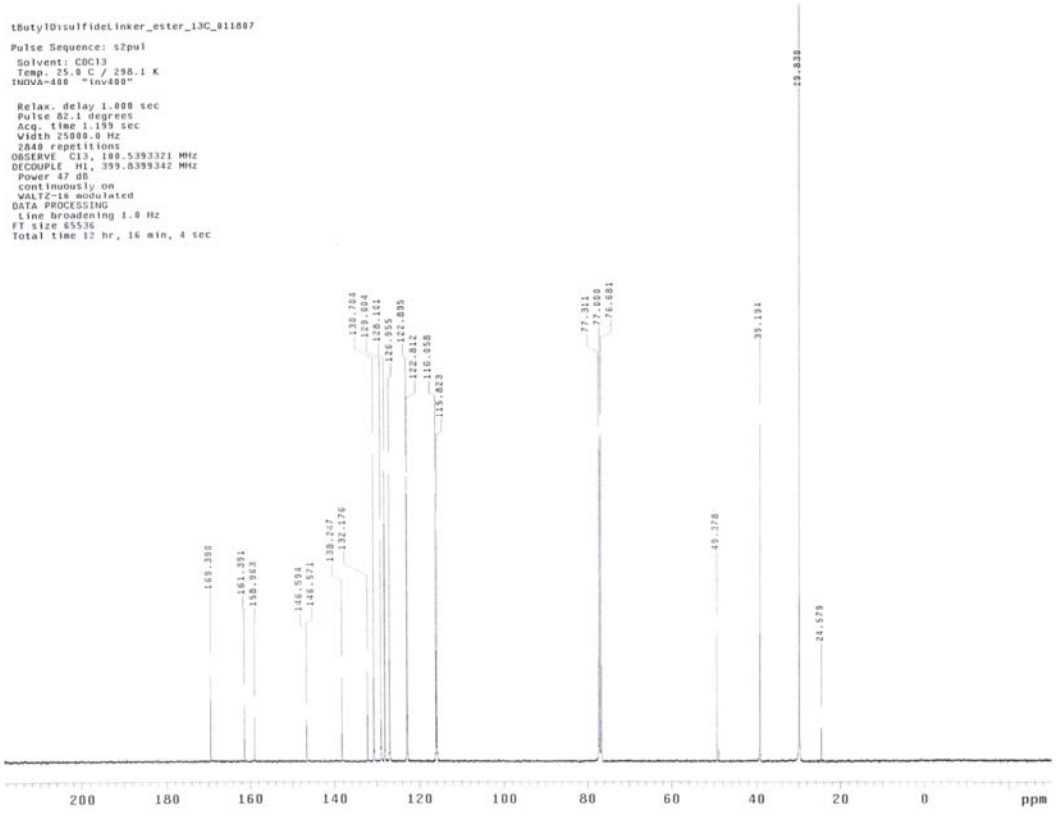

^{19}F NMR Spectrum of **3-11**

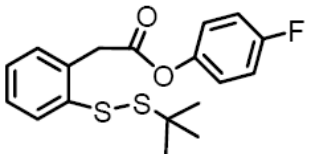

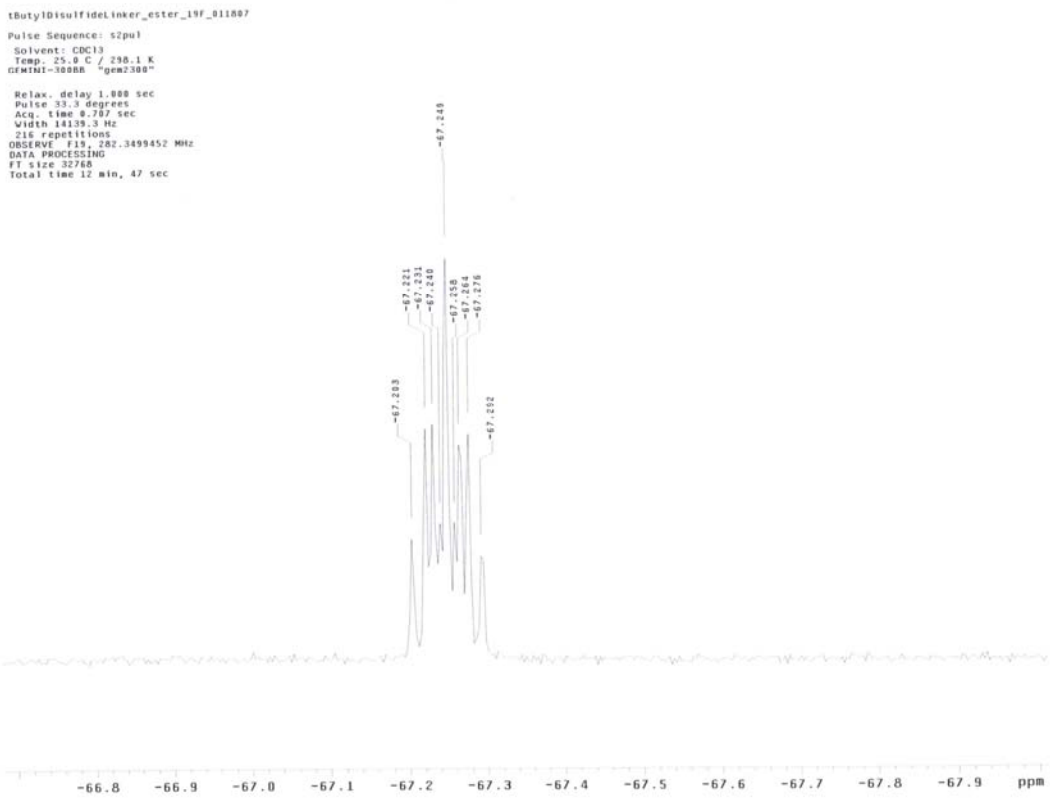

^{1}H NMR Spectrum of **3-12**

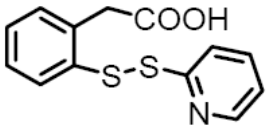

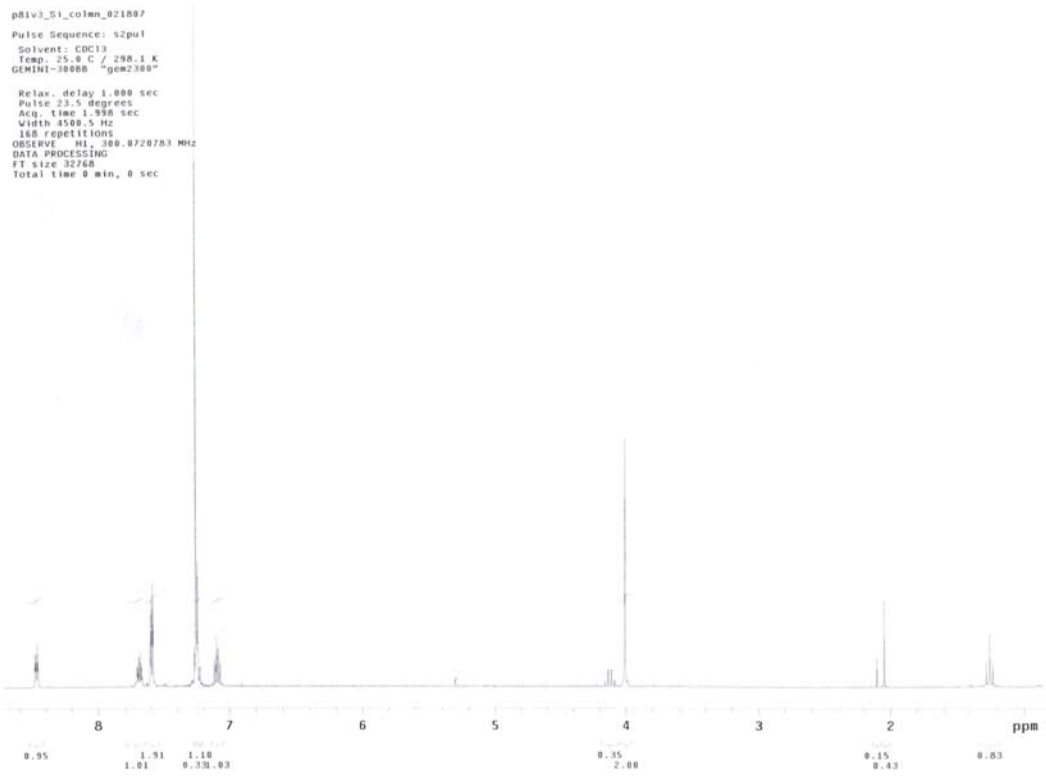

^{13}C NMR Spectrum of **3-12**

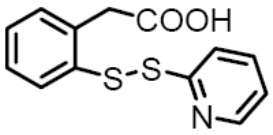

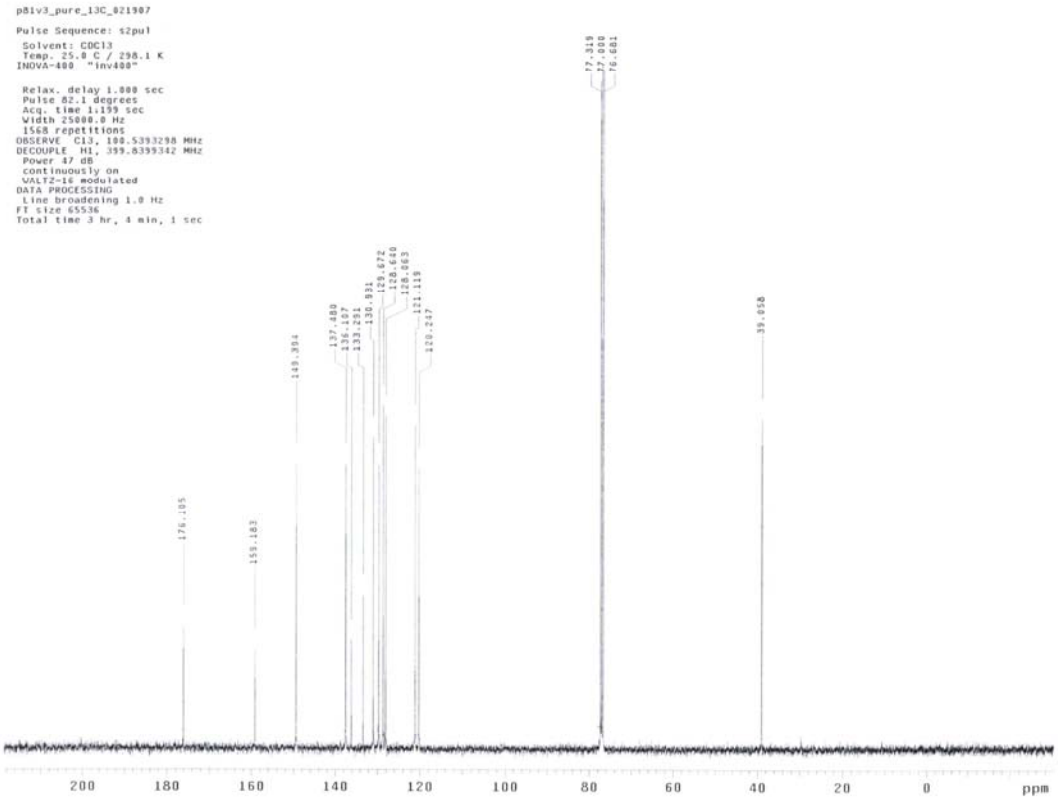

^{1}H NMR Spectrum of **3-13**

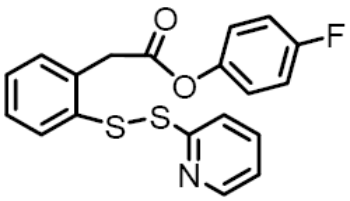

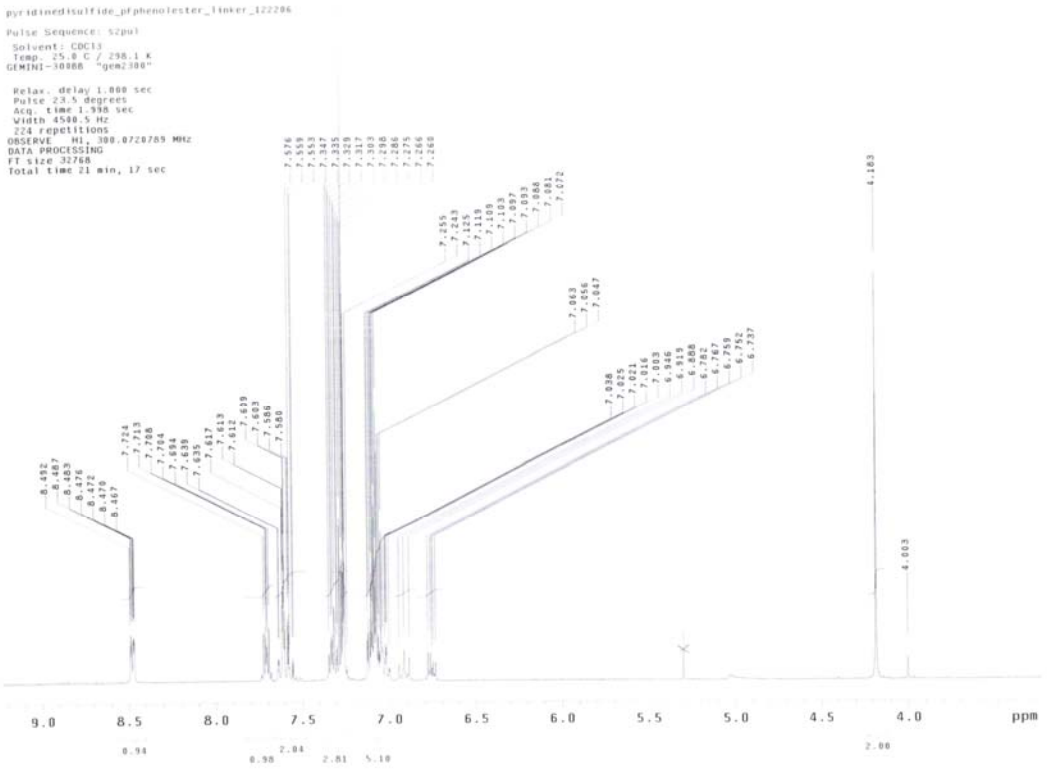

^{13}C NMR Spectrum of **3-13**

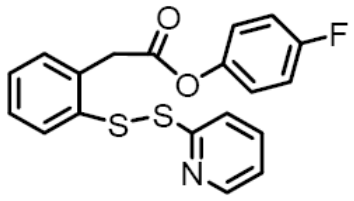

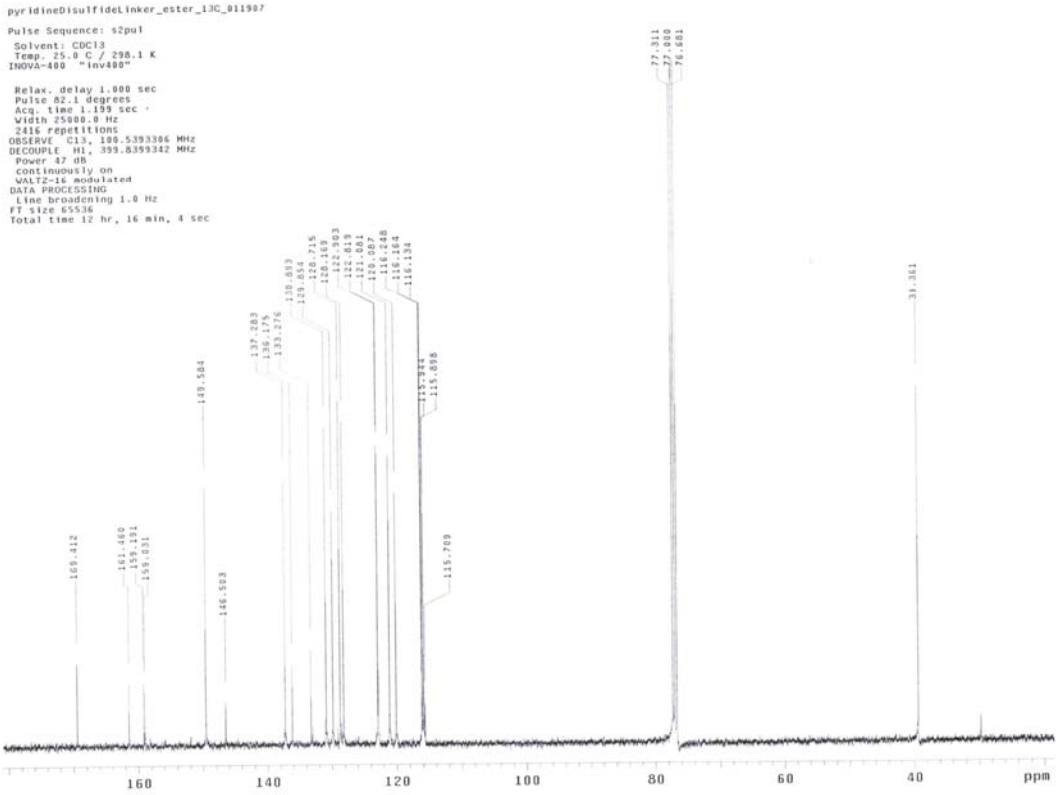

^{19}F NMR Spectrum of **3-13**

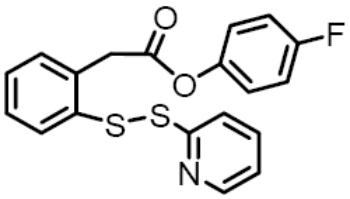

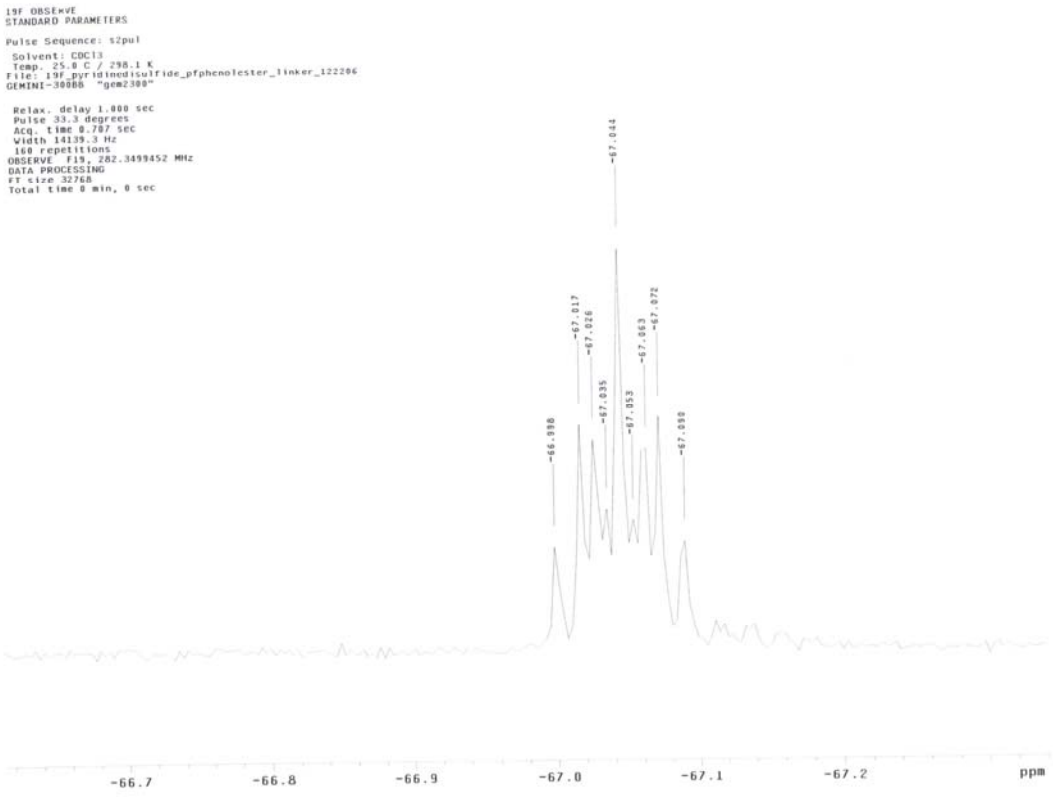

^{1}H NMR Spectrum of **4-5**

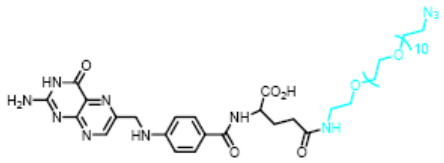

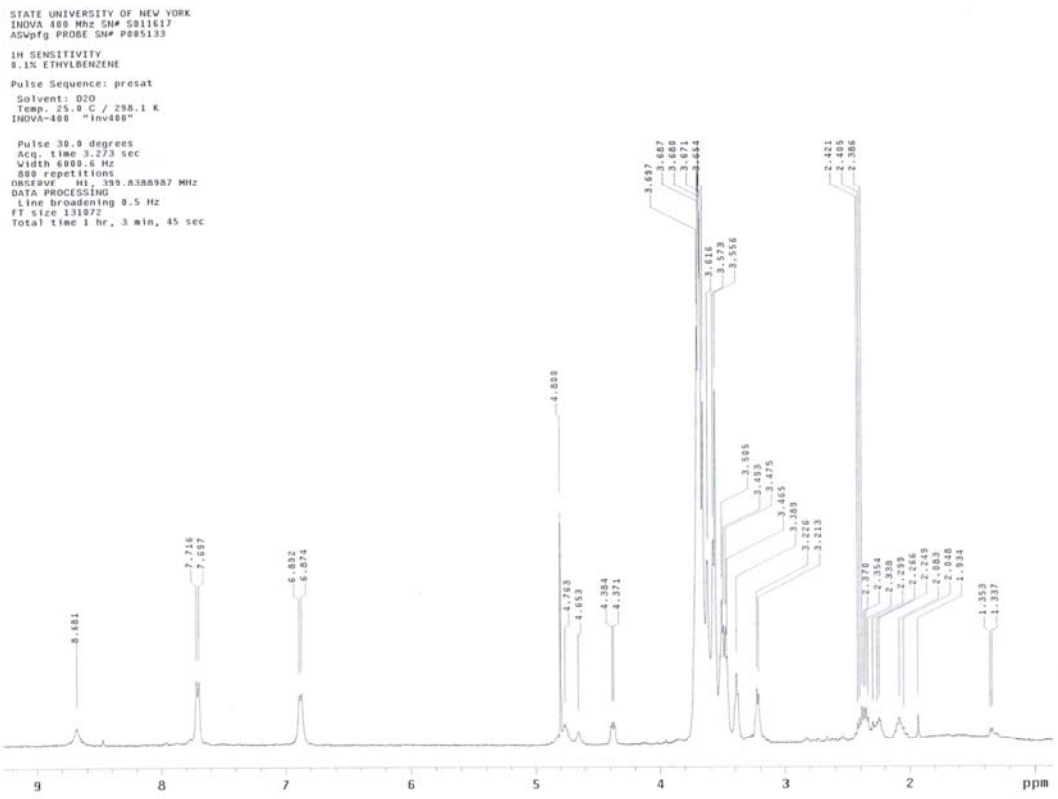

^{1}H NMR Spectrum of **4-6**

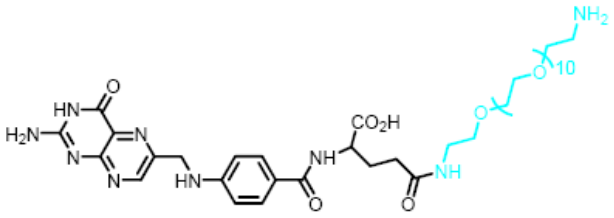

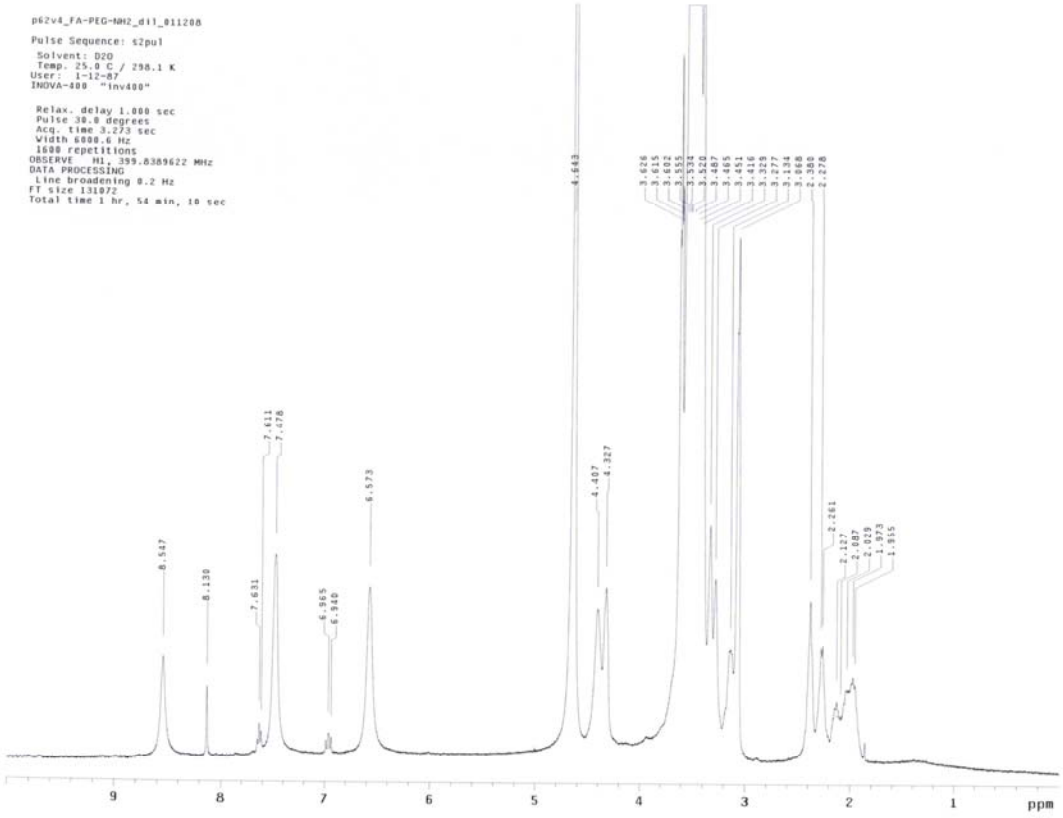

^{1}H NMR Spectrum of **4-9**

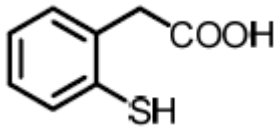

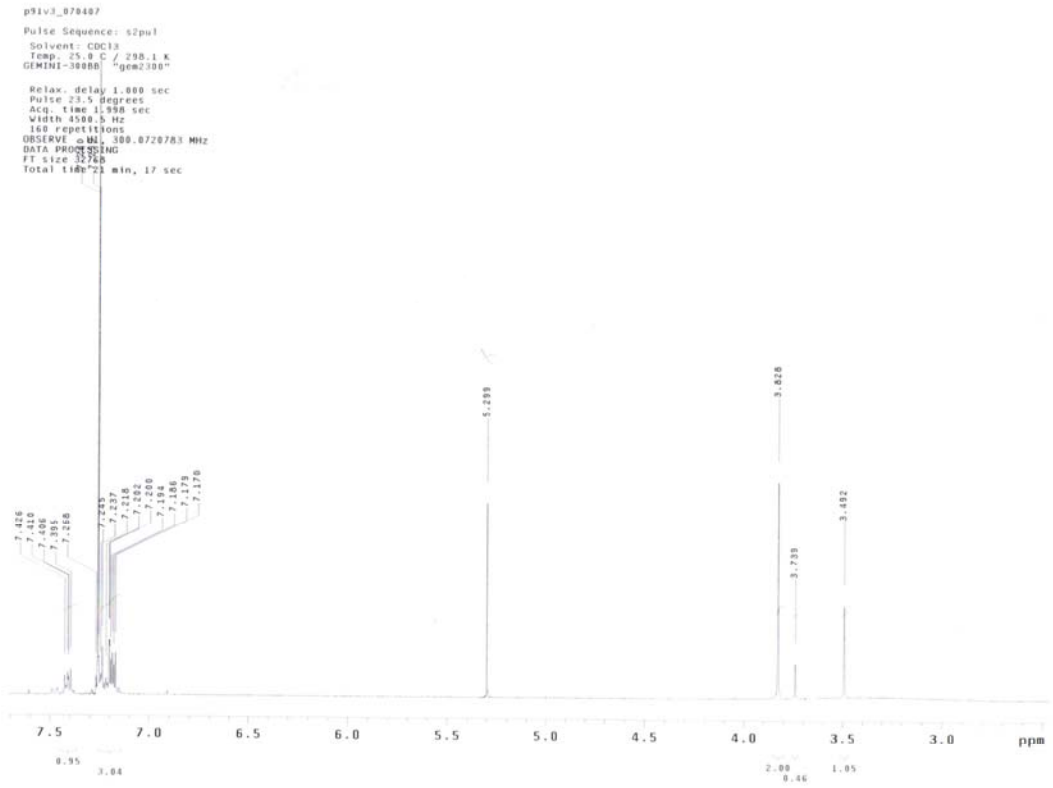

^{1}H NMR Spectrum of **4-12**

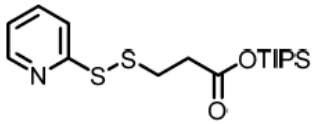

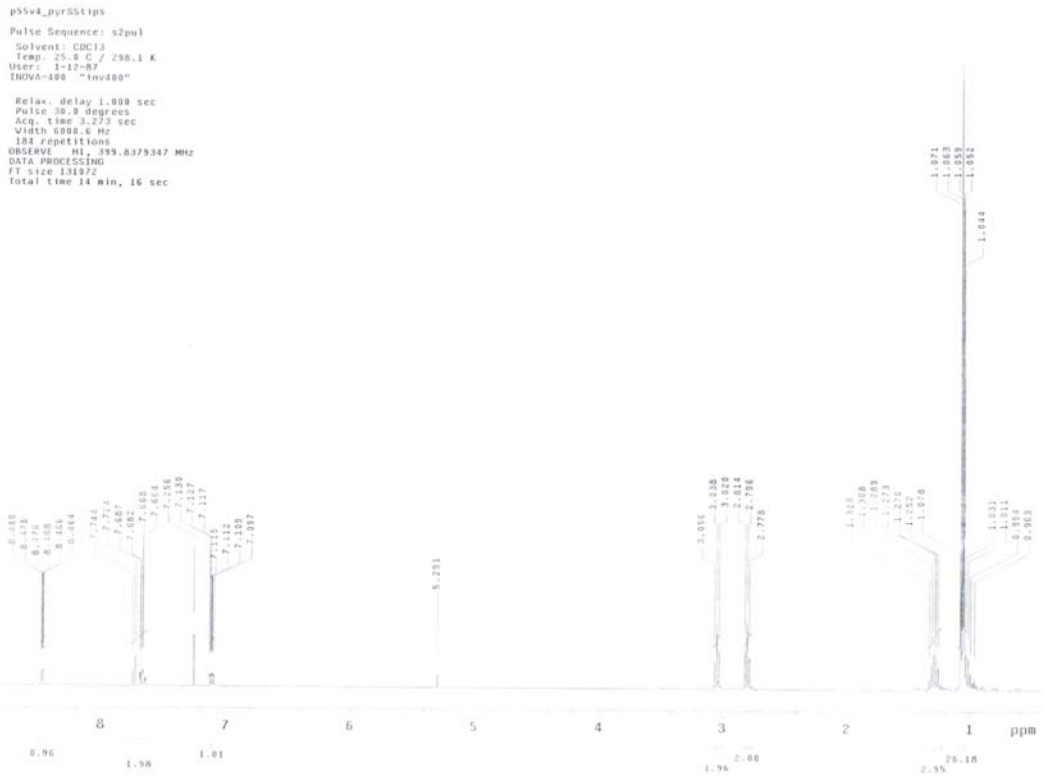

^{1}H NMR Spectrum of **4-13**

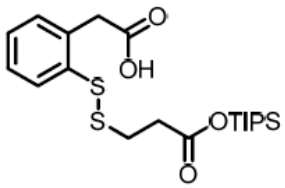

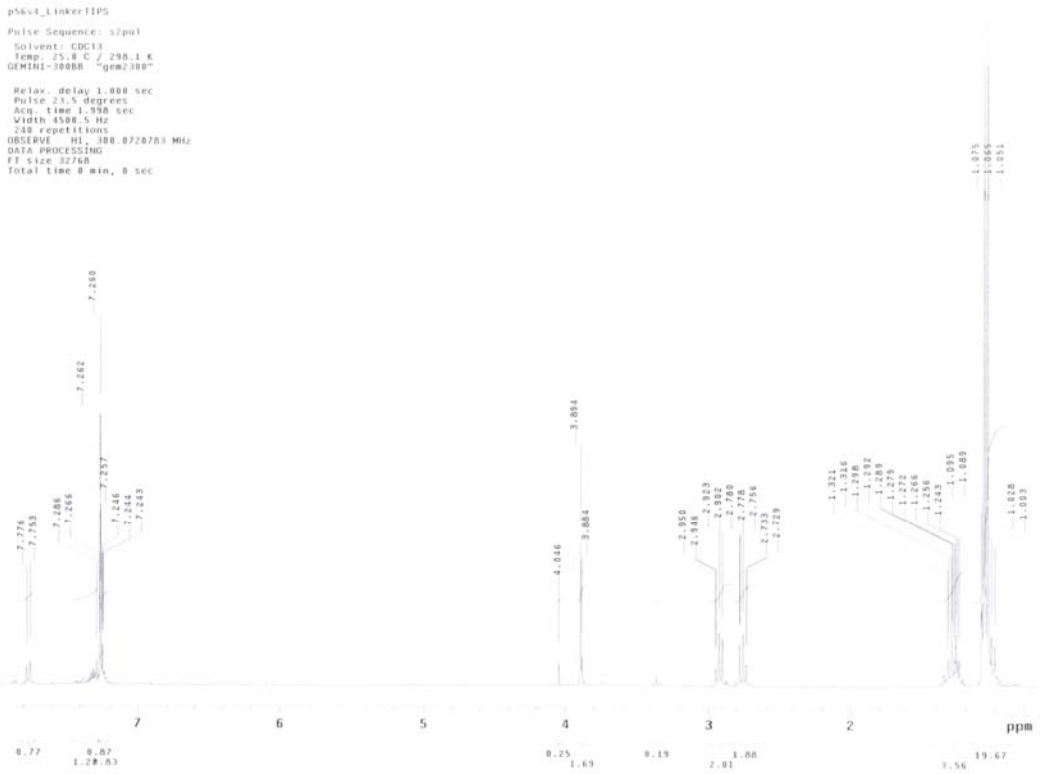

^{1}H NMR Spectrum of **4-14**

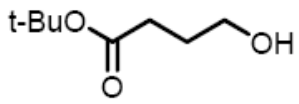

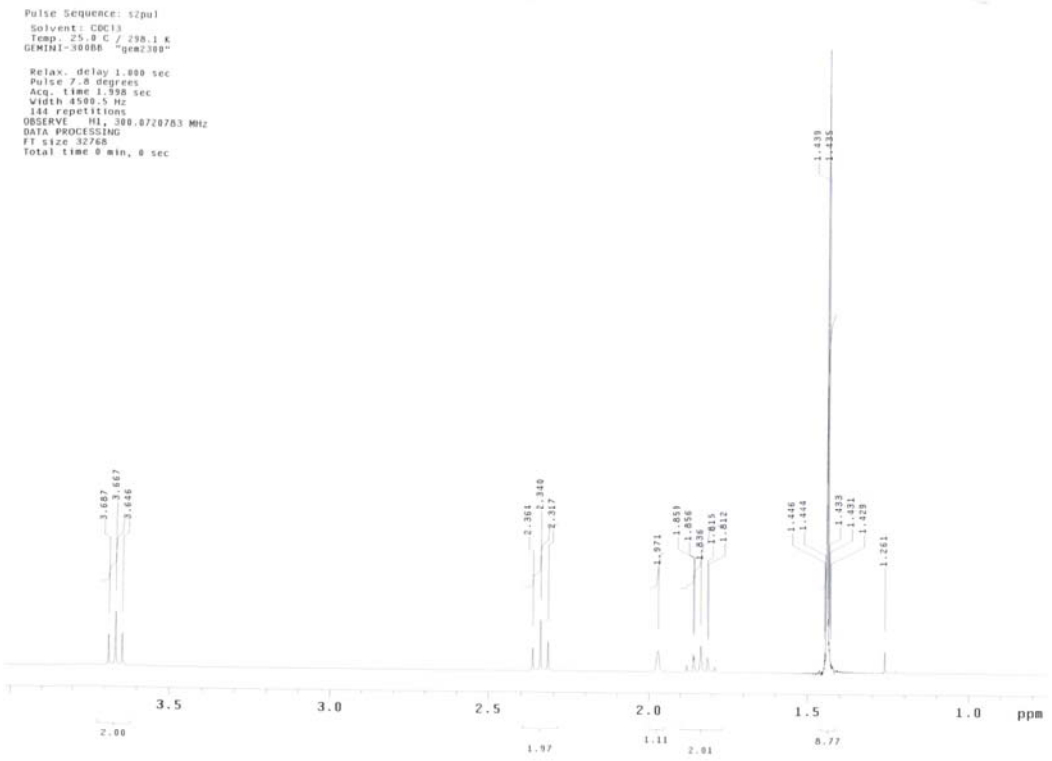

^{1}H NMR Spectrum of **4-15**

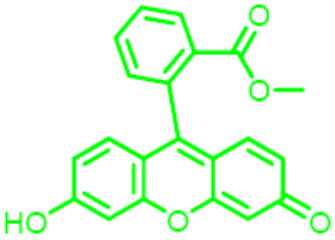

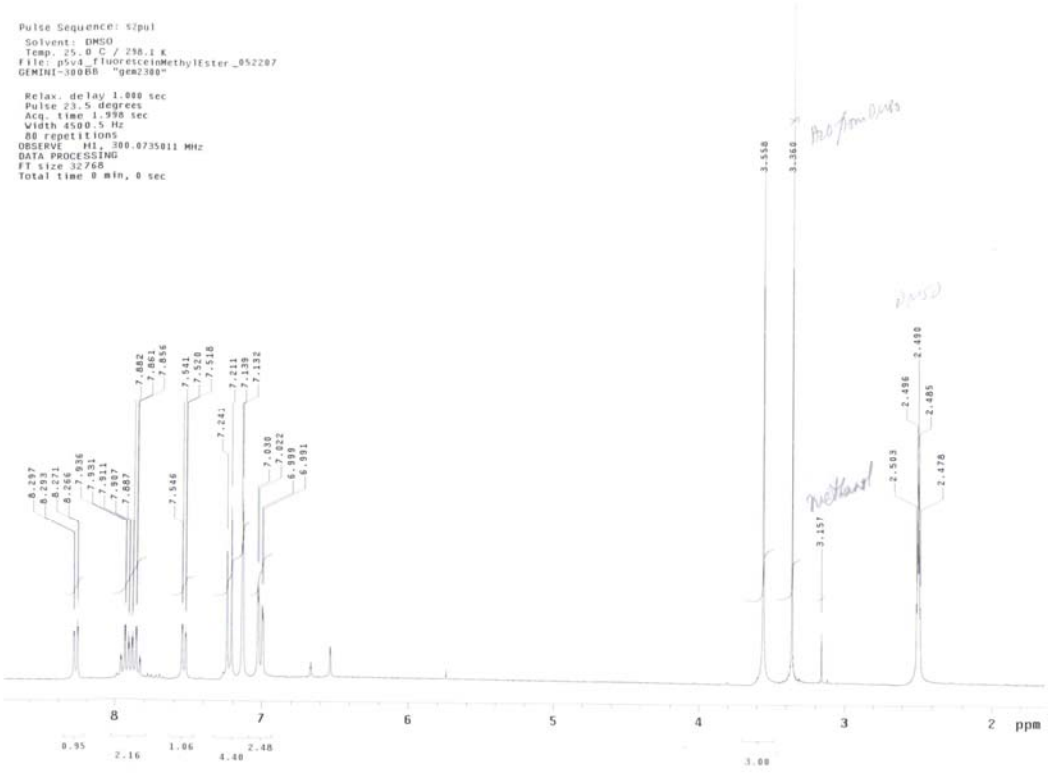

^{1}H NMR Spectrum of **4-16**

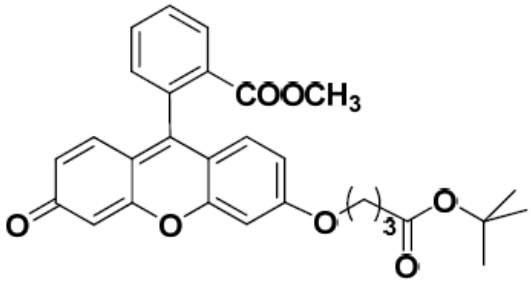

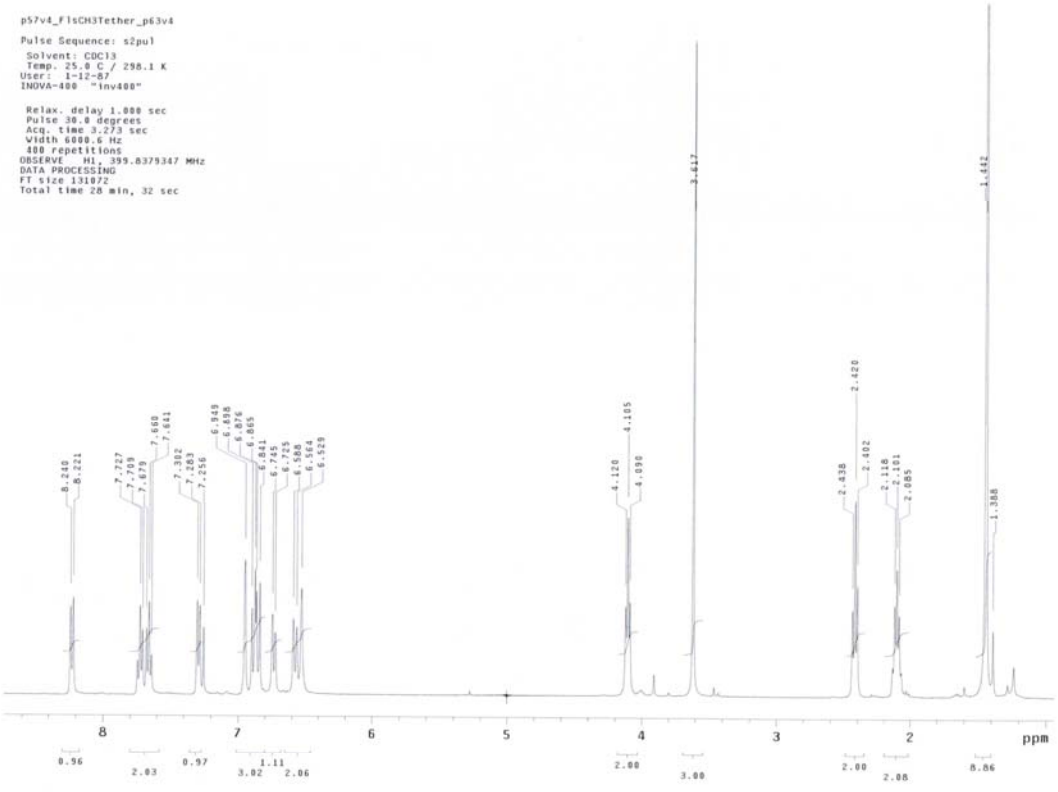

^{1}C NMR Spectrum of **4-16**

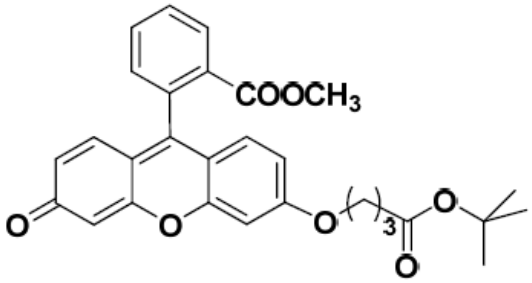

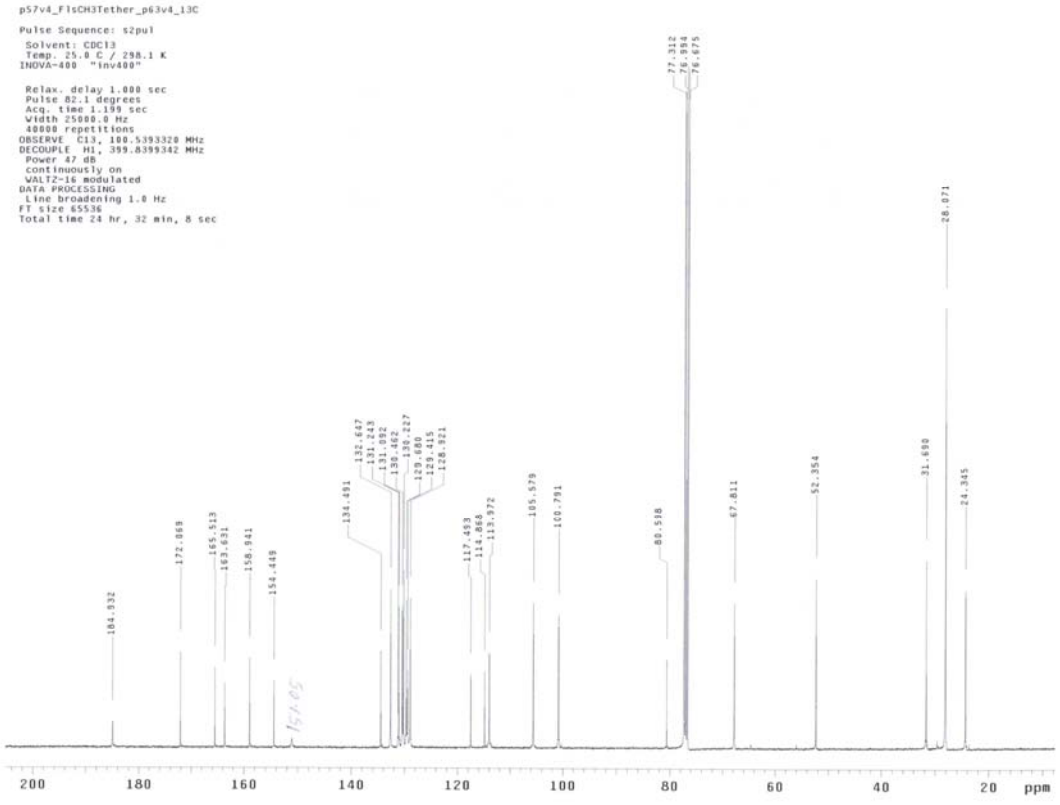

^{1}H NMR Spectrum of **4-17**

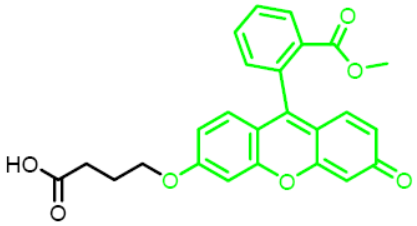

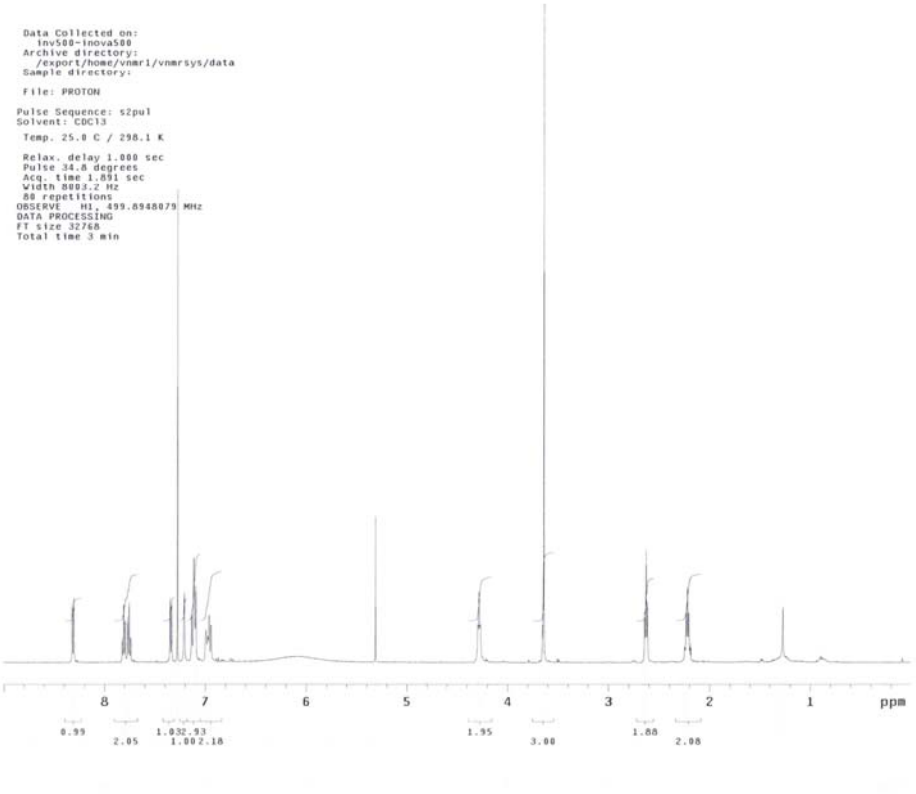

^{13}C NMR Spectrum of **4-17**

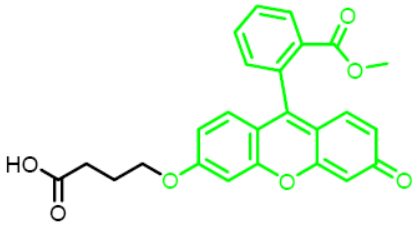

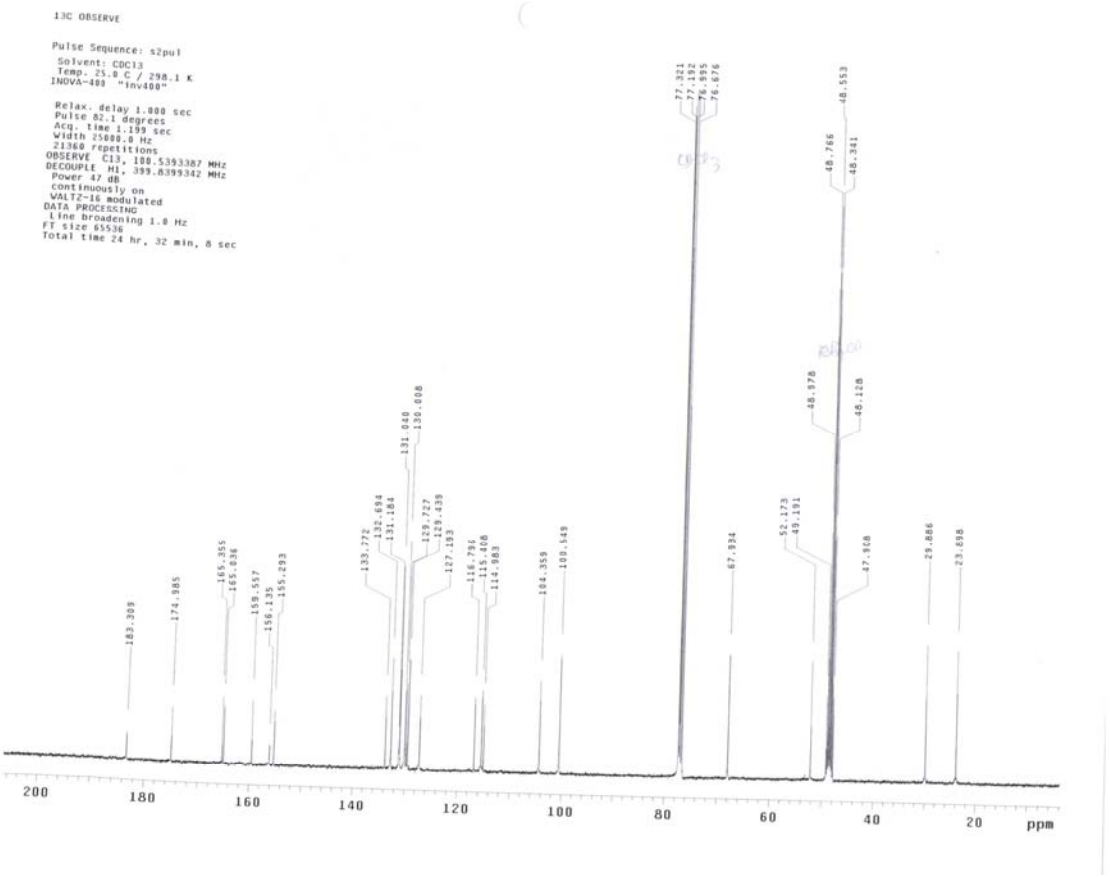

^{1}H NMR Spectrum of **4-18**

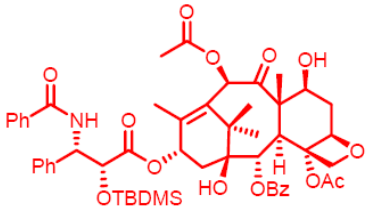

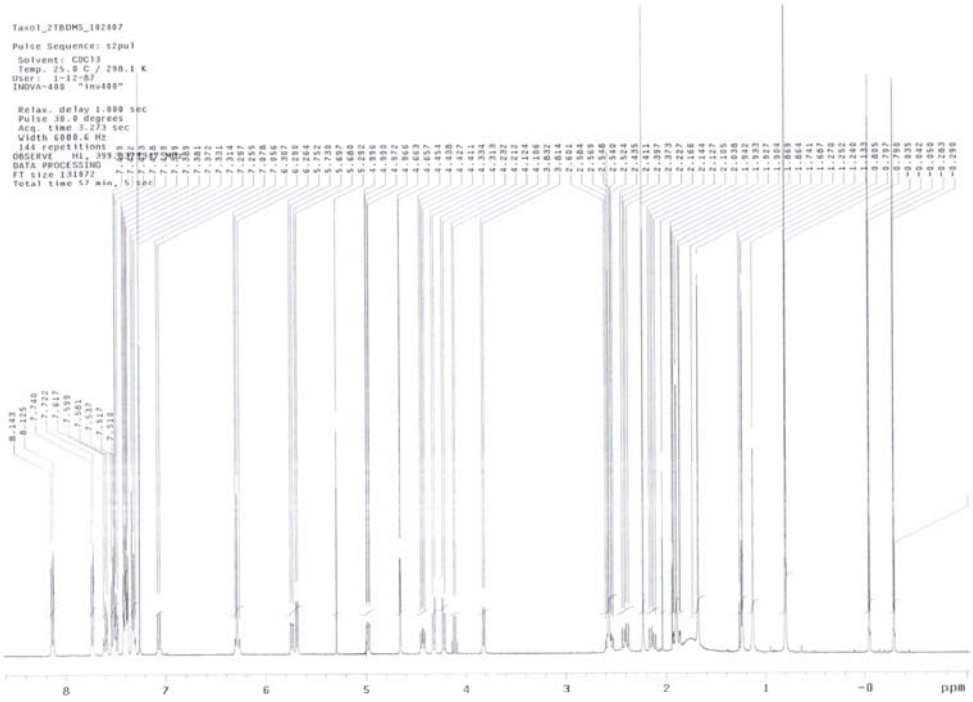

^{1}H NMR Spectrum of **4-19**

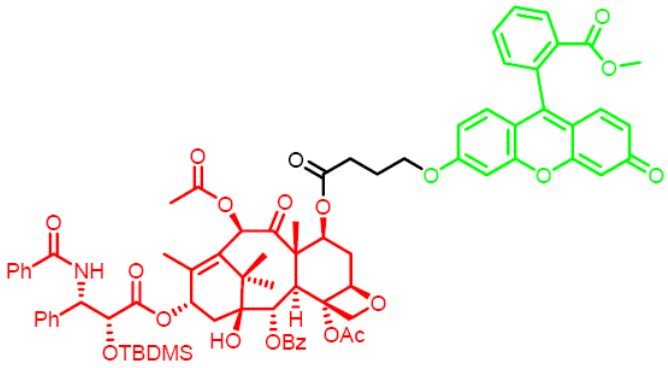

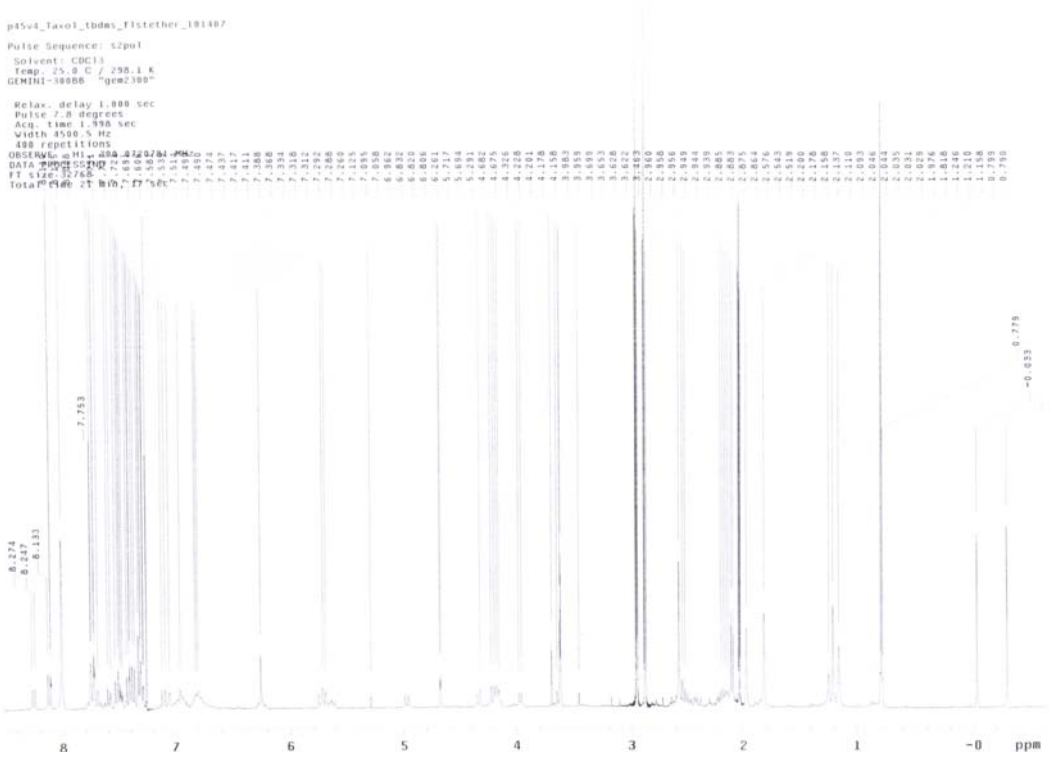

^{13}C NMR Spectrum of **4-19**

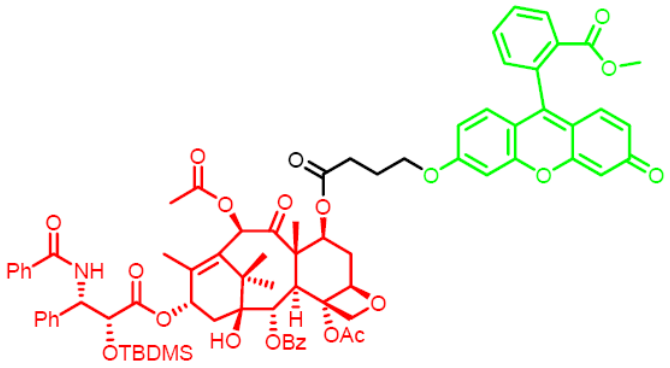

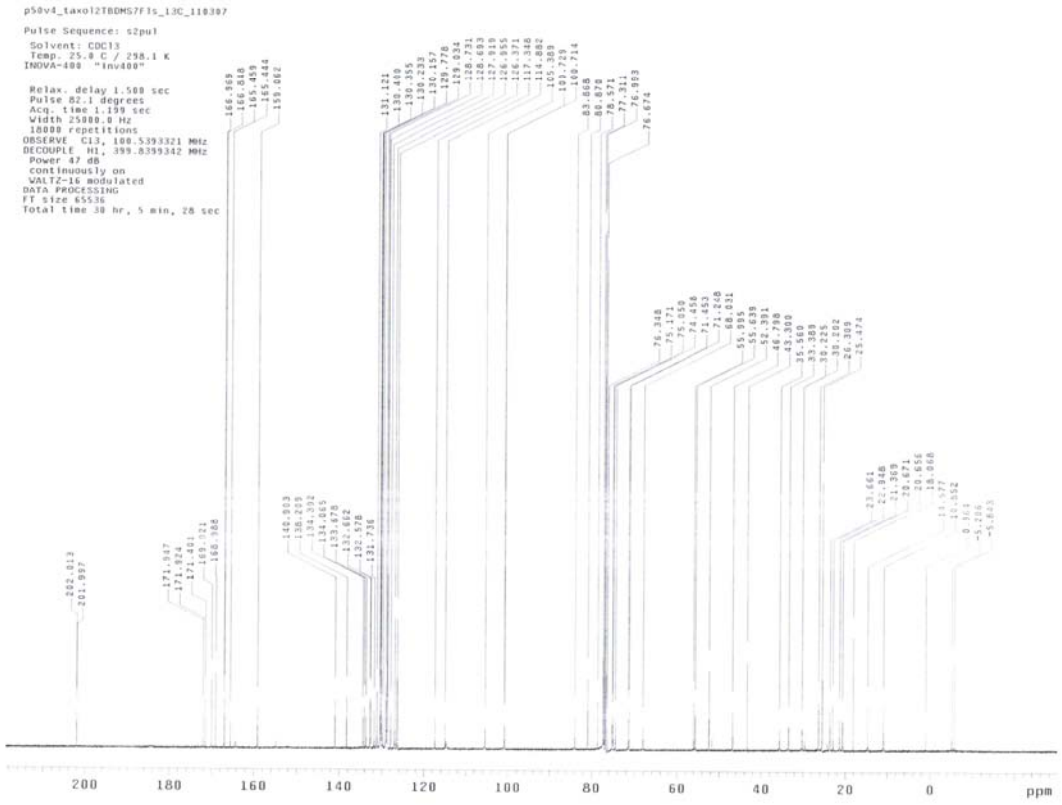

^{1}H NMR Spectrum of **4-20**

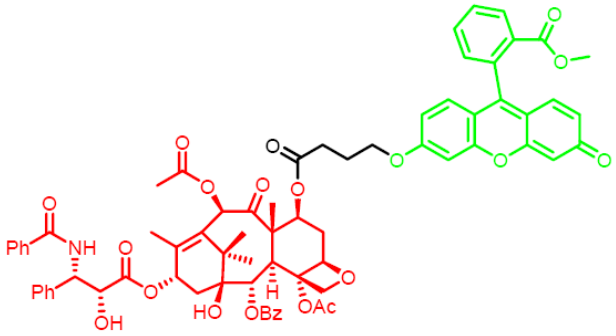

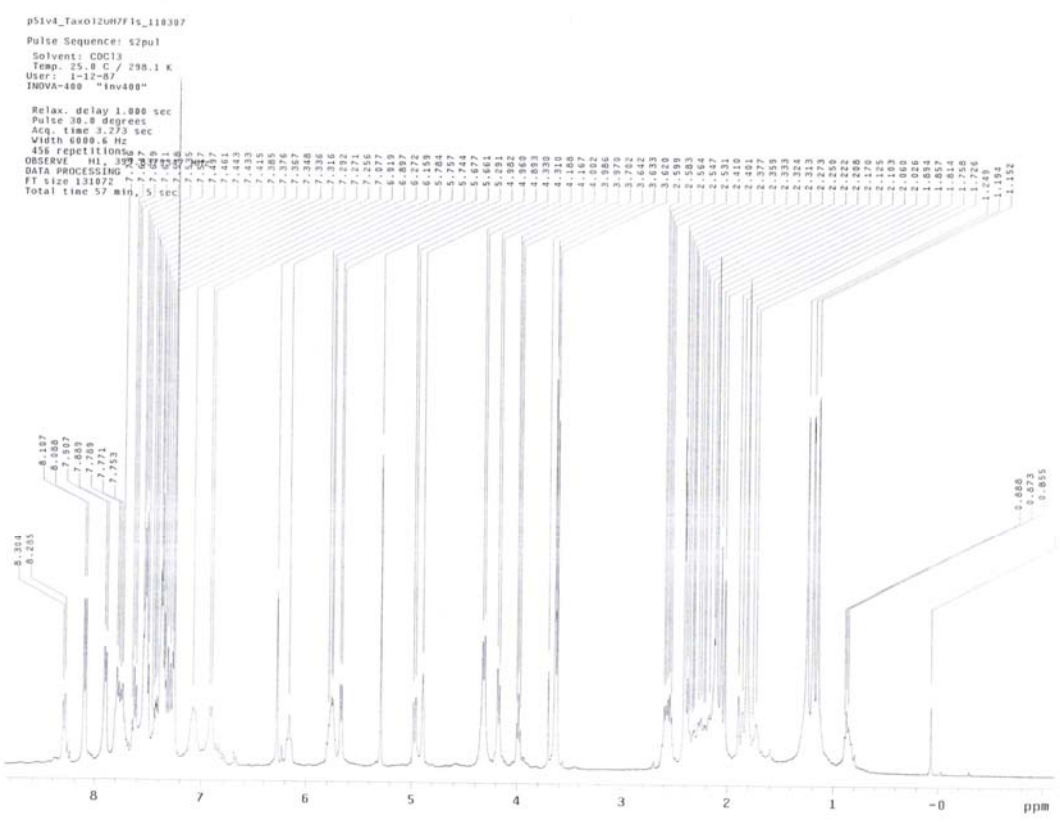

^{13}C NMR Spectrum of **4-20**

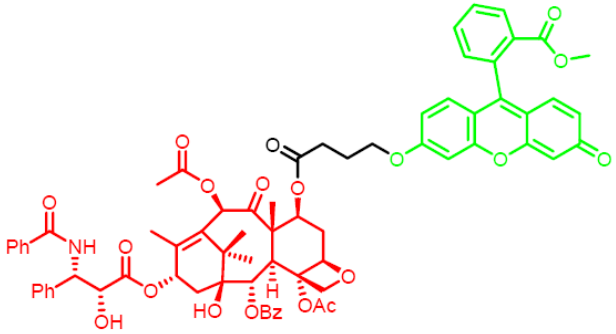

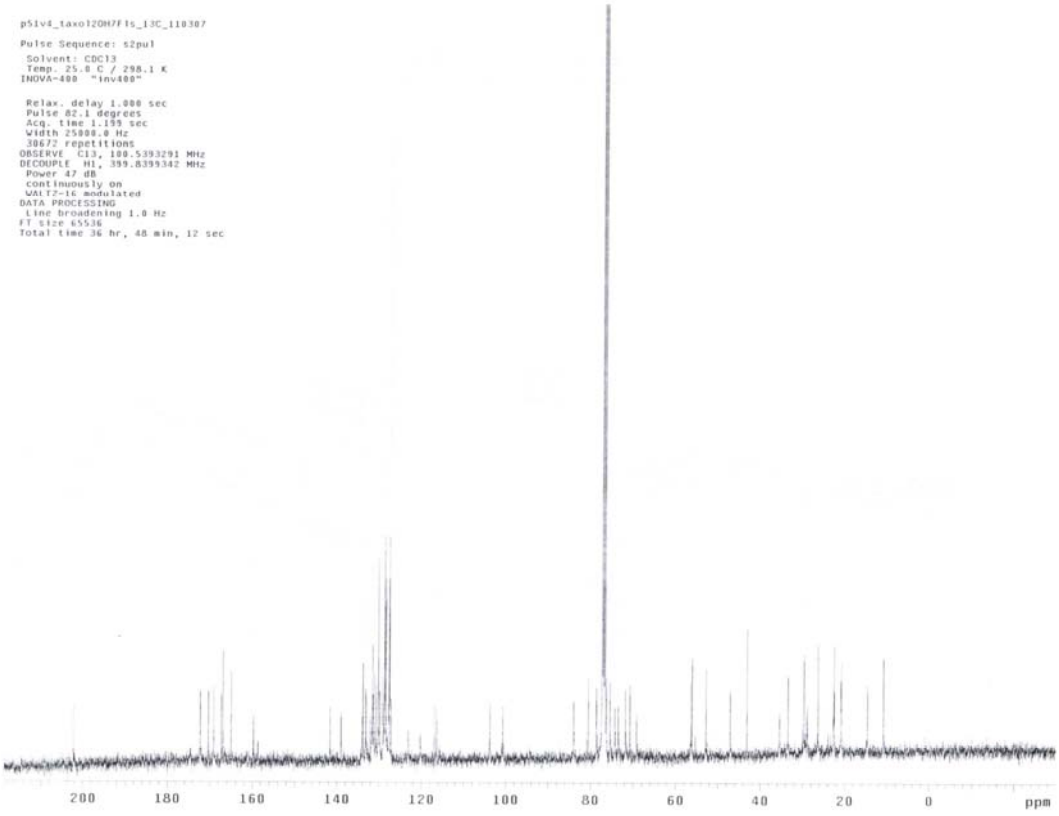

^{1}H NMR Spectrum of **4-21**

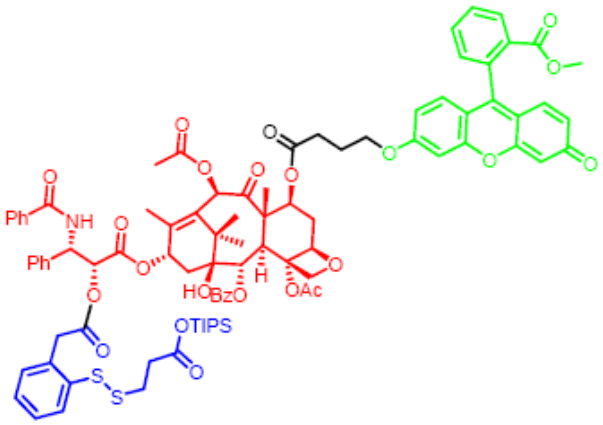

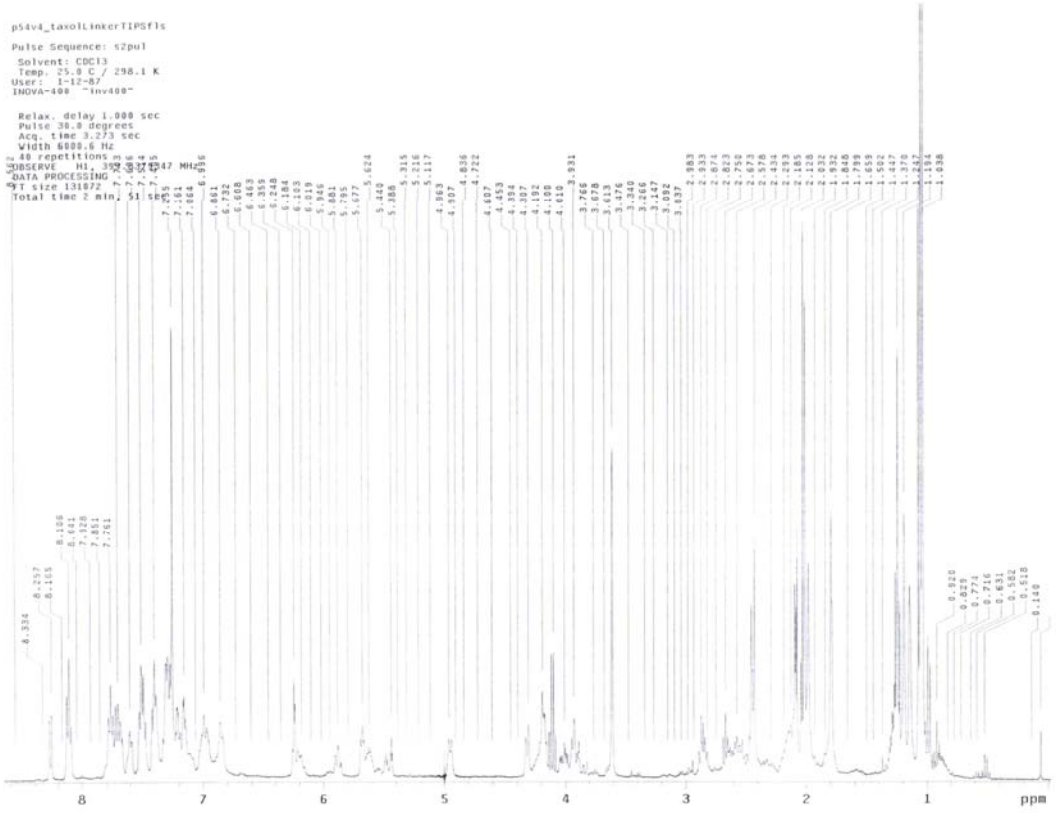

^{13}C NMR Spectrum of **4-21**

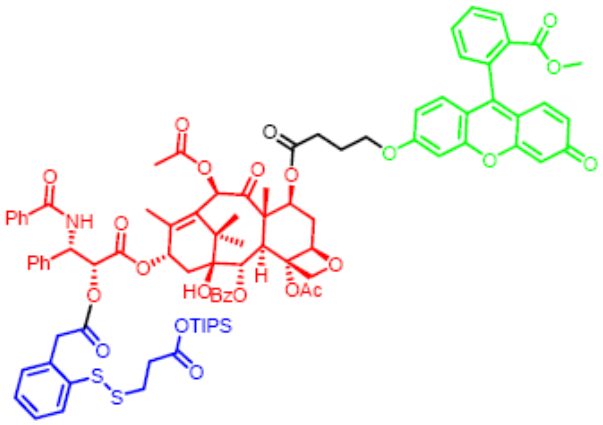

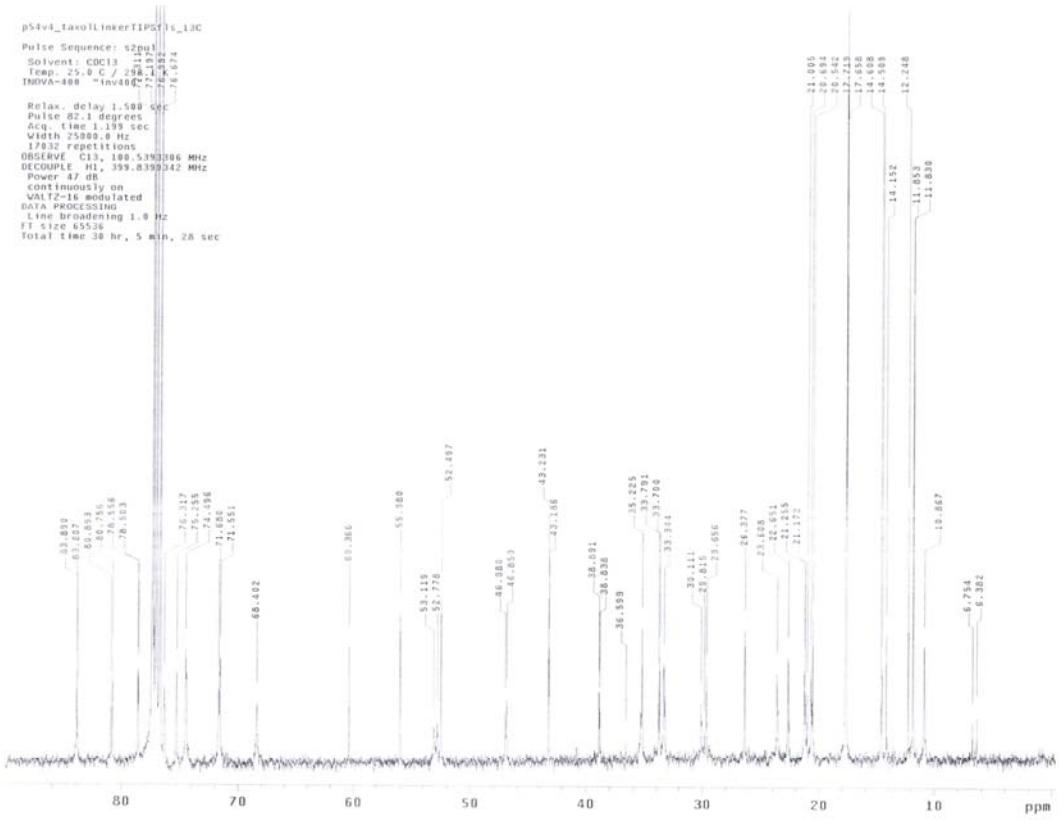

^{1}H NMR Spectrum of **4-25**

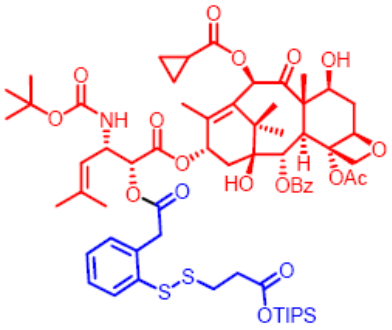

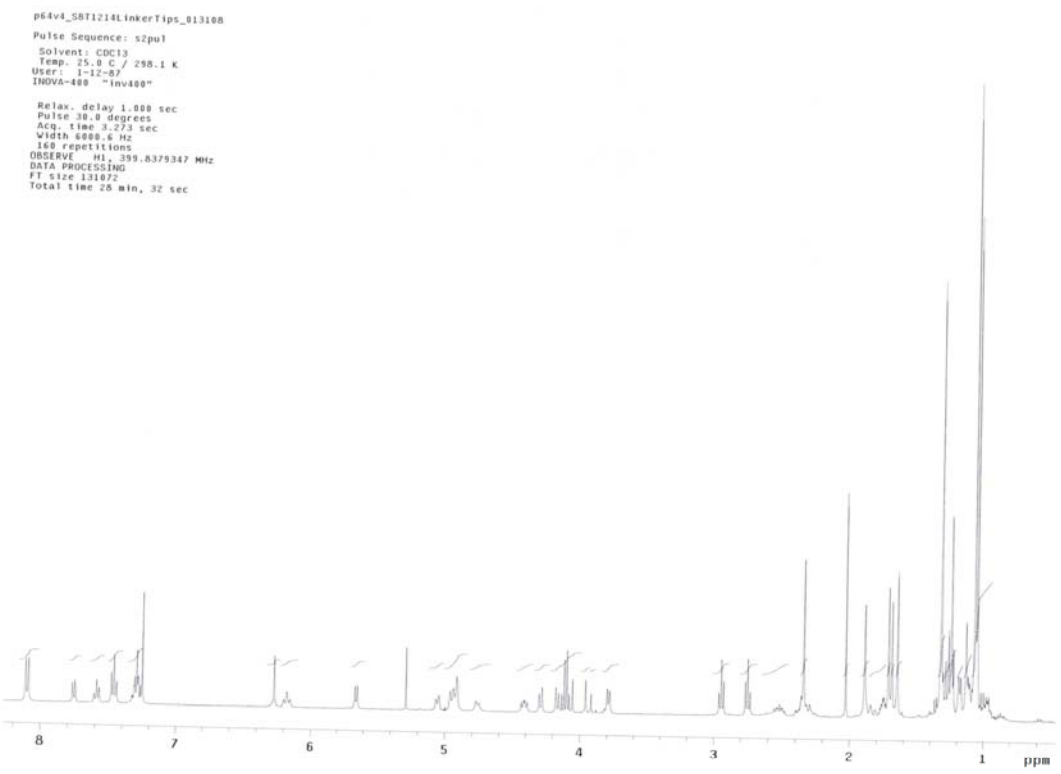

^{13}C NMR Spectrum of **4-25**

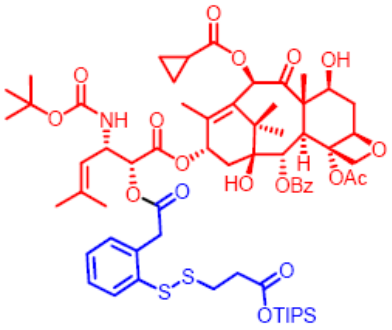

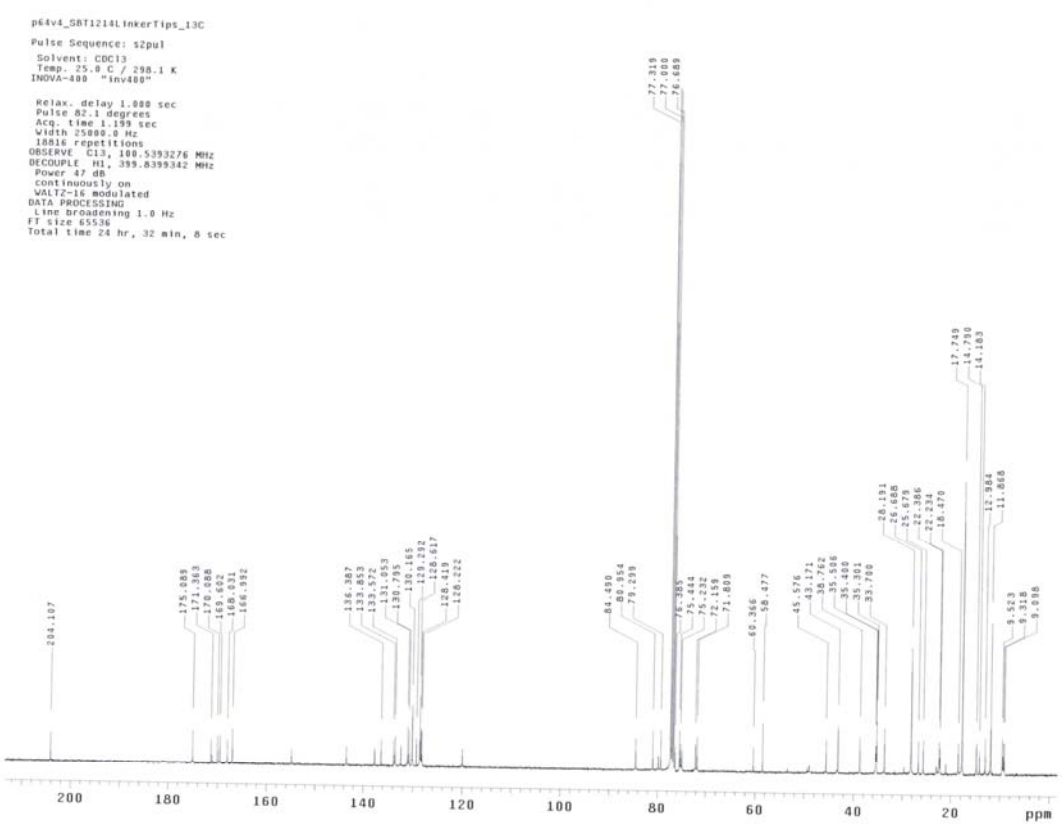

^{1}H NMR Spectrum of **4-26**

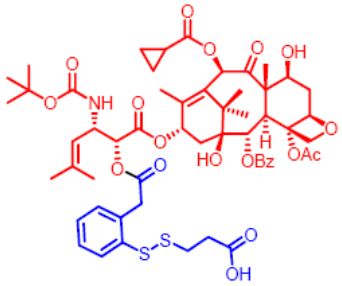

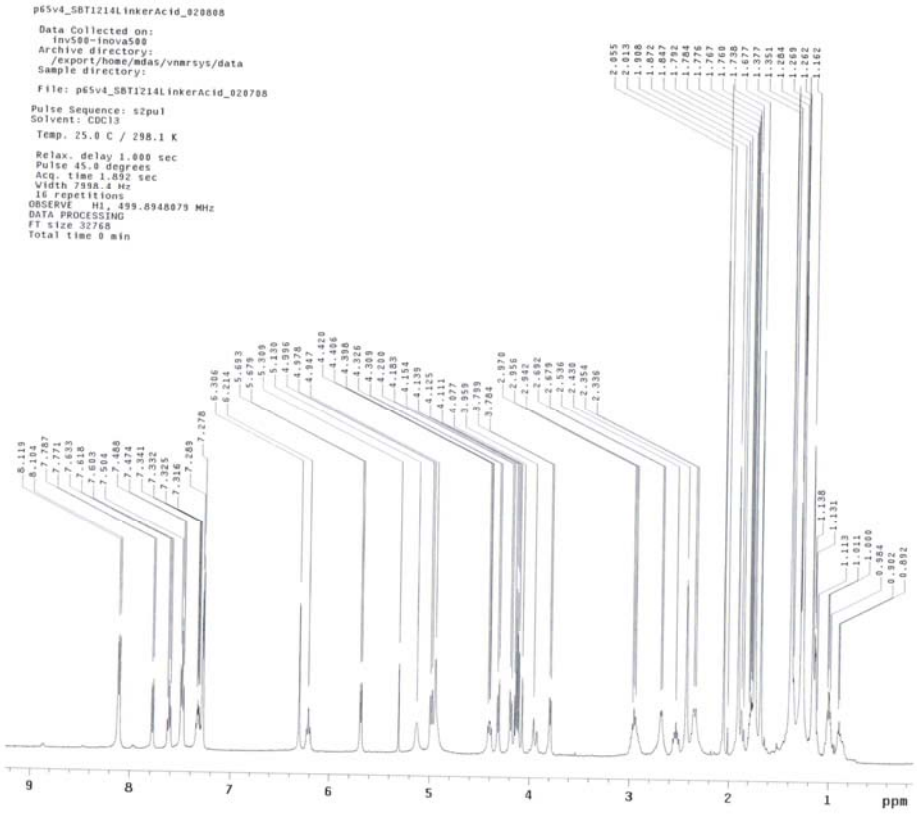

^{13}C NMR Spectrum of **4-26**

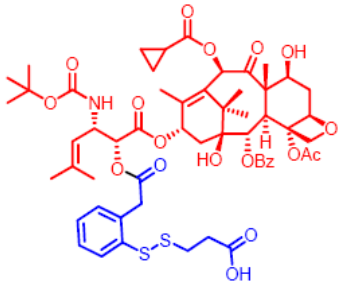

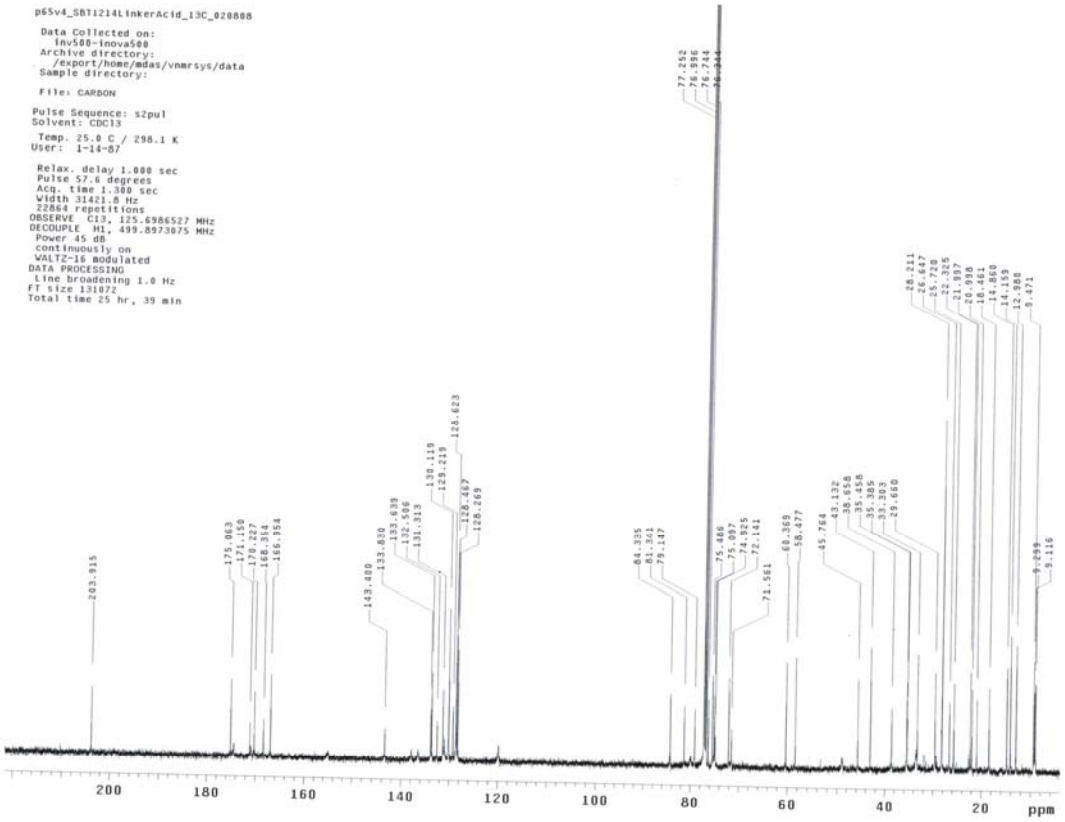

^{1}H NMR Spectrum of **4-27**

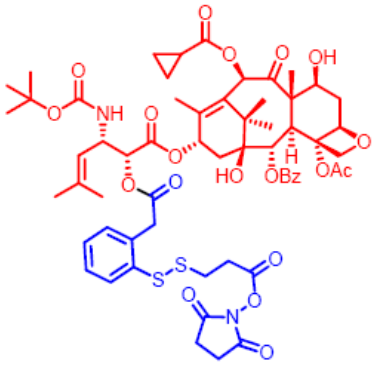

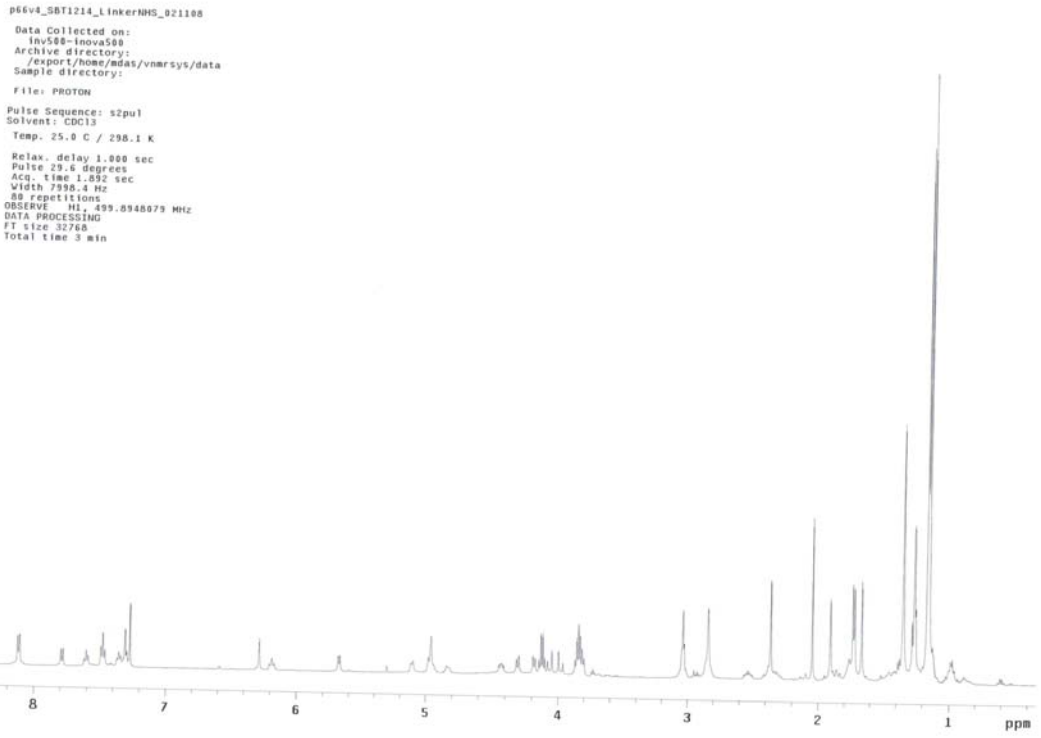

^{1}H NMR Spectrum of **6-1**

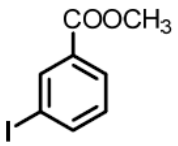

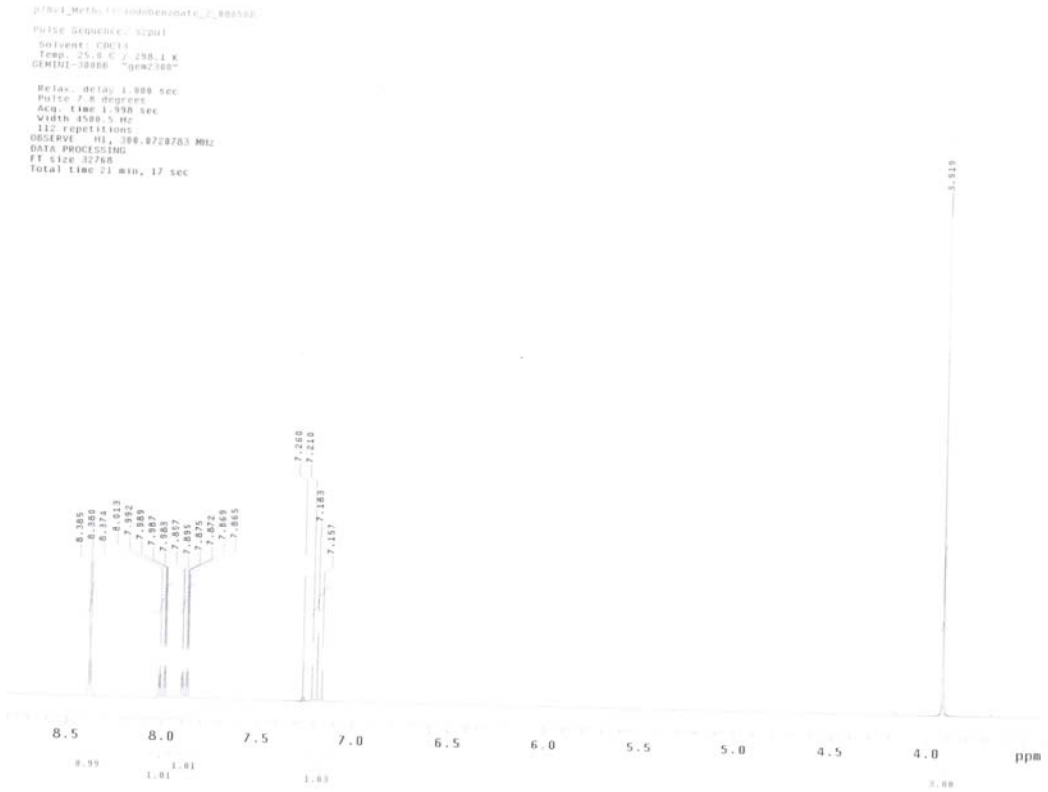

^{1}H NMR Spectrum of **6-2**

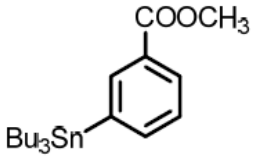

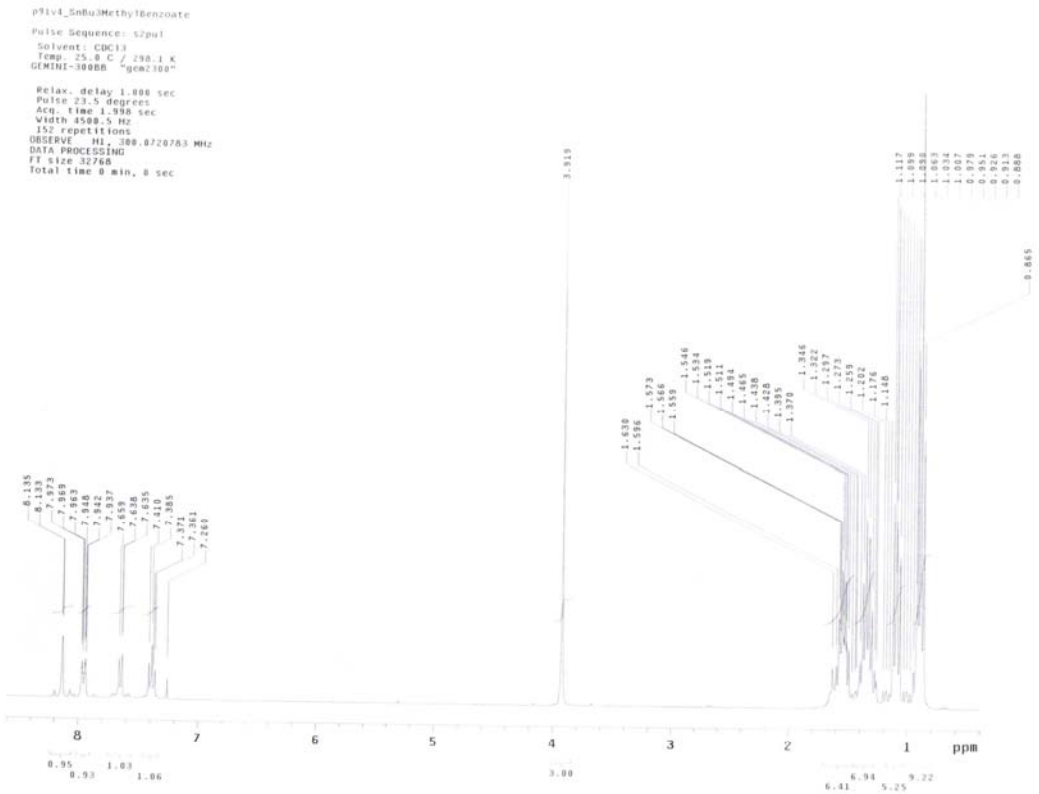

^{13}C NMR Spectrum of **6-2**

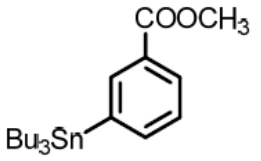

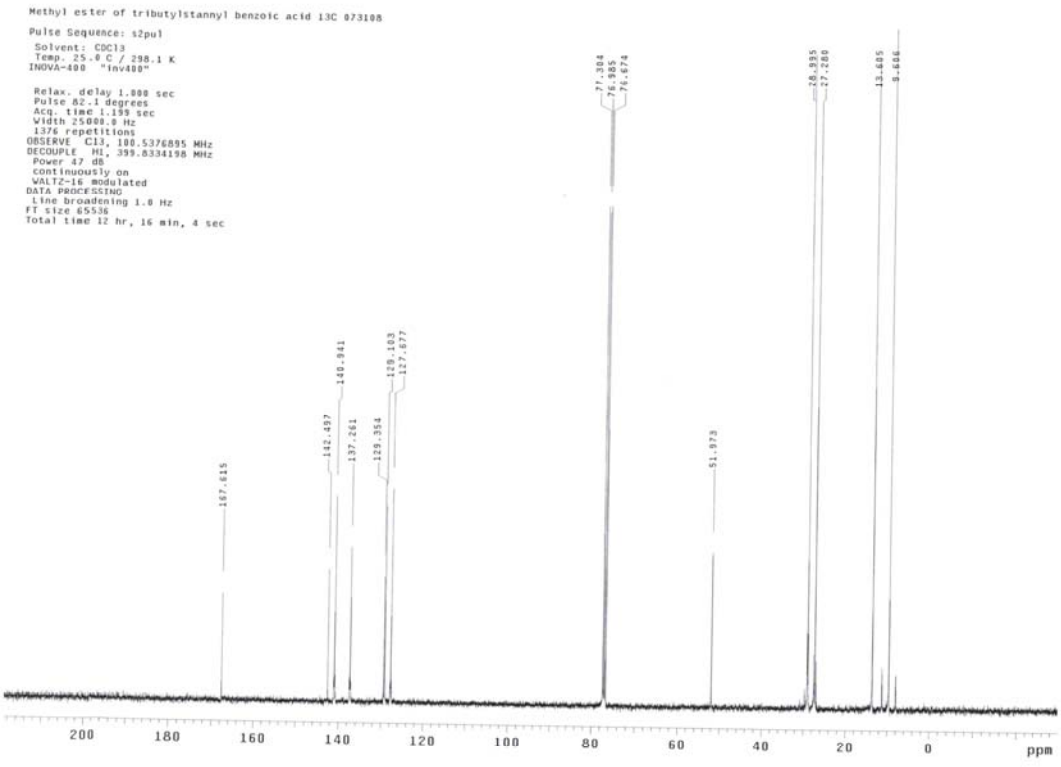

^{1}H NMR Spectrum of **6-3**

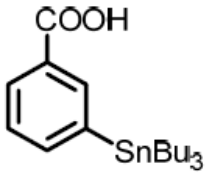

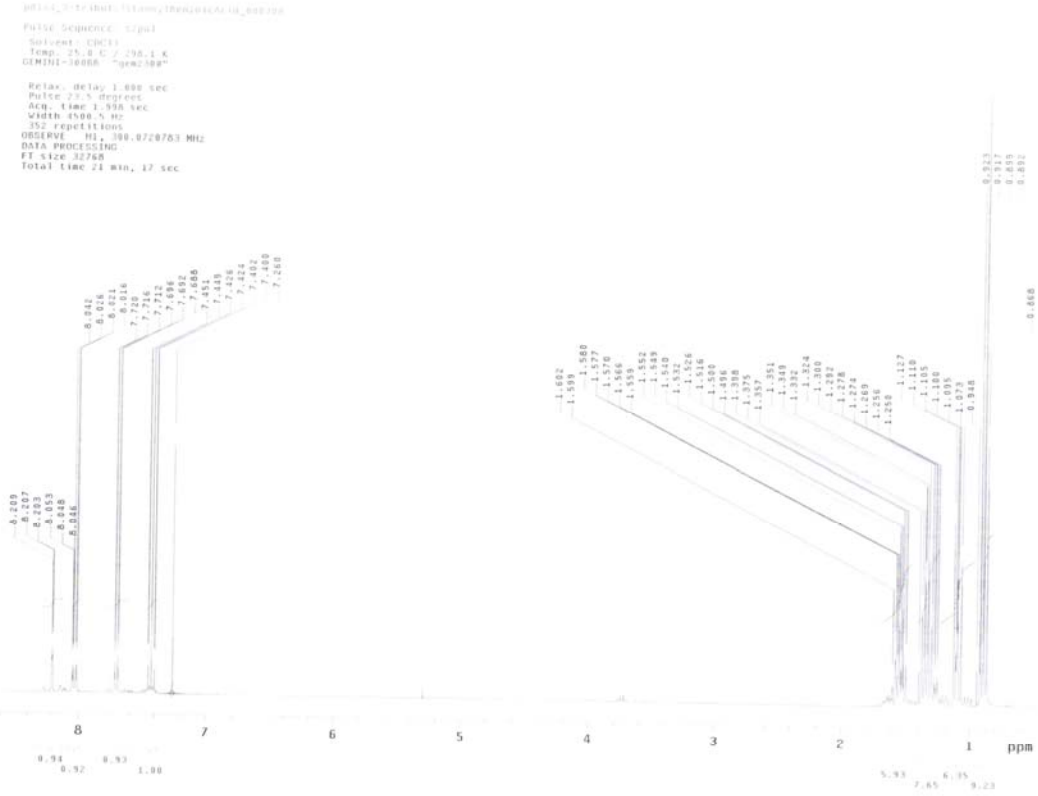

^{13}C NMR Spectrum of **6-3**

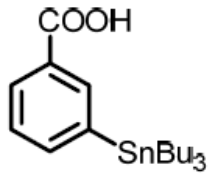

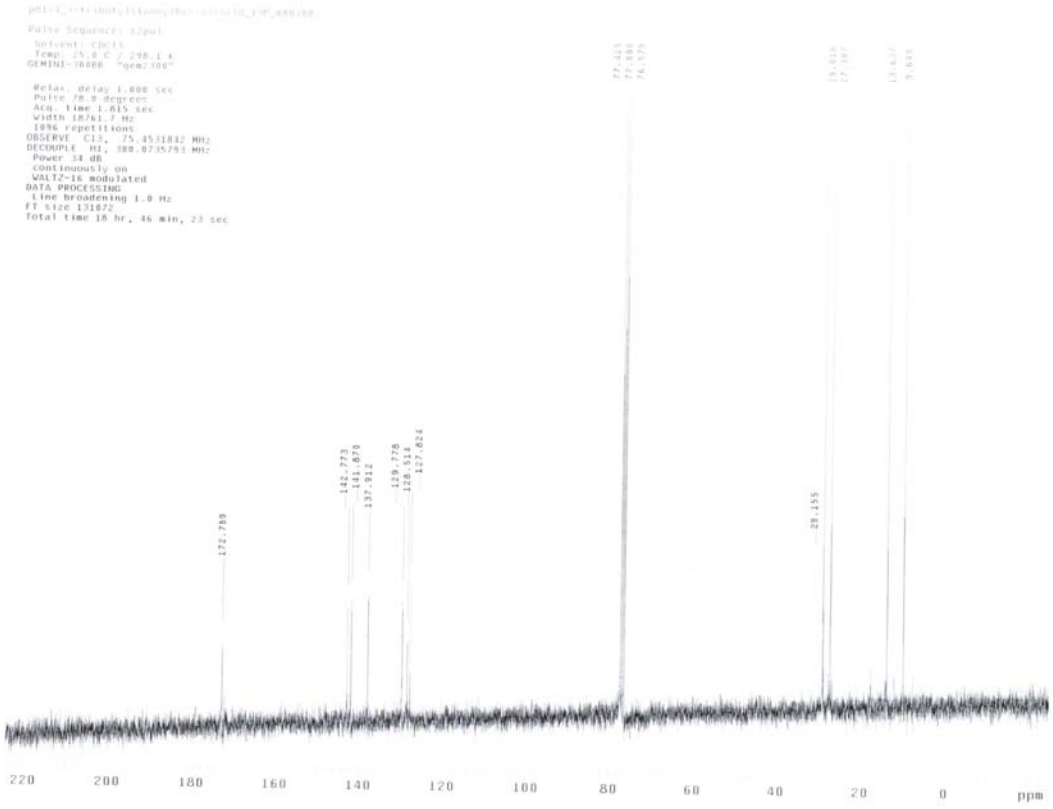

^{1}H NMR Spectrum of **6-5**

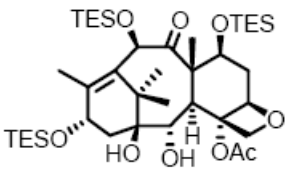

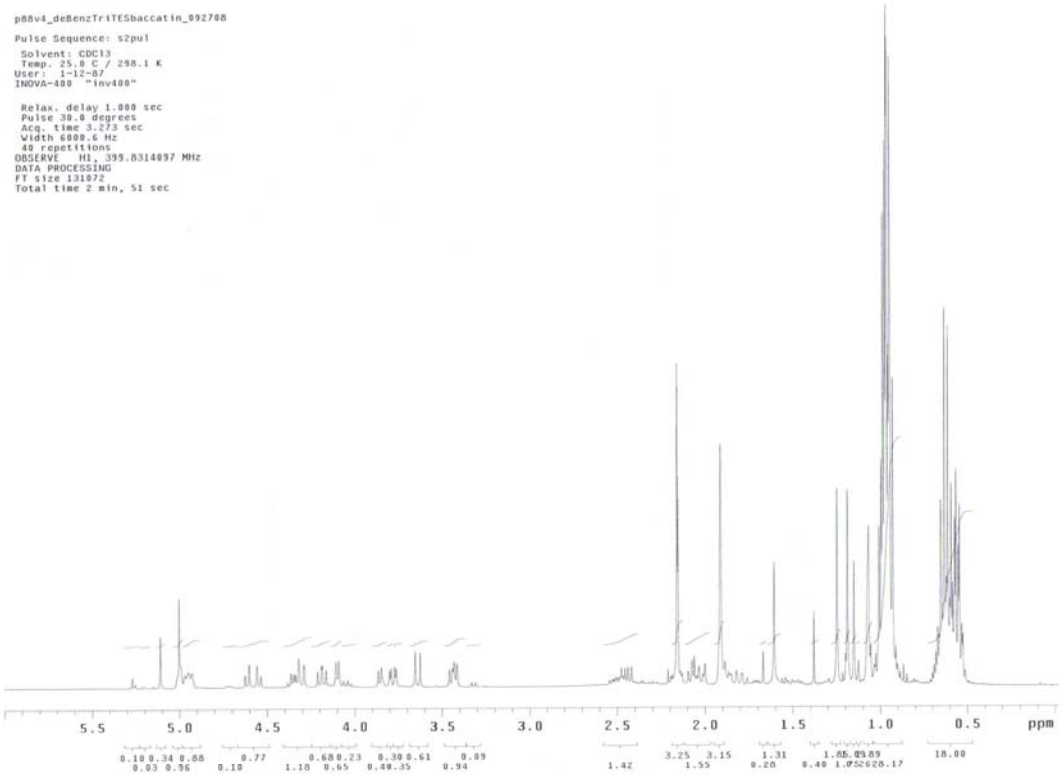

^{13}C NMR Spectrum of **6-5**

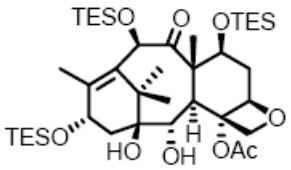

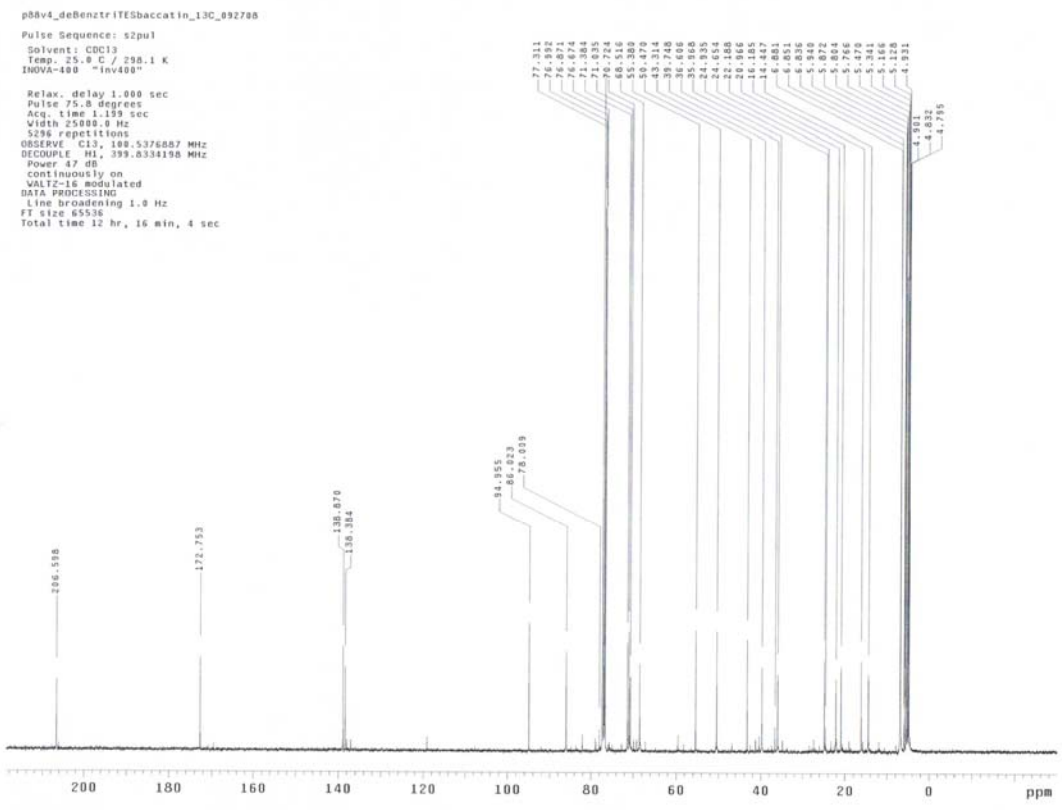

^{1}H NMR Spectrum of **6-6**

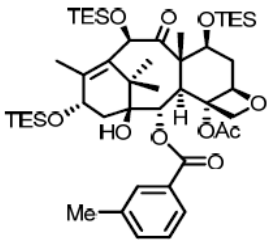

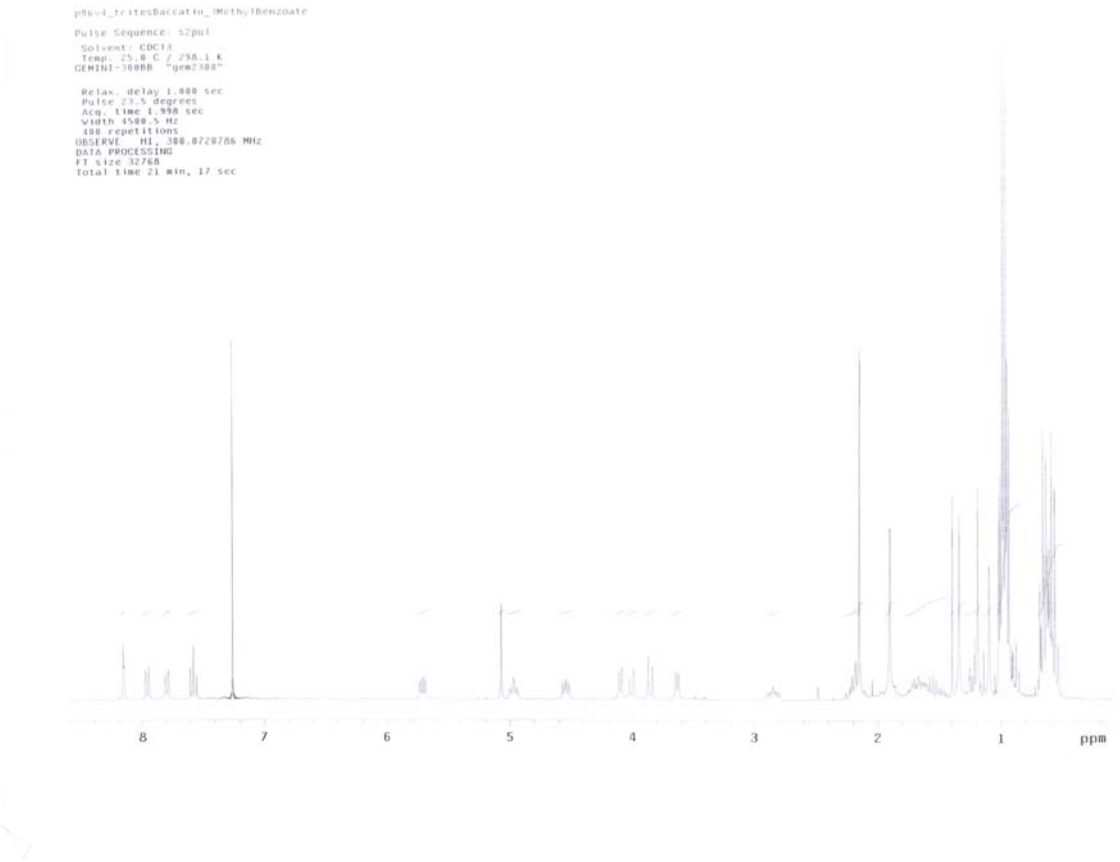

^{1}H NMR Spectrum of **6-7**

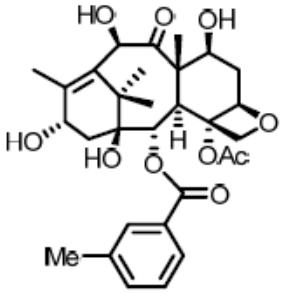

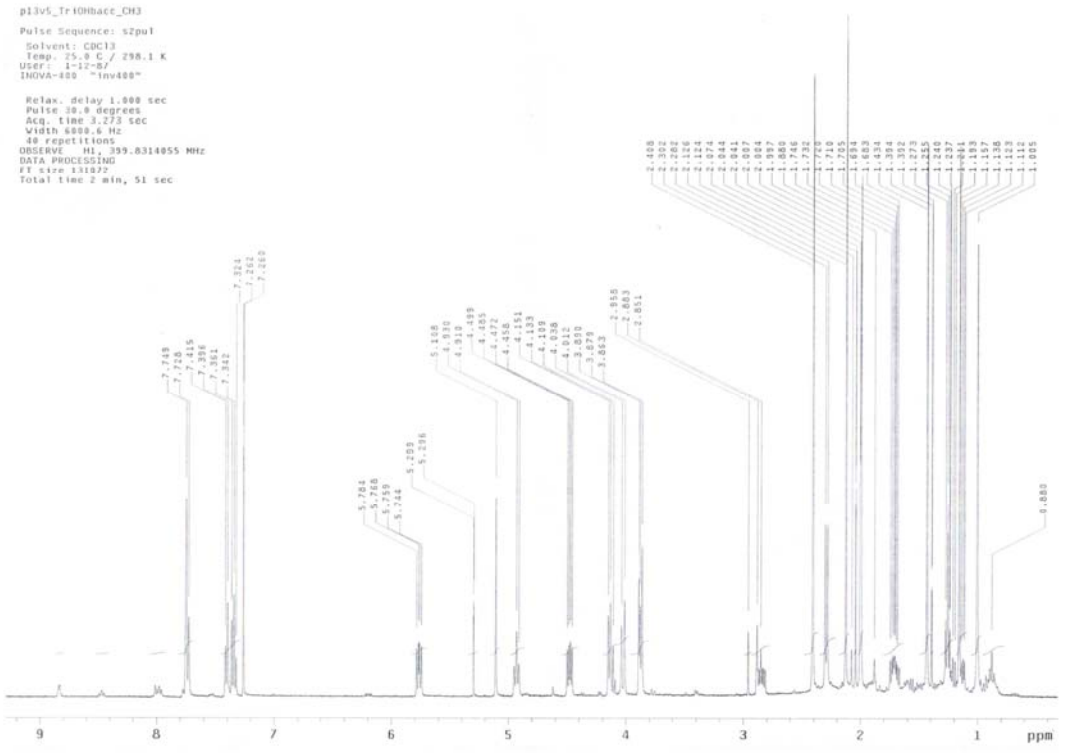

^{13}C NMR Spectrum of **6-7**

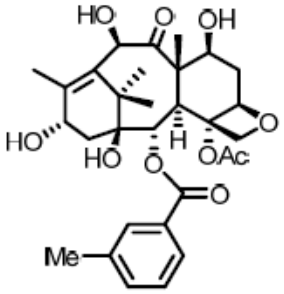

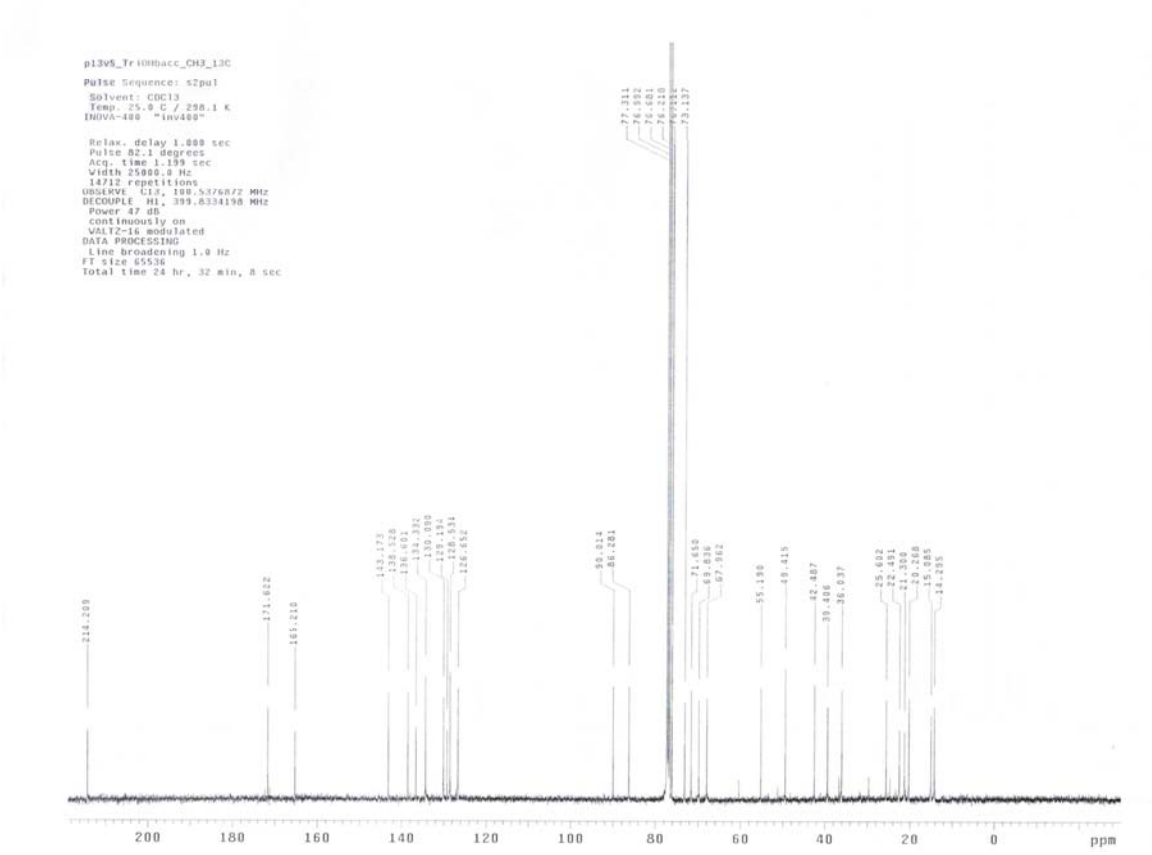

^{1}H NMR Spectrum of **6-8**

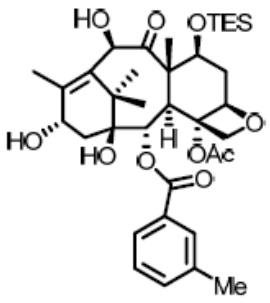

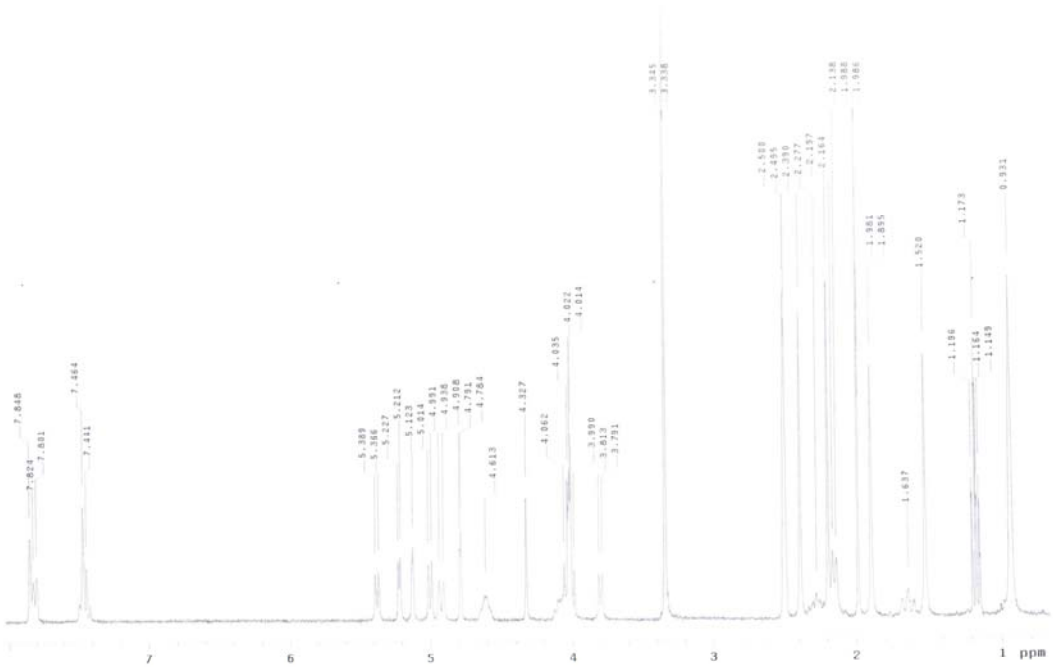

^{1}H NMR Spectrum of **6-9**

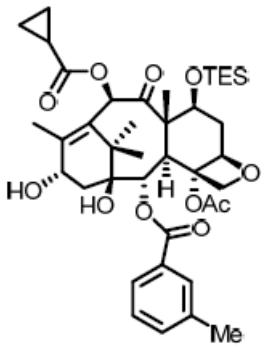

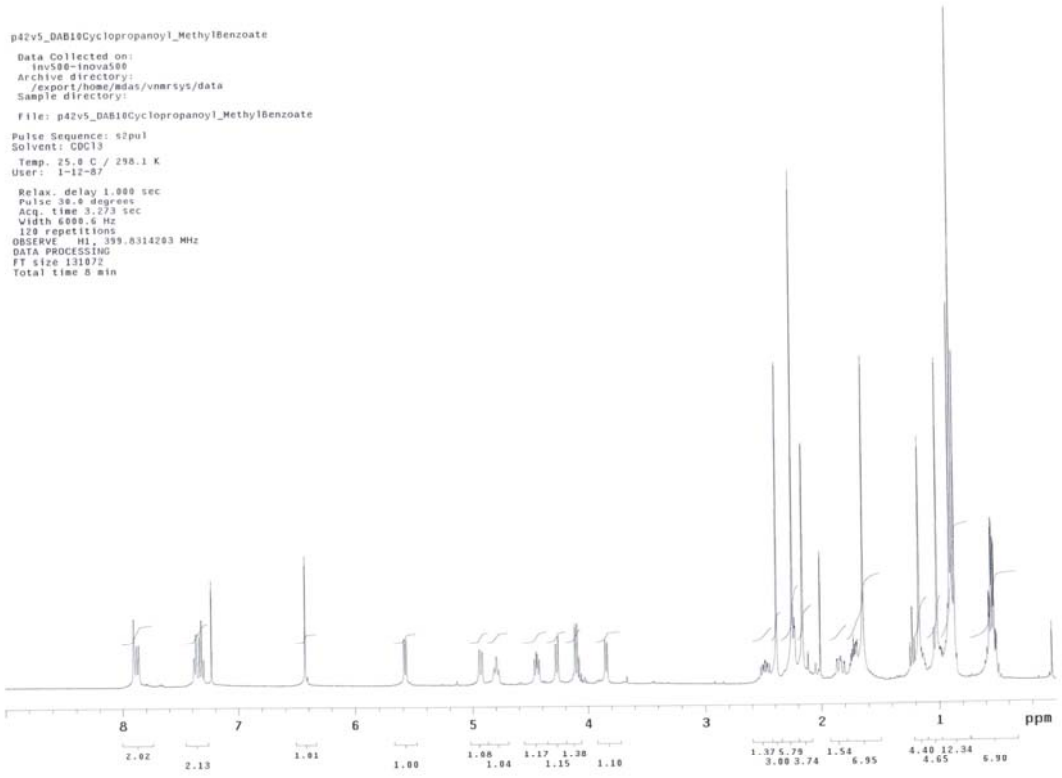

^{13}C NMR Spectrum of **6-9**

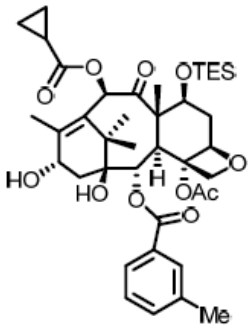

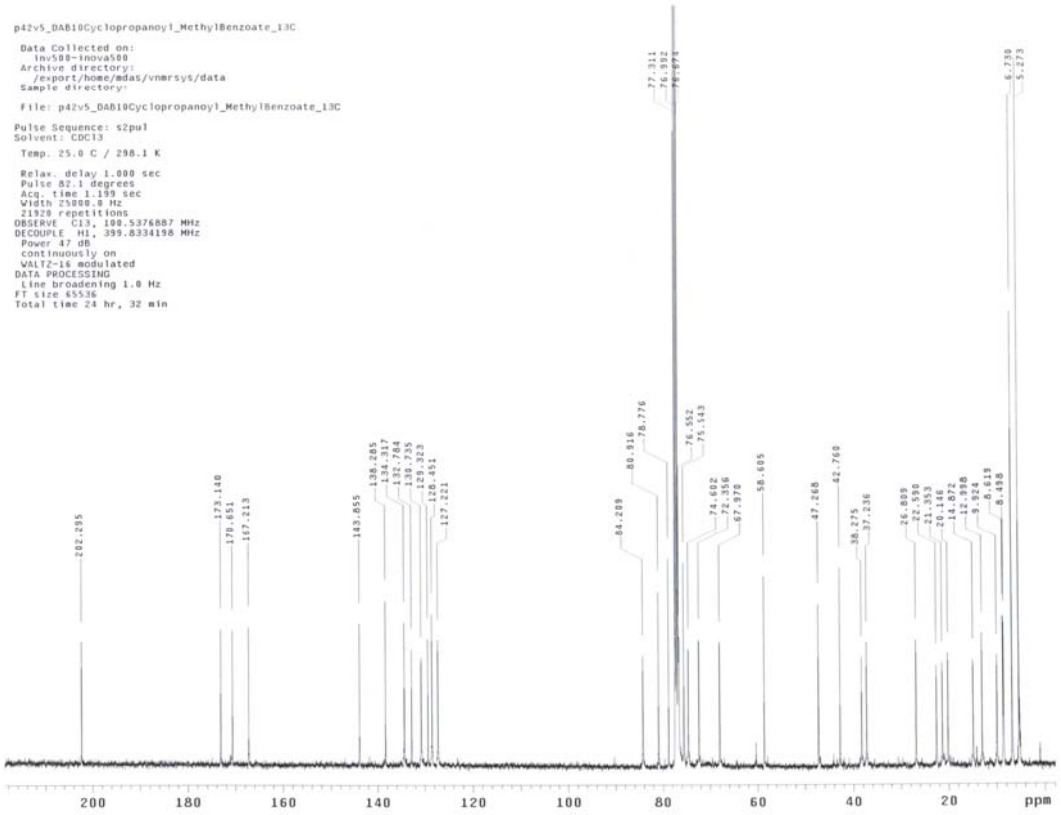

^{1}H NMR Spectrum of **6-10**

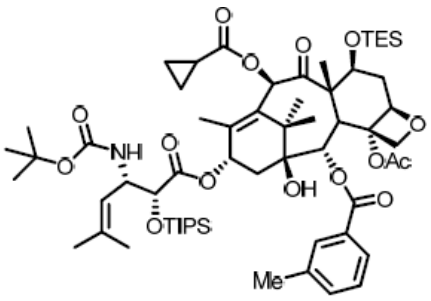

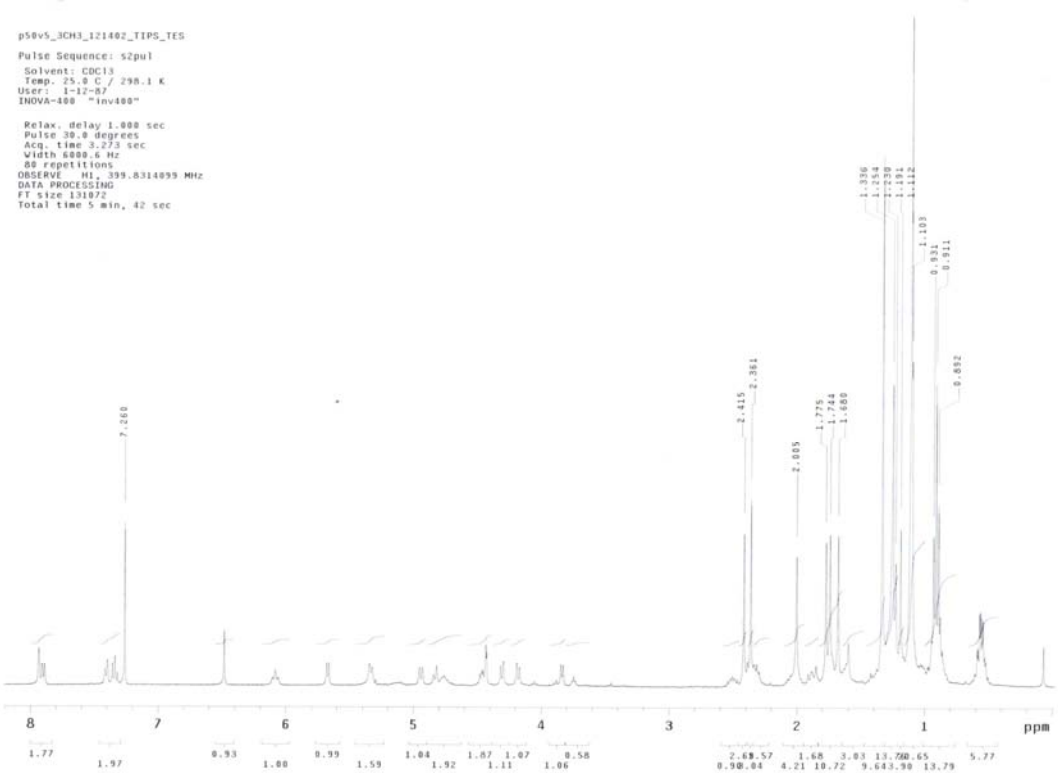

^{13}C NMR Spectrum of **6-10**

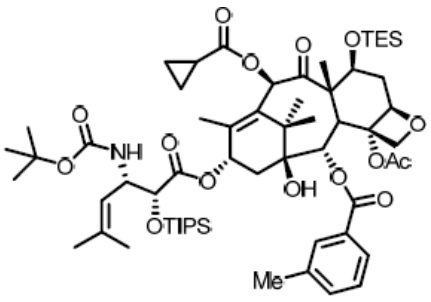

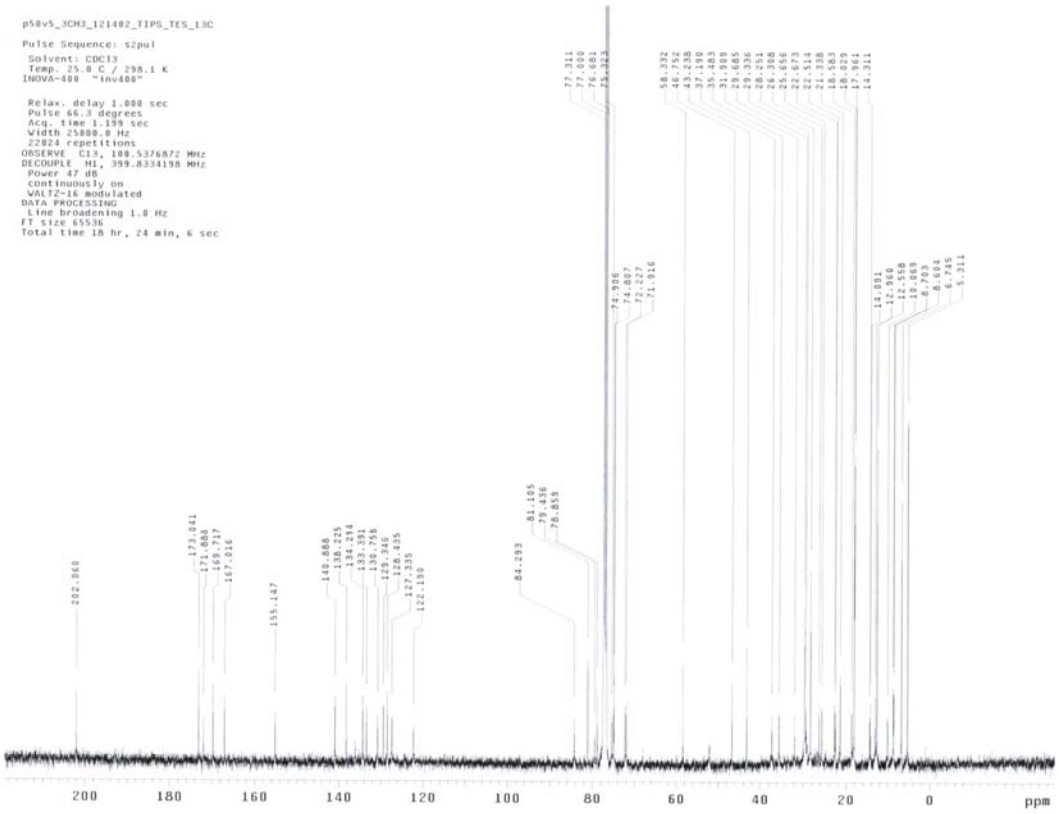

^{1}H NMR Spectrum of **SB-T-121402**

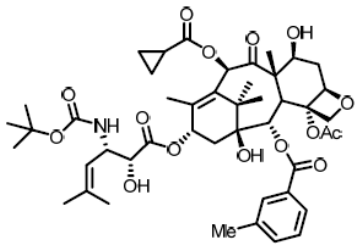

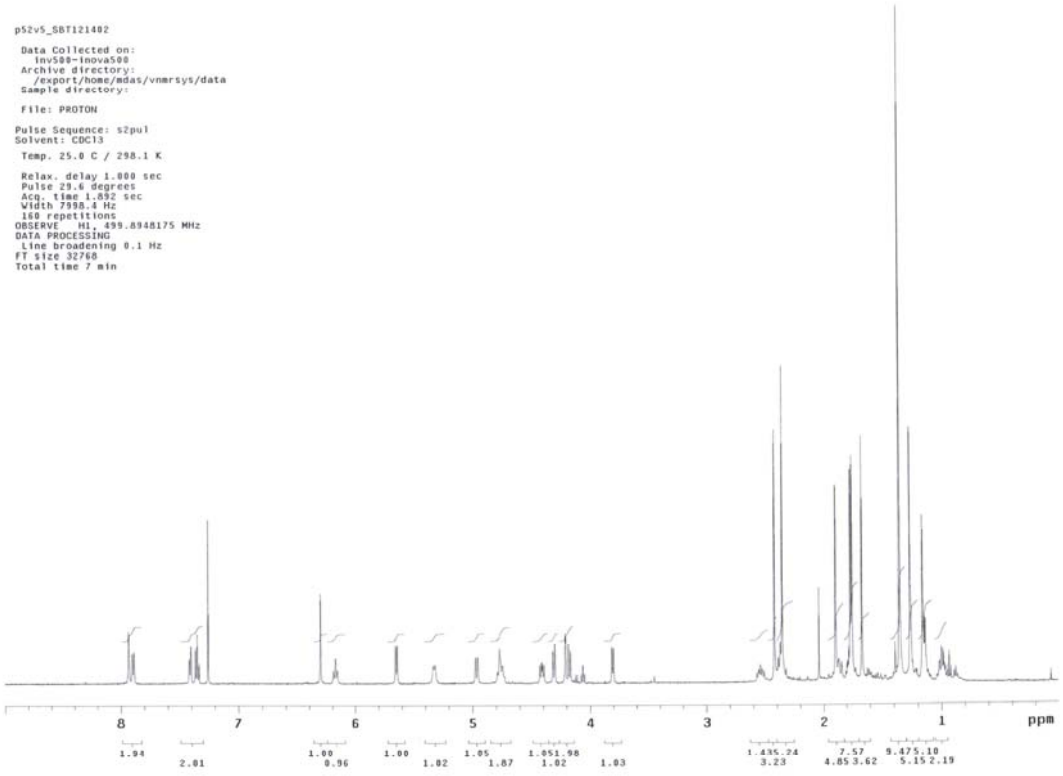

^{13}C NMR Spectrum of **SB-T-121402**

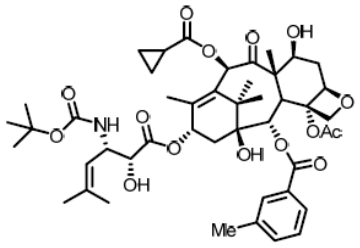

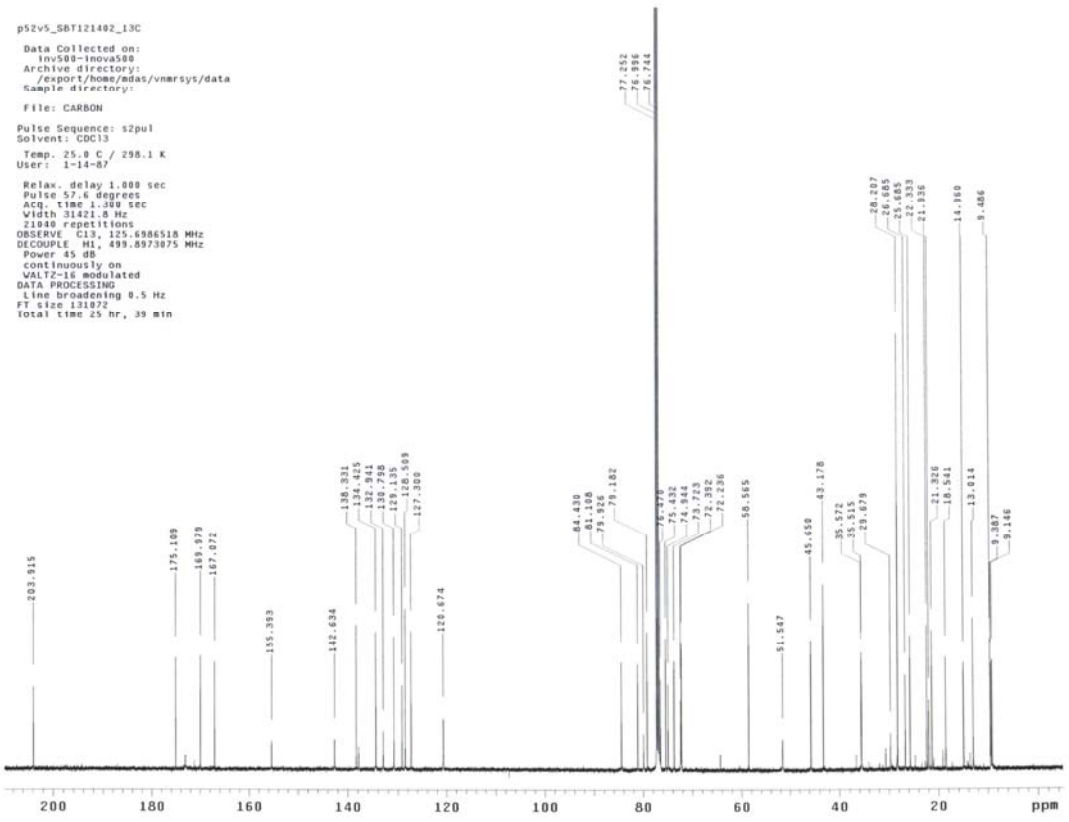

^{1}H NMR Spectrum of **6-11**

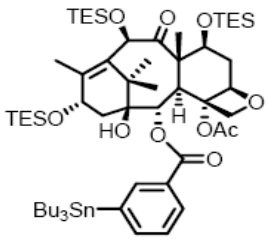

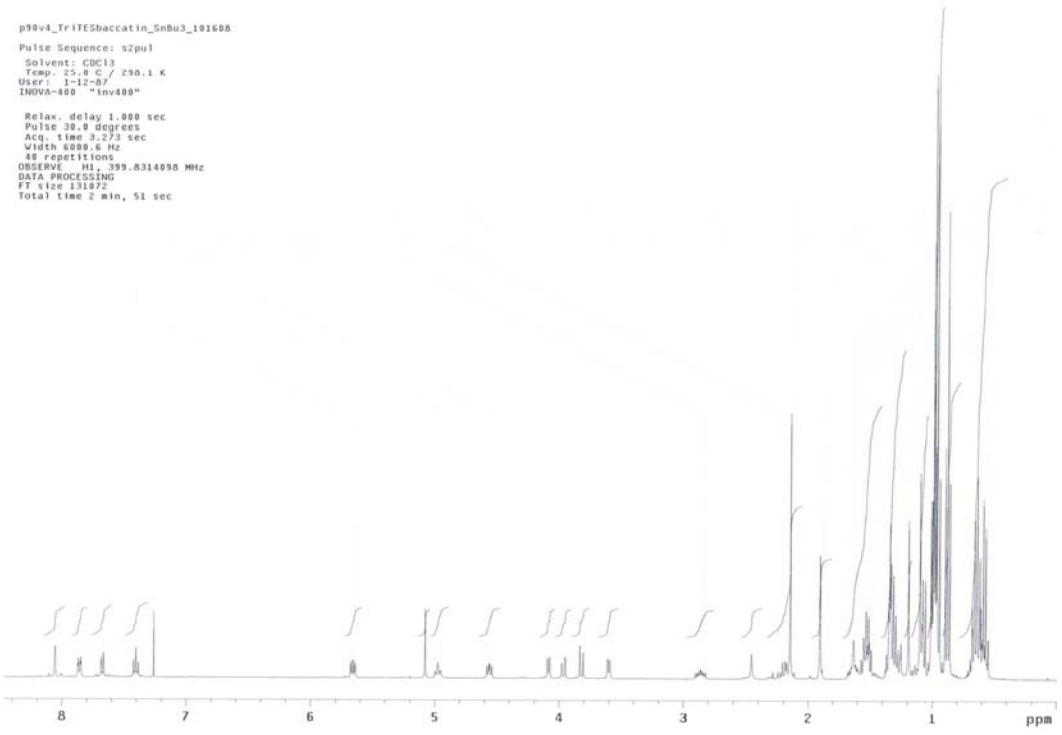

^{13}C NMR Spectrum of **6-11**

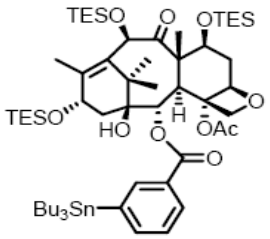

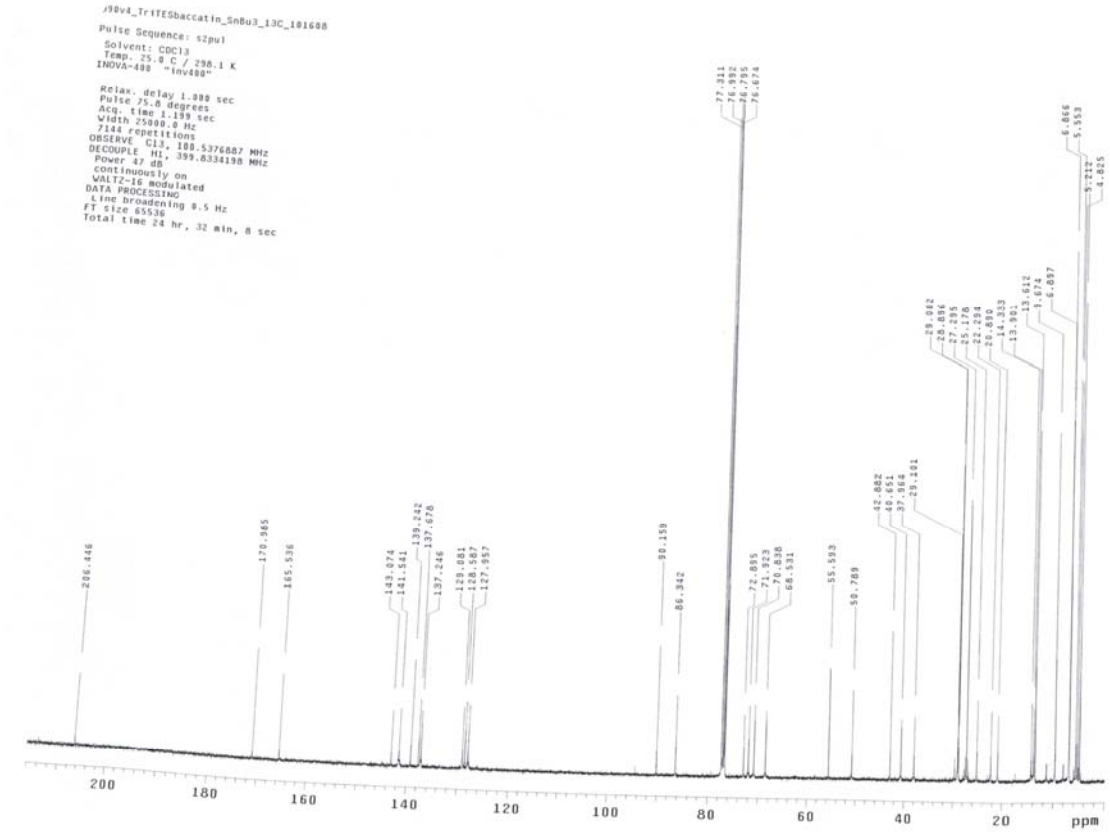

^{1}H NMR Spectrum of **6-12**

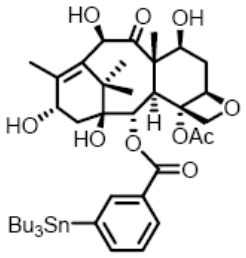

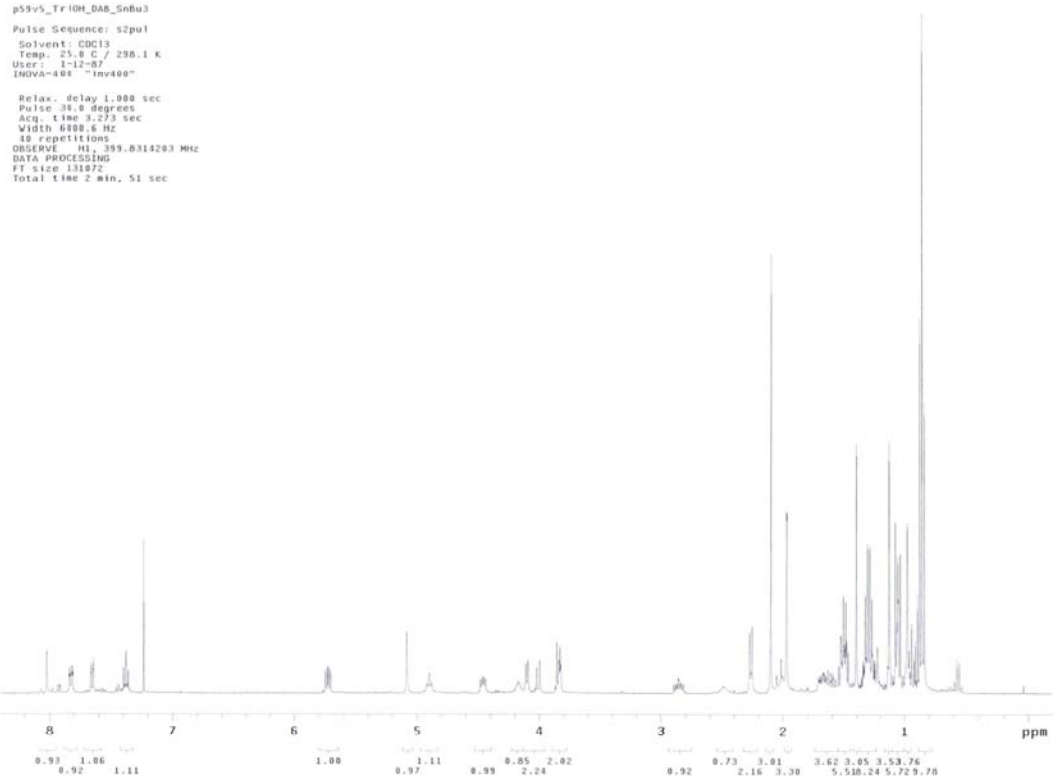

^{13}C NMR Spectrum of **6-12**

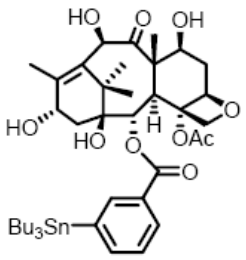

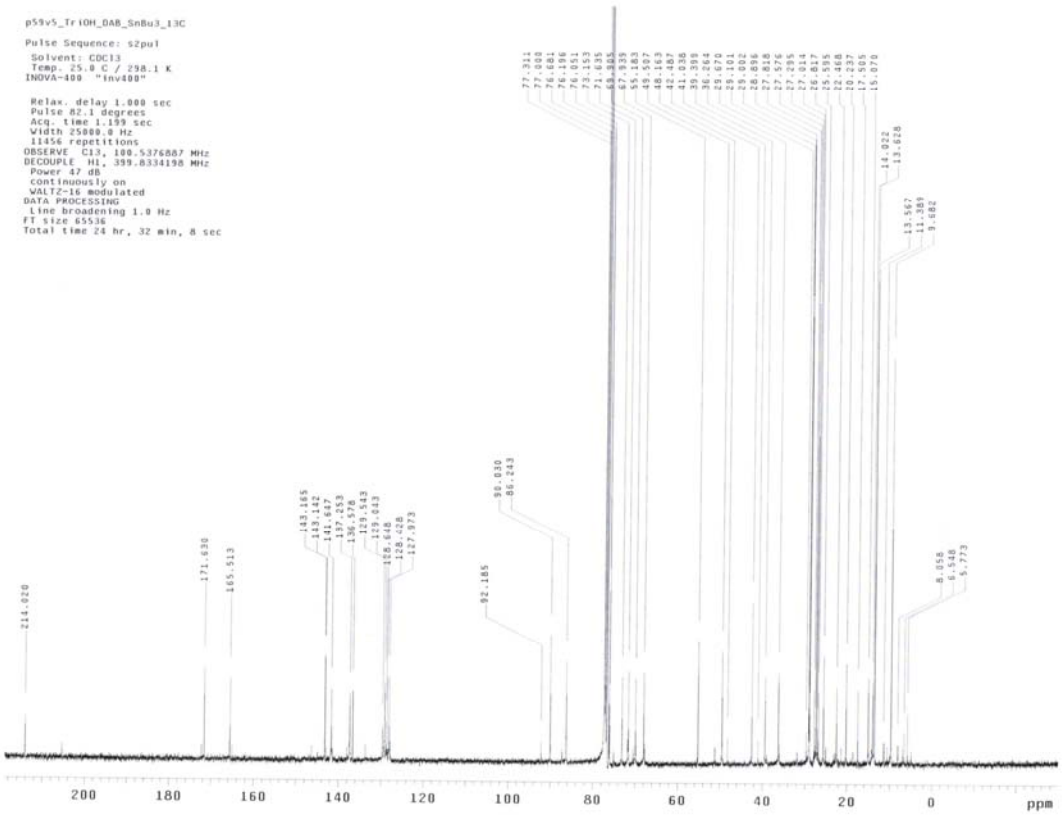

^{1}H NMR Spectrum of **6-13**

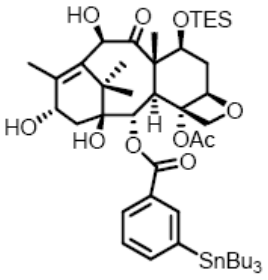

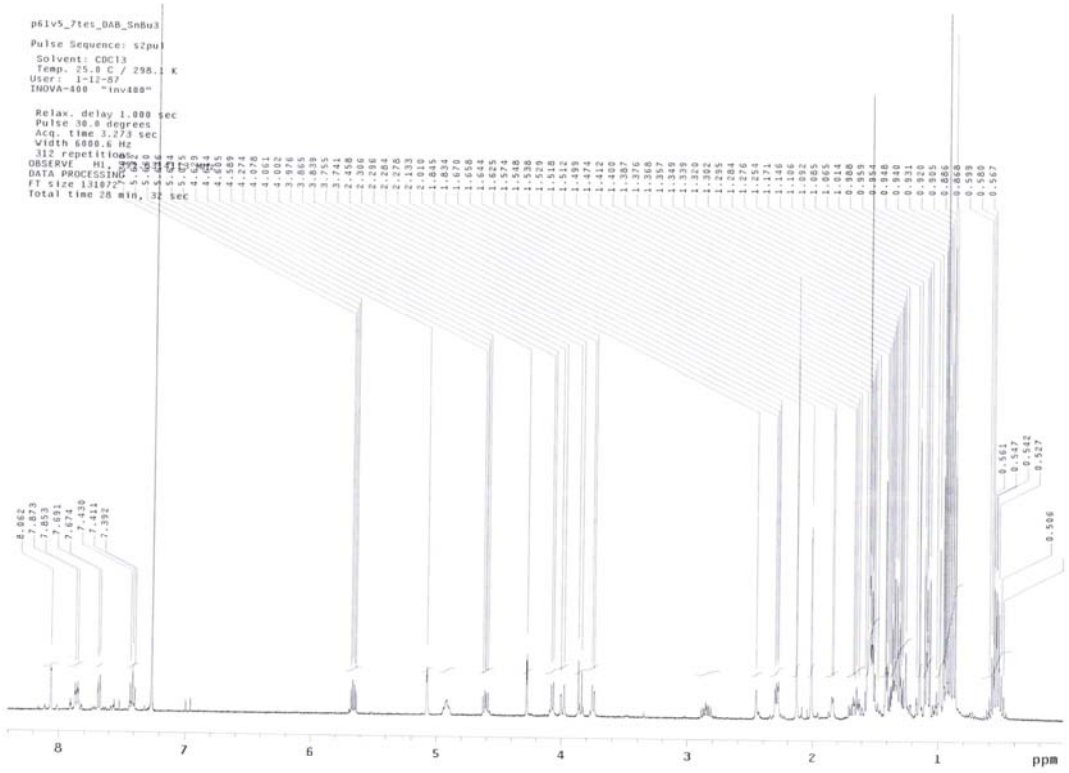

^{1}H NMR Spectrum of **6-14**

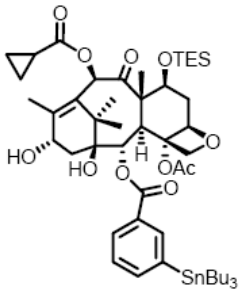

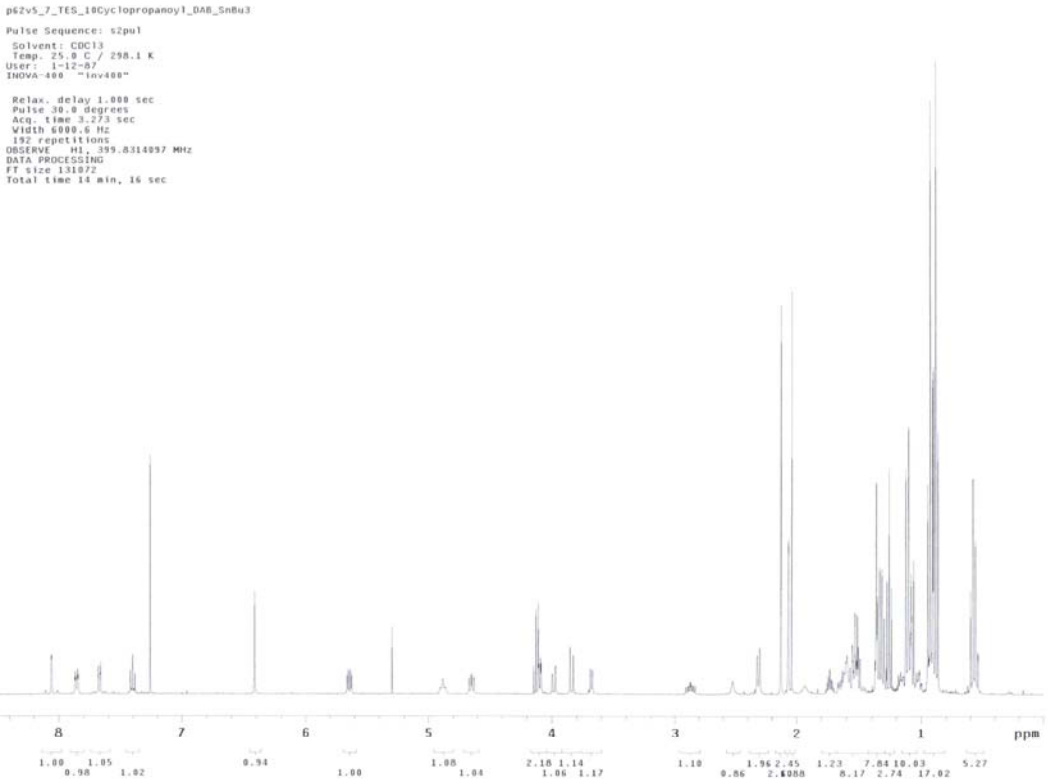

^{13}C NMR Spectrum of **6-14**

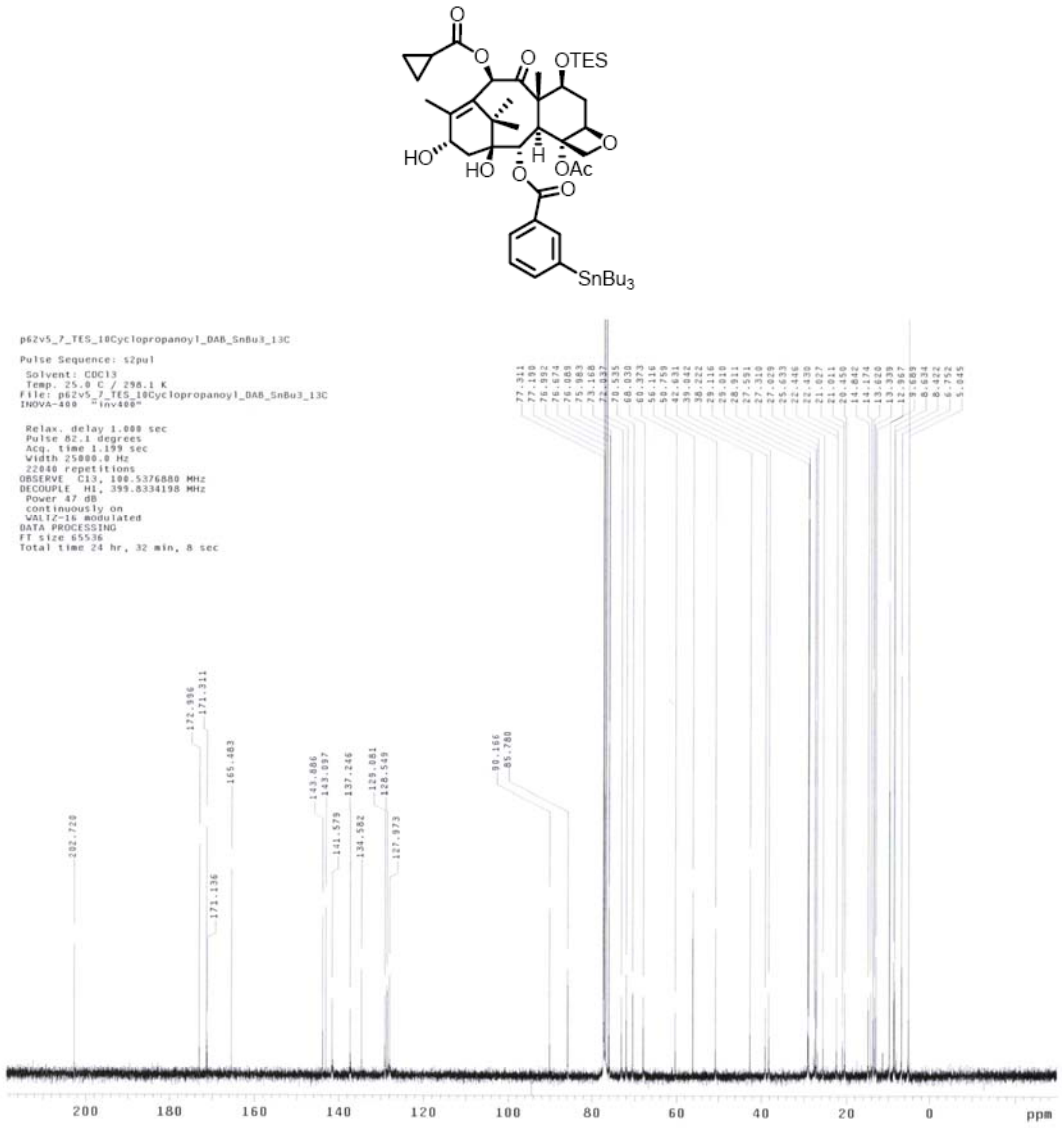

^{1}H NMR Spectrum of **6-15**

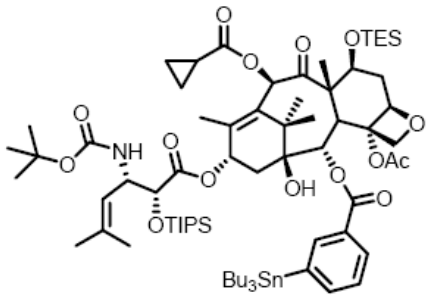

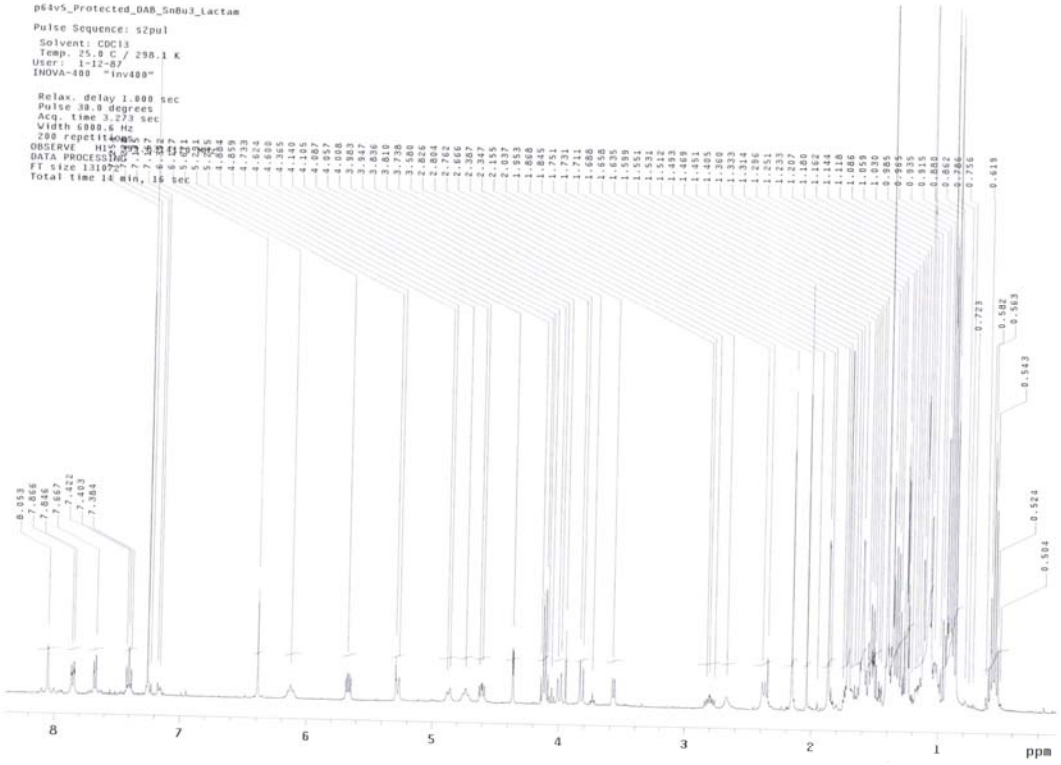

^{13}C NMR Spectrum of **6-15**

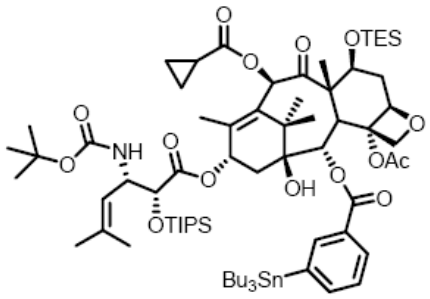

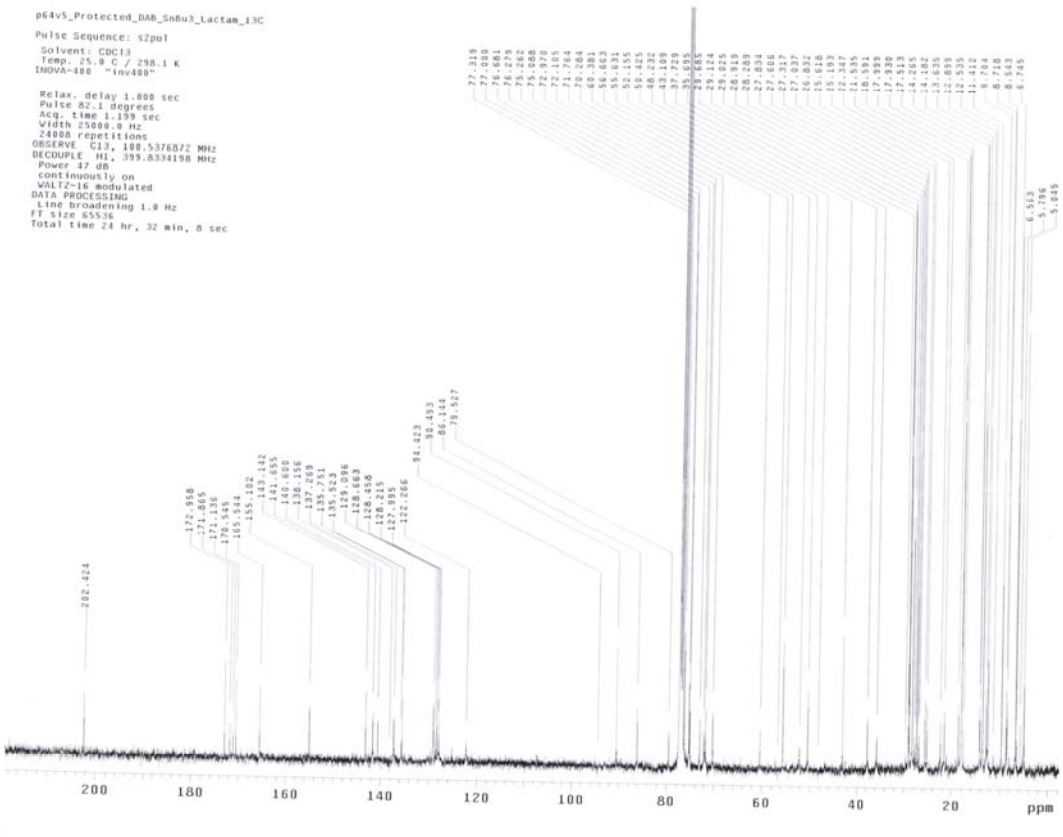

^{1}H NMR Spectrum of **6-16**

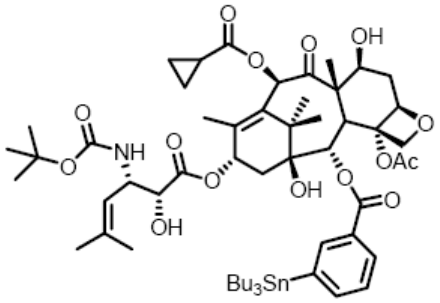

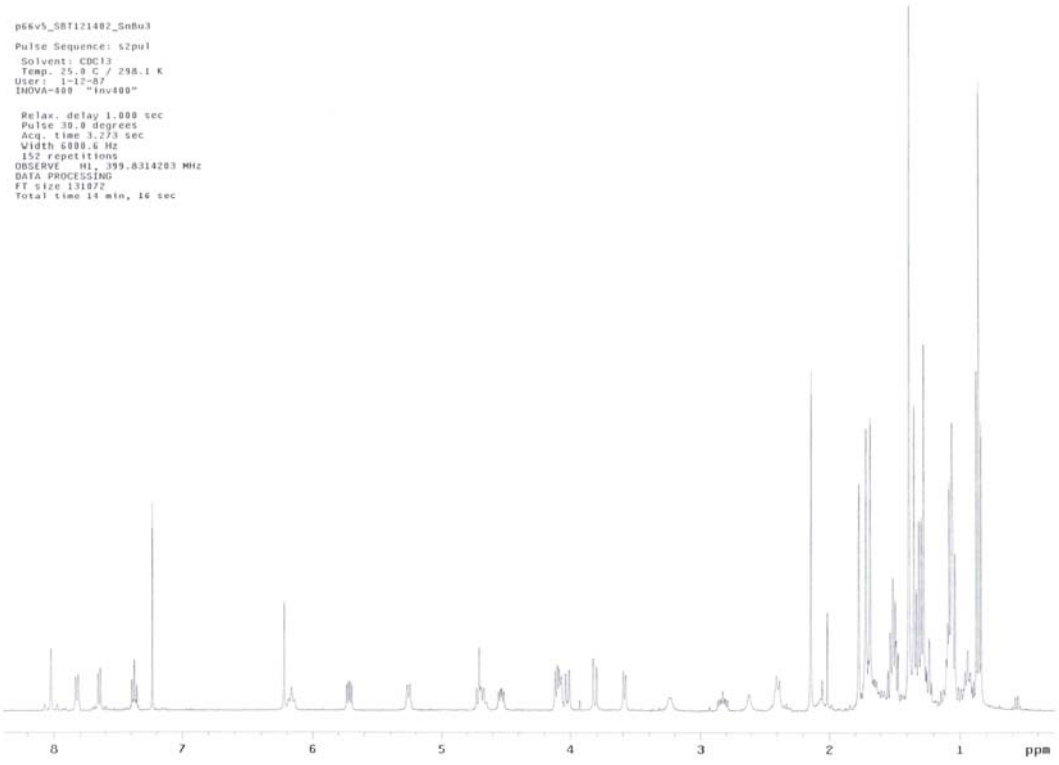

^{13}C NMR Spectrum of **6-16**